CONTENTS

	Page
SUMMARY	259
INTRODUCTION	259
SYMBOLS	259
HISTORICAL DEVELOPMENT	260
DESCRIPTION OF AIRFOILS	261
Method of Combining Mean Lines and Thickness Distributions	261
NACA Four-Digit Series Airfoils	262
Numbering system	262
Thickness distributions	263
Mean lines	263
NACA Five-Digit Series Airfoils	263
Numbering system	263
Thickness distributions	263
Mean lines	263
NACA 1-Series Airfoils	263
Numbering system	263
Thickness distributions	263
Mean lines	263
NACA 6-Series Airfoils	263
Numbering system	263
Thickness distributions	264
Mean lines	264
NACA 7-Series Airfoils	265
Numbering system	265
Thickness distributions	265
THEORETICAL CONSIDERATIONS	266
Pressure Distributions	266
Methods of derivation of thickness distributions	266
Rapid estimation of pressure distributions	268
Numerical examples	270
Effect of camber on pressure distribution	271
Critical Mach Number	271
Moment Coefficients	272
Methods of calculation	272
Numerical examples	272
Angle of Zero Lift	272
Methods of calculation	272
Numerical examples	272
Description of Flow around Airfoils	273
EXPERIMENTAL CHARACTERISTICS	274
Sources of Data	274
Drag Characteristics of Smooth Airfoils	274
Drag characteristics in low-drag range	274
Drag characteristics outside low-drag range	276
EXPERIMENTAL CHARACTERISTICS—Continued	
Drag Characteristics of Smooth Airfoils—Continued	
Effects of type of section on drag characteristics	276
Effective aspect ratio	279
Effect of surface irregularities on drag	280
Permissible roughness	280
Permissible waviness	280
Drag with fixed transition	282
Drag with practical construction methods	282
Effects of propeller slipstream and airplane vibration	287
Lift Characteristics of Smooth Airfoils	288
Two-dimensional data	288
Three-dimensional data	295
Lift Characteristics of Rough Airfoils	295
Two-dimensional data	295
Three-dimensional data	296
Unconservative Airfoils	297
Pitching Moment	298
Position of Aerodynamic Center	301
High-Lift Devices	301
Lateral-Control Devices	301
Leading-Edge Air Intakes	307
Interference	308
APPLICATION TO WING DESIGN	309
Application of Section Data	309
Selection of Root Section	309
Selection of Tip Section	310
CONCLUSIONS	310
APPENDIX—METHODS OF OBTAINING DATA IN THE LANGLEY TWO-DIMENSIONAL LOW-TURBULENCE TUNNELS	312
Description of Tunnels	312
Symbols	312
Measurement of Lift	313
Measurement of Drag	314
Tunnel-Wall Corrections	315
Correction for Blocking at High Lifts	317
Comparison with Experiment	317
REFERENCES	319
TABLES	321
SUPPLEMENTARY DATA:	
I—Basic Thickness Forms	327
II—Data for Mean Lines	347
III—Airfoil Ordinates	357
IV—Predicted Critical Mach Numbers	371
V—Aerodynamic Characteristics of Various Airfoil Sections	387

REPORT No. 824

SUMMARY OF AIRFOIL DATA

By Ira H. Abbott, Albert E. von Doenhoff, and Louis S. Stivers, Jr.

SUMMARY

Recent airfoil data for both flight and wind-tunnel tests have been collected and correlated insofar as possible. The flight data consist largely of drag measurements made by the wake-survey method. Most of the data on airfoil section characteristics were obtained in the Langley two-dimensional low-turbulence pressure tunnel. Detail data necessary for the application of NACA 6-series airfoils to wing design are presented in supplementary figures, together with recent data for the NACA 00-, 14-, 24-, 44-, and 230-series airfoils. The general methods used to derive the basic thickness forms for NACA 6- and 7-series airfoils and their corresponding pressure distributions are presented. Data and methods are given for rapidly obtaining the approximate pressure distributions for NACA four-digit, five-digit, 6-, and 7-series airfoils.

The report includes an analysis of the lift, drag, pitching-moment, and critical-speed characteristics of the airfoils, together with a discussion of the effects of surface conditions. Data on high-lift devices are presented. Problems associated with lateral-control devices, leading-edge air intakes, and interference are briefly discussed. The data indicate that the effects of surface condition on the lift and drag characteristics are at least as large as the effects of the airfoil shape and must be considered in airfoil selection and the prediction of wing characteristics. Airfoils permitting extensive laminar flow, such as the NACA 6-series airfoils, have much lower drag coefficients at high speed and cruising lift coefficients than earlier types of airfoils if, and only if, the wing surfaces are sufficiently smooth and fair. The NACA 6-series airfoils also have favorable critical-speed characteristics and do not appear to present unusual problems associated with the application of high-lift and lateral-control devices.

INTRODUCTION

A considerable amount of airfoil data has been accumulated from tests in the Langley two-dimensional low-turbulence tunnels. Data have also been obtained from tests both in other wind tunnels and in flight and include the effects of high-lift devices, surface irregularities, and interference. Some data are also available on the effects of airfoil section on aileron characteristics. Although a large amount of these data has been published, the scattered nature of the data and the limited objectives of the reports have prevented adequate analysis and interpretation of the results. The purpose of this report is to summarize these data and to correlate and interpret them insofar as possible.

Recent information on the aerodynamic characteristics of NACA airfoils is presented. The historical development of NACA airfoils is briefly reviewed. New data are presented that permit the rapid calculation of the approximate pressure distributions for the older NACA four-digit and five-digit airfoils by the same methods used for the NACA 6-series airfoils. The general methods used to derive the basic thickness forms for NACA 6- and 7-series airfoils together with their corresponding pressure distributions are presented. Detail data necessary for the application of the airfoils to wing design are presented in supplementary figures placed at the end of the paper. The report includes an analysis of the lift, drag, pitching-moment, and critical-speed characteristics of the airfoils, together with a discussion of the effects of surface conditions. Available data on high-lift devices are presented. Problems associated with lateral-control devices, leading-edge air intakes, and interference are briefly discussed, together with aerodynamic problems of application.

Numbered figures are used to illustrate the text and to present miscellaneous data. Supplementary figures and tables are not numbered but are conveniently arranged at the end of the report according to the numerical designation of the airfoil section within the following headings:

I—Basic Thickness Forms
II—Data for Mean Lines
III—Airfoil Ordinates
IV—Predicted Critical Mach Numbers
V—Aerodynamic Characteristics of Various Airfoil Sections

These supplementary figures and tables present the basic data for the airfoils.

SYMBOLS

A	aspect ratio
A_n, B_n	Fourier series coefficients
a	mean-line designation, fraction of chord from leading edge over which design load is uniform; in derivation of thickness distributions, basic length usually considered unity
b	wing span
b_{f_i}	flap span, inboard
b_{f_o}	flap span, outboard
C_D	drag coefficient
$C_{D_{L=0}}$	drag coefficient at zero lift
C_L	lift coefficient
ΔC_{L_f}	increment of maximum lift caused by flap deflection

c chord
c_a aileron chord
c_d section drag coefficient
$c_{d_{min}}$ minimum section drag coefficient
c_{f_i} flap chord, inboard
c_{f_o} flap chord, outboard
$\frac{c_f}{c}$ flap-chord ratio
c_H section aileron hinge-moment coefficient $\left(\frac{h}{q_0 c^2}\right)$
Δc_H increment of aileron hinge-moment coefficient at constant lift
$\Delta c_H \delta$ hinge-moment parameter
c_l section lift coefficient
c_{l_i} design section lift coefficient
$c_{m_{a.c.}}$ moment coefficient about aerodynamic center
$c_{m_{c/4}}$ moment coefficient about quarter-chord point
c_n section normal-force coefficient
D drag
ΔH loss of total pressure
H_0 free-stream total pressure
h section aileron hinge moment
h_e exit height
k constant
L lift
M Mach number
M_{cr} critical Mach number
0_U, 0_L typical points on upper and lower surfaces of airfoil
P pressure coefficient $\left(\frac{p-p_0}{q_0}\right)$
P_{cr} critical pressure coefficient
P_R resultant pressure coefficient; difference between local upper- and lower-surface pressure coefficients
p local static pressure; also, angular velocity in roll in $pb/2V$
p_0 free-stream static pressure
$pb/2V$ helix angle of wing tip
q_0 free-stream dynamic pressure
R Reynolds number
R_{cr} critical Reynolds number
S pressure coefficient $\left(\frac{H_0-p}{q_0}\right)$
t_1 first airfoil thickness ratio
t_2 second airfoil thickness ratio
V free-stream velocity
V_i inlet velocity
v local velocity
Δv increment of local velocity
Δv_a increment of local velocity caused by additional type of load distribution
$\left(\frac{v}{V}\right)_{t_1}$ velocity ratio corresponding to thickness t_1
$\left(\frac{v}{V}\right)_{t_2}$ velocity ratio corresponding to thickness t_2
x distance along chord
x_c mean-line abscissa
x_L abscissa of lower surface
x_U abscissa of upper surface
$\left(\frac{x}{c}\right)_{tr}$ chordwise position of transition
y distance perpendicular to chord
y_c mean-line ordinate
y_L ordinate of lower surface
y_t ordinate of symmetrical thickness distribution
y_U ordinate of upper surface
z complex variable in circle plane
z' complex variable in near-circle plane
α angle of attack
$\frac{\Delta\alpha_0}{\Delta\delta}$ section aileron effectiveness parameter, ratio of change in section angle of attack to increment of aileron deflection at a constant value of lift coefficient
α_{l_0} angle of zero lift
α_0 section angle of attack
$\Delta\alpha_0$ increment of section angle of attack
α_i section angle of attack corresponding to design lift coefficient
δ flap or aileron deflection; down deflection is positive
δ_{f_i} flap deflection, inboard
δ_{f_o} flap deflection, outboard
ϵ airfoil parameter $(\phi-\theta)$
ϵ_{TE} value of ϵ at trailing edge
ζ complex variable in airfoil plane
θ angular coordinate of z'; also, angle of which tangent is slope of mean line
λ taper ratio $\left(\frac{\text{Tip chord}}{\text{Root chord}}\right)$
τ turbulence factor $\left(\frac{\text{Effective Reynolds number}}{\text{Test Reynolds number}}\right)$
ϕ angular coordinate of z
ψ airfoil parameter determining radial coordinate of z
ψ_0 average value of ψ $\left(\frac{1}{2\pi}\int_0^{2\pi}\psi\, d\phi\right)$

HISTORICAL DEVELOPMENT

The development of types of NACA airfoils now in common use was started in 1929 with a systematic investigation of a family of airfoils in the Langley variable-density tunnel. Airfoils of this family were designated by numbers having four digits, such as the NACA 4412 airfoil. All airfoils of this family had the same basic thickness distribution (reference 1), and the amount and type of camber was systematically varied to produce the family of related airfoils. This investigation of the NACA airfoils of the four-digit series produced airfoil sections having higher maximum lift coefficients and lower minimum drag coefficients than those of sections developed before that time. The investigation also provided information on the changes in aerodynamic characteristics resulting from variations of geometry of the mean line and thickness ratio (reference 1).

The investigation was extended in references 2 and 3 to include airfoils with the same thickness distribution but with positions of the maximum camber far forward on the airfoil. These airfoils were designated by numbers having five digits, such as the NACA 23012 airfoil. Some airfoils of this family showed favorable aerodynamic characteristics except for a large sudden loss in lift at the stall.

Although these investigations were extended to include a limited number of airfoils with varied thickness distributions (references 1 and 3 to 6), no extensive investigations of thickness distribution were made. Comparison of experimental drag data at low lift coefficients with the skin-friction coefficients for flat plates indicated that nearly all of the profile drag under such conditions was attributable to skin friction. It was therefore apparent that any pronounced reduction of the profile drag must be obtained by a reduction of the skin friction through increasing the relative extent of the laminar boundary layer.

Decreasing pressures in the direction of flow and low air-stream turbulence were known to be favorable for laminar flow. An attempt was accordingly made to increase the relative extent of laminar flow by the development of airfoils having favorable pressure gradients over a greater proportion of the chord than the airfoils developed in references 1, 2, 3, and 6. The actual attainment of extensive laminar boundary layers at large Reynolds numbers was a previously unsolved experimental problem requiring the development of new test equipment with very low air-stream turbulence. This work was greatly encouraged by the experiments of Jones (reference 7), who demonstrated the possibility of obtaining extensive laminar layers in flight at relatively large Reynolds numbers. Uncertainty with regard to factors affecting separation of the turbulent boundary layer required experiments to determine the possibility of making the rather sharp pressure recoveries required over the rear portion of the new type of airfoil.

New wind tunnels were designed specifically for testing airfoils under conditions closely approaching flight conditions of air-stream turbulence and Reynolds number. The resulting wind tunnels, the Langley two-dimensional low-turbulence tunnel (LTT) and the Langley two-dimensional low-turbulence pressure tunnel (TDT), and the methods used for obtaining and correcting data are briefly described in the appendix. In these tunnels the models completely span the comparatively narrow test sections; two-dimensional flow is thus provided, which obviates difficulties previously encountered in obtaining section data from tests of finite-span wings and in correcting adequately for support interference (reference 8).

Difficulty was encountered in attempting to design airfoils having desired pressure distributions because of the lack of adequate theory. The Theodorsen method (reference 9), as ordinarily used for calculating the pressure distributions about airfoils, was not sufficiently accurate near the leading edge for prediction of the local pressure gradients. In the absence of a suitable theoretical method, the 9-percent-thick symmetrical airfoil of the NACA 16-series (reference 10) was obtained by empirical modification of the previously used thickness distributions (reference 4). These NACA 16-series sections represented the first family of the low-drag high-critical-speed sections.

Successive attempts to design airfoils by approximate theoretical methods led to families of airfoils designated NACA 2- to 5-series sections (reference 11). Experience with these sections showed that none of the approximate methods tried was sufficiently accurate to show correctly the effect of changes in profile near the leading edge. Wind-tunnel and flight tests of these airfoils showed that extensive laminar boundary layers could be maintained at comparatively large values of the Reynolds number if the airfoil surfaces were sufficiently fair and smooth. These tests also provided qualitative information on the effects of the magnitude of the favorable pressure gradient, leading-edge radius, and other shape variables. The data also showed that separation of the turbulent boundary layer over the rear of the section, especially with rough surfaces, limited the extent of laminar layer for which the airfoils should be designed. The airfoils of these early families generally showed relatively low maximum lift coefficients and, in many cases, were designed for a greater extent of laminar flow than is practical. It was learned that, although sections designed for an excessive extent of laminar flow gave extremely low drag coefficients near the design lift coefficient when smooth, the drag of such sections became unduly large when rough, particularly at lift coefficients higher than the design lift. These families of airfoils are accordingly considered obsolete.

The NACA 6-series basic thickness forms were derived by new and improved methods described herein in the section "Methods of Derivation of Thickness Distributions," in accordance with design criterions established with the objective of obtaining desirable drag, critical Mach number, and maximum-lift characteristics. The present report deals largely with the characteristics of these sections. The development of the NACA 7-series family has also been started. This family of airfoils is characterized by a greater extent of laminar flow on the lower than on the upper surface. These sections permit low pitching-moment coefficients with moderately high design lift coefficients at the expense of some reduction in maximum lift and critical Mach number.

Acknowledgement is gratefully expressed for the expert guidance and many original contributions of Mr. Eastman N. Jacobs, who initiated and supervised this work.

DESCRIPTION OF AIRFOILS

METHOD OF COMBINING MEAN LINES AND THICKNESS DISTRIBUTIONS

The cambered airfoil sections of all NACA families considered herein are obtained by combining a mean line and a thickness distribution. The necessary geometric data and some theoretical aerodynamic data for the mean lines and thickness distributions may be obtained from the supplementary figures by the methods described for each family of airfoils.

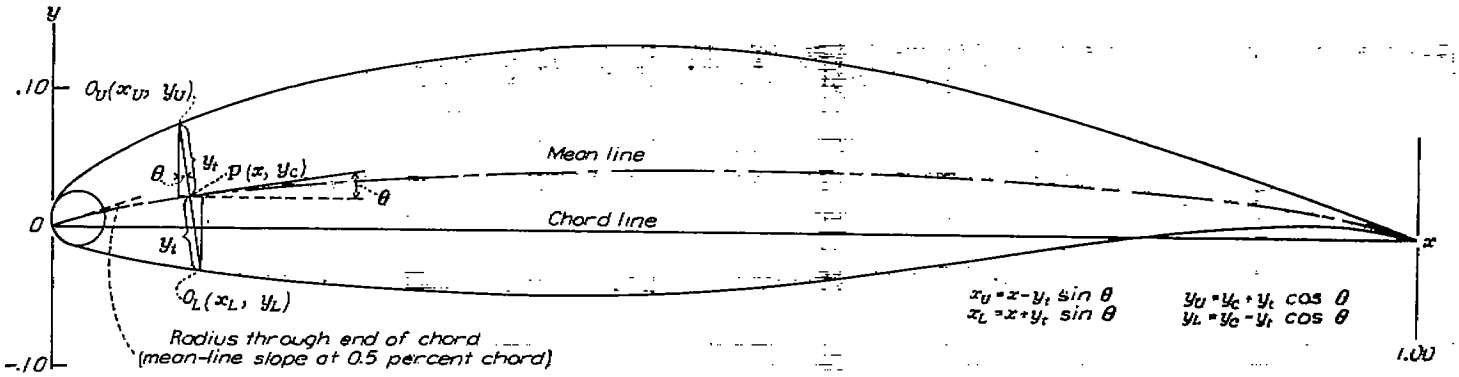

SAMPLE CALCULATIONS FOR DERIVATION OF THE NACA 65,3-818, a=1.0 AIRFOIL

x	y_t [a]	y_c [b]	$\tan\theta$	$\sin\theta$	$\cos\theta$	$y_t \sin\theta$	$y_t \cos\theta$	x_U	y_U	x_L	y_L
0	0	0	----------	----------	----------	0	0	0	0	0	0
.005	.01324	.00200	[c] 0.33696	0.31932	0.94765	.00423	.01255	.00077	.01455	.00923	−.01055
.05	.03831	.01264	.18744	.18422	.98288	.00706	.03765	.04294	.05029	.05706	−.02501
.25	.08093	.03580	.06996	.06979	.99756	.00566	.08078	.24435	.11653	.25565	−.01193
.50	.08593	.04412	0	0	1.00000	0	.08593	.50000	.13005	.50000	−.04181
.75	.04456	.03580	−.06996	−.06979	.99756	−.00311	.04445	.75311	.08026	.74689	−.00805
1.00	0	0	----------	----------	----------	0	0	1.00000	0	1.00000	0

[a] Thickness distribution obtained from ordinates of the NACA 65,3-018 airfoil.
[b] Ordinates of the mean line, 0.8 of the ordinate for c_{l_i}=1.0.
[c] Slope of radius through end of chord.

FIGURE 1.—Method of combining mean lines and basic thickness forms.

The process for combining a mean line and a thickness distribution to obtain the desired cambered airfoil section is illustrated in figure 1. The leading and trailing edges are defined as the forward and rearward extremities, respectively, of the mean line. The chord line is defined as the straight line connecting the leading and trailing edges. Ordinates of the cambered airfoil are obtained by laying off the thickness distribution perpendicular to the mean line. The abscissas, ordinates, and slopes of the mean line are designated as x_c, y_c, and tan θ, respectively. If x_U and y_U represent, respectively, the abscissa and ordinate of a typical point of the upper surface of the airfoil and y_t is the ordinate of the symmetrical thickness distribution at chordwise position x, the upper-surface coordinates are given by the following relations:

$$x_U = x - y_t \sin\theta \quad (1)$$

$$y_U = y_c + y_t \cos\theta \quad (2)$$

The corresponding expressions for the lower-surface coordinates are

$$x_L = x + y_t \sin\theta \quad (3)$$

$$y_L = y_c - y_t \cos\theta \quad (4)$$

The center for the leading-edge radius is found by drawing a line through the end of the chord at the leading edge with the slope equal to the slope of the mean line at that point and laying off a distance from the leading edge along this line equal to the leading-edge radius. This method of construction causes the cambered airfoils to project slightly forward of the leading-edge point. Because the slope at the leading edge is theoretically infinite for the mean lines having a theoretically finite load at the leading edge, the slope of the radius through the end of the chord for such mean lines is usually taken as the slope of the mean line at $\frac{x}{c}$=0.005. This procedure is justified by the manner in which the slope increases to the theoretically infinite value as x/c approaches 0. The slope increases slowly until very small values of x/c are reached. Large values of the slope are thus limited to values of x/c very close to 0 and may be neglected in practical airfoil design.

Tables of ordinates are included in the supplementary data for all airfoils for which standard characteristics are presented.

NACA FOUR-DIGIT-SERIES AIRFOILS

Numbering system.—The numbering system for the NACA airfoils of the four-digit series (reference 1) is based on the airfoil geometry. The first integer indicates the maximum value of the mean-line ordinate y_c in percent of the chord. The second integer indicates the distance from the leading edge to the location of the maximum camber in tenths of the chord. The last two integers indicate the airfoil thickness in percent of the chord. Thus, the NACA 2415 airfoil has 2-percent camber at 0.4 of the chord from the leading edge and is 15 percent thick.

The first two integers taken together define the mean line, for example, the NACA 24 mean line. The symmetrical airfoil sections representing the thickness distribution for a family of airfoils are designated by zeros for the first two integers, as in the case of the NACA 0015 airfoil.

Thickness distributions.—Data for the NACA 0006, 0008, 0009, 0010, 0012, 0015, 0018, 0021, and 0024 thickness distributions are presented in the supplementary figures. Ordinates for intermediate thicknesses may be obtained correctly by scaling the tabulated ordinates in proportion to the thickness ratio (reference 1). The leading-edge radius varies as the square of the thickness ratio. Values of $(v/V)^2$, which is equivalent to the low-speed pressure distribution, and of v/V are also presented. These data were obtained by Theodorsen's method (reference 9). Values of the velocity increments $\Delta v_a/V$ induced by changing angle of attack (see section "Rapid Estimation of Pressure Distributions") are also presented for an additional lift coefficient of approximately unity. Values of the velocity ratio v/V for intermediate thickness ratios may be obtained approximately by linear scaling of the velocity increments obtained from the tabulated values of v/V for the nearest thickness ratio; thus,

$$\left(\frac{v}{V}\right)_{t_2}=\left[\left(\frac{v}{V}\right)_{t_1}-1\right]\frac{t_2}{t_1}+1 \tag{5}$$

Values of the velocity-increment ratio $\Delta v_a/V$ may be obtained for intermediate thicknesses by interpolation.

Mean lines.—Data for the NACA 62, 63, 64, 65, 66, and 67 mean lines are presented in the supplementary figures. The data presented include the mean-line ordinates y_c, the slope dy_c/dx, the design lift coefficient c_{l_i} and the corresponding design angle of attack α_i, the moment coefficient $c_{m_{c/4}}$, the resultant pressure coefficient P_R, and the velocity ratio $\Delta v/V$. The theoretical aerodynamic characteristics were obtained from thin-airfoil theory. All tabulated values for each mean line, accordingly, vary linearly with the maximum ordinate y_c, and data for similar mean lines with different amounts of camber within the usual range may be obtained simply by scaling the tabulated values. Data for the NACA 22 mean line may thus be obtained by multiplying the data for the NACA 62 mean line by the ratio 2:6, and for the NACA 44 mean line by multiplying the data for the NACA 64 mean line by the ratio 4:6.

NACA FIVE-DIGIT-SERIES AIRFOILS

Numbering system.—The numbering system for airfoils of the NACA five-digit series is based on a combination of theoretical aerodynamic characteristics and geometric characteristics (references 2 and 3). The first integer indicates the amount of camber in terms of the relative magnitude of the design lift coefficient; the design lift coefficient in tenths is thus three-halves of the first integer. The second and third integers together indicate the distance from the leading edge to the location of the maximum camber; this distance in percent of the chord is one-half the number represented by these integers. The last two integers indicate the airfoil thickness in percent of the chord. The NACA 23012 airfoil thus has a design lift coefficient of 0.3, has its maximum camber at 15 percent of the chord, and has a thickness ratio of 12 percent.

Thickness distributions.—The thickness distributions for airfoils of the NACA five-digit series are the same as those for airfoils of the NACA four-digit series.

Mean lines.—Data for the NACA 210, 220, 230, 240, and 250 mean lines are presented in the supplementary figures in the same form as for the mean lines given herein for the four-digit series. All tabulated values for each mean line vary linearly with the maximum ordinate or with the design lift coefficient. Thus, data for the NACA 430 mean line may be obtained by multiplying the data for the NACA 230 mean line by the ratio 4:2 and for the NACA 640 mean line by multiplying the data for the NACA 240 mean line by the ratio 6:2.

NACA 1-SERIES AIRFOILS

Numbering system.—The NACA 1-series airfoils are designated by a five-digit number—as, for example, the NACA 16–212 section. The first integer represents the series designation. The second integer indicates the distance in tenths of the chord from the leading edge to the position of minimum pressure for the symmetrical section at zero lift. The first number following the dash indicates the amount of camber expressed in terms of the design lift coefficient in tenths, and the last two numbers together indicate the thickness in percent of the chord. The commonly used sections of this family have minimum pressure at 0.6 of the chord from the leading edge and are usually referred to as the NACA 16-series sections.

Thickness distributions.—Data for the NACA 16–006, 16–009, 16–012, 16–015, 16–018, and 16–021 thickness distributions (reference 10) are presented in the supplementary figures. These data are similar in form to the data for those airfoils of the NACA four-digit series, and data for intermediate thickness ratios may be obtained in the same manner.

Mean lines.—The NACA 16-series airfoils as commonly used are cambered with a mean line of the uniform-load type ($a=1.0$), which is described under the section for the NACA 6-series airfoils that follows. If any other type of mean line is used, this fact should be stated in the airfoil designation.

NACA 6-SERIES AIRFOILS

Numbering system.—The NACA 6-series airfoils are usually designated by a six-digit number together with a statement showing the type of mean line used. For example, in the designation NACA 65,3–218, $a=0.5$, the "6" is the series designation. The "5" denotes the chordwise position of minimum pressure in tenths of the chord behind the leading edge for the basic symmetrical section at zero lift. The "3" following the comma gives the range of lift coefficient in tenths above and below the design lift coefficient in which favorable pressure gradients exist on both surfaces. The "2" following the dash gives the design lift coefficient in tenths. The last two digits indicate the airfoil thickness in percent of the chord. The designation "$a=0.5$" shows the type of mean line used. When the mean-line designation is not given, it is understood that the uniform-load mean line ($a=1.0$) has been used.

When the mean line used is obtained by combining more than one mean line, the design lift coefficient used in the designation is the algebraic sum of the design lift coefficients of the mean lines used, and the mean lines are described in the statement following the number as in the following case:

$$\text{NACA } 65,3\text{–}218\begin{Bmatrix} a=0.5,\ c_{l_i}=0.3 \\ a=1.0,\ c_{l_i}=-0.1 \end{Bmatrix}$$

Airfoils having a thickness distribution obtained by linearly increasing or decreasing the ordinates of one of the originally derived thickness distributions are designated as in the following example:

$$\text{NACA } 65(318)\text{–}217,\ a=0.5$$

The significance of all of the numbers except those in the parentheses is the same as before. The first number and the last two numbers enclosed in the parentheses denote, respectively, the low-drag range and the thickness in percent of the chord of the originally derived thickness distribution.

The more recent NACA 6-series airfoils are derived as members of thickness families having a simple relationship between the conformal transformations for airfoils of different thickness ratios but having minimum pressure at the same chordwise position. These airfoils are distinguished from the earlier individually derived airfoils by writing the number indicating the low-drag range as a subscript; for example,

$$\text{NACA } 65_3\text{–}218,\ a=0.5$$

For NACA 6-series airfoils having a thickness ratio less than 0.12 of the chord, the subscript number indicating the low-drag range should be less than unity. Rather than use a fractional number, a subscript of unity was originally employed for these airfoils. Since this usage is not consistent with the previous definition of a number indicating the low-drag range, the designations of airfoil sections having a thickness ratio less than 0.12 of the chord are now given without such a number. As an example, an NACA 6-series airfoil having a thickness ratio of 0.10 of the chord would be designated:

$$\text{NACA } 65\text{–}210$$

Ordinates for the basic thickness distributions designated by a subscript are slightly different from those for the corresponding individually derived thickness distributions. As before, if the ordinates of the basic thickness distribution have been changed by a factor, the low-drag range and thickness ratio of the original thickness distribution are enclosed in parentheses as follows:

$$\text{NACA } 65_{(318)}\text{–}217,\ a=0.5$$

If, however, the ordinates of a basic thickness distribution having a thickness ratio less than 0.12 of the chord have been changed by a factor, the number indicating the low-drag range is eliminated and only the original thickness ratio is enclosed in parentheses as follows:

$$\text{NACA } 65_{(10)}\text{–}211$$

If the design lift coefficient in tenths or the airfoil thickness in percent of chord are not whole integers, the numbers giving these quantities are usually enclosed in parentheses as in the following designation:

$$\text{NACA } 65_{(318)}\text{–}(1.5)(16.5),\ a=0.5$$

Some early experimental airfoils are designated by the insertion of the letter "x" immediately preceding the hyphen as in the designation 66,2x–115.

Thickness distributions.—Data for available NACA 6-series thickness forms are presented in the supplementary figures. These data are comparable with the similar data for airfoils of the NACA four-digit series, except that ordinates for intermediate thicknesses may not be correctly obtained by scaling the tabulated ordinates proportional to the thickness ratio. This method of changing the ordinates by a factor will, however, produce shapes satisfactorily approximating members of the family if the change in thickness ratio is small. Values of v/V and $\Delta v_e/V$ for intermediate thickness ratios may be approximated as described for the NACA four-digit series.

Mean lines.—The mean lines commonly used with the NACA 6-series airfoils produce a uniform chordwise loading from the leading edge to the point $\frac{x}{c}=a$ and a linearly decreasing load from this point to the trailing edge. Data for NACA mean lines with values of a equal to 0, 0.1, 0.2, 0.3, 0.4, 0.5, 0.6, 0.7, 0.8, 0.9, and 1.0 are presented in the supplementary figures. The ordinates were computed by the following formula, which represents a simplification of the original expression for mean-line ordinates given in reference 11:

$$\frac{y_c}{c}=\frac{c_{l_i}}{2\pi(a+1)}\left\{\frac{1}{1-a}\left[\frac{1}{2}\left(a-\frac{x}{c}\right)^2\log_e\left|a-\frac{x}{c}\right|-\frac{1}{2}\left(1-\frac{x}{c}\right)^2\log_e\left(1-\frac{x}{c}\right)+\frac{1}{4}\left(1-\frac{x}{c}\right)^2-\frac{1}{4}\left(a-\frac{x}{c}\right)^2\right]-\frac{x}{c}\log_e\frac{x}{c}+g-h\,\frac{x}{c}\right\} \tag{6}$$

where

$$g=-\frac{1}{1-a}\left[a^2\left(\frac{1}{2}\log_e a-\frac{1}{4}\right)+\frac{1}{4}\right]$$

$$h=\frac{1}{1-a}\left[\frac{1}{2}(1-a)^2\log_e(1-a)-\frac{1}{4}(1-a)^2\right]+g$$

The ideal angle of attack α_i corresponding to the design lift coefficient is given by

$$\alpha_i=-h\,\frac{c_{l_i}}{2\pi(a+1)}$$

The data are presented for a design lift coefficient c_{l_i} equal to unity. All tabulated values vary directly with the design lift coefficient. Corresponding data for similar mean lines with other design lift coefficients may accordingly be obtained simply by multiplying the tabulated values by the desired design lift coefficient.

In order to camber NACA 6-series airfoils, mean lines are usually used having values of a equal to or greater than the distance from the leading edge to the location of minimum pressure for the selected thickness distribution at zero lift. For special purposes, load distributions other than those corresponding to the simple mean lines may be obtained by combining two or more types of mean line having positive or negative values of the design lift coefficient. The geometric

and aerodynamic characteristics of such combinations may be obtained by algebraic addition of the values for the component mean lines.

NACA 7-SERIES AIRFOILS

Numbering system.—The NACA 7-series airfoils are designated by a number of the following type (reference 12):

NACA 747A315

The first number "7" indicates the series number. The second number "4" indicates the extent over the upper surface, in tenths of the chord from the leading edge, of the region of favorable pressure gradient at the design lift coefficient. The third number "7" indicates the extent over the lower surface, in tenths of the chord from the leading edge, of the region of favorable pressure gradient at the design lift coefficient. The significance of the last group of three numbers is the same as for the previous NACA 6-series airfoils. The letter "A" which follows the first three numbers is a serial letter to distinguish different airfoils having parameters that would correspond to the same numerical designation. For example, a second airfoil having the same extent of favorable pressure gradient over the upper and lower surfaces, the same design lift coefficient, and the same maximum thickness as the original airfoil but having a different mean-line combination or thickness distribution would have the serial letter "B." Mean lines used for the NACA 7-series airfoils are obtained by combining two or more of the previously described mean lines. A list of the thickness distributions and mean lines used to form these airfoils is presented in table I. The basic thickness distribution is given a designation similar to those of the final cambered airfoils. For example, the basic thickness distribution for the NACA 747A315 and 747A415 airfoils is given the designation NACA 747A015 even though minimum pressure occurs at $0.4c$ on both upper and lower surfaces at zero lift. Combination of this thickness distribution with the mean lines listed in table I for the NACA 747A315 airfoil changes the pressure distribution to the desired type as shown in figure 2.

Thickness distributions.—Data for available NACA 7-series thickness distributions are presented in the supplementary figures. These thickness distributions are individually derived and do not form thickness families. The thickness ratio may, however, be changed a moderate amount—say 1 or 2 percent—by multiplying the tabulated ordinates by a suitable factor without seriously altering their characteristic features. Values of $(v/V)^2$ and of v/V for thinner or thicker thickness distributions may be approximated by the method of equation (5). If the change in thickness ratio is small, tabulated values of $\Delta v_a/V$ may be applied directly with reasonable accuracy.

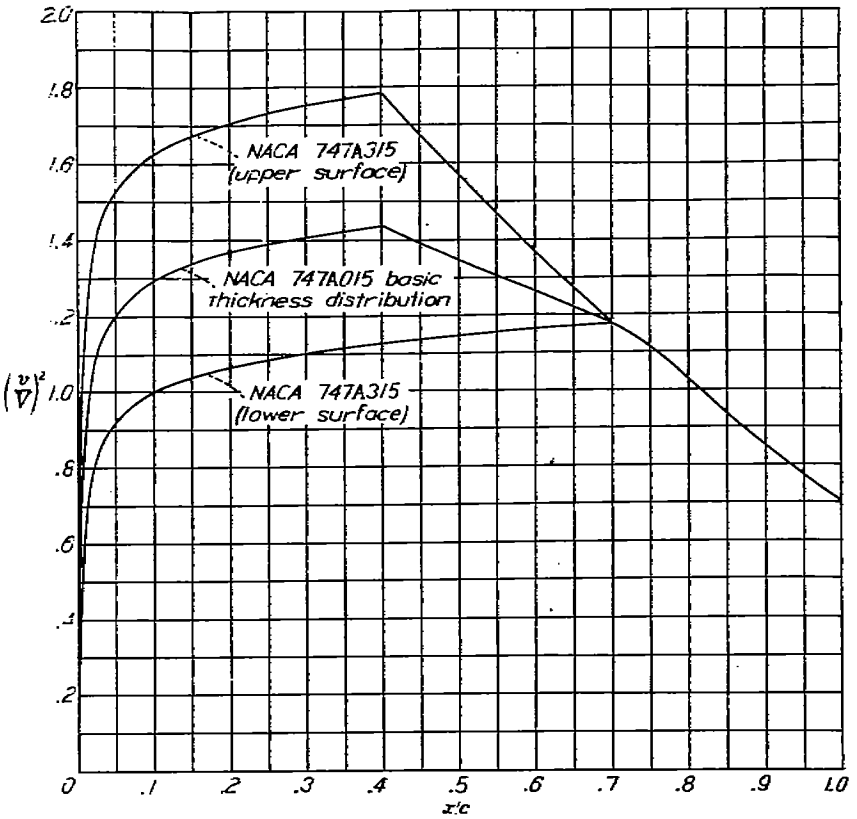

FIGURE 2.—Theoretical pressure distribution for the NACA 747A315 airfoil section at the design lift coefficient and the NACA 747A015 basic thickness distribution.

TABLE I.—ANALYSIS OF AIRFOIL DERIVATION

Airfoil designation	Basic thickness form	Mean-line combination [1]										
		$a=0$	$a=0.1$	$a=0.2$	$a=0.3$	$a=0.4$	$a=0.5$	$a=0.6$	$a=0.7$	$a=0.8$	$a=0.9$	$a=1.0$
747A315	747A015					0.763			−0.463			
747A415	747A015					.763			−.463			0.100

[1] The numbers in the various columns headed "Mean-line combination" indicate the magnitude of the design lift coefficient used.

THEORETICAL CONSIDERATIONS

PRESSURE DISTRIBUTIONS

A knowledge of the pressure distribution over an airfoil is desirable for structural design and for estimation of the critical Mach number and moment coefficient if tests are not available. The pressure distribution also exerts a strong or predominant influence on the boundary-layer flow and, hence, on the airfoil characteristics. It is therefore usually advisable to relate the airfoil characteristics to the pressure distribution rather than directly to the airfoil geometry.

Methods of derivation of thickness distributions.—As mentioned in the section "Historical Development," the basic symmetrical thickness distributions of the NACA 6- and 7-series airfoils, together with their corresponding pressure distributions, are derived by means of conformal transformations. The transformations used to relate the known flow about a circle to that about an airfoil section were developed by Theodorsen in reference 9. Figure 3 shows schematically the significance of the various phases of the process.

The circle about which the flow is originally calculated has its center at the origin and a radius of ae^{ψ_0}. The equation of this circle in complex coordinates is

$$z=ae^{\psi_0+i\phi} \tag{7}$$

where

z complex variable in circle plane

ϕ angular coordinate of z

a basic length usually considered unity

ψ_0 constant determining radius of circle

This true circle is transformed into an arbitrary, almost circular curve by the relation

$$\frac{z'}{z}=e^{(\psi-\psi_0)+i(\theta-\phi)} \tag{8}$$

the equation of the almost circular curve is

$$z'=ae^{\psi+i\theta} \tag{9}$$

where

z' complex variable in near-circle plane

ae^{ψ} radial coordinate of z'

θ angular coordinate of z'

In order for the transformation (8) to be conformal, it is necessary that the quantity $(\theta-\phi)$ (given the symbol $-\epsilon$) be the conjugate function of $(\psi-\psi_0)$; that is, if ϵ is represented by a Fourier series of the form

$$\epsilon=\sum_1^\infty A_n \sin n\phi-\sum_1^\infty B_n \cos n\phi$$

then $(\psi-\psi_0)$ is given by the relation

$$(\psi-\psi_0)=\sum_1^\infty A_n \cos n\phi+\sum_1^\infty B_n \sin n\phi$$

This relationship indicates that, if the function $\epsilon(\phi)$ is given, $(\psi-\psi_0)$ can be calculated as a function of ϕ. Means of performing this calculation are presented in reference 13. The transformation relating the almost circular curve to the airfoil shape is

$$\zeta=z'+\frac{a^2}{z'} \tag{10}$$

where ζ is the complex variable in the airfoil plane. The coordinates of the airfoil x and y are the real and imaginary parts of ζ, respectively. These coordinates are given by the relations

$$x=2a\cosh\psi\cos\theta \tag{11}$$

$$y=2a\sinh\psi\sin\theta \tag{12}$$

The velocity distribution in terms of the airfoil parameters ψ and ϵ is given exactly for perfect fluid flow by the expression

$$\frac{v}{V}=\frac{[\sin(\alpha_0+\phi)+\sin(\alpha_0+\epsilon_{TE})]\,e^{\psi_0}}{\sqrt{(\sinh^2\psi+\sin^2\theta)\left[\left(1-\frac{d\epsilon}{d\phi}\right)^2+\left(\frac{d\psi}{d\phi}\right)^2\right]}} \tag{13}$$

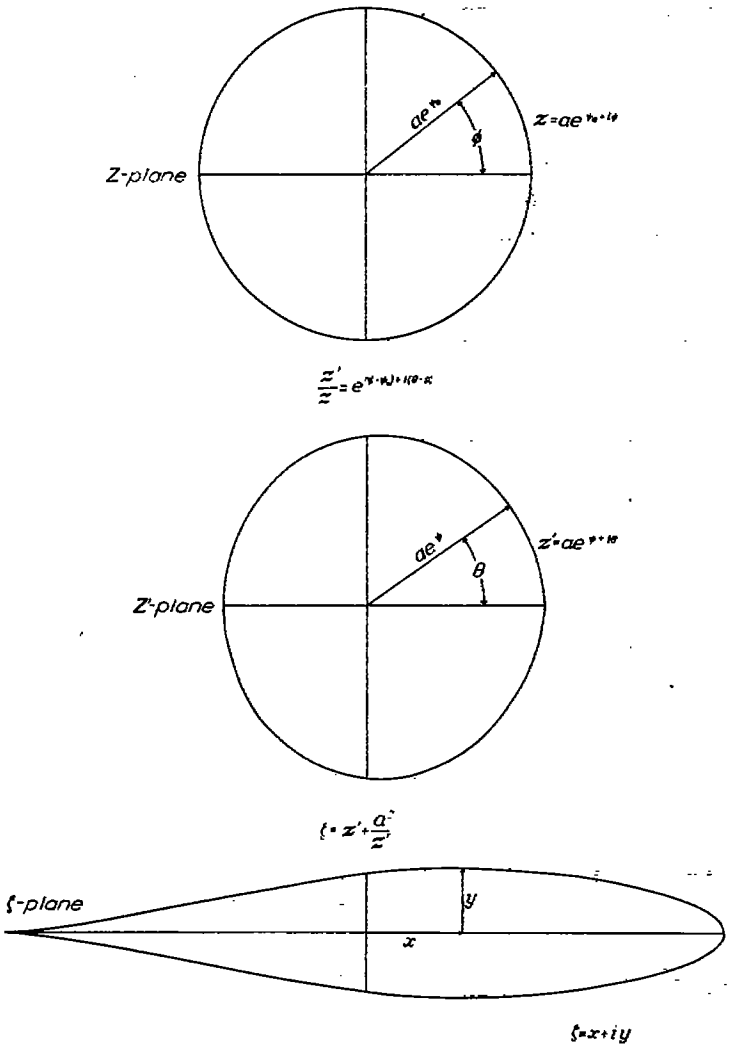

FIGURE 3.—Transformations used to derive airfoils and calculate pressure distributions.

where

v local velocity over surface of airfoil

V free-stream velocity

α_0 section angle of attack

ψ_0 average value of ψ $\left(\frac{1}{2\pi}\int_0^{2\pi}\psi\,d\phi\right)$

ϵ_{TE} value of ϵ at trailing edge

The basic symmetrical shapes were derived by assuming suitable values of $d\epsilon/d\phi$ as a function of ϕ. These values were chosen on the basis of previous experience and are subject to the conditions that

$$\int_0^{\pi}\frac{d\epsilon}{d\phi}=0$$

and $d\epsilon/d\phi$ at ϕ is equal to $d\epsilon/d\phi$ at $-\phi$. These conditions are necessary for obtaining closed symmetrical shapes. Values of $\epsilon(\phi)$ were obtained simply by integrating $\frac{d\epsilon}{d\phi}\,d\phi$. Values of $\psi(\phi)$ were found by obtaining the conjugate of the curve of $\epsilon(\phi)$ and adding a value ψ_0 sufficient to make the value of ψ equal to zero at $\phi=\pi$. This condition assures a sharp trailing-edge shape.

Inasmuch as small changes in the velocity distribution at any point of the surface are approximately proportional to $1+\frac{d\epsilon}{d\phi}$ (see reference 14), the initially assumed values of $d\epsilon/d\phi$ were altered by a process of successive approximations until the desired type of velocity distribution was obtained. After the final values of ψ and ϵ were obtained, the ordinates of the basic thickness distribution were computed by equations (11) and (12).

When these computations were made, it appeared that there was an optimum value of the leading-edge radius dependent upon the airfoil thickness and the position of minimum pressure. If the leading-edge radius was too small, a premature peak in the pressure distribution occurred in the immediate vicinity of the leading edge as the angle of attack was increased. If the leading-edge radius was too large, a premature peak occurred a few percent of the chord behind the leading edge. With the correct leading-edge radius, the pressure distribution became nearly flat over the forward portion of the airfoil before the normal leading-edge peak formed at the higher lift coefficients. Curves of the parameters ψ, ϵ, $d\psi/d\phi$, $d\epsilon/d\phi$ plotted against ϕ for the NACA 64_3–018 airfoil section are given in figure 4.

Experience has shown that, when the thickness ratio of an originally derived basic form was increased merely by multiplying all the ordinates by a constant factor, an unnecessarily large decrease in the critical speed of the resulting section occurred. Reducing the thickness ratio in a similar manner caused an unnecessarily large decrease in the low-drag range. For this reason, each of the earlier NACA 6-series sections was individually derived. It was later found that it was possible

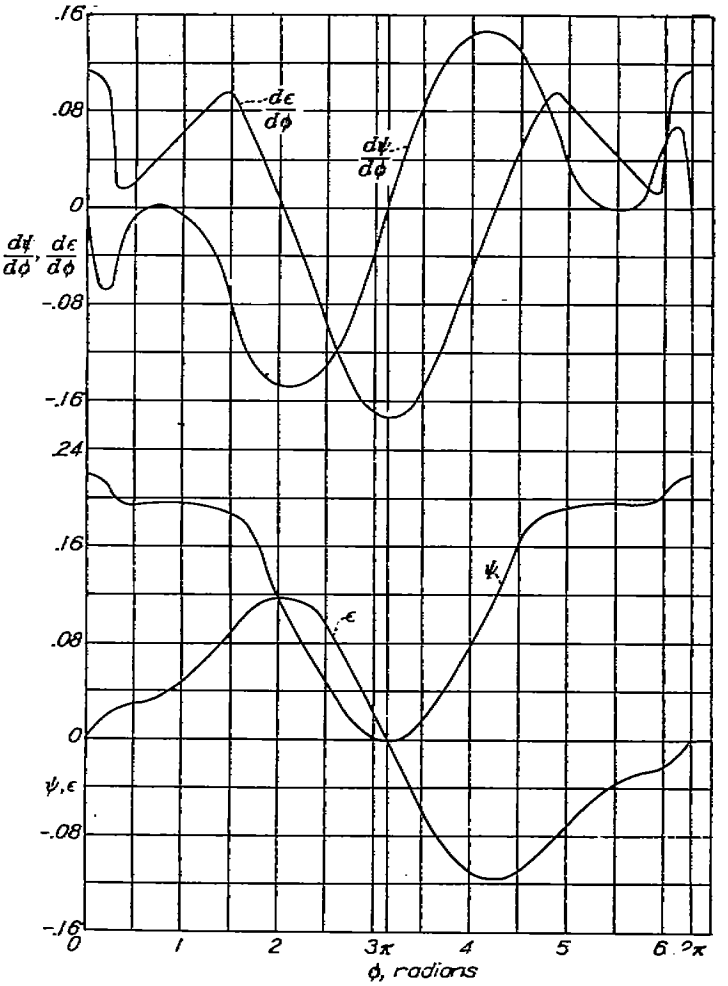

FIGURE 4.—Variation of airfoil parameters ψ, ϵ, $\frac{d\psi}{d\phi}$, $\frac{d\epsilon}{d\phi}$ with ϕ for the NACA 64_3-018 airfoil section basic thickness form.

to derive basic airfoil parameters ψ and ϵ that could be multiplied by a constant factor to obtain airfoils of various thickness ratios, without having the aforementioned limitations in the resulting sections. Each of the more recent families of NACA 6-series airfoils, in which numerical subscripts are used in the designation, having minimum pressure at a given chordwise position was obtained by scaling up and down the basic values of the airfoil parameters ψ and ϵ.

Theoretical pressure distributions $\left(\text{indicated by } \left(\frac{v}{V}\right)^2\right)$ for a family of NACA 65-series airfoils covering a range of thickness ratios are given in figure 5 (a). This figure shows the typical increase in the magnitude of the favorable pressure gradient, increase in maximum velocity over the surface, and increase in the relative pressure recovery over the rear portion of the airfoil with increase in thickness ratio. Figure 5 (b) shows the pressure distribution for a series of basic thickness forms having a thickness ratio of 0.15 and having minimum pressure at various chordwise positions. The value of the minimum pressure coefficient is seen to decrease and the magnitude of the pressure recovery over the rear portion of the airfoil to increase with the rearward movement of the point of minimum pressure.

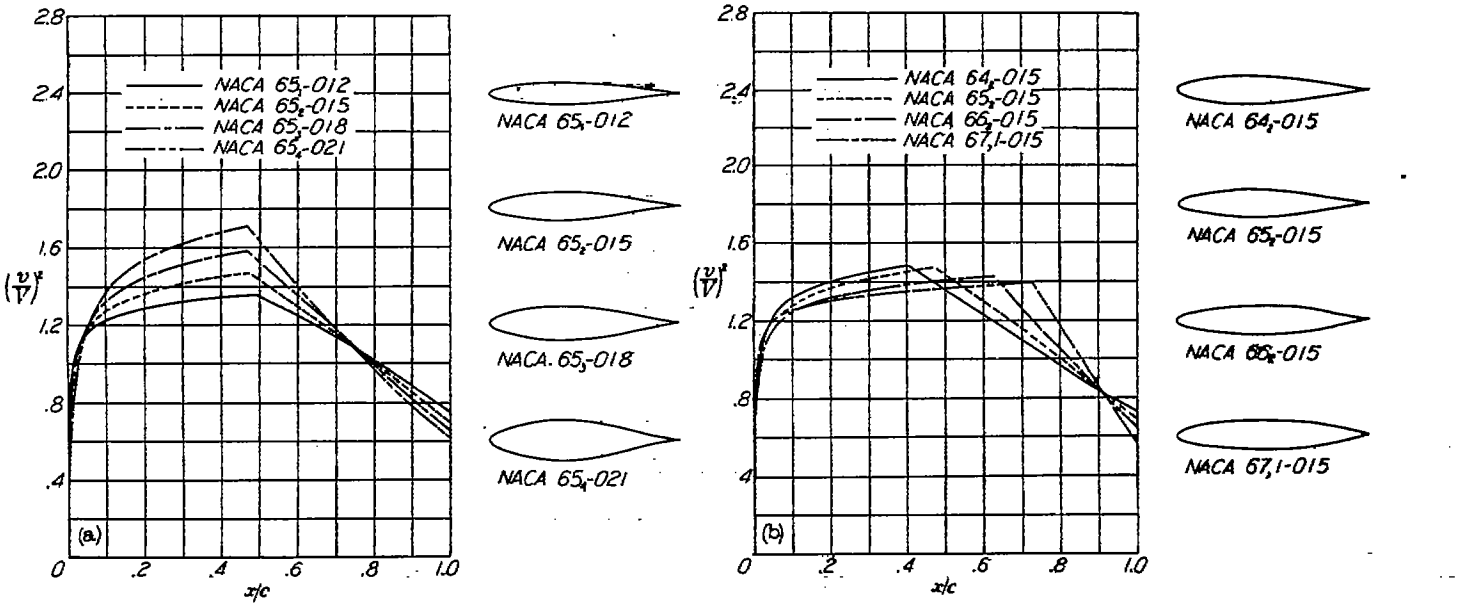

(a) Variation with thickness. (b) Variation with position of minimum pressure.

FIGURE 5.—Theoretical pressure distributions for some basic symmetrical NACA 6-series airfoils at zero lift.

The pressure distribution for one of the basic symmetrical thickness distributions at various lift coefficients is shown in figure 6. At zero lift the pressure distributions over the upper and lower surfaces are the same. As the lift coefficient is increased, the slope of the pressure distribution over the forward portion of the upper surface decreases until it becomes flat at a lift coefficient of 0.22 (the end of the low-drag range). As the lift coefficient is increased beyond this value, the usual peak in the pressure distribution forms at the leading edge.

Rapid estimation of pressure distributions.—In the discussion that follows, the term "pressure distribution" is used to signify the distribution of the static pressures on the upper and lower surfaces of the airfoil along the chord. The term "load distribution" is used to signify the distribution along the chord of the normal force resulting from the difference in pressure on the upper and lower surfaces.

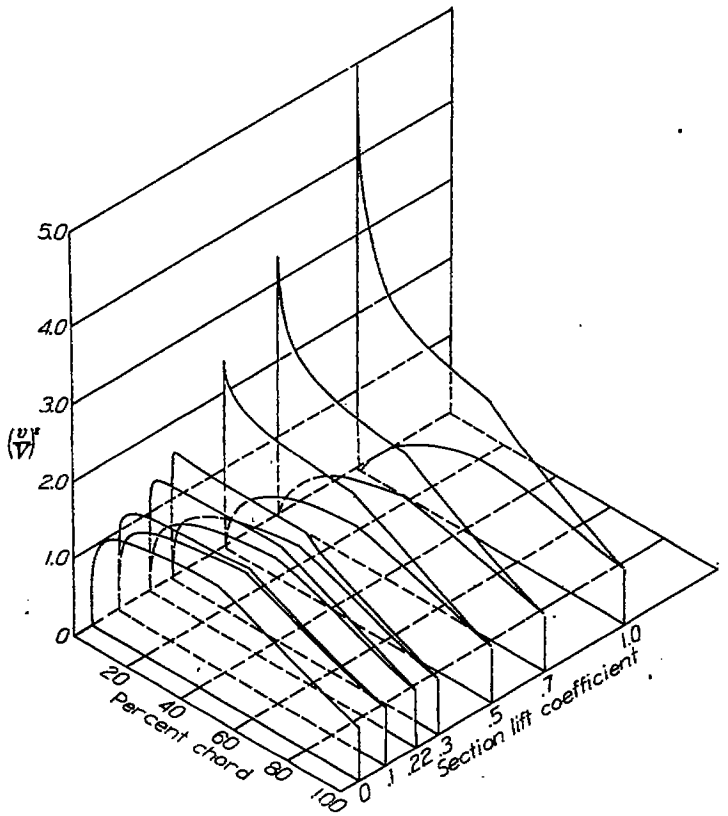

FIGURE 6.—Theoretical pressure distribution for the NACA 65₂-015 airfoil at several lift coefficients.

The pressure distribution about any airfoil in potential flow may be calculated accurately by a generalization of the methods of the previous section. Although this method is not unduly laborious, the computations required are too long to permit quick and easy calculations for large numbers of airfoils. The need for a simple method of quickly obtaining pressure distributions with engineering accuracy has led to the development of a method (reference 15) combining features of thin- and thick-airfoil theory. This simple method makes use of previously calculated characteristics of a limited number of mean lines and thickness distributions that may be combined to form large numbers of airfoils.

Thin-airfoil theory (references 16 to 18) shows that the load distribution of a thin airfoil may be considered to consist of: (1) a basic distribution at the ideal angle of attack and (2) an additional distribution proportional to the angle of attack as measured from the ideal angle of attack.

The first load distribution is a function only of the shape of the thin airfoil, or (if the thin airfoil is considered to be a mean line) of the mean-line geometry. Integration of this load distribution along the chord results in a normal-force coefficient which, at small angles of attack, is substantially equal to a lift coefficient c_{l_i}, which is designated the ideal or design lift coefficient. If, moreover, the camber of the mean line is changed by multiplying the mean-line ordinates by a constant factor, the resulting load distribution, the ideal or design angle of attack α_i and the design lift coefficient c_{l_i} may be obtained simply by multiplying the original values by the same factor. The characteristics of a large number of mean lines are presented in both graphical and tabular form in the supplementary figures. The load-distribution data are presented both in the form of the resultant pressure coefficient P_R and in the form of the corresponding velocity-increment ratios $\Delta v/V$. For positive design lift coefficients, these velocity-increment ratios are positive on the upper

surface and negative on the lower surface; the opposite is true for negative design lift coefficients.

The second load distribution, which results from changing the angle of attack, is designated herein the "additional load distribution" and the corresponding lift coefficient is designated the "additional lift coefficient." This additional load distribution contributes no moment about the quarter-chord point and, according to thin-airfoil theory, is independent of the airfoil geometry except for angle of attack. The additional load distribution obtained from thin-airfoil theory is of limited practical application, however, because this simple theory leads to infinite values of the velocity at the leading edge. This difficulty is obviated by the exact thick-airfoil theory (reference 9) which also shows that the additional load distribution is neither completely independent of the airfoil shape nor exactly a linear function of the lift coefficient. For this reason, the additional load distribution has been calculated by the methods of reference 9 for each of the thickness distributions presented in the supplementary figures. These data are presented in the form of velocity-increment ratios $\Delta v_a/V$ corresponding to an additional lift coefficient of approximately unity. For positive additional lift coefficients, these velocity-increment ratios are positive on the upper surfaces and negative on the lower surfaces; the opposite is true for negative additional lift coefficients.

In addition to the pressure distributions associated with these two load distributions, another pressure distribution exists which is associated with the basic symmetrical thickness form or thickness distribution of the airfoil. This pressure distribution has been calculated by the methods described in the previous section for the condition of zero lift and is presented in the supplementary figures as $\left(\frac{v}{V}\right)^2$, which is equivalent at low Mach numbers to the pressure coefficient S, and as the local velocity ratio v/V. This local velocity ratio is always positive and is the same for corresponding points on the upper and lower surfaces of the thickness form.

The velocity distribution about the airfoil is thus considered to be composed of three separate and independent components as follows:

(1) The distribution corresponding to the velocity distribution over the basic thickness form at zero angle of attack

(2) The distribution corresponding to the design load distribution of the mean line

(3) The distribution corresponding to the additional load distribution associated with angle of attack

The velocity-increment ratios $\Delta v/V$ and $\Delta v_a/V$ corresponding to components (2) and (3) are added to the velocity ratio corresponding to component (1) to obtain the total velocity at one point, from which the pressure coefficient S is obtained; thus,

$$S=\left(\frac{v}{V}\pm\frac{\Delta v}{V}\pm\frac{\Delta v_a}{V}\right)^2 \tag{14}$$

When this formula is used, values of the ratios corresponding to one value of x are added together and the resulting value of the pressure coefficient S is assigned to the airfoil surface at the same value of x.

The values of v/V and of $\Delta v/V$ in equation (14) should, of course, correspond to the airfoil geometry. Methods of obtaining the proper values of these ratios from the values tabulated in the supplementary figures are presented in the previous section "Description of Airfoils."

When the ratio $\Delta v_a/V$ has the value of zero, the resulting distribution of the pressure coefficient S will correspond approximately to the pressure distribution of the airfoil section at the design lift coefficient c_{l_i} of the mean line, and the lift coefficient may be assigned this value as a first approximation. If the pressure-distribution diagram is integrated, however, the value of c_l will be found to be greater than c_{l_i} by an amount dependent on the thickness ratio of the basic thickness form.

The pressure distribution will usually be desired at some specified lift coefficient not corresponding to c_{l_i}. For this purpose the ratio $\Delta v_a/V$ must be assigned some value obtained by multiplying the tabulated value of this ratio by a factor $f(\alpha)$. For a first approximation this factor may be assigned the value

$$f(\alpha)=c_l-c_{l_i} \tag{15}$$

where c_l is the lift coefficient for which the pressure distribution is desired. If greater accuracy is desired, the value of $f(\alpha)$ may be adjusted by trial and error to produce the actual desired lift coefficient as determined by integration of the pressure-distribution diagram.

Although this method of superposition of velocities has inadequate theoretical justification, experience has shown that the results obtained are adequate for engineering use. In fact, the results of even the first approximations agree well with experimental data and are adequate for at least preliminary consideration and selection of airfoils. A comparison of a first-approximation theoretical pressure distribution with an experimental distribution is shown in figure 7.

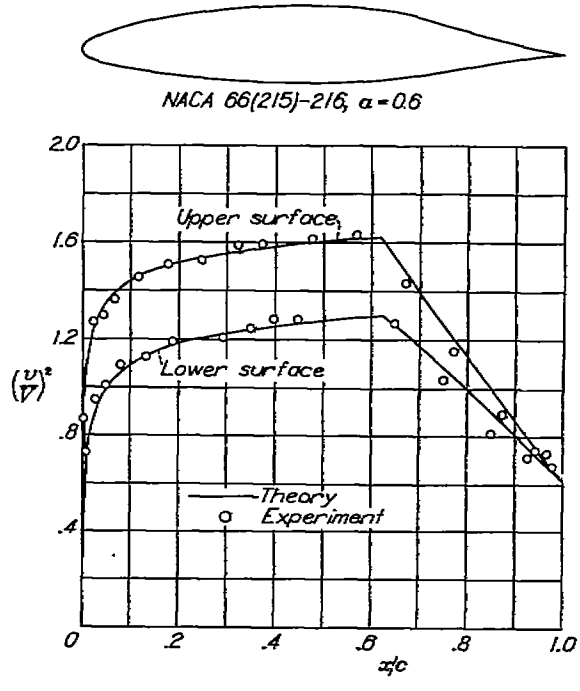

FIGURE 7.—Comparison of theoretical and experimental pressure distributions for the NACA 66(215)-216, $\alpha = 0.6$ airfoil. $c_l = 0.23$.

Some discrepancy naturally occurs between the results of experiment and of any theoretical method based on potential flow because of the presence of the boundary layer. These effects are small, however, over the range of lift coefficients for which the boundary layer is thin and the drag coefficient is low.

Numerical examples.—The following numerical examples are included to illustrate the method of obtaining the first-approximation pressure distributions:

Example 1: Find the pressure coefficient S at the station $x=0.50$ on the upper and lower surfaces of the NACA 65_3–418 airfoil at a lift coefficient of 0.2.

From the description of the NACA 6-series airfoils, it is determined that this airfoil is obtained by combining the NACA 65_3–018 basic thickness form with the $a=1.0$ type mean line cambered to a design lift coefficient of 0.4. The following data are obtained from the supplementary figures for this thickness form and mean line at $x=0.50$:

$$\frac{v}{V}=1.235$$

$$\frac{\Delta v_a}{V}=0.157$$

$$\frac{\Delta v}{V}=0.250$$

The desired value of $\Delta v_a/V$ is computed as follows by use of equation (15):

$$\frac{\Delta v_a}{V}=(0.157)\ (0.2-0.4)$$

$$=-0.031$$

The desired value of $\Delta v/V$ is obtained by multiplying the tabulated value by the design lift coefficient as stated in the description of the NACA 6-series airfoils. Thus,

$$\frac{\Delta v}{V}=(0.250)\ (0.4)$$

$$=0.100$$

Substituting these values in equation (14) gives the following values of S:

For the upper surface

$$S=(1.235+0.100-0.031)^2$$

$$=1.700$$

For the lower surface

$$S=(1.235-0.100+0.031)^2$$

$$=1.360$$

Example 2: Find the pressure coefficient S at the station $x=0.25$ on the upper and lower surfaces of the NACA $65_{(215)}$–214, $a=0.5$ airfoil at a lift coefficient of 0.6.

The airfoil designation shows that this airfoil was obtained by combining a thickness form obtained by multiplying the ordinates of the NACA 65_2–015 form by the factor 14/15 with the $a=0.5$ type mean line cambered to a design lift coefficient of 0.2.

The supplementary figures give a value of 1.182 for v/V at $x=0.25$ for the NACA 65_2–015 basic thickness form. The desired value of v/V is obtained by applying formula (5) as follows:

$$\frac{v}{V}=(1.182-1)\ \frac{14}{15}+1$$

$$=1.170$$

From the supplementary figures the following values of $\Delta v_a/V$ are obtained at $x=0.25$ for the following basic thickness forms:

Thickness form	$\frac{\Delta v_a}{V}$ at $x=0.25$
NACA 65_2–015	0.290
NACA 65_1–012	.252

By interpolation the value of $\Delta v_a/V$ of 0.287 may be assigned to the 14-percent-thick form. The desired value of $\Delta v_a/V$ is then computed as follows by use of equation (15):

$$\frac{\Delta v_a}{V}=(0.287)\ (0.6-0.2)$$

$$=0.115$$

Data presented in the supplementary figures for the $a=0.5$ type mean lines give the value of 0.333 for $\Delta v/V$ at $x=0.25$. As stated in the description of the NACA 6-series airfoils, the desired value of $\Delta v/V$ is obtained by multiplying the tabulated value by the design lift coefficient. Thus,

$$\frac{\Delta v}{V}=(0.333)\ (0.2)$$

$$=0.067$$

Substituting the foregoing values in equation (14) gives the values of S as follows:

For the upper surface

$$S=(1.170+0.067+0.115)^2$$

$$=1.828$$

For the lower surface

$$S=(1.170-0.067-0.115)^2$$

$$=0.976$$

Example 3: Find the pressure coefficient S at the station $x=0.30$ on the upper and lower surfaces of the NACA 2412 airfoil at a lift coefficient of 0.5.

The description of airfoils of the NACA four-digit series shows that the necessary data may be found from the NACA 0012 thickness form and 64 mean line in the supplementary figures. From these figures the following data are obtained:

At $x=0.30$

$$\frac{v}{V}=1.162$$

At $x=0.30$

$$\frac{\Delta v_a}{V}=0.239$$

For the NACA 64 mean line at $x=0.30$

$$\frac{\Delta v}{V}=0.260$$

For the NACA 64 mean line

$$c_{l_i}=0.76$$

The values of $\Delta v/V$ and c_{l_i} corresponding to the airfoil geometry are obtained by multiplying the foregoing values by the factor 2/6 as explained in the description of these airfoils; thus,

$$\frac{\Delta v}{V}=(0.260)\left(\frac{2}{6}\right)$$

$$=0.087$$

$$c_{l_i}=(0.76)\left(\frac{2}{6}\right)$$

$$=0.253$$

The desired value of $\Delta v_a/V$ is obtained from equation (15) as follows:

$$\frac{\Delta v_a}{V}=(0.239)(0.5-0.253)$$

$$=0.059$$

Substituting the proper values in equation (14) gives the values of S as follows:

For the upper surface

$$S=(1.162+0.087+0.059)^2$$

$$=1.712$$

For the lower surface

$$S=(1.162-0.087-0.059)^2$$

$$=1.032$$

Effect of camber on pressure distribution.—At zero lift the pressure distributions over the upper and lower surfaces of a basic symmetrical thickness distribution are, of course, identical. The effect of camber on the pressure distribution at the design lift coefficient is to separate the pressures on the upper and lower surfaces by an amount corresponding approximately to the design load distribution of the mean line. When the local value of the design load distribution is positive, the pressure coefficient S on the upper surface is increased (decreased absolute pressure) whereas that on the lower surface is decreased. This effect is shown in figure 8 (a) for various amounts of camber.

The maximum value of the pressure coefficient on the upper surface at the design lift coefficient increases with the design lift coefficient and for a given design lift coefficient increases with decreasing values of a. The result is to cause the critical Mach number at the design lift coefficient to decrease with increasing camber or with the use of types of mean line concentrating the load near the leading edge. Figure 8 (b) shows that the location of minimum pressure on both surfaces is not affected if a type of mean line is used having a value of a at least as large as the value of x/c at the position of minimum pressure on the basic thickness distribution. If a mean line with a smaller value of a is used, the possible extent of laminar flow along the upper surface will be reduced.

CRITICAL MACH NUMBER

The critical speed is defined as the free-stream speed at which the velocity at any point along the surface of the airfoil reaches the local velocity of sound. If the maximum value of the low-speed pressure coefficient S is known either experimentally or from theoretical methods, the critical Mach number may be predicted approximately by the Von Kármán method (reference 19). A curve relating the critical Mach number and the low-speed pressure coefficient S has been calculated from the equations of reference 19 and included in the supplementary figures. These predicted critical Mach numbers are useful for preliminary considerations in the absence of test data and appear to correspond fairly well to the Mach numbers at which the local velocity of sound is reached in the high-critical-speed range of lift coefficient. This criterion does not, however, appear to predict accurately

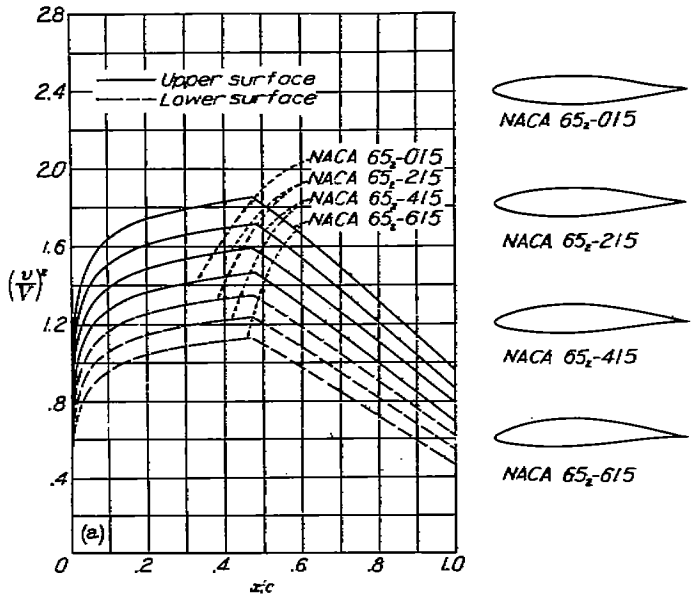

(a) Amount of camber.

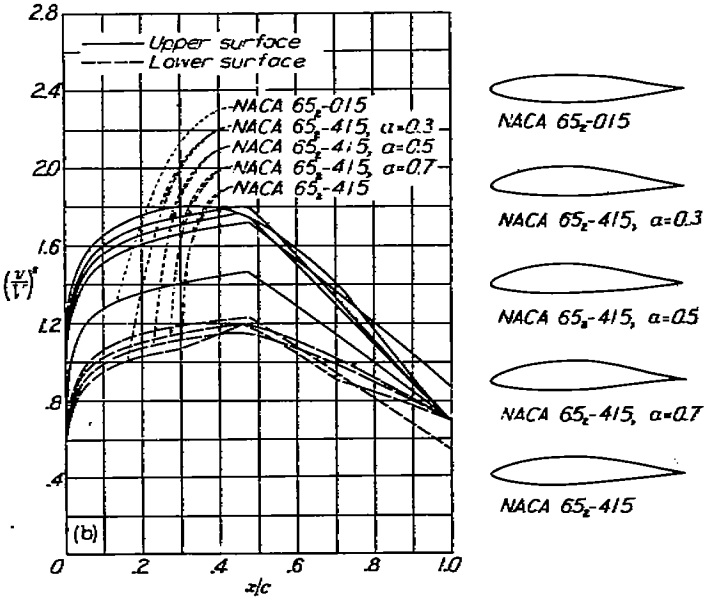

(b) Type of camber.

FIGURE 8.—Effect of amount and type of camber on pressure distribution at design lift.

the Mach numbers at which large changes in airfoil characteristics occur, especially when sharp pressure peaks exist at the leading edge. A discussion of the characteristics of airfoil sections at supercritical Mach numbers is beyond the scope of this report.

For convenience, curves of predicted critical Mach number plotted against the low-speed section lift coefficient have been included in the supplementary figures for a number of airfoils. High-speed lift coefficients may be obtained by multiplying the low-speed lift coefficient by the factor $\frac{1}{\sqrt{1-M^2}}$. The critical Mach numbers have been predicted from theoretical pressure distributions. For airfoils of the NACA four- and five-digit series and for the NACA 7-series airfoils, the theoretical pressure distributions were obtained by Theodorsen's method. For the other airfoils the theoretical pressure distributions were obtained by the approximate method described in the preceding section.

The data in the supplementary figures show that, for any one type of airfoil, the maximum critical Mach number decreases rapidly as the thickness is increased. The effect of camber is to lower the maximum critical Mach number and to shift the range of high critical Mach numbers in the same manner as for the low drag range. For common types of camber the minimum reduction in critical speed for a given design lift coefficient is obtained with a uniform load type of mean line. A comparison of the data presented in the supplementary figures shows that NACA 6-series sections have considerably higher maximum critical Mach numbers than NACA 24-, 44-, and 230-series airfoils of corresponding thickness ratios.

MOMENT COEFFICIENTS

Methods of calculation.—Theoretical moment coefficients may be approximated directly from the values presented in the supplementary figures for the various mean lines. These values were obtained from thin-airfoil theory and may be scaled up or down linearly with the design lift coefficient or with the mean-line ordinates. These theoretical values are sufficiently accurate for preliminary considerations, but experimental values should be used for stability and control calculations.

Numerical examples.—The following numerical examples illustrate the methods of calculating the moment coefficients:

Example 1: Find the theoretical moment coefficient about the quarter-chord point for the NACA 65_2-215, $a=0.5$ airfoil.

The designation of the airfoil shows that the design lift coefficient of this airfoil is 0.2. From the data on the NACA $a=0.5$ type mean line included in the supplementary figures, the value of $c_{m_{c/4}}$ is -0.139 for a design lift coefficient of 1.0. The desired value of the moment coefficient is accordingly

$$c_{m_{c/4}}=(-0.139)\ (0.2)$$
$$=-0.028$$

Example 2: Find the theoretical moment coefficient about the quarter-chord point for the NACA 4415 airfoil.

From the description of the NACA four-digit series airfoils, the required data is found to be presented for the NACA 64 mean line in the supplementary figures. The moment coefficient for this mean line is -0.157. The required value is then

$$c_{m_{c/4}}=(-0.157)\frac{4}{6}$$
$$=-0.105$$

ANGLE OF ZERO LIFT

Methods of calculation.—Values of the ideal or design angle of attack α_i corresponding to the design lift coefficient c_{l_i} are included among the data for the various mean lines presented in the supplementary figures. The approximate values of the angle of zero lift may be obtained from the data by using the theoretical value of the lift-curve slope for thin airfoils, 2π per radian. The value of α_{l_0} in degrees is then

$$\alpha_{l_0}=\alpha_i-\frac{57.3}{2\pi}c_{l_i} \tag{16}$$

The tabulated values of α_i may be scaled linearly with the design lift coefficient or with the mean-line ordinates.

Although these theoretical angles of zero lift may be useful in preliminary design, they should not be used without experimental verification for such purposes as establishing the washout of a wing.

Numerical examples.—The method of computing α_{l_0} is illustrated in the following examples:

Example 1: Find the theoretical angle of zero lift of the NACA 65_2-515, $a=0.5$ airfoil.

This airfoil number indicates a design lift coefficient of 0.5. Data for the NACA $a=0.5$ mean line indicate that $\alpha_i=3.04°$ when $c_{l_i}=1.0$. The desired value of α_i is then

$$\alpha_i=(3.04)\ (0.5)$$
$$=1.52°$$

Substituting in equation (16) gives

$$\alpha_{l_0}=1.52-\frac{(57.3)\ (0.5)}{2\pi}$$
$$=-3.0°$$

Example 2: Find the theoretical angle of zero lift for the NACA 2415 airfoil.

The description of the NACA four-digit-series airfoils shows that the required values of α_i and c_{l_i} may be obtained by multiplying the corresponding values for the NACA 64 mean line (see supplementary figures) by a factor 2/6; then

$$\alpha_i=(0.74)\left(\frac{2}{6}\right)$$
$$=0.25°$$

$$c_{l_i}=(0.76)\left(\frac{2}{6}\right)$$
$$=0.253$$

and from equation (16)

$$\alpha_{l_0}=0.25-\frac{(57.3)\ (0.253)}{2\pi}$$
$$=-2.0°$$

DESCRIPTION OF FLOW AROUND AIRFOILS

Perfect-fluid theory postulates that the flow follow the airfoil contour smoothly at all angles of attack with no loss of energy. Consequently, perfect-fluid theory itself gives no information concerning the profile drag or the maximum lift of airfoil sections. The explanation of these phenomena is found from a consideration of the effects of viscosity, which are of primary importance in a thin region near the surface of the airfoil called the boundary layer.

Boundary layers in general are of two types, namely, laminar and turbulent. The flow in the laminar layer is smooth and free from any eddying motion. The flow in the turbulent layer is characterized by the presence of a large number of relatively small eddies. Because the eddies in the turbulent layer produce a transfer of momentum from the relatively fast-moving outer parts of the boundary layer to the portions closer to the surface, the distribution of average velocity is characterized by relatively higher velocities near the surface and a greater total boundary-layer thickness in a turbulent boundary layer than in a laminar boundary layer developed under otherwise identical conditions. Skin friction is therefore higher for turbulent boundary-layer flow than for laminar flow.

When the pressures along the airfoil surface are increasing in the direction of flow, a general deceleration takes place. At the outer limits of the boundary layer this deceleration takes place in accordance with Bernoulli's law. Closer to the surface, no such simple law can be given because of the action of the viscous forces within the boundary layer. In general, however, the relative loss of speed is somewhat greater for particles of fluid within the boundary layer than for those at the outer limits of the layer because the reduced kinetic energy of the boundary-layer air limits its ability to flow against the adverse pressure gradient. If the rise in pressure is sufficiently great, portions of the fluid within the boundary layer may actually have their direction of motion reversed and may start moving upstream. When this reverse occurs, the flow in the boundary layer is said to be "separated." Because of the increased interchange of momentum from different parts of the layer, turbulent boundary layers are much more resistant to separation than are laminar layers. Laminar boundary layers can only exist for a relatively short distance in a region in which the pressure increases in the direction of flow. Formulas for calculating many of the boundary-layer characteristics are given in references 20 to 22.

After laminar separation occurs, the flow may either leave the surface permanently or reattach itself in the form of a turbulent boundary layer. Not much is known concerning the factors controlling this phenomenon. Laminar separation on wings is usually not permanent at flight values of the Reynolds number except when it occurs near the leading edge under conditions corresponding to maximum lift. The size of the locally separated region that is formed when the laminar boundary layer separates and the flow returns to the surface decreases with increasing Reynolds number at a given angle of attack.

The flow over aerodynamically smooth airfoils at low and moderate lift coefficients is characterized by laminar boundary layers from the leading edge back to approximately the location of the first minimum-pressure point on both upper and lower surfaces. If the region of laminar flow is extensive, separation occurs immediately downstream from the location of minimum pressure (reference 20) and the flow returns to the surface almost immediately at flight Reynolds numbers as a turbulent boundary layer. This turbulent boundary layer extends to the trailing edge. If the surfaces are not sufficiently smooth and fair, if the air stream is turbulent, or perhaps if the Reynolds number is sufficiently large, transition from laminar to turbulent flow may occur anywhere upstream of the calculated laminar separation point.

For low and moderate lift coefficients where inappreciable separation occurs, the airfoil profile drag is largely caused by skin friction and the value of the drag coefficient depends mainly on the relative amounts of laminar and turbulent flow. If the location of transition is known or assumed, the drag coefficient may be calculated with reasonable accuracy from boundary-layer theory by use of the methods of references 23 and 24.

As the lift coefficient of the airfoil is increased by changing the angle of attack, the resulting application of the additional type of lift distribution moves the minimum-pressure point upstream on the upper surface, and the possible extent of laminar flow is thus reduced. The resulting greater proportion of turbulent flow, together with the larger average velocity of flow over the surfaces, causes the drag to increase with lift coefficient.

In the case of many of the older types of airfoils, this forward movement of transition is gradual and the resulting variation of drag with lift coefficient occurs smoothly. The pressure distributions for NACA 6-series airfoils are such as to cause transition to move forward suddenly at the end of the low-drag range of lift coefficients. A sharp increase in drag coefficient to the value corresponding to a forward location of transition on the upper surface results. Such sudden shifts in transition give the typical drag curve for these airfoils with a "sag" or "bucket" in the low-drag range. The same characteristic is shown to a smaller degree by some of the earlier airfoils such as the NACA 23015 when tested in a low-turbulence stream.

At high lift coefficients, a large part of the drag is contributed by pressure or form drag resulting from separation of the flow from the surface. The flow over the upper surface is characterized by a negative pressure peak near the leading edge, which causes laminar separation. The onset of turbulence causes the flow to return to the surface as a turbulent boundary layer. High Reynolds numbers are favorable to the development of turbulence and aid in this process. If the lift coefficient is sufficiently high or if the reestablishment of flow following laminar separation is unduly delayed by low Reynolds numbers, the turbulent layer will separate from the surface near the trailing edge and will cause large drag increases. The eventual loss in lift with increasing angle of attack may result either from relatively sudden permanent separation of the laminar boundary layer near the leading edge or from progressive forward movement of turbulent separation. Under the latter condition, the flow over a relatively large portion of the surface may be separated prior to maximum lift. A more extended discussion of the flow conditions associated with maximum lift is given in reference 5.

EXPERIMENTAL CHARACTERISTICS

SOURCES OF DATA

The primary source of the wind-tunnel data presented is from tests in the Langley two-dimensional low-turbulence pressure tunnel (TDT). The methods used to obtain and correct the data are summarized in the appendix. Design data obtained from tests of 2-foot-chord models in this tunnel are presented in the supplementary figures.

Some wind-tunnel data presented were obtained in other NACA wind tunnels. In each case, the source of the data is indicated and the testing techniques and corrections used were conventional unless otherwise indicated.

Most of the flight data consist of drag measurements made by the wake-survey method on either the airplane wing or a "glove" fitted over the wing as the test specimen. Whenever the measurements were obtained for a glove, this fact is indicated in the presentation of the data. All data obtained at high speeds have been reduced to coefficient form by compressible-flow methods. In the case of all such NACA flight data, precautions have been taken to ensure that the results presented are not invalidated by cross flows of low-energy air into or out of the survey plane.

DRAG CHARACTERISTICS OF SMOOTH AIRFOILS

Drag characteristics in low-drag range.—The value of the drag coefficient in the low-drag range for smooth airfoils is mainly a function of the Reynolds number and the relative extent of the laminar layer and is moderately affected by the airfoil thickness ratio and camber. The effect on minimum drag of the position of minimum pressure which determines the possible extent of laminar flow is shown in figure 9 for some NACA 6-series airfoils. The data show a regular decrease in drag coefficient with rearward movement of minimum pressure.

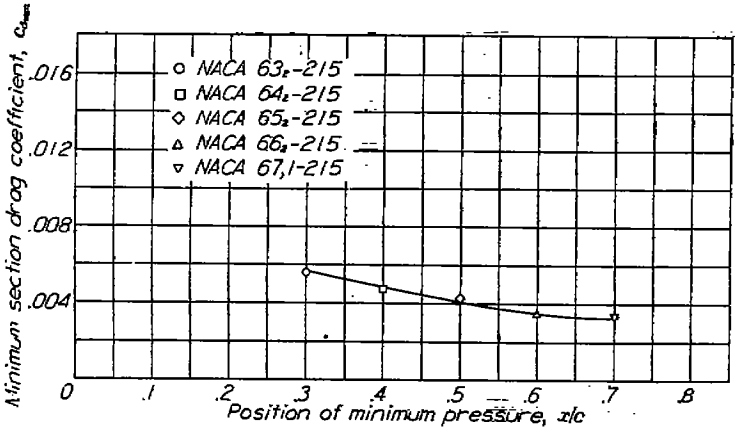

FIGURE 9.—Variation of minimum drag coefficient with position of minimum pressure for some NACA 6-series airfoils of the same camber and thickness. $R = 6 \times 10^6$.

The variation of minimum drag coefficient with Reynolds number for several airfoils is shown in figure 10. The drag coefficient generally decreases with increasing Reynolds number up to Reynolds numbers of the order of 20×10^6. Above this Reynolds number the drag coefficient of the NACA $65_{(421)}$–420 airfoil remained substantially constant up to a Reynolds number of nearly 40×10^6. The earlier increase in drag coefficient shown by the NACA 66(2x15)–116 airfoil may be caused by surface irregularities because the specimen

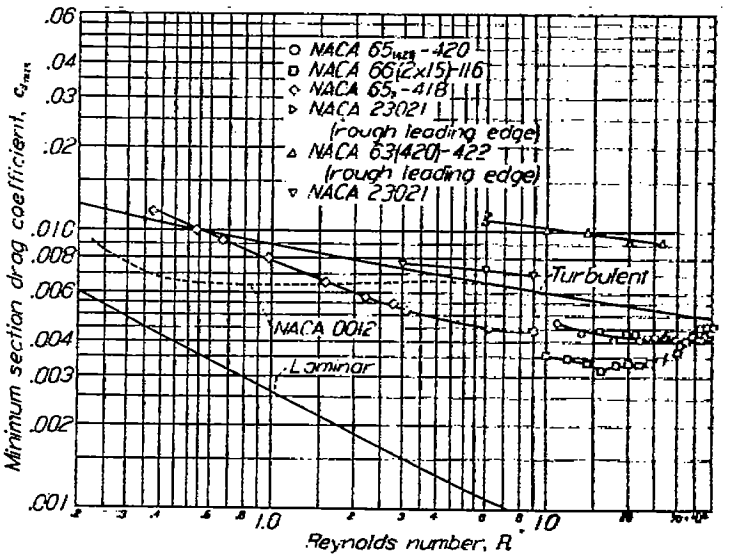

FIGURE 10.—Variation of minimum section drag coefficient with Reynolds number for several airfoils, together with laminar and turbulent skin-friction coefficients for a flat plate.

tested was a practical-construction model. It may be noted that the drag coefficient for the NACA 65_3–418 airfoil at low Reynolds numbers is substantially higher than that of the NACA 0012, whereas at high Reynolds numbers the opposite is the case. The higher drag of the NACA 65_3–418 airfoil section at low Reynolds numbers is caused by a relatively extensive region of laminar separation downstream of the point of minimum pressure. This region decreases in size with increasing Reynolds number. These data illustrate the inadequacy of low Reynolds number test data either to estimate the full-scale characteristics or to determine the relative merits of airfoil sections at flight Reynolds numbers (references 25 and 26).

The variation of minimum drag coefficient with camber is shown in figure 11 for a number of smooth 18-percent-thick NACA 6-series airfoils. These data show very little change

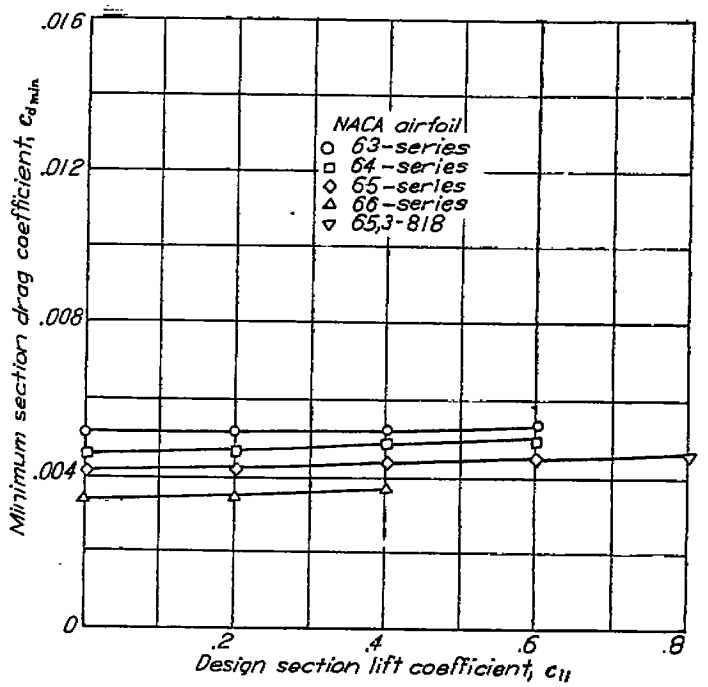

FIGURE 11.—Variation of minimum section drag coefficient with camber for several NACA 6-series airfoil sections of 18-percent thickness ratio. $R = 9 \times 10^6$.

in minimum drag coefficient with increase in camber. A large amount of systematic data is included in figure 12 to show the variation of minimum drag coefficient with thickness ratio for a number of NACA airfoil sections ranging in thickness from 6 percent to 24 percent of the chord. The minimum drag coefficient is seen to increase with increase in thickness ratio for each airfoil series. This increase, however, is greater for the NACA four- and five-digit-series airfoils (fig. 12 (a)) than for the NACA 6-series airfoils (figs. 12 (b) to 12 (e)).

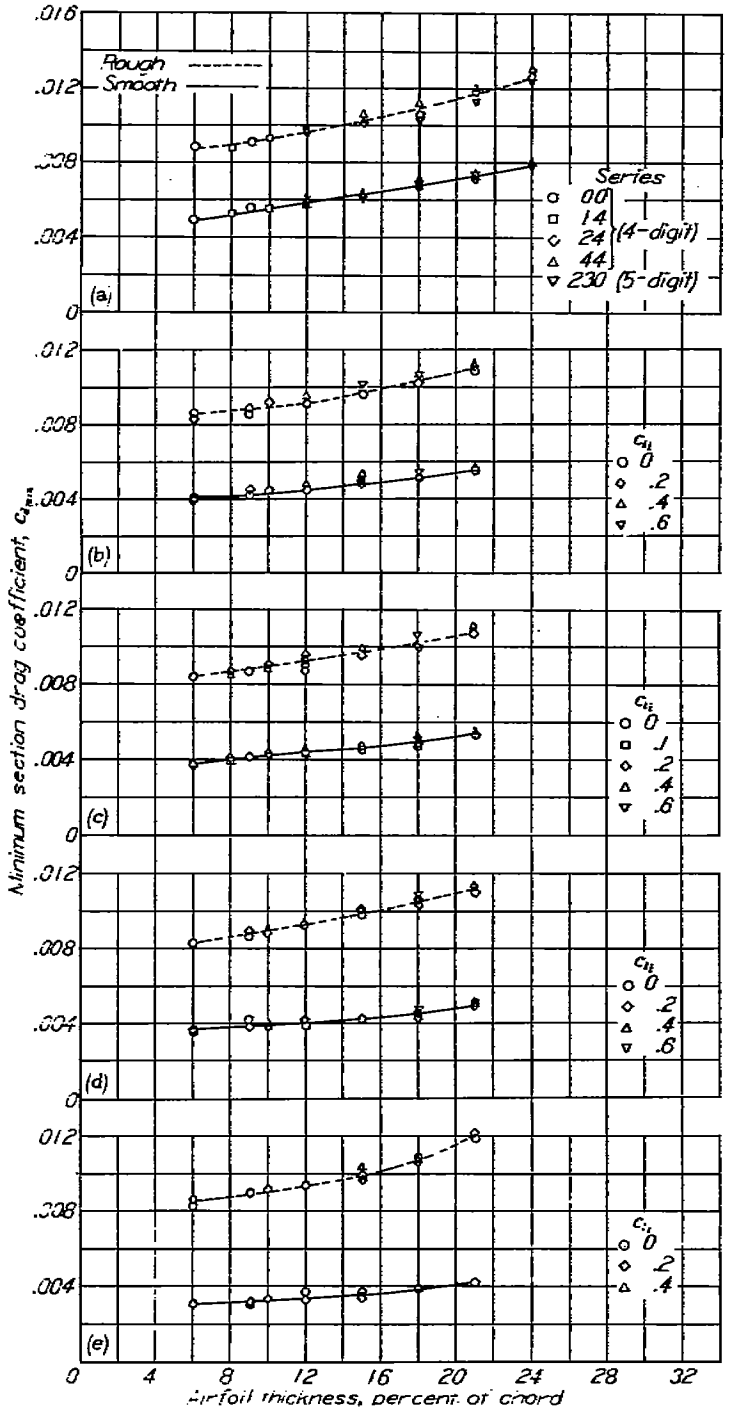

(a) NACA four- and five-digit series.
(b) NACA 63-series.
(c) NACA 64-series.
(d) NACA 65-series.
(e) NACA 66-series.

FIGURE 12.—Variation of minimum section drag coefficient with airfoil thickness ratio for several NACA airfoil sections of different cambers in both smooth and rough conditions. $R = 6 \times 10^6$.

The data presented in the supplementary figures for the NACA 6-series thickness forms show that the range of lift coefficients for low drag varies markedly with airfoil thickness. It has been possible to design airfoils of 12-percent thickness with a total theoretical low-drag range of lift coefficients of 0.2. This theoretical range increases by approximately 0.2 for each 3-percent increase of airfoil thickness. Figure 13 shows that the theoretical extent of the low-drag range is approximately realized at a Reynolds number of 9×10^6. Figure 13 also shows a characteristic tendency for the drag to increase to some extent toward the upper end of the low-drag range for moderately cambered airfoils, particularly for the thicker airfoils. All data for the NACA 6-series airfoils show a decrease in the extent of the low-drag range with increasing Reynolds number. Extrapolation of the rate of decrease observed at Reynolds numbers below 9×10^6 would indicate a vanishingly small low-drag range at flight values of the Reynolds number. Tests of a carefully constructed model of the NACA $65_{(421)}$–420 airfoil showed, however, that the rate of reduction of the low-drag range with increasing Reynolds number decreased markedly at Reynolds numbers above 9×10^6 (fig. 14). These data indicate that the extent of the low-drag range of this airfoil is reduced to about one-half the theoretical value at a Reynolds number of 35×10^6.

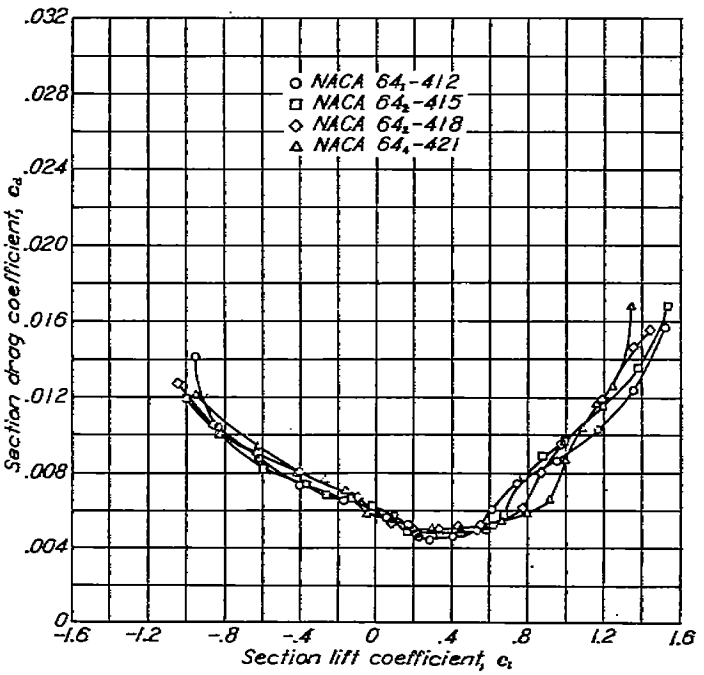

FIGURE 13.—Drag characteristics of some NACA 64-series airfoil sections of various thicknesses, cambered to a design lift coefficient of 0.4. $R = 9 \times 10^6$; TDT tests 652, 733, 735, and 691.

The values of the lift coefficient for which low drag is obtained are determined largely by the amount of camber. The lift coefficient at the center of the low-drag range corresponds approximately to the design lift coefficient of the mean line. The effect on the drag characteristics of various amounts of camber is shown in figure 15. Section data indicate that the location of the low-drag range may be shifted by even such crude camber changes as those caused by small deflections of a plain flap. (See supplementary fig.)

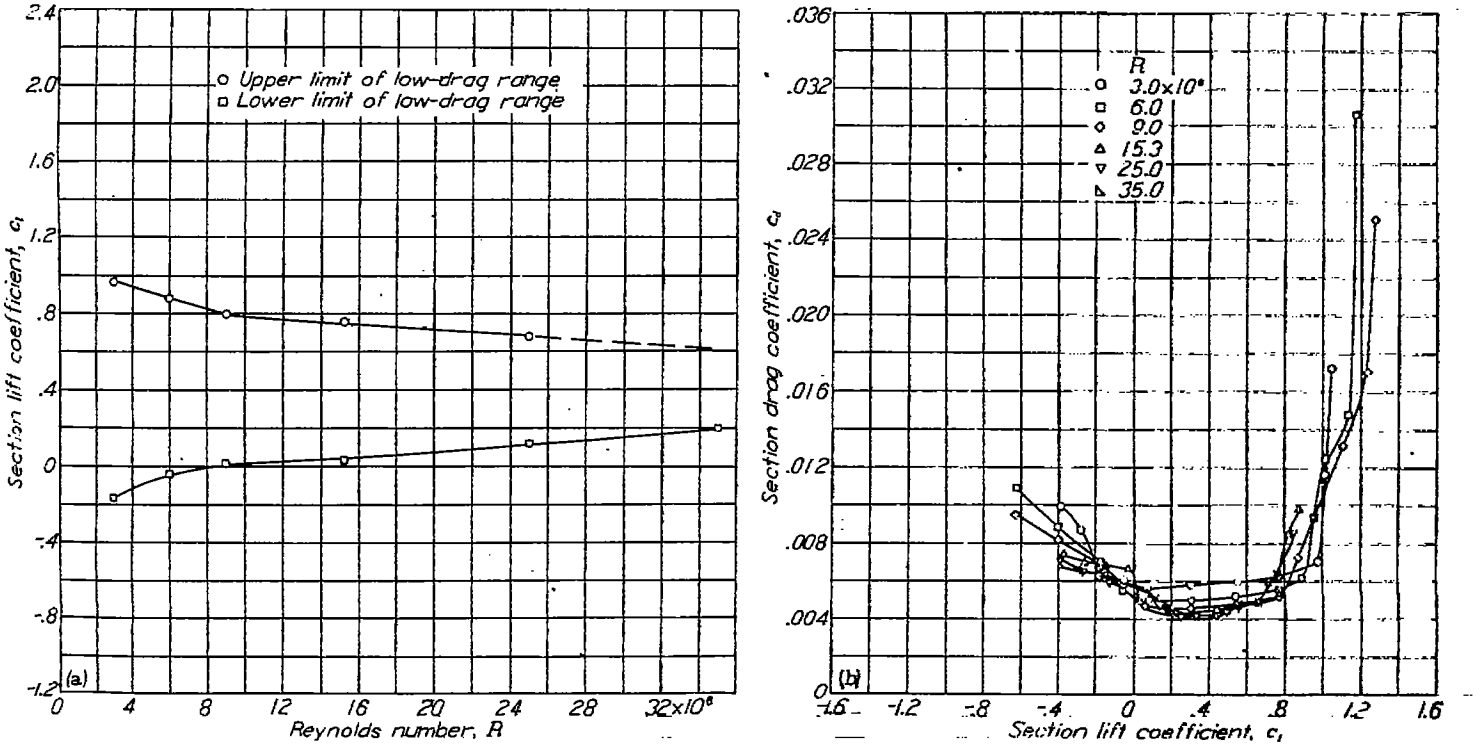

(a) Variation of upper and lower limits of low-drag range with Reynolds number. (b) Section drag characteristics at various Reynolds numbers.

FIGURE 14.—Variation of low-drag range with Reynolds number for the NACA 65(421)-420 airfoil. TDT tests 300, 312, and 328.

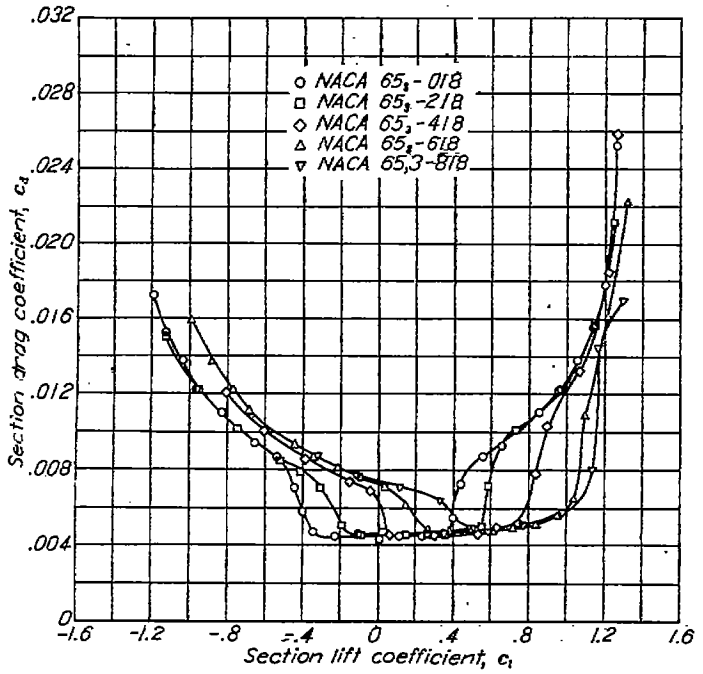

FIGURE 15.—Drag characteristics of some NACA 65-series airfoil sections of 18 percent thickness with various amounts of camber. $R = 6 \times 10^6$; TDT tests 163, 314, 802, 813, and 830.

The location of the low-drag range shows some variation from that predicted by simple thin-airfoil theory. This departure appears to be a function of the type of mean line used (reference 27) and the airfoil thickness. The effect of airfoil thickness is shown in figure 13, from which the center of the low-drag range is seen to shift to higher lift coefficients with increasing airfoil thickness. This shift is partly explained by the increase in lift coefficient above the design lift coefficient for the mean line obtained when the velocity increments caused by the mean line are combined with the velocity distribution for the basic thickness form according to the approximate methods previously described.

Drag characteristics outside low-drag range.—At the end of the low-drag range the drag increases rapidly with increase in lift coefficient. For symmetrical and low-cambered airfoils, for which the lift coefficient at the upper end of the low-drag range is moderate, this high rate of increase does not continue. (See fig. 15.) For highly cambered sections, for which the lift at the upper end of the low-drag range is already high, the drag coefficient shows a continued rapid increase.

Comparison of data for airfoils cambered with a uniform-load mean line with data for airfoils cambered to carry the load farther forward shows that the uniform-load mean line is favorable for obtaining low drag coefficients at high lift coefficients (fig. 16 and reference 27).

Data for many of the airfoils given in the supplementary figures show large reductions in drag with increasing Reynolds number at high lift coefficients. This scale effect is too large to be accounted for by the normal variation in skin friction and appears to be associated with the effect of Reynolds number on the onset of turbulent flow following laminar separation near the leading edge (reference 28).

Effects of type of section on drag characteristics.—A comparison of the drag characteristics of the NACA 23012 and of three NACA 6-series airfoils is presented in figure 17. The drag for the NACA 6-series sections is substantially lower than for the NACA 23012 section in the range of lift coefficients corresponding to high-speed flight, and this margin may usually be maintained through the range of lift coefficients useful for cruising by suitable choice of camber. The NACA 6-series sections show the higher maximum values of the lift-drag ratio. At high values of the lift coefficient, however, the earlier NACA sections have generally lower drag coefficients than the NACA 6-series airfoils.

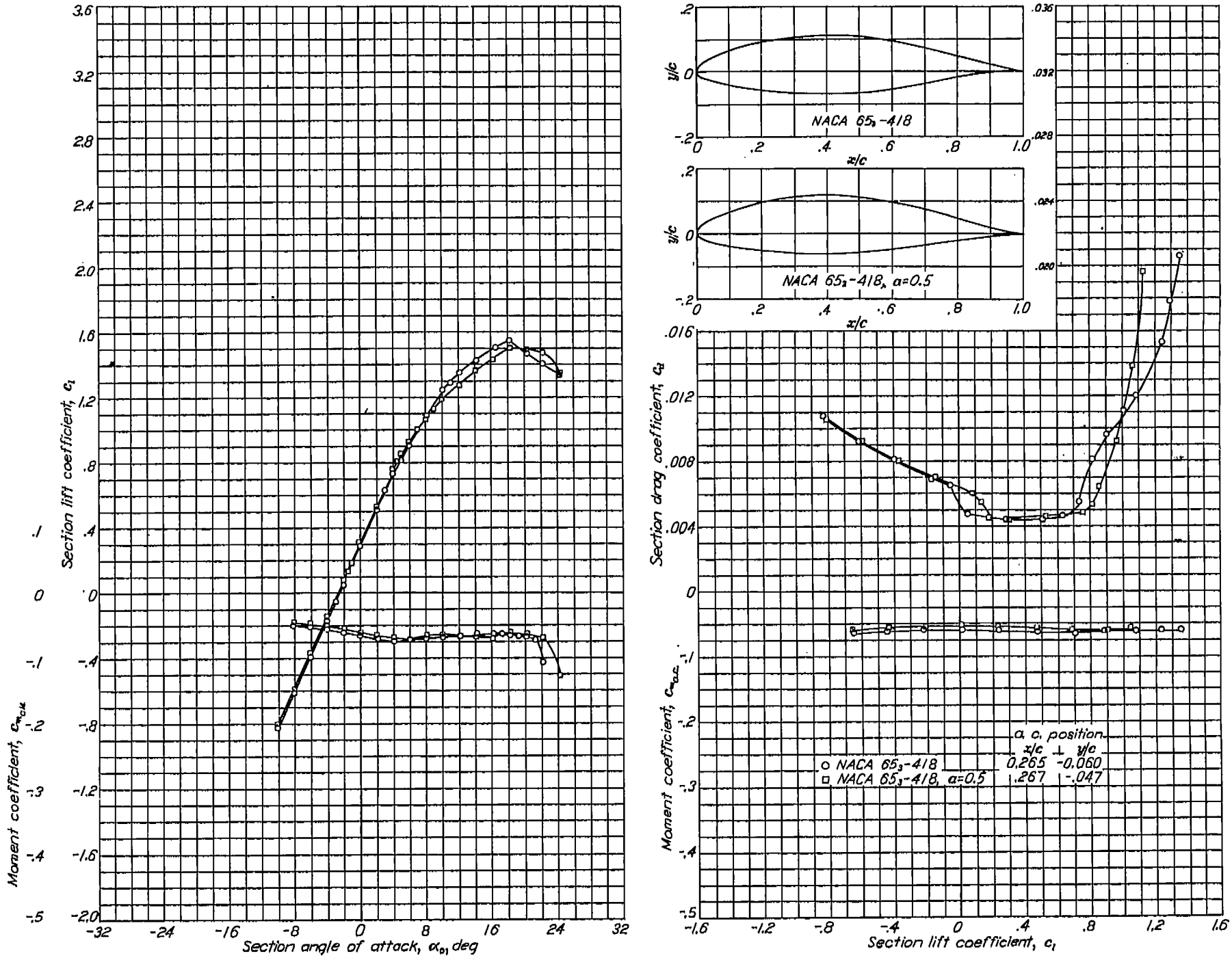

FIGURE 16.—Comparison of the aerodynamic characteristics of the NACA 65_3-418 and NACA 65_3-418, a = 0.5 airfoils at a Reynolds number of 9 × 10^6. TDT tests 314, 320, 406, and 411.

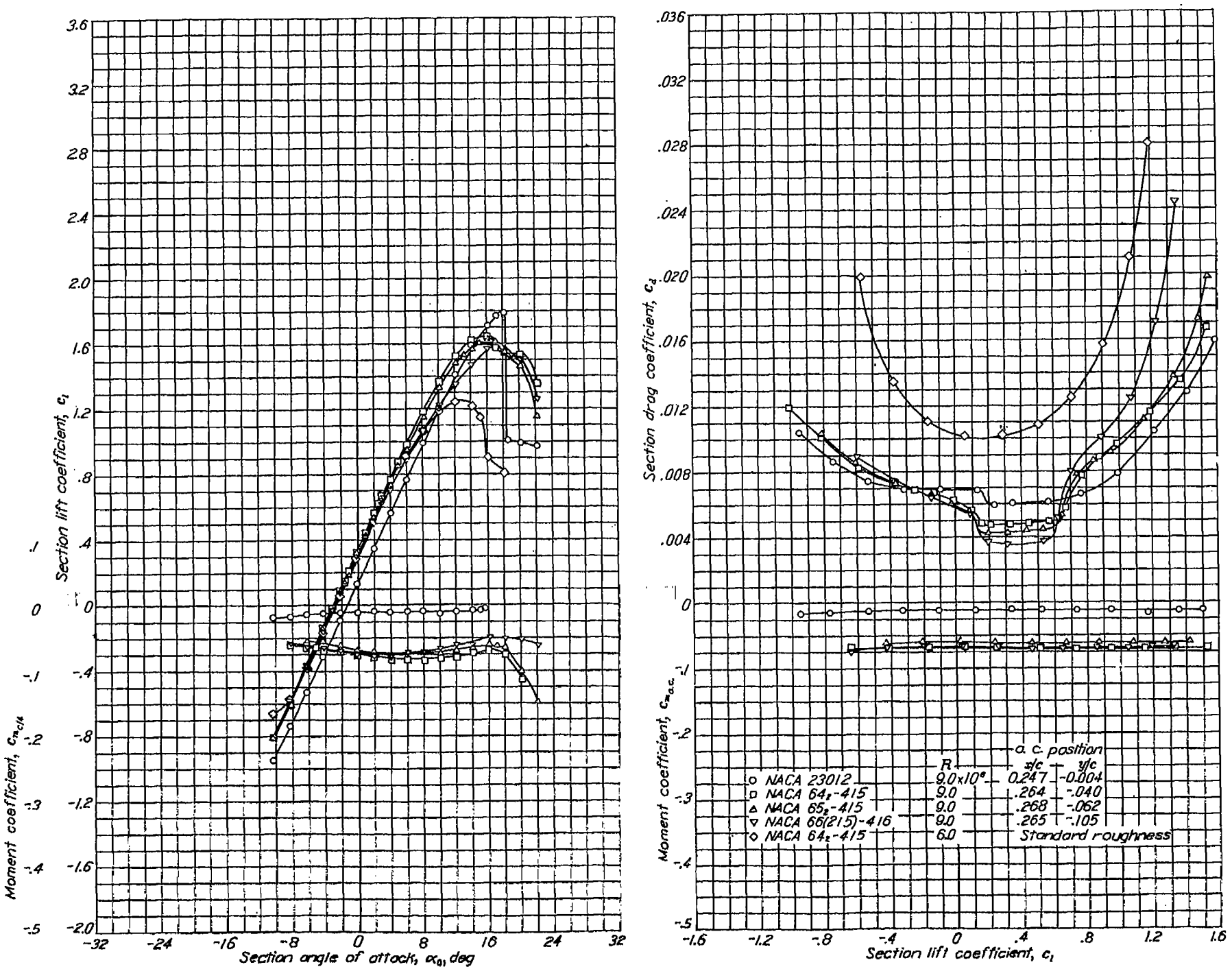

FIGURE 17.—Comparison of the aerodynamic characteristics of some NACA airfoils from tests in the Langley two-dimensional low-turbulence pressure tunnel.

Effective aspect ratio.—The combination of high drags at high lift coefficients, low drags at moderate lift coefficients, and the nonregular variation of drag with lift coefficient shown by the NACA 6-series airfoils may lead to paradoxical results when the span-efficiency concept (reference 29) is used for the calculation of airplane performance. In the usual application of this concept, the airplane drag characteristics are approximated by a curve of the type

$$C_D = C_{D_{L=0}} + kC_L^2 \qquad (17)$$

This curve is usually matched to the actual drag characteristics at a rather low and at a moderately high value of the lift coefficient (reference 30).

The application of this concept to two hypothetical airplanes with NACA 230- and 65-series sections, respectively, is illustrated in figure 18 (a). The wing drags of the airplanes have been calculated by adding the induced drags corresponding to an aspect ratio of 10 with elliptical loading to the profile-drag coefficients of the NACA 23018 and 65_3–418 airfoils. These sections are considered representative of average wing sections for a large airplane of this aspect ratio. Ordinate scales are given in figure 18 (a) for the wing drag and for the total airplane drag coefficients obtained by adding a representative constant value of 0.0150 to the wing drag coefficients. The resulting drag coefficients have been approximated by two curves corresponding to equation (17) and matched to the drag curves at lift coefficients of 0.2 and 1.0. These two curves correspond to effective aspect ratios of 9.29 for the airplane with NACA 23018 sections and of 8.30 for the airplane with NACA 65_3–418 sections and illustrate the typical large reduction in the effective aspect ratio obtained with such sections.

It should be noted, however, that although equation (17) provides a reasonably satisfactory approximation to the drag of the airplane with NACA 23018 sections, such is not the case for the airplane with the NACA 65_3–418 section. The most important reason for using high aspect ratios on large airplanes is to reduce the drag at cruising lift coefficients and to obtain high maximum values of the lift-drag ratio. For the two wings considered, the maximum value of this ratio is appreciably higher for the airplane with NACA 65_3–418 sections (19.8 as compared with 18.5) despite the fact that this airplane shows the lower effective aspect ratio. Figure 18 (b) shows a similar comparison with similar results for two airplanes of aspect ratio 8 and NACA 2415 and 65_2–415 airfoils. It is accordingly concluded that the effective aspect ratio is not a satisfactory criterion for use in airfoil selection.

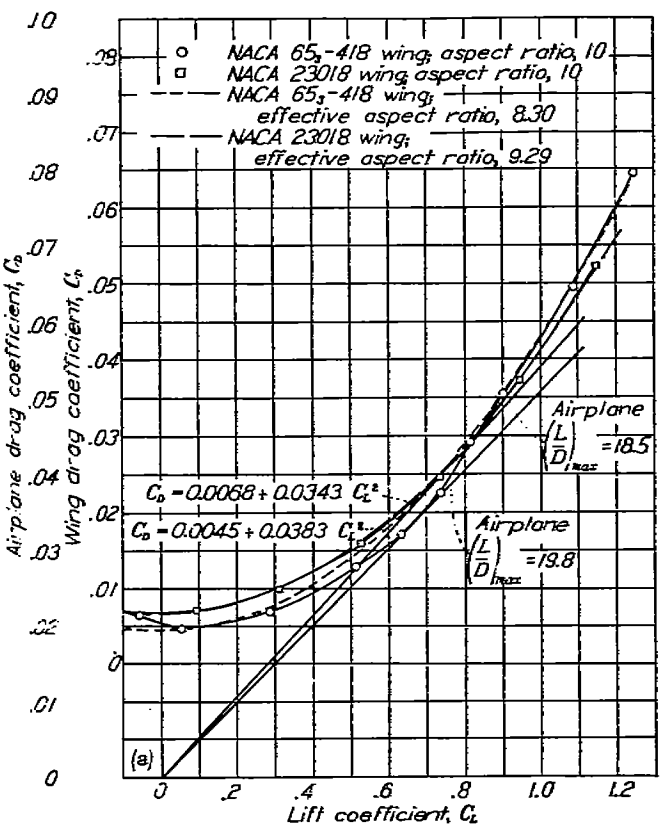

(a) NACA 65_3–418 and 23018 wings of aspect ratio 10.

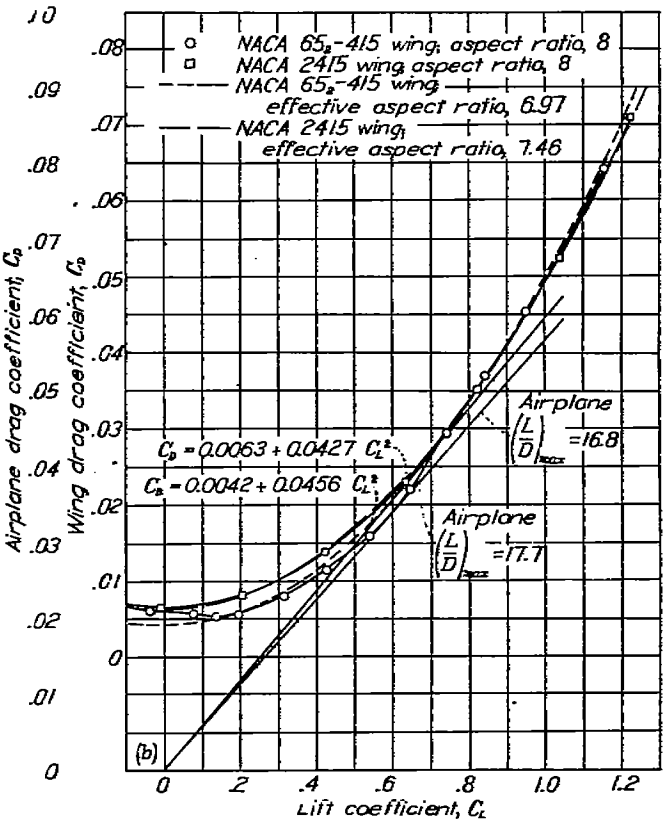

(b) NACA 65_2–415 and 2415 wings of aspect ratio 8.

FIGURE 18.—Comparison of finite aspect-ratio drag characteristics for two types of airfoils obtained by adding the induced drag corresponding to an elliptical span loading to the section drag coefficients.

EFFECT OF SURFACE IRREGULARITIES ON DRAG

Permissible roughness.—Previous work has shown large drag increments resulting from surface roughness (reference 31). Although a large part of these drag increments was shown to result from forward movement of transition, substantial drag increments resulted from surface roughness in the region of turbulent flow. It is accordingly important to maintain smooth surfaces even when extensive laminar flow cannot be expected, but the gains that may be expected from maintaining smooth surfaces are greater for NACA 6- or 7-series airfoils when extensive laminar flows are possible.

No accurate method of specifying the surface condition necessary for extensive laminar flow at high Reynolds numbers has been developed, although some general conclusions have been reached. It may be presumed that for a given Reynolds number and chordwise position, the size of the permissible roughness will vary directly with the chord of the airfoil. It is known, at one extreme, that the surfaces do not have to be polished or optically smooth. Such polishing or waxing has shown no improvement in tests in the Langley two-dimensional low-turbulence tunnels when applied to satisfactorily sanded surfaces. Polishing or waxing a surface that is not aerodynamically smooth will, of course, result in improvement and such finishes may be of considerable practical value because deterioration of the finish may be easily seen and possibly postponed. Large models having chord lengths of 5 to 8 feet tested in the Langley two-dimensional low-turbulence tunnels are usually finished by sanding in the chordwise direction with No. 320 carborundum paper when an aerodynamically smooth surface is desired. Experience has shown the resulting finish to be satisfactory at flight values of the Reynolds number. Any rougher surface texture should be considered as a possible source of transition, although slightly rougher surfaces have appeared to produce satisfactory results in some cases.

Wind-tunnel experience in testing NACA 6-series sections and data of reference 32 show that small protuberances extending above the general surface level of an otherwise satisfactory surface are more likely to cause transition than small depressions. Dust particles, for example, are more effective than small scratches in producing transition if the material at the edges of the scratches is not forced above the general surface level. Dust particles adhering to the oil left on airfoil surfaces by fingerprints may be expected to cause transition at high Reynolds numbers.

Transition spreads from an individual disturbance with an included angle of about 15° (references 31 and 33). A few scattered specks, especially near the leading edge, will cause the flow to be largely turbulent. This fact makes necessary an extremely thorough inspection if low drags are to be realized. Specks sufficiently large to cause premature transition on full-size wings can be felt by hand. The inspection procedure used in the Langley two-dimensional low-turbulence tunnels is to feel the entire surface by hand after which the surface is thoroughly wiped with a dry cloth.

It has been noticed that transition resulting from individual small sharp protuberances, in contrast to waves, tends to occur at the protuberance. Transition caused by surface waviness appears to approach the wave gradually as the Reynolds number or wave size is increased. The height of a small cylindrical protuberance necessary to cause transition when located at 5 percent of the chord with its axis normal to the surface is shown in figure 19. These data were

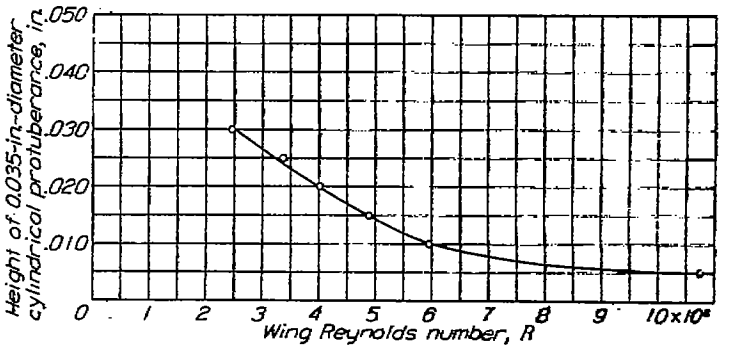

FIGURE 19.—Variation with wing Reynolds number of the minimum height of a cylindrical protuberance necessary to cause premature transition. Protuberance has 0.035-inch diameter with axis normal to wing surface and is located at 5 percent chord of a 90-inch-chord symmetrical 6-series airfoil section of 15-percent thickness and with minimum pressure at 70 percent chord.

obtained at rather low values of the Reynolds number and show a large decrease in allowable height with increase in Reynolds number. This effect of Reynolds number on permissible surface roughness is also evident in figure 20, in which a sharp increase in drag at a Reynolds number of approximately 20×10^6 occurs for the model painted with camouflage lacquer.

The magnitude of the favorable gradient appears to have a small effect on the permissible surface roughness for laminar flow. Figure 21 shows that the roughness becomes more important at the extremities of the low-drag range where the favorable pressure gradient is reduced on one surface. The effect of increasing the Reynolds number for a surface of marginal smoothness, which has an effect similar to increasing the surface roughness for a given Reynolds number, is to reduce rapidly the extent of the low-drag range and then to increase the minimum drag coefficient (fig. 21). The data of figure 21 were specially chosen to show this effect. In most cases, the effect of Reynolds number predominates over the effect of decreasing the magnitude of the favorable pressure gradient to such an extent that the only effect is the elimination of the low-drag range (reference 34).

Permissible waviness.—More difficulty is generally encountered in reducing the waviness to permissible values for the maintenance of laminar flow than in obtaining the required surface smoothness. In addition, the specification of the required freedom from surface waviness is more difficult than that of the required surface smoothness. The problem is not limited merely to finding the minimum wave size that will cause transition under given conditions because the number of waves and the shape of the waves require consideration.

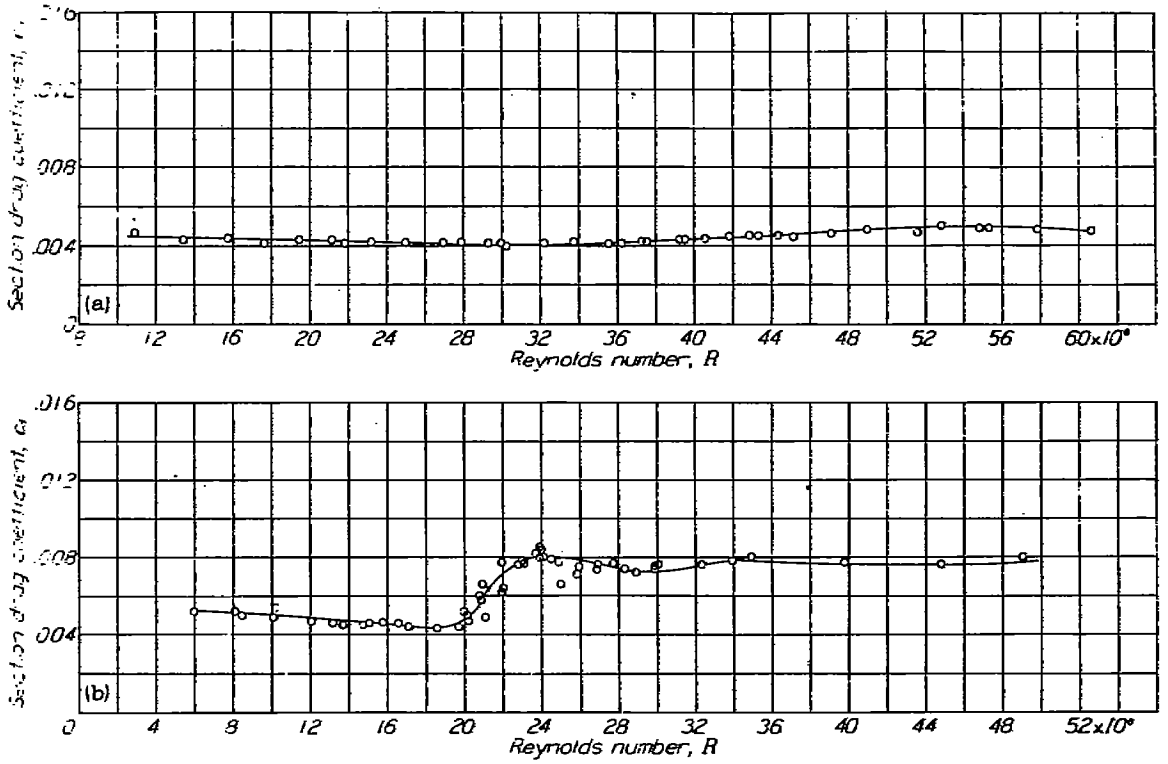

(a) Smooth condition; TDT test 328.
(b) Lacquer camouflage unimproved after painting; TDT test 461.

FIGURE 20.—Variation of drag coefficient with Reynolds number for a 60-inch-chord model of the NACA $65_{(421)}$-420 airfoil for two surface conditions.

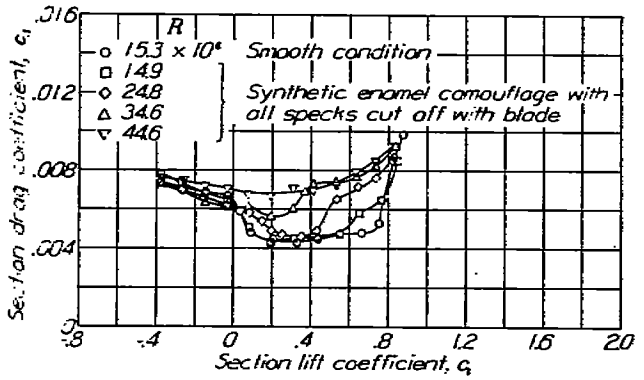

FIGURE 21.—Drag characteristics of NACA $65_{(421)}$-420 airfoil for two surface conditions. TDT tests 300 and 436.

If the wave is sufficiently large to affect the pressure distribution in such a manner that laminar separation is encountered, there is little doubt that such a wave will cause premature transition at all useful Reynolds numbers. A relation between the dimensions of a wave and the pressure distribution may be found by the method of reference 35. The size of the wave required to reverse the favorable pressure gradient increases with the pressure gradient. Large negative pressure gradients would therefore appear to be favorable for wavy surfaces. Experimental results have shown this conclusion to be qualitatively correct.

Little information is available on waves too small to cause laminar separation or even reversal of the pressure gradient. Data for an airfoil section having a relatively long wave on the upper surface are given in figure 22. Marked increases in the drag corresponding to a rapid forward movement of the transition point were not noticeable below a Reynolds number of 44×10^6. On the other hand, transition has been caused at comparatively low Reynolds numbers by a series of small waves with a wave height of the order of a few ten-thousandths of an inch and a wave length of the order of 2 inches on the same 60-inch-chord model.

For the types of wave usually encountered on practical-construction wings, the test of rocking a straightedge over the surface in a chordwise direction is a fairly satisfactory criterion. The straightedge should rock smoothly without jarring or clicking. The straightedge test will not show the existence of waves that leave the surface convex, such as the wave of figure 22 and the series of small waves previously mentioned. Tests of a large number of practical-construction models, however, have shown that those models which passed the straightedge test were sufficiently free of small waves to permit low drags to be obtained at flight values of the Reynolds number.

It is not feasible to specify construction tolerances on airfoil ordinates with sufficient accuracy to ensure adequate freedom from waviness. If care is taken to obtain fair surfaces, normal tolerances may be used without causing serious alteration of the drag characteristics.

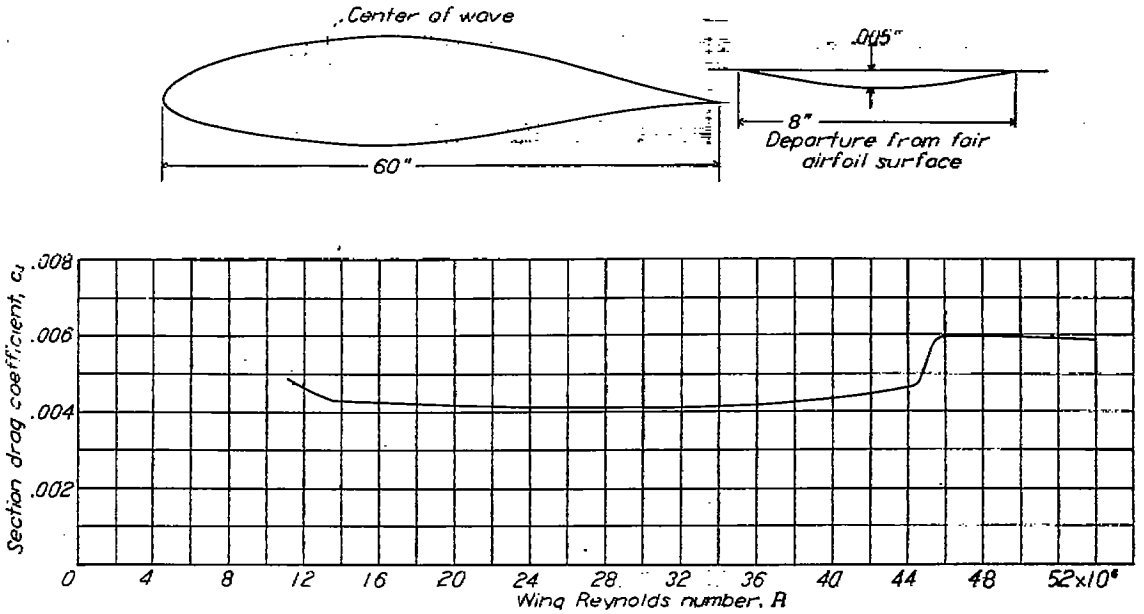

FIGURE 22.—Experimental curve showing variation of drag coefficient with Reynolds number for the NACA 65(420)-420 airfoil section with a small amount of surface waviness.

Drag with fixed transition.—If the airfoil surface is sufficiently rough to cause transition near the leading edge, large drag increases are to be expected. Figure 23 shows that, although the degree of roughness has some effect, the increment in minimum drag coefficient caused by the smallest roughness capable of producing transition is nearly as great as that caused by much larger grain roughness when the roughness is confined to the leading edge. The degree of roughness has a much larger effect on the drag at high lift coefficients. If the roughness is sufficiently large to cause transition at all Reynolds numbers considered, the drag of the airfoil with roughness only at the leading edge decreases with increasing Reynolds number (fig. 10 and reference 36).

The effect of fixing transition by means of a roughness strip of carborundum of 0.011-inch grain is shown in figure 24. The minimum drag increases progressively with forward movement of the roughness strip. The effect on the drag at high lift coefficients is not progressive; the drag increases rapidly when the roughness is at the leading edge. Figure 25 shows that the drag coefficients for the NACA 65(223)-422 and 63(420)-422 airfoils were nearly the same throughout most of the lift range when the extent of laminar flow was limited to 0.30c.

All recent airfoil data obtained in the Langley two-dimensional low-turbulence pressure tunnel include results with roughened leading edge, and these data are included in the supplementary figures. Tests with roughened leading edge were formerly made only for a limited number of airfoil sections, especially those having large thickness ratios (reference 37). The standard roughness selected for 24-inch-chord models consists of 0.011-inch carborundum grains applied to the airfoil surface at the leading edge over a surface length of 0.08c measured from the leading edge on both surfaces. The grains are thinly spread to cover 5 to 10 percent of this area. This standard roughness is considerably more severe than that caused by the usual manufacturing irregularities or deterioration in service but is considerably less severe than that likely to be encountered in service as a result of accumulation of ice or mud or damage in military combat.

The variation of minimum drag coefficient with thickness ratio for a number of NACA airfoils with standard roughness is shown in figure 12. These data show that the magnitudes of the minimum drag coefficients for the NACA 6-series airfoils are less than the values for the NACA four- and five-digit-series airfoils. The rate of increase of drag with thickness is greater for the airfoils in the rough condition than in the smooth condition.

Drag with practical-construction methods.—The section drag coefficients of several airplane wings have been measured in flight by the wake-survey method (reference 38), and a number of practical-construction wing sections have been tested in the Langley two-dimensional low-turbulence pressure tunnel at flight values of the Reynolds number. Flight data obtained by the NACA (reference 38) are summarized in figure 26 and some data obtained by the Consolidated Vultee Aircraft Corporation are presented in figure 27. Data obtained in the Langley two-dimensional low-turbulence pressure tunnel for typical practical-construction sections are presented in figures 28 to 32. Figure 33 presents a comparison of the drag coefficients obtained in this wind tunnel for a model of the NACA 0012 section and in flight for the same model mounted on an airplane. For this case, the wind-tunnel and flight data agree to within the experimental error.

All wings for which flight data are presented in figure 26 were carefully finished to produce smooth surfaces. Great care was taken to reduce surface waviness to a minimum for all the sections except the NACA 2414.5, the N-22, the Republic S-3,13, and the NACA 27-212. Curvature-gage measurements of surface waviness for some of these airfoils are presented in reference 38. Surface conditions corresponding to the data of figure 27 are described in the figure. These data show that the sections permitting extensive laminar flow had substantially lower drag coefficients when smooth than the other sections.

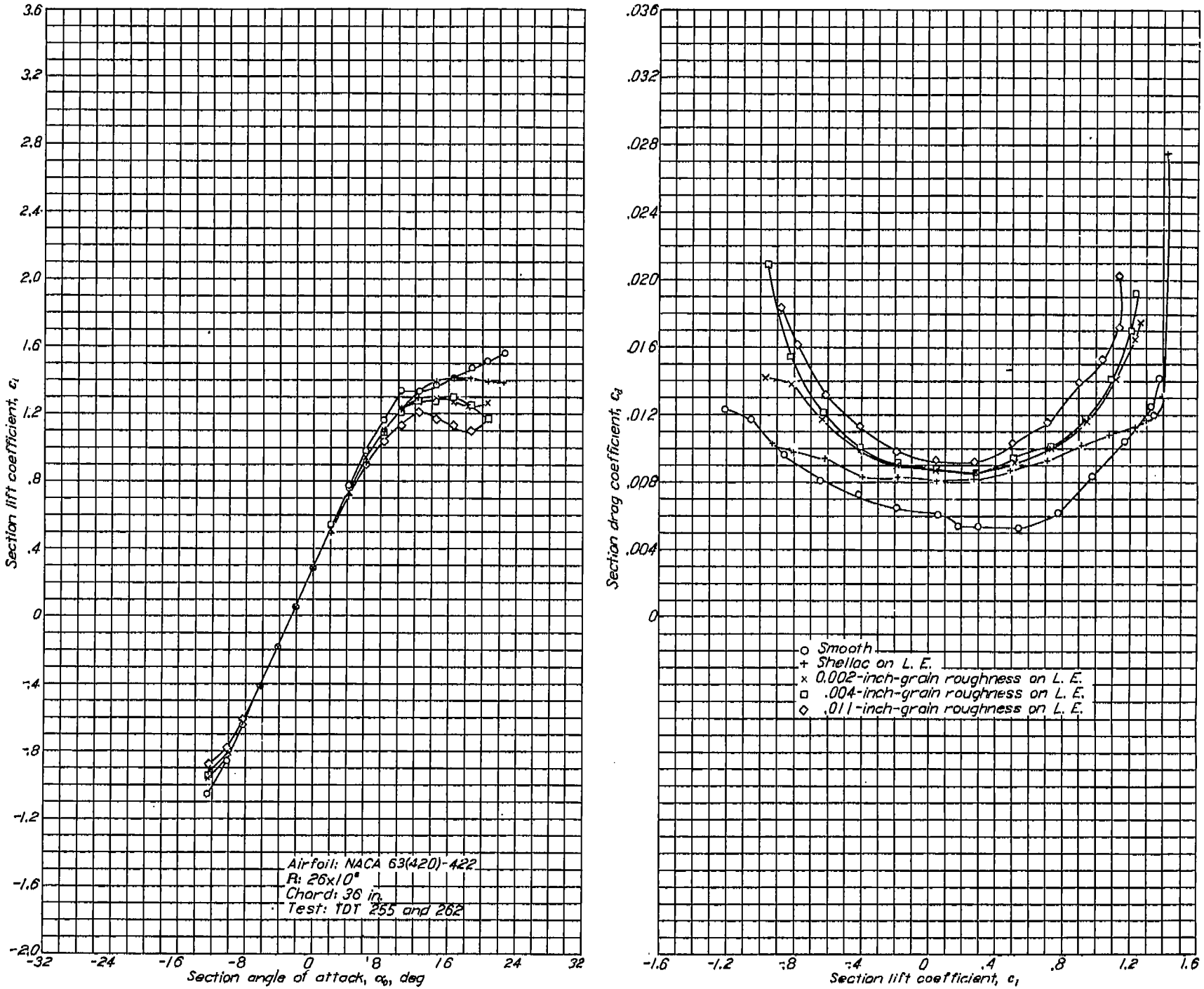

FIGURE 23.—Lift and drag characteristics of an NACA 63(420)-422 airfoil with various degrees of roughness at the leading edge.

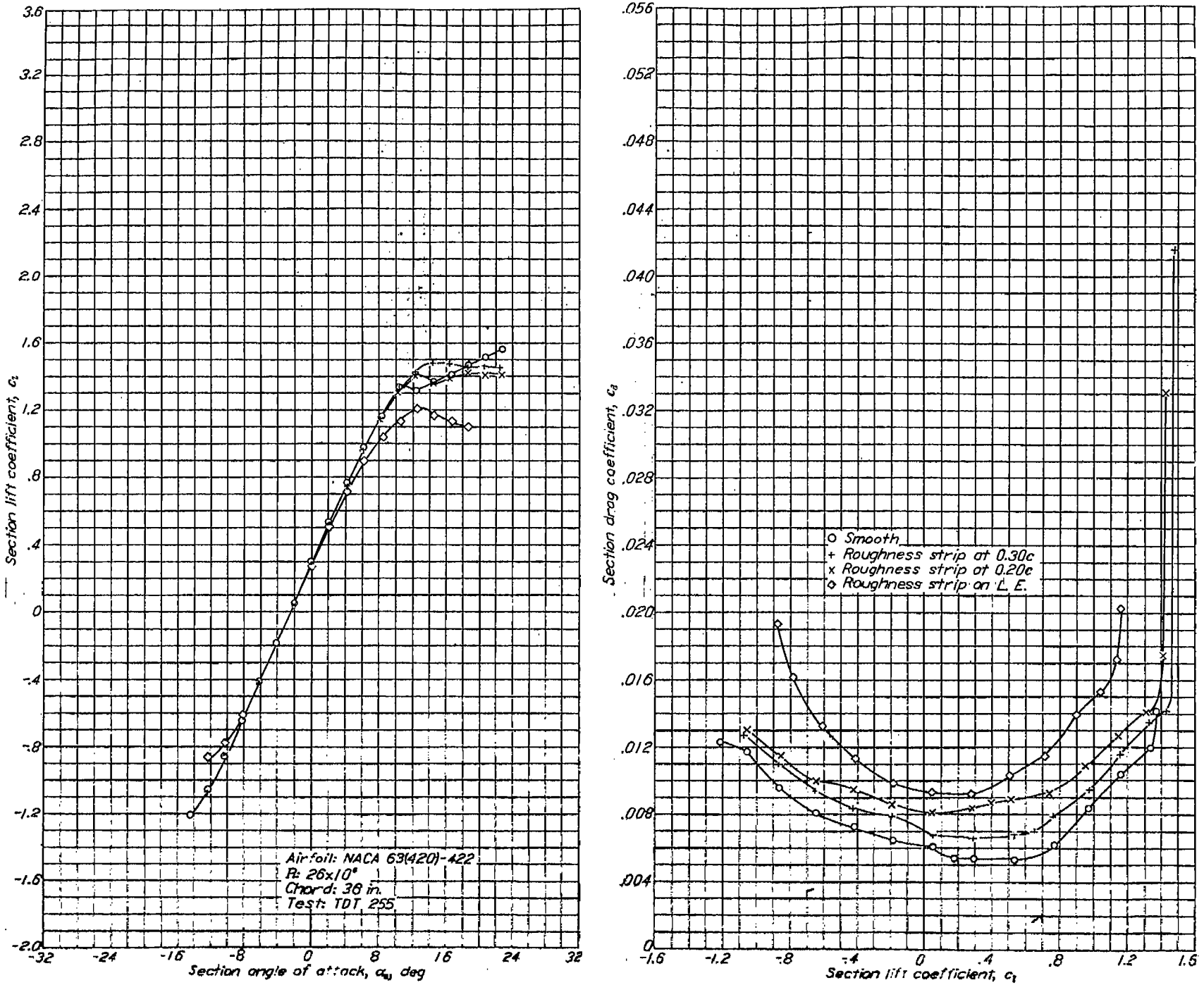

FIGURE 24.—Lift and drag characteristics of an NACA 63(420)-422 airfoil with 0.011-inch-grain roughness at various chordwise locations.

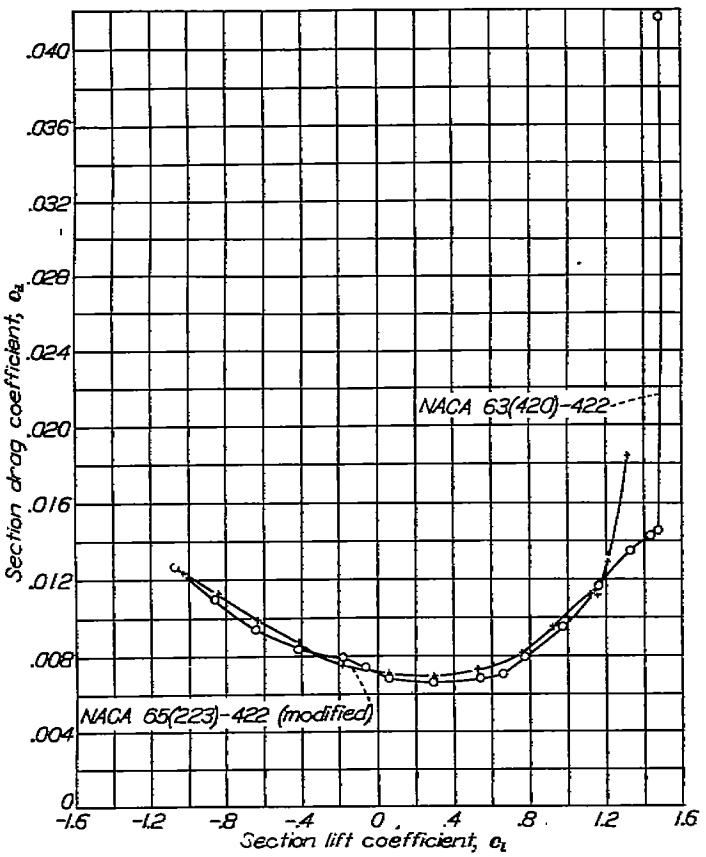

FIGURE 25.—Drag characteristics of two NACA 6-series airfoils with 0.011-inch-grain roughness at 0.30c. $R=26\times10^6$.

The wind-tunnel tests of practical-construction wing sections as delivered by the manufacturer showed minimum drag coefficients of the order of 0.0070 to 0.0080 in nearly all cases regardless of the airfoil section used (figs. 28 to 32). Such values may be regarded as typical for good current construction practice. Finishing the sections to produce smooth surfaces always produced substantial drag reductions although considerable waviness usually remained. None of the sections tested had fair surfaces at the front spar. Unless special care is taken to produce fair surfaces at the front spar, the resulting wave may be expected to cause transition either at the spar location or a short distance behind it. One practical-construction specimen tested with smooth surfaces maintained relatively low drags up to Reynolds numbers of approximately 30×10^6 (NACA 66(2x15)–116 airfoil of fig. 10). This specimen had no spar forward of about 35 percent chord from the leading edge and no spanwise stiffeners forward of the spars. This type of construction resulted in unusually fair surfaces and is being used on some modern high-performance airplanes.

A comparison of the effect of airfoil section on the minimum drag with practical-construction surfaces is very difficult because the quality of the surface has more effect on the drag than the type of section. Probably the best comparison can be obtained from pairs of models constructed at

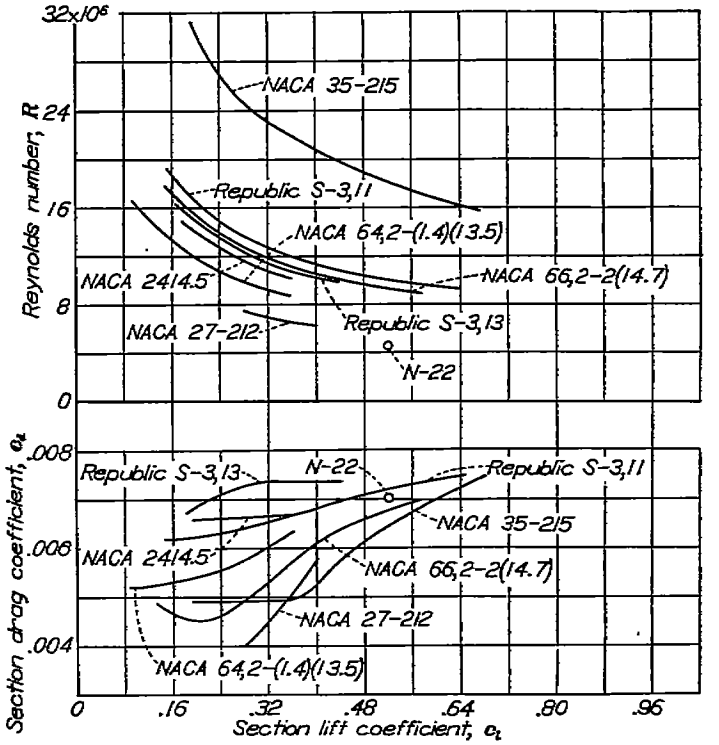

FIGURE 26.—Comparison of section drag coefficients obtained in flight on various airfoils. Tests of NACA 27-212 and 35-215 sections made on gloves.

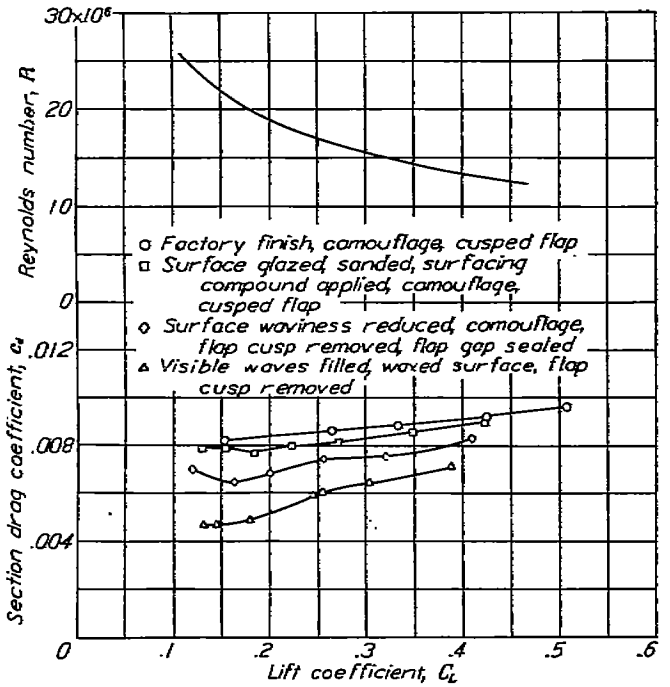

FIGURE 27.—Consolidated-Vultee flight measurements of the effect of wing surface condition on drag of an NACA 66(215)-1(14.5) wing section.

the same time by the same manufacturers. Data for such pairs of models are presented in figures 30 to 32. The results indicate that as long as current construction practices are used the type of section has relatively little effect at flight values of the Reynolds number for military airplanes.

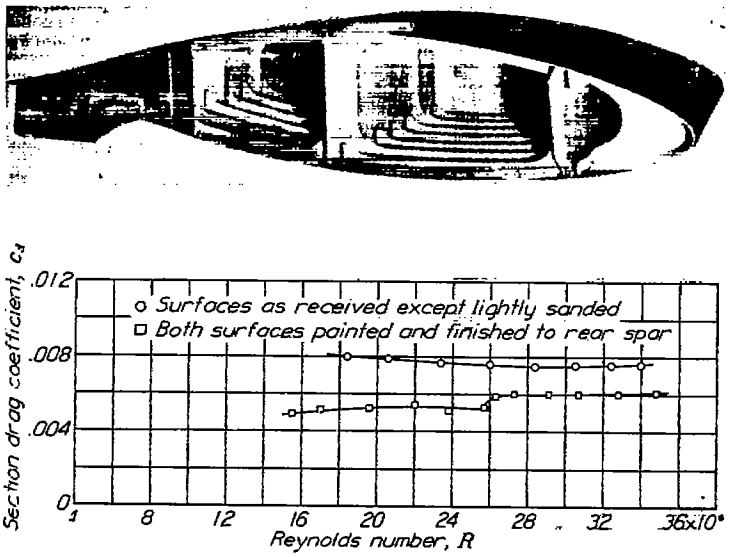

FIGURE 28.—Drag scale effect on 100-inch-chord practical-construction model of the NACA 65(216)-3(16.5) (approx.) airfoil section. c_l=0.2 (approx.).

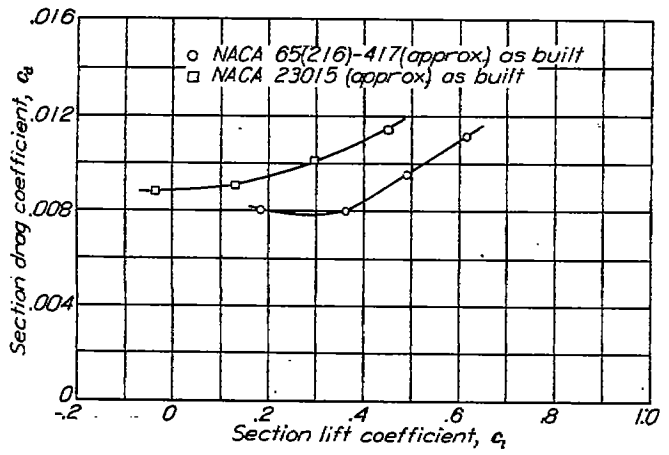

FIGURE 30.—Drag characteristics of the NACA 65(216)-417 (approx.) and NACA 23015 (approx.) airfoil sections built by practical-construction methods by the same manufacturer. R=10.23×10⁶.

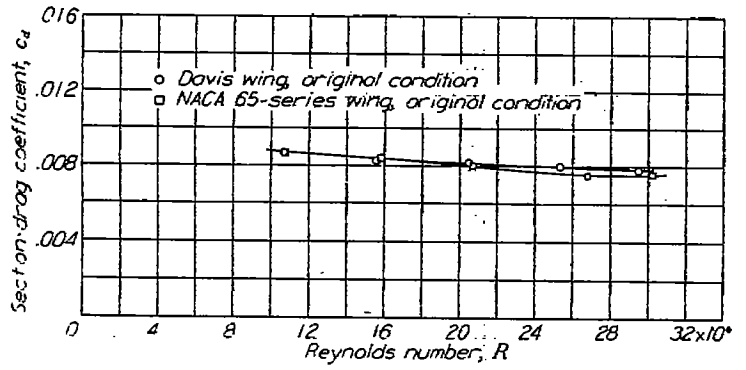

FIGURE 32.—Drag scale effect for a model of the NACA 65-series airfoil section, 18.27 percent thick, and the Davis airfoil section, 18.27 percent thick, built by practical-construction methods by the same manufacturer. c_l=0.46 (approx.).

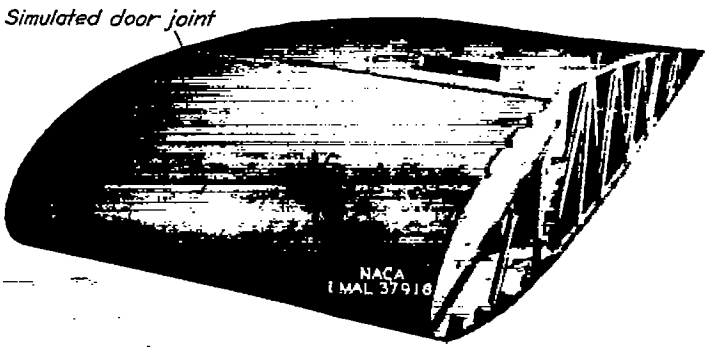

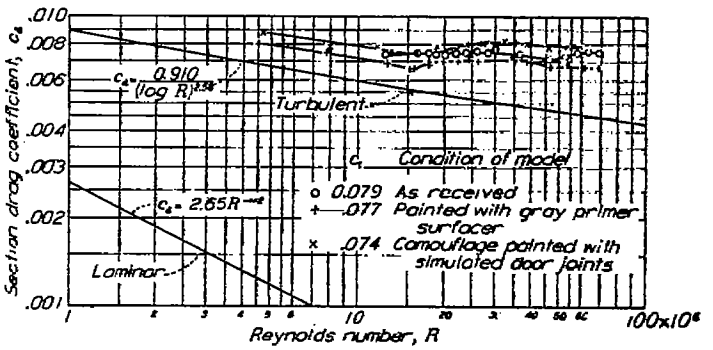

FIGURE 29.—Variation of drag coefficient with Reynolds number for the NACA 23016 airfoil section together with laminar and turbulent skin-friction coefficients for a flat plate.

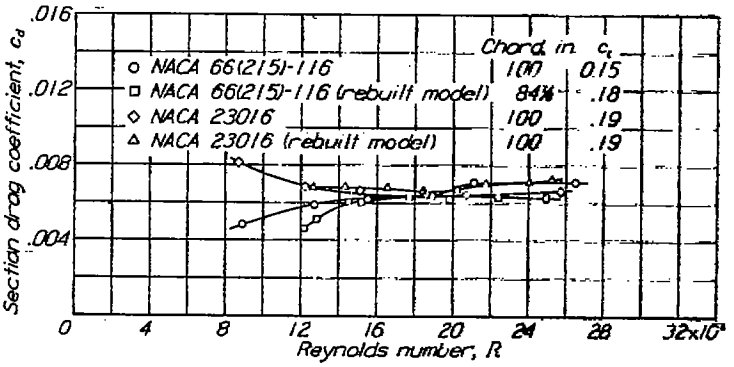

FIGURE 31.—Scale effect on drag of the NACA 66(215)-116 and NACA 23016 airfoil sections built by practical-construction methods by the same manufacturer and tested as received.

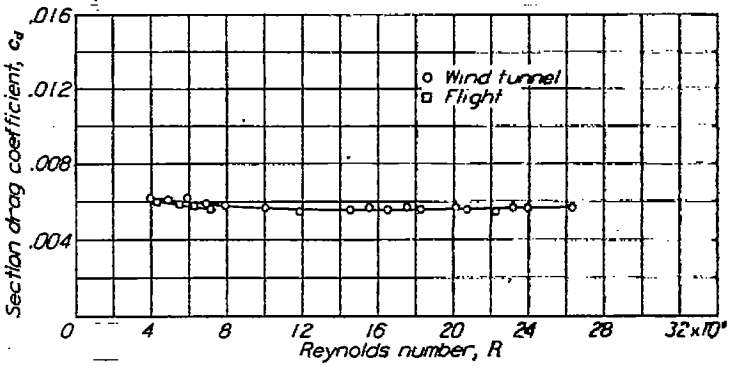

FIGURE 33.—Comparison of drag coefficients measured in flight and wind tunnel for the NACA 0012 airfoil section at zero lift.

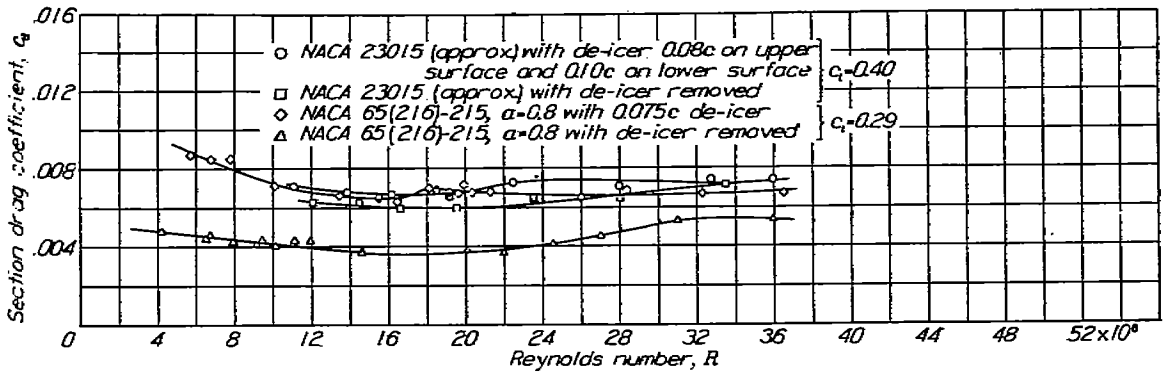

FIGURE 34.—Effect of de-icers on the drag of two practical-construction airfoil sections with relatively smooth surfaces.

Important savings in drag may be obtained at high Reynolds numbers by keeping the surfaces smooth even if extensive laminar flow is not realized. Drag increments resulting from surface roughness in turbulent flow have been shown to be important (reference 31). The effects of surface roughness on the variation of drag with Reynolds number are shown in figure 29, in which the favorable scale effect usually expected at high Reynolds numbers was not realized. This type of scale effect may be compared with that shown for the NACA 63(420)–422 airfoil with rough leading edge but otherwise smooth surfaces (fig. 10). Drag increments obtained in flight resulting from roughness in the turbulent boundary layer with fixed transition are presented in reference 39.

The effect of the application of de-icers to the leading edge of two smooth airfoils is shown in figure 34. The de-icer "boots" were installed in both cases by the manufacturer to represent good typical installations. The minimum drag coefficients for both sections with de-icers installed were of the order of 0.0070 at high Reynolds numbers.

Effects of propeller slipstream and airplane vibration.— Very few data are available on the effect of propeller slipstream on transition or airfoil drag; the data that are available do not show consistent results. This inconsistency may result from variations in lift coefficient, surface condition, air-stream turbulence, propeller advance-diameter ratio, and number of blades. Tests in the Langley 8-foot high-speed tunnel indicated transition occurring from 5 to 10 percent of the chord from the leading edge (reference 40). Drag measurements made in the Langley 19-foot pressure tunnel (fig. 35) indicated only moderate drag increments resulting from a windmilling propeller. Although the data of figure 35 may not be very accurate because of the difficulty of making wake surveys in the slipstream, these data seem to preclude very large drag increments such as would result from movement of the transition to a position close to the leading edge. These data also seem to be confirmed by recent NACA flight data (fig. 36), which show transition as far back as 20 percent

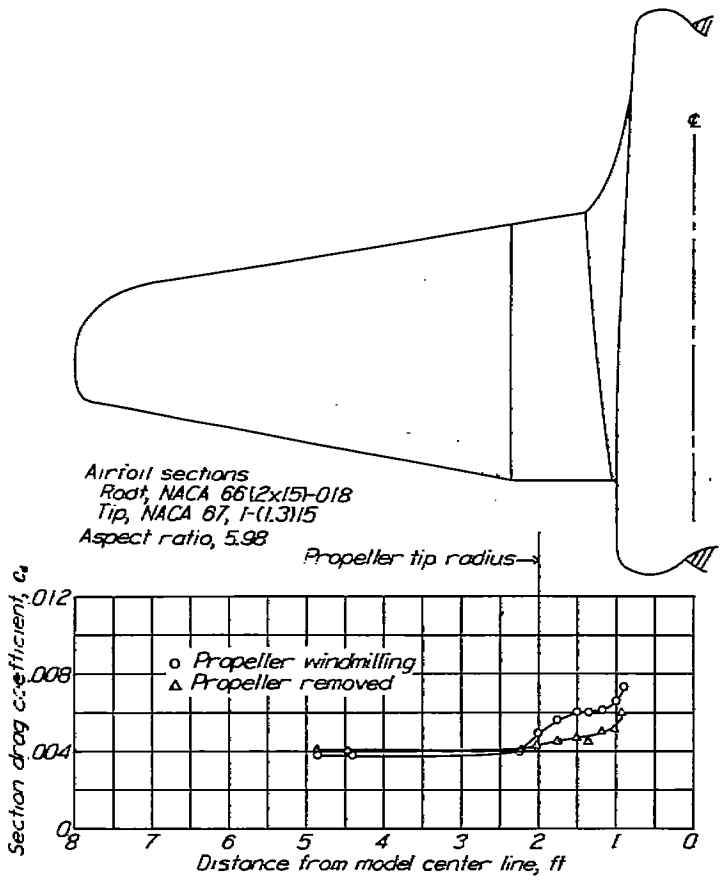

FIGURE 35.—The effect of propeller operation on section drag coefficient of a fighter-type airplane from tests of a model in the Langley 19-foot pressure tunnel. C_L=0.10; R=3.7×10⁶.

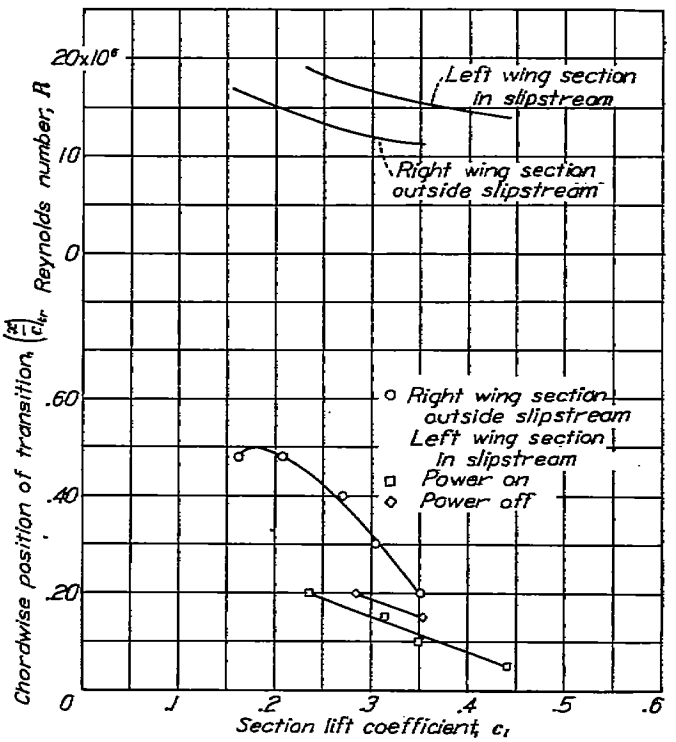

FIGURE 36.—Flight measurements of transition on an NACA 66-series wing within and outside the slipstream.

of the chord in the slipstream. Other unpublished NACA flight data on transition on an S–3,14.6 airfoil in the slipstream indicated that laminar flow occurred as far back as 0.2c.

Even less data are available on the effects of vibration on transition. Tests in the Langley 8-foot high-speed tunnel (reference 40) showed negligible effects, but the range of frequencies tested may not have been sufficiently wide. Some unpublished flight data showed small but consistent rearward movements of transition outside the slipstream when the propellers were feathered. This effect was noticed even when the propeller on the opposite side of the airplane from the survey plane was feathered and was accordingly attributed to vibration. Recent tests in the Ames full-scale tunnel showed premature adverse scale effect on drag coefficients measured by the wake-survey method when a model-support strut vibrated.

LIFT CHARACTERISTICS OF SMOOTH AIRFOILS

Two-dimensional data.—As explained in the section "Angle of Zero Lift," the angle of zero lift of an airfoil is largely determined by the camber. Thin-airfoil theory provides a means for computing the angle of zero lift from the mean-line data presented in the supplementary figures. The agreement between the calculated and the experimental angle of zero lift depends on the type of mean line used. Comparison of the experimental values of the angle of zero lift obtained from the supplementary figures and the theoretical values taken from the mean-line data shows that the agreement is good except for the uniform-load type ($a=1.0$) mean line. The angles of zero lift for this type mean line generally have values more positive than those predicted. The experimental values of the angles of zero lift for a number of NACA four- and five-digit and NACA 6-series airfoils are presented in figure 37. The airfoil thickness appears to have little effect on the value of the angle of zero lift regardless of the airfoil series. For the NACA four-digit-series airfoils, the angles of zero lift are approximately 0.93 of the value given by thin-airfoil theory; for the NACA 230-series airfoils, this factor is approximately 1.08; and for the NACA 6-series airfoils with uniform-load type mean line, this factor is approximately 0.74.

The lift-curve slopes (fig. 38) for airfoils tested in the Langley two-dimensional low-turbulence pressure tunnel are higher than those previously obtained in the tests reported in reference 8. It is not clear whether this difference in slope is caused by the difference in air-stream turbulence or by the differences in test methods, since the section data of reference 8 were inferred from tests of models of aspect ratio 6. The present values of the lift-curve slope were measured for a Reynolds number of 6×10^6 and at values of the lift coefficient approximately equal to the design lift coefficient of the airfoil section. For the NACA 6-series airfoils this lift coefficient is approximately in the center of the low-drag range. For airfoils having thicknesses in the range from 6 to 10 percent, the NACA four- and five-digit series and the NACA 64-series airfoil sections have values of lift-curve slope very close to the value for thin airfoils (2π per radian or 0.110 per degree). Variation in Reynolds number between 3×10^6 and 9×10^6 and variations in airfoil camber up to 4 percent chord appear to have no systematic effect on values of lift-curve slope. The airfoil thickness and the type of thickness distribution appear to be the primary variables. For the NACA four- and five-digit-series airfoil sections, the lift-curve slope decreases with increase in airfoil thickness. For the NACA 6-series airfoil sections, however, the lift-curve slope increases with increase in thickness and forward movement of the position of minimum pressure of the basic thickness form at zero lift.

Some NACA 6-series airfoils show jogs in the lift curve at the end of the low-drag range, especially at low Reynolds numbers. This jog becomes more pronounced with increase of camber or thickness and with rearward movement of the position of minimum pressure on the basic thickness form. This jog decreases rapidly in severity with increasing Reynolds number, becomes merely a change in lift-curve slope, and is practically nonexistent at a Reynolds number of 9×10^6 for most airfoils that would be considered for practical application. This jog may be a consideration in the selection of airfoils for small low-speed airplanes. An analysis of the flow conditions leading to this jog is presented in reference 28.

The variation of maximum lift coefficient with airfoil thickness ratio at a Reynolds number of 6×10^6 is shown in figure 39 for a number of NACA airfoil sections. The airfoils for which data are presented in this figure have a range of thickness ratio from 6 to 24 percent and cambers up to 4 percent chord. From the data for the NACA four- and five-digit-series airfoil sections (fig. 39 (a)), the maximum lift coefficients for the plain airfoils appear to be the greatest for a thickness of 12 percent. In general, the rate of change of maximum lift coefficient with thickness ratio appears to be greatest for airfoils having a thickness less than 12 percent. The data for the NACA 6-series airfoils (figs. 39 (b) to 39 (e)) also show a rapid increase in maximum lift coefficient with increasing thickness ratio for thickness ratios of less than 12 percent. For NACA 6-series airfoil sections cambered to give a design lift coefficient of not more than 0.2, the optimum thickness ratio for maximum lift coefficient appears to be between 12 and 15 percent, except for the airfoils having the position of minimum pressure at 60 percent chord. The optimum thickness ratio for the NACA 66-series sections cambered for a design lift coefficient of not more than 0.2 appears to be 15 percent or greater.

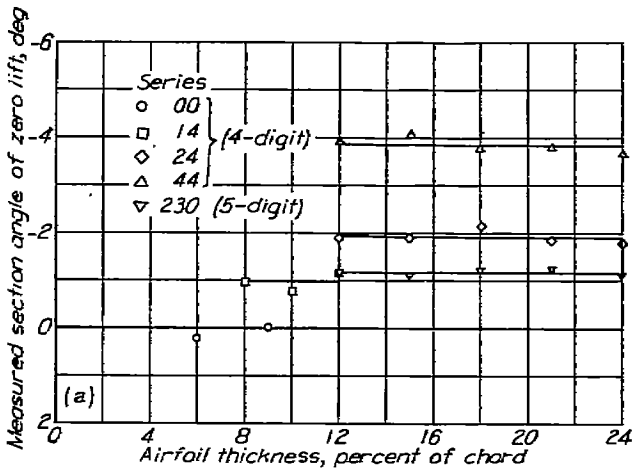

(a) NACA four- and five-digit series.

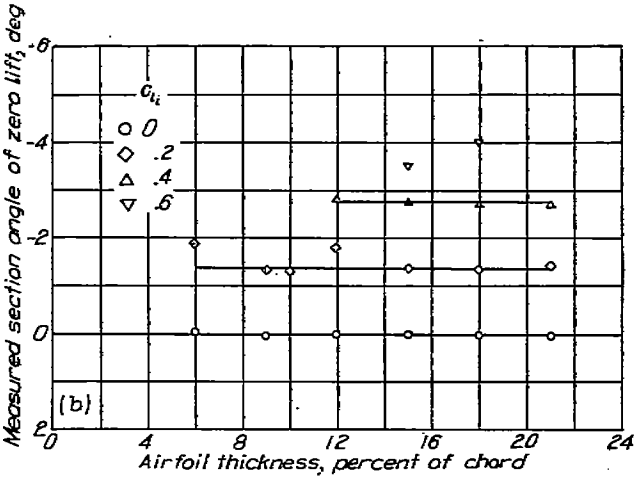

(b) NACA 63-series.

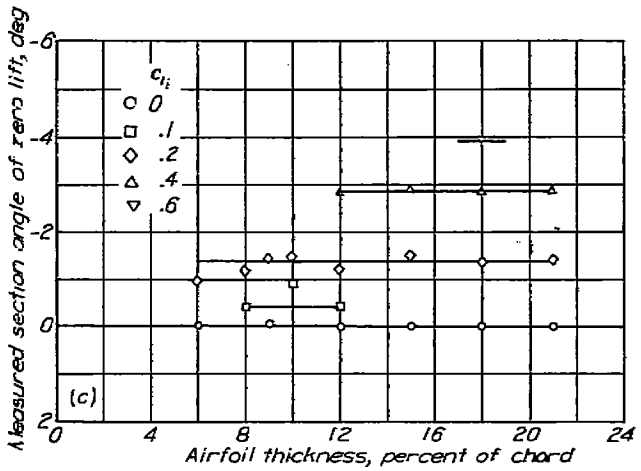

(c) NACA 64-series.

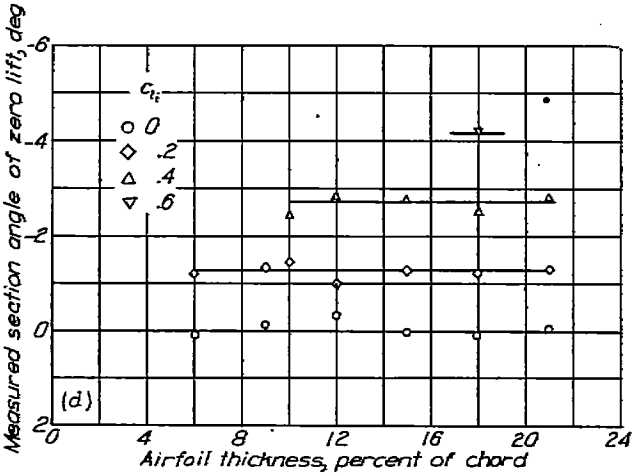

(d) NACA 65-series.

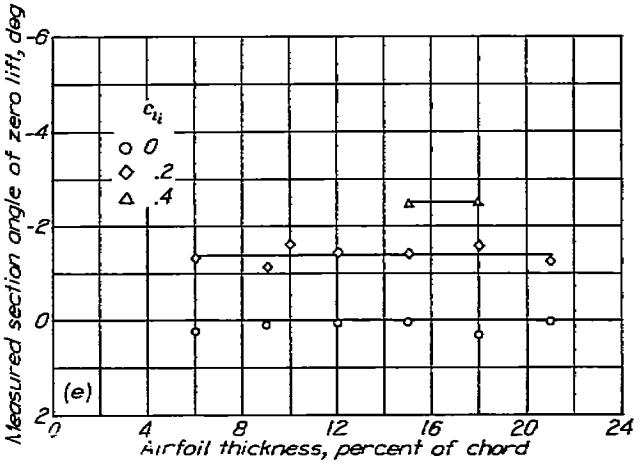

(e) NACA 66-series.

FIGURE 37.—Measured section angles of zero lift for a number of NACA airfoil sections of various thicknesses and camber, $R=6\times10^6$.

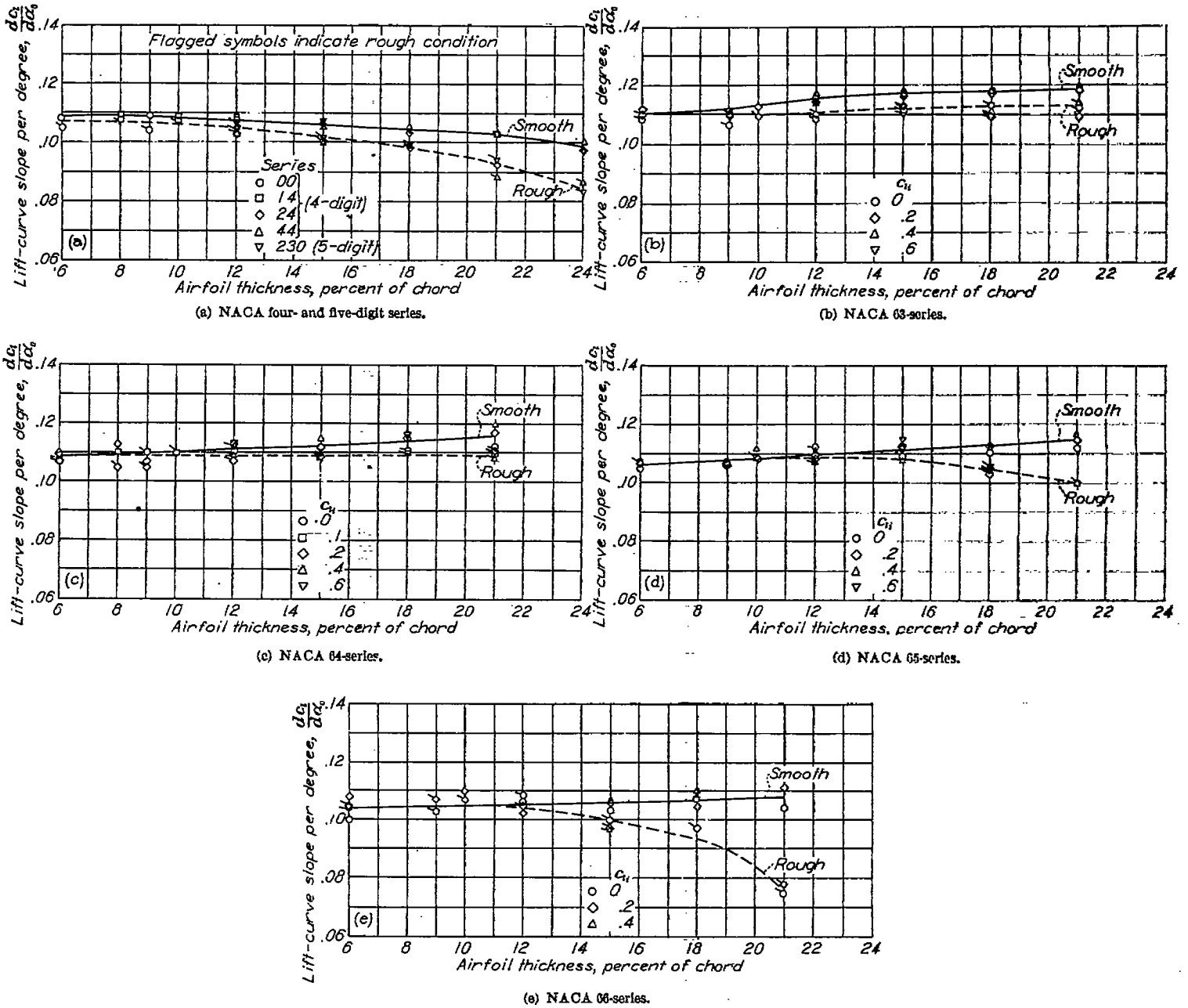

FIGURE 38.—Variation of lift-curve slope with airfoil thickness ratio and camber for a number of NACA airfoil sections in both the smooth and rough conditions. $R=6\times10^6$.

The available data indicate that a thickness ratio of 12 percent or less is optimum for airfoils having a design lift coefficient of 0.4.

The maximum lift coefficient is least sensitive to variations in position of minimum pressure on the basic thickness form for airfoils having thickness ratios of 6, 18, or 21 percent. The maximum lift coefficients corresponding to intermediate thickness ratios increase with forward movement of the position of minimum pressure, particularly for those airfoils having design lift coefficients of 0.2 or less.

The maximum lift coefficients of moderately cambered NACA 6-series sections increase with increasing camber (fig. 39 (b) to 39 (e)). The addition of camber to the symmetrical airfoils causes the greatest increments of maximum lift coefficient for airfoil thickness ratios varying from 6 to 12 percent. The effectiveness of camber as a means of increasing the maximum lift coefficient generally decreases as the airfoil thickness increases beyond 12 or 15 percent. The available data indicate that the combination of a 12-percent-thick section and a mean line cambered for a design lift coefficient of 0.4 yields the highest maximum lift coefficient.

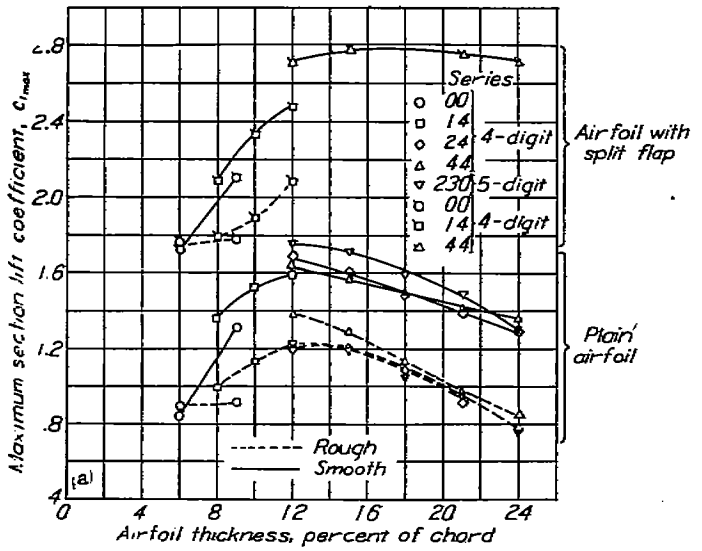

(a) NACA four- and five-digit series.

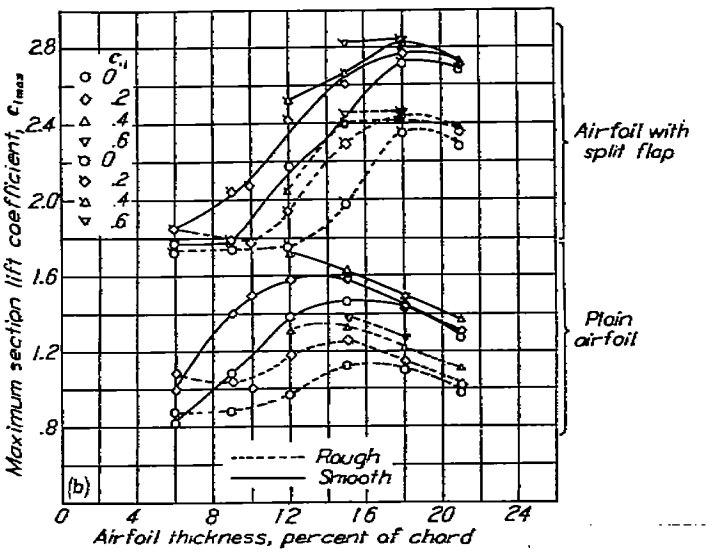

(b) NACA 63-series.

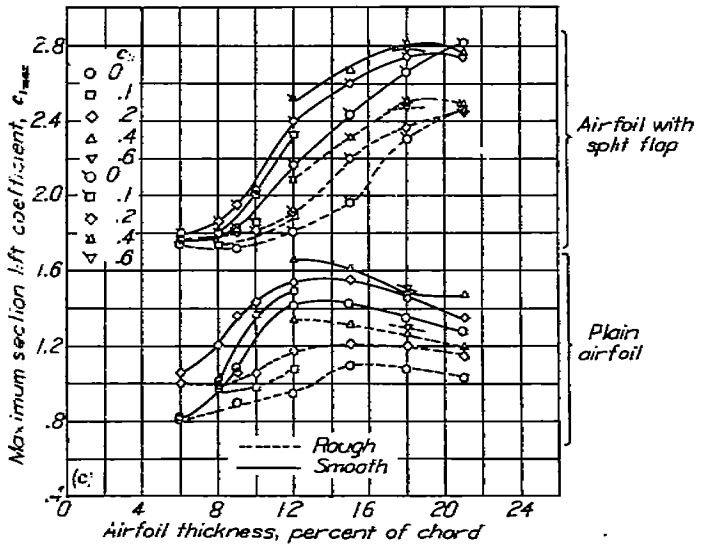

(c) NACA 64-series.

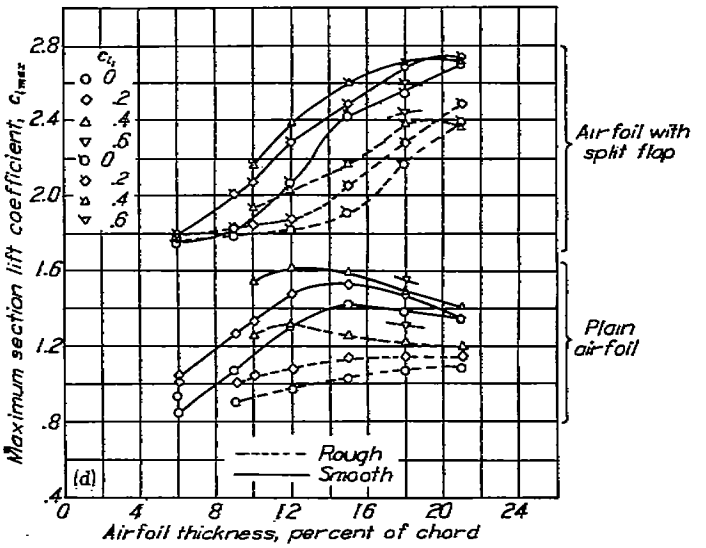

(d) NACA 65-series.

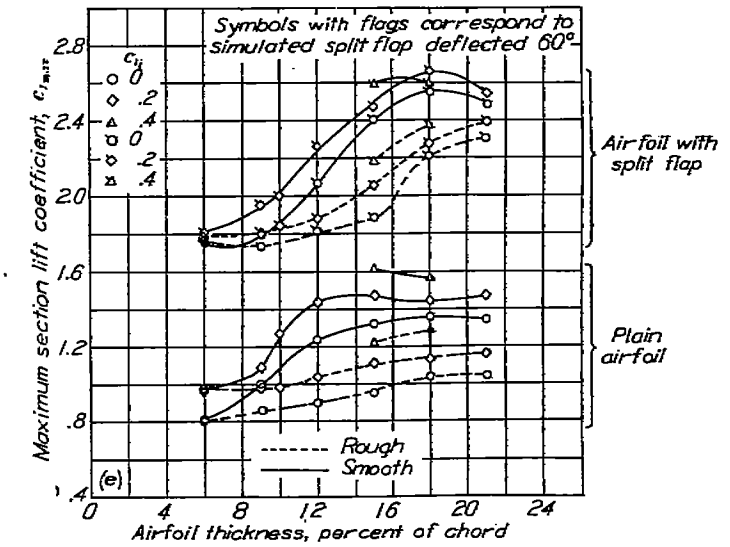

(e) NACA 66-series.

FIGURE 39.—Variation of maximum section lift coefficient with airfoil thickness ratio and camber for several NACA airfoil sections with and without simulated split flaps and standard roughness. $R=6\times10^6$.

The variation of maximum lift with type of mean line is shown in figure 40 for one 6-series thickness distribution. No systematic data are available for mean lines with values of a less than 0.5. It should be noted, however, that airfoils such as the NACA 230-series sections with the maximum camber far forward show large values of maximum lift. Airfoil sections with maximum camber far forward and with thickness ratios of 6 to 12 percent usually stall from the leading edge with large sudden losses in lift. A more desirable gradual stall is obtained when the location of maximum camber is farther back, as for the NACA 24-, 44-, and 6-series sections with normal types of camber.

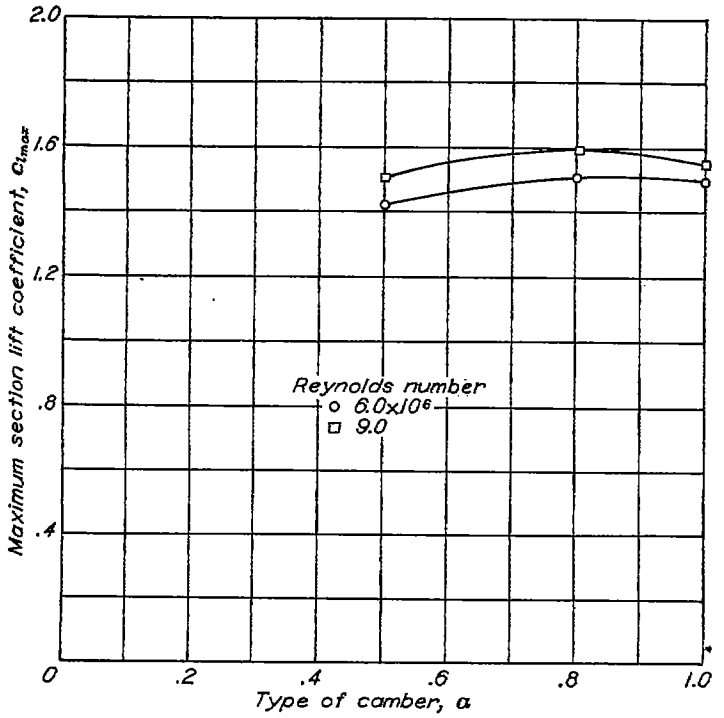

FIGURE 40.—Variation of maximum lift coefficient with type of camber for some NACA 65a-418 airfoil sections from tests in the Langley two-dimensional low-turbulence pressure tunnel.

A comparison of the maximum lift coefficients of NACA 64-series airfoil sections cambered for a design lift coefficient of 0.4 with those of the NACA 44- and 230-series sections (fig. 39) shows that the maximum lift coefficients of the NACA 64-series airfoils are as high or higher than those of the NACA 44-series sections in all cases. The NACA 230-series airfoil sections have maximum lift coefficients somewhat higher than those of the NACA 64-series sections.

The scale effect on the maximum lift coefficient of a large number of NACA airfoil sections for Reynolds numbers from 3×10^6 to 9×10^6 is shown in figure 41. The scale effect for the NACA 24-, 44-, and 230-series airfoils (figs. 41 (a) and 41 (b)) having thickness ratios from 12 to 24 percent is favorable and nearly independent of the airfoil thickness. Increasing the Reynolds number from 3×10^6 to 9×10^6 results in an increase in the maximum lift coefficient of approximately 0.15 to 0.20. The scale effect on the NACA 00- and 14-series airfoils having thickness ratios less than $0.12c$ is very small.

The scale-effect data for the NACA 6-series airfoils (figs. 41 (c) to 41 (f)) do not show an entirely systematic variation. In general, the scale effect is favorable for these airfoil sections. For the NACA 63- and 64-series airfoils with small camber, the increase in maximum lift coefficient with increase in Reynolds number is generally small for thickness ratios of less than 12 percent but is somewhat larger for the thicker sections. The character of the scale effect for the NACA 65- and 66-series airfoil sections is similar to that for the NACA 63- and 64-series airfoils but the trends are not so well defined. In most cases the scale effect for NACA 6-series airfoil sections cambered for a design lift coefficient of 0.4 or 0.6 does not vary much with airfoil thickness ratio. The data of figure 42 show that the maximum lift coefficient for the NACA 63(420)–422 airfoil continues to increase with Reynolds number, at least up to a Reynolds number of 26×10^6.

The values of the maximum lift coefficient presented were obtained for steady conditions. The maximum lift coefficient may be higher when the angle of attack is increasing. Such a condition might occur during gusts and landing maneuvers. (See reference 41.)

The systematic investigation of NACA 6-series airfoils included tests of the airfoils with a simulated split flap deflected 60°. It was believed that these tests would serve as an indication of the effectiveness of more powerful types of trailing-edge high-lift devices although sufficient data to verify this assumption have not been obtained. The maximum lift coefficients for a large number of NACA airfoil sections obtained from tests with the simulated split flap are presented in figure 39.

The data for the NACA 00- and 14-series airfoils equipped with split flap for thickness ratios from 6 to 12 percent show a considerable increase in maximum lift coefficient with increase in thickness ratio. Corresponding data for the NACA 44-series airfoils with thickness ratios from 12 to 24 percent show very little variation in maximum lift coefficient with thickness. For NACA 6-series airfoils equipped with split flaps the maximum lift coefficients increase rapidly with increasing thickness over a range of thickness ratio, the range beginning at thickness ratios between 6 and 9 percent, depending upon the camber. The upper limit of this range for the symmetrical NACA 64- and 65-series airfoils appears to be greater than 21 percent and for the NACA 63- and 66-series airfoils, approximately 18 percent. Between thickness ratios of 6 and 9 percent the values of maximum lift coefficient for the symmetrical NACA 6-series airfoils are essentially the same regardless of thickness ratio and position of minimum pressure on the basic thickness form. The maximum lift coefficient decreases with rearward movement of minimum pressure for the airfoils having thickness ratios between 9 and 18 percent.

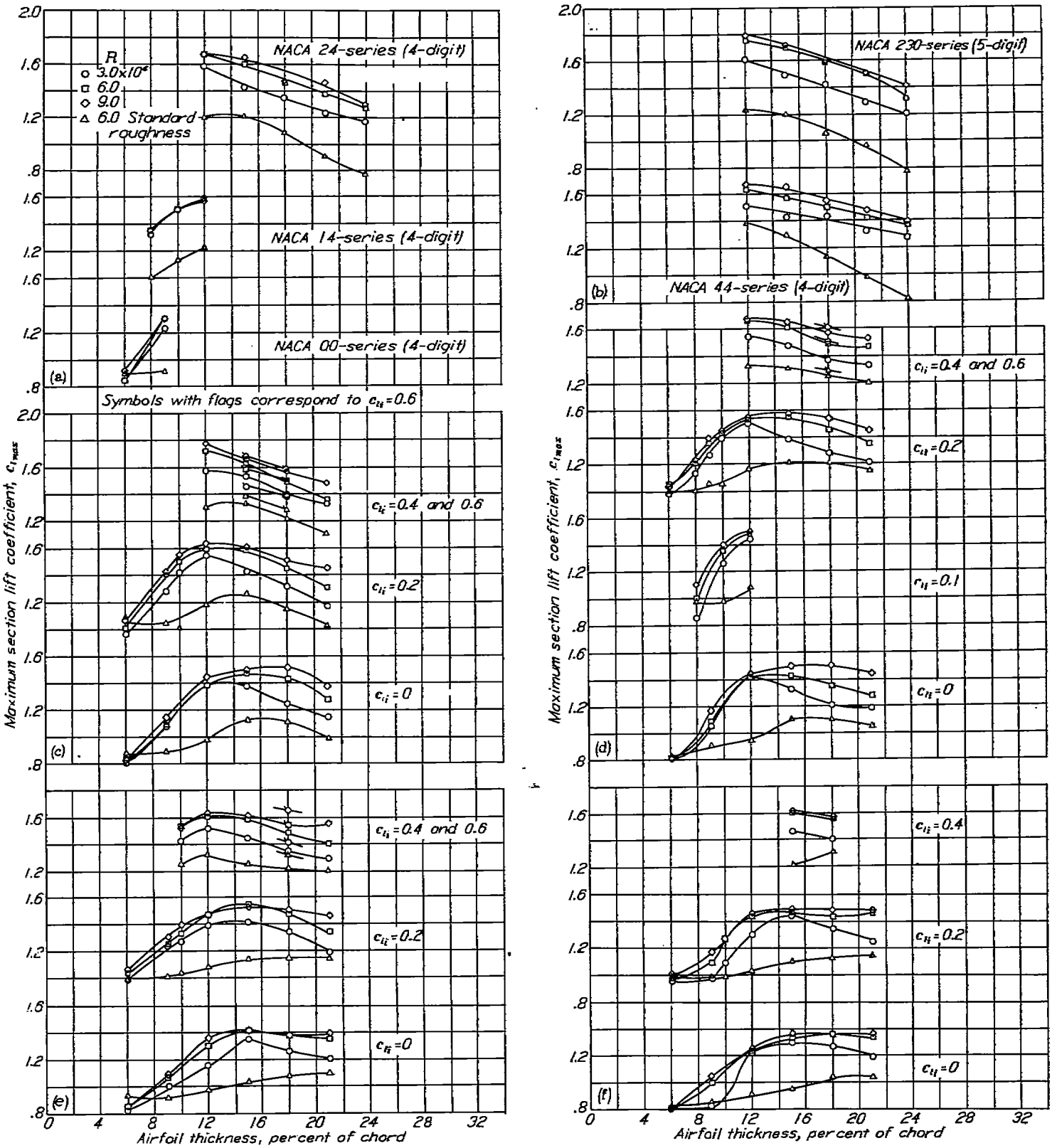

(a) NACA four-digit series.
(b) NACA four- and five-digit series.
(c) NACA 63-series.
(d) NACA 64-series.
(e) NACA 65-series.
(f) NACA 66-series.

FIGURE 41.—Variation of maximum section lift coefficient with airfoil thickness ratio at several Reynolds numbers for a number of NACA airfoil sections of different cambers.

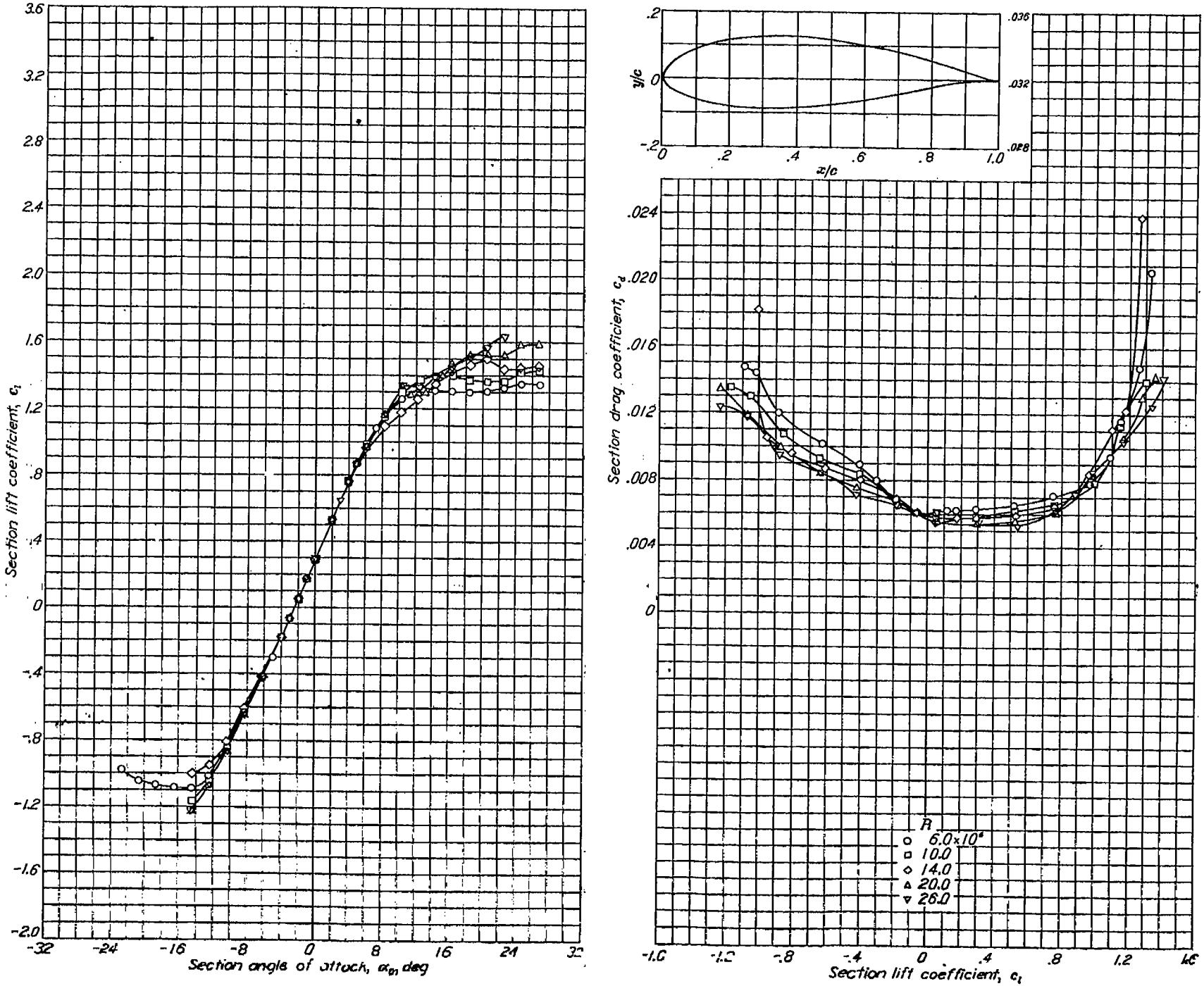

FIGURE 42.—Lift and drag characteristics of the NACA 63(420)-422 airfoil at high Reynolds number TDT tests 228 and 255.

Substantial increments in maximum lift coefficient with increase in camber are shown for the NACA 6-series airfoils of moderate thickness ratios (10 to 15 percent chord) with split flaps. For the airfoils having thickness ratios of 6 percent and for the airfoils having thickness ratios of 18 or 21 percent, the maximum lift coefficient is affected very little by a change in camber. For thickness ratios greater than 15 percent, the maximum lift coefficients of the NACA 63- and 64-series airfoils cambered for a design lift coefficient of 0.4 equipped with split flaps are greater than the corresponding maximum lift coefficients of the NACA 44-series airfoils.

Three-dimensional data.—No recent systematic three-dimensional wing data obtained at high Reynolds numbers are available, so that it is difficult to make any comparison with the section data. When the maximum-lift data for three-dimensional wings are compared with section data, account should be taken of the span load distribution over the wing. The predicted maximum lift coefficient for the wing will be somewhat lower than the maximum lift coefficients of the sections used because of the nonuniformity of the spanwise distribution of lift coefficient. The difference amounts to about 4 to 7 percent for a rectangular wing with an aspect ratio of 6.

Maximum-lift data obtained from tests of a number of wings and airplane models in the Langley 19-foot pressure tunnel are presented in table II. Although section data at the Reynolds numbers necessary to permit a detailed comparison are not available, the maximum lift coefficient for plain wings given in table II appears to be in general agreement with values expected from section data. The data for the airplane models are presented to indicate the maximum lift coefficients obtained with various airfoils and configurations.

LIFT CHARACTERISTICS OF ROUGH AIRFOILS

Two-dimensional data.—Most recent airfoil tests, especially of airfoils with the thicker sections, have included tests with roughened leading edge (reference 37), and the available data are included in the supplementary figures.

The effect on maximum lift coefficient of various degrees of roughness applied to the leading edge of the NACA 63(420)–422 airfoil is shown in figure 23. The maximum lift coefficient decreases progressively with increasing roughness (reference 36). For a given surface condition at the leading edge, the maximum lift coefficient increases slowly with increasing Reynolds number (fig. 43). Figure 24 shows that roughness strips located more than 0.20c from the leading edge have little effect on the maximum lift coefficient or lift-curve slope. The results presented in figure 38 show that the effect of standard leading edge roughness is to decrease the lift-curve slope, particularly for the thicker airfoils having the position of minimum pressure far back. These data are for a Reynolds number of 6×10^6. Maximum-lift-coefficient data at a Reynolds number of 6×10^6 for a large number of NACA airfoil sections with standard roughness are presented in figures 39 and 41. The variation of maximum lift coefficient with thickness for the NACA four- and five-digit-series airfoil sections shows the same trends for the airfoils with roughness as for the smooth airfoils except that the values are considerably reduced for all of these airfoils other than the NACA 00-series airfoils of 6 percent thickness. For a given thickness ratio greater than 15 percent, the values of maximum lift coefficient for the four- and five-digit-series airfoils are substantially the same.

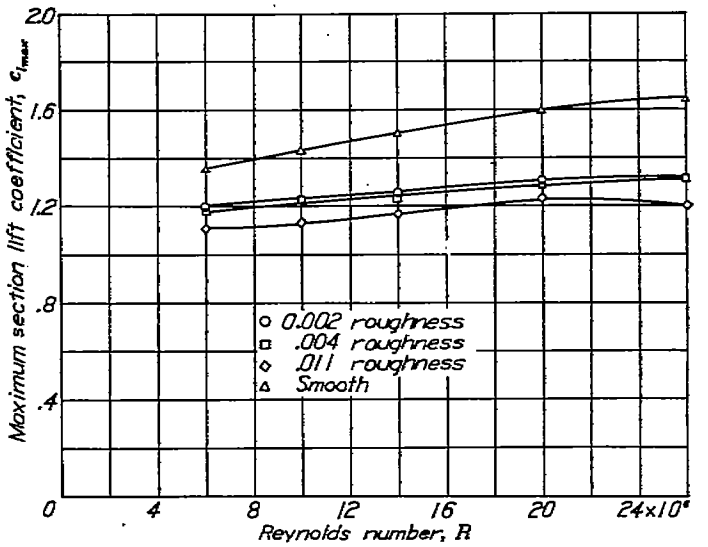

FIGURE 43.—Effects of Reynolds number on maximum section lift coefficient $c_{l_{max}}$ of the NACA 63(420)-422 airfoil with roughened and smooth leading edge.

Much less variation in maximum lift coefficient with thickness ratio is shown by the NACA 6-series airfoil sections in the rough condition than with smooth leading edge. The maximum lift coefficients of the 6-percent-thick airfoils are essentially the same for both smooth and rough conditions. The variation of maximum lift coefficient with camber, however, is about the same for the airfoils with standard roughness as for the smooth sections. The maximum lift coefficient of airfoils with standard roughness generally decreases somewhat with rearward movement of the position of minimum pressure except for airfoils having thickness ratios greater than 18 percent, in which case some slight gain in maximum lift coefficient results from a rearward movement of the position of minimum pressure.

Except for the NACA 44-series airfoils of 12 to 15 percent thickness, the present data indicate that the rough NACA 64-series airfoil sections cambered for a design lift coefficient of 0.4 have maximum lift coefficients consistently higher than the rough airfoils of the NACA 24-, 44-, and 230-series airfoils of comparable thickness. Standard roughness causes decrements in maximum lift coefficient of the airfoils with split flaps that are substantially the same as those observed for the plain airfoils.

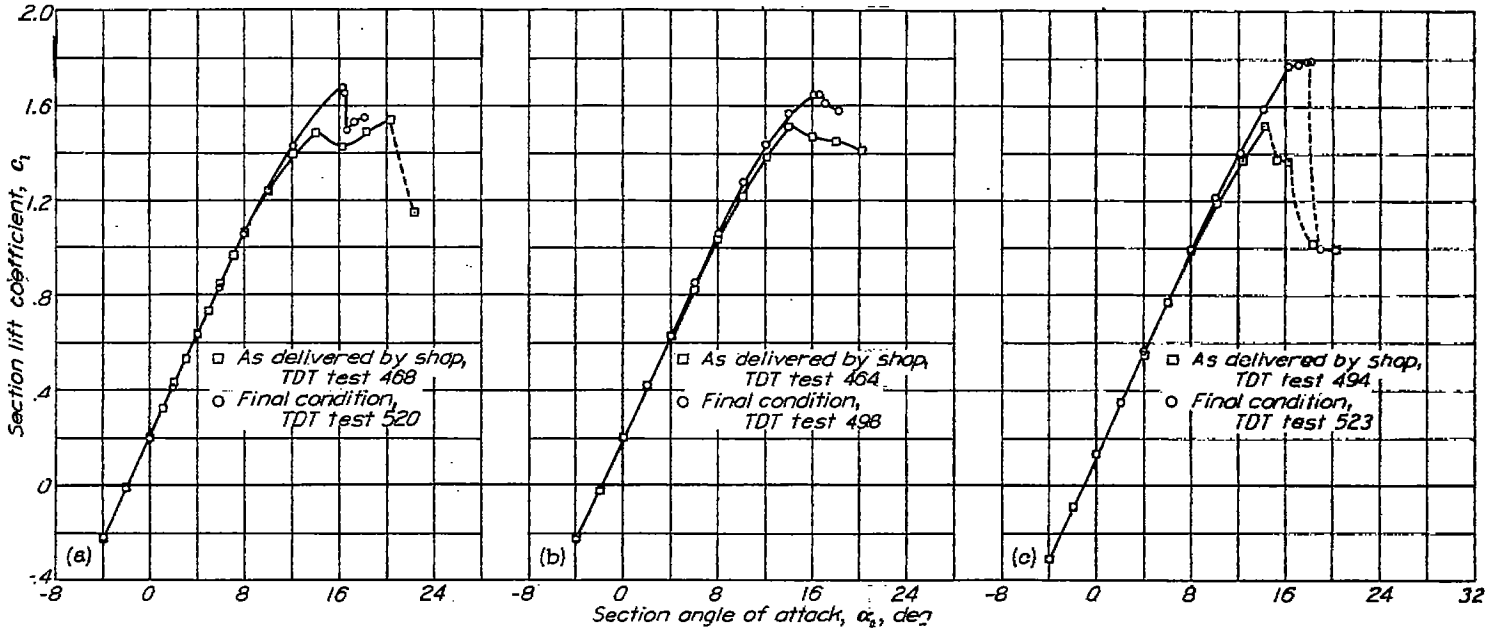

(a) NACA 2412. (b) NACA 2415. (c) NACA 23012.

FIGURE 44.—Lift characteristics of the NACA 23012, 2412, and 2415 airfoil sections as affected by normal model inaccuracies. $R=9\times10^6$ (approx.).

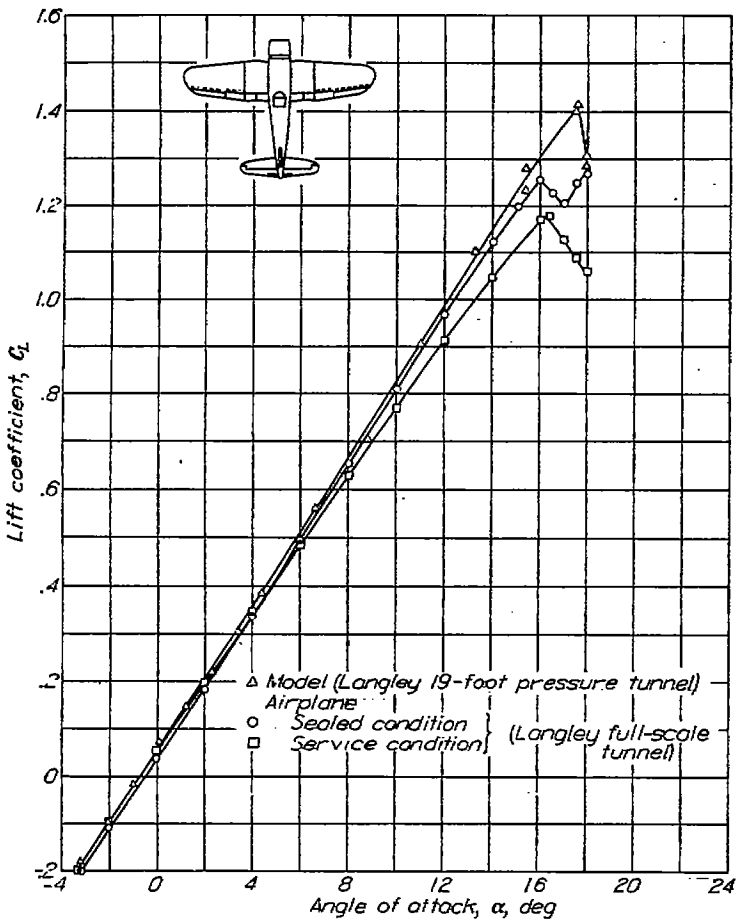

FIGURE 45.—The effects of surface conditions on the lift characteristics of a fighter-type airplane. $R=2.8\times10^6$.

The maximum lift coefficient may be lowered by failure to maintain the true airfoil contour near the leading edge, but no systematic data on this effect have been obtained. Examples of this effect that were accidentally encountered are presented in figure 44, in which lift characteristics are given for accurate and slightly inaccurate models. The model inaccuracies were so small that they were not found previous to the tests.

Three-dimensional data.—Tests of several airplanes in the Langley full-scale tunnel (reference 42) show that many factors besides the airfoil sections affect the maximum lift coefficient of airplanes. Such factors as roughness, leakage, leading-edge air intakes, armament installations, nacelles, and fuselages make it difficult to correlate the airplane maximum lift with the airfoils used, even when the flaps are retracted. The various flap configurations used make such a correlation even more difficult when the flaps are deflected. When the flaps were retracted, both the highest and the lowest maximum lift coefficients obtained in recent tests of airplanes and complete mock-ups of conventional configurations in the Langley full-scale tunnel were those obtained with NACA 6-series airfoils.

Results obtained from tests of a model of an airplane in the Langley 19-foot pressure tunnel and of the airplane in the Langley full-scale tunnel are presented in figure 45. Both tests were made at approximately the same Reynolds number. The results show that the airplane in the service condition had a maximum lift coefficient more than 0.2 lower than that of the model, as well as a lower lift-curve slope. Some improvement in the airplane lift characteristics was obtained by sealing leaks. These results show that airplane lift characteristics are strongly affected by details not reproduced on large-scale smooth models.

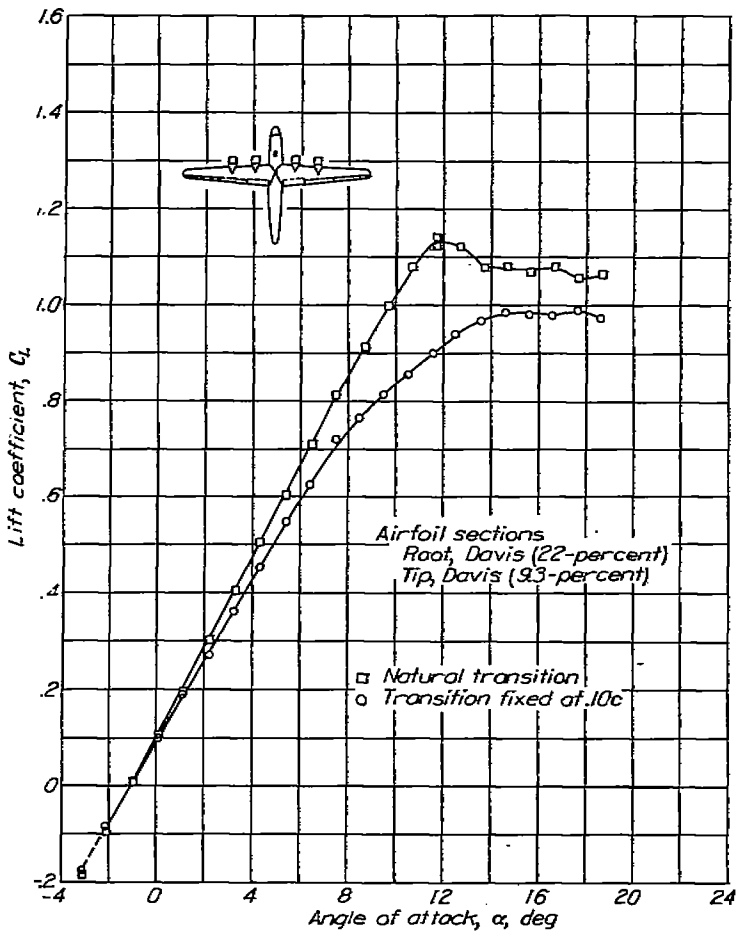

FIGURE 46.—The effect on the lift characteristics of fixing the transition on a model in the Langley 19-foot pressure tunnel. $R=2.7\times10^6$. (Model with Davis airfoil sections.)

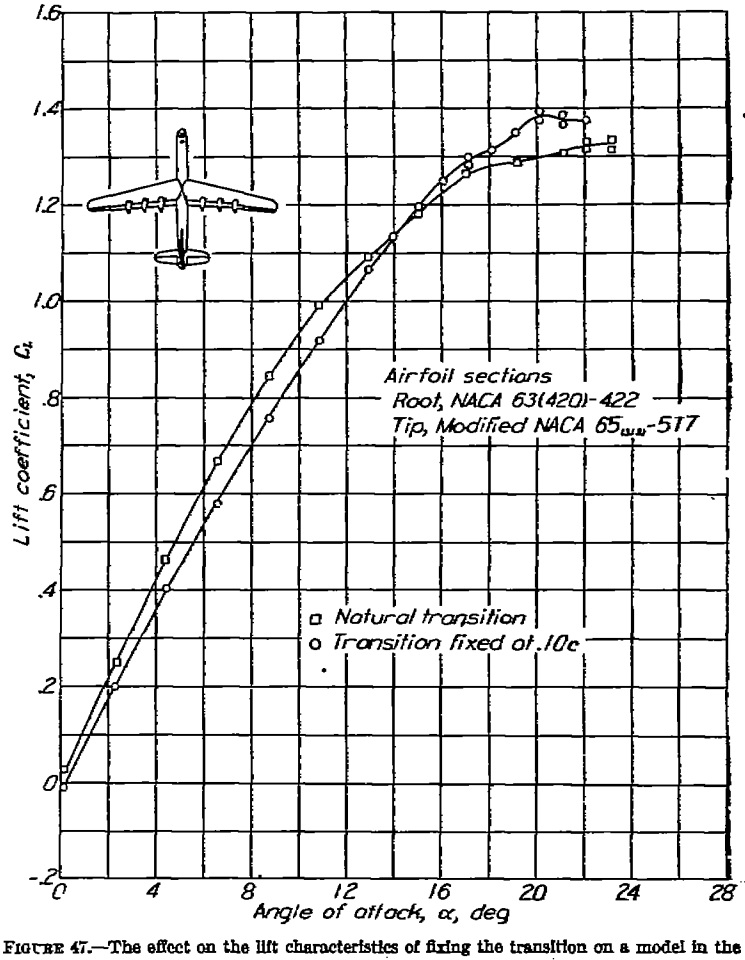

FIGURE 47.—The effect on the lift characteristics of fixing the transition on a model in the Langley 19-foot pressure tunnel. $R=2.7\times10^6$. (Model with NACA airfoil sections.)

Lift characteristics obtained in the Langley 19-foot pressure tunnel for two airplane models in the smooth condition and with transition fixed at the front spar are presented in figures 46 and 47. In both cases, the lift-curve slope was decreased throughout most of the lift range with fixed transition. The maximum lift coefficient was decreased in one case but was increased in the other case.

UNCONSERVATIVE AIRFOILS

The attempt to obtain low drags, especially for long-range airplanes, leads to high wing loadings together with relatively low span loadings. This tendency results in wings of high aspect ratio that require large spar depths for structural efficiency. The large spar depths require the use of thick root sections.

This trend to thick root sections has been encouraged by the relatively small increase in drag coefficient with thickness ratio of smooth airfoils (fig. 12). Unfortunately, airplane wings are not usually constructed with smooth surfaces and, in any case, the surfaces cannot be relied upon to stay smooth under all service conditions. The effect of roughening the leading edges of thick airfoils is to cause large increases in the drag coefficient at high lift coefficients. The resulting drag coefficients may be excessive at cruising lift coefficients for heavily loaded, high-altitude airplanes. Airfoil sections that have suitable characteristics when smooth but have excessive drag coefficients when rough at lift coefficients corresponding to cruising or climbing conditions are classified as unconservative.

The decision as to whether a given airfoil section is conservative will depend upon the power and the wing loading of the airplane. The decision may be affected by expected service and operating conditions. For example, the ability of a multiengine airplane to fly with one or more engines inoperative in icing conditions or after suffering damage in combat may be a consideration.

As an aid in judging whether the sections are conservative, the lift coefficient corresponding to a drag coefficient of 0.02 was determined from the supplementary figures for a large number of NACA airfoil sections with roughened leading edges. The variation of this critical lift coefficient with airfoil thickness ratio and camber is shown in figure 48. These data show that, in general, the lift coefficient at which the drag coefficient is 0.02 decreases with rearward movement of

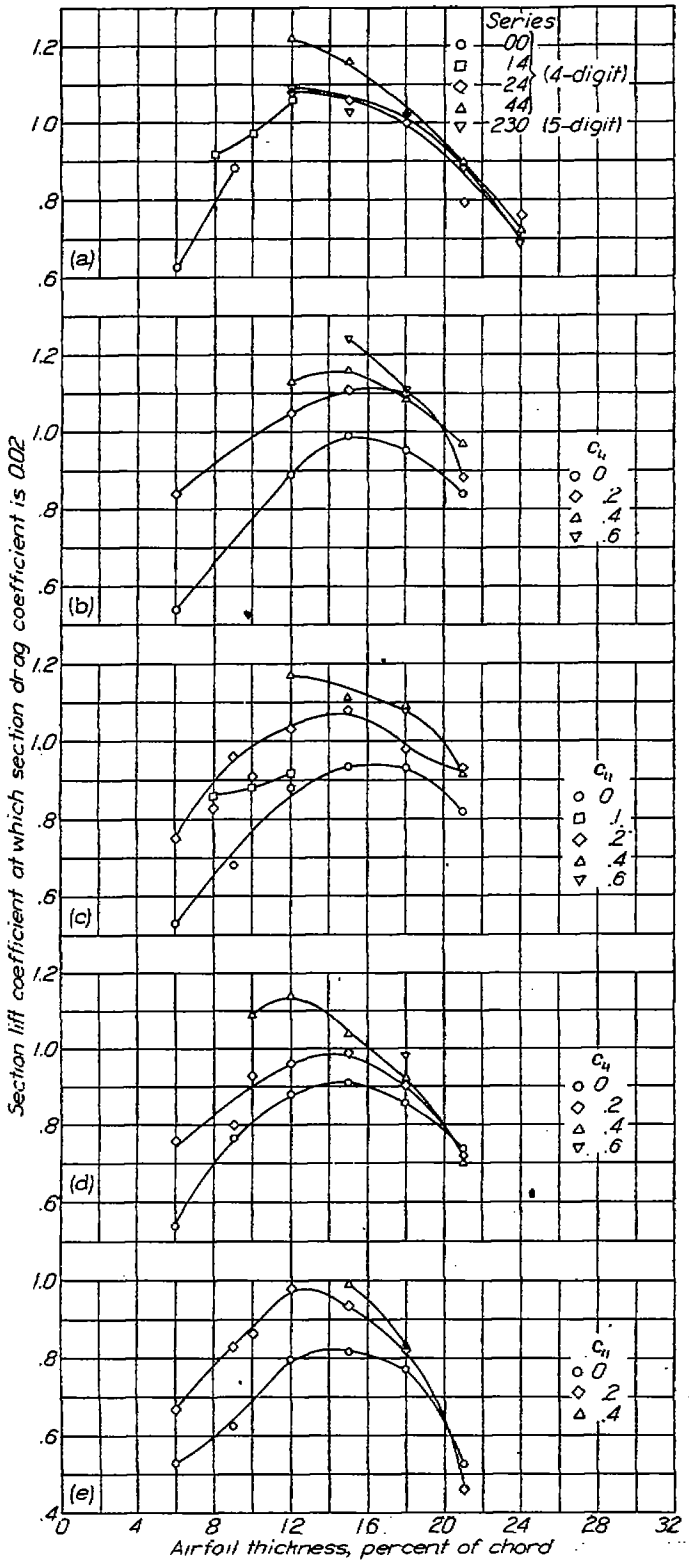

(a) NACA four- and five-digit series.
(b) NACA 63-series.
(c) NACA 64-series.
(d) NACA 65-series.
(e) NACA 66-series.

FIGURE 48.—Variation of the lift coefficient corresponding to a drag coefficient of 0.02 with thickness and camber for a number of NACA airfoil sections with roughened leading edges. $R=6\times10^6$.

position of minimum pressure. The thickness ratio for which this lift coefficient is a maximum usually lies between 12 and 15 percent; variations in thickness ratio from this optimum range generally cause rather sharp decreases in the critical lift coefficient. The addition of camber to the symmetrical airfoils usually causes an increase in the critical lift coefficient except for the very thick sections, in which case increasing the camber becomes relatively ineffectual and may be actually harmful. All the data of figure 48 correspond to a Reynolds number of 6×10^6. As shown in figure 49, the drag coefficient at flight values of the Reynolds number may be considerably lower than the drag coefficient at a Reynolds number of 6×10^6 if the roughness is confined to the leading edge.

PITCHING MOMENT

The variation of the quarter-chord pitching-moment coefficient at zero angle of attack with airfoil thickness ratio and camber is presented in figure 50 for several NACA airfoil sections. The quarter-chord pitching-moment coefficients of the NACA four- and five-digit-series airfoils become less negative with increasing airfoil thickness. Almost no variation in quarter-chord pitching-moment coefficient with airfoil thickness ratio or position of minimum pressure is shown by the NACA 6-series airfoil sections. As might be expected, increasing the amount of camber causes an almost uniform negative increase in the pitching-moment coefficient.

As discussed previously, the pitching moment of an airfoil section is primarily a function of its camber, and thin-airfoil theory provides a means for estimating the pitching moment from the mean-line data presented in the supplementary figures. A comparison of the experimental moment coefficient and theoretical values for the mean lines is presented in figure 51. The experimental values of the moment coefficients for NACA 6-series airfoils cambered with the uniform-load type mean line are usually about three-quarters of the theoretical values (figs. 50 and 51). Airfoils employing mean lines with values of a less than unity, however, have moment coefficients somewhat more negative than those indicated by theory. The use of a mean line having a value of a less than unity, therefore, brings about only a slight reduction in pitching-moment coefficient for a given design lift coefficient when compared with the value obtained with a uniform-load type mean line. The experimental moment coefficients for the NACA 24-, 44-, and 230-series airfoils are also less negative than those indicated by theory but the agreement is closer than for airfoils having the uniform-load type mean line.

The pitching-moment data for the airfoils equipped with simulated split flaps deflected 60° (fig. 50) indicate that the value of the quarter-chord pitching-moment coefficient becomes more negative with increasing thickness for all the airfoils tested. For the thicker NACA 6-series sections the magnitude of the moment coefficient increases with rearward movement of the position of minimum pressure.

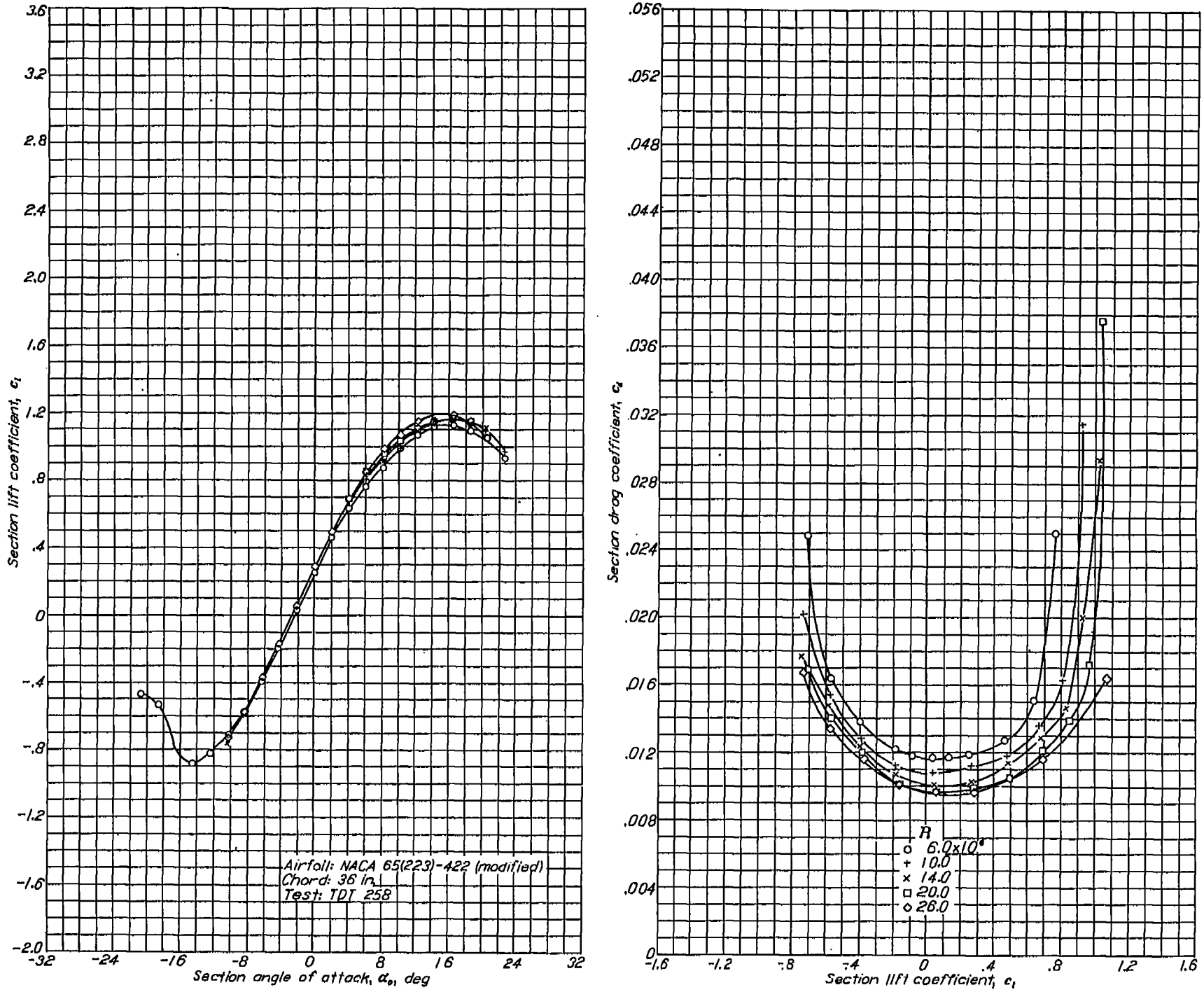

FIGURE 49.—Lift and drag characteristics of an NACA 65(223)-422 (modified) airfoil with standard roughness applied to the leading edge.

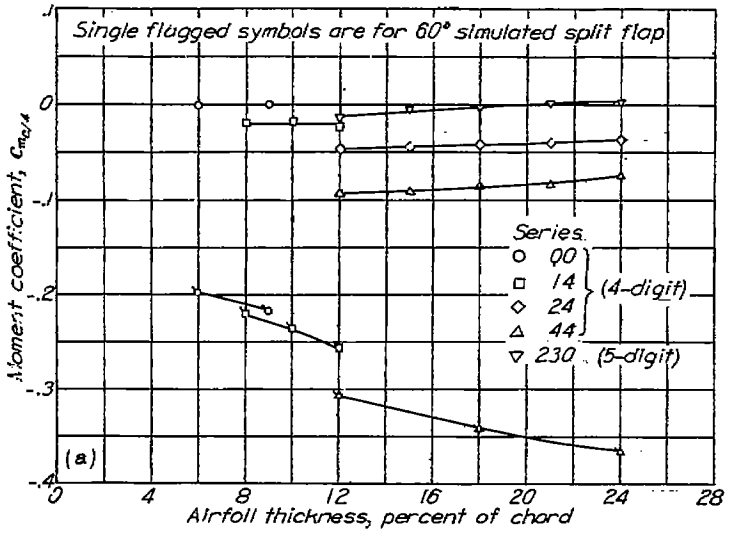

(a) NACA four- and five-digit series.

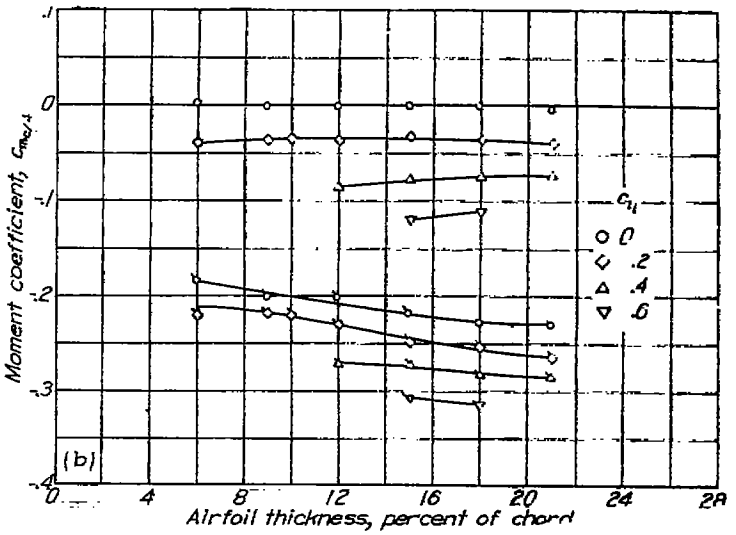

(b) NACA 63 series.

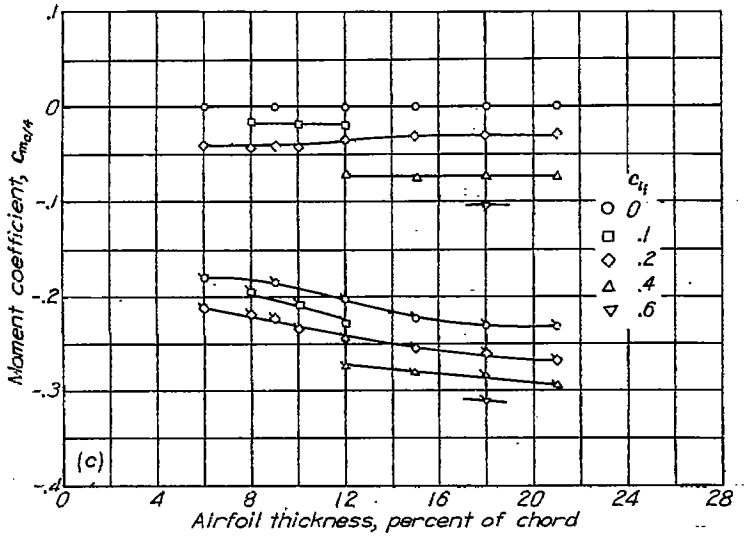

(c) NACA 64-series.

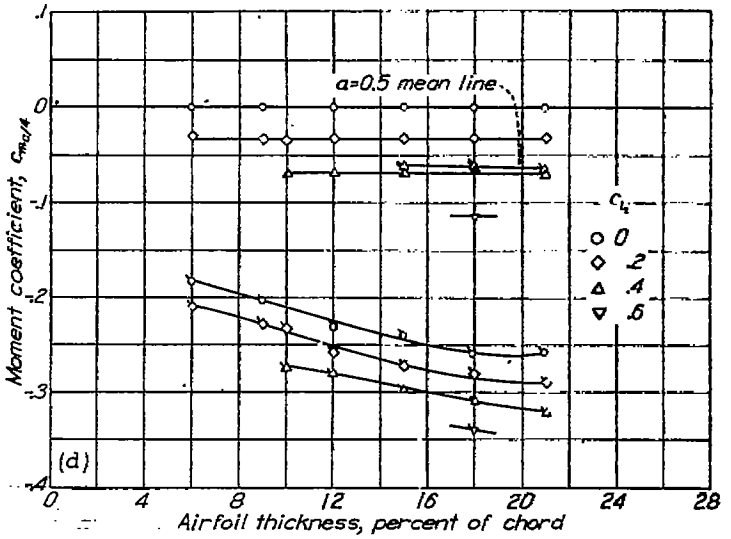

(d) NACA 65-series.

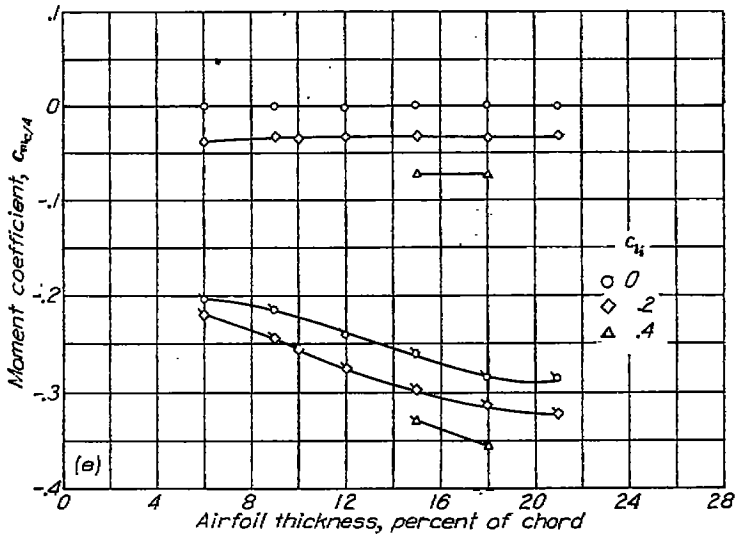

(e) NACA 66-series.

FIGURE 50.—Variation of section quarter-chord pitching-moment coefficient (measured at an angle of attack of 0°) with airfoil thickness ratio for several NACA airfoil sections of different camber. $R=6\times10^6$.

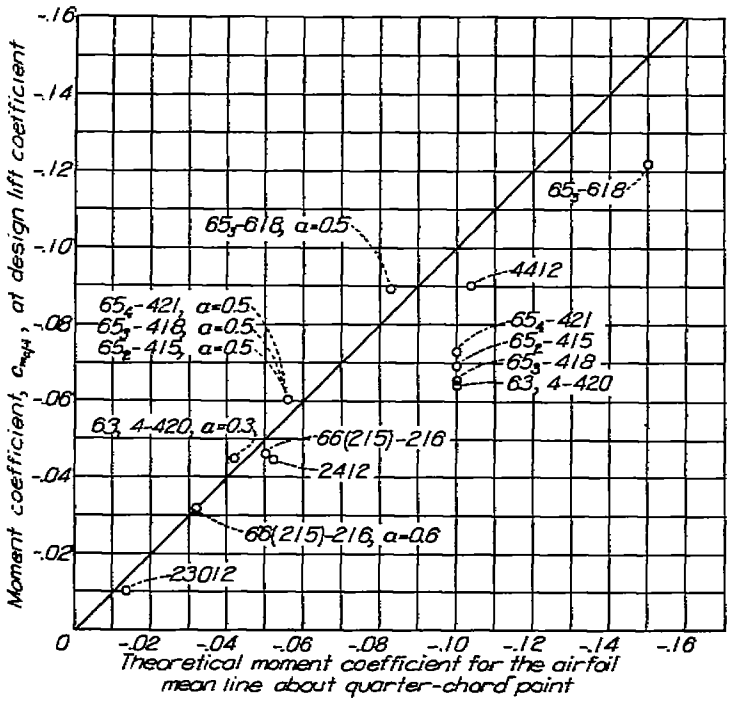

FIGURE 51.—Comparison of theoretical and measured pitching-moment coefficients for some NACA airfoils. $R=6\times10^6$.

POSITION OF AERODYNAMIC CENTER

The variation of chordwise position of the aerodynamic center corresponding to a Reynolds number of 6×10^6 for a large number of NACA airfoils is presented in figure 52. From the data given in the supplementary figures there appears to be no systematic variation of chordwise position of aerodynamic center with Reynolds number. The data for the NACA 00- and 14-series airfoils, presented for thickness ratios less than 12 percent, show that the chordwise position of the aerodynamic center is at the quarter-chord point and does not vary with airfoil thickness. For the NACA 24-, 44-, and 230-series airfoils with thickness ratios ranging from 12 to 24 percent, the chordwise position of the aerodynamic center is ahead of the quarter-chord point and moves forward with increase in thickness ratio.

The chordwise position of the aerodynamic center is behind the quarter-chord point for the NACA 6-series airfoils and moves rearward with increase in airfoil thickness, which is in accordance with the trends indicated by perfect-fluid theory. There appears to be no systematic variation of chordwise position of the aerodynamic center with camber or position of minimum pressure on the basic thickness form for these airfoils.

The data of reference 43 show important forward movements of the aerodynamic center with increasing trailing-edge angle for a given airfoil thickness. For the NACA 24-, 44-, and 230-series airfoils (fig. 52) the effect of increasing trailing-edge angle is apparently greater than the effect of increasing thickness. For the NACA 6-series airfoils, the opposite appears to be the case.

HIGH-LIFT DEVICES

Lift characteristics for two NACA 6-series airfoils equipped with plain flaps are presented in figure 53. These data show that the maximum lift coefficient increases less rapidly with flap deflection for the more highly cambered section. Lift characteristics of three NACA 6-series airfoils with split flaps are presented in reference 44 and figure 54. The maximum-lift increments for the 12-percent-thick sections were only about three-fourths of that increment for the 16-percent-thick section. The maximum lift coefficient for the thicker section with flap deflected is about the same as that obtained for the NACA 23012 airfoil in the now obsolete Langley variable-density tunnel (reference 45) and in the Langley 7- by 10-foot tunnel (reference 46).

Tests of a number of slotted flaps on NACA 6-series airfoils (supplementary figures and reference 47) indicate that the design parameters necessary to obtain high maximum lifts are essentially similar to those for the NACA 230-series sections (references 48 and 49). Lift data obtained for typical hinged single slotted 0.25c flaps (fig. 55 (a)) on the NACA 63,4–420 airfoil are presented in figure 55 (b). A maximum lift coefficient of approximately 2.95 was obtained for one of the flaps. Lift characteristics for the NACA 65_3–118 airfoil fitted with a double slotted flap (reference 47 and fig. 56 (a)) are presented in figure 56 (b). A maximum lift coefficient of 3.28 was obtained. It may be concluded that no special difficulties exist in obtaining high maximum lift coefficients with slotted flaps on moderately thick NACA 6-series sections.

Tests of airplanes in the Langley full-scale tunnel (reference 42) have shown that expected increments of maximum lift coefficient are obtained for split flaps (fig. 57) but not for slotted flaps (fig. 58). This failure to obtain the expected maximum-lift increments with slotted flaps may be attributed to inaccuracies of flap contour and location, roughness near the flap leading edge, leakage, interference from flap supports, and deflection of flap and lip under load.

LATERAL-CONTROL DEVICES

An adequate discussion of lateral-control devices is outside the scope of this report. The following brief discussion is therefore limited to considerations of effects of airfoil shape on aileron characteristics.

The effect of airfoil shape on aileron effectiveness may be inferred from the data of figure 59 and reference 50. The section aileron effectiveness parameter $\Delta\alpha_0/\Delta\delta$ is plotted against the aileron-chord ratio c_a/c for a number of airfoils of different type in figure 59. Also shown in this figure are the theoretical values of the parameter for thin airfoils.

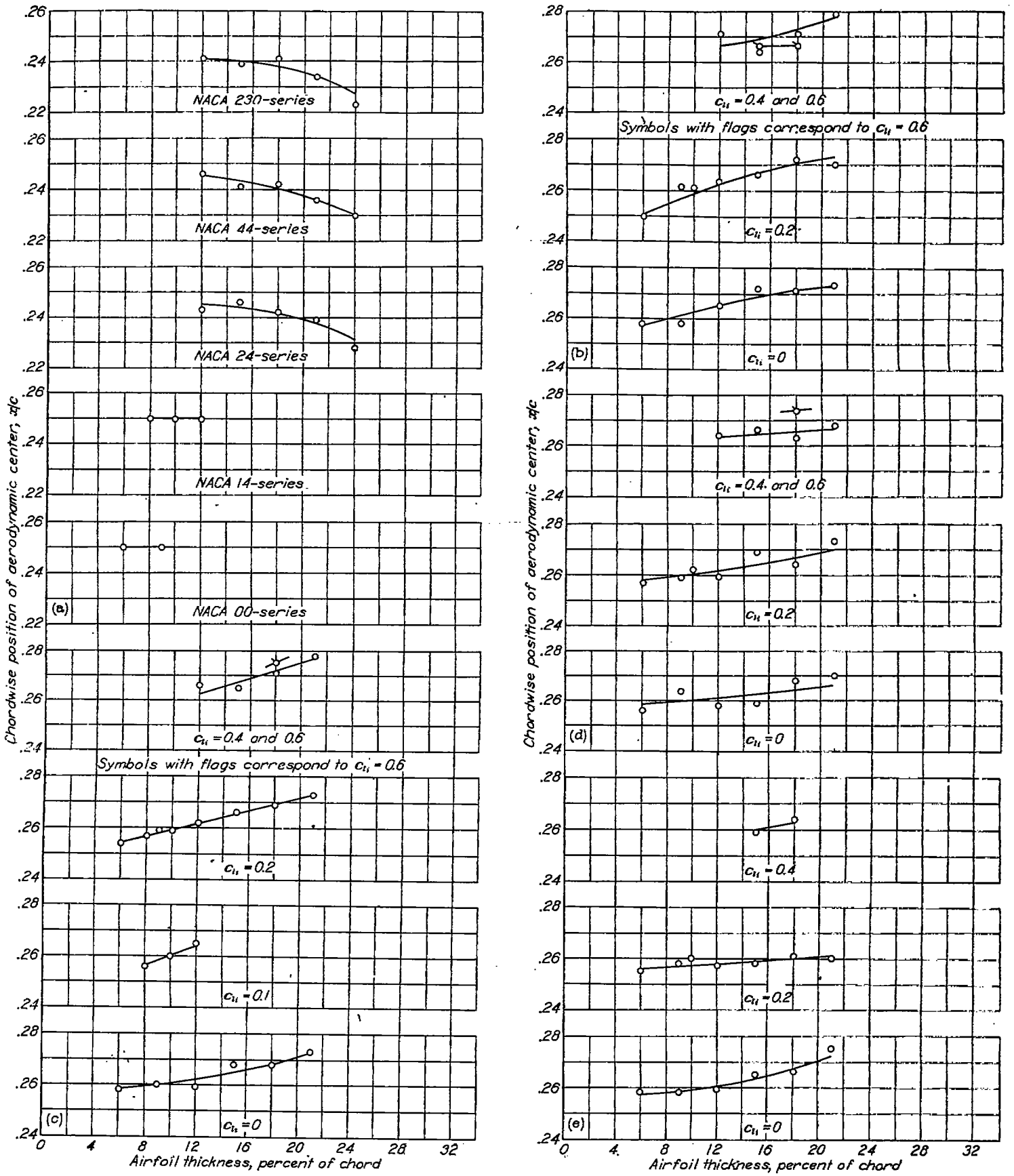

(a) NACA four- and five-digit series.
(c) NACA 64-series.

(b) NACA 63-series.
(d) NACA 65-series.
(e) NACA 66-series.

FIGURE 52.—Variation of section chordwise position of the aerodynamic center with airfoil thickness ratio for several NACA airfoil sections of different cambers. $R = 6 \times 10^6$.

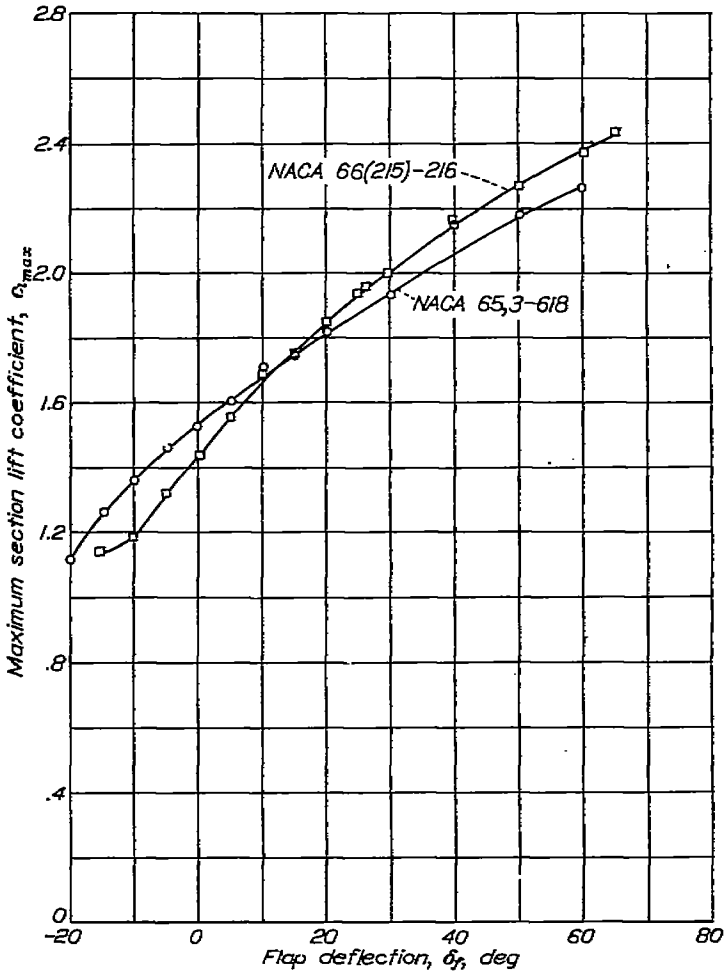

FIGURE 53.—Maximum lift coefficients for the NACA 65,3-618 and NACA 66(215)-216 airfoils fitted with 0.20-airfoil-chord plain flaps. $R=6\times10^6$.

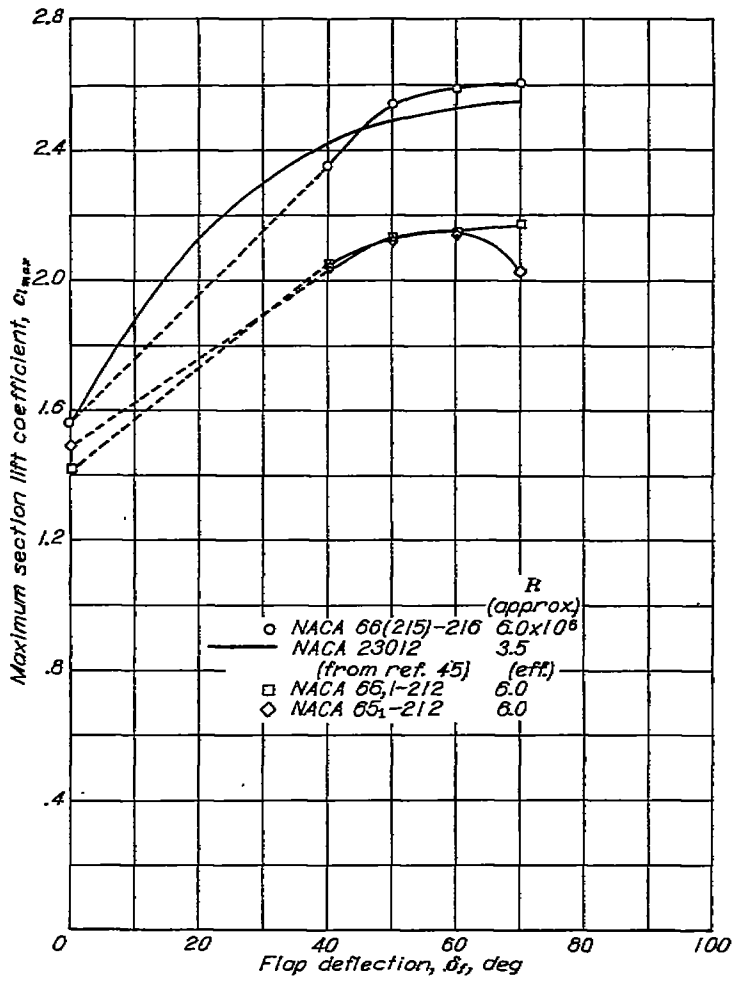

FIGURE 54.—Maximum lift coefficients for some NACA airfoils fitted with 0.20-airfoil-chord split flaps.

The data show no large consistent trends of aileron-effectiveness variation with airfoil section for a wide range of thickness distributions and thickness ratios. In order to evaluate aileron characteristics from section data, a method of analysis is necessary that will lead to results comparable to the usual curves of stick force against helix angle $pb/2V$ for three-dimensional data. The analysis that follows is considered suitable for comparing the relative merits of ailerons from two-dimensional data.

Two-dimensional data are presented in the form of the equivalent change in section angle of attack $\Delta\alpha_0$ required to maintain a constant section lift coefficient for various deflections of the aileron from neutral. This equivalent change in angle of attack is plotted against the hinge-moment parameter $\Delta c_H\delta$, which is the product of the aileron deflection from neutral and the resulting increment of hinge-moment coefficient based on the wing chord. This method of analysis takes into account the aileron effectiveness, the hinge moments, and the possible mechanical advantage between the controls and the ailerons. The larger the value of $\Delta\alpha_0$ for a given value of the hinge-moment parameter, the more advantageous the combination should be for providing a large value of $pb/2V$ for a given control force. The assumption that the aileron operates at a constant lift coefficient as the airplane rolls is not entirely correct, however, and involves an overestimation of the effect of changing angle of attack on the hinge-moment coefficient. In addition, the span of the ailerons and other possible three-dimensional effects are not considered. In spite of these inaccuracies, the method provides a useful means of comparing the two-dimensional characteristics of different ailerons.

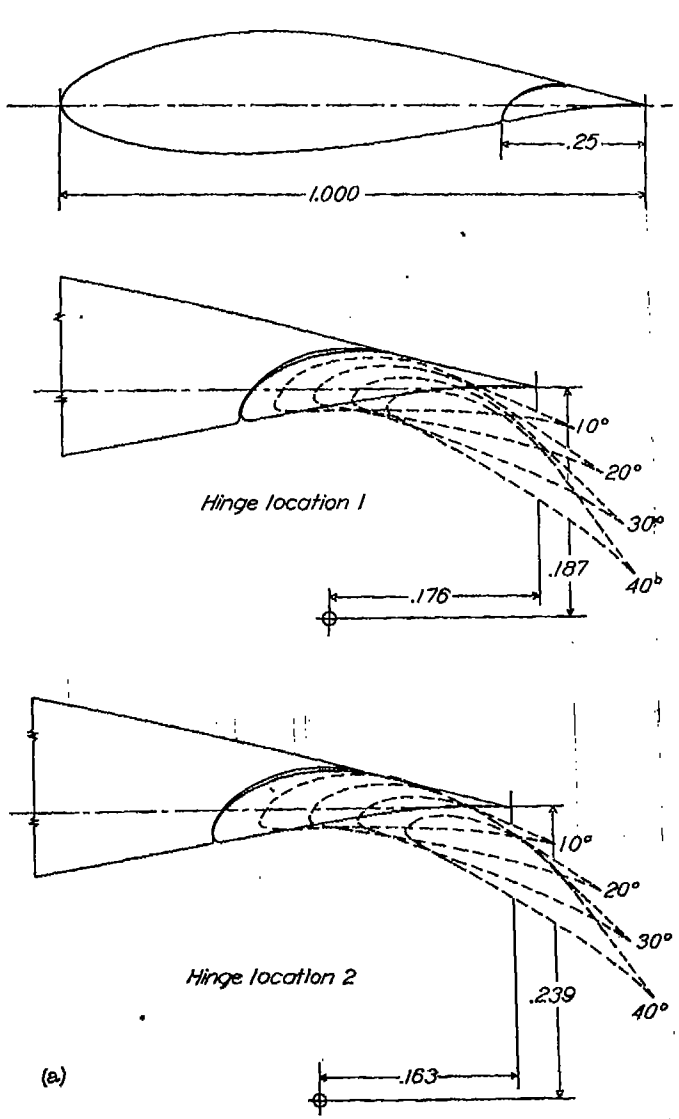

(a) Flap configuration.

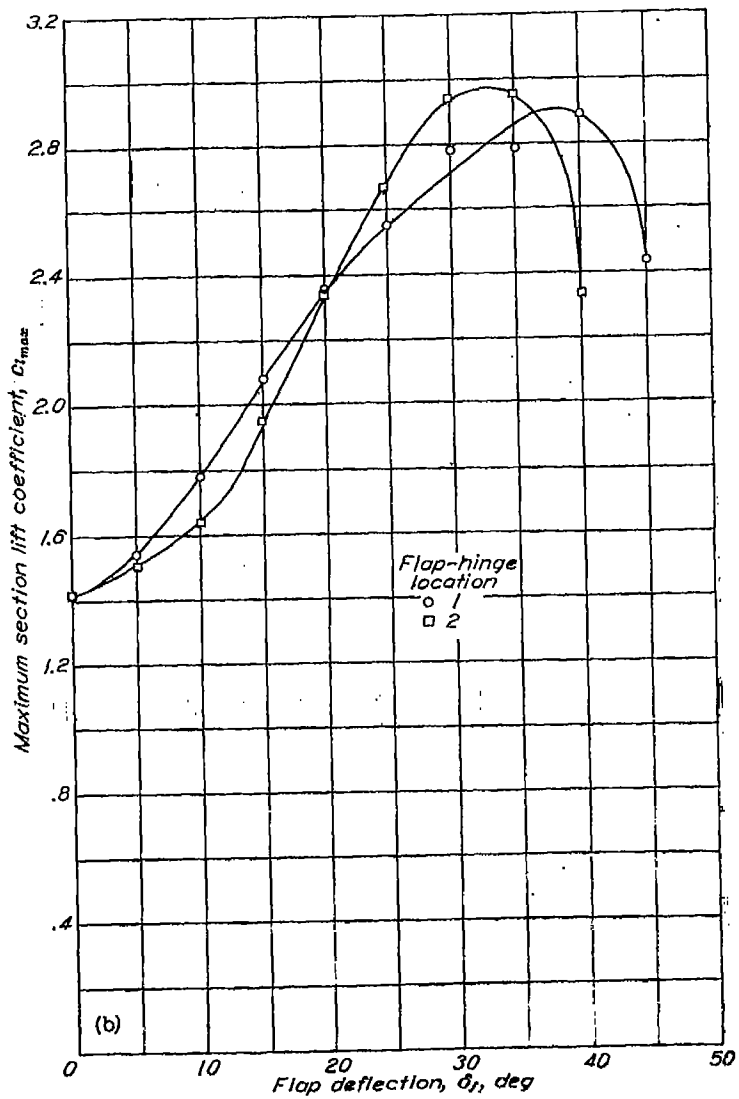

(b) Maximum lift characteristics.

FIGURE 55.—Flap configuration and maximum lift coefficients for the NACA 63,4-420 airfoil with a 0.25-airfoil-chord hinged slotted flap. $R=6\times10^6$

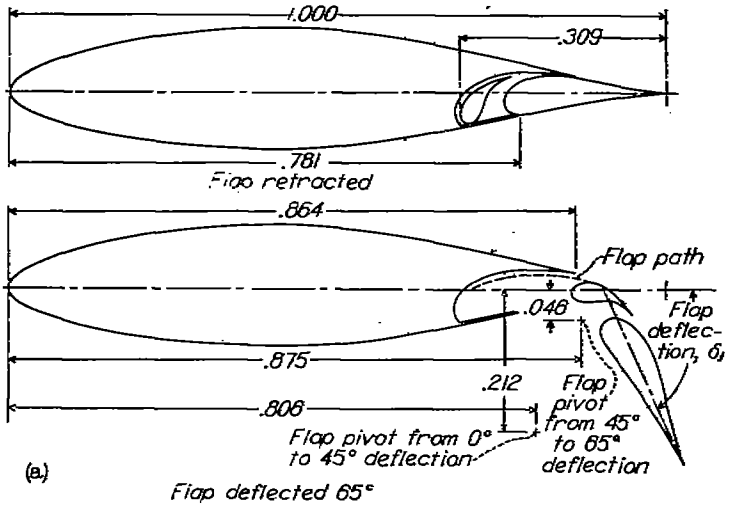

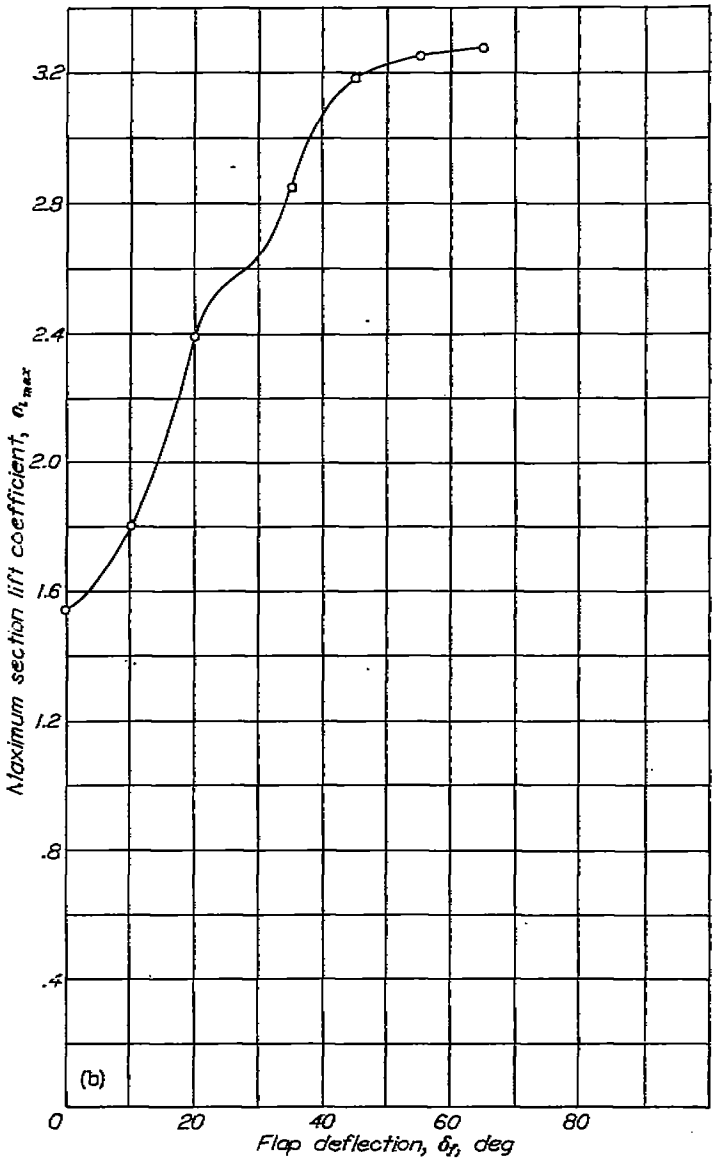

(a) Flap configuration.
(b) Maximum lift characteristics.

FIGURE 56.—Flap configuration and maximum lift coefficients for the NACA 65$_3$-118 airfoil with a double slotted flap. $R=6\times10^6$.

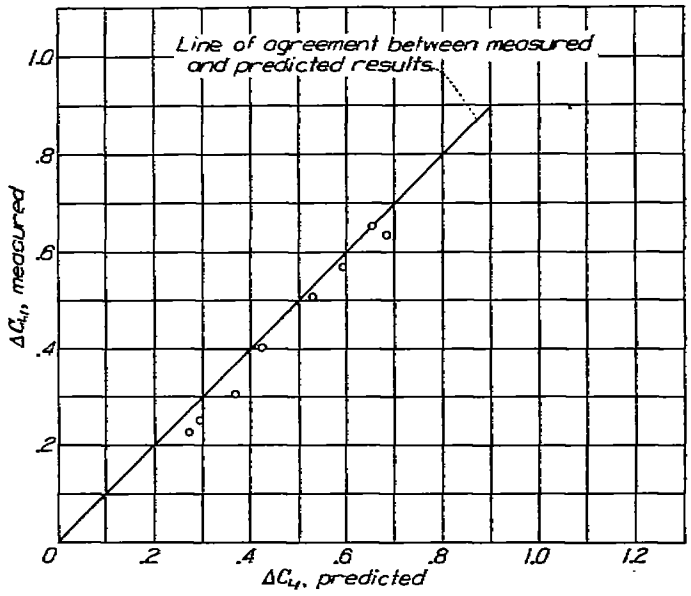

FIGURE 57.—Comparison between measured values of the increments in lift coefficients due to flap deflection and values predicted from two-dimensional data. Split flap.

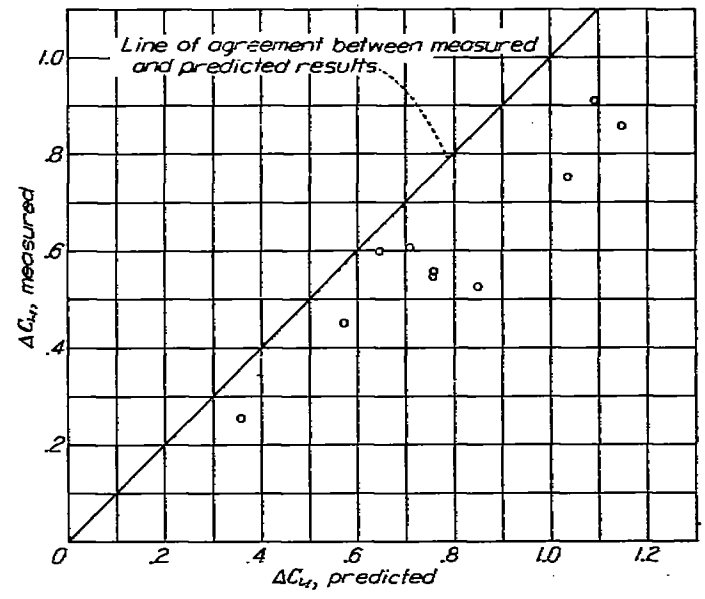

FIGURE 58.—Comparison between measured values of the increments in lift coefficients due to flap deflection and values predicted from two-dimensional data. Slotted flap.

SUPPLEMENTARY INFORMATION REGARDING TESTS OF TWO-DIMENSIONAL MODELS

Symbol	Basic airfoil	Type of flap	Air-flow characteristics			Reference
			τ	M	R	
○	NACA 0009	Plain	1.93	0.08	----------	51 to 55
+	NACA 0015	do	1.93	.10	1.4×10^6	56
×	NACA 23012	do	1.60	.11	2.2×10^6	57, 48
□	NACA 66(2x15)-009	Plain, straight contour	1.93	.10	1.4×10^6	--------
◇	NACA 66-009	Plain	1.93	.11	1.4×10^6	58
△	NACA 63,4-4(17.8) (approx.)	Internally balanced	(1)	.17	2.5×10^6	59
▽	NACA 66(2x15)-216, a=0.6	do	(1)	.18	5.3×10^6	59
▷	NACA 66(2x15)-116, a=0.6	do	(1)	.14	6.0×10^6	59
◁	NACA 64,2-(1.4) (13.5)	Plain	(1)	--------	13.0×10^6	--------
▽	NACA 65,2-318 (approx.)	Internally balanced	(1)	.14	6.0×10^6	59
◁	NACA 63(420)-521 (approx.)	do	(1)	--------	8.0×10^6	--------
▷	NACA 66(216)-216, a=0.6	do	(1)	.20 to .48	2.8×10^6 to 6.8×10^6	60
◁	NACA 66(215)-014	Plain	1.93	.09	1.2×10^6	61
○	NACA 66(215)-216, a=0.6	do	(1)	--------	6.0×10^6	--------
□	NACA 65_8-415	do	(1)	.13	6.0×10^6	62
□	NACA 65_8-418	do	(1)	.13	6.0×10^6	62
□	NACA 65_8-421	do	(1)	.13	6.0×10^6	62
◇	NACA $65_{(21)}$-213	Internally balanced	(1)	.14	8.0×10^6	--------
◇	NACA 745A317 (approx.)	do	(1)	.13	6.0×10^6	--------
◇	NACA 64,3-013 (approx.)	do	(1)	.13	6.0×10^6	--------
◇	NACA 64,3-1(15.5) (approx.)	do	(1)	.13	6.0×10^6	--------

[1] Approaching 1.00.

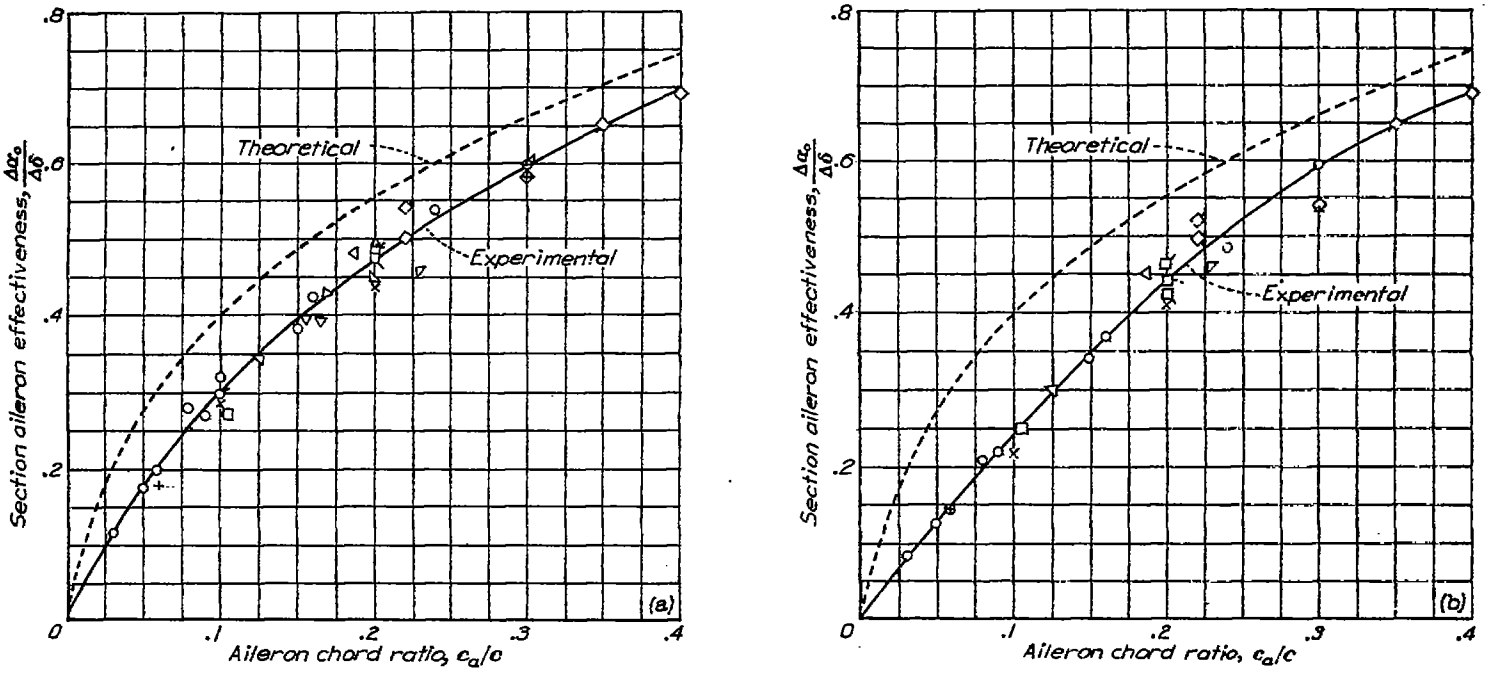

(a) δ range from 0° to 10°.

(b) δ range from 0° to 20°.

FIGURE 59.—Variation of section aileron effectiveness with aileron chord ratio for true-airfoil-contour ailerons without exposed overhang balance on a number of airfoil sections. Gaps sealed; c_l=0.

Basic airfoil	c_l	Type of aileron [1]	Air-flow characteristics			Reference
			ϵ	M	R	
NACA 0009	0	0.20c plain	1.93	0.10	1.4×10^6	63
NACA 64,2–(1.4) (13.5)	.150	0.187c plain	[2]	.18	4.0×10^6	----
NACA 66(215)–216, α=0.6	.100	0.20c plain	[2]	.33	9.0×10^6	64

[1] True airfoil contour.
[2] Approaching 1.00.

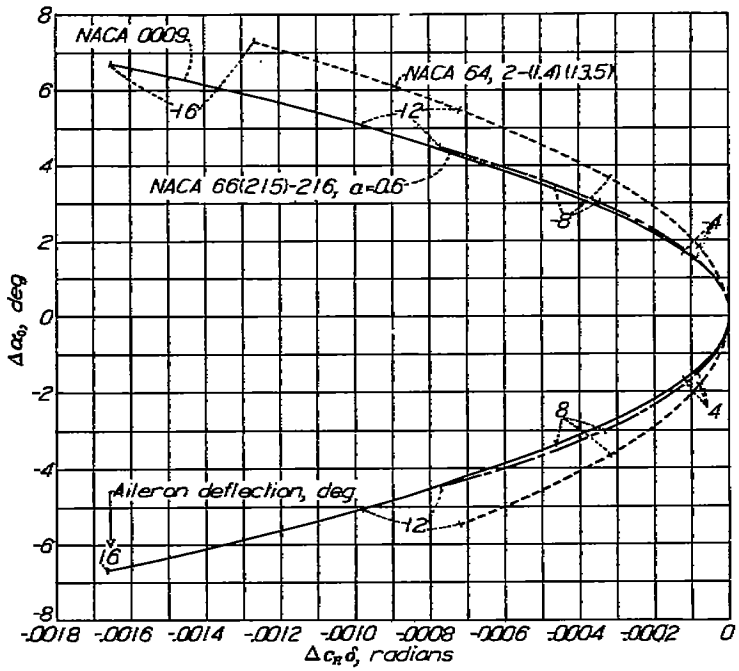

FIGURE 60.—Variation of the hinge-moment parameter $\Delta c_{H\delta}$ with the equivalent change in section angle of attack required to maintain a constant section lift coefficient for deflection of the aileron on the NACA 0009, NACA 64,2-(1.4)(13.5), and NACA 66(215)–216, α=0.6 airfoil sections. Gaps sealed.

For the purpose of evaluating the effect of airfoil shape on the aileron characteristics, it is desirable to make the comparison with unbalanced ailerons to avoid confusion. Plots of the parameters for plain unbalanced flaps of true airfoil contour on three airfoil sections are shown in figure 60. The characteristics of the NACA 66(215)–216, α=0.6 section are essentially the same as those for the NACA 0009 airfoil within the range of deflection for which data are available. The NACA 64,2–(1.4)(13.5) airfoil shows appreciably smaller values of $\Delta c_H\delta$ for a given value of $\Delta\alpha_0$ than the other sections presented. No explanation for this difference can be offered, although some of the difference may result from the slightly smaller chord of the flap for this combination.

The effects of using straight-sided ailerons instead of ailerons of true airfoil contour are shown in figure 61 for two NACA 6-series airfoils. One of the two combinations for which data are available was provided with an internal balance whereas the other combination was without balance. This difference prevents any comparison between the two combinations but does not affect comparison of the two contours for each case. For the NACA 66(215)–216, α=0.6 airfoil, the straight-sided aileron has more desirable characteristics for the range of deflections for which data are available. It appears, however, that the straight-sided aileron would be less advantageous than the aileron of true contour for positive deflections greater than 12°. In the case of the NACA 63,4–4(17.8) (approx.) airfoil, the straight-sided aileron appears to have no advantage over the aileron of true airfoil contour. The advantage of using straight-sided ailerons appears to depend markedly on the airfoil used but sufficient data are not available to determine the significant airfoil parameters. Figure 62 shows that in one case the effect of leading-edge roughness on the aileron characteristics is unfavorable.

Basic airfoil	c_l	Type of aileron	Reference
NACA 66(215)–216, α=0.6	0.100	0.20c plain	64
NACA 63,4–4(17.8) (approx.)	.450	0.20c with 0.43c_f internal balance	----

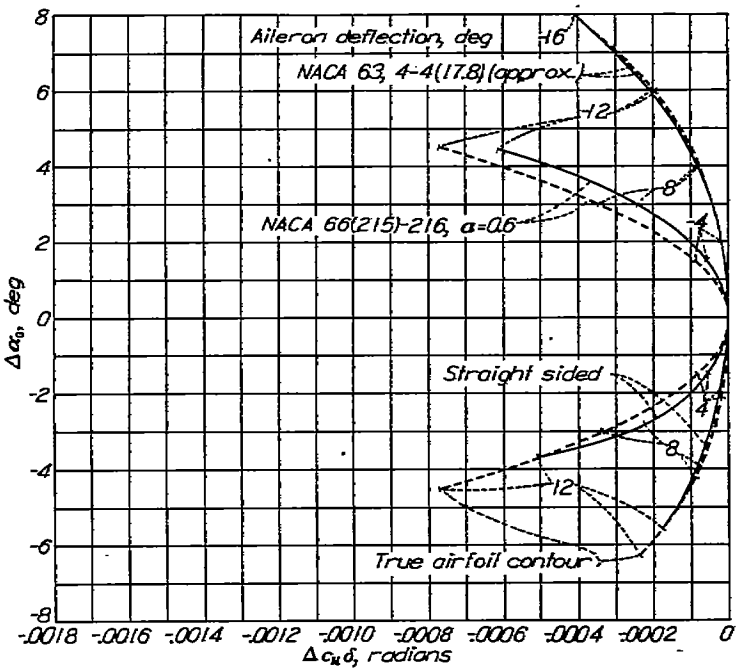

FIGURE 61.—Variation of the hinge-moment parameter $\Delta c_{H\delta}$ with the equivalent change in section angle of attack required to maintain a constant section lift coefficient for deflection of true-airfoil-contour and straight-sided ailerons on the NACA 63,4–4(17.8) (approx.) and the NACA 66(215)–216, α=0.6 airfoil sections. Gaps sealed.

LEADING-EDGE AIR INTAKES

The problem of designing satisfactory leading-edge air intakes is to maintain the lift, drag, and critical-speed characteristics of the sections while providing low intake losses over a wide range of lift coefficients and intake velocity ratios. The data of reference 65 show that desirable intake and drag characteristics can easily be maintained over a rather small range of lift coefficients for NACA 6-series airfoils. The data of reference 65 show that the intake losses increase rapidly at moderately high lift coefficients for the shapes tested. Unpublished data taken at the Langley Laboratory indicate that shapes such as those of reference 65 have low maximum lift coefficients. Recent data show

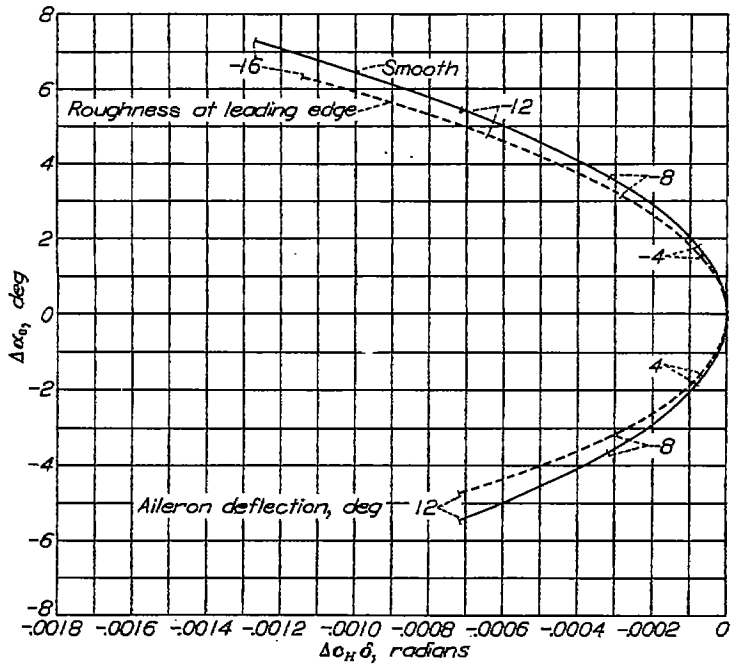

FIGURE 62.—Variation of the hinge-moment parameter $\Delta c_{H\delta}$ with the equivalent change in section angle of attack required to maintain a constant section lift coefficient for deflection of the aileron on the NACA 64,2-(1.4)(13.5) airfoil section, smooth and with roughness at the leading edge of the airfoil. (For description of aileron, see fig. 60.)

that air-intake shapes can be provided for such airfoil sections with desirable air-intake characteristics and without loss in maximum lift coefficient (fig. 63). Some pressure-distribution data for the air intakes shown in figure 63 indicate that the critical speed of the section has been lowered only slightly and that falling pressures in the direction of flow were maintained for some distance from the leading edge on both surfaces at lift coefficients near the design lift coefficient for the section. Sufficient information is not available to permit such desirable configurations to be designed without experimental development.

INTERFERENCE

The main problem of interference at low Mach numbers is considered to be that of avoiding boundary-layer separation resulting from rapid flow expansions caused by the addition of induced velocities about bodies and the boundary-layer accumulations near intersections. No recent systematic investigations of interference such as the investigation of reference 66 have been made.

Some tests have been made of airfoil sections with intersecting flat plates (reference 67). These configurations may be considered to represent approximately the condition of a wing intersection with a large flat-sided fuselage. In

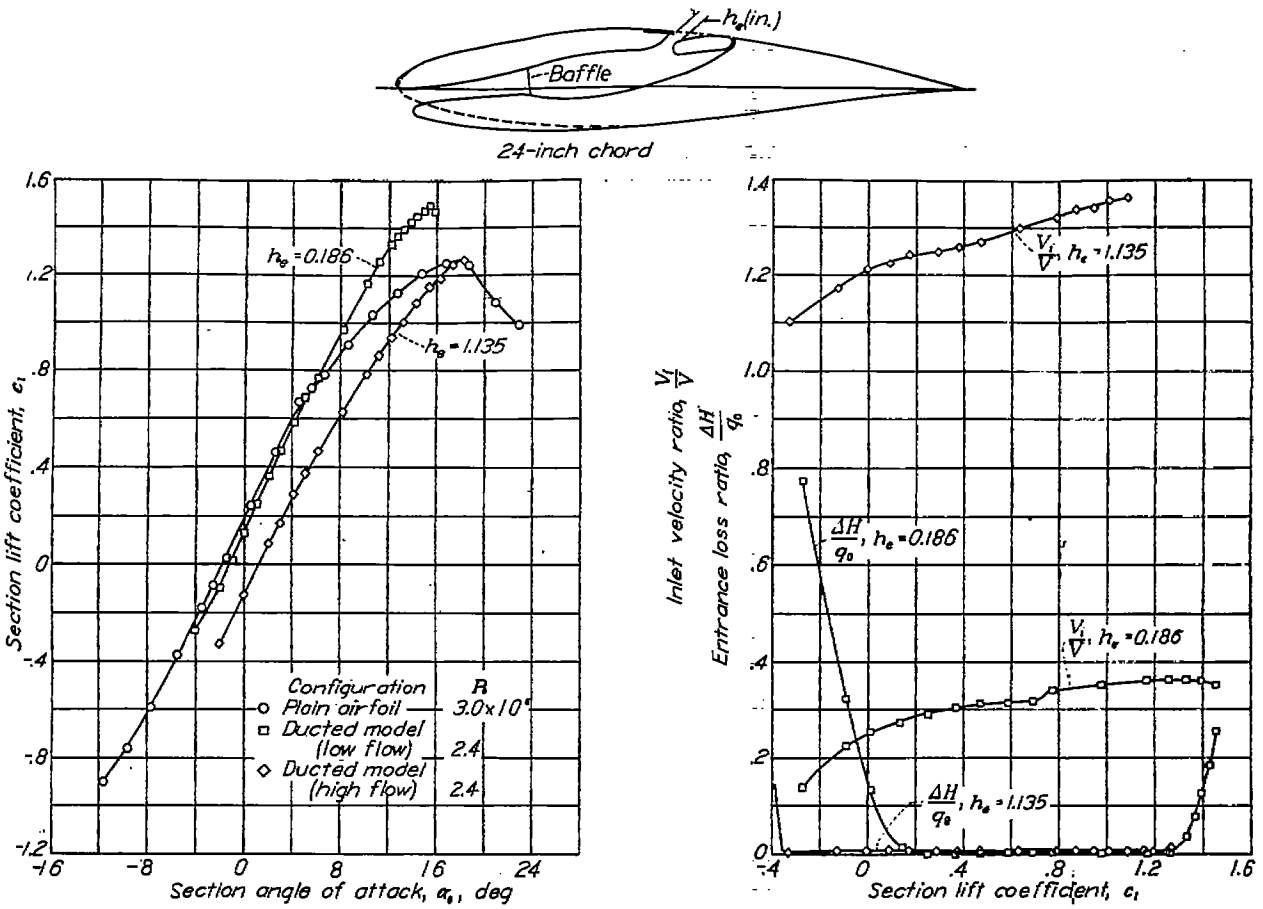

FIGURE 63.—Lift and flow characteristics of an NACA 7-series type airfoil section with leading-edge air intake.

this case, the interference may be considered to result from the effect on the wing of the fully developed turbulent boundary layer on the fuselage or flat plate and the accumulation of boundary layer in the intersection. These tests showed little interference except in cases for which the boundary layer on the airfoil alone was approaching conditions of separation such as were noted with the less conservative airfoils at moderately high lift coefficients.

Some scattered data on the characteristics of nacelles mounted on airfoils permitting extensive laminar flow are presented in references 68 to 70. The data appear to indicate that the interference problems for conservative NACA 6-series sections are similar to those encountered with other types of airfoil. The detail shapes for optimum interfering bodies and fillets may, however, be different for various sections if local excessive expansions in the flow are to be avoided.

Some lift and drag data for an airfoil with pusher-propeller-shaft housings are presented in reference 71. These results indicate that protuberances near the trailing edge of wings should be carefully designed to avoid unnecessary drag increments.

Another type of interference of particular importance for high-speed airplanes results in the reduction of the critical Mach number of the combination because of the addition of the induced velocities associated with each body (reference 72). This effect may be kept to a minimum by the use of bodies with low induced velocities, by separation of interfering bodies to the greatest possible extent, and by such selection and arrangement of combinations that the points of maximum induced velocity for each body do not coincide.

APPLICATION TO WING DESIGN

Detail consideration of the various factors affecting wing design lies outside the scope of this report. The following discussion is therefore limited to some important aerodynamic features that must be considered in the application of the data presented.

APPLICATION OF SECTION DATA

Wing characteristics are usually predicted from airfoil-section data by use of methods based on simple lifting-line theory (references 73 to 76). Application of such methods to wings of conventional plan form without spanwise discontinuities yields results of reasonable engineering accuracy (reference 77), especially with regard to such important characteristics as the angle of zero lift, the lift-curve slope, the pitching moment, and the drag. Basically similar methods not requiring the assumption of linear section lift characteristics (references 78 and 79) appear capable of yielding results of greater accuracy, especially at high lift coefficients. Further refinement may be made by consideration of the chordwise distribution of lift (reference 80). Wings with large amounts of sweep require special consideration (reference 81).

The usual wing theory assumes that the resultant air force and moment on any wing section are functions of only the section lift coefficient (or angle of attack) and the section shape. According to this assumption, the air forces and moments on any section are not affected by adjacent sections or other features of the wing except as such sections or features affect the lift distribution and thus the local lift of the section under consideration. These assumptions obviously are not valid near wing tips, near discontinuities in deflected flaps or ailerons, near disturbing bodies, or for wings with pronounced sweep or sudden changes in plan form, section, or twist. Under such circumstances, cross flows result in a breakdown of the concept of two-dimensional flow over the airfoil sections. In addition to these cross flows, induced effects exist that are equivalent to a change in camber. Such effects are particularly marked near the wing tips for wings of normal plan form and for wings of low aspect ratio or unusual plan form. Lifting-surface theory (see, for example, reference 81) provides a means for calculating wing characteristics more accurately than the simple lifting-line theory.

Although span load distributions calculated for wings with discontinuities such as are found with partial-span flaps (references 82 and 83) may be sufficiently accurate for structural design, such distributions are not suitable for predicting maximum-lift and stalling characteristics. Until sufficient data are obtained to permit the prediction of the maximum-lift and stalling characteristics of wings with discontinuities, these characteristics may best be estimated from previous results with similar wings or, in the case of unusual configurations, should be obtained by test.

The characteristics of intermediate wing sections must be known for the application of wing theory, but data for such sections are seldom available. Tests of a number of such intermediate sections obtained by several manufacturers for wings formed by straight-line fairing have indicated that the characteristics of such sections may be obtained with reasonable accuracy by interpolation of the root and tip characteristics according to the thickness variation.

SELECTION OF ROOT SECTION

The characteristics of a wing are affected to a large extent by the root section. In the case of tapered wings formed by straight-line fairing, the resulting nonlinear variation of section along the span causes the shapes of the sections to be predominantly affected by the root section over a large part of the wing area. The desirability of having a thick wing that provides space for housing fuel and equipment and reduces structural weight or permits large spans usually leads to the selection of the thickest root section that is aerodynamically feasible. The comparatively small variation of minimum drag coefficient with thickness ratio for smooth airfoils in the normal range of thickness ratios and the maintenance of high lift coefficient for thick sections with flaps deflected usually result in limitation of thickness ratio by characteristics other than maximum lift and minimum drag.

The critical Mach number of the section is the most serious limitation of thickness ratio for high-speed airplanes. It is desirable to select a root section with a critical Mach number sufficiently high to avoid serious drag increases resulting from compressibility effects at the highest level-flight speed of the airplane, allowance being made for the increased velocity of flow over the wing resulting from interference of bodies and slipstream. Available data indicate that a small margin exists between the critical Mach number and the Mach number at which the drag increases sharply. As airplane speeds increase, it becomes increasingly difficult and finally impossible to avoid the drag increases resulting from compressibility effects by reduction of the airfoil thickness ratio.

In the cases of airplanes of such low speeds that compressibility considerations do not limit the thickness ratio to values less than about 0.20, the maximum thickness ratio is limited by excessive drag coefficients at moderate and high lift coefficients with the surfaces rough. In these cases, the actual surface conditions expected for the airplane should be considered in selecting the section. Consideration should also be given to unusual conditions such as ice, mud, and damage caused in military combat, especially in the case of multiengine airplanes for which ability to fly under such conditions is desired with one or more engines inoperative. In cases for which root sections having large thickness ratios are under consideration to permit the use of high aspect ratios, a realistic appraisal of the drag coefficients of such sections with the expected surface conditions at moderately high lift coefficients will indicate an optimum aspect ratio beyond which corresponding increases in aspect ratio and root thickness ratio will result in reduced performance.

Inboard sections of wings on conventional airplanes are subject to interference effects and may be in the propeller slipstream. The wing surfaces are likely to be roughened by access doors, landing-gear retraction wells, and armament installations. Attainment of extensive laminar flows is, therefore, less likely on the inboard wing panels than on the outboard panels. Unless such effects are minimized, little drag reduction is to be expected from the use of sections permitting extensive laminar flow. Under these conditions, the use of sections such as the NACA 63-series will provide advantages if the sections are thick, because such sections are more conservative than those permitting more extensive laminar flow.

SELECTION OF TIP SECTION

In order to promote desirable stalling characteristics, the tip section should have a high maximum lift coefficient and a large range of angle of attack between zero and maximum lift as compared with the root section. It is also desirable that the tip section stall without a large sudden loss in lift. The attainment of a high maximum lift coefficient is often more difficult at the tip section than at the root section for tapered wings because of the lower Reynolds number of the tip section. For wings with small camber, the most effective way of increasing the section maximum lift coefficient is to increase the camber. The amount of camber used will be limited in most cases by either the critical-speed requirements or by the requirement that the section have low drag at the high-speed lift coefficient.

The selection of the optimum type of camber for the tip section presents problems for which no categorical answers can be given on the basis of existing data. The use of a type of camber that imposes heavy loads on the ailerons complicates the design of the lateral-control system and increases its weight. The use of a type of camber that carries the lift farther forward on the section and thus relieves the ailerons will, however, have little effect on the maximum lift coefficient of the section unless the maximum-camber position is well forward, as for the NACA 230-series sections. In this case a sudden loss of lift at the stall may be expected. The effects on the camber of modifications to the airfoil contour near the trailing edge, which may be made in designing the ailerons, should not be overlooked in estimating the characteristics of the wing.

If the root sections are at least moderately thick, it is usually desirable to select a tip section with a somewhat reduced thickness ratio. This reduction in thickness ratio, together with the absence of induced velocities from interfering bodies, gives a margin in critical speed that permits the camber of the tip section to be increased. This reduction in thickness ratio will probably be limited by the loss in maximum lift coefficient resulting from too thin a section.

A small amount of aerodynamic washout may also be useful as an aid in the avoidance of tip stalling. The permissible amount of washout may not be limited by the increase in induced drag, which is small for 1° or 2° of washout (reference 73). The limiting washout may be that which causes the tip section to operate outside the low-drag range at the high-speed lift coefficient. This limitation may be so severe as to require some adjustment of the camber to permit the use of any washout.

A change in airfoil section between the root and tip may be desirable to obtain favorable stalling characteristics or to take advantage of the greater extent of laminar flow that may be possible on the outboard sections. Thus, such combinations as an NACA 230-series root section with an NACA 44-series tip section or an NACA 63-series root section with an NACA 65-series tip section may be desirable.

It should be noted that the tip sections may easily be so heavily loaded by the use of an unfavorable plan form as to cause tip stalling with any reasonable choice of section and washout. Both high taper ratios and large amounts of sweepback are unfavorable in this respect and are particularly bad when used together, because the resulting tip stall promotes longitudinal instability at the stall in addition to the usual lateral instability.

CONCLUSIONS

The following conclusions may be drawn from the data presented. Most of the data, particularly for the lift, drag, and pitching-moment characteristics, were obtained at Reynolds numbers from 3 to 9×10^6.

1. Airfoil sections permitting extensive laminar flow, such as the NACA 6- and 7-series sections, result in substantial reductions in drag at high-speed and cruising lift coefficients as compared with other sections if, and only if, the wing surfaces are fair and smooth.

2. Experience with full-size wings has shown that extensive laminar flows are obtainable if the surface finish is as smooth as that provided by sanding in the chordwise direction with No. 320 carborundum paper and if the surface is free from small scattered defects and specks. Satisfactory results are usually obtained if the surface is sufficiently fair to permit a straightedge to be rocked smoothly in the chordwise direction without jarring or clicking.

3. For wings of moderate thickness ratios with surface conditions corresponding to those obtained with current construction methods, minimum drag coefficients of the order of 0.0080 may be expected. The values of the minimum drag coefficient for such wings depend primarily on the surface condition rather than on the airfoil section.

4. Substantial reductions in drag coefficient at high Reynolds numbers may be obtained by smoothing the wing surfaces, even if extensive laminar flow is not obtained.

5. The maximum lift coefficients for moderately cambered smooth NACA 6-series airfoils with the uniform-load type of mean line are as high as those for NACA 24- and 44-series airfoils. The NACA 230-series airfoils have somewhat higher maximum lift coefficients for thickness ratios less than 0.20.

6. The maximum lift coefficients of airfoils with flaps are about the same for moderately thick NACA 6-series sections as for the NACA 23012 section but appear to be considerably lower for thinner NACA 6-series sections.

7. The lift-curve slopes for smooth NACA 6-series airfoils are slightly higher than for NACA 24-, 44-, and 230-series airfoils and usually exceed the theoretical value for thin airfoils.

8. Leading-edge roughness causes large reductions in maximum lift coefficient for both plain airfoils and airfoils equipped with split flaps deflected 60°. The decrement in maximum lift coefficient resulting from standard roughness is essentially the same for the plain airfoils as for the airfoils equipped with the 60° split flaps.

9. The effect of leading-edge roughness is to decrease the lift-curve slope, particularly for the thicker sections having the position of minimum pressure far back.

10. Characteristics of airfoil sections with the expected surface conditions must be known or estimated to provide a satisfactory basis for the prediction of the characteristics of practical-construction wings and the selection of airfoils for such wings.

11. The NACA 6-series airfoils provide higher critical Mach numbers for high-speed and cruising lift coefficients than earlier types of sections and have a reasonable range of lift coefficients within which high critical Mach numbers may be obtained.

12. The NACA 6-series sections provide lower predicted critical Mach numbers at moderately high lift coefficients than the earlier types of sections. The limited data available suggest, however, that the NACA 6-series sections retain satisfactory lift characteristics up to higher Mach numbers than the earlier sections.

13. The NACA 6-series airfoils do not appear to present unusual problems with regard to the application of ailerons.

14. Problems associated with the avoidance of boundary-layer separation caused by interference are expected to be similar for conservative NACA 6-series sections and other good airfoils. Detail shapes for optimum interfering bodies and fillets may be different for various sections if local excessive expansions in the flow are to be avoided.

15. Satisfactory leading-edge air intakes may be provided for NACA 6-series sections, but insufficient information exists to allow such intakes to be designed without experimental development.

LANGLEY MEMORIAL AERONAUTICAL LABORATORY,
NATIONAL ADVISORY COMMITTEE FOR AERONAUTICS,
LANGLEY FIELD, VA., *March 5, 1945*.

APPENDIX

METHODS OF OBTAINING DATA IN THE LANGLEY TWO-DIMENSIONAL LOW-TURBULENCE TUNNELS

By MILTON M. KLEIN

DESCRIPTION OF TUNNELS

The Langley two-dimensional low-turbulence tunnels are closed-throat wind tunnels having rectangular test sections 3 feet wide and 7½ feet high and are designed to test models completely spanning the width of the tunnel in two-dimensional flow. The low-turbulence level of these tunnels, amounting to only a few hundredths of 1 percent, is achieved by the large contraction ratio in the entrance cone (approx. 20:1) and by the introduction of a number of fine-wire small-mesh turbulence-reducing screens in the widest part of the entrance cone. The chord of models tested in these tunnels is usually about 2 feet, although the characteristics at low lift coefficients of models having chords as large as 8 feet may be determined.

The Langley two-dimensional low-turbulence tunnel operates at atmospheric pressure and has a maximum speed of approximately 155 miles per hour. The Langley two-dimensional low-turbulence pressure tunnel operates at pressures up to 10 atmospheres absolute and has a maximum speed of approximately 300 miles per hour at atmospheric pressure. Standard airfoil tests in this tunnel are made of 2-foot-chord wooden models up to Reynolds numbers of approximately 9×10^6 at a pressure of 4 atmospheres absolute.

The lift and drag characteristics of airfoils tested in these tunnels are usually measured by methods other than the use of balances. The lift is evaluated from measurements of the pressure reactions on the floor and ceiling of the tunnel. The drag is obtained from measurements of static and total pressures in the wake. Moments are usually measured by a balance.

SYMBOLS

$A_1, A_2, \ldots A_n$ coefficients of potential function for a symmetrical body

a fraction of chord from leading edge over which design load is uniform

B dimensionless constant determining width of wake

c chord

c_d drag coefficient corrected for tunnel-wall effects

c_d' drag coefficient uncorrected for tunnel-wall effects

c_{d_T} drag coefficient measured in tunnel

c_l section lift coefficient corrected for tunnel-wall effects

c_l' section lift coefficient uncorrected for tunnel-wall effects

c_{l_i} design lift coefficient

c_{l_T} lift coefficient measured in tunnel

$c_{m_{c/4}}$ moment coefficient about quarter-chord point corrected for tunnel-wall effects

$c_{m_{c/4}}'$ moment coefficient about quarter-chord point measured in tunnel

F average of velocity readings of orifices on floor and ceiling used to measure blocking at high lifts

F_0 average value of F in low-lift range

f potential function used to obtain η-factor

H_0 total pressure in front of airfoil

H_1 total pressure in wake of airfoil

H_c coefficient of loss of total pressure in the wake $\left(\frac{H_0-H_1}{q_0}\right)$

$H_{c_{max}}$ maximum value of H_c

h_T tunnel height

$K=\frac{c_d'}{c_{d_T}}$

L true lift resulting from a point vortex

L' lift associated with a point vortex as measured by integrating manometers

m upstream limit of integration of floor and ceiling pressures

n downstream limit of integration of floor and ceiling pressures

P_R resultant pressure coefficient; difference between local upper- and lower-surface pressure coefficients

p_1 static pressure in the wake

q_0 free-stream dynamic pressure

S static-pressure coefficient $\left(\frac{H_0-p}{q_0}\right)$

S_1 static-pressure coefficient in the wake $\left(\frac{H_0-p_1}{q_0}\right)$

s distance along airfoil surface

u velocity, due to row of vortices, at any point along tunnel walls

V free-stream velocity

ΔV increment in free-stream velocity due to blocking

V' corrected indicated tunnel velocity
V'' tunnel velocity measured by static-pressure orifices
v local velocity at any point on airfoil surface
w potential function for flow past a symmetrical body
x distance along chord or center line of tunnel
Y variable of integration $\left(\frac{By_w}{c}\right)$
y distance perpendicular to stream direction
y_t ordinate of symmetrical thickness distribution
y_w distance perpendicular to stream direction from position of $H_{c_{max}}$
$\frac{dy_t}{dx}$ slope of surface of symmetrical thickness distribution
z complex variable $(x+iy)$
α_{t_0} angle of zero lift
α_0 section angle of attack corrected for tunnel-wall effects
α_0' section angle of attack measured in tunnel
Γ strength of a single vortex
η ratio of measured lift to actual lift for any type of lift distribution
η_a η-factor for additional-type loading
η_b η-factor for basic mean-line loading
η_x η-factor applying to a point vortex
Λ component of blocking factor dependent on shape of body
ξ quantity used for correcting effect of body upon velocity measured by static-pressure orifices
σ component of blocking factor dependent on size of body
ϕ potential function
ψ stream function

MEASUREMENT OF LIFT

The lift carried by the airfoil induces an equal and opposite reaction upon the floor and ceiling of the tunnel. The lift may therefore be obtained by integrating the pressure distribution along the floor and ceiling of the tunnel, the integration being accomplished with an integrating manometer. Because the pressure field theoretically extends to infinity in both the upstream and the downstream directions, not all the lift is included in the length over which the integration is performed. It is therefore necessary to apply a correction factor η that gives the ratio of the measured lift to the actual lift for any lift distribution. The calculation was performed by first finding the correction factor η_x applying to a point vortex and then determining the weighted average of this factor over the chord of the model.

The factor η_x was obtained as follows: The image system which gives only a tangential component of velocity along the tunnel walls is made up of an infinite vertical row of vortices of alternating sign as shown in figure 64. If the sign of the vortex at the origin is assumed to be positive, the complex potential function f for this image system is

$$f=\frac{i\Gamma}{2\pi}\log\sinh\frac{\pi z}{2h_T}-\frac{i\Gamma}{2\pi}\log\sinh\pi\left(\frac{z-ih_T}{2h_T}\right) \qquad (18)$$

where

Γ strength of a single vortex

z complex variable $(x+iy)$

h_T tunnel height

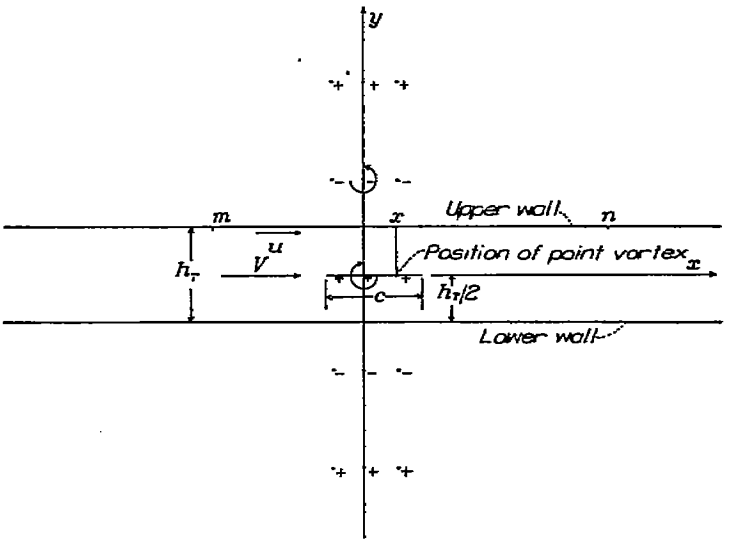

FIGURE 64.—Image system for calculation of η-factor in the Langley two-dimensional low-turbulence tunnels.

The velocity u, due to the row of vortices, at any point along the tunnel walls where

$$y=\frac{h_T}{2}$$

is then obtained as

$$u=\frac{\Gamma}{2h_T}\operatorname{sech}\frac{\pi x}{h_T} \qquad (19)$$

where x is the horizontal distance from the point on the wall to the origin. The resultant pressure coefficient P_R is then given by

$$P_R=\frac{4u}{V}$$

$$=\frac{2\Gamma}{h_T V}\operatorname{sech}\frac{\pi x}{h_T} \qquad (20)$$

where V is the free-stream velocity.

The lift manometers integrate the pressure distribution along the floor and ceiling from the downstream position n to the upstream position m (fig. 64). For a point vortex

located a distance x from the origin along the center line of the tunnel, the limits of integration become $n-x$ and $m-x$. The lift L' associated with a point vortex, as measured by the integrating manometers, is given by

$$L'=\int_{m-x}^{n-x} q_0 P_R\, dx \tag{21}$$

where q_0 is the free-stream dynamic pressure.

The true lift L resulting from the point vortex is given by

$$L=\frac{2q_0\Gamma}{V}$$

The correction factor η_x is then

$$\eta_x=\frac{L'}{L}$$

$$=\frac{1}{h_T}\int_{m-x}^{n-x} \operatorname{sech}\frac{\pi x}{h_T}\,dx$$

which yields

$$\eta_x=\frac{2}{\pi}\tan^{-1}\left[\frac{e^{-\pi x/h_T}(e^{\pi n/h_T}-e^{\pi m/h_T})}{1+e^{-2\pi x/h_T}e^{\pi(m+n)/h_T}}\right] \tag{22}$$

In the Langley two-dimensional low-turbulence tunnels, the orifices in the floor and ceiling of the tunnel used to measure the lift extend over a length of approximately 13 feet. A plot of η_x against x for the Langley two-dimensional low-turbulence pressure tunnel is shown in figure 65. The η-factor for a given lift distribution is obtained from the expression

$$\eta=\frac{\int_{chord} P_R\eta_x\, d\left(\frac{x}{c}\right)}{\int_{chord} P_R\, d\left(\frac{x}{c}\right)} \tag{23}$$

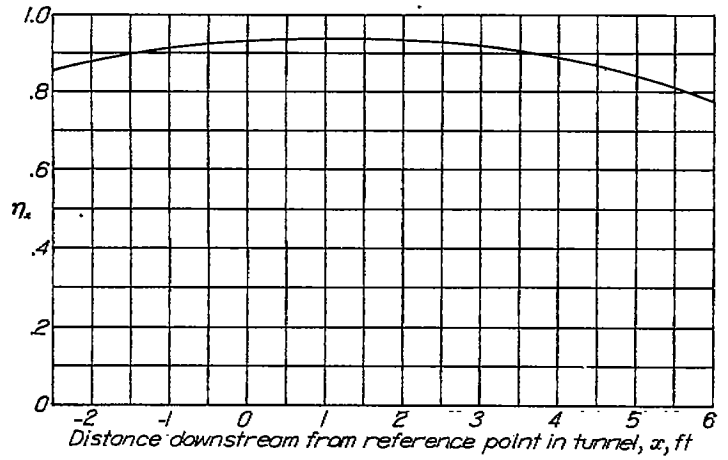

FIGURE 65.—Lift efficiency factor η_x for a point vortex situated at various positions along the center line of the tunnel.

The values of η_b and η_a for the Langley two-dimensional low-turbulence pressure tunnel are given in the following table for a model having a chord length of 2 feet, where η_b is the η-factor corresponding to the basic mean-line loading (indicated by the value of a) and η_a is the η-factor for the additional type of loading as given by thin-airfoil theory:

a	η_b
1.0	0.9347
.8	.9342
.6	.9336
.4	.9330
.2	.9325
0	.9322

η_a=0.9296

In order to check the variation of η_a with variations in the additional type of lift distribution, the value of η_a was recalculated for the class C additional lift distribution given in figure 6 of reference 74. The value of η_a for this case was 0.9304, as compared with 0.9296 for a thin airfoil. Because of the small variation of η_a with the type of additional lift, the value for thin-airfoil additional lift was used for all calculations. The lift coefficient of the model in the tunnel uncorrected for blocking c_l' is given in terms of the lift coefficient measured in the tunnel c_{l_T} and the design lift coefficient of the airfoil c_{l_t} by the following expression:

$$c_l'=\frac{c_{l_T}}{\eta_a}-\left(\frac{\eta_b}{\eta_a}-1\right)c_{l_t} \tag{24}$$

Because η_b does not differ much from η_a, it is not necessary that the basic loading or the design lift coefficient be known with great accuracy.

Because of tunnel-wall and other effects, the lift distribution over the airfoil in the tunnel does not agree exactly with the assumed lift distribution. Because of the small variations of η with lift distribution, errors caused by this effect are considered negligible. It can also be shown that errors caused by neglecting the effect of airfoil thickness on the distribution of the lift reaction along the tunnel walls are small.

MEASUREMENT OF DRAG

The drag of an airfoil may be obtained from observations of the pressures in the wake (reference 84). An approximation to the drag is given by the loss in total pressure of the air in the wake of the airfoil. The loss of total pressure is measured by a rake of total-pressure tubes in the wake. When the total pressures in front of the airfoil and in the wake are represented by H_0 and H_1, respectively, the drag coefficient obtained from loss of total pressure c_{d_T} is

$$c_{d_T}=\int_{wake} H_c\frac{dy_w}{c} \tag{25}$$

where

H_c coefficient of loss of total pressure in the wake $\left(\frac{H_0-H_1}{q_0}\right)$

y_w distance perpendicular to stream direction from position of $H_{c_{max}}$

If the static pressure in the wake is represented by p_1, the true drag coefficient uncorrected for blocking c_d' may be shown to be (reference 84)

$$c_d' = \int_{wake} 2\sqrt{S_1 - H_c}\left(1 - \sqrt{1 - H_c}\right)\frac{dy_w}{c} \tag{26}$$

where S_1 is the static-pressure coefficient in the wake $\frac{H_0 - p_1}{q_0}$. The assumption is made that the variation of total pressure across the wake can be represented by a normal probability curve. The drag coefficient c_d' is then easily obtainable from measurements of c_{d_T} by means of a factor K, the ratio of c_d' to c_{d_T}, which depends only on S_1 and the maximum value of H_c. If the maximum value of H_c is represented by $H_{c_{max}}$, the equation of the normal probability curve is

$$H_c = H_{c_{max}} e^{-\left(\frac{By_w}{c}\right)^2}$$

where B is a dimensionless constant that determines the width of the wake. If a convenient variable of integration $Y = \frac{By_w}{c}$ is used, the ratio K is

$$K = \frac{c_d'}{c_{d_T}}$$

$$= \frac{2}{\sqrt{\pi}} \frac{1}{H_{c_{max}}} \int_{-\infty}^{\infty} \sqrt{S_1 - H_c}\left(1 - \sqrt{1 - H_c}\right) dY \tag{27}$$

and is independent of the width of the wake. The quantity K has been evaluated for various values of $H_{c_{max}}$ and S_1 by assuming S_1 to be constant across the wake. The drag coefficient c_d' may thus be obtained from tunnel measurements of c_{d_T}, $H_{c_{max}}$, and S_1. A plot of K as a function of $H_{c_{max}}$ with S_1 as parameter is given in figure 66. A parallel treatment of this problem is given in reference 85.

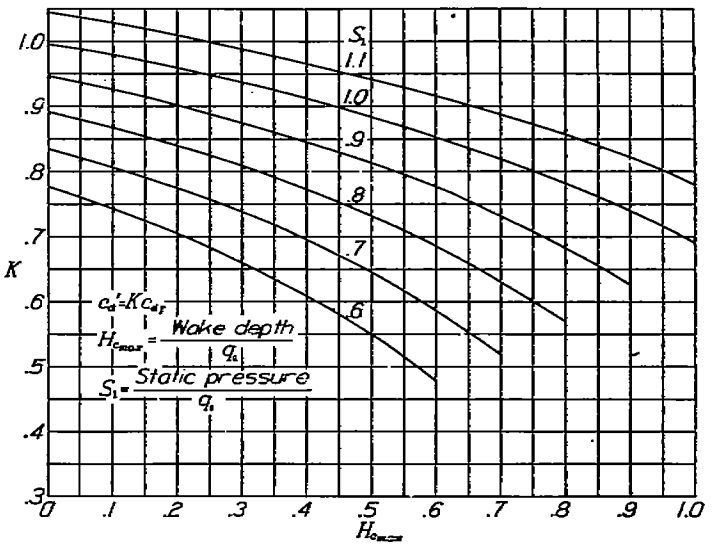

FIGURE 66.—Plot of K as a function of $H_{c_{max}}$ with S_1 as a parameter.

TUNNEL-WALL CORRECTIONS

In two-dimensional flow, the tunnel walls may be conveniently considered as having two distinct effects upon the flow over a model in a tunnel: (1) an increase in the free-stream velocity in the neighborhood of the model because of a constriction of the flow and (2) a distortion of the lift distribution from the induced curvature of the flow.

The increase in free-stream velocity caused by the tunnel walls (blocking effect) is obtained from consideration of an infinite vertical row of images of a symmetrical body as given in reference 86; the images represent the effect of the tunnel walls.

The potential function w for a symmetrical body is given by

$$w = Vz + \frac{A_1}{z} + \frac{A_2}{z^2} + \cdots + \frac{A_n}{z^n} \tag{28}$$

where V is the free-stream velocity and the coefficients A_1, A_2, . . . are complex. If the tunnel height is large compared to the size of the body, powers of $1/z$ greater than 1 may be neglected and

$$w = Vz + \frac{A_1}{z} \tag{29}$$

This operation is equivalent to replacing the body by a circle of which the doublet strength is $2\pi A_1$; the term A_1/z represents the disturbance to the free-stream flow. The total induced velocity at the center of the body due to all the images is expressed in reference 86 as

$$\Delta V = \frac{A_1}{h_T^2}\frac{\pi^2}{3} \tag{30}$$

where the term A_1 is the same as the term $\frac{1}{4}\lambda l^2 V$ of reference 86.

For convenience in tunnel calculations, the expression of ΔV may be written

$$\frac{\Delta V}{V} = \Lambda\sigma \tag{31}$$

where

$$\sigma = \frac{\pi^2}{48}\left(\frac{c}{h_T}\right)^2 \tag{32}$$

$$\Lambda = \frac{16A_1}{c^2 V} \tag{33}$$

The factor σ depends only on the size of the body and is easily calculated. The factor Λ depends on the shape of the body and is more difficult to calculate. For bodies such as

Rankine ovals and ellipses, simple formulas may be obtained for calculating Λ. In the general case, the value of Λ may be obtained from the velocity distribution over the body by the expression

$$\Lambda=\frac{16}{\pi}\int_0^1 \frac{y}{c}\frac{v}{V}\sqrt{1+\left(\frac{dy_t}{dx}\right)^2}\,d\left(\frac{x}{c}\right) \tag{34}$$

where v is the velocity at any point on the airfoil surface and dy_t/dx is the slope of the airfoil surface at any point of which the ordinate is y_t.

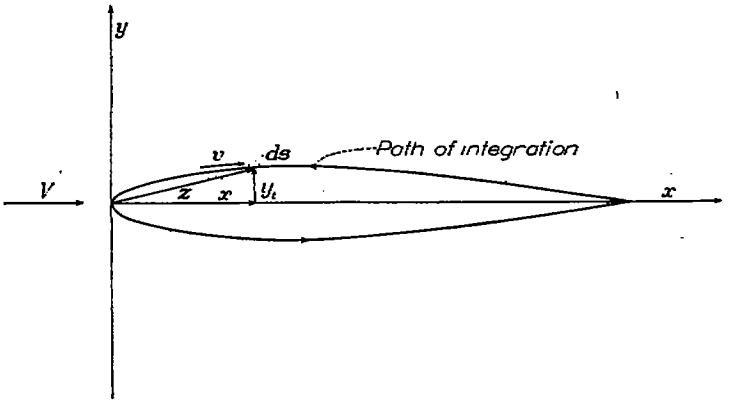

FIGURE 67.—Sketch for derivation of Λ-factor.

In order to obtain this expression, consider the flow past a symmetrical body as shown in figure 67. The potential function for this flow is given by equation (28). Differentiating and multiplying equation (28) by z gives

$$z\frac{dw}{dz}=Vz-\frac{A_1}{z}-\frac{2A_2}{z^2}\cdots-\frac{nA_n}{z^n}$$

The line integral about a closed curve $\int_C z\frac{dw}{dz}\,dz$ will depend only on the term $-A_1/z$ and, from the theory of residues, is given by

$$\int_C z\frac{dw}{dz}\,dz=-2\pi i A_1$$

but

$$z\frac{dw}{dz}\,dz=z\,dw$$
$$=(x+iy)(d\phi+i\,d\psi)$$

where ϕ is the potential function and ψ is the stream function. On the surface of the body $d\psi=0$, so that

$$\int_C z\frac{dw}{dz}\,dz=\int_C x\,d\phi+i\int_C y\,d\phi \tag{35}$$

Since the body is symmetrical, the term $x\,d\phi$ will have equal numerical values but opposite signs at corresponding points of the upper and lower surfaces, and $\int_C x\,d\phi$ will vanish. The term $y\,d\phi$ will have equal values at corresponding points of the upper and lower surfaces, and $\int_C y\,d\phi$ may be replaced by an integration over the upper surface; therefore,

$$\int_C z\frac{dw}{dz}\,dz=2i\int y\,d\phi \text{ (counterclockwise direction)}$$

or

$$A_1=-\frac{1}{\pi}\int y\,d\phi$$

Reversing the path of integration, replacing $d\phi$ by $v\,ds$, replacing ds by $\sqrt{1+\frac{dy_t^2}{dx}}\,dx$, and solving for $\Lambda=\frac{16A_1}{c^2V}$ gives

$$\Lambda=\frac{16}{\pi}\int_0^1 \frac{y}{c}\frac{v}{V}\sqrt{1+\left(\frac{dy_t}{dx}\right)^2}\,d\left(\frac{x}{c}\right)$$

where the integration is taken from the leading edge to the trailing edge over the upper surface.

In addition to the error caused by blocking, an error exists in the measured tunnel velocity because of the interference effects of the model upon the velocity indicated by the static-pressure orifices located a few feet upstream of the model and halfway between floor and ceiling. In order to correct for this error, an analysis was made of the velocity distribution along the streamline halfway between the upper and the lower tunnel walls for Rankine ovals of various sizes and thickness ratios. The analysis showed that the correction could be expressed, within the range of conventional-airfoil thickness ratios, as a product of a thickness factor given by the blocking factor Λ and a factor ξ which depended upon the size of the model and the distance from the static-pressure orifices to the midchord point of the model. The corrected indicated tunnel velocity V' could then be written

$$V'=V''(1+\Lambda\xi) \tag{36}$$

where V'' is the velocity measured by the static-pressure orifices. In the Langley two-dimensional low-turbulence tunnels, the distance from the static-pressure orifices to the midchord point of the model is approximately 5.5 feet; the corresponding value of ξ for a 2-foot-chord model is approximately 0.002.

In order to calculate the effect of the tunnel walls upon the lift distribution, a comparison is made of the lift distribution of a given airfoil in a tunnel and in free air on the basis of thin-airfoil theory. It is assumed that the flow conditions in the tunnel correspond most closely to those in free air when the additional lift in the tunnel and in free air are the same (reference 87). On this basis the following corrections are derived (reference 87), in which the primed quantities refer to the coefficients measured in the tunnel:

$$c_l=[1-2\Lambda(\sigma+\xi)-\sigma]c_l' \tag{37}$$

$$\alpha_0=(1+\sigma)\alpha_0'+\frac{4\sigma c_{m_{c/4}}'}{dc_l'/d\alpha_0'}-\sigma\alpha_{l_0}' \tag{38}$$

$$c_{m_{c/4}}=[1-2\Lambda(\sigma+\xi)]c_{m_{c/4}}'+\sigma\frac{c_l'}{4} \tag{39}$$

In the foregoing equations, the terms $\frac{4\sigma c_{m_{c/4}}'}{dc_l'/d\alpha_0'}$, $\sigma\alpha_{l_0}$, and $\sigma c_l'/4$ are usually negligible for 2-foot-chord models in the Langley two-dimensional low-turbulence tunnels.

When the effect of the tunnel walls on the pressure distribution over the model is small, the wall effect on the drag is merely that corresponding to an increase in the tunnel speed. The correction to the drag coefficient is therefore given by the following relation:

$$c_d=[1-2\Lambda(\sigma+\xi)]c_d' \tag{40}$$

Similar considerations have been applied to the development of corrections for the pressure distribution in reference 87.

Equation (40) neglects the blocking due to the wake, such blocking being small at low to moderate drags. The effect of a pressure gradient in the tunnel upon loss of total pressure in the wake is not easily analyzed but is estimated to be small. The effect of the pressure gradient upon the drag has therefore been disregarded. When the drag is measured by a balance, the effect of the pressure gradient upon the drag is directly additive and a correction should be applied. For large models, especially at high lift coefficients, the effect of the tunnel walls is to distort the pressure distribution appreciably. Such distortions of the pressure distribution may cause large changes in the boundary flow and no adequate corrections to any of the coefficients, particularly the drag, can be found.

CORRECTION FOR BLOCKING AT HIGH LIFTS

So long as the flow follows the airfoil surface, the foregoing relations account for the effects of the tunnel walls with sufficient accuracy. When the flow leaves the surface, the blocking increases because of the predominant effect of the wake upon the free-stream velocity. Since the wake effect shows up primarily in the drag, the increase in blocking would logically be expressed in terms of the drag. The accurate measurement of drag under these conditions by means of a rake is impractical because of spanwise movements of low-energy air. A method of correcting for increased blocking at high angles of attack without drag measurements has therefore been devised for use in the Langley two-dimensional low-turbulence tunnels.

Readings of the floor and ceiling velocities are taken a few inches ahead of the quarter-chord point and averaged to remove the effect of lift. This average F, which is a measure of the effective tunnel velocity, is essentially constant in the low-lift range. The quantity F/F_0, where F_0 is the average value of F in the low-lift range, however, shows a variation from unity in the high-lift range for any airfoil tested in the tunnel; this variation indicates a change in blocking at high lifts. A plot of F/F_0 against angle of attack α_0' for a 2-foot-chord model of the NACA 64$_2$–418 airfoil is given in figure 68. The quantity F/F_0 is nearly constant for values of α_0' up to 12°; but for values of α_0' greater than 12°, F/F_0 increases and the increase is particularly noticeable at and over the stall.

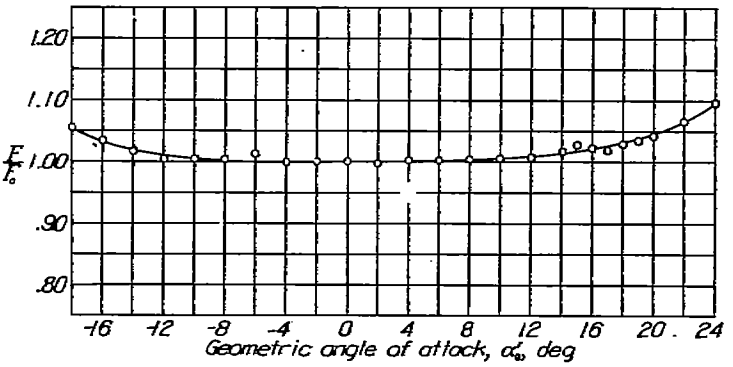

FIGURE 68.—Additional blocking factor at the tunnel walls plotted against angle of attack for the NACA 64$_2$–418 airfoil.

A theoretical comparison was made of the blocking factor $\Lambda\sigma$ and the velocity measured by the floor and ceiling orifices for a series of Rankine ovals of various sizes and thickness ratios. The quarter-chord point of each oval was located at the pivot point, the usual position of an airfoil in the tunnel. The analysis showed the relation between the blocking factor $\Lambda\sigma$ and the change in F to be unique for chord lengths up to 50 inches in that different bodies having the same blocking factor $\Lambda\sigma$ gave approximately the same value of F. For chords up to 50 inches, the relationship is

$$\frac{\Delta V}{V}=0.45\left(\frac{F}{F_0}-1\right) \tag{41}$$

where $\Delta V/V$ is the true increment in tunnel velocity due to blocking. The foregoing relation was adopted to obtain the correction to the blocking in the range of lifts where $\frac{F}{F_0}>1$.

Considerable uncertainty exists regarding the correct numerical value of the coefficient occurring in equation (41). If a row of sources, rather than the Rankine ovals used in the present analysis, is considered to represent the effect of the wake, the value of the coefficient in equation (41) would be approximately twice the value used. Fortunately, the correction amounts to only about 2 percent at maximum lift for an extreme condition with a 2-foot-chord model. Further refinement of this correction has therefore not been attempted.

COMPARISON WITH EXPERIMENT

A check of the validity of the tunnel-wall corrections has been made in reference 87, which gives lift and moment curves for models having various ratios of chord to tunnel height, uncorrected and corrected for tunnel-wall effects.

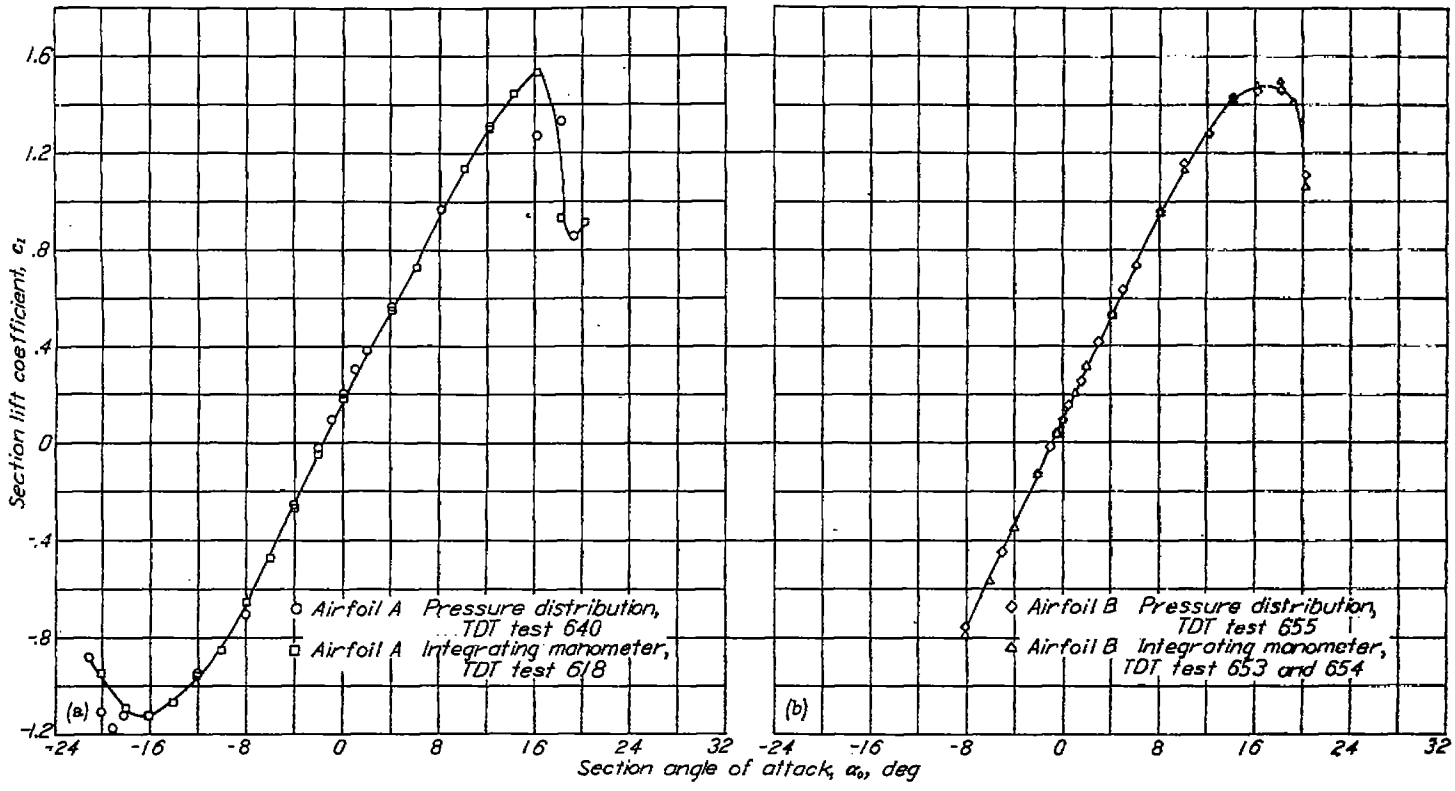

(a) Comparison for airfoil A.

(b) Comparison for airfoil B.

FIGURE 69.—Comparison between lifts obtained from pressure-distribution measurements and lifts obtained from reactions on the floor and ceiling of the tunnel

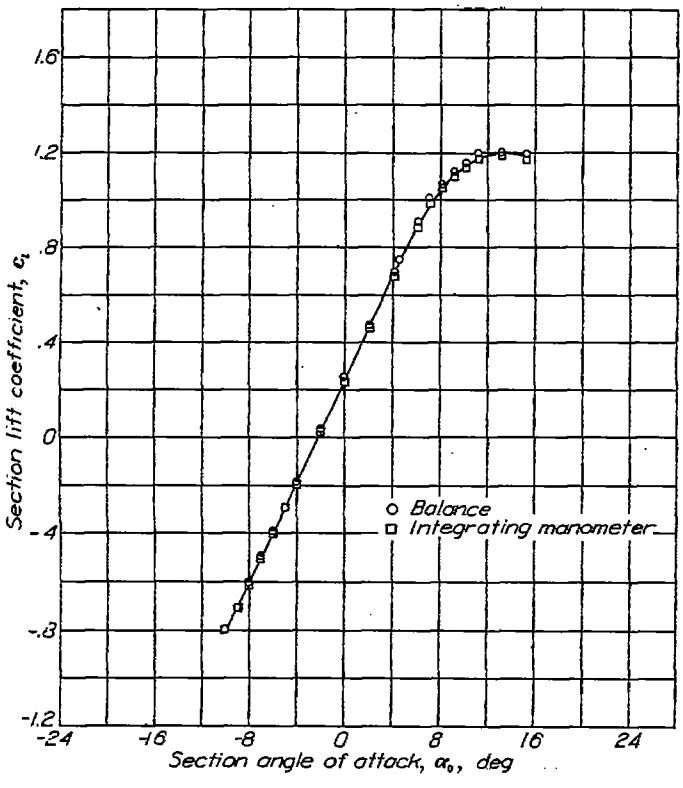

FIGURE 70.—Comparison between lifts obtained from balance measurements and from reactions on the floor and ceiling of the tunnel.

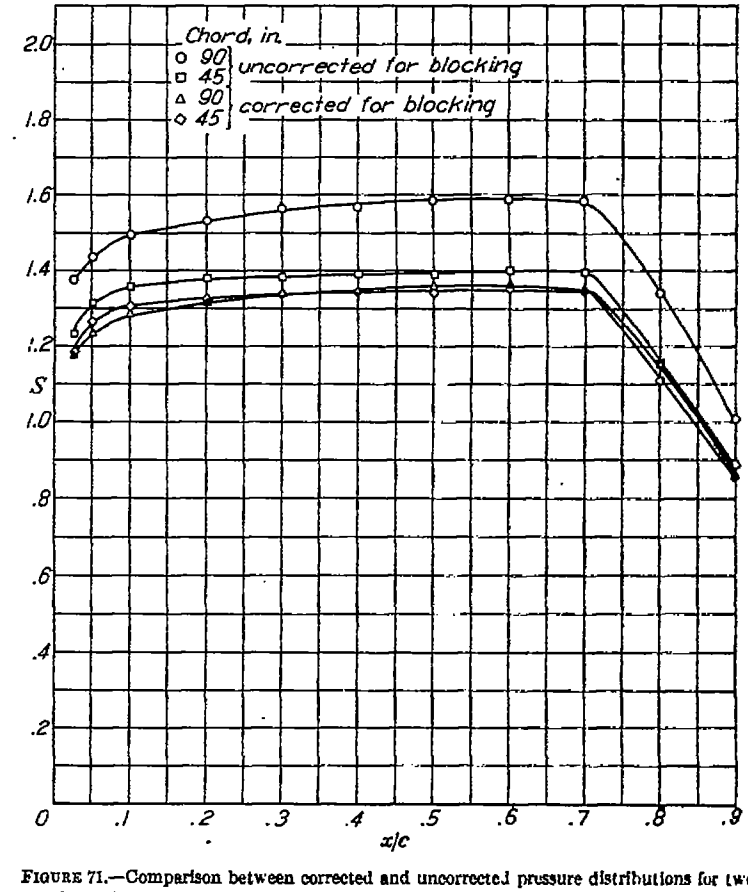

FIGURE 71.—Comparison between corrected and uncorrected pressure distributions for two chord sizes of a symmetrical NACA 6-series airfoil of 15-percent thickness. $\alpha_c = 0°$

The general agreement of the corrected curves shows that the method of correcting the lifts and moments is valid.

A comparison is made in reference 87 between the theoretical correction factor (equation (40)) and the experimentally derived corrections of reference 88. The theoretical correction factors were found to be in good agreement with those obtained experimentally.

In order to check the validity of the η-factor, a comparison has been made of lift values obtained from pressure distributions with those obtained from the integration of the floor and ceiling pressures in the tunnel. A comparison for two airfoils given in figure 69 shows that the two methods of measuring lift give results that are in good agreement. The η-factor has also been checked by comparison of the lift obtained from balance measurements with the integrating-manometer values in figure 70.

Finally, a check has been made of the method of correcting pressure distributions (reference 87) for NACA 6-series airfoils of two chord lengths at zero angle of attack in figure 71, in which the pressure coefficients are plotted against chordwise position x/c. The agreement between the corrected pressure distributions for both models verifies the method of making the tunnel-wall corrections.

REFERENCES

1. Jacobs, Eastman N., Ward, Kenneth E., and Pinkerton, Robert M.: The Characteristics of 78 Related Airfoil Sections from Tests in the Variable-Density Wind Tunnel. NACA Rep. No. 460, 1933.
2. Jacobs, Eastman N., and Pinkerton, Robert M.: Tests in the Variable-Density Wind Tunnel of Related Airfoils Having the Maximum Camber Unusually Far Forward. NACA Rep. No. 537, 1935.
3. Jacobs, Eastman N., Pinkerton, Robert M., and Greenberg, Harry: Tests of Related Forward-Camber Airfoils in the Variable-Density Wind Tunnel. NACA Rep. No. 610, 1937.
4. Stack, John, and Von Doenhoff, Albert E.: Tests of 16 Related Airfoils at High Speeds. NACA Rep. No. 492, 1934.
5. Jacobs, Eastman N., and Sherman, Albert: Airfoil Section Characteristics as Affected by Variations of the Reynolds Number. NACA Rep. No. 586, 1937.
6. Pinkerton, Robert M., and Greenberg, Harry: Aerodynamic Characteristics of a Large Number of Airfoils Tested in the Variable-Density Wind Tunnel. NACA Rep. No. 628, 1938.
7. Jones, B. Melvill: Flight Experiments on the Boundary Layer. Jour. Aero. Sci., vol. 5, no. 3, Jan. 1938, pp. 81–94.
8. Jacobs, Eastman N., and Abbott, Ira H.: Airfoil Section Data Obtained in the N.A.C.A. Variable-Density Tunnel as Affected by Support Interference and Other Corrections. NACA Rep. No. 669, 1939.
9. Theodorsen, Theodore: Theory of Wing Sections of Arbitrary Shape. NACA Rep. No. 411, 1931.
10. Stack, John: Tests of Airfoils Designed to Delay the Compressibility Burble. NACA Rep. No. 763, 1943.
11. Jacobs, Eastman N.: Preliminary Report on Laminar-Flow Airfoils and New Methods Adopted for Airfoil and Boundary-Layer Investigations. NACA ACR, June 1939.
12. Von Doenhoff, Albert E., and Stivers, Louis S., Jr.: Aerodynamic Characteristics of the NACA 747A315 and 747A415 Airfoils from Tests in the NACA Two-Dimensional Low-Turbulence Pressure Tunnel. NACA CB No. L4I25, 1944.
13. Naiman, Irven: Numerical Evaluation by Harmonic Analysis of the ϵ-Function of the Theodorsen Arbitrary-Airfoil Potential Theory. NACA ARR No. L5H18, 1945.
14. Theodorsen, Theodore: Airfoil-Contour Modification Based on ϵ-Curve Method of Calculating Pressure Distribution. NACA ARR No. L4G05, 1944.
15. Allen, H. Julian: A Simplified Method for the Calculation of Airfoil Pressure Distribution. NACA TN No. 708, 1939.
16. Munk, Max M.: Elements of the Wing Section Theory and of the Wing Theory. NACA Rep. No. 191, 1924.
17. Glauert, H.: The Elements of Aerofoil and Airscrew Theory. Cambridge Univ. Press, 1926, pp. 87–93.
18. Theodorsen, Theodore: On the Theory of Wing Sections with Particular Reference to the Lift Distribution. NACA Rep. No. 383, 1931.
19. Von Kármán, Th.: Compressibility Effects in Aerodynamics. Jour. Aero. Sci., vol. 8, no. 9, July 1941, pp. 337–356.
20. Von Doenhoff, Albert E.: A Method of Rapidly Estimating the Position of the Laminar Separation Point. NACA TN No. 671, 1938.
21. Jacobs, E. N., and Von Doenhoff, A. E.: Formulas for Use in Boundary-Layer Calculations on Low-Drag Wings. NACA ACR, Aug. 1941.
22. Von Doenhoff, Albert E., and Tetervin, Neal: Determination of General Relations for the Behavior of Turbulent Boundary Layers. NACA Rep. No. 772, 1943.
23. Squire, H. B., and Young, A. D.: The Calculation of the Profile Drag of Aerofoils. R. & M. No. 1838, British A. R. C., 1938.
24. Tetervin, Neal: A Method for the Rapid Estimation of Turbulent Boundary-Layer Thicknesses for Calculating Profile Drag. NACA ACR No. L4G14, 1944.
25. Quinn, John H., Jr., and Tucker, Warren A.: Scale and Turbulence Effects on the Lift and Drag Characteristics of the NACA 65_3–418, $a=1.0$ Airfoil Section. NACA ACR No. L4H11, 1944.
26. Tucker, Warren A., and Wallace, Arthur R.: Scale-Effect Tests in a Turbulent Tunnel of the NACA 65_3–418, $a=1.0$ Airfoil Section with 0.20-Airfoil-Chord Split Flap. NACA ACR No. L4I22, 1944.
27. Davidson, Milton, and Turner, Harold R., Jr.: Effects of Mean-Line Loading on the Aerodynamic Characteristics of Some Low-Drag Airfoils. NACA ACR No. 3I27, 1943.
28. Von Doenhoff, Albert E., and Tetervin, Neal: Investigation of the Variation of Lift Coefficient with Reynolds Number at a Moderate Angle of Attack on a Low-Drag Airfoil. NACA CB, Nov. 1942.
29. Oswald, W. Bailey: General Formulas and Charts for the Calculation of Airplane Performance. NACA Rep. No. 408, 1932.
30. Millikan, Clark B.: Aerodynamics of the Airplane. John Wiley & Sons, Inc., 1941, pp. 108–109.
31. Hood, Manley J.: The Effects of Some Common Surface Irregularities on Wing Drag. NACA TN No. 695, 1939.
32. Loftin, Laurence K., Jr.: Effects of Specific Types of Surface Roughness on Boundary-Layer Transition. NACA ACR No. L5J29a, 1946.
33. Charters, Alex C., Jr.: Transition between Laminar and Turbulent Flow by Transverse Contamination. NACA TN No. 891, 1943.
34. Braslow, Albert L.: Investigation of Effects of Various Camouflage Paints and Painting Procedures on the Drag Characteristics of an NACA $65_{(421)}$–420, $a=1.0$ Airfoil Section. NACA CB No. L4G17, 1944.

35. Jones, Robert T., and Cohen, Doris: A Graphical Method of Determining Pressure Distribution in Two-Dimensional Flow. NACA Rep. No. 722, 1941.
36. Abbott, Frank T., Jr., and Turner, Harold R., Jr.: The Effects of Roughness at High Reynolds Numbers on the Lift and Drag Characteristics of Three Thick Airfoils. NACA ACR No. L4H21, 1944.
37. Jacobs, Eastman N., Abbott, Ira H., and Davidson, Milton: Investigation of Extreme Leading-Edge Roughness on Thick Low-Drag Airfoils to Indicate Those Critical to Separation. NACA CB, June 1942.
38. Zalovcik, John A.: Profile-Drag Coefficients of Conventional and Low-Drag Airfoils as Obtained in Flight. NACA ACR No. L4E31, 1944.
39. Zalovcik, John A., and Wood, Clotaire: A Flight Investigation of the Effect of Surface Roughness on Wing Profile Drag with Transition Fixed. NACA ARR No. L4I25, 1944.
40. Hood, Manley J., and Gaydos, M. Edward: Effects of Propellers and of Vibration on the Extent of Laminar Flow on the N. A. C. A. 27–212 Airfoil. NACA ACR, Oct. 1939.
41. Silverstein, Abe, Katzoff, S., and Hootman, James A.: Comparative Flight and Full-Scale Wind-Tunnel Measurements of the Maximum Lift of an Airplane. NACA Rep. No. 618, 1938.
42. Sweberg, Harold H., and Dingeldein, Richard C.: Summary of Measurements in Langley Full-Scale Tunnel of Maximum Lift Coefficients and Stalling Characteristics of Airplanes. NACA Rep. No. 829, 1945.
43. Purser, Paul E., and Johnson, Harold S.: Effects of Trailing-Edge Modifications on Pitching-Moment Characteristics of Airfoils. NACA CB No. L4I30, 1944.
44. Fullmer, Felicien F., Jr.: Wind-Tunnel Investigation of NACA 66(215)–216, 66,1–212, and 65_1–212 Airfoils with 0.20-Airfoil-Chord Split Flaps. NACA CB No. L4G10, 1944.
45. Abbott, Ira H., and Greenberg, Harry: Tests in the Variable-Density Wind Tunnel of the N. A. C. A. 23012 Airfoil with Plain and Split Flaps. NACA Rep. No. 661, 1939.
46. Wenzinger, Carl J., and Harris, Thomas A.: Wind-Tunnel Investigation of N. A. C. A. 23012, 23021, and 23030 Airfoils with Various Sizes of Split Flap. NACA Rep. No. 668, 1939.
47. Bogdonoff, Seymour M.: Wind-Tunnel Investigation of a Low-Drag Airfoil Section with a Double Slotted Flap. NACA ACR No. 3I20, 1943.
48. Wenzinger, Carl J., and Harris, Thomas A.: Wind-Tunnel Investigation of an N. A. C. A. 23012 Airfoil with Various Arrangements of Slotted Flaps. NACA Rep. No. 664, 1939.
49. Wenzinger, Carl J., and Harris, Thomas A.: Wind-Tunnel Investigation of an N. A. C. A. 23021 Airfoil with Various Arrangements of Slotted Flaps. NACA Rep. No. 677, 1939.
50. Swanson, Robert S., and Crandall, Stewart M.: Analysis of Available Data on the Effectiveness of Ailerons without Exposed Overhang Balance. NACA ACR No. L4E01, 1944.
51. Street, William G., and Ames, Milton B., Jr.: Pressure-Distribution Investigation of an N. A. C. A. 0009 Airfoil with a 50-Percent-Chord Plain Flap and Three Tabs. NACA TN No. 734, 1939.
52. Ames, Milton B., Jr., and Sears, Richard I.: Pressure-Distribution Investigation of an N. A. C. A. 0009 Airfoil with an 80-Percent-Chord Plain Flap and Three Tabs. NACA TN No. 761, 1940.
53. Ames, Milton B., Jr., and Sears, Richard I.: Pressure-Distribution Investigation of an N. A. C. A. 0009 Airfoil with a 30-Percent-Chord Plain Flap and Three Tabs. NACA TN No. 759, 1940.
54. Sears, Richard I.: Wind-Tunnel Investigation of Control-Surface Characteristics. I—Effect of Gap on the Aerodynamic Characteristics of an NACA 0009 Airfoil with a 30-Percent-Chord Plain Flap. NACA ARR, June 1941.
55. Jones, Robert T., and Ames, Milton B., Jr.: Wind-Tunnel Investigation of Control-Surface Characteristics. V—The Use of a Beveled Trailing Edge to Reduce the Hinge Moment of a Control Surface. NACA ARR, March 1942.
56. Sears, Richard I., and Liddell, Robert B.: Wind-Tunnel Investigation of Control-Surface Characteristics. VI—A 30-Percent-Chord Plain Flap on the NACA 0015 Airfoil. NACA ARR, June 1942.
57. Wenzinger, Carl J., and Delano, James B.: Pressure Distribution over an N. A. C. A. 23012 Airfoil with a Slotted and a Plain Flap. NACA Rep. No. 633, 1938.
58. Gillis, Clarence L., and Lockwood, Vernard E.: Wind-Tunnel Investigation of Control-Surface Characteristics. XIII—Various Flap Overhangs Used with a 30-Percent-Chord Flap on an NACA 66–009 Airfoil. NACA ACR No. 3G20, 1943.
59. Rogallo, F. M.: Collection of Balanced-Aileron Test Data. NACA ACR No. 4A11, 1944.
60. Denaci, H. G., and Bird, J. D.: Wind-Tunnel Tests of Ailerons at Various Speeds. II—Ailerons of 0.20 Airfoil Chord and True Contour with 0.60 Aileron-Chord Sealed Internal Balance on the NACA 66,2–216 Airfoil. NACA ACR No. 3F18, 1943.
61. Purser, Paul E., and Riebe, John M.: Wind-Tunnel Investigation of Control-Surface Characteristics. XV—Various Contour Modifications of a 0.30-Airfoil-Chord Plain Flap on an NACA 66(215)–014 Airfoil. NACA ACR No. 3L20, 1943.
62. Braslow, Albert L.: Wind-Tunnel Investigation of Aileron Effectiveness of 0.20-Airfoil-Chord Plain Ailerons of True Airfoil Contour on NACA 65_2–415, 65_3–418, and 65_4–421 Airfoil Sections. NACA CB No. L4H12, 1944.
63. Sears, Richard I., and Purser, Paul E.: Wind-Tunnel Investigation of Control-Surface Characteristics. XIV—NACA 0009 Airfoil with a 20-Percent-Chord Double Plain Flap. NACA ARR No. 3F29, 1943.
64. Crane, Robert M., and Holtzclaw, Ralph W.: Wind-Tunnel Investigation of the Effects of Profile Modifications and Tabs on the Characteristics of Ailerons on a Low Drag Airfoil. NACA Rep. No. 803, 1944.
65. Von Doenhoff, Albert E., and Horton, Elmer A.: Preliminary Investigation in the NACA Low-Turbulence Tunnel of Low-Drag-Airfoil Sections Suitable for Admitting Air at the Leading Edge. NACA ACR, July 1942
66. Jacobs, Eastman N., and Ward, Kenneth E.: Interference of Wing and Fuselage from Tests of 209 Combinations in the N. A. C. A. Variable-Density Tunnel. NACA Rep. No. 540, 1935.
67. Abbott, Ira H.: Interference Effects of Longitudinal Flat Plates on Low-Drag Airfoils. NACA CB, Nov. 1942.
68. Ellis, Macon C., Jr.: Some Lift and Drag Measurements of a Representative Bomber Nacelle on a Low-Drag Wing—II. NACA CB, Sept. 1942.
69. Ellis, Macon C., Jr.: Effects of a Typical Nacelle on the Characteristics of a Thick Low-Drag Airfoil Critically Affected by Leading-Edge Roughness. NACA CB No. 3D27, 1943.
70. Allen, H. Julian, and Frick, Charles W., Jr.: Experimental Investigation of a New Type of Low-Drag Wing-Nacelle Combination. NACA ACR, July 1942.
71. Abbott, Frank T., Jr.: Lift and Drag Data for 30 Pusher-Propeller Shaft Housings on an NACA 65,3-018 Airfoil Section. NACA ACR No. 3K13, 1943.
72. Robinson, Russell G., and Wright, Ray H.: Estimation of Critical Speeds of Airfoils and Streamline Bodies. NACA ACR, March 1940.
73. Anderson, Raymond F.: Determination of the Characteristics of Tapered Wings. NACA Rep. No. 572, 1936.
74. Jacobs, Eastman N., and Rhode, R. V.: Airfoil Section Characteristics as Applied to the Prediction of Air Forces and Their Distribution on Wings. NACA Rep. No. 631, 1938.

75. Soulé, H. A., and Anderson, R. F.: Design Charts Relating to the Stalling of Tapered Wings. NACA Rep. No. 703, 1940.
76. Harmon, Sidney M.: Additional Design Charts Relating to the Stalling of Tapered Wings. NACA ARR, Jan. 1943.
77. Anderson, Raymond F.: The Experimental and Calculated Characteristics of 22 Tapered Wings. NACA Rep. No. 627, 1938.
78. Tani, Itiro: A Simple Method of Calculating the Induced Velocity of a Monoplane Wing. Rep. No. 111 (Vol. IX, 3), Aero. Res. Inst., Tokyo Imperial Univ., Aug. 1934.
79. Sherman, Albert: A Simple Method of Obtaining Span Load Distributions. NACA TN No. 732, 1939.
80. Jones, Robert T.: Correction of the Lifting-Line Theory for the Effect of the Chord. NACA TN No. 817, 1941.
81. Cohen, Doris: Theoretical Distribution of Load over a Swept-Back Wing. NACA ARR, Oct. 1942.
82. Pearson, H. A.: Span Load Distribution for Tapered Wings with Partial-Span Flaps. NACA Rep. No. 585, 1937.
83. Pearson, Henry A., and Anderson, Raymond F.: Calculation of the Aerodynamic Characteristics of Tapered Wings with Partial-Span Flaps. NACA Rep. No. 665, 1939.
84. The Cambridge University Aeronautics Laboratory: The Measurement of Profile Drag by the Pitot-Traverse Method. R. & M. No. 1688, British A. R. C., 1936.
85. Silverstein, A., and Katzoff, S.: A Simplified Method for Determining Wing Profile Drag in Flight. Jour. Aero. Sci., vol. 7, no. 7, May 1940, pp. 295–301.
86. Glauert, H.: Wind Tunnel Interference on Wings, Bodies and Airscrews. R. & M. No. 1566, British A. R. C., 1933.
87. Allen, H. Julian, and Vincenti, Walter G.: Interference in a Two-Dimensional-Flow Wind Tunnel with the Consideration of the Effect of Compressibility. NACA Rep. No. 782, 1944.
88. Fage, A.: On the Two-Dimensional Flow past a Body of Symmetrical Cross-Section Mounted in a Channel of Finite Breadth. R. & M. No. 1223, British A. R. C., 1929.

TABLE II.—MAXIMUM LIFT AND STALLING CHARACTERISTICS OF MODELS TESTED IN THE NACA 19-FOOT PRESSURE TUNNEL

Model	Configuration		Geometric characteristics	Flap		Flap angle (deg)		Flap chord (percent c)		Flap span (percent b)		R	$C_{L_{max}}$	Stalling characteristics
	Plan view	Front view		Inboard	Outboard	δ_{f_i}	δ_{f_o}	c_{f_i}	c_{f_o}	b_{f_i}	b_{f_o}			
I	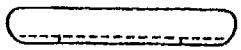		Sections: Root: NACA 66(215)-216 Tip: NACA 66(215)-216 A=7.00 λ=1.00 Geometric washout, 0.0°	None	None	----	----	None	None	None	None	2.6×10^6 3.6 4.6	1.26 1.36 1.41	Abrupt stall progresses from root toward tip for flaps neutral and partial-span flaps deflected; no data for full-span flaps
				Split	↓	60	↓	10	↓	53	↓	2.6 3.6 4.6	1.72 1.78 1.84	
								20				2.6 3.6 4.6	1.94 1.98 2.07	
								30				2.6 3.6 4.6	1.97 2.03 2.06	
					Split		60	10	10		37	2.6 3.6 4.6	2.04 2.11 2.15	
								20	20			2.6 3.6 4.6	2.40 2.50 2.51	
								30	30			2.6 3.6 4.6	2.43 2.49 2.52	
II	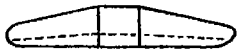		Sections: Root: NACA 66(215)-116 Tip: NACA 66(215)-216 A=7.0 λ=0.5 Geometric washout, 1.5°	Fowler	Fowler	0	0	30	30	53	37	2.1×10^6 2.8 3.8	1.15 1.29 1.27	With flaps neutral, satisfactory; with flaps deflected, extremely abrupt stall envelops entire wing
						30						2.1 2.9 3.4	2.29 2.44 2.49	
						35						2.1 2.9 3.4	2.36 2.49 2.54	
						60	30					2.1 2.9 3.4	3.13 3.31 3.29	
III			Sections: Root: NACA 65(318)-019 Tip: NACA 65(318)-015 A=7.36 λ=0.25 Geometric washout; 3.6°	None	None	----	----	----	----	----	----	3.0×10^6 5.1 7.4	1.18 1.37 1.43	Abrupt stall with satisfactory progression toward tips
IV	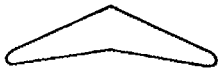		Sections: Root: NACA 65(318)-019 Tip: NACA 65(318)-015 A=7.36 λ=0.25 Geometric washout, 4.0° Sweepback of 0.25 chord line 21.98°	None	None	----	----	----	----	----	----	3.3×10^6 5.6 7.2	1.17 1.31 1.34	Unsatisfactory stall; a strong outflow resulted in severe tip stall
V		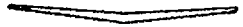	Sections: Root: NACA 66(215)-(1.8)(15.5), a=0.6 Tip: NACA 66(215)-(1.8)12, a=0.6 A=5.32 λ=0.46 Geometric washout, 2.5°	Plain	None	0	----	25	----	60	----	3.2×10^6 5.4 7.8	1.40 1.52 1.55	Abrupt stall with satisfactory progression toward tips
						50	----		----		----	3.3 5.2 5.8 7.0	2.10 2.19 2.21 2.23	

VI	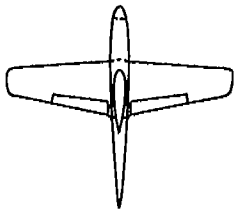		Sections: Root: NACA 66(215)-(1.8) (15.5), a=0.6 Tip: NACA 66(215)-(1.8)12, a=0.6 A=5.82 λ=0.46 Geometric washout, 2.5°	Plain ↓	None ↓	0 50	------ ------	25 ↓ ↓	------ ------	60 ↓ ↓	------ ------	3.3×10⁶ 5.3 6.0 3.3 5.1 5.8	1.34 1.39 1.39 1.87 1.91 1.92	Abrupt stall with satisfactory progression toward tips
VII	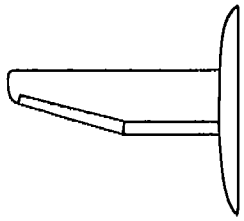		Sections: Root: Mod. NACA 65, 3-318, a=0.8 Tip: Mod. NACA 65(318)-316, a=0.8 A=8.09 λ=0.5 Geometric washout, 0.0°	Double slotted ↓	Double slotted ↓	0 55	0 30	25 ↓ ↓	25 ↓ ↓	50 ↓ ↓	48 ↓ ↓	5.1×10⁶ 5.1	1.88 2.85	Satisfactory
VIII	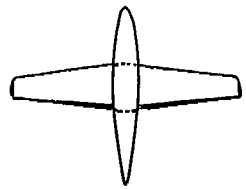		Sections: Root: NACA 67(115)-116 Tip: NACA 67, 1-115 A=6.7 λ=0.4 Geometric washout, 2.0°	Zap ↓ ↓ Split ↓	Zap ↓ ↓ None Split	0 48 ↓ 60 ↓	0 ↓ 48 ------ 60	35 ↓ ↓ 20 ↓	35 ↓ ↓ 20 ↓	60 ↓ ↓ 60 ↓	38 ↓ ↓ 38 ↓	2.4×10⁶ 2.4 2.4 2.5 2.5	1.82 2.25 2.77 1.91 2.22	No data
IX	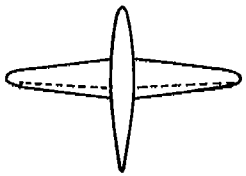		Sections: Root: NACA 64(215)-418 Tip: NACA 66,2x-415 A=8.92 λ=0.33 Geometric washout, 1.0°	None Split ↓	None ↓	------ 55	------ ------	------ 20	------ ------	------ 60	------ ------	3.5×10⁶ 3.6	1.38 1.97	Satisfactory
X	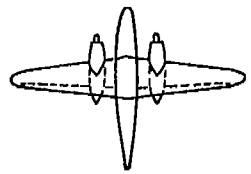		Sections: Root: NACA 64(215)-418 Tip: NACA 66,2x-415 A=8.92 λ=0.33 Geometric washout, 1.0°	None Split ↓	None Split	------ 55 ↓	------ 55	------ 20 ↓	------ 20	------ 60 ↓	------ 60	3.5×10⁶ 3.6 3.5	1.42 1.87 2.11	Satisfactory
XI	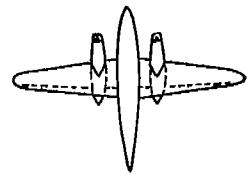	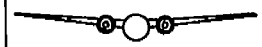	Sections: Root: NACA 64(215)-418 Tip: NACA 66,2x-415 A=8.92 λ=0.33 Geometric washout, 1.0°	None Split	None ↓	------ 55	------ ------	------ 20	------ ------	------ 60	------ ------	4.0×10⁶ 4.1	1.47 1.95	Satisfactory
XII	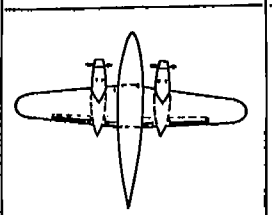	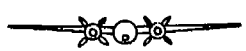	Sections: Root: NACA 63(420)-418, a=1.0 Tip: NACA 65₂-415, a=1.0 A=7.77 λ=0.50 Geometric washout, 2.8°	Extensible slotted ↓ Split	None ↓	0 35 60	------ ------ ------	25 ↓ ↓	------ ------ ------	70 ↓ ↓	------ ------ ------	3.1×10⁶ 4.1 4.8 3.1 4.0 4.9 3.1 4.1 4.8	*1.87 *1.42 *1.45 *2.19 *2.20 *2.21 *2.00 *2.06 *2.06	Satisfactory

* Propellers windmilling.

TABLE II.—MAXIMUM LIFT AND STALLING CHARACTERISTICS OF MODELS TESTED IN THE NACA 19-FOOT PRESSURE TUNNEL—Concluded

Model	Configuration: Plan view	Configuration: Front view	Geometric characteristics	Flap: Inboard	Flap: Outboard	Flap angle (deg): δ_{f_i}	Flap angle (deg): δ_{f_o}	Flap chord (percent c): c_{f_i}	Flap chord (percent c): c_{f_o}	Flap span (percent b): b_{f_i}	Flap span (percent b): b_{f_o}	R	$C_{L_{max}}$	Stalling characteristics
XIII	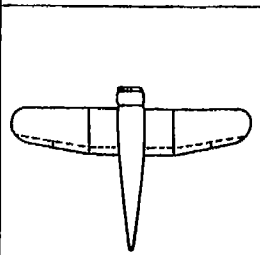		Sections: Roots: NACA 66(215)-016 Tip: NACA 66(215)-016 A=5.34 λ=0.68 Geometric washout, 0.0°	None	None							2.4×10^6 3.8 5.3	1.21 1.37 1.45	Satisfactory
				Split		60		20		65		2.4 3.8 5.4	1.76 1.89 1.96	
				Extensible trailing edge		45						2.5 3.7 5.2	1.72 1.86 1.98	
					Split		60		20		30	2.4 3.6 5.3	1.99 2.03 2.13	
				Split		60						2.4 3.8 5.8	2.01 2.15 2.21	
XIV	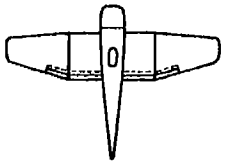		Sections: Root: NACA 65(318)-1(18.5) Tip: NACA 66(215)-216 A=5.52 λ=0.48 Geometric washout, 3.0°	Extensible slotted	None	0		20		60		3.6×10^6 5.1 6.1	1.32 1.42 1.46	Abrupt stall with satisfactory progression toward tips
						35						3.6 5.2 6.3	2.27 2.34 2.37	
				Slotted		50						3.5 4.9 5.9	2.04 2.13 2.16	
				Split		50						3.5 4.8 5.9	2.02 2.12 2.17	
XV	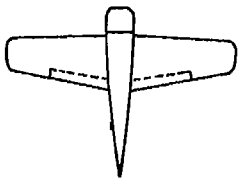		Sections: Root: NACA 23015.6 Tip: NACA 23009 A=5.5 λ=0.52 Geometric washout, 0.0°	Slotted	None	0		20		60		3.4×10^6 4.8 5.6	1.55 1.58 1.60	Very abrupt stall, left wing stalling very rapidly, for all conditions
						50						3.4 4.8 5.6	2.46 2.50 2.52	
XVI	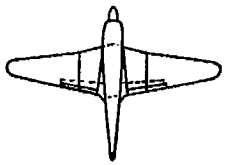		Sections: Root: NACA 66,2-118 Tip: NACA 66(2x15)-116 A=6.9 Geometric washout, 2.0°	Extensible slotted	None	0		24		50		3.0×10^6 4.1 5.0	1.34 1.47 1.50	Extremely abrupt stall, left wing stalls first for the extensible slotted flap, satisfactory for split flap
						38						2.9 4.0 4.9	2.01 2.15 2.21	
				Split		45						4.9 4.9	[b]2.29 [b]1.98	
XVII	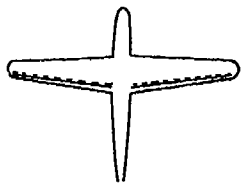		Sections: Root: NACA 65 (216)-215, α=0.8 Tip: NACA 65(216)-215 α=0.5 A=9.08 λ=0.45 Geometric washout, 1.0° 0.2 chord line straight	Double slotted	Double slotted	0 55	0 25	25	25	65	31	3.6×10^6 2.1 2.8	1.38 2.45 2.69	Satisfactory
XVIII	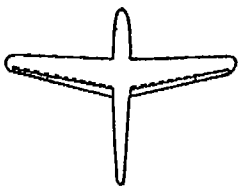		Sections: Root: NACA 65 (216)-215, α=0.8 Tip: NACA 65(216)-215, α=0.5 A=9.06 λ=0.45 Geometric washout, 1.0° —0.10 chord line straight	Double slotted	Double slotted	0 55	0 25	25	25	65	31	3.6×10^6 3.1 2.8	1.37 2.44 2.76	Satisfactory

XIX	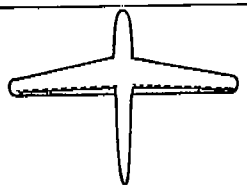		Sections: Root: NACA 65(216)-215, a=0.8 Tip: NACA 65(216)-215, a=0.5 A=9.08 λ=0.45 Geometric washout, 1.0° 1.1 chord line straight	Double slotted ↓	Double slotted ↓	0 55 ↓	0 ↓ 25	25 ↓	25 ↓	65 ↓	31 ↓	3.6×10^6 3.1 2.8	1.45 2.57 2.86	Unsatisfactory, severe tip stall for all conditions except full-span flap
XX	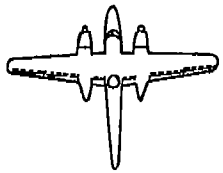		Sections: Root: NACA 65(216)-215, a=0.8 Tip: NACA 65(216)-215, a=0.5 A=9.08 λ=0.45 Geometric washout, 1.0° 0.20 chord line straight	Double slotted ↓	Double slotted ↓	0 55 ↓	0 ↓ 55	25 ↓	25 ↓	65 ↓	31 ↓	5.5×10^6 5.5 5.5	1.45 2.37 2.65	Satisfactory
XXI	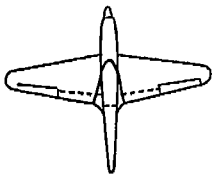		Sections: Root: NACA 66,2-118 Tip: NACA 66(2x15)-116 A=6.25 λ=0.35 Geometric washout, 2.5° 0.375 chord line straight	None Split ↓ Split	None ↓	------ 45 ↓ 60 ↓	------ ------ 60	------ 20 ↓	------ ------ 20	------ 50 ↓	------ ------ 40	2.9×10^6 4.0 4.9 3.0 4.0 4.9 3.0 4.3 5.1 5.2	1.23 1.43 1.51 1.80 1.85 1.96 1.90 2.01 2.04 2.48	Satisfactory
XXII	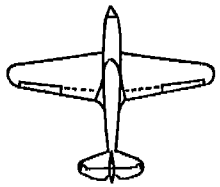		Sections: Root: NACA 66,2-118 Tip: NACA 66(2x15)-116 A=6.25 λ=0.35 Geometric washout, 2.5° 0.375 chord line straight	None Split	None ↓	------ 45	------ ------	------ 20	------ ------	------ 50	------ ------	4.1×10^6 4.9 4.1	1.50 1.60 2.02	Satisfactory
XXIII	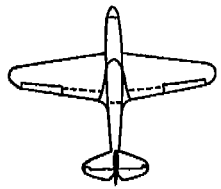		Sections: Root: NACA 66,2-118 Tip: NACA 66(2x15)-116 A=6.25 λ=0.35 Geometric washout, 2.5° 0.375 chord line swept forward 3.5°	None Split	None ↓	------ 45	------ ------	------ 20	------ ------	------ 50	------ ------	2.9×10^6 4.1 4.9 2.9 4.1 5.0	1.88 1.57 1.61 1.83 1.99 2.02	Satisfactory
XXIV	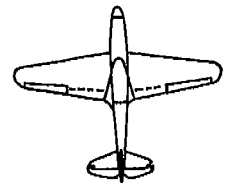		Sections: Root: NACA 66,2-118 Tip: NACA 66(2x15)-116 A=6.1 λ=0.47 Geometric washout, 2.5° 0.375 chord line straight	None Split	None ↓	------ 45	------ ------	------ 20	------ ------	------ 50	------ ------	2.9×10^6 4.2 5.0 3.0 4.2 5.1	1.84 1.56 1.63 1.85 1.92 2.01	Satisfactory
XXV	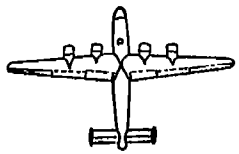	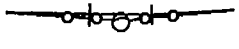	Sections: Root: NACA 65(223)-221, a=1.0 Tip: NACA 66(215)-316, a=0.6 A=12.8 λ=0.33 Geometric washout, 0.0°	Fowler ↓	None ↓	0 40	------ ------	18 ↓ ------	------ ------	53 ↓ ------	------ ------	1.5×10^6 2.2 2.8 1.4 1.9 2.7	1.17 1.27 1.37 2.21 2.23 2.30	Poor, initial stall occurs at tips

* Fillets removed.

SUPPLEMENTARY DATA

I—BASIC THICKNESS FORMS

	Page
NACA 0006	328
NACA 0008	328
NACA 0009	328
NACA 0010	329
NACA 0012	329
NACA 0015	329
NACA 0018	330
NACA 0021	330
NACA 0024	330
NACA 16–006	331
NACA 16–009	331
NACA 16–012	331
NACA 16–015	332
NACA 16–018	332
NACA 16–021	332
NACA 63,4–020	333
NACA 63–006	333
NACA 63–009	333
NACA 63–010	334
NACA 63_1–012	334
NACA 63_2–015	334
NACA 63_3–018	335
NACA 63_4–021	335
NACA 64,2–015	335
NACA 64–006	336
NACA 64–008	336
NACA 64–009	336
NACA 64–010	337
NACA 64_1–012	337
NACA 64_2–015	337
NACA 64_3–018	338
NACA 64_4–021	338
NACA 65,2–016	338
NACA 65,2–023	339
NACA 65,3–018	339
NACA 65–006	339
NACA 65–008	340
NACA 65–009	340
NACA 65–010	340
NACA 65_1–012	341
NACA 65_2–015	341
NACA 65_3–018	341
NACA 65_4–021	342
NACA 66,1–012	342
NACA 66,2–015	342
NACA 66,2–018	343
NACA 66–006	343
NACA 66–008	343
NACA 66–009	344
NACA 66–010	344
NACA 66_1–012	344
NACA 66_2–015	345
NACA 66_3–018	345
NACA 66_4–021	345
NACA 67,1–015	346
NACA 747A015	346

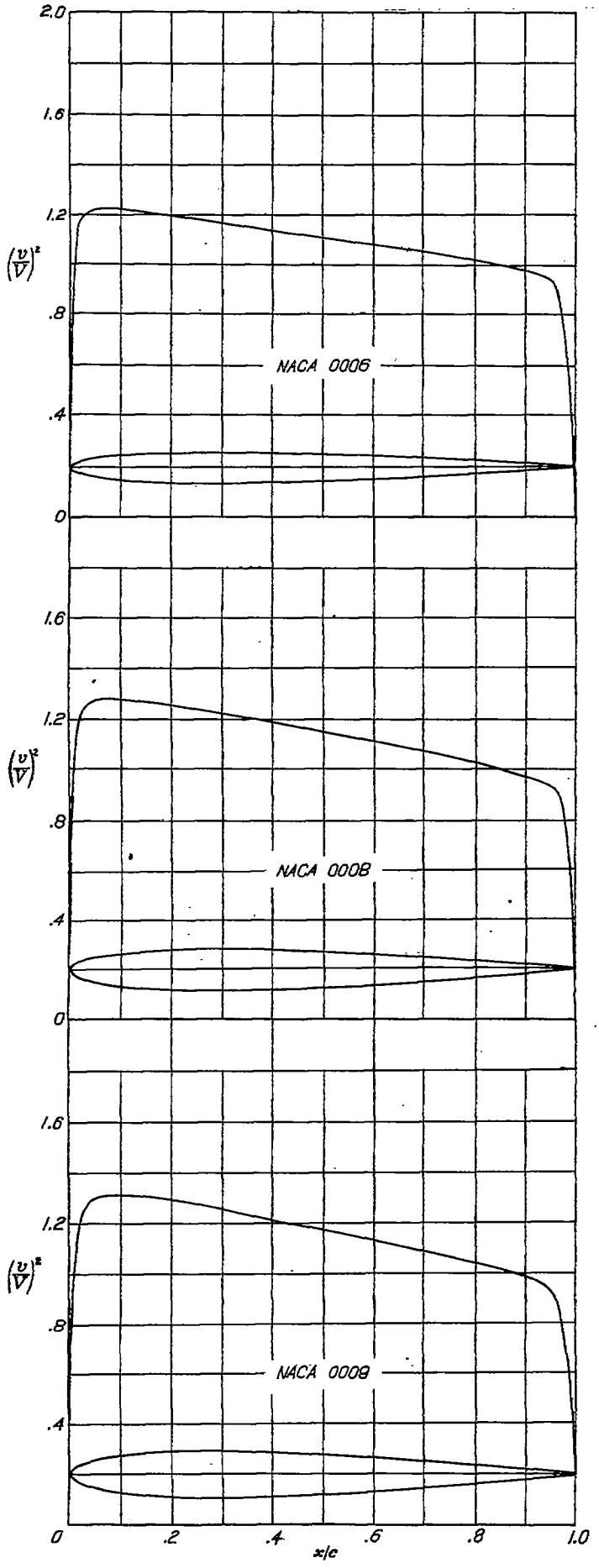

NACA 0006 BASIC THICKNESS FORM

x (percent c)	y (percent c)	$(v/V)^2$	v/V	$\Delta s_a/V$
0	0	0	0	2.392
.5	----------	.880	.938	2.015
1.25	.947	1.117	1.057	1.364
2.5	1.307	1.186	1.089	.984
5.0	1.777	1.217	1.103	.626
7.5	2.100	1.225	1.107	.562
10	2.341	1.212	1.101	.478
15	2.673	1.206	1.098	.378
20	2.869	1.190	1.091	.316
25	2.971	1.179	1.086	.272
30	3.001	1.162	1.078	.239
40	2.902	1.136	1.066	.189
50	2.647	1.109	1.053	.152
60	2.282	1.086	1.042	.123
70	1.832	1.057	1.028	.097
80	1.312	1.026	1.013	.073
90	.724	.980	.990	.047
95	.403	.949	.974	.032
100	.063	0	0	0

L. E. radius: 0.40 percent c

NACA 0008 BASIC THICKNESS FORM

x (percent c)	y (percent c)	$(v/V)^2$	v/V	$\Delta s_a/V$
0	0	0	0	2.900
.5	----------	.792	.890	1.795
1.25	1.263	1.103	1.050	1.210
2.5	1.743	1.221	1.105	.971
5.0	2.369	1.272	1.128	.694
7.5	2.800	1.284	1.133	.561
10	3.121	1.277	1.130	.479
15	3.564	1.272	1.128	.379
20	3.825	1.259	1.122	.318
25	3.961	1.241	1.114	.273
30	4.001	1.223	1.106	.239
40	3.869	1.186	1.089	.188
50	3.529	1.149	1.072	.152
60	3.043	1.111	1.054	.121
70	2.443	1.080	1.039	.096
80	1.749	1.034	1.017	.071
90	.965	.968	.984	.047
95	.537	.939	.969	.031
100	.084	----------	----------	0

L. E. radius: 0.70 percent c

NACA 0009 BASIC THICKNESS FORM

x (percent c)	y (percent c)	$(v/V)^2$	v/V	$\Delta s_a/V$
0	0	0	0	0.598
.5	----------	.750	.866	1.700
1.25	1.420	1.083	1.041	1.253
2.5	1.961	1.229	1.109	.963
5.0	2.666	1.299	1.140	.692
7.5	3.150	1.310	1.145	.560
10	3.512	1.309	1.144	.479
15	4.009	1.304	1.142	.390
20	4.303	1.293	1.137	.318
25	4.456	1.275	1.129	.273
30	4.501	1.252	1.119	.239
40	4.352	1.209	1.100	.188
50	3.971	1.170	1.082	.151
60	3.423	1.126	1.061	.120
70	2.748	1.087	1.043	.095
80	1.967	1.037	1.018	.070
90	1.086	.984	.992	.046
95	.605	.933	.966	.030
100	.095	0	0	0

L. E. radius: 0.89 percent c

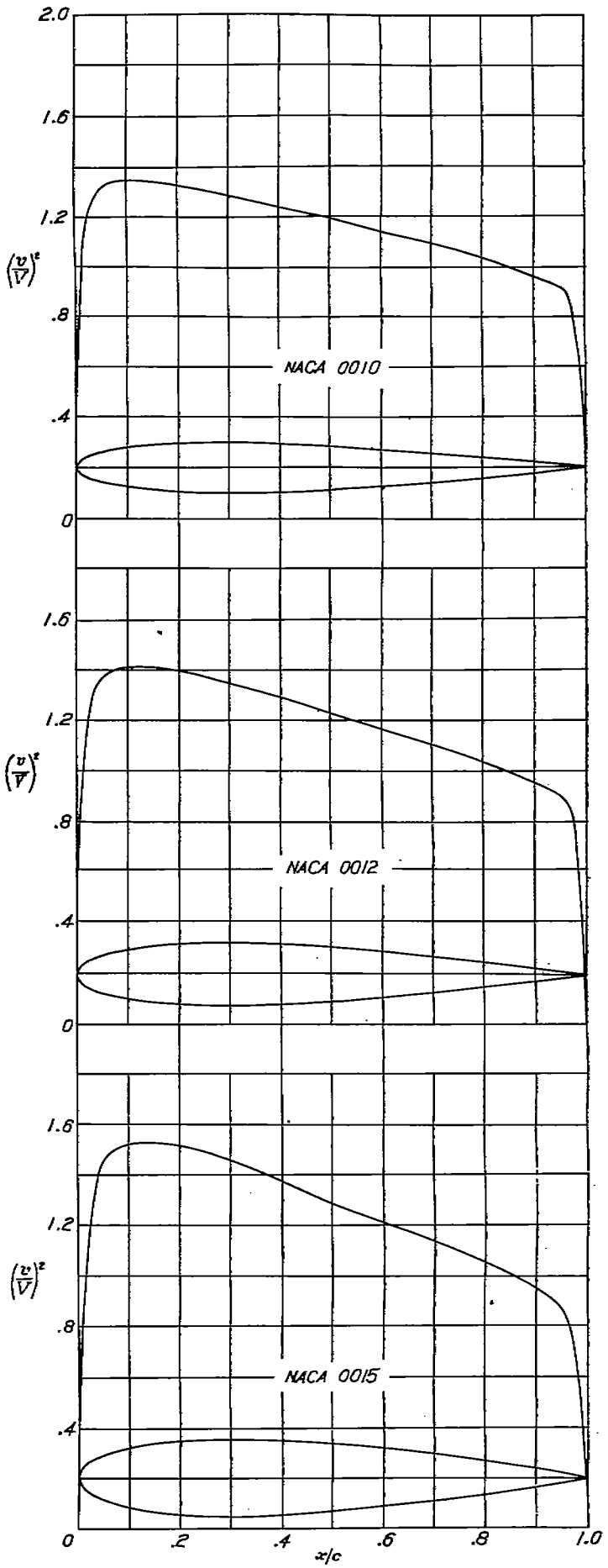

NACA 0010 BASIC THICKNESS FORM

x (percent c)	y (percent c)	$(v/V)^2$	v/V	$\Delta s_s/V$
0	0	0	0	1.372
.5	----------	.712	.844	1.618
1.25	1.578	1.061	1.030	1.255
2.5	2.178	1.237	1.112	.955
5.0	2.962	1.325	1.151	.630
7.5	3.500	1.341	1.158	.539
10	3.902	1.341	1.158	.479
15	4.455	1.341	1.158	.380
20	4.782	1.329	1.153	.318
25	4.952	1.309	1.144	.278
30	5.002	1.284	1.133	.239
40	4.837	1.237	1.112	.188
50	4.412	1.190	1.091	.150
60	3.803	1.138	1.067	.119
70	3.053	1.094	1.046	.094
80	2.187	1.040	1.020	.069
90	1.207	.960	.980	.046
95	.672	.925	.962	.030
100	.105	----------	----------	0

L. E. radius: 1.10 percent c

NACA 0012 BASIC THICKNESS FORM

x (percent c)	y (percent c)	$(v/V)^2$	v/V	$\Delta s_s/V$
0	0	0	0	1.988
.5	----------	.640	.800	1.475
1.25	1.894	1.010	1.005	1.199
2.5	2.615	1.241	1.114	.934
5.0	3.555	1.378	1.174	.685
7.5	4.200	1.402	1.184	.558
10	4.683	1.411	1.188	.479
15	5.345	1.411	1.188	.381
20	5.738	1.399	1.183	.319
25	5.941	1.378	1.174	.278
30	6.002	1.350	1.162	.239
40	5.803	1.288	1.135	.187
50	5.294	1.228	1.108	.149
60	4.563	1.166	1.080	.118
70	3.664	1.109	1.053	.092
80	2.623	1.044	1.022	.068
90	1.448	.956	.978	.044
95	.807	.906	.952	.029
100	.126	0	0	0

L. E. radius: 1.58 percent c

NACA 0015 BASIC THICKNESS FORM

x (percent c)	y (percent c)	$(v/V)^2$	v/V	$\Delta s_s/V$
0	0	0	0	1.600
.5	----------	.546	.739	1.312
1.25	2.367	.933	.966	1.112
2.5	3.203	1.237	1.112	.900
5.0	4.443	1.450	1.204	.675
7.5	5.250	1.498	1.224	.557
10	5.853	1.520	1.233	.479
15	6.682	1.520	1.233	.381
20	7.172	1.510	1.229	.320
25	7.427	1.484	1.218	.274
30	7.502	1.450	1.204	.239
40	7.254	1.369	1.170	.185
50	6.617	1.279	1.131	.146
60	5.704	1.206	1.098	.115
70	4.580	1.132	1.064	.090
80	3.279	1.049	1.024	.065
90	1.810	.945	.972	.041
95	1.008	.872	.934	.027
100	.158	0	0	0

L. E. radius: 2.48 percent c

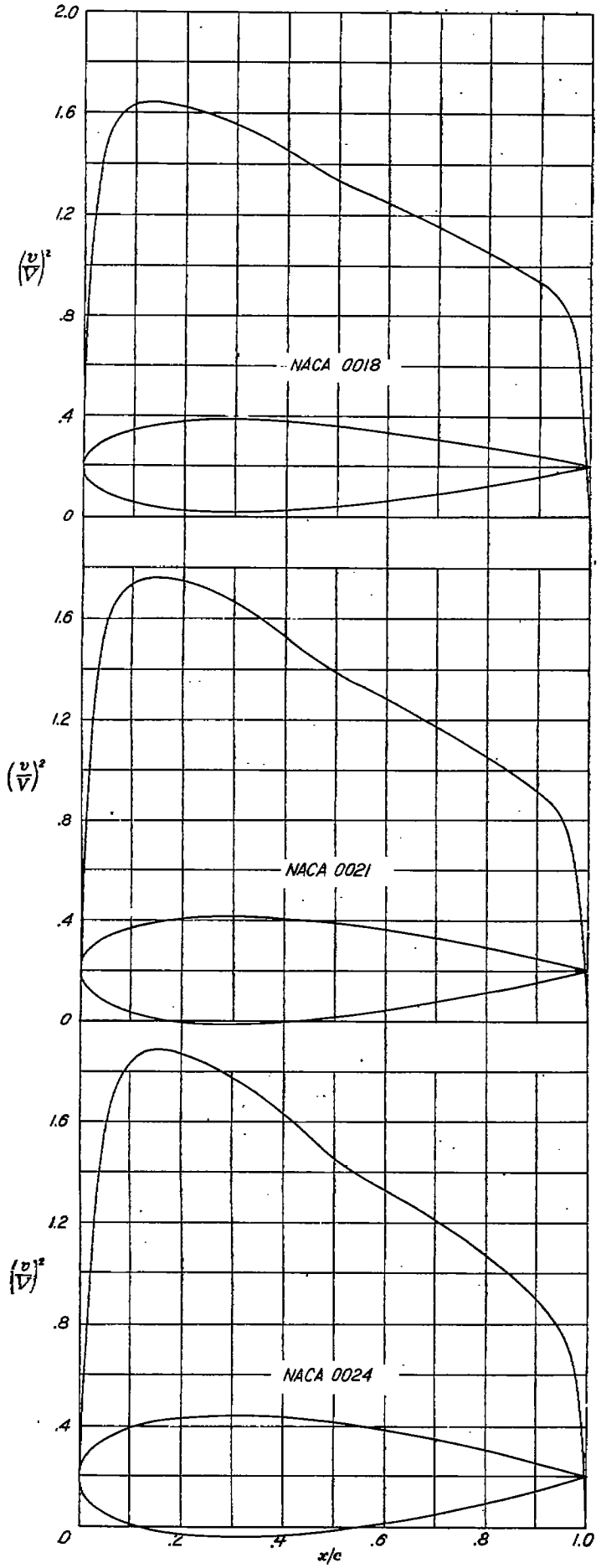

NACA 0018 BASIC THICKNESS FORM

x (percent c)	y (percent c)	$(v/V)^2$	v/V	$\Delta v_a/V$
0	0	0	0	1.342
.5	----------	.465	.682	1.178
1.25	2.841	.857	.926	1.028
2.5	3.922	1.217	1.103	.851
5.0	5.332	1.507	1.228	.662
7.5	6.300	1.598	1.264	.555
10	7.024	1.628	1.276	.479
15	8.018	1.633	1.278	.381
20	8.608	1.625	1.275	.320
25	8.912	1.592	1.262	.274
30	9.002	1.556	1.247	.238
40	8.705	1.483	1.205	.184
50	7.941	1.331	1.154	.144
60	6.845	1.246	1.116	.113
70	5.496	1.153	1.074	.087
80	3.935	1.051	1.025	.063
90	2.172	.933	.966	.039
95	1.210	.836	.914	.025
100	.189	0	0	0

L. E. radius: 3.56 percent c

NACA 0021 BASIC THICKNESS FORM

x (percent c)	y (percent c)	$(v/V)^2$	v/V	$\Delta v_a/V$
0	0	0	0	1.167
.5	----------	.397	.630	1.065
1.25	3.815	.787	.887	.946
2.5	4.576	1.182	1.087	.818
5	6.221	1.543	1.242	.648
7.5	7.350	1.682	1.297	.550
10	8.195	1.734	1.317	.478
15	9.364	1.756	1.325	.381
20	10.040	1.742	1.320	.320
25	10.397	1.706	1.306	.274
30	10.504	1.664	1.290	.238
40	10.156	1.538	1.240	.183
50	9.266	1.388	1.178	.142
60	7.986	1.284	1.133	.111
70	6.412	1.177	1.085	.084
80	4.591	1.056	1.027	.061
90	2.534	.916	.957	.037
95	1.412	.801	.895	.023
100	.221	0	0	0

L. E. radius: 4.85 percent c

NACA 0024 BASIC THICKNESS FORM

x (percent c)	y (percent c)	$(v/V)^2$	v/V	$\Delta v_a/V$
0	0	0	0	1.030
.5	----------	.335	.579	.964
1.25	3.788	.719	.848	.870
2.5	5.229	1.130	1.063	.771
5.0	7.109	1.548	1.244	.632
7.5	8.400	1.748	1.322	.542
10	9.366	1.833	1.354	.476
15	10.691	1.889	1.374	.383
20	11.475	1.871	1.368	.321
25	11.883	1.822	1.350	.274
30	12.004	1.777	1.333	.238
40	11.607	1.631	1.277	.181
50	10.588	1.450	1.204	.140
60	9.127	1.325	1.151	.109
70	7.328	1.203	1.097	.082
80	5.247	1.065	1.032	.059
90	2.896	.891	.944	.035
95	1.613	.773	.879	.022
100	.252	0	0	0

L. E. radius: 6.38 percent c

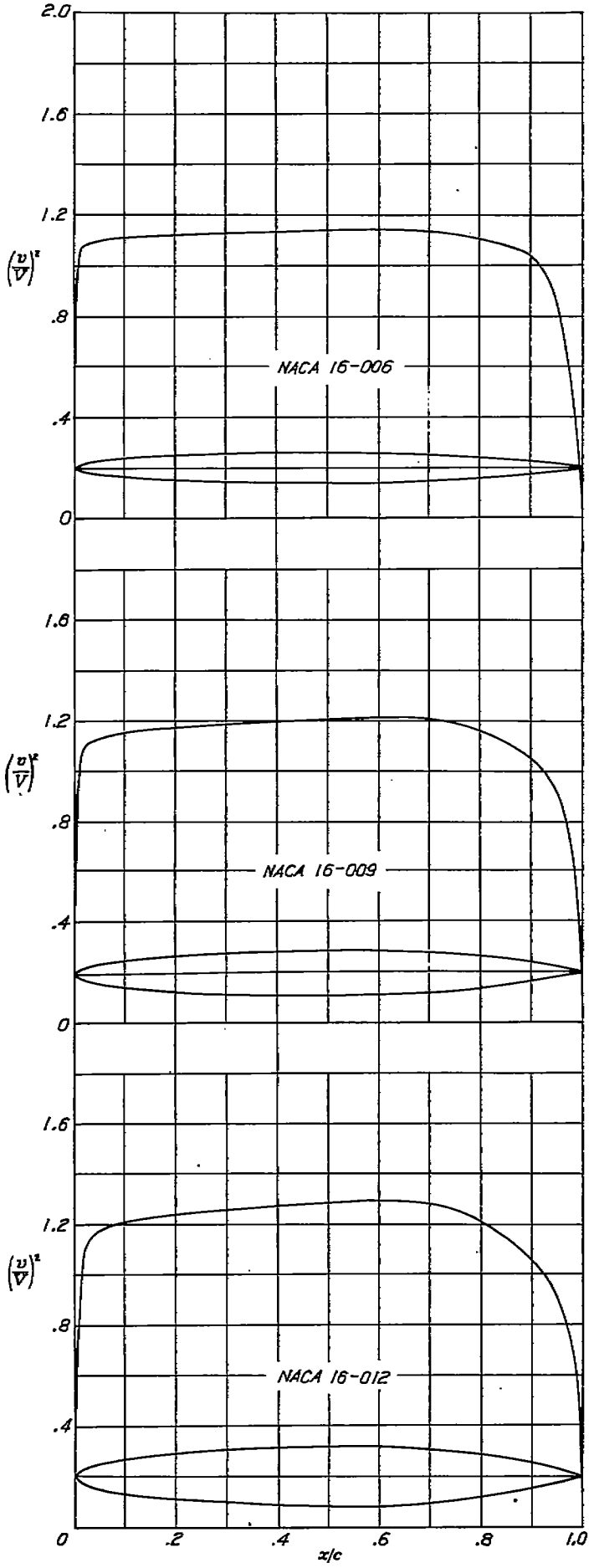

NACA 16-006 BASIC THICKNESS FORM

x (percent c)	y (percent c)	$(v/V)^2$	v/V	$\Delta x_s/V$
0	0	0	0	5.471
1.25	.646	1.059	1.029	1.376
2.5	.903	1.085	1.042	.960
5.0	1.255	1.097	1.047	.689
7.5	1.516	1.105	1.051	.557
10	1.729	1.108	1.053	.476
15	2.067	1.112	1.055	.379
20	2.332	1.116	1.057	.319
30	2.709	1.123	1.060	.244
40	2.927	1.132	1.064	.196
50	3.000	1.137	1.066	.160
60	2.917	1.141	1.068	.130
70	2.635	1.132	1.064	.104
80	2.099	1.104	1.051	.077
90	1.259	1.035	1.017	.049
95	.707	.962	.981	.032
100	.060	0	0	0

L. E. radius: 0.176 percent c

NACA 16-009 BASIC THICKNESS FORM

x (percent c)	y (percent c)	$(v/V)^2$	v/V	$\Delta x_s/V$
0	0	0	0	3.644
1.25	.969	1.042	1.021	1.330
2.5	1.354	1.109	1.053	.964
5.0	1.882	1.139	1.067	.684
7.5	2.274	1.152	1.073	.554
10	2.593	1.158	1.076	.475
15	3.101	1.168	1.081	.378
20	3.498	1.177	1.085	.319
30	4.063	1.190	1.091	.245
40	4.391	1.202	1.096	.197
50	4.500	1.211	1.100	.160
60	4.376	1.214	1.106	.131
70	3.952	1.206	1.099	.103
80	3.149	1.156	1.075	.076
90	1.888	1.043	1.022	.047
95	1.061	.939	.969	.030
100	.090	0	0	0

L. E. radius: 0.396 percent c

NACA 16-012 BASIC THICKNESS FORM

x (percent c)	y (percent c)	$(v/V)^2$	v/V	$\Delta x_s/V$
0	0	0	0	2.624
1.25	1.292	1.002	1.001	1.268
2.5	1.805	1.109	1.053	.942
5.0	2.509	1.173	1.083	.677
7.5	3.032	1.197	1.094	.551
10	3.457	1.208	1.099	.473
15	4.135	1.223	1.106	.378
20	4.664	1.237	1.112	.319
30	5.417	1.257	1.121	.245
40	5.855	1.271	1.128	.197
50	6.000	1.286	1.134	.161
60	5.835	1.298	1.137	.131
70	5.269	1.275	1.129	.102
80	4.199	1.203	1.097	.075
90	2.517	1.051	1.025	.045
95	1.415	.908	.953	.027
100	.120	0	0	0

L. E. radius: 0.703 percent c

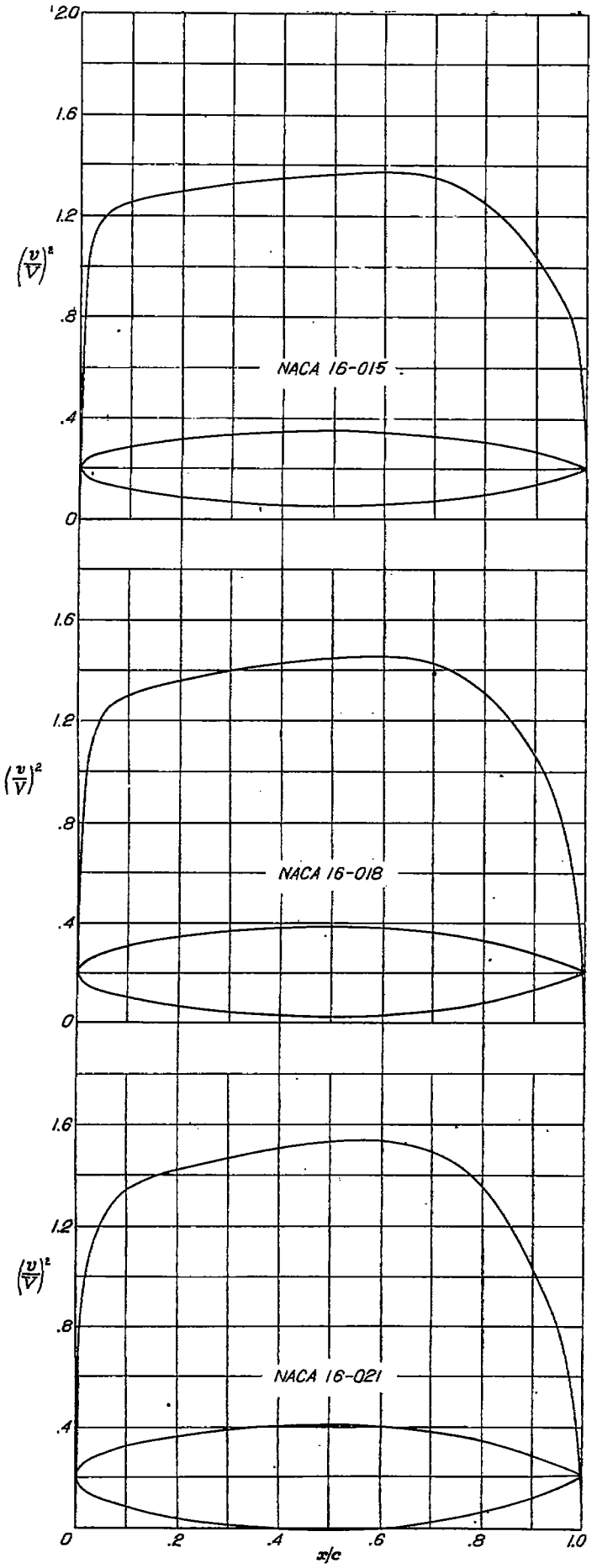

NACA 16-015 BASIC THICKNESS FORM

x (percent c)	y (percent c)	$(v/V)^2$	v/V	$\Delta r_c/V$
0	0	0	0	2.041
1.25	1.615	.956	.978	1.209
2.5	2.257	1.105	1.051	.916
5.0	3.137	1.200	1.095	.663
7.5	3.790	1.239	1.113	.547
10	4.322	1.256	1.121	.471
15	5.168	1.278	1.130	.377
20	5.830	1.297	1.139	.318
30	6.772	1.327	1.152	.245
40	7.318	1.349	1.161	.197
50	7.500	1.364	1.168	.161
60	7.293	1.374	1.172	.131
70	6.587	1.348	1.161	.102
80	5.248	1.254	1.120	.074
90	3.147	1.053	1.026	.043
95	1.763	.878	.935	.026
100	.150	0	0	0

L. E. radius: 1.100 percent c

NACA 16-018 BASIC THICKNESS FORM

x (percent c)	y (percent c)	$(v/V)^2$	v/V	$\Delta r_c/V$
0	0	0	0	1.744
1.25	1.938	.903	.950	1.140
2.5	2.708	1.092	1.045	.883
5.0	3.764	1.217	1.103	.637
7.5	4.548	1.271	1.128	.541
10	5.186	1.302	1.141	.468
15	6.202	1.332	1.154	.376
20	6.996	1.357	1.165	.318
30	8.126	1.399	1.183	.245
40	8.782	1.426	1.194	.198
50	9.000	1.447	1.203	.162
60	8.752	1.452	1.205	.131
70	7.904	1.421	1.192	.102
80	6.298	1.306	1.143	.078
90	3.776	1.051	1.025	.042
95	2.122	.837	.915	.024
100	.180	0	0	0

L. E. radius: 1.584 percent c

NACA 16-021 BASIC THICKNESS FORM

x (percent c)	y (percent c)	$(v/V)^2$	v/V	$\Delta r_c/V$
0	0	0	0	1.574
1.25	2.261	.826	.909	1.059
2.5	3.159	1.062	1.031	.828
5.0	4.391	1.221	1.105	.610
7.5	5.306	1.295	1.138	.504
10	6.050	1.342	1.159	.433
15	7.236	1.391	1.179	.374
20	8.162	1.419	1.191	.317
30	9.450	1.474	1.214	.245
40	10.246	1.506	1.227	.198
50	10.500	1.535	1.239	.162
60	10.211	1.536	1.239	.131
70	9.221	1.495	1.223	.102
80	7.348	1.351	1.166	.079
90	4.405	1.039	1.019	.041
95	2.476	.801	.895	.023
100	.210	0	0	0

L. E. radius: 2.156 percent c

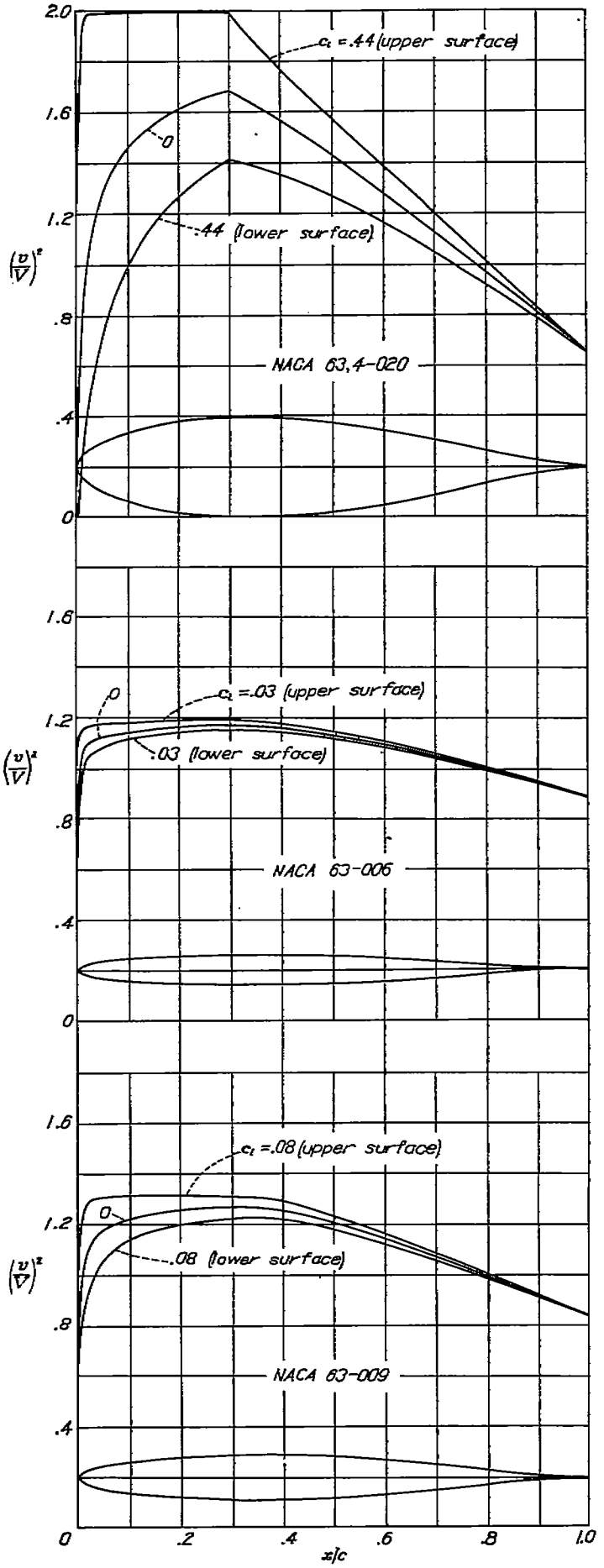

NACA 63,4-020 BASIC THICKNESS FORM

x (percent c)	y (percent c)	$(v/V)^2$	v/V	$\Delta s_d/V$
0	0	0	0	1.395
.5	1.714	.444	.666	1.280
.75	2.081	.605	.778	1.201
1.25	2.638	.820	.906	1.072
2.5	3.606	1.080	1.039	.846
5.0	4.947	1.277	1.130	.645
7.5	5.964	1.383	1.176	.543
10	6.800	1.456	1.207	.475
15	8.090	1.551	1.245	.386
20	9.006	1.614	1.270	.330
25	9.630	1.659	1.288	.289
30	9.955	1.689	1.300	.257
35	9.978	1.630	1.277	.219
40	9.765	1.567	1.252	.192
45	9.366	1.500	1.225	.169
50	8.819	1.433	1.197	.148
55	8.143	1.362	1.167	.128
60	7.351	1.288	1.135	.112
65	6.464	1.213	1.101	.097
70	5.496	1.137	1.066	.084
75	4.466	1.059	1.029	.071
80	3.401	.978	.989	.059
85	2.342	.896	.947	.046
90	1.348	.811	.901	.036
95	.501	.728	.853	.023
100	0	.661	.807	0

L. E. radius: 3.16 percent c

NACA 63-006 BASIC THICKNESS FORM

x (percent c)	y (percent c)	$(v/V)^2$	v/V	$\Delta s_d/V$
0	0	0	0	4.453
.5	.503	.973	.986	2.110
.75	.609	1.050	1.025	1.778
1.25	.771	1.080	1.039	1.399
2.5	1.057	1.110	1.054	.981
5	1.482	1.130	1.063	.692
7.5	1.796	1.142	1.069	.562
10	2.010	1.149	1.072	.484
15	2.386	1.159	1.077	.384
20	2.656	1.165	1.079	.321
25	2.841	1.170	1.082	.279
30	2.954	1.174	1.084	.245
35	3.000	1.170	1.082	.218
40	2.971	1.164	1.079	.196
45	2.877	1.161	1.073	.176
50	2.723	1.137	1.066	.158
55	2.517	1.118	1.057	.141
60	2.267	1.096	1.047	.125
65	1.982	1.074	1.036	.111
70	1.670	1.046	1.023	.093
75	1.342	1.020	1.010	.085
80	1.008	.994	.997	.073
85	.683	.965	.982	.060
90	.383	.936	.967	.047
95	.138	.910	.954	.032
100	0	.886	.941	0

L. E. radius: 0.297 percent c

NACA 63-009 BASIC THICKNESS FORM

x (percent c)	y (percent c)	$(v/V)^2$	v/V	$\Delta s_d/V$
0	0	0	0	3.058
.5	.749	.885	.941	1.889
.75	.906	1.002	1.001	1.647
1.25	1.151	1.051	1.025	1.339
2.5	1.582	1.130	1.063	.961
5	2.196	1.180	1.086	.689
7.5	2.655	1.205	1.098	.560
10	3.024	1.221	1.105	.484
15	3.591	1.241	1.114	.386
20	3.997	1.256	1.120	.324
25	4.275	1.264	1.124	.281
30	4.442	1.269	1.126	.248
35	4.500	1.265	1.125	.220
40	4.447	1.255	1.120	.196
45	4.296	1.235	1.111	.175
50	4.056	1.208	1.099	.156
55	3.739	1.175	1.084	.140
60	3.358	1.141	1.068	.124
65	2.928	1.104	1.051	.109
70	2.458	1.065	1.032	.095
75	1.966	1.025	1.012	.082
80	1.471	.984	.992	.069
85	.990	.942	.971	.057
90	.550	.903	.950	.044
95	.196	.868	.932	.030
100	0	.838	.915	0

L. E. radius: 0.631 percent c

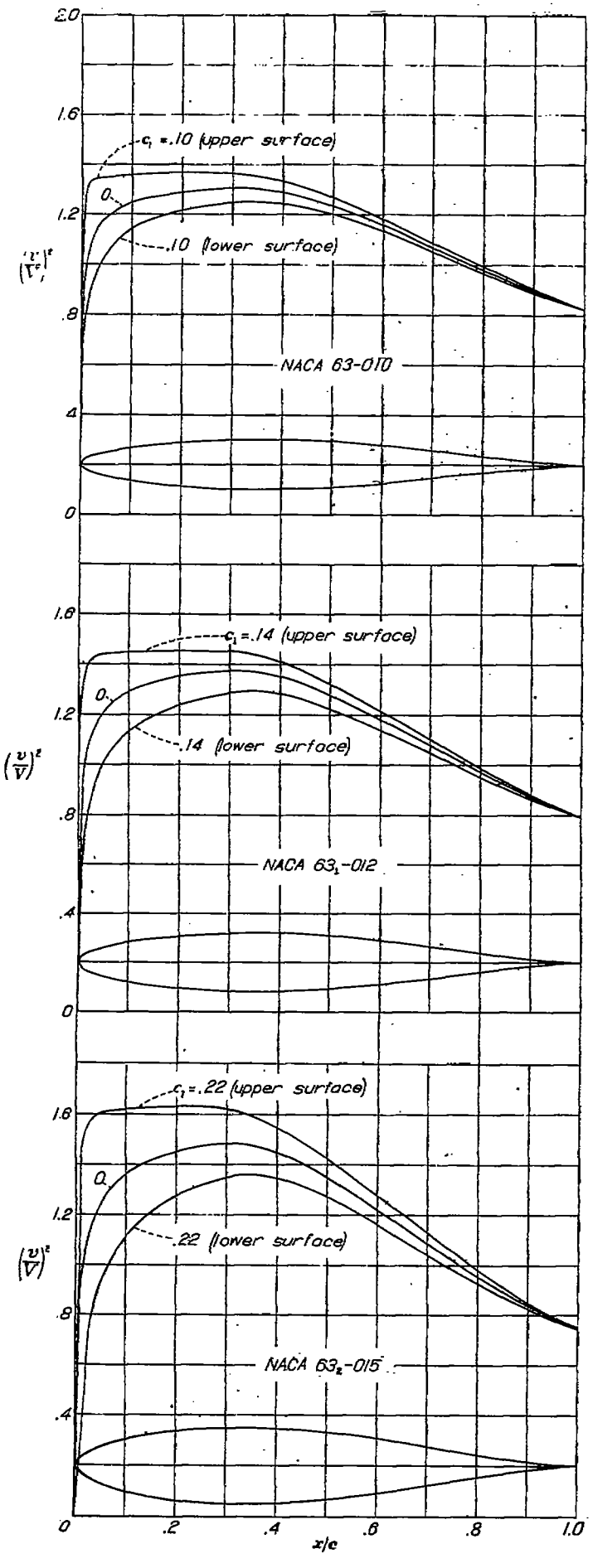

NACA 63-010 BASIC THICKNESS FORM

x (percent c)	y (percent c)	$(v/V)^2$	v/V	$\Delta v_a/V$
0	0	0	0	2.775
.5	.829	.841	.917	1.825
.75	1.004	.978	.989	1.603
1.25	1.275	1.037	1.018	1.316
2.5	1.756	1.131	1.063	.952
5.0	2.440	1.193	1.092	.657
7.5	2.960	1.223	1.106	.500
10	3.362	1.245	1.116	.484
15	3.994	1.270	1.127	.396
20	4.445	1.285	1.134	.325
25	4.753	1.296	1.138	.272
30	4.938	1.302	1.141	.218
35	5.000	1.299	1.140	.220
40	4.938	1.286	1.134	.193
45	4.766	1.262	1.123	.178
50	4.496	1.231	1.110	.156
55	4.140	1.193	1.092	.139
60	3.715	1.154	1.074	.123
65	3.234	1.113	1.055	.108
70	2.712	1.069	1.034	.094
75	2.166	1.025	1.012	.081
80	1.618	.979	.989	.069
85	1.088	.935	.967	.056
90	.604	.893	.945	.043
95	.214	.853	.924	.030
100	0	.822	.937	0

L. E. radius: 0.770 percent c

NACA 63$_1$-012 BASIC THICKNESS FORM

x (percent c)	y (percent c)	$(v/V)^2$	v/V	$\Delta v_a/V$
0	0	0	0	2.336
.5	.935	.750	.866	1.695
.75	1.194	.825	.902	1.513
1.25	1.519	1.005	1.003	1.256
2.5	2.102	1.129	1.063	.933
5	2.925	1.217	1.103	.682
7.5	3.542	1.261	1.123	.559
10	4.039	1.294	1.138	.481
15	4.799	1.330	1.153	.387
20	5.342	1.349	1.161	.328
25	5.712	1.362	1.167	.283
30	5.930	1.370	1.170	.249
35	6.000	1.368	1.169	.221
40	5.920	1.348	1.161	.196
45	5.704	1.317	1.148	.174
50	5.370	1.276	1.130	.155
55	4.935	1.229	1.109	.137
60	4.420	1.181	1.087	.121
65	3.840	1.131	1.063	.106
70	3.210	1.076	1.037	.091
75	2.556	1.023	1.011	.079
80	1.902	.969	.984	.067
85	1.274	.920	.959	.055
90	.707	.871	.933	.042
95	.250	.826	.909	.029
100	0	.791	.889	0

L. E. radius: 1.087 percent c

NACA 63$_2$-015 BASIC THICKNESS FORM

x (percent c)	y (percent c)	$(v/V)^2$	v/V	$\Delta v_a/V$
0	0	0	0	1.918
.5	1.204	.600	.775	1.613
.75	1.462	.822	.907	1.379
1.25	1.878	.938	.969	1.182
2.5	2.610	1.105	1.051	.903
5	3.648	1.244	1.115	.674
7.5	4.427	1.315	1.147	.557
10	5.055	1.360	1.166	.484
15	6.011	1.415	1.190	.388
20	6.663	1.446	1.202	.330
25	7.155	1.467	1.211	.286
30	7.421	1.481	1.217	.251
35	7.500	1.475	1.214	.222
40	7.396	1.446	1.202	.196
45	7.099	1.401	1.184	.174
50	6.665	1.345	1.160	.153
55	6.108	1.281	1.132	.135
60	5.453	1.220	1.105	.118
65	4.721	1.155	1.075	.102
70	3.934	1.085	1.042	.088
75	3.119	1.019	1.009	.076
80	2.310	.953	.976	.063
85	1.541	.894	.946	.051
90	.852	.839	.916	.039
95	.300	.789	.888	.026
100	0	.750	.866	0

L. E. radius: 1.594 percent c

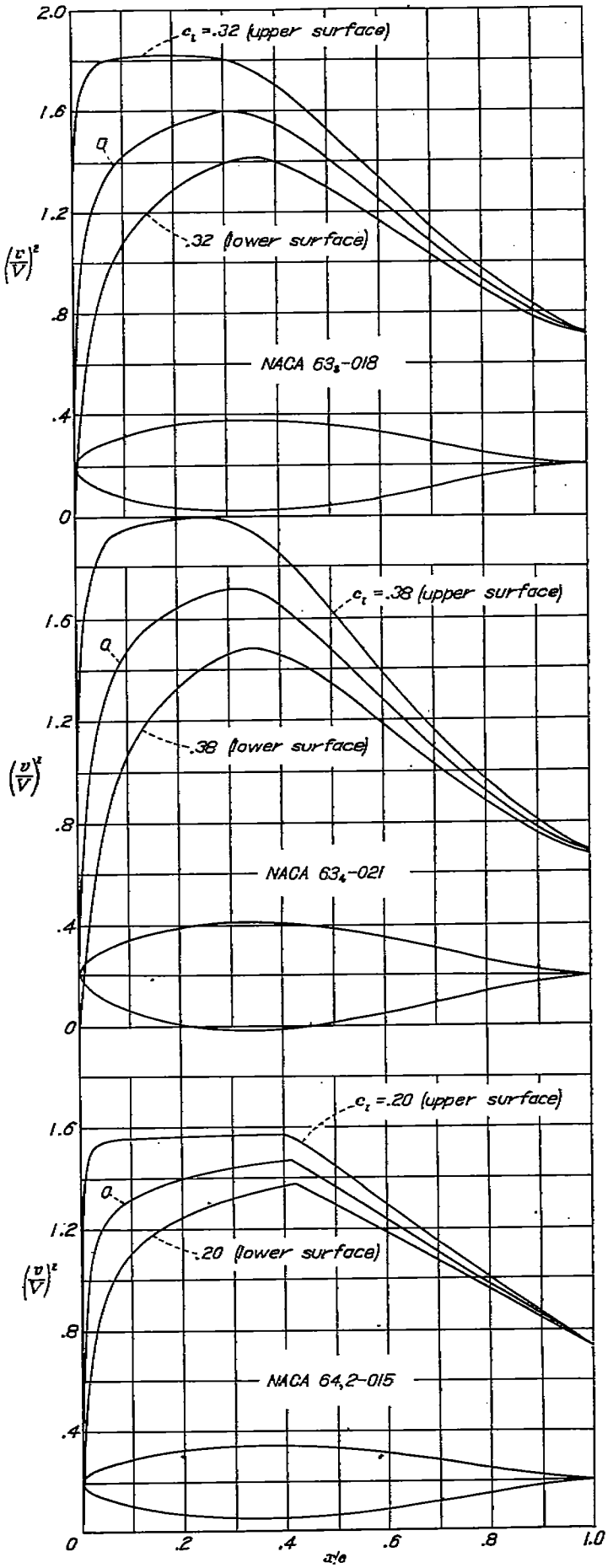

NACA 63$_3$-018 BASIC THICKNESS FORM

x (percent c)	y (percent c)	$(v/V)^2$	v/V	$\Delta p_a/V$
0	0	0	0	1.639
.5	1.404	.441	.664	1.361
.75	1.713	.700	.837	1.258
1.25	2.217	.848	.921	1.105
2.5	3.104	1.065	1.032	.871
5	4.362	1.260	1.122	.663
7.5	5.308	1.360	1.166	.553
10	6.068	1.424	1.193	.484
15	7.225	1.500	1.225	.390
20	8.048	1.547	1.244	.333
25	8.600	1.579	1.257	.292
30	8.913	1.598	1.264	.253
35	9.000	1.585	1.259	.223
40	8.845	1.550	1.245	.197
45	8.482	1.490	1.221	.173
50	7.942	1.411	1.188	.152
55	7.256	1.330	1.153	.133
60	6.455	1.252	1.119	.115
65	5.567	1.170	1.082	.099
70	4.622	1.087	1.043	.084
75	3.650	1.009	1.004	.072
80	2.691	.933	.966	.059
85	1.787	.868	.932	.048
90	.985	.807	.898	.036
95	.348	.753	.868	.024
100	0	.712	.844	0

L. E. radius: 2.120 percent c

NACA 63$_4$-021 BASIC THICKNESS FORM

x (percent c)	y (percent c)	$(v/V)^2$	v/V	$\Delta p_a/V$
0	0	0	0	1.439
.5	1.583	.275	.524	1.236
.75	1.937	.564	.751	1.126
1.25	2.527	.725	.851	1.034
2.5	3.577	1.010	1.005	.842
5	5.065	1.260	1.122	.653
7.5	6.182	1.394	1.181	.550
10	7.080	1.487	1.219	.484
15	8.441	1.592	1.262	.392
20	9.410	1.655	1.286	.335
25	10.053	1.698	1.303	.291
30	10.412	1.721	1.312	.255
35	10.500	1.709	1.307	.225
40	10.298	1.654	1.286	.198
45	9.854	1.578	1.256	.173
50	9.206	1.479	1.216	.150
55	8.390	1.380	1.175	.130
60	7.441	1.281	1.132	.112
65	6.396	1.180	1.086	.096
70	5.290	1.084	1.041	.081
75	4.160	.994	.997	.068
80	3.054	.911	.954	.057
85	2.021	.839	.916	.046
90	1.113	.774	.880	.035
95	.392	.721	.849	.023
100	0	.676	.822	0

L. E. radius: 2.650 percent c

NACA 64,2-015 BASIC THICKNESS FORM

x (percent c)	y (percent c)	$(v/V)^2$	v/V	$\Delta p_a/V$
0	0	0	0	1.930
.5	1.216	.710	.843	1.500
.75	1.453	.825	.908	1.359
1.25	1.829	.962	.981	1.161
2.5	2.538	1.122	1.059	.911
5.0	3.514	1.234	1.111	.678
7.5	4.243	1.288	1.135	.553
10	4.838	1.323	1.150	.477
15	5.781	1.371	1.171	.383
20	6.464	1.401	1.184	.325
25	6.967	1.422	1.192	.285
30	7.307	1.441	1.200	.253
35	7.481	1.458	1.207	.227
40	7.480	1.471	1.213	.202
45	7.268	1.432	1.197	.175
50	6.850	1.366	1.169	.156
55	6.311	1.299	1.140	.137
60	5.670	1.234	1.111	.122
65	4.944	1.168	1.081	.102
70	4.158	1.102	1.050	.086
75	3.338	1.039	1.019	.080
80	2.506	.973	.986	.071
85	1.693	.910	.954	.056
90	.961	.849	.921	.039
95	.351	.791	.889	.027
100	0	.739	.860	0

L. E. radius: 1.65 percent c

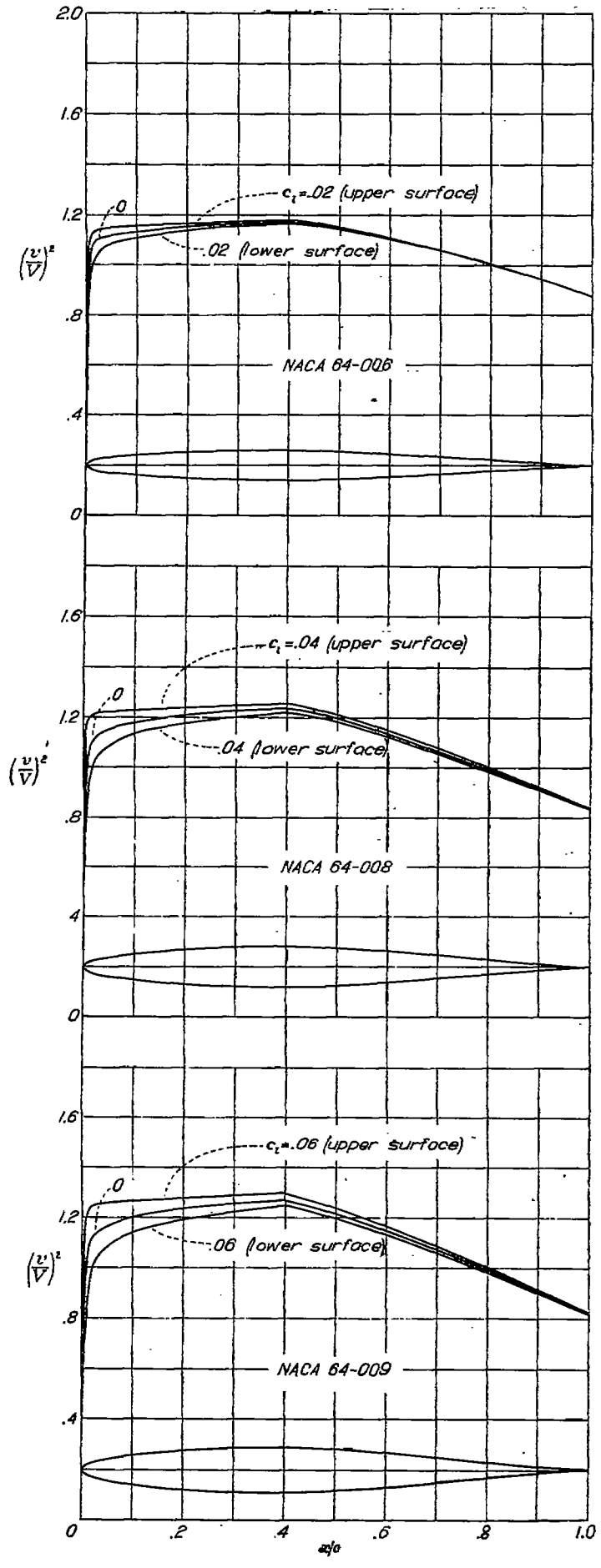

NACA 64-006 BASIC THICKNESS FORM

x (percent c)	y (percent c)	$(v/V)^2$	v/V	$\Delta p_a/V$
0	0	0	0	4.623
.5	.494	.995	.997	2.175
.75	.596	1.058	1.029	1.780
1.25	.754	1.085	1.042	1.418
2.5	1.024	1.108	1.053	.982
5.0	1.405	1.119	1.058	.692
7.5	1.692	1.128	1.062	.500
10	1.928	1.134	1.065	.433
15	2.298	1.146	1.071	.385
20	2.572	1.154	1.074	.321
25	2.772	1.160	1.077	.279
30	2.907	1.164	1.079	.246
35	2.981	1.168	1.081	.220
40	2.995	1.171	1.082	.198
45	2.919	1.160	1.077	.178
50	2.775	1.143	1.069	.158
55	2.575	1.124	1.060	.142
60	2.331	1.102	1.050	.126
65	2.050	1.079	1.039	.112
70	1.740	1.054	1.027	.098
75	1.412	1.028	1.014	.085
80	1.072	1.000	1.000	.079
85	.737	.970	.985	.060
90	.423	.939	.969	.047
95	.187	.908	.953	.031
100	0	.876	.936	0

L. E. radius: 0.256 percent c

NACA 64-008 BASIC THICKNESS FORM

x (percent c)	y (percent c)	$(v/V)^2$	v/V	$\Delta p_a/V$
0	0	0	0	3.514
.5	.658	.912	.955	1.924
.75	.794	1.016	1.008	1.656
1.25	1.005	1.084	1.041	1.307
2.5	1.365	1.127	1.062	.909
5.0	1.875	1.152	1.073	.638
7.5	2.259	1.167	1.080	.500
10	2.574	1.179	1.086	.430
15	3.069	1.195	1.093	.385
20	3.437	1.208	1.099	.323
25	3.704	1.217	1.103	.279
30	3.884	1.225	1.107	.246
35	3.979	1.230	1.109	.220
40	3.992	1.235	1.111	.198
45	3.883	1.220	1.105	.176
50	3.684	1.191	1.091	.158
55	3.411	1.163	1.078	.141
60	3.081	1.133	1.064	.125
65	2.704	1.102	1.050	.110
70	2.291	1.069	1.034	.096
75	1.854	1.033	1.016	.083
80	1.404	.995	.997	.071
85	.961	.957	.978	.059
90	.550	.918	.958	.046
95	.206	.878	.937	.031
100	0	.839	.916	0

L. E. radius: 0.455 percent c

NACA 64-009 BASIC THICKNESS FORM

x (percent c)	y (percent c)	$(v/V)^2$	v/V	$\Delta p_a/V$
0	0	0	0	3.130
.5	.739	.872	.934	1.905
.75	.892	.990	.995	1.537
1.25	1.128	1.075	1.037	1.310
2.5	1.533	1.131	1.063	.903
5.0	2.109	1.166	1.080	.636
7.5	2.543	1.186	1.089	.500
10	2.898	1.200	1.095	.479
15	3.455	1.221	1.105	.383
20	3.868	1.236	1.112	.323
25	4.170	1.246	1.116	.281
30	4.373	1.256	1.120	.248
35	4.479	1.262	1.123	.221
40	4.490	1.267	1.126	.198
45	4.364	1.246	1.116	.176
50	4.136	1.217	1.103	.158
55	3.826	1.183	1.088	.140
60	3.452	1.149	1.072	.125
65	3.026	1.112	1.055	.109
70	2.561	1.073	1.036	.095
75	2.069	1.033	1.016	.082
80	1.564	.992	.996	.070
85	1.059	.950	.975	.057
90	.611	.907	.952	.044
95	.237	.865	.930	.030
100	0	.822	.907	0

L. E. radius: 0.579 percent c

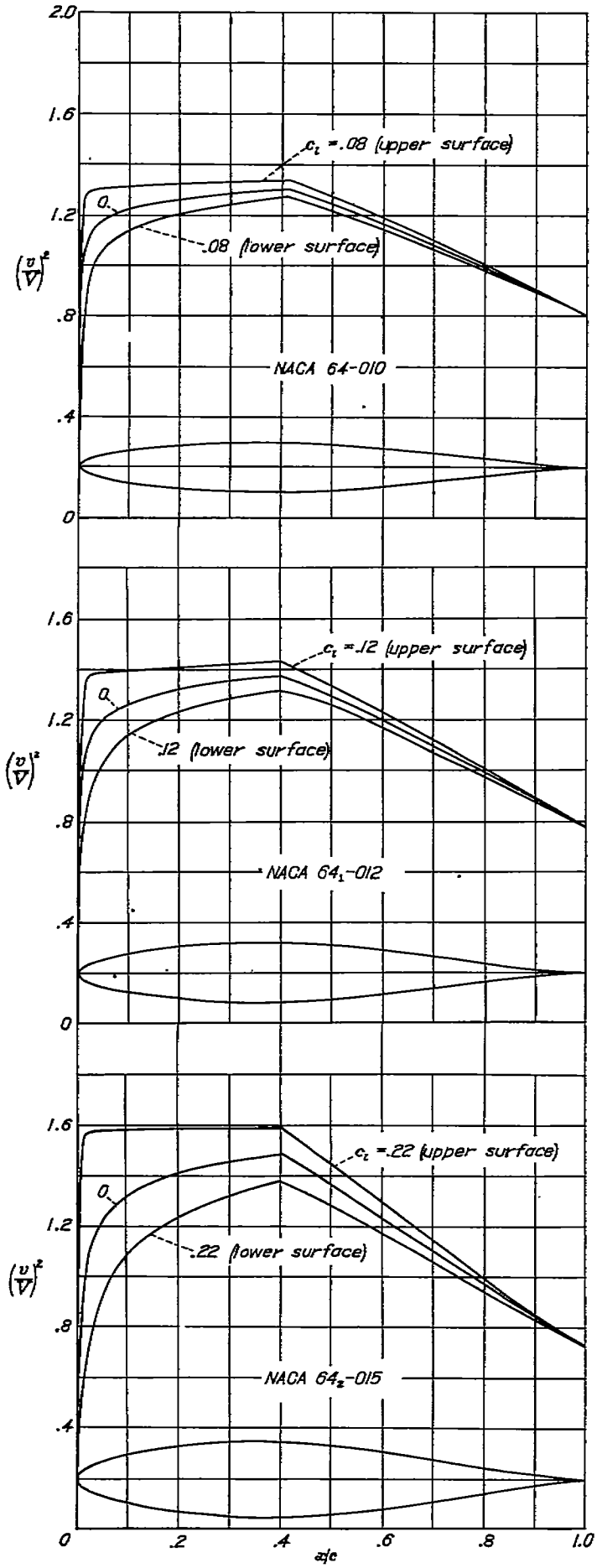

NACA 64-010 BASIC THICKNESS FORM

x (percent c)	y (percent c)	$(v/V)^2$	v/V	$\Delta v_a/V$
0	0	0	0	2.815
.5	.820	.834	.913	1.817
.75	.989	.962	.981	1.586
1.25	1.250	1.061	1.030	1.313
2.5	1.701	1.130	1.063	.957
5	2.343	1.181	1.087	.684
7.5	2.826	1.206	1.098	.559
10	3.221	1.221	1.105	.480
15	3.842	1.245	1.116	.386
20	4.302	1.262	1.123	.325
25	4.639	1.275	1.129	.280
30	4.864	1.286	1.134	.246
35	4.980	1.295	1.138	.220
40	4.988	1.300	1.140	.199
45	4.843	1.279	1.131	.176
50	4.536	1.241	1.114	.158
55	4.238	1.201	1.096	.139
60	3.820	1.161	1.077	.124
65	3.345	1.120	1.058	.109
70	2.827	1.080	1.039	.096
75	2.281	1.036	1.018	.081
80	1.722	.990	.995	.069
85	1.176	.944	.972	.057
90	.671	.900	.949	.044
95	.248	.850	.922	.030
100	0	.805	.897	0

L. E. radius: 0.720 percent c

NACA 64_1-012 BASIC THICKNESS FORM

x (percent c)	y (percent c)	$(v/V)^2$	v/V	$\Delta v_a/V$
0	0	0	0	2.379
.5	.978	.750	.866	1.663
.75	1.179	.885	.941	1.508
1.25	1.490	1.020	1.010	1.271
2.5	2.035	1.129	1.063	.943
5.0	2.810	1.204	1.097	.685
7.5	3.394	1.240	1.114	.559
10	3.871	1.264	1.124	.482
15	4.620	1.296	1.139	.388
20	5.173	1.320	1.149	.328
25	5.576	1.338	1.156	.281
30	5.844	1.351	1.162	.247
35	5.978	1.362	1.167	.221
40	5.981	1.372	1.171	.199
45	5.798	1.335	1.156	.177
50	5.450	1.289	1.136	.158
55	5.056	1.243	1.115	.138
60	4.548	1.195	1.093	.122
65	3.974	1.144	1.070	.103
70	3.350	1.091	1.044	.088
75	2.695	1.037	1.018	.074
80	2.029	.981	.990	.063
85	1.382	.928	.963	.052
90	.786	.874	.935	.045
95	.288	.825	.908	.028
100	0	.775	.880	0

L. E. radius: 1.040 percent c

NACA 64_2-015 BASIC THICKNESS FORM

x (percent c)	y (percent c)	$(v/V)^2$	v/V	$\Delta v_a/V$
0	0	0	0	1.939
.5	1.208	.670	.819	1.476
.75	1.456	.762	.873	1.354
1.25	1.842	.896	.947	1.188
2.5	2.528	1.113	1.055	.916
5.0	3.504	1.231	1.109	.670
7.5	4.240	1.284	1.133	.559
10	4.842	1.323	1.150	.482
15	5.785	1.375	1.172	.389
20	6.480	1.410	1.187	.326
25	6.955	1.434	1.198	.285
30	7.319	1.454	1.206	.250
35	7.482	1.470	1.213	.225
40	7.473	1.495	1.218	.202
45	7.224	1.426	1.195	.179
50	6.810	1.365	1.168	.158
55	6.266	1.300	1.140	.135
60	5.620	1.233	1.110	.121
65	4.895	1.167	1.080	.105
70	4.113	1.101	1.049	.090
75	3.296	1.033	1.016	.078
80	2.472	.967	.983	.065
85	1.677	.902	.950	.054
90	.950	.841	.917	.041
95	.346	.785	.886	.031
100	0	.730	.855	0

L. E. radius: 1.590 percent c

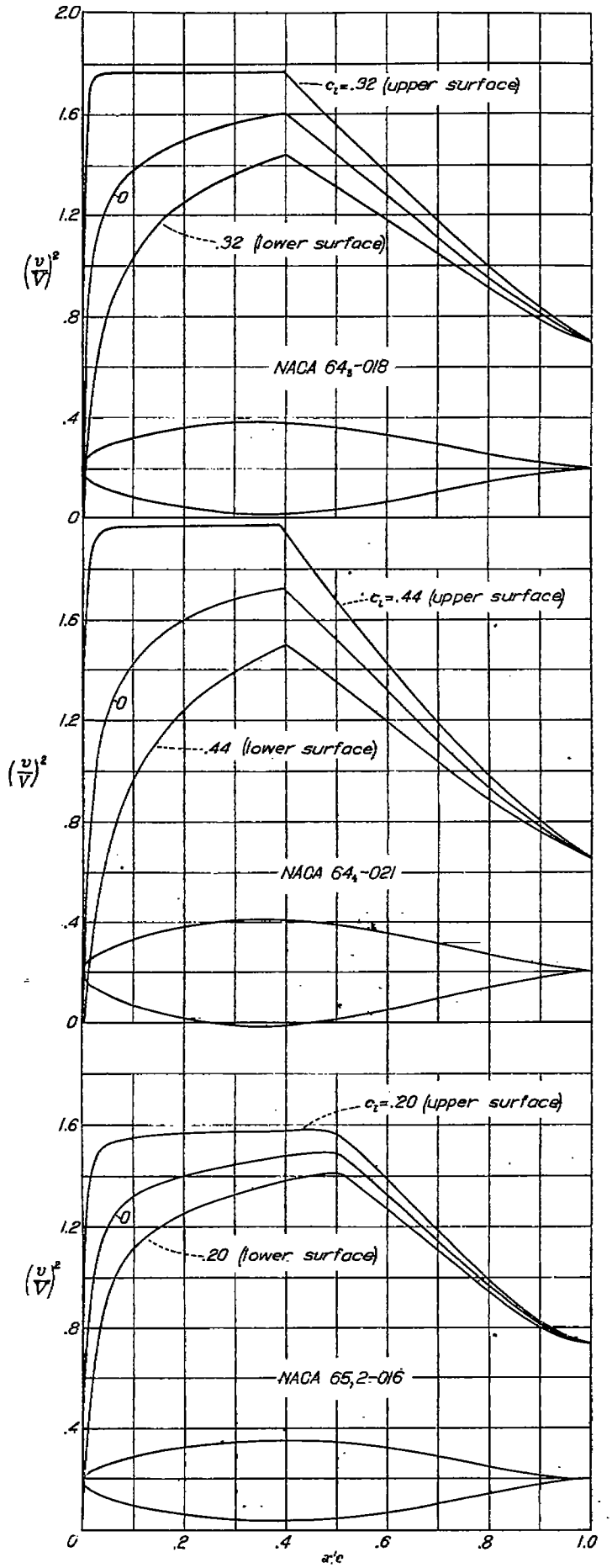

NACA 64$_3$-018 BASIC THICKNESS FORM

x (percent c)	y (percent c)	$(y/l')^2$	y/l'	$\Delta r_a/l'$
0	0	0	0	1.616
.5	1.428	.546	.739	1.360
.75	1.720	.705	.840	1.269
1.25	2.177	.802	.920	1.128
2.5	3.005	1.079	1.039	.904
5.0	4.186	1.244	1.115	.669
7.5	5.076	1.327	1.152	.558
10	5.803	1.350	1.175	.486
15	6.942	1.450	1.204	.391
20	7.782	1.497	1.224	.331
25	8.391	1.535	1.239	.288
30	8.789	1.562	1.250	.256
35	8.979	1.585	1.259	.228
40	8.952	1.600	1.265	.200
45	8.030	1.518	1.232	.177
50	8.114	1.436	1.198	.154
55	7.445	1.354	1.164	.134
60	6.658	1.272	1.128	.117
65	5.782	1.190	1.091	.102
70	4.842	1.109	1.053	.088
75	3.866	1.028	1.014	.074
80	2.888	.952	.976	.063
85	1.951	.879	.937	.051
90	1.101	.812	.901	.039
95	.400	.747	.864	.027
100	0	.695	.834	0

L. E. radius: 2.208 percent c

NACA 64$_4$-021 BASIC THICKNESS FORM

x (percent c)	y (percent c)	$(y/l')^2$	y/l'	$\Delta r_a/l'$
0	0	0	0	1.488
.5	1.646	.462	.680	1.274
.75	1.985	.603	.776	1.203
1.25	2.517	.759	.871	1.084
2.5	3.495	1.010	1.005	.878
5.0	4.871	1.248	1.117	.665
7.5	5.916	1.358	1.165	.557
10	6.709	1.431	1.196	.480
15	8.108	1.527	1.236	.395
20	9.096	1.593	1.262	.336
25	9.807	1.654	1.281	.293
30	10.269	1.681	1.297	.259
35	10.481	1.712	1.308	.232
40	10.431	1.709	1.307	.202
45	10.030	1.607	1.268	.178
50	9.404	1.507	1.228	.155
55	8.607	1.406	1.186	.134
60	7.678	1.307	1.143	.116
65	6.649	1.209	1.099	.099
70	5.549	1.112	1.055	.084
75	4.416	1.020	1.010	.071
80	3.287	.932	.965	.059
85	2.213	.851	.923	.047
90	1.245	.778	.882	.036
95	.449	.711	.844	.022
100	0	.653	.808	0

L. E. radius: 2.584 percent c

NACA 65,2-016 BASIC THICKNESS FORM

x (percent c)	y (percent c)	$(y/l')^2$	y/l'	$\Delta r_a/l'$
0	0	0	0	1.950
.5	1.202	.500	.718	1.650
.75	1.423	.690	.831	1.500
1.25	1.796	.842	.918	1.275
2.5	2.507	1.068	1.033	.920
5.0	3.543	1.217	1.103	.680
7.5	4.316	1.287	1.134	.545
10	4.954	1.328	1.152	.450
15	5.958	1.379	1.174	.360
20	6.701	1.409	1.187	.328
25	7.262	1.433	1.197	.285
30	7.645	1.453	1.205	.256
35	7.892	1.469	1.212	.236
40	7.995	1.484	1.218	.200
45	7.938	1.497	1.224	.180
50	7.672	1.491	1.221	.160
55	7.184	1.421	1.192	.140
60	6.495	1.328	1.152	.125
65	5.647	1.235	1.111	.110
70	4.718	1.147	1.071	.095
75	3.738	1.056	1.028	.080
80	2.759	.970	.985	.065
85	1.817	.886	.941	.050
90	.932	.816	.903	.040
95	.340	.769	.877	.025
100	0	.733	.856	0

L. E. radius: 1.704 percent c

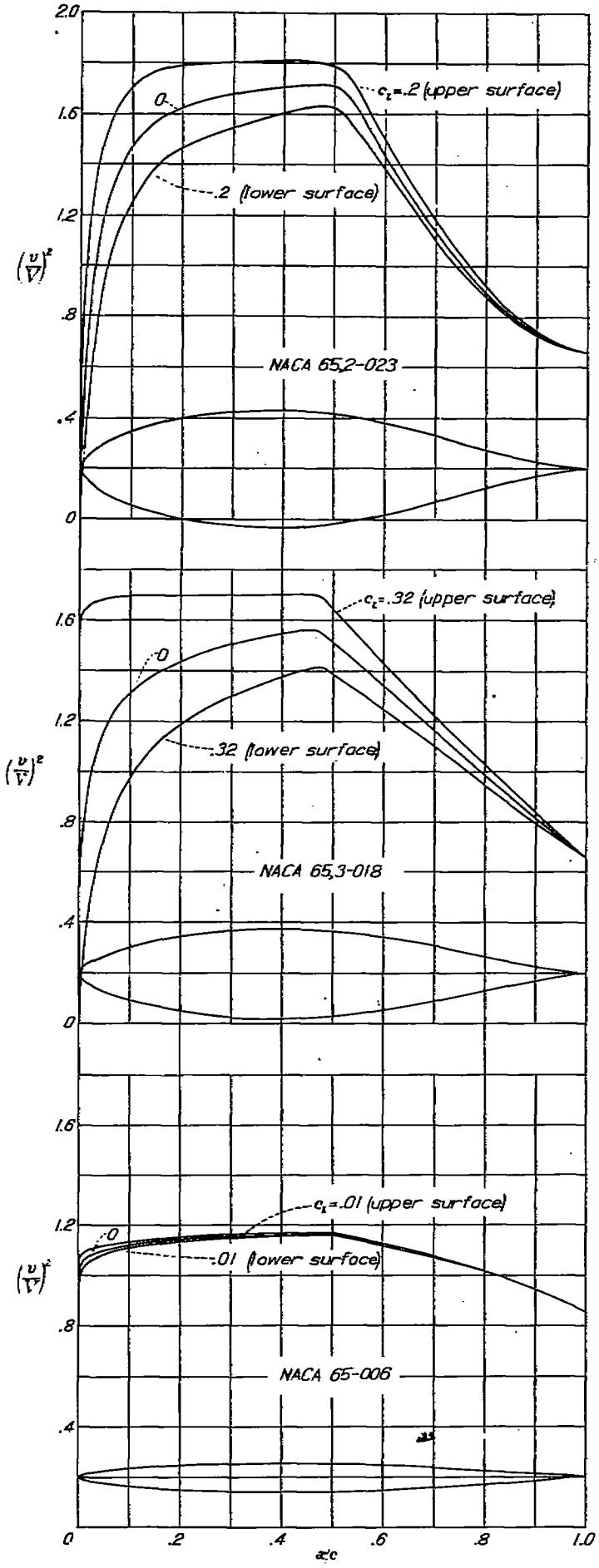

NACA 65,2-023 BASIC THICKNESS FORM

x (percent c)	y (percent c)	$(v/V)^2$	v/V	$\Delta x_s/V$
0	0	0	0	1.414
.5	1.664	.400	.632	1.161
.75	2.040	.500	.707	1.084
1.25	2.628	.632	.826	.967
2.5	3.715	.943	.971	.811
5.0	5.300	1.232	1.110	.633
7.5	6.478	1.375	1.173	.539
10	7.433	1.467	1.211	.479
15	8.889	1.577	1.256	.390
20	9.917	1.628	1.276	.324
25	10.648	1.655	1.286	.281
30	11.142	1.677	1.295	.247
35	11.423	1.694	1.302	.220
40	11.499	1.708	1.307	.198
45	11.361	1.716	1.310	.178
50	10.949	1.712	1.308	.161
55	10.179	1.606	1.267	.147
60	9.108	1.428	1.195	.110
65	7.845	1.274	1.129	.096
70	6.461	1.135	1.065	.093
75	5.015	1.003	1.001	.090
80	3.618	.893	.945	.053
85	2.345	.803	.896	.035
90	1.258	.732	.856	.022
95	.439	.682	.826	.018
100	0	.651	.807	0

L. E. radius: 2.955 percent c

NACA 65,3-018 BASIC THICKNESS FORM

x (percent c)	y (percent c)	$(v/V)^2$	v/V	$\Delta x_s/V$
0	0	0	0	1.750
.5	1.324	.650	.806	1.387
.75	1.599	.760	.866	1.268
1.25	2.004	.872	.934	1.106
2.5	2.728	1.020	1.010	.890
5.0	3.831	1.179	1.086	.677
7.5	4.701	1.263	1.124	.568
10	5.424	1.320	1.149	.489
15	6.568	1.393	1.180	.395
20	7.434	1.439	1.200	.334
25	8.093	1.473	1.214	.292
30	8.568	1.502	1.226	.260
35	8.868	1.526	1.235	.232
40	8.990	1.546	1.243	.209
45	8.916	1.562	1.250	.186
50	8.598	1.513	1.230	.165
55	8.045	1.423	1.193	.142
60	7.317	1.348	1.161	.123
65	6.450	1.258	1.122	.107
70	5.456	1.169	1.081	.093
75	4.456	1.079	1.039	.080
80	3.390	.992	.996	.066
85	2.325	.905	.951	.054
90	1.324	.818	.904	.040
95	.492	.738	.859	.024
100	0	.658	.811	0

L. E. radius: 1.92 percent c

NACA 65-006 BASIC THICKNESS FORM

x (percent c)	y (percent c)	$(v/V)^2$	v/V	$\Delta x_s/V$
0	0	0	0	4.815
.5	.476	1.044	1.022	2.110
.75	.574	1.055	1.027	1.780
1.25	.717	1.063	1.031	1.390
2.5	.956	1.081	1.040	.965
5.0	1.310	1.100	1.049	.695
7.5	1.589	1.112	1.055	.560
10	1.824	1.120	1.058	.474
15	2.197	1.134	1.065	.381
20	2.482	1.143	1.069	.322
25	2.697	1.149	1.072	.281
30	2.852	1.155	1.075	.247
35	2.962	1.159	1.077	.220
40	2.998	1.163	1.078	.198
45	2.983	1.166	1.080	.178
50	2.900	1.165	1.079	.160
55	2.741	1.145	1.070	.144
60	2.518	1.124	1.060	.128
65	2.246	1.100	1.049	.114
70	1.935	1.073	1.036	.100
75	1.594	1.044	1.022	.086
80	1.233	1.013	1.006	.074
85	.865	.981	.990	.060
90	.510	.944	.972	.046
95	.195	.902	.950	.031
100	0	.858	.926	0

L. E. radius: 0.240 percent c

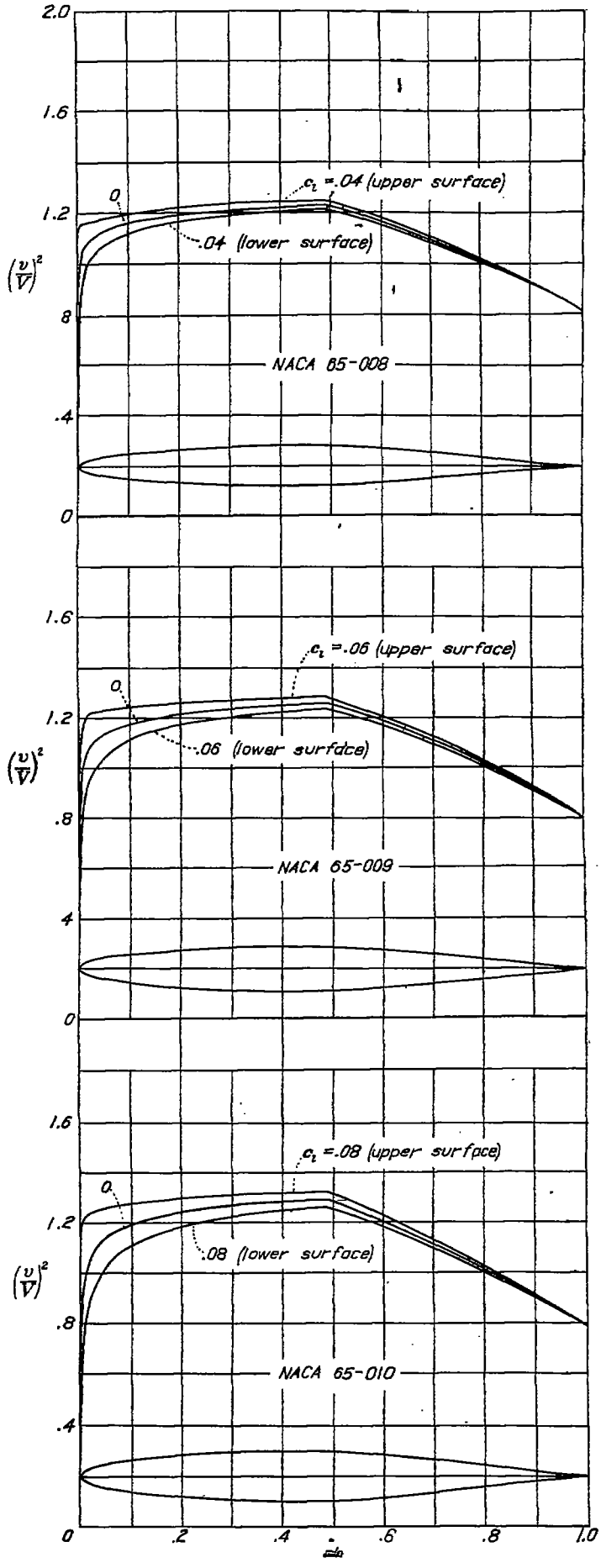

NACA 65-008 BASIC THICKNESS FORM

x (percent c)	y (percent c)	$(v/V)^2$	v/V	$\Delta r_s/V$
0	0	0	0	3.695
.5	.627	.978	.989	2.010
.75	.756	1.010	1.005	1.636
1.25	.945	1.043	1.021	1.340
2.5	1.267	1.086	1.042	.958
5.0	1.745	1.125	1.061	.689
7.5	2.118	1.145	1.070	.560
10	2.432	1.158	1.076	.477
15	2.931	1.178	1.085	.382
20	3.312	1.192	1.092	.323
25	3.599	1.203	1.097	.281
30	3.805	1.210	1.100	.248
35	3.938	1.217	1.103	.221
40	3.998	1.222	1.105	.199
45	3.974	1.226	1.107	.178
50	3.857	1.222	1.105	.160
55	3.638	1.193	1.092	.145
60	3.337	1.163	1.078	.128
65	2.971	1.130	1.063	.113
70	2.553	1.094	1.046	.098
75	2.096	1.055	1.027	.084
80	1.617	1.014	1.007	.072
85	1.131	.971	.985	.059
90	.664	.923	.961	.044
95	.262	.873	.934	.031
100	0	.817	.904	0

L. E. radius: 0.434 percent c

NACA 65-009 BASIC THICKNESS FORM

x (percent c)	y (percent c)	$(v/V)^2$	v/V	$\Delta r_s/V$
0	0	0	0	3.270
.5	.700	.945	.972	1.902
.75	.845	.985	.992	1.655
1.25	1.058	1.037	1.018	1.315
2.5	1.421	1.089	1.044	.930
5.0	1.961	1.134	1.065	.687
7.5	2.383	1.159	1.077	.560
10	2.736	1.177	1.085	.477
15	3.299	1.200	1.095	.382
20	3.727	1.216	1.103	.323
25	4.050	1.229	1.109	.280
30	4.282	1.238	1.113	.248
35	4.431	1.246	1.116	.220
40	4.496	1.252	1.119	.198
45	4.469	1.258	1.122	.178
50	4.338	1.250	1.118	.160
55	4.086	1.220	1.105	.144
60	3.743	1.185	1.089	.128
65	3.328	1.145	1.070	.111
70	2.856	1.103	1.050	.097
75	2.342	1.059	1.029	.084
80	1.805	1.013	1.006	.071
85	1.260	.963	.981	.059
90	.738	.912	.955	.044
95	.280	.856	.925	.030
100	0	.797	.893	0

L. E. radius: 0.552 percent c

NACA 65-010 BASIC THICKNESS FORM

x (percent c)	y (percent c)	$(v/V)^2$	v/V	$\Delta r_s/V$
0	0	0	0	2.967
.5	.772	.911	.954	1.911
.75	.932	.960	.980	1.614
1.25	1.169	1.025	1.012	1.292
2.5	1.574	1.085	1.042	.932
5.0	2.177	1.143	1.069	.679
7.5	2.647	1.177	1.085	.558
10	3.040	1.197	1.094	.490
15	3.666	1.224	1.106	.393
20	4.143	1.242	1.114	.321
25	4.503	1.257	1.121	.280
30	4.760	1.268	1.126	.248
35	4.924	1.277	1.130	.222
40	4.996	1.284	1.133	.199
45	4.963	1.290	1.136	.179
50	4.812	1.284	1.133	.160
55	4.530	1.244	1.115	.141
60	4.146	1.202	1.096	.126
65	3.682	1.158	1.076	.110
70	3.156	1.112	1.055	.097
75	2.584	1.062	1.031	.082
80	1.987	1.011	1.005	.070
85	1.385	.958	.979	.058
90	.810	.903	.950	.045
95	.306	.844	.919	.030
100	0	.781	.884	0

L. E. radius: 0.687 percent c

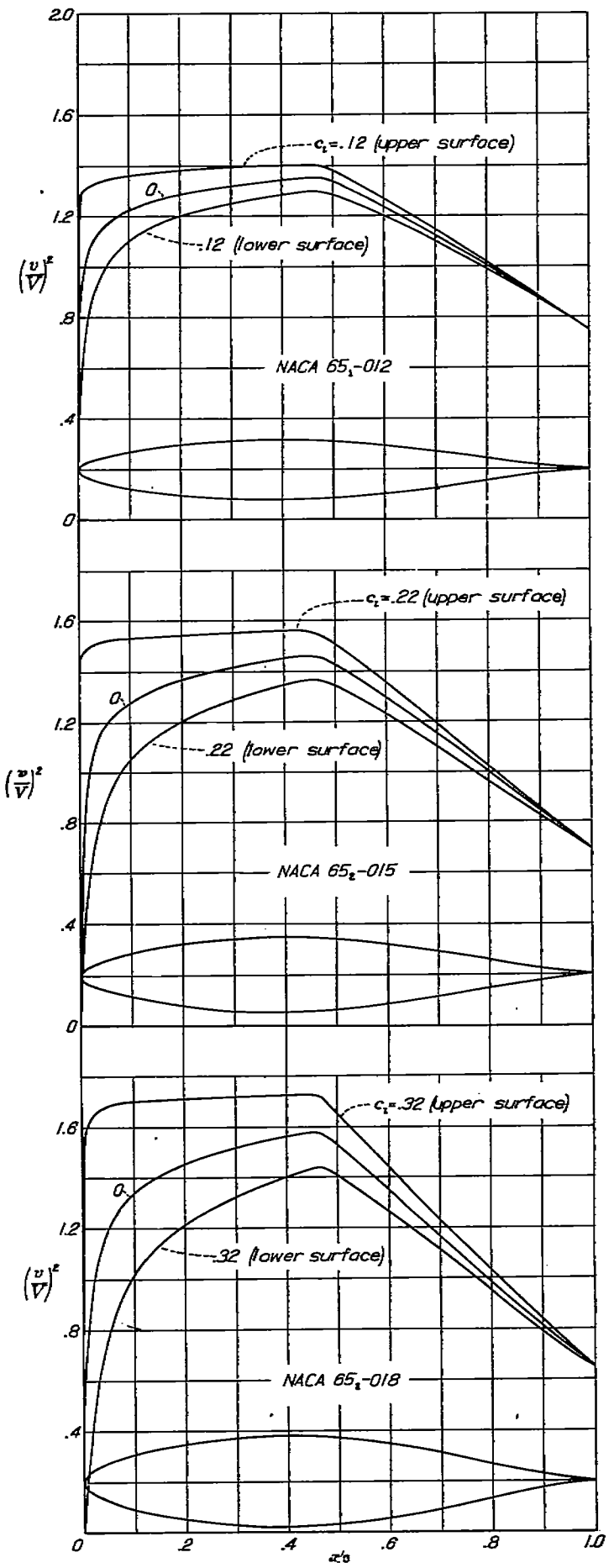

NACA 65$_1$-012 BASIC THICKNESS FORM

x (percent c)	y (percent c)	$(v/V)^2$	v/V	$\Delta x_s/V$
0	0	0	0	2.444
.5	.923	.848	.921	1.776
.75	1.109	.935	.967	1.465
1.25	1.357	1.000	1.000	1.200
2.5	1.875	1.082	1.040	.931
5.0	2.603	1.162	1.078	.702
7.5	3.172	1.201	1.096	.568
10	3.647	1.232	1.110	.480
15	4.402	1.268	1.126	.359
20	4.975	1.295	1.138	.326
25	5.403	1.316	1.147	.262
30	5.716	1.332	1.154	.251
35	5.912	1.343	1.159	.223
40	5.997	1.350	1.162	.204
45	5.949	1.357	1.165	.188
50	5.757	1.343	1.159	.169
55	5.412	1.295	1.138	.145
60	4.943	1.243	1.115	.127
65	4.381	1.188	1.090	.111
70	3.743	1.134	1.065	.094
75	3.059	1.073	1.036	.074
80	2.345	1.010	1.005	.062
85	1.630	.949	.974	.049
90	.947	.884	.940	.038
95	.356	.819	.905	.025
100	0	.748	.865	0

L. E. radius: 1.000 percent c

NACA 65$_2$-015 BASIC THICKNESS FORM

x (percent c)	y (percent c)	$(v/V)^2$	v/V	$\Delta x_s/V$
0	0	0	0	2.038
.5	1.124	.654	.809	1.729
.75	1.356	.817	.904	1.390
1.25	1.702	.939	.969	1.156
2.5	2.324	1.063	1.031	.920
5.0	3.245	1.184	1.088	.682
7.5	3.959	1.241	1.114	.563
10	4.555	1.281	1.132	.487
15	5.504	1.336	1.156	.393
20	6.223	1.374	1.172	.334
25	6.764	1.397	1.182	.290
30	7.182	1.418	1.191	.255
35	7.396	1.438	1.199	.227
40	7.498	1.452	1.205	.203
45	7.427	1.464	1.210	.184
50	7.168	1.433	1.197	.160
55	6.720	1.369	1.170	.143
60	6.118	1.297	1.139	.127
65	5.403	1.228	1.108	.109
70	4.600	1.151	1.073	.096
75	3.744	1.077	1.038	.078
80	2.858	1.002	1.001	.068
85	1.977	.924	.961	.052
90	1.144	.846	.920	.038
95	.428	.773	.879	.026
100	0	.697	.835	0

L. E. radius: 1.505 percent c

NACA 65$_3$-018 BASIC THICKNESS FORM

x (percent c)	y (percent c)	$(v/V)^2$	v/V	$\Delta x_s/V$
0	0	0	0	1.746
.5	1.337	.625	.791	1.437
.75	1.608	.702	.838	1.302
1.25	2.014	.817	.904	1.123
2.5	2.751	1.020	1.010	.858
5.0	3.866	1.192	1.092	.650
7.5	4.733	1.275	1.129	.542
10	5.457	1.329	1.153	.474
15	6.606	1.402	1.184	.385
20	7.476	1.452	1.205	.327
25	8.129	1.488	1.220	.285
30	8.595	1.515	1.231	.251
35	8.886	1.539	1.241	.225
40	8.999	1.561	1.249	.203
45	8.901	1.578	1.256	.182
50	8.568	1.526	1.235	.157
55	8.008	1.440	1.200	.137
60	7.267	1.353	1.163	.118
65	6.395	1.262	1.123	.104
70	5.426	1.170	1.082	.087
75	4.396	1.076	1.037	.074
80	3.338	.985	.992	.062
85	2.295	.896	.947	.050
90	1.319	.813	.902	.039
95	.490	.730	.854	.026
100	0	.657	.811	0

L. E. radius: 1.96 percent c

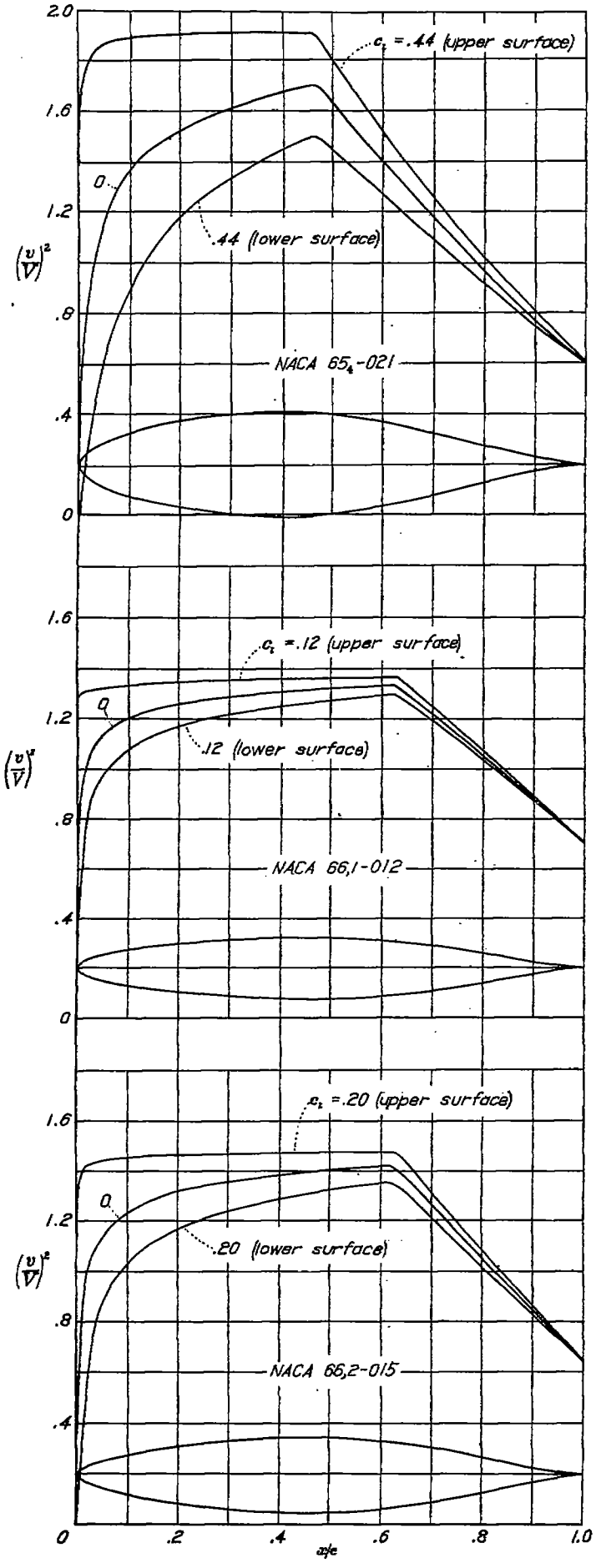

NACA 65$_4$-021 BASIC THICKNESS FORM

x (percent c)	y (percent c)	$(v/V)^2$	z/V'	$\Delta r_z/V'$
0	0	0	0	1.531
.5	1.522	.514	.717	1.333
.75	1.838	.607	.779	1.215
1.25	2.301	.710	.860	1.062
2.5	3.154	.900	.090	.838
5.0	4.472	1.136	1.089	.649
7.5	5.498	1.283	1.137	.544
10	6.352	1.371	1.171	.478
15	7.700	1.469	1.212	.388
20	8.720	1.533	1.238	.330
25	9.487	1.580	1.257	.289
30	10.036	1.621	1.273	.255
35	10.375	1.654	1.286	.229
40	10.499	1.680	1.296	.206
45	10.366	1.700	1.304	.184
50	9.952	1.633	1.278	.158
55	9.277	1.508	1.228	.139
60	8.390	1.397	1.182	.120
65	7.360	1.286	1.134	.101
70	6.224	1.177	1.085	.087
75	5.024	1.073	1.036	.073
80	3.800	.970	.985	.058
85	2.598	.872	.934	.047
90	1.484	.778	.882	.035
95	.646	.694	.833	.020
100		.616	.785	0

L. E. radius: 2.50 percent c

NACA 66,1-012 BASIC THICKNESS FORM

x (percent c)	y (percent c)	$(v/V')^2$	z/V'	$\Delta r_z/V'$
0	0	0	0	2.555
.5	.900	.854	.924	1.790
.75	1.083	.902	.950	1.510
1.25	1.343	.964	.982	1.247
2.5	1.803	1.069	1.034	.926
5.0	2.484	1.138	1.067	.673
7.5	3.019	1.175	1.084	.552
10	3.482	1.201	1.096	.474
15	4.214	1.237	1.112	.381
20	4.779	1.257	1.121	.319
25	5.218	1.272	1.128	.280
30	5.550	1.284	1.133	.248
35	5.786	1.293	1.137	.220
40	5.934	1.302	1.141	.195
45	5.998	1.309	1.144	.178
50	5.972	1.313	1.146	.161
55	5.844	1.320	1.149	.144
60	5.594	1.327	1.152	.130
65	5.165	1.297	1.139	.117
70	4.535	1.221	1.105	.099
75	3.789	1.143	1.069	.083
80	2.964	1.061	1.030	.069
85	2.098	.974	.987	.053
90	1.244	.885	.941	.041
95	.477	.792	.890	.028
100	0	.701	.837	0

L. E. radius: 0.893 percent c

NACA 66,2-015 BASIC THICKNESS FORM

x (percent c)	y (percent c)	$(v/V')^2$	z/V'	$\Delta r_z/V'$
0	0	0	0	2.085
.5	1.110	.700	.837	1.703
.75	1.329	.870	.933	1.382
1.25	1.645	.940	.970	1.156
2.5	2.229	1.048	1.024	.898
5.0	3.086	1.154	1.074	.656
7.5	3.757	1.210	1.100	.547
10	4.337	1.244	1.115	.473
15	5.255	1.290	1.136	.382
20	5.964	1.323	1.150	.323
25	6.516	1.342	1.158	.283
30	6.933	1.359	1.166	.248
35	7.230	1.374	1.172	.222
40	7.415	1.387	1.178	.199
45	7.495	1.397	1.182	.179
50	7.460	1.407	1.186	.161
55	7.294	1.416	1.190	.145
60	6.961	1.421	1.192	.131
65	6.405	1.372	1.171	.122
70	5.597	1.267	1.126	.102
75	4.652	1.162	1.078	.090
80	3.616	1.057	1.028	.066
85	2.545	.953	.976	.050
90	1.488	.848	.921	.037
95	.560	.743	.862	.025
100	0	.640	.800	0

L. E. radius: 1.384 percent c

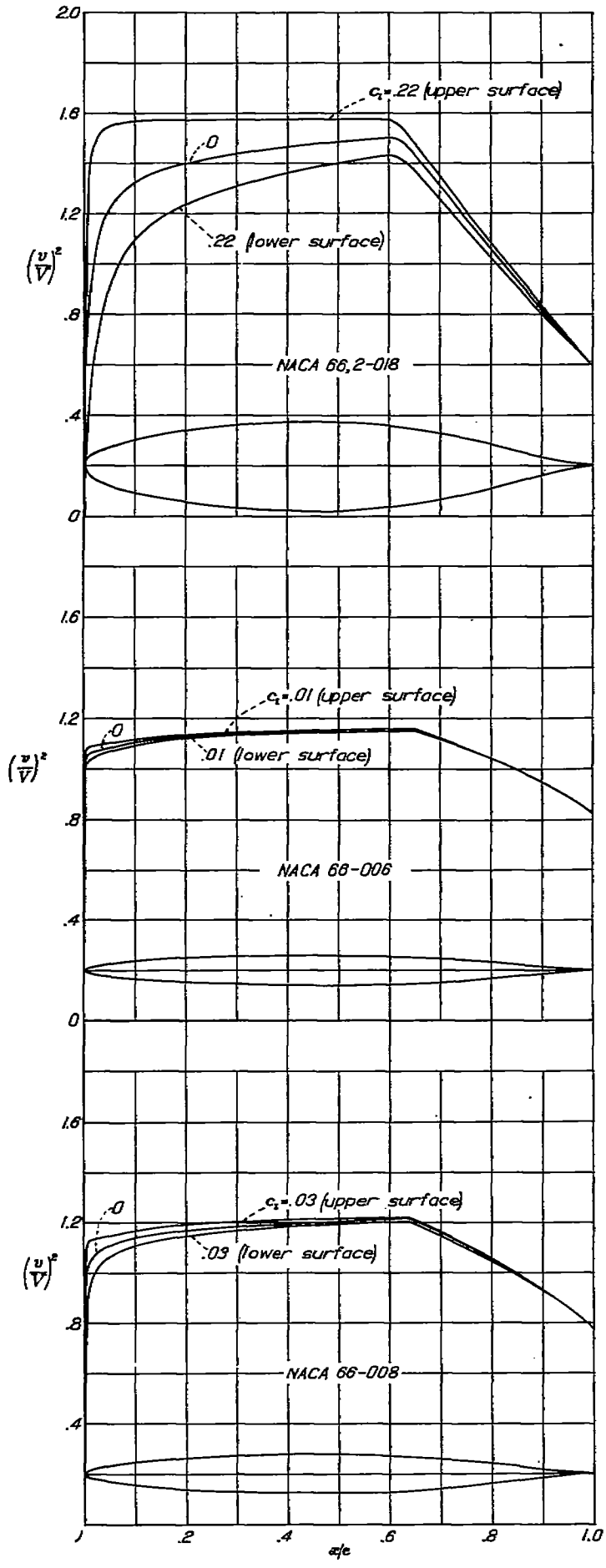

NACA 66,2-018 BASIC THICKNESS FORM

x (percent c)	y (percent c)	$(v/V)^2$	v/V	$\Delta s_a/V$
0	0	0	0	1.659
.5	1.438	.590	.768	1.317
.75	1.730	.740	.860	1.209
1.25	2.180	.918	.958	1.091
2.5	2.938	1.084	1.041	.887
5.0	3.984	1.217	1.103	.665
7.5	4.804	1.285	1.134	.544
10	5.456	1.325	1.151	.469
15	6.541	1.373	1.172	.379
20	7.342	1.401	1.184	.323
25	7.957	1.422	1.192	.282
30	8.419	1.440	1.200	.251
35	8.741	1.456	1.207	.224
40	8.933	1.468	1.212	.201
45	8.998	1.478	1.216	.181
50	8.934	1.488	1.220	.162
55	8.719	1.497	1.224	.146
60	8.316	1.502	1.226	.134
65	7.629	1.442	1.201	.102
70	6.657	1.314	1.146	.089
75	5.423	1.185	1.089	.078
80	4.296	1.059	1.029	.064
85	3.027	.936	.967	.052
90	1.789	.817	.904	.041
95	.672	.700	.837	.027
100	0	.594	.771	0

L. E. radius: 2.30 percent c

NACA 66-006 BASIC THICKNESS FORM

x (percent c)	y (percent c)	$(v/V)^2$	v/V	$\Delta s_a/V$
0	0	0	0	4.941
.5	.461	1.052	1.026	2.500
.75	.554	1.057	1.028	2.020
1.25	.693	1.062	1.031	1.500
2.5	.918	1.071	1.035	.967
5.0	1.257	1.056	1.042	.695
7.5	1.524	1.088	1.043	.554
10	1.752	1.107	1.052	.474
15	2.119	1.119	1.058	.379
20	2.401	1.128	1.062	.320
25	2.618	1.133	1.064	.278
30	2.782	1.138	1.067	.245
35	2.899	1.142	1.069	.219
40	2.971	1.145	1.070	.197
45	3.000	1.148	1.071	.178
50	2.985	1.151	1.073	.161
55	2.925	1.153	1.074	.145
60	2.815	1.155	1.075	.130
65	2.611	1.154	1.074	.116
70	2.316	1.118	1.057	.102
75	1.963	1.081	1.040	.089
80	1.543	1.040	1.020	.075
85	1.107	.996	.998	.061
90	.665	.948	.974	.047
95	.262	.890	.943	.030
100	0	.822	.907	0

L. E. radius: 0.223 percent c

NACA 66-008 BASIC THICKNESS FORM

x (percent c)	y (percent c)	$(v/V)^2$	v/V	$\Delta s_a/V$
0	0	0	0	3.794
.5	.610	.968	.984	2.220
.75	.735	1.023	1.011	1.825
1.25	.919	1.046	1.023	1.338
2.5	1.219	1.078	1.038	.949
5.0	1.673	1.107	1.052	.669
7.5	2.031	1.128	1.062	.522
10	2.335	1.141	1.068	.474
15	2.826	1.158	1.076	.379
20	3.201	1.171	1.082	.321
25	3.490	1.178	1.085	.278
30	3.709	1.186	1.089	.246
35	3.865	1.191	1.091	.220
40	3.962	1.196	1.094	.198
45	4.000	1.201	1.096	.178
50	3.978	1.205	1.098	.161
55	3.896	1.208	1.099	.145
60	3.740	1.213	1.101	.130
65	3.459	1.202	1.096	.115
70	3.062	1.155	1.075	.101
75	2.574	1.103	1.050	.087
80	2.027	1.048	1.024	.073
85	1.447	.989	.994	.058
90	.864	.926	.962	.045
95	.338	.855	.925	.029
100	0	.768	.876	0

L. E. radius: 0.411 percent c

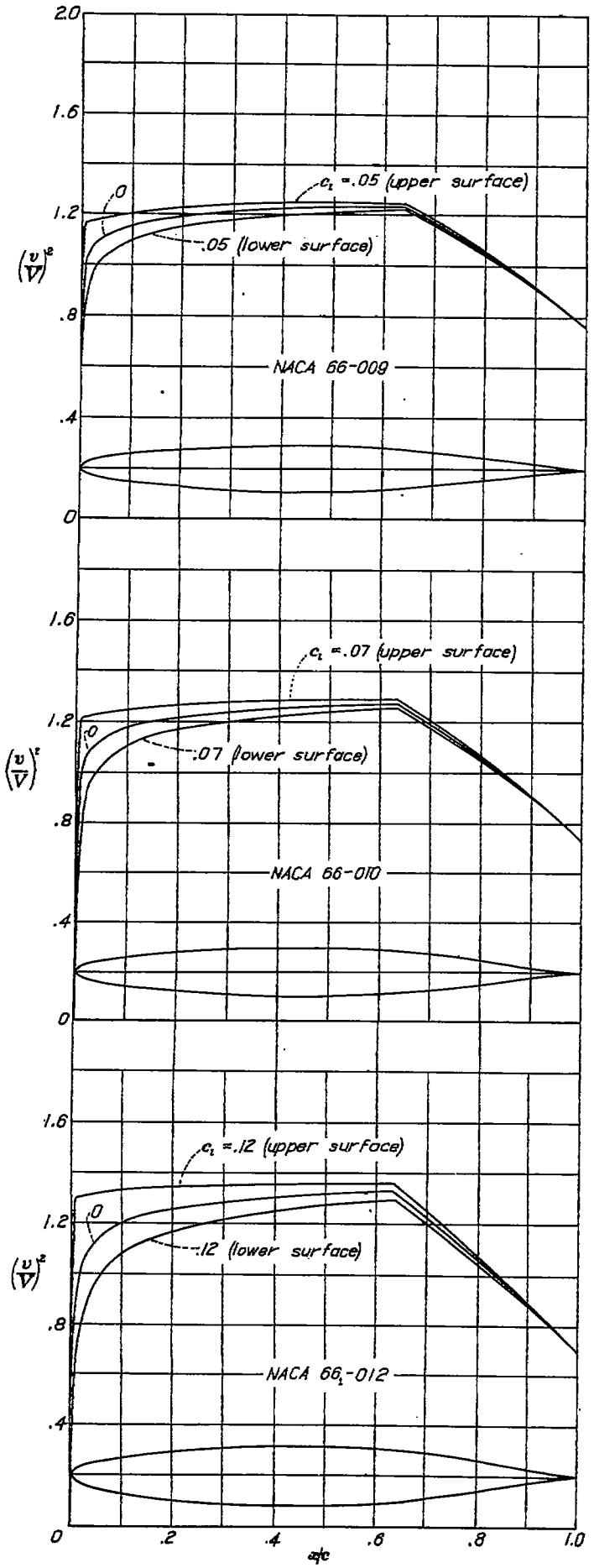

NACA 66-009 BASIC THICKNESS FORM

x (percent c)	y (percent c)	$(v/V)^2$	v/V	$\Delta p_s/V^2$
0	0	0	0	3.352
.5	.687	.930	.964	2.100
.75	.824	.999	.999	1.750
1.25	1.030	1.036	1.018	1.340
2.5	1.368	1.079	1.039	.910
5.0	1.880	1.119	1.058	.680
7.5	2.283	1.142	1.069	.552
10	2.626	1.159	1.077	.473
15	3.178	1.178	1.085	.379
20	3.601	1.190	1.091	.323
25	3.927	1.201	1.096	.280
30	4.173	1.210	1.100	.246
35	4.348	1.217	1.103	.220
40	4.457	1.221	1.105	.197
45	4.499	1.228	1.108	.178
50	4.475	1.232	1.110	.161
55	4.381	1.237	1.112	.145
60	4.204	1.240	1.114	.130
65	3.882	1.230	1.109	.116
70	3.428	1.172	1.083	.100
75	2.877	1.113	1.055	.085
80	2.263	1.050	1.026	.071
85	1.611	.985	.992	.057
90	.961	.916	.957	.043
95	.374	.839	.916	.028
100	0	.747	.864	0

L. E. radius: 0.530 percent c

NACA 66-010 BASIC THICKNESS FORM

x (percent c)	y (percent c)	$(v/V)^2$	v/V	$\Delta p_s/V^2$
0	0	0	0	3.002
.5	.759	.896	.947	2.012
.75	.913	.972	.986	1.630
1.25	1.141	1.023	1.011	1.266
2.5	1.516	1.078	1.038	.931
5.0	2.087	1.126	1.061	.682
7.5	2.536	1.154	1.074	.551
10	2.917	1.174	1.084	.473
15	3.530	1.198	1.095	.379
20	4.001	1.215	1.102	.322
25	4.363	1.226	1.107	.279
30	4.636	1.236	1.112	.246
35	4.832	1.243	1.115	.220
40	4.953	1.249	1.118	.198
45	5.000	1.255	1.120	.178
50	4.971	1.261	1.123	.161
55	4.865	1.265	1.125	.146
60	4.665	1.270	1.127	.130
65	4.302	1.250	1.118	.114
70	3.787	1.190	1.091	.099
75	3.176	1.121	1.059	.085
80	2.494	1.052	1.026	.070
85	1.773	.979	.989	.056
90	1.054	.904	.951	.043
95	.408	.821	.906	.027
100	0	.729	.854	0

L. E. radius: 0.662 percent c

NACA 66$_1$-012 BASIC THICKNESS FORM

x (percent c)	y (percent c)	$(v/V)^2$	v/V	$\Delta p_s/V^2$
0	0	0	0	2.569
.5	.906	.800	.894	1.847
.75	1.087	.915	.957	1.575
1.25	1.358	.980	.990	1.237
2.5	1.803	1.073	1.036	.913
5	2.496	1.138	1.067	.674
7.5	3.037	1.177	1.085	.549
10	3.496	1.204	1.097	.473
15	4.234	1.237	1.112	.380
20	4.801	1.259	1.122	.323
25	5.238	1.275	1.129	.280
30	5.568	1.287	1.134	.246
35	5.803	1.297	1.139	.221
40	5.947	1.303	1.142	.197
45	6.000	1.311	1.145	.178
50	5.965	1.318	1.148	.162
55	5.836	1.323	1.150	.147
60	5.588	1.331	1.154	.132
65	5.139	1.302	1.141	.113
70	4.515	1.221	1.105	.095
75	3.767	1.139	1.067	.084
80	2.944	1.053	1.026	.069
85	2.083	.968	.984	.053
90	1.234	.879	.938	.040
95	.474	.788	.888	.031
100	0	.687	.829	0

L. E. radius: 0.952 percent c

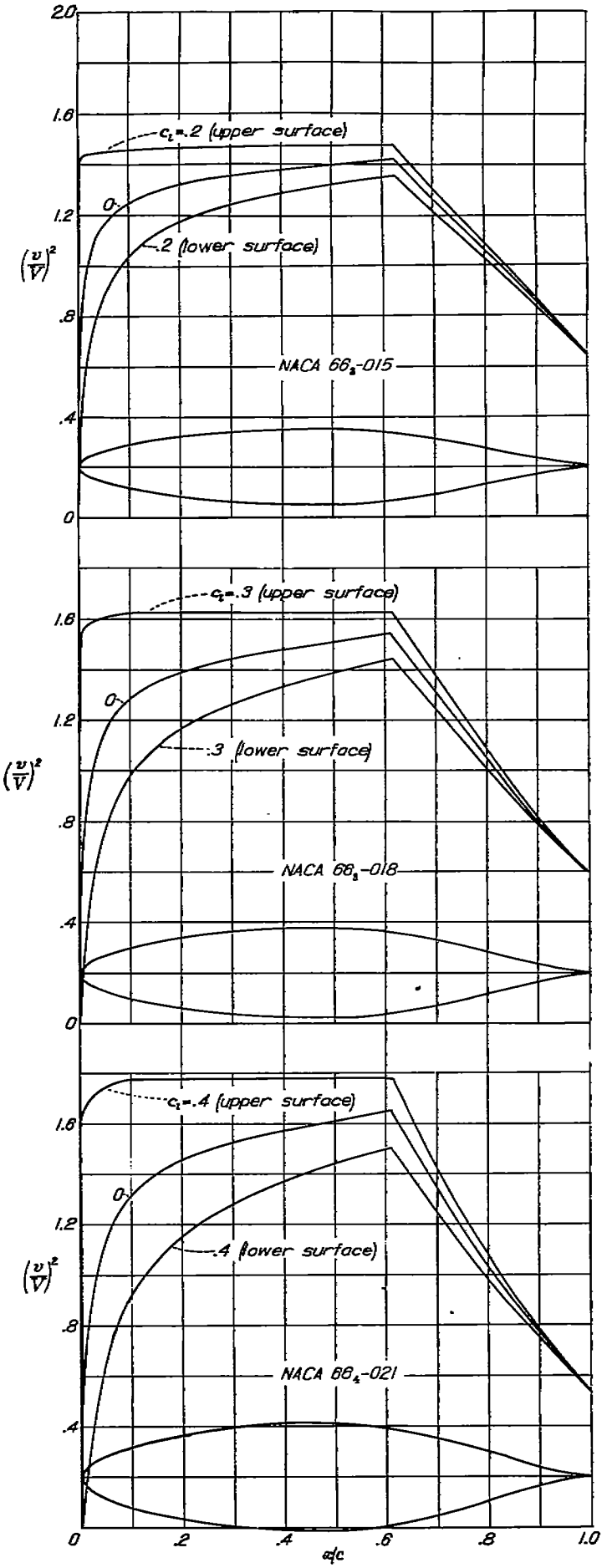

NACA 66$_2$-015 BASIC THICKNESS FORM

x (percent c)	y (percent c)	$(v/V)^2$	v/V	$\Delta v_a/V$
0	0	0	0	2.139
.5	1.122	.702	.838	1.652
.75	1.343	.840	.916	1.431
1.25	1.675	.929	.964	1.172
2.5	2.235	1.055	1.027	.895
5	3.100	1.163	1.078	.663
7.5	3.781	1.209	1.099	.547
10	4.352	1.254	1.114	.473
15	5.281	1.288	1.134	.381
20	5.997	1.317	1.148	.322
25	6.573	1.340	1.158	.280
30	6.998	1.356	1.164	.248
35	7.280	1.370	1.170	.222
40	7.430	1.380	1.175	.200
45	7.495	1.391	1.179	.180
50	7.450	1.401	1.184	.163
55	7.283	1.411	1.188	.146
60	6.959	1.420	1.192	.131
65	6.372	1.367	1.169	.113
70	5.576	1.260	1.122	.096
75	4.632	1.156	1.075	.080
80	3.598	1.053	1.026	.065
85	2.530	.949	.974	.051
90	1.489	.847	.920	.039
95	.566	.744	.863	.025
100	0	.639	.799	0

L. E. radius: 1.435 percent c

NACA 66$_2$-018 BASIC THICKNESS FORM

x (percent c)	y (percent c)	$(v/V)^2$	v/V	$\Delta v_a/V$
0	0	0	0	1.773
.5	1.323	.650	.806	1.456
.75	1.571	.735	.857	1.312
1.25	1.952	.850	.897	1.121
2.5	2.646	1.005	1.002	.858
5	3.690	1.154	1.074	.649
7.5	4.513	1.234	1.111	.545
10	5.210	1.285	1.134	.472
15	6.333	1.350	1.162	.381
20	7.188	1.393	1.180	.323
25	7.843	1.423	1.193	.282
30	8.346	1.445	1.202	.250
35	8.701	1.464	1.210	.223
40	8.918	1.481	1.217	.201
45	8.998	1.496	1.223	.181
50	8.942	1.509	1.228	.163
55	8.733	1.522	1.234	.147
60	8.323	1.534	1.238	.131
65	7.680	1.433	1.199	.114
70	6.597	1.302	1.141	.095
75	5.451	1.172	1.083	.077
80	4.206	1.045	1.022	.061
85	2.934	.922	.950	.048
90	1.714	.803	.896	.037
95	.646	.692	.832	.022
100	0	.587	.766	0

L. E. radius: 1.955 percent c

NACA 66$_2$-021 BASIC THICKNESS FORM

x (percent c)	y (percent c)	$(v/V)^2$	v/V	$\Delta v_a/V$
0	0	0	0	1.547
.5	1.525	.580	.761	1.314
.75	1.804	.635	.797	1.218
1.25	2.240	.755	.869	1.054
2.5	3.045	.952	.976	.828
5	4.269	1.143	1.069	.635
7.5	5.233	1.246	1.116	.542
10	6.052	1.318	1.148	.472
15	7.369	1.405	1.185	.381
20	8.376	1.459	1.208	.324
25	9.153	1.499	1.224	.283
30	9.738	1.528	1.236	.251
35	10.154	1.551	1.245	.224
40	10.407	1.574	1.255	.202
45	10.500	1.594	1.263	.183
50	10.434	1.611	1.269	.165
55	10.186	1.629	1.276	.148
60	9.692	1.648	1.284	.132
65	8.793	1.508	1.228	.114
70	7.610	1.335	1.155	.093
75	6.251	1.176	1.084	.073
80	4.796	1.031	1.015	.058
85	3.324	.891	.944	.046
90	1.924	.763	.873	.034
95	.717	.648	.805	.020
100	0	.589	.734	0

L. E. radius: 2.550 percent c

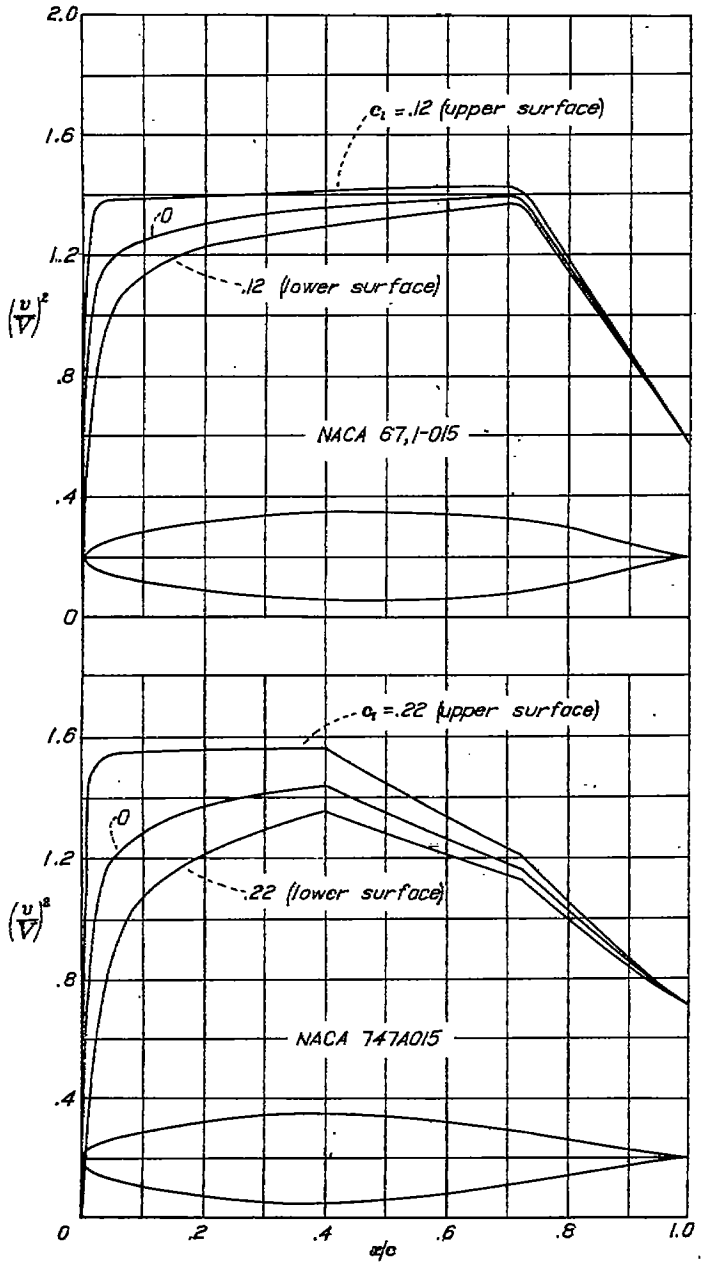

NACA 67,1-015 BASIC THICKNESS FORM

$\frac{x}{c}$ (percent c)	$\frac{y}{c}$ (percent c)	$(v/V)^2$	v/V	$\Delta r_u/V$
0	0	0	0	2.042
.5	1.167	.650	.800	1.660
.75	1.394	.970	.935	1.370
1.25	1.764	1.059	1.079	1.162
2.5	2.395	1.140	1.068	.906
5.0	3.245	1.209	1.101	.697
7.5	3.900	1.239	1.113	.548
10	4.433	1.259	1.122	.470
15	5.283	1.285	1.134	.370
20	5.940	1.304	1.142	.312
25	6.454	1.318	1.148	.270
30	6.854	1.330	1.153	.248
35	7.155	1.341	1.158	.221
40	7.359	1.351	1.162	.201
45	7.475	1.360	1.166	.180
50	7.497	1.368	1.170	.160
55	7.421	1.375	1.173	.142
60	7.231	1.381	1.175	.124
65	6.905	1.388	1.178	.111
70	6.402	1.390	1.179	.106
75	5.621	1.321	1.149	.094
80	4.540	1.176	1.084	.071
85	3.227	1.018	1.009	.000
90	2.021	.864	.930	.045
95	.788	.712	.844	.025
100	0	.570	.755	0

L. E. radius: 1.523 percent c.

NACA 747A015 BASIC THICKNESS FORM

$\frac{x}{c}$ (percent c)	$\frac{y}{c}$ (percent c)	$(v/V)^2$	v/V	$\Delta r_u/V$
0	0	0	0	2.028
.5	1.199	.660	.812	1.680
.75	1.435	.799	.894	1.500
1.25	1.801	.942	.971	1.326
2.5	2.462	1.100	1.049	.920
5	3.419	1.201	1.096	.695
7.5	4.143	1.259	1.122	.561
10	4.743	1.295	1.138	.465
15	5.684	1.339	1.156	.353
20	6.394	1.369	1.170	.324
25	6.808	1.390	1.179	.283
30	7.253	1.409	1.187	.252
35	7.454	1.423	1.193	.224
40	7.494	1.436	1.198	.199
45	7.316	1.391	1.179	.176
50	7.003	1.348	1.161	.156
55	6.584	1.308	1.143	.138
60	6.064	1.265	1.125	.122
65	5.449	1.221	1.105	.108
70	4.738	1.178	1.085	.093
75	3.921	1.115	1.056	.079
80	3.020	1.027	1.013	.065
85	2.036	.938	.969	.052
90	1.193	.852	.923	.040
95	.443	.774	.880	.028
100	0	.703	.838	.018

L. E. radius: 1.544 percent c

II—DATA FOR MEAN LINES

	Page		Page
NACA mean line 62	348	NACA mean line $a=0$	351
NACA mean line 63	348	NACA mean line $a=0.1$	352
NACA mean line 64	348	NACA mean line $a=0.2$	352
NACA mean line 65	349	NACA mean line $a=0.3$	352
NACA mean line 66	349	NACA mean line $a=0.4$	353
NACA mean line 67	349	NACA mean line $a=0.5$	353
NACA mean line 210	350	NACA mean line $a=0.6$	353
NACA mean line 220	350	NACA mean line $a=0.7$	354
NACA mean line 230	350	NACA mean line $a=0.8$	354
NACA mean line 240	351	NACA mean line $a=0.9$	354
NACA mean line 250	351	NACA mean line $a=1.0$	355

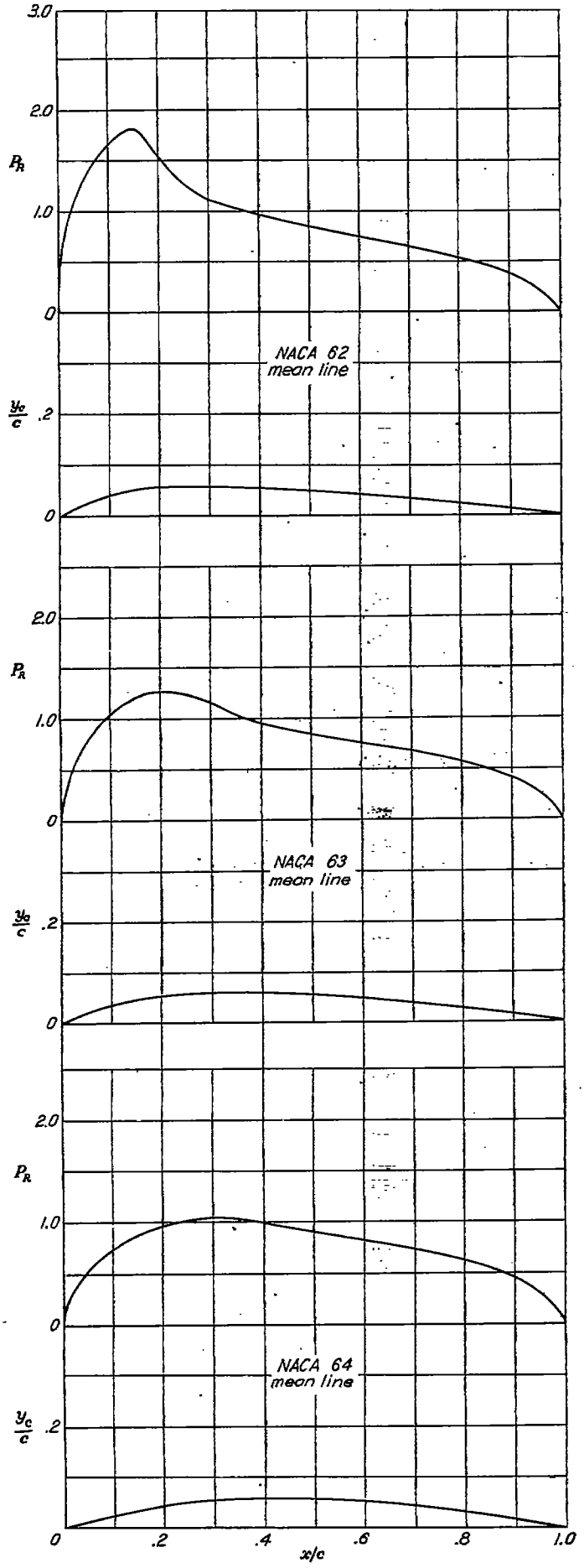

NACA MEAN LINE 62

	c_{l_i}=0.90	α_i=2.81°	$c_{m_{c/4}}$=−0.118	
x (percent c)	y_c (percent c)	dy_c/dx	P_R	$\Delta s/V=P_R/4$
0	0	0.60000	0	0
1.25	.726	.56250	.682	.171
2.5	1.406	.52500	1.031	.258
5.0	2.625	.45000	1.314	.328
7.5	3.656	.37500	1.503	.376
10	4.500	.30000	1.651	.412
15	5.625	.15000	1.802	.451
20	6.000	0	1.530	.383
25	5.977	−.09938	1.273	.318
30	5.906	−.01875	1.113	.279
40	5.625	−.03750	.951	.238
50	5.156	−.05625	.843	.211
60	4.500	−.07500	.741	.185
70	3.656	−.09375	.635	.159
80	2.625	−.11250	.525	.131
90	1.406	−.13125	.377	.094
95	.727	−.14062	.261	.065
100	0	−.15000	0	0

NACA MEAN LINE 63

	c_{l_i}=0.80	α_i=1.60°	$c_{m_{c/4}}$=−0.134	
x (percent c)	y_c (percent c)	dy_c/dx	P_R	$\Delta s/V=P_R/4$
0	0	0.40000	0	0
1.25	.489	.38333	.389	.097
2.5	.958	.36667	.553	.138
5.0	1.833	.33333	.788	.197
7.5	2.625	.30000	.940	.235
10	3.333	.26667	1.066	.267
15	4.500	.20000	1.220	.305
20	5.333	.13333	1.259	.315
25	5.833	.06667	1.233	.308
30	6.000	0	1.160	.290
40	5.878	−.02449	.949	.237
50	5.510	−.04898	.850	.213
60	4.898	−.07347	.762	.191
70	4.041	−.09796	.673	.168
80	2.939	−.12245	.560	.140
90	1.592	−.14694	.406	.102
95	.827	−.16918	.291	.073
100	0	−.17143	0	0

NACA MEAN LINE 64

	c_{l_i}=0.76	α_i=0.74°	$c_{m_{c/4}}$=−0.157	
x (percent c)	y_c (percent c)	dy_c/dx	P_R	$\Delta s/V=P_R/4$
0	0	0.30000	0	0
1.25	.369	.29062	.257	.064
2.5	.726	.28125	.391	.098
5.0	1.406	.26250	.548	.137
7.5	2.039	.24375	.668	.167
10	2.625	.22500	.748	.187
15	3.656	.18750	.871	.218
20	4.500	.15000	.966	.242
25	5.156	.11250	1.030	.258
30	5.625	.07500	1.040	.260
40	6.000	0	.999	.250
50	5.833	−.03333	.910	.228
60	5.333	−.06667	.827	.207
70	4.500	−.10000	.750	.188
80	3.333	−.13333	.635	.159
90	1.833	−.16667	.466	.117
95	.958	−.18333	.334	.084
100	0	−.20000	0	0

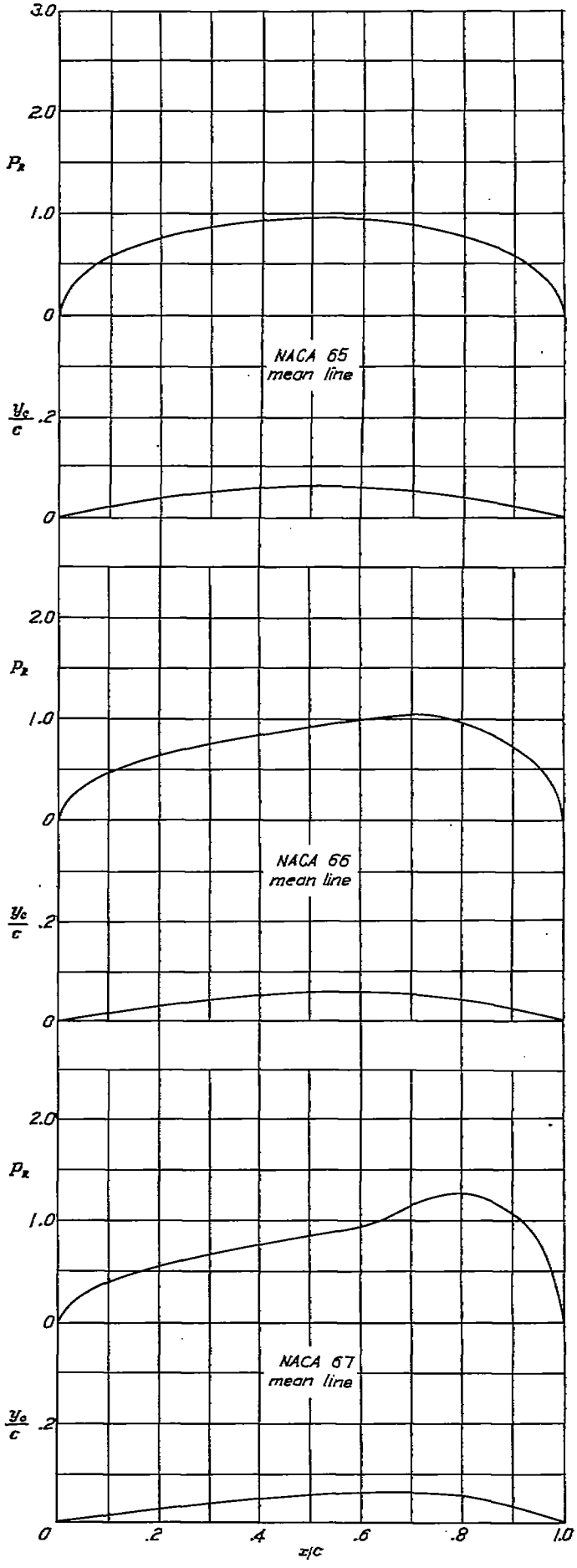

NACA MEAN LINE 65

$c_{l_i}=0.75$ $\alpha_i=0°$ $c_{m_{c/4}}=-0.187$

x (percent c)	y_c (percent c)	dy_c/dx	P_z	$\Delta s/V=P_z/4$
0	0	0.24000	0	0
1.25	.296	.23400	.205	.051
2.5	.585	.22800	.294	.074
5.0	1.140	.21600	.413	.103
7.5	1.665	.20400	.502	.126
10	2.160	.19200	.571	.143
15	3.060	.16800	.679	.170
20	3.840	.14400	.760	.190
25	4.500	.12000	.824	.206
30	5.040	.09600	.872	.218
40	5.760	.04800	.932	.233
50	6.000	0	.951	.238
60	5.760	−.04800	.932	.233
70	5.040	−.09600	.872	.218
80	3.840	−.14400	.760	.190
90	2.160	−.19200	.571	.143
95	1.140	−.21600	.413	.103
100	0	−.24000	0	0

NACA MEAN LINE 66

$c_{l_i}=0.76$ $\alpha_i=-0.74°$ $c_{m_{c/4}}=-0.222$

x (percent c)	y_c (percent c)	dy_c/dx	P_z	$\Delta s/V=P_z/4$
0	0	0.20000	0	0
1.25	.247	.19583	.135	.034
2.5	.490	.19167	.244	.061
5.0	.958	.18333	.334	.084
7.5	1.406	.17500	.408	.102
10	1.833	.16667	.466	.117
15	2.625	.15000	.557	.139
20	3.333	.13333	.635	.159
25	3.958	.11667	.700	.175
30	4.500	.10000	.750	.188
40	5.333	.06667	.827	.207
50	5.833	.03333	.910	.228
60	6.000	0	.999	.250
70	5.625	−.07500	1.040	.260
80	4.500	−.15000	.966	.242
90	2.625	−.22500	.748	.187
95	1.406	−.26250	.546	.137
100	0	−.30000	0	0

NACA MEAN LINE 67

$c_{l_i}=0.80$ $\alpha_i=-1.60°$ $c_{m_{c/4}}=-0.266$

x (percent c)	y_c (percent c)	dy_c/dx	P_z	$\Delta s/V=P_z/4$
0	0	0.17143	0	0
1.25	.212	.16837	.137	.034
2.5	.421	.16531	.195	.049
5	.827	.16918	.291	.073
7.5	1.217	.16306	.356	.089
10	1.592	.14694	.406	.102
15	2.293	.13469	.483	.121
20	2.939	.12245	.560	.140
25	3.520	.11020	.616	.154
30	4.041	.09796	.673	.168
40	4.898	.07347	.762	.191
50	5.510	.04898	.850	.213
60	5.878	.02449	.949	.237
70	6.000	0	1.160	.290
80	5.333	−.13333	1.259	.315
90	3.333	−.26667	1.066	.267
95	1.833	−.33333	.788	.197
100	0	−.40000	0	0

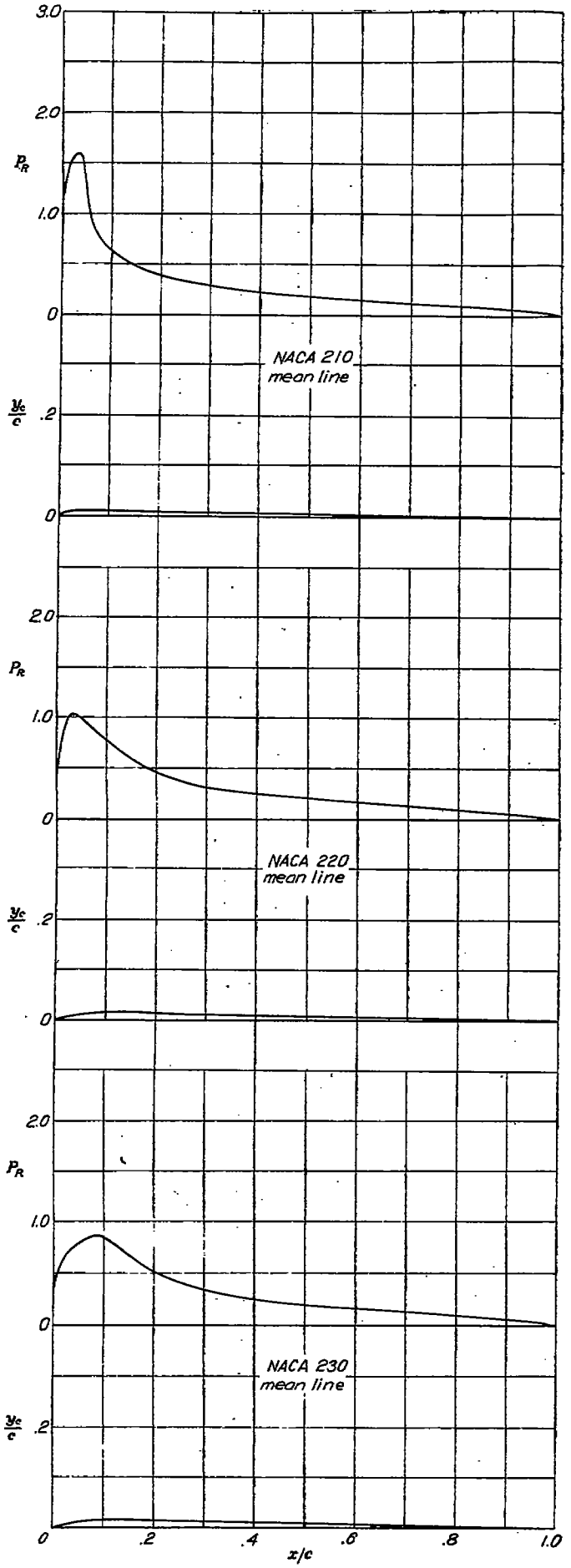

NACA MEAN LINE 210

c_{l_i}=0.30 α_i=2.09° $c_{m_{c/4}}$=−0.006

x (percent c)	y_c (percent c)	dy_c/dx	P_R	$\Delta v/V=P_R/4$
0	0	0.59613	0	0
1.25	.596	.36236	1.381	.345
2.5	.928	.18504	1.565	.391
5.0	1.114	−.00018	1.221	.305
7.5	1.087		.781	.195
10	1.058		.626	.156
15	.999		.489	.122
20	.940		.408	.102
25	.881		.348	.087
30	.823		.302	.075
40	.705		.242	.061
50	.588	−.01175	.198	.049
60	.470		.160	.040
70	.353		.128	.032
80	.235		.098	.025
90	.118		.065	.016
95	.059		.044	.011
100	0		0	0

NACA MEAN LINE 220

c_{l_i}=0.30 α_i=1.86° $c_{m_{c/4}}$=−0.010

x (percent c)	y_c (percent c)	dy_c/dx	P_R	$\Delta v/V=P_R/4$
0	0	0.39270	0	0
1.25	.442	.31541	.822	.206
2.5	.793	.24618	1.003	.251
5.0	1.257	.13192	.988	.247
7.5	1.479	.04904	.900	.225
10	1.535	.00024	.801	.200
15	1.463		.618	.154
20	1.377		.465	.116
25	1.291		.378	.095
30	1.205		.326	.082
40	1.033		.253	.063
50	.861		.205	.051
60	.689	−.01722	.169	.042
70	.516		.135	.034
80	.344		.100	.025
90	.172		.064	.016
95	.086		.040	.010
100	0		0	0

NACA MEAN LINE 230

c_{l_i}=0.30 α_i=1.65° $c_{m_{c/4}}$=−0.014

x (percent c)	y_c (percent c)	dy_c/dx	P_R	$\Delta v/V=P_R/4$
0	0	0.30508	0	0
1.25	.357	.26594	.528	.132
2.5	.666	.22929	.673	.168
5.0	1.155	.16347	.791	.198
7.5	1.492	.10762	.853	.213
10	1.701	.06174	.859	.215
15	1.838	−.00009	.678	.170
20	1.767	−.02203	.519	.130
25	1.656		.419	.105
30	1.546		.361	.090
40	1.325		.274	.069
50	1.104		.217	.054
60	.883		.177	.044
70	.662	−.02203	.144	.036
80	.442		.105	.026
90	.221		.069	.017
95	.110		.042	.011
100	0		0	0

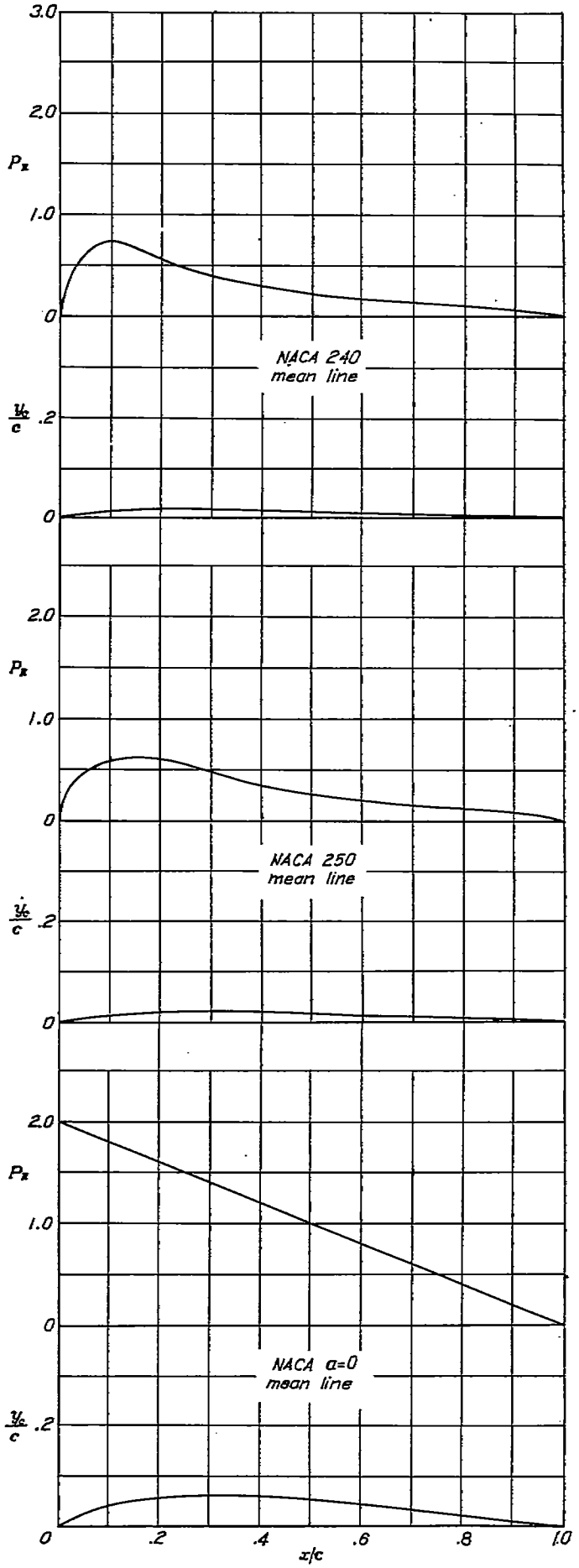

NACA MEAN LINE 240

c_{l_i}=0.30 α_i=1.45° $c_{m_{c/4}}$=−0.019

x (percent c)	y_c (percent c)	dy_c/dx	P_R	$\Delta s/V=P_R/4$
0	0	0.25233	0	0
1.25	.301	.22877	.377	.094
2.5	.572	.20625	.491	.123
5.0	1.035	.16432	.625	.156
7.5	1.397	.12653	.718	.180
10	1.671	.09290	.750	.188
15	1.991	.03810	.677	.169
20	2.079	−.00010	.566	.142
25	2.018	−.02169	.477	.119
30	1.890		.410	.103
40	1.620		.304	.076
50	1.350		.234	.059
60	1.080		.186	.047
70	.810	−.02700	.150	.038
80	.540		.110	.028
90	.270		.071	.018
95	.135		.047	.012
100	0		0	0

NACA MEAN LINE 250

c_{l_i}=0.30 α_i=1.26° $c_{m_{c/4}}$=−0.026

x (percent c)	y_c (percent c)	dy_c/dx	P_R	$\Delta s/V=P_R/4$
0	0	0.21472	0	0
1.25	.258	.19920	.281	.070
2.5	.498	.18416	.369	.092
5.0	.922	.15562	.477	.119
7.5	1.277	.12909	.552	.138
10	1.570	.10458	.592	.148
15	1.982	.06162	.624	.156
20	2.199	.02674	.610	.153
25	2.263	−.00007	.547	.137
30	2.212	−.01880	.470	.117
40	1.931		.346	.087
50	1.609		.255	.064
60	1.287		.197	.049
70	.965	−.03218	.154	.038
80	.644		.119	.030
90	.322		.076	.019
95	.161		.051	.013
100	0		0	0

NACA MEAN LINE a=0

c_{l_i}=1.0 α_i=4.58° $c_{m_{c/4}}$=−0.053

x (percent c)	y_c (percent c)	dy_c/dx	P_R	$\Delta s/V=P_R/4$
0	0			
.5	.460	0.75867	1.990	0.498
.75	.641	.69212	1.985	.496
1.25	.964	.60715	1.975	.494
2.5	1.641	.45892	1.950	.488
5.0	2.693	.36561	1.900	.475
7.5	3.507	.29028	1.850	.463
10	4.161	.23515	1.800	.450
15	5.124	.15508	1.700	.425
20	5.747	.09693	1.600	.400
25	6.114	.05156	1.500	.375
30	6.277	.01452	1.400	.350
35	6.273	−.01554	1.300	.325
40	6.130	−.04086	1.200	.300
45	5.871	−.06201	1.100	.275
50	5.516	−.07958	1.000	.250
55	5.081	−.09395	.900	.225
60	4.581	−.10639	.800	.200
65	4.032	−.11406	.700	.175
70	3.445	−.12003	.600	.150
75	2.836	−.12329	.500	.125
80	2.217	−.12371	.400	.100
85	1.604	−.12099	.300	.075
90	1.013	−.11455	.200	.050
95	.467	−.10301	.100	.025
100	0	−.07958	0	0

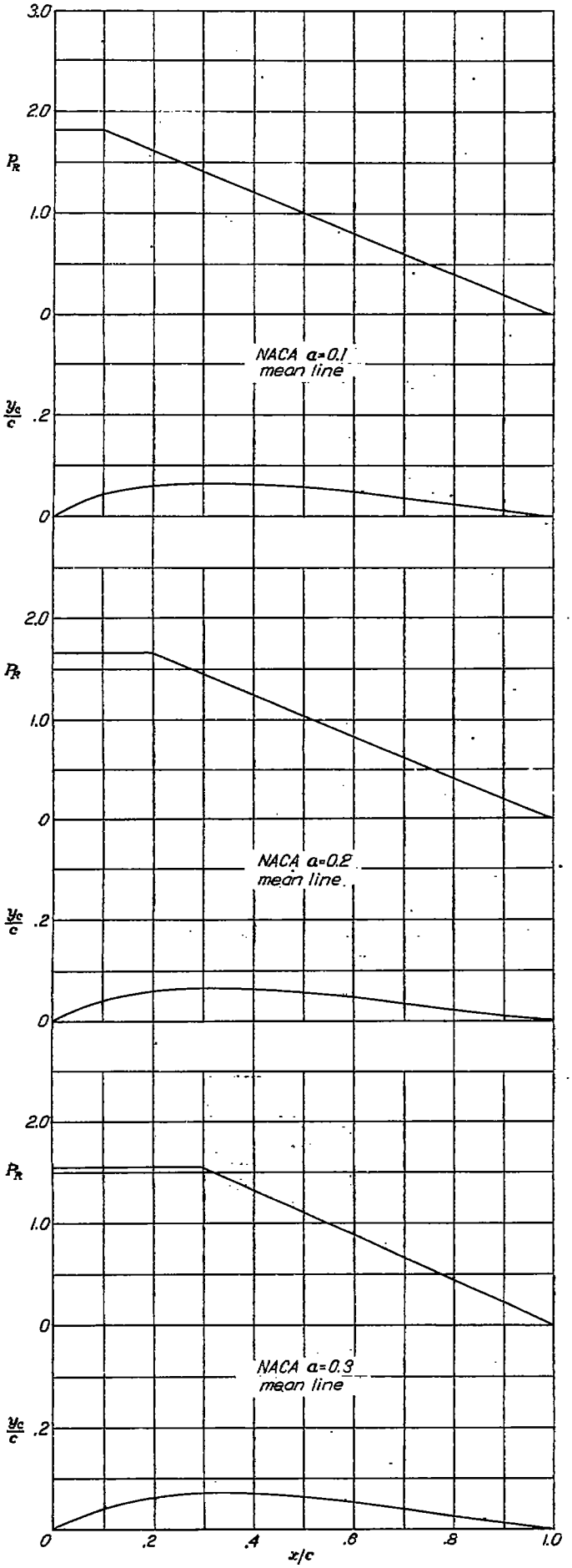

NACA MEAN LINE $a=0.1$

$c_{l_i}=1.0$ $\alpha_i=4.43°$ $c_{m_{c/4}}=-0.026$

x (percent c)	y_c (percent c)	dy_c/dx	P_R	$\Delta p/V=P_R/4$
0	0	----------	----------	----------
.5	.440	0.73441		
.75	.616	.67479		
1.25	.933	.59890		
2.5	1.608	.49366	1.818	0.456
5.0	2.689	.38235		
7.5	3.551	.31067		
10	4.253	.25057		
15	5.201	.16087	1.717	.429
20	5.905	.09981	1.616	.404
25	6.282	.05281	1.518	.379
30	6.449	.01498	1.414	.354
35	6.443	−.01017	1.313	.328
40	6.296	−.04210	1.212	.303
45	6.029	−.06373	1.111	.278
50	5.664	−.08168	1.010	.253
55	5.218	−.09637	.909	.227
60	4.706	−.10800	.808	.202
65	4.142	−.11694	.707	.177
70	3.541	−.12307	.606	.152
75	2.916	−.12644	.505	.126
80	2.281	−.12693	.404	.101
85	1.652	−.12425	.303	.076
90	1.045	−.11781	.202	.050
95	.482	−.10620	.101	.025
100	0	−.08258	0	0

NACA MEAN LINE $a=0.2$

$c_{l_i}=1.0$ $\alpha_i=4.17°$ $c_{m_{c/4}}=-0.094$

x (percent c)	y_c (percent c)	dy_c/dx	P_R	$\Delta p/V=P_R/4$
0	0	----------	----------	----------
.5	.414	0.60492		
.75	.581	.54047		
1.25	.882	.47138		
2.5	1.530	.37692		
5.0	2.583	.27661	1.667	0.417
7.5	3.443	.21487		
10	4.169	.16803		
15	5.317	.10373		
20	6.117	.06405		
25	6.572	.03345	1.563	.391
30	6.777	.01030	1.459	.365
35	6.789	−.00418	1.355	.339
40	6.646	−.01246	1.250	.313
45	6.373	−.01588	1.146	.287
50	5.994	−.01522	1.042	.260
55	5.527	−.01101	.938	.234
60	4.989	−.00559	.834	.208
65	4.396	−.00017	.729	.182
70	3.762	−.00655	.625	.156
75	3.102	−.01363	.521	.130
80	2.431	−.01440	.417	.104
85	1.764	−.01186	.313	.078
90	1.119	−.00841	.208	.052
95	.518	−.00461	.104	.026
100	0	−.00241	0	0

NACA MEAN LINE $a=0.3$

$c_{l_i}=1.0$ $\alpha_i=3.84°$ $c_{m_{c/4}}=-0.106$

x (percent c)	y_c (percent c)	dy_c/dx	P_R	$\Delta p/V=P_R/4$
0	0	----------	----------	----------
.5	.389	0.55536		
.75	.546	.50524		
1.25	.832	.44158		
2.5	1.448	.35399		
5.0	2.458	.26344		
7.5	3.293	.20780	1.538	0.385
10	4.008	.16621		
15	5.172	.10246		
20	6.052	.06063		
25	6.685	.03278		
30	7.072	.01333		
35	7.176	−.00205	1.429	.357
40	7.074	−.01710	1.319	.330
45	6.816	−.02492	1.209	.302
50	6.433	−.02746	1.099	.275
55	5.949	−.02567	.989	.247
60	5.383	−.02014	.879	.220
65	4.753	−.01319	.769	.192
70	4.076	−.00601	.659	.165
75	3.368	−.00035	.549	.137
80	2.645	.00300	.440	.110
85	1.924	.00279	.330	.082
90	1.224	.00138	.220	.055
95	.570	.00030	.110	.028
100	0	−.00307	0	0

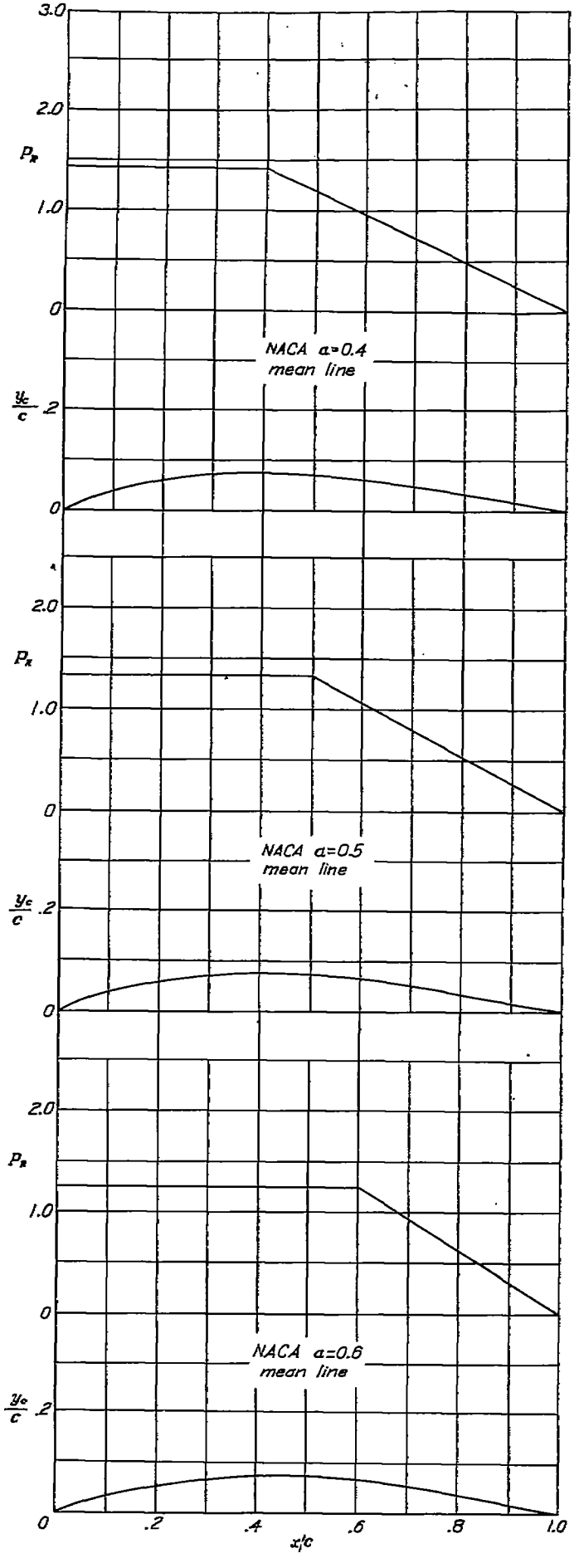

NACA MEAN LINE $a=0.4$

$c_{l_i}=1.0$ $\alpha_i=3.46°$ $c_{m_{c/4}}=-0.121$

x (percent c)	y_c (percent c)	dy_c/dx	P_R	$\Delta p/V=P_R/4$
0	0	----------	----------	----------
.5	.366	0.61759		
.75	.514	.57105		
1.25	.784	.51210		
2.5	1.367	.43106		
5.0	2.330	.34764		
7.5	3.131	.29871		
10	3.824	.25892	1.429	0.357
15	4.968	.20185		
20	5.862	.15682		
25	6.546	.11733		
30	7.039	.07968		
35	7.343	.04136		
40	7.439	−.00721		
45	7.276	−.05321	1.310	.327
50	6.929	−.08330	1.190	.298
55	6.449	−.10734	1.071	.268
60	5.864	−.12567	.952	.238
65	5.199	−.13962	.833	.208
70	4.475	−.14963	.714	.179
75	3.709	−.15589	.595	.149
80	2.922	−.15837	.476	.119
85	2.132	−.15683	.357	.089
90	1.361	−.15062	.238	.060
95	.630	−.13816	.119	.030
100	0	−.11138	0	0

NACA MEAN LINE $a=0.5$

$c_{l_i}=1.0$ $\alpha_i=3.04°$ $c_{m_{c/4}}=-0.139$

x (percent c)	y_c (percent c)	dy_c/dx	P_R	$\Delta p/V=P_R/4$
0	0	----------	----------	----------
.5	.345	0.58195		
.75	.485	.53855		
1.25	.735	.48360		
2.5	1.295	.40815		
5.0	2.205	.33070		
7.5	2.970	.28365		
10	3.630	.24890		
15	4.740	.19690	1.333	0.333
20	5.620	.15650		
25	6.310	.12180		
30	6.840	.09000		
35	7.215	.05930		
40	7.430	.02890		
45	7.490	−.00630		
50	7.350	−.05305		
55	6.965	−.09763	1.200	.300
60	6.405	−.12550	1.067	.267
65	5.725	−.14570	.933	.233
70	4.955	−.16015	.800	.200
75	4.130	−.16960	.667	.167
80	3.285	−.17435	.533	.133
85	2.395	−.17415	.400	.100
90	1.535	−.16850	.267	.067
95	.720	−.15565	.133	.033
100	0	−.12660	0	0

NACA MEAN LINE $a=0.6$

$c_{l_i}=1.0$ $\alpha_i=2.68°$ $c_{m_{c/4}}=-0.153$

x (percent c)	y_c (percent c)	dy_c/dx	P_R	$\Delta p/V=P_R/4$
0	0	----------	----------	----------
.5	.325	0.54825		
.75	.455	.50760		
1.25	.695	.45615		
2.5	1.220	.38556		
5.0	2.080	.31325		
7.5	2.805	.26950		
10	3.435	.23730		
15	4.495	.18935		
20	5.345	.15250	1.250	0.312
25	6.035	.12125		
30	6.570	.09310		
35	6.965	.06860		
40	7.235	.04060		
45	7.370	.01405		
50	7.370	−.01435		
55	7.220	−.04700		
60	6.880	−.09470		
65	6.275	−.14015	1.094	.273
70	5.505	−.16595	.938	.234
75	4.630	−.18270	.781	.195
80	3.695	−.19225	.625	.156
85	2.720	−.19515	.469	.117
90	1.755	−.19095	.312	.078
95	.825	−.17790	.156	.039
100	0	−.14550	0	0

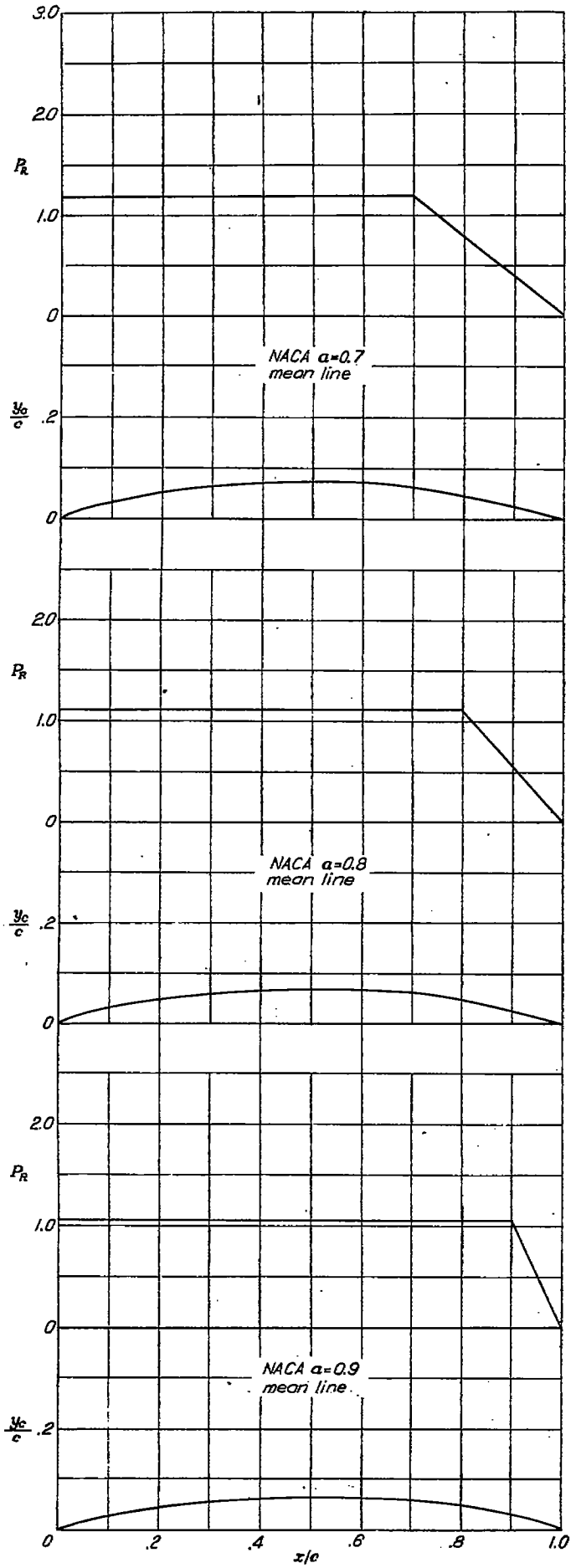

NACA MEAN LINE $a=0.7$

$c_{l_i}=1.0$ $\alpha_i=2.09°$ $c_{m_{c/4}}=-0.179$

x (percent c)	y_c (percent c)	dy_c/dx	P_R	$\Delta s/V=P_R/4$
0	0	----------	----------	----------
.5	.305	0.51620		
.75	.425	.47795		
1.25	.655	.42960		
2.5	1.160	.36325		
5.0	1.955	.29545		
7.5	2.645	.25450		
10	3.240	.22443		
15	4.245	.17995		
20	5.060	.14595		
25	5.715	.11740	1.176	0.294
30	6.240	.09200		
35	6.635	.06840		
40	6.925	.04570		
45	7.095	.02315		
50	7.155	0		
55	7.090	−.02455		
60	6.900	−.05185		
65	6.585	−.08475		
70	6.030	−.13650		
75	5.205	−.18510	.980	.245
80	4.215	−.20855	.784	.196
85	3.140	−.21955	.588	.147
90	2.035	−.21960	.392	.098
95	.965	−.20725	.196	.049
100	0	−.16985	0	0

NACA MEAN LINE $a=0.8$

$c_{l_i}=1.0$ $\alpha_i=1.54°$ $c_{m_{c/4}}=-0.202$

x (percent c)	y_c (percent c)	dy_c/dx	P_R	$\Delta s/V=P_R/4$
0	0	----------	----------	----------
.5	.287	0.48536		
.75	.404	.44925		
1.25	.616	.40359		
2.5	1.077	.34104		
5.0	1.841	.27718		
7.5	2.483	.23868		
10	3.043	.21050		
15	3.985	.16892		
20	4.748	.13734		
25	5.367	.11101		
30	5.863	.08775	1.111	0.278
35	6.248	.06634		
40	6.528	.04601		
45	6.709	.02613		
50	6.790	.00620		
55	6.770	−.01433		
60	6.644	−.03611		
65	6.405	−.06010		
70	6.037	−.08790		
75	5.514	−.12311		
80	4.771	−.18412		
85	3.683	−.23921	.833	.208
90	2.435	−.25583	.556	.139
95	1.103	−.24004	.278	.069
100	0	−.20385	0	0

NACA MEAN LINE $a=0.9$

$c_{l_i}=1.0$ $\alpha_i=0.90°$ $c_{m_{c/4}}=-0.225$

x (percent c)	y_c (percent c)	dy_c/dx	P_R	$\Delta s/V=P_R/4$
0	0	----------	----------	----------
.5	.269	0.45182		
.75	.379	.42064		
1.25	.577	.37740		
2.5	1.008	.31821		
5.0	1.720	.25786		
7.5	2.316	.22158		
10	2.835	.19500		
15	3.707	.15595		
20	4.410	.12644		
25	4.980	.10190		
30	5.435	.08047		
35	5.787	.06084	1.053	0.263
40	6.045	.04234		
45	6.212	.02447		
50	6.290	.00678		
55	6.279	−.01111		
60	6.178	−.02965		
65	5.981	−.04938		
70	5.681	−.07103		
75	5.265	−.09583		
80	4.714	−.12605		
85	3.987	−.16727		
90	2.984	−.25204		
95	1.503	−.31403	.526	.132
100	0	−.26086	0	0

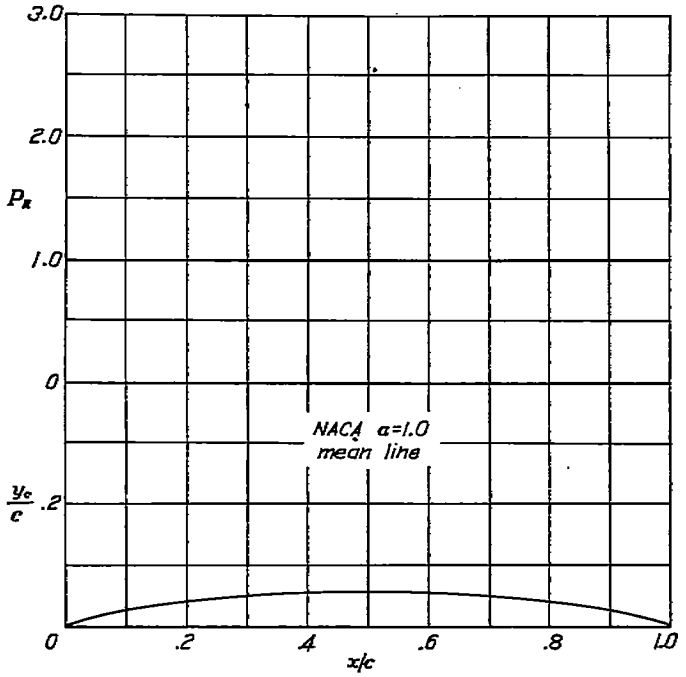

NACA MEAN LINE $\alpha=1.0$

$c_{l_i}=1.0$ $\alpha_i=0°$ $c_{m_{c/4}}=-0.250$

x (percent c)	y_c (percent c)	dy_c/dx	P_R	$\Delta\varepsilon_i/V=P_R/4$
0	0	----------	----------	----------
.5	.250	0.42120		
.75	.350	.38875		
1.25	.535	.34770		
2.5	.930	.29156		
5.0	1.580	.23430		
7.5	2.120	.19995		
10	2.585	.17485		
15	3.365	.13905		
20	3.980	.11030		
25	4.475	.08745		
30	4.860	.06745		
35	5.150	.04925	1.000	0.250
40	5.355	.03225		
45	5.475	.01595		
50	5.515	0		
55	5.475	−.01595		
60	5.355	−.03225		
65	5.150	−.04925		
70	4.860	−.06745		
75	4.475	−.08745		
80	3.980	−.11030		
85	3.365	−.13905		
90	2.585	−.17485		
95	1.580	−.23430		
100	0	----------	----------	----------

III—AIRFOIL ORDINATES

	Page
NACA 0006	358
NACA 0009	358
NACA 1408	358
NACA 1410	358
NACA 1412	358
NACA 2412	358
NACA 2415	358
NACA 2418	358
NACA 2421	358
NACA 2424	358
NACA 4412	359
NACA 4415	359
NACA 4418	359
NACA 4421	359
NACA 4424	359
NACA 23012	359
NACA 23015	359
NACA 23018	359
NACA 23021	359
NACA 23024	359
NACA 63, 4–420	360
NACA 63, 4–420, $a=0.3$	360
NACA 63(420)–422	360
NACA 63(420)–517	360
NACA 63–006	360
NACA 63–009	360
NACA 63–206	360
NACA 63–209	360
NACA 63–210	360
NACA 63_1–012	360
NACA 63_1–212	361
NACA 63_1–412	361
NACA 63_2–015	361
NACA 63_2–215	361
NACA 63_2–415	361
NACA 63_2–615	361
NACA 63_3–018	361
NACA 63_3–218	361
NACA 63_3–418	361
NACA 63_3–618	361
NACA 63_4–021	362
NACA 63_4–221	362
NACA 63_4–421	362
NACA 64–006	362
NACA 64–009	362
NACA 64–108	362
NACA 64–110	362
NACA 64–206	362
NACA 64–208	362
NACA 64–209	362
NACA 64–210	363
NACA 64_1–012	363
NACA 64_1–112	363
NACA 64_1–212	363
NACA 64_1–412	363
NACA 64_2–015	363
NACA 64_2–215	363
NACA 64_2–415	363
NACA 64_3–018	363
NACA 64_3–218	363
NACA 64_3–418	364
NACA 64_3–618	364
NACA 64_4–021	364
NACA 64_4–221	364
NACA 64_4–421	364
NACA 65, 3–018	364
NACA 65, 3–418, $a=0.8$	364
NACA 65, 3–618	364
NACA 65(216)–415, $a=0.5$	364
NACA 65–006	364
NACA 65–009	365
NACA 65–206	365
NACA 65–209	365
NACA 65–210	365
NACA 65–410	365
NACA 65_1–012	365
NACA 65_1–212	365
NACA 65_1–212, $a=0.6$	365
NACA 65_1–412	365
NACA 65_2–015	365
NACA 65_2–215	366
NACA 65_2–415	366
NACA 65_2–415, $a=0.5$	366
NACA 65_2–018	366
NACA 65_3–218	366
NACA 65_3–418	366
NACA 65_3–418, $a=0.5$	366
NACA 65_3–618	366
NACA 65_3–618, $a=0.5$	366
NACA 65_4–021	366
NACA 65_4–221	367
NACA 65_4–421	367
NACA 65_4–421, $a=0.5$	367
NACA 65(a=0)–114	367
NACA 65(a=0)–420	367
NACA 66,1–212	367
NACA 66(215)–016	367
NACA 66(215)–216	367
NACA 66(215)–216, $a=0.6$	367
NACA 66(215)–416	367
NACA 66–006	368
NACA 66–009	368
NACA 66–206	368
NACA 66–209	368
NACA 66–210	368
NACA 66_1–012	368
NACA 66_1–212	368
NACA 66_2–015	368
NACA 66_2–215	368
NACA 66_2–415	368
NACA 66_3–018	369
NACA 66_3–218	369
NACA 66_3–418	369
NACA 66_4–021	369
NACA 66_4–221	369
NACA 67,1–215	369
NACA 747A315	369
NACA 747A415	369

843107—50——24

NACA 0006

[Stations and ordinates given in percent of airfoil chord]

Upper surface		Lower surface	
Station	Ordinate	Station	Ordinate
0	0	0	0
1.25	.95	1.25	−.95
2.5	1.31	2.5	−1.31
5.0	1.78	5.0	−1.78
7.5	2.10	7.5	−2.10
10	2.34	10	−2.34
15	2.67	15	−2.67
20	2.87	20	−2.87
25	2.97	25	−2.97
30	3.00	30	−3.00
40	2.90	40	−2.90
50	2.65	50	−2.65
60	2.28	60	−2.28
70	1.83	70	−1.83
80	1.31	80	−1.31
90	.72	90	−.72
95	.40	95	−.40
100	(.06)	100	(−.06)
100	0	100	0

L. E. radius: 0.40

NACA 0009

[Stations and ordinates given in percent of airfoil chord]

Upper surface		Lower surface	
Station	Ordinate	Station	Ordinate
0	0	0	0
1.25	1.42	1.25	−1.42
2.5	1.96	2.5	−1.96
5.0	2.67	5.0	−2.67
7.5	3.15	7.5	−3.15
10	3.51	10	−3.51
15	4.01	15	−4.01
20	4.30	20	−4.30
25	4.46	25	−4.46
30	4.50	30	−4.50
40	4.35	40	−4.35
50	3.97	50	−3.97
60	3.42	60	−3.42
70	2.75	70	−2.75
80	1.97	80	−1.97
90	1.09	90	−1.09
95	.60	95	−.60
100	(.10)	100	(−.10)
100	0	100	0

L. E. radius: 0.89

NACA 1408

[Stations and ordinates given in percent of airfoil chord]

Upper surface		Lower surface	
Station	Ordinate	Station	Ordinate
0	0	0	0
1.189	1.824	1.311	−1.200
2.418	1.862	2.562	−1.620
4.896	2.602	5.104	−2.184
7.386	3.138	7.614	−2.458
9.883	3.558	10.117	−2.682
14.889	4.171	15.111	−2.953
19.904	4.574	20.096	−3.074
24.926	4.819	25.074	−3.101
29.950	4.939	30.050	−3.063
40.000	4.869	40.000	−2.869
50.020	4.502	49.980	−2.556
60.034	3.931	59.966	−2.153
70.041	3.193	69.959	−1.698
80.039	2.305	79.961	−1.193
90.027	1.271	89.973	−.659
95.016	.698	94.984	−.378
100.000	.084	100.000	−.084

L. E. radius: 0.70
Slope of radius through L. E.: 0.05

NACA 1410

[Stations and ordinates given in percent of airfoil chord]

Upper surface		Lower surface	
Station	Ordinate	Station	Ordinate
0	0	0	0
1.174	1.639	1.326	−1.515
2.398	2.297	2.602	−2.055
4.870	3.194	5.130	−2.726
7.358	3.837	7.642	−3.157
9.854	4.338	10.146	−3.462
14.861	5.062	15.139	−3.844
19.880	5.531	20.120	−4.031
24.907	5.809	25.093	−4.091
29.937	5.940	30.063	−4.064
40.000	5.836	40.000	−3.836
50.025	5.385	49.975	−3.439
60.042	4.692	59.958	−2.914
70.051	3.804	69.949	−2.304
80.049	2.741	79.951	−1.629
90.034	1.513	89.966	−.901
95.021	.832	94.979	−.512
100.000	.105	100.000	−.105

L. E. radius: 1.10
Slope of radius through L. E.: 0.05

NACA 1412

[Stations and ordinates given in percent of airfoil chord]

Upper surface		Lower surface	
Station	Ordinate	Station	Ordinate
0	0	0	0
1.158	1.954	1.342	−1.830
2.378	2.733	2.622	−2.491
4.845	3.786	5.155	−3.318
7.330	4.537	7.670	−3.857
9.824	5.118	10.176	−4.242
14.833	5.951	15.167	−4.733
19.857	6.486	20.143	−4.986
24.889	6.799	25.111	−5.081
29.925	6.940	30.075	−5.064
40.000	6.803	40.000	−4.803
50.029	6.267	49.971	−4.321
60.051	5.453	59.949	−3.675
70.061	4.413	69.939	−2.913
80.058	3.178	79.942	−2.066
90.040	1.753	89.960	−1.141
95.028	.966	94.975	−.646
100.000	.126	100.000	−.126

L. E. radius: 1.58
Slope of radius through L. E.: 0.05

NACA 2412

[Stations and ordinates given in percent of airfoil chord]

Upper surface		Lower surface	
Station	Ordinate	Station	Ordinate
0	-----	0	0
1.25	2.15	1.25	−1.65
2.5	2.99	2.5	−2.27
5.0	4.13	5.0	−3.01
7.5	4.96	7.5	−3.46
10	5.63	10	−3.75
15	6.61	15	−4.10
20	7.26	20	−4.28
25	7.67	25	−4.22
30	7.88	30	−4.12
40	7.80	40	−3.80
50	7.24	50	−3.34
60	6.36	60	−2.76
70	5.18	70	−2.14
80	3.75	80	−1.50
90	2.08	90	−.82
95	1.14	95	−.48
100	(.13)	100	(−.13)
100	-----	100	0

L. E. radius: 1.58
Slope of radius through L. E.: 0.10

NACA 2415

[Stations and ordinates given in percent of airfoil chord]

Upper surface		Lower surface	
Station	Ordinate	Station	Ordinate
0	-----	0	0
1.25	2.71	1.25	−2.06
2.5	3.71	2.5	−2.86
5.0	5.07	5.0	−3.84
7.5	6.06	7.5	−4.47
10	6.83	10	−4.90
15	7.97	15	−5.42
20	8.70	20	−5.66
25	9.17	25	−5.70
30	9.38	30	−5.62
40	9.25	40	−5.25
50	8.87	50	−4.67
60	7.80	60	−3.90
70	6.10	70	−3.05
80	4.41	80	−2.15
90	2.45	90	−1.17
95	1.34	95	−.68
100	(.16)	100	(−.16)
100	-----	100	0

L. E. radius: 2.48
Slope of radius through L. E.: 0.10

NACA 2418

[Stations and ordinates given in percent of airfoil chord]

Upper surface		Lower surface	
Station	Ordinate	Station	Ordinate
0	-----	0	0
1.25	3.28	1.25	−2.45
2.5	4.45	2.5	−3.44
5.0	6.08	5.0	−4.68
7.5	7.17	7.5	−5.48
10	8.05	10	−6.03
15	9.34	15	−6.74
20	10.15	20	−7.09
25	10.65	25	−7.18
30	10.88	30	−7.12
40	10.71	40	−6.71
50	9.89	50	−5.99
60	8.65	60	−5.04
70	7.02	70	−3.97
80	5.08	80	−2.80
90	2.81	90	−1.53
95	1.55	95	−.87
100	(.19)	100	(−.19)
100	-----	100	0

L. E. radius: 3.56
Slope of radius through L. E.: 0.10

NACA 2421

[Stations and ordinates given in percent of airfoil chord]

Upper surface		Lower surface	
Station	Ordinate	Station	Ordinate
0	-----	0	0
1.25	3.87	1.25	−2.82
2.5	5.21	2.5	−4.02
5.0	7.00	5.0	−5.51
7.5	8.29	7.5	−6.48
10	9.28	10	−7.18
15	10.70	15	−8.05
20	11.59	20	−8.52
25	12.15	25	−8.67
30	12.38	30	−8.62
40	12.16	40	−8.16
50	11.22	50	−7.31
60	9.79	60	−6.17
70	7.94	70	−4.87
80	5.74	80	−3.44
90	3.18	90	−1.88
95	1.76	95	−1.06
100	(.22)	100	(−.22)
100	-----	100	0

L. E. radius: 4.85
Slope of radius through L. E.: 0.10

NACA 2424

[Stations and ordinates given in percent of airfoil chord]

Upper surface		Lower surface	
Station	Ordinate	Station	Ordinate
0	0	0	0
.885	3.892	1.615	−3.646
2.012	5.449	2.988	−4.965
4.380	7.552	5.620	−6.614
6.820	9.052	8.180	−7.692
9.300	10.215	10.700	−8.465
14.333	11.888	15.667	−9.450
19.427	12.959	20.573	−9.959
24.555	13.593	25.445	−10.155
29.700	13.874	30.300	−10.124
40.000	13.606	40.000	−9.606
50.118	12.532	49.882	−8.644
60.203	10.903	59.797	−7.347
70.244	8.824	69.756	−5.824
80.233	6.352	79.767	−4.130
90.161	3.502	89.839	−2.280
95.098	1.930	94.902	−1.292
100.000	-------	100.000	0

L. E. radius: 6.33
Slope of radius through L. E.: 0.10

NACA 4412

[Stations and ordinates given in percent of airfoil chord]

Upper surface		Lower surface	
Station	Ordinate	Station	Ordinate
0	0	0	0
1.25	2.44	1.25	−1.48
2.5	3.39	2.5	−1.95
5.0	4.73	5.0	−2.49
7.5	5.76	7.5	−2.74
10	6.59	10	−2.86
15	7.89	15	−2.88
20	8.80	20	−2.74
25	9.41	25	−2.50
30	9.76	30	−2.26
40	9.80	40	−1.80
50	9.19	50	−1.40
60	8.14	60	−1.00
70	6.69	70	−.65
80	4.89	80	−.39
90	2.71	90	−.22
95	1.47	95	−.16
100	(.13)	100	(−.13)
100	-------	100	0

L. E. radius: 1.58
Slope of radius through L. E.: 0.20

NACA 4415

[Stations and ordinates given in percent of airfoil chord]

Upper surface		Lower surface	
Station	Ordinate	Station	Ordinate
0	-------	0	0
1.25	3.07	1.25	−1.79
2.5	4.17	2.5	−2.48
5.0	5.74	5.0	−3.27
7.5	6.91	7.5	−3.71
10	7.84	10	−3.98
15	9.27	15	−4.18
20	10.25	20	−4.15
25	10.92	25	−3.98
30	11.25	30	−3.75
40	11.25	40	−3.25
50	10.53	50	−2.72
60	9.30	60	−2.14
70	7.63	70	−1.55
80	5.55	80	−1.03
90	3.08	90	−.57
95	1.67	95	−.36
100	(.16)	100	(−.16)
100	-------	100	0

L. E. radius: 2.48
Slope of radius through L. E.: 0.20

NACA 4418

[Stations and ordinates given in percent of airfoil chord]

Upper surface		Lower surface	
Station	Ordinate	Station	Ordinate
0	-------	0	0
1.25	3.76	1.25	−2.11
2.5	5.00	2.5	−2.99
5.0	6.75	5.0	−4.06
7.5	8.06	7.5	−4.67
10	9.11	10	−5.06
15	10.66	15	−5.49
20	11.72	20	−5.56
25	12.40	25	−5.49
30	12.76	30	−5.26
40	12.70	40	−4.70
50	11.85	50	−4.02
60	10.44	60	−3.24
70	8.55	70	−2.45
80	6.22	80	−1.67
90	3.46	90	−.93
95	1.89	95	−.55
100	(.19)	100	(−.19)
100	-------	100	0

L. E. radius: 3.56
Slope of radius through L. E.: 0.20

NACA 4421

[Stations and ordinates given in percent of airfoil chord]

Upper surface		Lower surface	
Station	Ordinate	Station	Ordinate
0	-----	0	0
1.25	4.45	1.25	−2.42
2.5	5.84	2.5	−3.48
5.0	7.82	5.0	−4.78
7.5	9.24	7.5	−5.62
10	10.35	10	−6.15
15	12.04	15	−6.75
20	13.17	20	−6.98
25	13.88	25	−6.92
30	14.27	30	−6.70
40	14.16	40	−6.16
50	13.18	50	−5.34
60	11.60	60	−4.40
70	9.50	70	−3.35
80	6.91	80	−2.31
90	3.85	90	−1.27
95	2.11	95	−.74
100	(.22)	100	(−.22)
100	-----	100	0

L. E. radius: 4.85
Slope of radius through L. E.: 0.20

NACA 4424

[Stations and ordinates given in percent of airfoil chord]

Upper surface		Lower surface	
Station	Ordinate	Station	Ordinate
0	0	0	0
.580	3.904	1.970	−3.472
1.536	5.624	3.464	−4.650
3.775	7.942	6.225	−6.086
6.153	9.651	8.847	−6.981
8.611	11.012	11.389	−7.512
13.674	13.045	16.326	−8.169
18.858	14.416	21.142	−8.416
24.111	15.287	25.889	−8.411
29.401	15.738	30.599	−8.238
40.000	15.606	40.000	−7.606
50.235	14.474	49.765	−6.698
60.405	12.674	59.595	−5.562
70.487	10.312	69.513	−4.312
80.464	7.447	79.536	−3.003
90.320	4.099	89.680	−1.655
95.196	2.240	94.804	−.964
100.000	-----	100.000	0

L. E. radius: 6.33
Slope of radius through L. E.: 0.20

NACA 23012

[Stations and ordinates given in percent of airfoil chord]

Upper surface		Lower surface	
Station	Ordinate	Station	Ordinate
0	-----	0	0
1.25	2.67	1.25	−1.23
2.5	3.61	2.5	−1.71
5.0	4.91	5.0	−2.26
7.5	5.80	7.5	−2.61
10	6.43	10	−2.92
15	7.19	15	−3.50
20	7.50	20	−3.97
25	7.60	25	−4.28
30	7.55	30	−4.46
40	7.14	40	−4.48
50	6.41	50	−4.17
60	5.47	60	−3.67
70	4.36	70	−3.00
80	3.08	80	−2.16
90	1.68	90	−1.23
95	.92	95	−.70
100	(.13)	100	(−.13)
100	-----	100	0

L. E. radius: 1.58
Slope of radius through L. E.: 0.305

NACA 23015

[Stations and ordinates given in percent of airfoil chord]

Upper surface		Lower surface	
Station	Ordinate	Station	Ordinate
0	-----	0	0
1.25	3.84	1.25	−1.54
2.5	4.44	2.5	−2.25
5.0	5.89	5.0	−3.04
7.5	6.90	7.5	−3.61
10	7.64	10	−4.00
15	8.52	15	−4.84
20	8.92	20	−5.41
25	9.08	25	−5.78
30	9.05	30	−5.96
40	8.59	40	−5.92
50	7.74	50	−5.50
60	6.61	60	−4.81
70	5.25	70	−3.91
80	3.73	80	−2.83
90	2.04	90	−1.59
95	1.12	95	−.90
100	(.16)	100	(−.16)
100	-----	100	0

L. E. radius: 2.48
Slope of radius through L. E.: 0.305

NACA 23018

[Stations and ordinates given in percent of airfoil chord]

Upper surface		Lower surface	
Station	Ordinate	Station	Ordinate
0	-----	0	0
1.25	4.09	1.25	−1.83
2.5	5.29	2.5	−2.71
5.0	6.92	5.0	−3.80
7.5	8.01	7.5	−4.60
10	8.83	10	−5.22
15	9.86	15	−6.18
20	10.36	20	−6.86
25	10.56	25	−7.27
30	10.55	30	−7.47
40	10.04	40	−7.37
50	9.05	50	−6.81
60	7.75	60	−5.94
70	6.18	70	−4.82
80	4.40	80	−3.48
90	2.39	90	−1.94
95	1.32	95	−1.09
100	(.19)	100	(−.19)
100	-----	100	0

L. E. radius: 3.56
Slope of radius through L. E.: 0.305

NACA 23021

[Stations and ordinates given in percent of airfoil chord]

Upper surface		Lower surface	
Station	Ordinate	Station	Ordinate
0	-----	0	0
1.25	4.87	1.25	−2.08
2.5	6.14	2.5	−3.14
5.0	7.93	5.0	−4.52
7.5	9.13	7.5	−5.55
10	10.08	10	−6.32
15	11.19	15	−7.51
20	11.80	20	−8.30
25	12.05	25	−8.76
30	12.06	30	−8.95
40	11.49	40	−8.83
50	10.40	50	−8.14
60	8.90	60	−7.07
70	7.09	70	−5.72
80	5.05	80	−4.13
90	2.76	90	−2.30
95	1.53	95	−1.30
100	(.22)	100	(−.22)
100	-----	100	0

L. E. radius: 4.85
Slope of radius through L. E.: 0.305

NACA 23024

[Stations and ordinates given in percent of airfoil chord]

Upper surface		Lower surface	
Station	Ordinate	Station	Ordinate
0	0	0	0
.277	4.017	2.223	−3.308
1.331	5.764	3.669	−4.482
3.858	8.172	6.147	−5.862
6.601	9.884	8.399	−6.880
9.423	11.049	10.577	−7.647
15.001	12.528	14.999	−8.852
20.258	13.237	19.747	−9.703
25.262	13.535	24.738	−10.223
30.265	13.546	29.735	−10.454
40.256	12.928	39.744	−10.278
50.235	11.690	49.766	−9.482
60.202	10.008	59.798	−8.242
70.162	7.988	69.838	−6.664
80.116	5.687	79.884	−4.803
90.064	3.115	89.936	−2.673
95.036	1.724	94.964	−1.504
100	-----	100	0

L. E. radius: 6.33
Slope of radius through L. E.: 0.305

NACA 63,4-420

[Stations and ordinates given in percent of airfoil chord]

Upper surface		Lower surface	
Station	Ordinate	Station	Ordinate
0	0	0	0
.215	1.790	.785	−1.590
.430	2.196	1.070	−1.916
.887	2.827	1.613	−2.399
2.082	3.954	2.918	−3.210
4.538	5.557	5.462	−4.298
7.024	6.793	7.976	−5.097
9.526	7.817	10.474	−5.749
14.554	9.424	15.446	−6.732
19.603	10.589	20.397	−7.405
24.663	11.414	25.337	−7.834
29.732	11.895	30.268	−8.007
34.808	12.036	35.197	−7.916
39.874	11.906	40.126	−7.622
44.940	11.556	45.060	−7.176
50.000	11.025	50.000	−6.613
55.052	10.333	54.948	−5.953
60.095	9.492	59.905	−5.208
65.127	8.523	64.873	−4.403
70.148	7.438	69.852	−3.550
75.156	6.258	74.844	−2.673
80.150	4.990	79.850	−1.806
85.129	3.684	84.871	−.992
90.094	2.379	89.906	−.311
95.047	1.131	94.953	.133
100	0	100	0

L. E. radius: 3.16
Slope of radius through L. E.: 0.168

NACA 63,4-420

$a = 0.3$

[Stations and ordinates given in percent of airfoil chord]

Upper surface		Lower surface	
Station	Ordinate	Station	Ordinate
0	0	0	0
.065	1.814	.935	−1.502
.260	2.241	1.240	−1.805
.691	2.912	1.809	−2.244
1.856	4.128	3.144	−2.968
4.288	5.878	5.712	−3.914
6.771	7.237	8.229	−4.601
9.280	8.366	10.720	−5.128
14.347	10.132	15.653	−5.996
19.458	11.410	20.542	−6.570
24.604	12.296	25.396	−6.948
29.808	12.781	30.192	−7.125
35.008	12.848	34.992	−7.108
40.145	12.594	39.855	−6.934
45.243	12.089	44.757	−6.637
50.308	11.388	49.692	−6.240
55.344	10.516	54.656	−5.756
60.353	9.497	59.647	−5.189
65.339	8.357	64.661	−4.553
70.305	7.120	69.695	−3.856
75.250	5.807	74.744	−3.111
80.197	4.458	79.803	−2.337
85.134	3.108	84.866	−1.568
90.073	1.836	89.927	−.856
95.025	.728	94.975	−.272
100.000	0	100.000	0

L. E. radius: 3.16
Slope of radius through L. E.: 0.262

NACA 63(420)-422

[Stations and ordinates given in percent of airfoil chord]

Upper surface		Lower surface	
Station	Ordinate	Station	Ordinate
0	0	0	0
.187	1.959	.813	−1.769
3.98	2.402	1.102	−2.122
.850	3.088	1.650	−2.660
2.041	4.312	2.959	−3.568
4.492	6.050	5.508	−4.786
6.977	7.387	8.023	−5.691
9.478	8.496	10.522	−6.428
14.509	10.231	15.491	−7.539
19.563	11.489	20.437	−8.305
24.630	12.377	25.370	−8.797
29.705	12.890	30.295	−9.002
34.784	13.034	35.216	−8.914
39.861	12.883	40.139	−8.599
44.934	12.498	45.066	−8.113
50.000	11.907	50.000	−7.495
55.057	11.147	54.943	−6.767
60.104	10.227	59.896	−5.948
65.140	9.169	64.860	−5.049
70.163	7.988	69.837	−4.100
75.172	6.700	74.828	−3.120
80.165	5.329	79.835	−2.145
85.142	3.918	84.858	−1.226
90.103	2.513	89.897	−.446
95.051	1.181	94.949	.033
100.000	0	100.000	0

L. E. radius: 3.82
Slope of radius through L. E.: 0.198

NACA 63(420)-517

[Stations and ordinates given in percent of airfoil chord]

Upper surface		Lower surface	
Station	Ordinate	Station	Ordinate
0	0	0	0
.200	1.551	.800	−1.301
.412	1.912	1.088	−1.562
.868	2.477	1.634	−1.941
2.058	3.498	2.942	−2.508
4.511	4.966	5.489	−3.336
6.996	6.104	8.004	−3.924
9.497	7.050	10.503	−4.466
14.527	8.542	15.473	−5.178
19.578	9.633	20.422	−5.653
24.642	10.416	25.358	−5.940
29.715	10.887	30.285	−6.027
34.791	11.053	35.209	−5.903
39.866	10.977	40.134	−5.621
44.936	10.699	45.064	−5.223
50.000	10.254	50.000	−4.738
55.055	9.660	54.945	−4.184
60.101	8.925	59.899	−3.569
65.135	8.067	64.865	−2.917
70.157	7.099	69.843	−2.239
75.166	6.030	74.834	−1.554
80.159	4.877	79.841	−.897
85.137	3.668	84.863	−.304
90.100	2.434	89.900	.150
95.050	1.218	94.950	.367
100.000	0	100.000	0

L. E. radius: 2.283
Slope of radius through L. E.: 0.211

NACA 63-006

[Stations and ordinates given in percent of airfoil chord]

Upper surface		Lower surface	
Station	Ordinate	Station	Ordinate
0	0	0	0
.5	.508	.5	−.508
.75	.609	.75	−.609
1.25	.771	1.25	−.771
2.5	1.057	2.5	−1.057
5.0	1.462	5.0	−1.462
7.5	1.766	7.5	−1.766
10	2.010	10	−2.010
15	2.386	15	−2.386
20	2.656	20	−2.656
25	2.841	25	−2.841
30	2.954	30	−2.954
35	3.000	35	−3.000
40	2.971	40	−2.971
45	2.877	45	−2.877
50	2.723	50	−2.723
55	2.517	55	−2.517
60	2.267	60	−2.267
65	1.982	65	−1.982
70	1.670	70	−1.670
75	1.342	75	−1.342
80	1.008	80	−1.008
85	.683	85	−.683
90	.383	90	−.383
95	.138	95	−.138
100	0	100	0

L. E. radius: 0.297

NACA 63-009

[Stations and ordinates given in percent of airfoil chord]

Upper surface		Lower surface	
Station	Ordinate	Station	Ordinate
0	0	0	0
.5	.749	.5	−.749
.75	.906	.75	−.906
1.25	1.151	1.25	−1.151
2.5	1.582	2.5	−1.582
5.0	2.196	5.0	−2.196
7.5	2.655	7.5	−2.655
10	3.024	10	−3.024
15	3.591	15	−3.591
20	3.997	20	−3.997
25	4.275	25	−4.275
30	4.442	30	−4.442
35	4.500	35	−4.500
40	4.447	40	−4.447
45	4.296	45	−4.296
50	4.056	50	−4.056
55	3.739	55	−3.739
60	3.358	60	−3.358
65	2.928	65	−2.928
70	2.458	70	−2.458
75	1.966	75	−1.966
80	1.471	80	−1.471
85	.990	85	−.990
90	.550	90	−.550
95	.196	95	−.196
100	0	100	0

L. E. radius: 0.631

NACA 63-206

[Stations and ordinates given in percent of airfoil chord]

Upper surface		Lower surface	
Station	Ordinate	Station	Ordinate
0	0	0	0
.458	.551	.542	−.451
.703	.677	.797	−.537
1.197	.876	1.303	−.662
2.438	1.241	2.562	−.869
4.932	1.776	5.068	−1.144
7.429	2.189	7.571	−1.341
9.930	2.526	10.070	−1.492
14.934	3.058	15.066	−1.712
19.941	3.451	20.059	−1.859
24.950	3.736	25.050	−1.946
29.960	3.920	30.040	−1.982
34.970	4.030	35.030	−1.970
39.981	4.042	40.019	−1.900
44.991	3.972	45.009	−1.782
50.000	3.826	50.000	−1.620
55.008	3.612	54.992	−1.422
60.015	3.338	59.985	−1.196
65.020	3.012	64.980	−.952
70.023	2.642	69.977	−.698
75.023	2.237	74.977	−.447
80.022	1.804	79.978	−.212
85.019	1.356	84.981	−.010
90.013	.900	89.987	.134
95.000	.454	94.994	.178
100.000	0	100.000	0

L. E. radius: 0.297
Slope of radius through L. E.: 0.0842

NACA 63-209

[Stations and ordinates given in percent of airfoil chord]

Upper surface		Lower surface	
Station	Ordinate	Station	Ordinate
0	0	0	0
.437	.796	.563	−.696
.680	1.107	.820	−.833
1.170	1.255	1.330	−1.041
2.408	1.765	2.592	−1.398
4.897	2.510	5.103	−1.878
7.394	3.077	7.606	−2.229
9.894	3.539	10.106	−2.505
14.901	4.263	15.099	−2.917
19.912	4.792	20.088	−3.200
24.925	5.169	25.075	−3.379
29.940	5.414	30.060	−3.470
34.956	5.530	35.044	−3.470
39.971	5.518	40.029	−3.376
44.986	5.391	45.014	−3.201
50.000	5.169	50.000	−2.953
55.012	4.854	54.988	−2.644
60.022	4.429	59.978	−2.287
65.029	3.928	64.971	−1.896
70.033	3.430	69.967	−1.488
75.034	2.861	74.966	−1.071
80.032	2.267	79.968	−.675
85.027	1.663	84.973	−.317
90.019	1.067	89.981	−.033
95.009	.512	94.991	.120
100.000	0	100.000	0

L. E. radius: 0.631
Slope of radius through L. E.: 0.0842

NACA 63-210

[Stations and ordinates given in percent of airfoil chord]

Upper surface		Lower surface	
Station	Ordinate	Station	Ordinate
0	0	0	0
.430	.876	.570	−.776
.669	1.207	.831	−.967
1.162	1.379	1.338	−1.165
2.395	1.939	2.602	−1.567
4.886	2.753	5.114	−2.121
7.382	3.372	7.618	−2.524
9.882	3.877	10.118	−2.843
14.890	4.665	15.110	−3.319
19.902	5.240	20.098	−3.648
24.917	5.647	25.083	−3.857
29.933	5.910	30.067	−3.966
34.951	6.030	35.049	−3.970
39.968	6.009	40.032	−3.867
44.985	5.861	45.015	−3.671
50.000	5.599	50.000	−3.393
55.013	5.235	54.987	−3.045
60.024	4.786	59.976	−2.644
65.032	4.264	64.968	−2.204
70.036	3.684	69.964	−1.740
75.038	3.061	74.962	−1.271
80.036	2.414	79.964	−.822
85.030	1.761	84.970	−.415
90.021	1.121	89.979	−.087
95.010	.530	94.990	.102
100.000	0	100.000	0

L. E. radius: 0.770
Slope of radius through L. E.: 0.0842

NACA 631-012

[Stations and ordinates given in percent of airfoil chord]

Upper surface		Lower surface	
Station	Ordinate	Station	Ordinate
0	0	0	0
.5	.985	.5	−.985
.75	1.194	.75	−1.194
1.25	1.519	1.25	−1.519
2.5	2.102	2.5	−2.102
5.0	2.925	5.0	−2.925
7.5	3.542	7.5	−3.542
10	4.039	10	−4.039
15	4.799	15	−4.799
20	5.342	20	−5.342
25	5.712	25	−5.712
30	5.930	30	−5.930
35	6.000	35	−6.000
40	5.920	40	−5.920
45	5.704	45	−5.704
50	5.370	50	−5.370
55	4.935	55	−4.935
60	4.420	60	−4.420
65	3.840	65	−3.840
70	3.210	70	−3.210
75	2.556	75	−2.556
80	1.902	80	−1.902
85	1.274	85	−1.274
90	.707	90	−.707
95	.250	95	−.250
100	0	100	0

L. E. radius: 1.087

NACA 63$_1$-212

[Stations and ordinates given in percent of airfoil chord]

Upper surface		Lower surface	
Station	Ordinate	Station	Ordinate
0	0	0	0
.417	1.032	.583	−.932
.587	1.260	.843	−1.120
1.145	1.622	1.355	−1.408
2.378	2.284	2.622	−1.912
4.868	3.238	5.137	−2.606
7.358	3.963	7.642	−3.115
9.859	4.554	10.141	−3.520
14.868	5.470	15.132	−4.124
19.882	6.137	20.118	−4.545
24.900	6.600	25.100	−4.816
29.920	6.901	30.080	−4.957
34.941	7.080	35.059	−4.970
39.962	6.991	40.038	−4.849
44.982	6.799	45.018	−4.609
50.000	6.473	50.000	−4.267
55.016	6.030	54.984	−3.840
60.029	5.491	59.971	−3.349
65.038	4.870	64.962	−2.810
70.043	4.182	69.957	−2.238
75.045	3.451	74.955	−1.661
80.042	2.698	79.958	−1.106
85.036	1.947	84.965	−.601
90.025	1.224	89.975	−.190
95.012	.560	94.988	.008
100.000	0	100.000	0

L. E. radius: 1.087
Slope of radius through L. E.: 0.0842

NACA 63$_1$-412

[Stations and ordinates given in percent of airfoil chord]

Upper surface		Lower surface	
Station	Ordinate	Station	Ordinate
0	0	0	0
.336	1.071	.664	−.871
.567	1.320	.933	−1.040
1.041	1.719	1.459	−1.291
2.287	2.460	2.743	−1.716
4.727	3.344	5.278	−2.380
7.218	4.079	7.782	−2.885
9.718	5.003	10.282	−2.995
14.735	6.138	15.265	−3.446
19.765	6.929	20.235	−3.745
24.800	7.409	25.200	−3.919
29.840	7.672	30.160	−3.984
34.882	8.069	35.118	−3.939
39.924	8.002	40.076	−3.778
44.964	7.804	45.036	−3.514
50.000	7.576	50.000	−3.164
55.031	7.125	54.969	−2.745
60.057	6.502	59.943	−2.278
65.076	5.899	64.924	−1.779
70.087	5.133	69.913	−1.265
75.089	4.344	74.911	−.764
80.084	3.492	79.916	−.308
85.070	2.618	84.930	.074
90.049	1.739	89.951	.329
95.023	.881	94.977	.383
100.000	0	100.000	0

L. E. radius: 1.087
Slope of radius through L. E.: 0.1685

NACA 63$_2$-015

[Stations and ordinates given in percent of airfoil chord]

Upper surface		Lower surface	
Station	Ordinate	Station	Ordinate
0	0	0	0
.5	1.204	.5	−1.204
.75	1.462	.75	−1.462
1.25	1.878	1.25	−1.878
2.5	2.610	2.5	−2.610
5.0	3.648	5.0	−3.648
7.5	4.427	7.5	−4.427
10	5.055	10	−5.055
15	6.011	15	−6.011
20	6.693	20	−6.693
25	7.155	25	−7.155
30	7.421	30	−7.421
35	7.500	35	−7.500
40	7.386	40	−7.386
45	7.099	45	−7.099
50	6.665	50	−6.665
55	6.103	55	−6.103
60	5.453	60	−5.453
65	4.721	65	−4.721
70	3.934	70	−3.934
75	3.119	75	−3.119
80	2.310	80	−2.310
85	1.541	85	−1.541
90	.852	90	−.852
95	.300	95	−.300
100	0	100	0

L. E. radius: 1.594

NACA 63$_2$-215

[Stations and ordinates given in percent of airfoil chord]

Upper surface		Lower surface	
Station	Ordinate	Station	Ordinate
0	0	0	0
.399	1.250	.601	−1.150
.687	1.528	.863	−1.388
1.120	1.980	1.380	−1.766
2.348	2.792	2.652	−2.420
4.829	3.960	5.171	−3.328
7.323	4.847	7.677	−3.999
9.823	5.569	10.177	−4.535
14.834	6.682	15.166	−5.336
19.852	7.437	20.148	−5.895
24.875	8.049	25.125	−6.259
29.900	8.392	30.100	−6.448
34.926	8.530	35.074	−6.470
39.952	8.457	40.048	−6.315
44.977	8.194	45.023	−6.004
50.000	7.768	50.000	−5.562
55.019	7.203	54.981	−5.013
60.035	6.524	59.965	−4.382
65.047	5.751	64.953	−3.691
70.053	4.906	69.947	−2.962
75.055	4.014	74.945	−2.224
80.051	3.105	79.949	−1.513
85.043	2.213	84.957	−.857
90.030	1.368	89.970	−.384
95.014	.616	94.986	−.016
100.000	0	100.000	0

L. E. radius: 1.594
Slope of radius through L. E.: 0.0842

NACA 63$_2$-415

Stations and ordinates given in percent of airfoil chord]

Upper surface		Lower surface	
Station	Ordinate	Station	Ordinate
0	0	0	0
.300	1.287	.700	−1.087
.525	1.585	.975	−1.305
.991	2.074	1.509	−1.646
2.198	2.964	2.802	−2.220
4.660	4.264	5.340	−3.000
7.147	5.251	7.853	−3.595
9.647	6.077	10.353	−4.009
14.669	7.348	15.331	−4.656
19.705	8.279	20.295	−5.095
24.750	8.941	25.250	−5.361
29.800	9.362	30.200	−5.474
34.852	9.589	35.148	−5.439
39.905	9.527	40.095	−5.243
44.955	9.249	45.045	−4.909
50.000	8.771	50.000	−4.459
55.039	8.298	54.961	−3.918
60.070	7.595	59.930	−3.311
65.093	6.780	64.907	−2.660
70.106	5.877	69.894	−1.989
75.109	4.907	74.891	−1.327
80.102	3.900	79.898	−.716
85.085	2.885	84.915	−.193
90.059	1.884	89.941	.184
95.028	.931	94.972	.333
100.000	0	100.000	0

L. E. radius: 1.594
Slope of radius through L. E.: 0.1685

NACA 63$_2$-615

Stations and ordinates given in percent of airfoil chord]

Upper surface		Lower surface	
Station	Ordinate	Station	Ordinate
0	0	0	0
.205	1.317	.795	−1.017
.418	1.634	1.082	−1.214
.866	2.189	1.634	−1.517
2.050	3.129	2.950	−2.013
4.492	4.500	5.508	−2.664
6.973	5.607	8.027	−3.128
9.473	6.578	10.527	−3.476
14.504	8.010	15.496	−3.972
19.558	9.066	20.442	−4.290
24.625	9.830	25.375	−4.480
29.700	10.331	30.300	−4.499
34.778	10.587	35.222	−4.407
39.857	10.598	40.143	−4.172
44.932	10.384	45.068	−3.814
50.000	9.974	50.000	−3.350
55.058	9.393	54.942	−2.823
60.105	8.665	59.895	−2.239
65.139	7.809	64.861	−1.629
70.159	6.847	69.841	−1.015
75.163	5.800	74.837	−.430
80.153	4.693	79.847	.033
85.127	3.555	84.873	.433
90.089	2.398	89.911	.704
95.042	1.245	94.958	.651
100.000	0	100.000	0

L. E. radius: 1.594
Slope of radius through L. E.: 0.2527

NACA 63$_3$-018

[Stations and ordinates given in percent of airfoil chord]

Upper surface		Lower surface	
Station	Ordinate	Station	Ordinate
0	0	0	0
.5	1.404	.5	−1.404
.75	1.718	.75	−1.718
1.25	2.217	1.25	−2.217
2.5	3.104	2.5	−3.104
5.0	4.362	5.0	−4.362
7.5	5.308	7.5	−5.308
10	6.068	10	−6.068
15	7.225	15	−7.225
20	8.048	20	−8.048
25	8.600	25	−8.600
30	8.913	30	−8.913
35	9.000	35	−9.000
40	8.845	40	−8.845
45	8.432	45	−8.432
50	7.942	50	−7.942
55	7.256	55	−7.256
60	6.455	60	−6.455
65	5.567	65	−5.567
70	4.622	70	−4.622
75	3.650	75	−3.650
80	2.691	80	−2.691
85	1.787	85	−1.787
90	.985	90	−.985
95	.348	95	−.848
100	0	100	0

L. E. radius: 2.120

NACA 63$_3$-218

[Stations and ordinates given in percent of airfoil chord]

Upper surface		Lower surface	
Station	Ordinate	Station	Ordinate
0	0	0	0
.382	1.440	.618	−1.849
.617	1.778	.883	−1.688
1.096	2.319	1.404	−2.105
2.319	3.285	2.681	−2.913
4.796	4.673	5.204	−4.041
7.288	5.728	7.712	−4.880
9.788	6.581	10.212	−5.547
14.801	7.895	15.199	−6.549
19.822	8.842	20.178	−7.250
24.850	9.494	25.150	−7.704
29.880	9.884	30.120	−7.940
34.911	10.030	35.089	−7.970
39.943	9.916	40.057	−7.774
44.973	9.577	45.027	−7.387
50.000	9.045	50.000	−6.839
55.023	8.351	54.977	−6.161
60.042	7.520	59.958	−5.384
65.055	6.597	64.945	−4.537
70.062	5.594	69.938	−3.650
75.064	4.544	74.936	−2.754
80.059	3.486	79.941	−1.894
85.049	2.459	84.951	−1.118
90.034	1.501	89.966	−.467
95.016	.664	94.984	−.082
100.000	0	100.000	0

L. E. radius: 2.120
Slope of radius through L. E.: 0.0842

NACA 63$_3$-418

[Stations and ordinates given in percent of airfoil chord]

Upper surface		Lower surface	
Station	Ordinate	Station	Ordinate
0	0	0	0
.287	1.484	.733	−1.284
.487	1.833	1.013	−1.553
.945	2.410	1.555	−1.982
2.140	3.455	2.860	−2.711
4.593	4.975	5.407	−3.711
7.077	6.139	7.923	−4.443
9.577	7.087	10.423	−5.019
14.602	8.560	15.398	−5.868
19.645	9.632	20.355	−6.448
24.699	10.385	25.301	−6.805
29.760	10.854	30.240	−6.966
34.828	11.058	35.177	−6.938
39.886	10.986	40.114	−6.702
44.940	10.672	45.054	−6.292
50.000	10.148	50.000	−5.736
55.046	9.446	54.954	−5.066
60.083	8.590	59.917	−4.312
65.110	7.626	64.890	−3.506
70.125	6.564	69.875	−2.670
75.128	5.438	74.872	−1.858
80.119	4.280	79.881	−1.096
85.099	3.130	84.901	−.438
90.069	2.017	89.931	.051
95.032	.978	94.968	.286
100.000	0	100.000	0

L. E. radius: 2.120
Slope of radius through L. E.: 0.1685

NACA 63$_3$-618

[Stations and ordinates given in percent of airfoil chord]

Upper surface		Lower surface	
Station	Ordinate	Station	Ordinate
0	0	0	0
.156	1.511	.844	−1.211
.361	1.878	1.139	−1.458
.797	2.491	1.708	−1.840
1.995	3.610	3.005	−2.500
4.393	5.268	5.607	−3.372
6.868	6.542	8.132	−3.998
9.367	7.586	10.633	−4.484
14.404	9.219	15.596	−5.181
19.469	10.418	20.531	−5.642
24.549	11.278	25.451	−5.903
29.640	11.822	30.360	−5.990
34.734	12.080	35.266	−5.908
39.829	12.066	40.171	−5.680
44.919	11.767	45.081	−5.107
50.000	11.251	50.000	−4.633
55.069	10.541	54.931	−3.971
60.125	9.667	59.875	−3.241
65.164	8.655	64.836	−2.475
70.187	7.534	69.813	−1.702
75.191	6.330	74.809	−.960
80.178	5.073	79.822	−.297
85.147	3.800	84.853	.233
90.103	2.531	89.897	.571
95.048	1.293	94.952	.603
100.000	0	100.000	0

L. E. radius: 2.120
Slope of radius through L. E.: 0.2527

NACA 63$_4$-021

[Stations and ordinates given in percent of airfoil chord]

Upper surface		Lower surface	
Station	Ordinate	Station	Ordinate
0	0	0	0
.5	1.583	.5	−1.583
.75	1.937	.75	−1.937
1.25	2.527	1.25	−2.527
2.5	3.577	2.5	−3.577
5.0	5.065	5.0	−5.065
7.5	6.182	7.5	−6.182
10	7.080	10	−7.080
15	8.441	15	−8.441
20	9.410	20	−9.410
25	10.058	25	−10.058
30	10.412	30	−10.412
35	10.500	35	−10.500
40	10.298	40	−10.298
45	9.854	45	−9.854
50	9.206	50	−9.206
55	8.390	55	−8.390
60	7.441	60	−7.441
65	6.396	65	−6.396
70	5.290	70	−5.290
75	4.160	75	−4.160
80	3.054	80	−3.054
85	2.021	85	−2.021
90	1.113	90	−1.113
95	.392	95	−.392
100	0	100	0

L. E. radius: 2.650

NACA 63$_4$-221

[Stations and ordinates given in percent of airfoil chord]

Upper surface		Lower surface	
Station	Ordinate	Station	Ordinate
0	0	0	0
.367	1.627	.633	−1.527
.600	2.001	.900	−1.861
1.075	2.628	1.425	−2.414
2.292	3.757	2.708	−3.385
4.763	5.375	5.237	−4.743
7.268	6.601	7.747	−5.753
9.753	7.593	10.247	−6.559
14.767	9.111	15.238	−7.765
19.792	10.204	20.208	−8.612
24.824	10.946	25.176	−9.156
29.860	11.383	30.140	−9.439
34.897	11.529	35.103	−9.469
39.934	11.369	40.066	−9.227
44.969	10.949	45.031	−8.759
50.000	10.309	50.000	−8.103
55.027	9.485	54.973	−7.296
60.048	8.512	59.952	−6.370
65.063	7.420	64.937	−5.366
70.071	6.262	69.929	−4.318
75.073	5.054	74.927	−3.264
80.067	3.849	79.933	−2.257
85.050	2.698	84.944	−1.347
90.039	1.629	89.961	−.595
95.018	.708	94.982	−.076
100.000	0	100.000	0

L. E. radius: 2.650
Slope of radius through L. E.: 0.0842

NACA 63$_4$-421

[Stations and ordinates given in percent of airfoil chord]

Upper surface		Lower surface	
Station	Ordinate	Station	Ordinate
0	0	0	0
.227	1.661	.773	−1.461
.452	2.054	1.048	−1.774
.902	2.717	1.598	−2.289
2.086	3.925	2.914	−3.181
4.527	5.675	5.473	−4.411
7.007	7.010	7.993	−5.314
9.506	8.097	10.494	−6.029
14.535	9.774	15.465	−7.082
19.585	10.993	20.415	−7.809
24.649	11.837	25.351	−8.257
29.719	12.352	30.281	−8.464
34.793	12.558	35.207	−8.438
39.867	12.459	40.133	−8.155
44.937	12.044	45.063	−7.664
50.000	11.412	50.000	−7.000
55.054	10.580	54.946	−6.200
60.096	9.582	59.904	−5.298
65.128	8.455	64.874	−4.335
70.148	7.232	69.857	−3.344
75.145	5.947	74.855	−2.367
80.135	4.643	79.805	−1.459
85.111	3.364	84.889	−.672
90.078	2.144	89.922	−.076
95.037	1.022	94.963	.242
100.000	0	100.000	0

L. E. radius: 2.650
Slope of radius through L. E.: 0.1685

NACA 64-006

[Stations and ordinates given in percent of airfoil chord]

Upper surface		Lower surface	
Station	Ordinate	Station	Ordinate
0	0	0	0
.50	.494	.50	−.494
.75	.596	.75	−.596
1.25	.754	1.25	−.754
2.5	1.024	2.5	−1.024
5.0	1.405	5.0	−1.405
7.5	1.692	7.5	−1.692
10	1.928	10	−1.928
15	2.298	15	−2.298
20	2.572	20	−2.572
25	2.772	25	−2.772
30	2.907	30	−2.907
35	2.981	35	−2.981
40	2.995	40	−2.995
45	2.919	45	−2.919
50	2.775	50	−2.775
55	2.575	55	−2.575
60	2.331	60	−2.331
65	2.050	65	−2.050
70	1.740	70	−1.740
75	1.412	75	−1.412
80	1.072	80	−1.072
85	.737	85	−.737
90	.423	90	−.423
95	.157	95	−.157
100	0	100	0

L. E. radius: 0.256

NACA 64-009

[Stations and ordinates given in percent of airfoil chord]

Upper surface		Lower surface	
Station	Ordinate	Station	Ordinate
0	0	0	0
.50	.739	.50	−.739
.75	.892	.75	−.892
1.25	1.128	1.25	−1.128
2.5	1.533	2.5	−1.533
5.0	2.109	5.0	−2.109
7.5	2.543	7.5	−2.543
10	2.898	10	−2.898
15	3.455	15	−3.455
20	3.868	20	−3.868
25	4.170	25	−4.170
30	4.373	30	−4.373
35	4.479	35	−4.479
40	4.490	40	−4.490
45	4.384	45	−4.384
50	4.136	50	−4.136
55	3.826	55	−3.826
60	3.452	60	−3.452
65	3.026	65	−3.026
70	2.561	70	−2.561
75	2.069	75	−2.069
80	1.564	80	−1.564
85	1.069	85	−1.069
90	.611	90	−.611
95	.227	95	−.227
100	0	100	0

L. E. radius: 0.572

NACA 64-108

[Stations and ordinates given in percent of airfoil chord]

Upper surface		Lower surface	
Station	Ordinate	Station	Ordinate
0	0	0	0
.472	.662	.528	−.662
.719	.828	.781	−.768
1.215	1.058	1.285	−.960
2.460	1.467	2.540	−1.271
4.956	2.032	5.044	−1.716
7.455	2.471	7.545	−2.047
9.955	2.832	10.045	−2.316
14.958	3.405	15.042	−2.733
19.962	3.835	20.038	−3.039
24.968	4.152	25.032	−3.256
29.974	4.370	30.026	−3.398
34.980	4.494	35.020	−3.464
39.987	4.528	40.013	−3.466
44.994	4.481	45.006	−3.335
50.000	4.236	50.000	−3.132
55.005	3.959	54.995	−2.863
60.010	3.617	59.990	−2.545
65.013	3.219	64.987	−2.189
70.015	2.777	69.985	−1.805
75.016	2.302	74.984	−1.406
80.015	1.803	79.985	−1.006
85.013	1.297	84.987	−.625
90.010	.805	89.990	−.292
95.005	.364	94.995	−.048
100.000	0	100.000	0

L. E. radius: 0.455
Slope of radius through L. E.: 0.042

NACA 64-110

[Stations and ordinates given in percent of airfoil chord]

Upper surface		Lower surface	
Station	Ordinate	Station	Ordinate
0	0	0	0
.465	.644	.535	−.794
.712	1.023	.788	−.958
1.207	1.303	1.293	−1.195
2.450	1.793	2.550	−1.607
4.945	2.500	5.055	−2.184
7.443	3.037	7.557	−2.613
9.944	3.479	10.050	−2.963
14.947	4.175	15.038	−3.506
19.953	4.700	20.047	−3.904
24.959	5.087	25.041	−4.191
29.967	5.350	30.033	−4.378
34.975	5.495	35.025	−4.465
39.984	5.524	40.016	−4.452
44.992	5.391	45.008	−4.295
50.000	5.138	50.000	−4.034
55.007	4.786	54.993	−3.690
60.012	4.356	59.988	−3.284
65.016	3.860	64.984	−2.830
70.019	3.313	69.981	−2.341
75.020	2.729	74.980	−1.833
80.019	2.120	79.981	−1.324
85.016	1.512	84.984	−.840
90.012	.929	89.988	−.413
95.006	.406	94.994	−.090
100.000	0	100.000	0

L. E. radius: 0.720
Slope of radius through L. E.: 0.042

NACA 64-206

[Stations and ordinates given in percent of airfoil chord]

Upper surface		Lower surface	
Station	Ordinate	Station	Ordinate
0	0	0	0
.459	.642	.541	−.442
.704	.864	.796	−.524
1.198	.859	1.302	−.645
2.440	1.208	2.560	−.836
4.934	1.719	5.066	−1.087
7.432	2.115	7.568	−1.267
9.933	2.444	10.067	−1.410
14.937	2.970	15.063	−1.624
19.943	3.367	20.057	−1.775
24.952	3.667	25.048	−1.877
29.961	3.879	30.039	−1.935
34.971	4.011	35.029	−1.951
39.981	4.066	40.019	−1.924
44.991	4.014	45.009	−1.824
50.000	3.878	50.000	−1.672
55.008	3.670	54.992	−1.480
60.015	3.402	59.985	−1.260
65.020	3.080	64.980	−1.020
70.023	2.712	69.977	−.768
75.025	2.307	74.975	−.517
80.024	1.866	79.976	−.276
85.020	1.410	84.980	−.064
90.015	.940	89.985	.094
95.007	.473	94.993	.159
100.000	0	100.000	0

L. E. radius: 0.366
Slope of radius through L. E.: 0.064

NACA 64-208

[Stations and ordinates given in percent of airfoil chord]

Upper surface		Lower surface	
Station	Ordinate	Station	Ordinate
0	0	0	0
.445	.706	.555	−.606
.688	.862	.812	−.722
1.180	1.110	1.320	−.890
2.421	1.549	2.579	−1.177
4.912	2.189	5.088	−1.557
7.410	2.681	7.590	−1.833
9.909	3.069	10.091	−2.055
14.915	3.741	15.085	−2.395
19.924	4.232	20.076	−2.640
24.935	4.598	25.065	−2.808
29.948	4.856	30.052	−2.912
34.961	5.009	35.039	−2.949
39.974	5.063	40.026	−2.921
44.988	4.978	45.012	−2.788
50.000	4.757	50.000	−2.581
55.011	4.506	54.989	−2.316
60.020	4.152	59.980	−2.010
65.027	3.733	64.973	−1.673
70.031	3.263	69.969	−1.319
75.032	2.749	74.968	−.959
80.031	2.200	79.969	−.608
85.027	1.634	84.973	−.288
90.019	1.067	89.981	−.033
95.010	.522	94.990	.110
100.000	0	100.000	0

L. E. radius: 0.455
Slope of radius through L. E.: 0.084

NACA 64-209

[Stations and ordinates given in percent of airfoil chord]

Upper surface		Lower surface	
Station	Ordinate	Station	Ordinate
0	0	0	0
.438	.736	.562	−.666
.680	.959	.820	−.819
1.172	1.282	1.328	−1.018
2.411	1.716	2.589	−1.344
4.901	2.423	5.099	−1.791
7.398	2.965	7.602	−2.117
9.899	3.413	10.101	−2.379
14.905	4.127	15.095	−2.781
19.915	4.663	20.085	−3.071
24.927	5.064	25.073	−3.274
29.941	5.345	30.059	−3.401
34.956	5.509	35.044	−3.449
39.971	5.561	40.029	−3.419
44.986	5.469	45.014	−3.289
50.000	5.239	50.000	−3.033
55.012	4.921	54.988	−2.731
60.022	4.523	59.978	−2.381
65.030	4.056	64.970	−1.996
70.035	3.533	69.965	−1.589
75.036	2.964	74.964	−1.174
80.035	2.360	79.965	−.768
85.030	1.742	84.970	−.396
90.021	1.128	89.979	−.094
95.011	.543	94.989	.089
100.000	0	100.000	0

L. E. radius: 0.579
Slope of radius through L. E.: 0.084

NACA 64-210

[Stations and ordinates given in percent of airfoil chord]

Upper surface		Lower surface	
Station	Ordinate	Station	Ordinate
0	0	0	0
.481	.867	.569	−.767
.673	1.056	.827	−.916
1.163	1.354	1.337	−1.140
2.401	1.884	2.590	−1.512
4.890	2.656	5.110	−2.024
7.387	3.248	7.613	−2.400
9.887	3.736	10.113	−2.702
14.894	4.514	15.106	−3.168
19.905	5.097	20.095	−3.505
24.919	5.533	25.081	−3.743
29.934	5.836	30.066	−3.892
34.951	6.010	35.049	−3.950
39.968	6.059	40.032	−3.917
44.985	5.933	45.015	−3.748
50.000	5.689	50.000	−3.483
55.014	5.333	54.987	−3.143
60.025	4.891	59.975	−2.749
65.038	4.375	64.967	−2.315
70.038	3.799	69.962	−1.855
75.040	3.176	74.960	−1.386
80.038	2.518	79.962	−.926
85.033	1.849	84.968	−.503
90.024	1.188	89.977	−.154
95.012	.564	94.988	−.068
100.000	0	100.000	0

L. E. radius: 0.720
Slope of radius through L. E.: 0.084

NACA 641-012

[Stations and ordinates given in percent of airfoil chord]

Upper surface		Lower surface	
Station	Ordinate	Station	Ordinate
0	0	0	0
.5	.978	.5	−.978
.75	1.179	.75	−1.179
1.25	1.490	1.25	−1.490
2.5	2.085	2.5	−2.085
5.0	2.810	5.0	−2.810
7.5	3.394	7.5	−3.394
10	3.871	10	−3.871
15	4.620	15	−4.620
20	5.173	20	−5.173
25	5.576	25	−5.576
30	5.844	30	−5.844
35	5.978	35	−5.978
40	5.981	40	−5.981
45	5.798	45	−5.798
50	5.480	50	−5.480
55	5.056	55	−5.056
60	4.548	60	−4.548
65	3.974	65	−3.974
70	3.350	70	−3.350
75	2.695	75	−2.695
80	2.029	80	−2.029
85	1.382	85	−1.382
90	.780	90	−.780
95	.288	95	−.288
100	0	100	0

L. E. radius: 1.040

NACA 641-112

[Stations and ordinates given in percent of airfoil chord]

Upper surface		Lower surface	
Station	Ordinate	Station	Ordinate
0	0	0	0
.459	1.002	.541	−.952
.704	1.213	.796	−1.143
1.198	1.543	1.302	−1.435
2.441	2.127	2.559	−1.941
4.934	2.967	5.066	−2.651
7.432	3.605	7.568	−3.181
9.932	4.128	10.068	−3.612
14.930	4.950	15.064	−4.284
19.943	5.571	20.057	−4.775
24.951	6.024	25.049	−5.128
29.961	6.330	30.039	−5.358
34.971	6.498	35.020	−5.468
39.981	6.517	40.019	−5.445
44.991	6.346	45.009	−5.250
50.000	6.032	50.000	−4.928
55.008	5.604	54.992	−4.508
60.015	5.084	59.985	−4.012
65.020	4.489	64.980	−3.459
70.023	3.836	69.977	−2.864
75.024	3.143	74.976	−2.247
80.022	2.427	79.978	−1.631
85.019	1.718	84.981	−1.046
90.014	1.044	89.986	−.528
95.007	.446	94.993	−.130
100.000	0	100.000	0

L. E. radius: 1.040
Slope of radius through L. E.: 0.042

NACA 641-212

[Stations and ordinates given in percent of airfoil chord]

Upper surface		Lower surface	
Station	Ordinate	Station	Ordinate
0	0	0	0
.418	1.025	.582	−.925
.650	1.245	.841	−1.105
1.147	1.593	1.358	−1.379
2.382	2.218	2.618	−1.846
4.868	3.123	5.132	−2.491
7.364	3.815	7.636	−2.967
9.865	4.386	10.135	−3.352
14.872	5.291	15.128	−3.945
19.880	5.968	20.114	−4.376
24.903	6.470	25.097	−4.680
29.921	6.815	30.079	−4.871
34.941	7.008	35.059	−4.948
39.961	7.052	40.039	−4.910
44.982	6.893	45.018	−4.708
50.000	6.583	50.000	−4.377
55.016	6.151	54.984	−3.961
60.029	5.619	59.971	−3.477
65.039	5.004	64.961	−2.944
70.045	4.322	69.955	−2.378
75.047	3.590	74.953	−1.800
80.045	2.825	79.955	−1.233
85.038	2.054	84.962	−.708
90.027	1.303	89.973	−.269
95.018	.604	94.987	−.028
100.000	0	100.000	0

L. E. radius: 1.040
Slope of radius through L. E.: 0.084

NACA 641-412

[Stations and ordinates given in percent of airfoil chord]

Upper surface		Lower surface	
Station	Ordinate	Station	Ordinate
0	0	0	0
.388	1.064	.662	−.864
.589	1.305	.931	−1.025
1.045	1.690	1.455	−1.262
2.264	2.393	2.736	−1.649
4.738	3.430	5.262	−2.166
7.229	4.281	7.771	−2.536
9.730	4.896	10.270	−2.828
14.745	5.959	15.255	−3.287
19.772	6.760	20.228	−3.576
24.805	7.363	25.195	−3.783
29.842	7.786	30.158	−3.898
34.882	8.037	35.118	−3.917
39.923	8.128	40.077	−3.839
44.963	7.983	45.037	−3.668
50.000	7.686	50.000	−3.374
55.032	7.246	54.968	−2.980
60.059	6.690	59.941	−2.496
65.078	6.033	64.922	−1.943
70.090	5.293	69.910	−1.345
75.094	4.483	74.906	−.908
80.089	3.619	79.911	−.435
85.076	2.722	84.924	−.088
90.055	1.818	89.945	.250
95.027	.919	94.973	.345
100.000	0	100.000	0

L. E. radius: 1.040
Slope of radius through L. E.: 0.168

NACA 642-015

[Stations and ordinates given in percent of airfoil chord]

Upper surface		Lower surface	
Station	Ordinate	Station	Ordinate
0	0	0	0
.50	1.208	.50	−1.208
.75	1.456	.75	−1.456
1.25	1.842	1.25	−1.842
2.5	2.528	2.5	−2.528
5.0	3.504	5.0	−3.504
7.5	4.240	7.5	−4.240
10	4.842	10	−4.842
15	5.785	15	−5.785
20	6.480	20	−6.480
25	6.985	25	−6.985
30	7.319	30	−7.319
35	7.482	35	−7.482
40	7.473	40	−7.473
45	7.294	45	−7.294
50	6.810	50	−6.810
55	6.266	55	−6.266
60	5.620	60	−5.620
65	4.895	65	−4.895
70	4.113	70	−4.113
75	3.296	75	−3.296
80	2.472	80	−2.472
85	1.677	85	−1.677
90	.950	90	−.950
95	.346	95	−.346
100	0	100	0

L. E. radius: 1.590

NACA 642-215

[Stations and ordinates given in percent of airfoil chord]

Upper surface		Lower surface	
Station	Ordinate	Station	Ordinate
0	0	0	0
.399	1.254	.601	−1.154
.637	1.522	.863	−1.382
1.122	1.945	1.378	−1.731
2.353	2.710	2.647	−2.338
4.836	3.816	5.164	−3.184
7.331	4.661	7.669	−3.813
9.831	5.356	10.169	−4.322
14.840	6.456	15.160	−5.110
19.857	7.274	20.143	−5.682
24.878	7.879	25.122	−6.089
29.901	8.290	30.099	−6.346
34.926	8.512	35.074	−6.462
39.952	8.544	40.048	−6.402
44.977	8.319	45.023	−6.129
50.000	7.913	50.000	−5.707
55.020	7.361	54.980	−5.171
60.036	6.691	59.964	−4.549
65.048	5.925	64.952	−3.865
70.055	5.085	69.945	−3.141
75.058	4.191	74.942	−2.401
80.055	3.267	79.945	−1.675
85.046	2.349	84.954	−1.008
90.033	1.466	89.967	−.432
95.016	.662	94.984	−.080
100.000	0	100.000	0

L. E. radius: 1.590
Slope of radius through L. E.: 0.084

NACA 642-415

[Stations and ordinates given in percent of airfoil chord]

Upper surface		Lower surface	
Station	Ordinate	Station	Ordinate
0	0	0	0
.299	1.291	.701	−1.091
.526	1.579	.974	−1.299
.996	2.088	1.504	−1.610
2.207	2.883	2.793	−2.189
4.673	4.121	5.327	−2.857
7.162	5.075	7.838	−3.379
9.662	5.884	10.338	−3.796
14.681	7.122	15.319	−4.480
19.714	8.060	20.286	−4.882
24.756	8.771	25.244	−5.191
29.803	9.260	30.197	−5.372
34.853	9.541	35.147	−5.421
39.904	9.614	40.096	−5.330
44.954	9.414	45.046	−5.084
50.000	9.016	50.000	−4.694
55.040	8.456	54.960	−4.076
60.072	7.762	59.928	−3.478
65.096	6.954	64.904	−2.854
70.111	6.055	69.889	−2.167
75.115	5.084	74.885	−1.504
80.109	4.062	79.891	−.878
85.092	3.020	84.908	−.328
90.066	1.982	89.934	−.086
95.032	.976	94.968	−.288
100.000	0	100.000	0

L. E. radius: 1.590
Slope of radius through L. E.: 0.168

NACA 643-018

[Stations and ordinates given in percent of airfoil chord]

Upper surface		Lower surface	
Station	Ordinate	Station	Ordinate
0	0	0	0
.50	1.428	.50	−1.428
.75	1.720	.75	−1.720
1.25	2.177	1.25	−2.177
2.5	3.005	2.5	−3.005
5.0	4.186	5.0	−4.186
7.5	5.076	7.5	−5.076
10	5.808	10	−5.808
15	6.942	15	−6.942
20	7.782	20	−7.782
25	8.391	25	−8.391
30	8.789	30	−8.789
35	8.979	35	−8.979
40	8.952	40	−8.952
45	8.680	45	−8.680
50	8.114	50	−8.114
55	7.445	55	−7.445
60	6.658	60	−6.658
65	5.782	65	−5.782
70	4.842	70	−4.842
75	3.866	75	−3.866
80	2.888	80	−2.888
85	1.951	85	−1.951
90	1.101	90	−1.101
95	.400	95	−.400
100	0	100	0

L. E. radius: 2.208

NACA 643-218

[Stations and ordinates given in percent of airfoil chord]

Upper surface		Lower surface	
Station	Ordinate	Station	Ordinate
0	0	0	0
.380	1.473	.620	−1.378
.617	1.785	.883	−1.645
1.099	2.279	1.401	−2.005
2.325	3.186	2.675	−2.814
4.804	4.497	5.196	−3.836
7.297	5.496	7.703	−4.648
9.797	6.310	10.203	−5.282
14.808	7.612	15.192	−6.266
19.828	8.576	20.172	−6.984
24.853	9.285	25.147	−7.495
29.881	9.760	30.119	−7.810
34.912	10.009	35.088	−7.949
39.942	10.023	40.058	−7.881
44.972	9.725	45.028	−7.535
50.000	9.217	50.000	−7.011
55.024	8.540	54.976	−6.350
60.043	7.729	59.957	−5.587
65.057	6.812	64.943	−4.752
70.065	5.814	69.935	−3.870
75.068	4.760	74.932	−2.970
80.064	3.683	79.936	−2.091
85.054	2.628	84.946	−1.277
90.038	1.617	89.962	−.588
95.019	.716	94.981	−.084
100.000	0	100.000	0

L. E. radius: 2.208
Slope of radius through L. E.: 0.084

NACA 643-418

[Stations and ordinates given in percent of airfoil chord]

Upper surface		Lower surface	
Station	Ordinate	Station	Ordinate
0	0	0	0
.263	1.508	.737	−1.306
.486	1.840	1.014	−1.560
.950	2.370	1.550	−1.942
2.152	3.357	2.848	−2.613
4.609	4.800	5.391	−3.536
7.095	5.908	7.905	−4.212
9.595	6.823	10.405	−4.755
14.617	8.277	15.383	−5.588
19.657	9.366	20.343	−6.182
24.707	10.176	25.293	−6.596
29.763	10.730	30.237	−6.842
34.823	11.037	35.177	−6.917
39.885	11.093	40.115	−6.809
44.945	10.820	45.055	−6.440
50.000	10.320	50.000	−5.908
55.047	9.635	54.953	−5.255
60.086	8.799	59.914	−4.515
65.114	7.841	64.886	−3.721
70.131	6.784	69.869	−2.896
75.135	5.654	74.865	−2.074
80.127	4.477	79.873	−1.293
85.108	3.294	84.892	−.602
90.077	2.132	89.923	−.064
95.037	1.030	94.963	.234
100.000	0	100.000	0

L. E. radius: 2.208
Slope of radius through L. E.: 0.168

NACA 643-618

[Stations and ordinates given in percent of airfoil chord]

Upper surface		Lower surface	
Station	Ordinate	Station	Ordinate
0	0	0	0
.150	1.534	.850	−1.234
.359	1.885	1.141	−1.485
.805	2.452	1.695	−1.810
1.982	3.518	3.018	−2.402
4.417	5.093	5.583	−3.197
6.895	6.312	8.105	−3.768
9.395	7.322	10.605	−4.220
14.427	8.937	15.573	−4.899
19.486	10.153	20.514	−5.377
24.560	11.065	25.440	−5.695
29.645	11.698	30.355	−5.866
34.735	12.065	35.265	−5.885
39.827	12.163	40.173	−5.737
44.917	11.915	45.083	−5.345
50.000	11.428	50.000	−4.805
55.071	10.730	54.929	−4.160
60.129	9.870	59.871	−3.444
65.171	8.870	64.829	−2.690
70.196	7.754	69.804	−1.922
75.203	6.544	74.797	−1.174
80.191	5.270	79.809	−.494
85.161	3.963	84.839	.075
90.115	2.646	89.885	.456
95.056	1.344	94.944	.552
100.000	0	100.000	0

L. E. radius: 2.208
Slope of radius through L. E.: 0.253

NACA 644-021

[Stations and ordinates given in percent of airfoil chord]

Upper surface		Lower surface	
Station	Ordinate	Station	Ordinate
0	0	0	0
.50	1.646	.50	−1.646
.75	1.985	.75	−1.985
1.25	2.517	1.25	−2.517
2.5	3.485	2.5	−3.485
5.0	4.871	5.0	−4.871
7.5	5.915	7.5	−5.915
10	6.769	10	−6.769
15	8.108	15	−8.108
20	9.095	20	−9.095
25	9.807	25	−9.807
30	10.269	30	−10.269
35	10.481	35	−10.481
40	10.431	40	−10.431
45	10.030	45	−10.030
50	9.404	50	−9.404
55	8.607	55	−8.607
60	7.678	60	−7.678
65	6.649	65	−6.649
70	5.549	70	−5.549
75	4.416	75	−4.416
80	3.287	80	−3.287
85	2.213	85	−2.213
90	1.245	90	−1.245
95	.449	95	−.449
100	0	100	0

L. E. radius: 2.884.

NACA 644-221

[Stations and ordinates given in percent of airfoil chord]

Upper surface		Lower surface	
Station	Ordinate	Station	Ordinate
0	0	0	0
.362	1.690	.638	−1.590
.896	2.049	.904	−1.909
1.075	2.618	1.425	−2.404
2.297	3.665	2.703	−3.293
4.772	5.182	5.228	−4.550
7.264	6.334	7.736	−5.486
9.763	7.282	10.237	−6.248
14.776	8.778	15.224	−7.432
19.799	9.889	20.201	−8.297
24.829	10.701	25.171	−8.911
29.861	11.240	30.139	−9.296
34.897	11.510	35.103	−9.450
39.933	11.502	40.067	−9.360
44.968	11.125	45.032	−8.935
50.000	10.507	50.000	−8.301
55.027	9.702	54.973	−7.512
60.050	8.749	59.950	−6.607
65.065	7.679	64.935	−5.619
70.075	6.521	69.925	−4.577
75.077	5.310	74.923	−3.520
80.073	4.082	79.927	−2.490
85.061	2.885	84.939	−1.539
90.044	1.761	89.956	−.727
95.021	.765	94.979	−.183
100.000	0	100.000	0

L. E. radius: 2.884
Slope of radius through L. E.: 0.084

NACA 644-421

[Stations and ordinates given in percent of airfoil chord]

Upper surface		Lower surface	
Station	Ordinate	Station	Ordinate
0	0	0	0
.227	1.723	.773	−1.523
.445	2.101	1.055	−1.821
.903	2.707	1.597	−2.279
2.096	3.834	2.904	−3.090
4.545	5.482	5.455	−4.218
7.028	6.744	7.972	−5.048
9.528	7.786	10.472	−5.718
14.553	9.442	15.447	−6.750
19.599	10.678	20.401	−7.494
24.657	11.591	25.343	−8.011
29.723	12.209	30.277	−8.321
34.794	12.539	35.206	−8.419
39.865	12.572	40.135	−8.288
44.936	12.220	45.064	−7.840
50.000	11.610	50.000	−7.198
55.055	10.797	54.945	−6.417
60.099	9.819	59.901	−5.535
65.131	8.708	64.869	−4.588
70.150	7.491	69.850	−3.603
75.154	6.203	74.846	−2.628
80.145	4.876	79.855	−1.692
85.122	3.556	84.878	−.864
90.087	2.276	89.913	−.208
95.042	1.079	94.958	.185
100.000	0	100.000	0

L. E. radius: 2.884
Slope of radius through L. E.: 0.168

NACA 65,3-018

[Stations and ordinates given in percent of airfoil chord]

Upper surface		Lower surface	
Station	Ordinate	Station	Ordinate
0	0	0	0
.5	1.324	.5	−1.324
.75	1.599	.75	−1.599
1.25	2.004	1.25	−2.004
2.5	2.728	2.5	−2.728
5.0	3.831	5.0	−3.831
7.5	4.701	7.5	−4.701
10	5.424	10	−5.424
15	6.568	15	−6.568
20	7.434	20	−7.434
25	8.093	25	−8.093
30	8.568	30	−8.568
35	8.868	35	−8.868
40	8.990	40	−8.990
45	8.916	45	−8.916
50	8.593	50	−8.593
55	8.045	55	−8.045
60	7.317	60	−7.317
65	6.450	65	−6.450
70	5.496	70	−5.496
75	4.456	75	−4.456
80	3.390	80	−3.390
85	2.326	85	−2.326
90	1.324	90	−1.324
95	.492	95	−.492
100	0	100	0

L. E. radius: 1.92

NACA 65,3-418 $a=0.8$

[Stations and ordinates given in percent of airfoil chord]

Upper surface		Lower surface	
Station	Ordinate	Station	Ordinate
0	0	0	0
.248	1.416	.752	−1.184
.467	1.736	1.033	−1.412
.931	2.224	1.569	−1.732
2.131	3.133	2.869	−2.273
4.578	4.542	5.422	−3.074
7.053	5.572	7.947	−3.688
9.544	6.617	10.456	−4.198
14.558	8.149	15.442	−4.957
19.592	9.319	20.408	−5.527
24.641	10.233	25.359	−5.937
29.700	10.909	30.300	−6.217
34.765	11.369	35.235	−6.361
39.835	11.600	40.165	−6.376
44.932	11.602	45.068	−6.230
49.979	11.307	50.021	−5.879
55.046	10.751	54.954	−5.339
60.106	9.974	59.894	−4.658
65.158	9.016	64.845	−3.880
70.198	7.899	69.807	−3.067
75.219	6.651	74.781	−2.251
80.249	5.289	79.751	−1.473
85.221	3.818	84.779	−.810
90.135	2.269	89.865	−.345
95.049	.930	94.951	−.090
100.000	0	100.000	0

L. E. radius: 1.92
Slope of radius through L. E.: 0.194

NACA 65,3-618

[Stations and ordinates given in percent of airfoil chord]

Upper surface		Lower surface	
Station	Ordinate	Station	Ordinate
0	0	0	0
.176	1.434	.824	−1.134
.387	1.767	1.113	−1.347
.841	2.283	1.659	−1.641
2.030	3.245	2.970	−2.129
4.467	4.742	5.533	−2.846
6.940	5.940	8.060	−3.396
9.434	6.945	10.566	−3.843
14.458	8.565	15.542	−4.527
19.509	9.806	20.491	−5.030
24.576	10.767	25.424	−5.397
29.654	11.477	30.346	−5.645
34.738	11.954	35.262	−5.774
39.826	12.201	40.174	−5.775
44.915	12.201	45.085	−5.631
50.000	11.902	50.000	−5.254
55.077	11.330	54.923	−4.760
60.142	10.529	59.858	−4.103
65.191	9.537	64.809	−3.357
70.222	8.398	69.778	−2.506
75.233	7.135	74.767	−1.765
80.224	5.771	79.776	−.995
85.192	4.336	84.808	−.298
90.138	2.868	89.862	.234
95.066	1.435	94.932	.461
100.000	0	100.000	0

L. E. radius: 1.92
Slope of radius through L. E.: 0.253

NACA 65(216)-415 $a=0.5$

[Stations and ordinates given in percent of airfoil chord]

Upper surface		Lower surface	
Station	Ordinate	Station	Ordinate
0	0	0	0
.244	1.286	.756	−.960
.469	1.498	1.031	−1.110
.930	1.947	1.570	−1.359
2.121	2.837	2.879	−1.801
4.564	4.175	5.436	−2.411
7.044	5.208	7.956	−2.832
9.540	6.073	10.460	−3.169
14.561	7.465	15.439	−3.673
19.608	8.518	20.392	−4.022
24.669	9.315	25.331	−4.267
29.742	9.900	30.258	−4.428
34.825	10.279	35.175	−4.507
39.916	10.467	40.084	−4.523
45.019	10.438	44.981	−4.446
50.158	10.131	49.847	−4.251
55.268	9.512	54.737	−3.940
60.305	8.645	59.695	−3.521
65.308	7.576	64.692	−2.995
70.231	6.373	69.719	−2.409
75.237	5.152	74.763	−1.848
80.180	3.890	79.820	−1.273
85.117	2.639	84.883	−.723
90.062	1.533	89.938	−.306
95.020	.606	94.980	−.030
100.000	0	100.000	0

L. E. radius: 1.496
Slope of radius through L. E.: 0.233

NACA 65-006

[Stations and ordinates given in percent of airfoil chord]

Upper surface		Lower surface	
Station	Ordinate	Station	Ordinate
0	0	0	0
.5	.476	.5	−.476
.75	.574	.75	−.574
1.25	.717	1.25	−.717
2.5	.956	2.5	−.956
5.0	1.310	5.0	−1.310
7.5	1.589	7.5	−1.589
10	1.824	10	−1.824
15	2.197	15	−2.197
20	2.482	20	−2.482
25	2.697	25	−2.697
30	2.853	30	−2.852
35	2.952	35	−2.952
40	2.998	40	−2.998
45	2.983	45	−2.983
50	2.900	50	−2.900
55	2.741	55	−2.741
60	2.518	60	−2.518
65	2.246	65	−2.246
70	1.935	70	−1.935
75	1.594	75	−1.594
80	1.233	80	−1.233
85	.865	85	−.865
90	.510	90	−.510
95	.195	95	−.195
100	0	100	0

L. E. radius: 0.240

NACA 65-009

[Stations and ordinates given in percent of airfoil chord]

Upper surface		Lower surface	
Station	Ordinate	Station	Ordinate
0	0	0	0
.5	.700	.5	−.700
.75	.845	.75	−.845
1.25	1.058	1.25	−1.058
2.5	1.421	2.5	−1.421
5.0	1.961	5.0	−1.961
7.5	2.383	7.5	−2.383
10	2.736	10	−2.736
15	3.299	15	−3.299
20	3.727	20	−3.727
25	4.050	25	−4.050
30	4.282	30	−4.282
35	4.431	35	−4.431
40	4.496	40	−4.496
45	4.469	45	−4.469
50	4.336	50	−4.336
55	4.086	55	−4.086
60	3.743	60	−3.743
65	3.328	65	−3.328
70	2.856	70	−2.856
75	2.343	75	−2.343
80	1.805	80	−1.805
85	1.260	85	−1.260
90	.738	90	−.738
95	.280	95	−.280
100	0	100	0

L. E. radius: 0.552

NACA 65-206

[Stations and ordinates given in percent of airfoil chord]

Upper surface		Lower surface	
Station	Ordinate	Station	Ordinate
0	0	0	0
.460	.524	.540	−.424
.708	.642	.794	−.502
1.200	.822	1.300	−.608
2.444	1.140	2.556	−.768
4.939	1.625	5.061	−.998
7.437	2.012	7.563	−1.164
9.936	2.340	10.064	−1.306
14.939	2.869	15.061	−1.523
19.945	3.277	20.055	−1.685
24.958	3.592	25.047	−1.802
29.962	3.824	30.038	−1.880
34.971	3.982	35.029	−1.922
39.981	4.069	40.019	−1.927
44.990	4.078	45.010	−1.888
50.000	4.003	50.000	−1.797
55.009	3.830	54.991	−1.640
60.016	3.589	59.984	−1.447
65.022	3.276	64.978	−1.216
70.026	2.907	69.974	−.963
75.028	2.489	74.972	−.699
80.027	2.029	79.973	−.437
85.024	1.538	84.976	−.192
90.018	1.027	89.982	.007
95.009	.511	94.991	.121
100.000	0	100.000	0

L. E. radius: 0.240
Slope of radius through L. E.: 0.084

NACA 65-209

[Stations and ordinates given in percent of airfoil chord]

Upper surface		Lower surface	
Station	Ordinate	Station	Ordinate
0	0	0	0
.441	.748	.559	−.648
.684	.912	.816	−.772
1.177	1.162	1.323	−.948
2.417	1.605	2.583	−1.233
4.908	2.275	5.092	−1.643
7.405	2.805	7.595	−1.957
9.904	3.251	10.096	−2.217
14.909	3.971	15.091	−2.625
19.918	4.522	20.082	−2.930
24.929	4.944	25.071	−3.154
29.942	5.254	30.058	−3.310
34.956	5.461	35.044	−3.401
39.971	5.567	40.029	−3.425
44.986	5.564	45.014	−3.374
50.000	5.439	50.000	−3.253
55.013	5.181	54.987	−2.991
60.024	4.814	59.976	−2.672
65.033	4.358	64.967	−2.298
70.039	3.828	69.961	−1.884
75.041	3.237	74.959	−1.447
80.040	2.601	79.960	−1.009
85.035	1.933	84.965	−.587
90.026	1.255	89.974	−.221
95.013	.596	94.987	.036
100.000	0	100.000	0

L. E. radius: 0.552
Slope of radius through L. E.: 0.084

NACA 65-210

[Stations and ordinates given in percent of airfoil chord]

Upper surface		Lower surface	
Station	Ordinate	Station	Ordinate
0	0	0	0
.485	.819	.565	−.719
.678	.999	.822	−.859
1.160	1.278	1.331	−1.059
2.408	1.757	2.592	−1.385
4.898	2.491	5.102	−1.859
7.394	3.090	7.606	−2.221
9.894	3.555	10.106	−2.521
14.899	4.338	15.101	−2.992
19.909	4.938	20.091	−3.346
24.921	5.397	25.079	−3.607
29.936	5.732	30.064	−3.788
34.951	5.954	35.049	−3.894
39.968	6.067	40.032	−3.925
44.984	6.058	45.016	−3.868
50.000	5.915	50.000	−3.709
55.014	5.625	54.986	−3.435
60.027	5.217	59.973	−3.075
65.036	4.712	64.964	−2.652
70.043	4.128	69.957	−2.184
75.045	3.479	74.955	−1.689
80.044	2.783	79.956	−1.191
85.038	2.057	84.962	−.711
90.028	1.327	89.972	−.298
95.014	.622	94.986	.010
100.000	0	100.000	0

L. E. radius: 0.687
Slope of radius through L. E.: 0.084

NACA 65-410

[Stations and ordinates given in percent of airfoil chord]

Upper surface		Lower surface	
Station	Ordinate	Station	Ordinate
0	0	0	0
.372	.861	.628	−.661
.607	1.061	.893	−.781
1.089	1.372	1.411	−.944
2.818	1.935	2.682	−1.191
4.797	2.800	5.203	−1.536
7.289	3.487	7.711	−1.791
9.788	4.067	10.212	−1.999
14.798	5.000	15.202	−2.314
19.817	5.731	20.183	−2.547
24.843	6.290	25.157	−2.710
29.872	6.702	30.128	−2.814
34.903	6.983	35.097	−2.863
39.936	7.138	40.064	−2.854
44.968	7.153	45.032	−2.778
50.000	7.018	50.000	−2.606
55.029	6.720	54.971	−2.340
60.053	6.288	59.947	−2.004
65.073	5.741	64.927	−1.621
70.085	5.099	69.915	−1.211
75.090	4.372	74.910	−.792
80.088	3.577	79.912	−.393
85.076	2.729	84.924	−.037
90.057	1.842	89.943	.220
95.029	.937	94.971	.327
100.000	0	100.000	0

L. E. radius: 0.687
Slope of radius through L. E.: 0.168

NACA 651-012

[Stations and ordinates given in percent of airfoil chord]

Upper surface		Lower surface	
Station	Ordinate	Station	Ordinate
0	0	0	0
.5	.928	.5	−.928
.75	1.109	.75	−1.109
1.25	1.387	1.25	−1.387
2.5	1.875	2.5	−1.875
5.0	2.606	5.0	−2.606
7.5	3.172	7.5	−3.172
10	3.647	10	−3.647
15	4.402	15	−4.402
20	4.975	20	−4.975
25	5.406	25	−5.406
30	5.716	30	−5.716
35	5.912	35	−5.912
40	5.997	40	−5.997
45	5.949	45	−5.949
50	5.757	50	−5.757
55	5.412	55	−5.412
60	4.943	60	−4.943
65	4.381	65	−4.381
70	3.743	70	−3.743
75	3.059	75	−3.059
80	2.345	80	−2.345
85	1.630	85	−1.630
90	.947	90	−.947
95	.356	95	−.356
100	0	100	0

L. E. radius: 1.000

NACA 651-212

[Stations and ordinates given in percent of airfoil chord]

Upper surface		Lower surface	
Station	Ordinate	Station	Ordinate
0	0	0	0
.428	.970	.577	−.870
.664	1.176	.836	−1.036
1.164	1.491	1.846	−1.277
2.391	2.058	2.609	−1.686
4.878	2.919	5.122	−2.287
7.373	3.598	7.627	−2.745
9.873	4.162	10.127	−3.128
14.879	5.073	15.121	−3.727
19.890	5.770	20.110	−4.178
24.906	6.300	25.094	−4.510
29.923	6.687	30.077	−4.748
34.942	6.942	35.058	−4.892
39.961	7.068	40.039	−4.926
44.981	7.044	45.019	−4.854
50.000	6.860	50.000	−4.654
55.017	6.507	54.983	−4.317
60.032	6.014	59.968	−3.872
65.043	5.411	64.957	−3.351
70.050	4.715	69.950	−2.771
75.053	3.954	74.947	−2.164
80.052	3.140	79.948	−1.548
85.045	2.302	84.955	−.956
90.033	1.463	89.967	−.429
95.017	.672	94.983	−.040
100.000	0	100.000	0

L. E. radius: 1.000
Slope of radius through L. E.: 0.084

NACA 651-212 $a=0.6$

[Stations and ordinates given in percent of airfoil chord]

Upper surface		Lower surface	
Station	Ordinate	Station	Ordinate
0	0	0	0
.899	.982	.601	−.852
.638	1.194	.862	−1.012
1.124	1.520	1.376	−1.242
2.356	2.118	2.644	−1.625
4.837	3.017	5.163	−2.185
7.329	3.728	7.671	−2.600
9.827	4.330	10.173	−2.956
14.833	5.298	15.167	−3.500
19.848	6.042	20.152	−3.904
24.869	6.611	25.131	−4.197
29.894	7.029	30.106	−4.401
34.921	7.304	35.079	−4.518
39.951	7.444	40.049	−4.550
44.983	7.423	45.017	−4.475
50.017	7.231	49.983	−4.283
55.051	6.856	54.949	−3.988
60.094	6.318	59.906	−3.566
65.123	5.634	64.877	−3.124
70.124	4.842	69.876	−2.640
75.112	3.983	74.888	−2.131
80.090	3.082	79.910	−1.604
85.064	2.173	84.936	−1.085
90.030	1.297	89.904	−.595
95.013	.521	94.987	−.191
100.000	0	100.000	0

L. E. radius: 1.000
Slope of radius through L. E.: 0.110

NACA 651-412

[Stations and ordinates given in percent of airfoil chord]

Upper surface		Lower surface	
Station	Ordinate	Station	Ordinate
0	0	0	0
.347	1.010	.653	−.810
.580	1.236	.920	−.956
1.059	1.588	1.441	−1.160
2.288	2.284	2.717	−1.490
4.757	3.227	5.243	−1.963
7.247	4.010	7.753	−2.314
9.746	4.672	10.254	−2.604
14.757	5.741	15.243	−3.049
19.781	6.562	20.219	−3.378
24.811	7.193	25.189	−3.613
29.840	7.658	30.154	−3.770
34.884	7.971	35.116	−3.851
39.928	8.139	40.077	−3.855
44.962	8.139	45.038	−3.759
50.000	7.963	50.000	−3.551
55.035	7.602	54.955	−3.222
60.064	7.085	59.936	−2.801
65.086	6.440	64.914	−2.320
70.101	5.686	69.899	−1.798
75.107	4.847	74.893	−1.267
80.108	3.935	79.897	−.751
85.090	2.974	84.910	−.282
90.060	1.979	89.934	.089
95.033	.950	94.967	.278
100.000	0	100.000	0

L. E. radius: 1.000
Slope of radius through L. E.: 0.168

NACA 652-015

[Stations and ordinates given in percent of airfoil chord]

Upper surface		Lower surface	
Station	Ordinate	Station	Ordinate
0	0	0	0
.5	1.124	.5	−1.124
.75	1.356	.75	−1.356
1.25	1.702	1.25	−1.702
2.50	2.324	2.50	−2.324
5.00	3.245	5.00	−3.245
7.50	3.959	7.50	−3.959
10	4.555	10	−4.555
15	5.504	15	−5.504
20	6.223	20	−6.223
25	6.764	25	−6.764
30	7.152	30	−7.152
35	7.390	35	−7.390
40	7.498	40	−7.498
45	7.427	45	−7.427
50	7.168	50	−7.168
55	6.720	55	−6.720
60	6.118	60	−6.118
65	5.403	65	−5.403
70	4.600	70	−4.600
75	3.744	75	−3.744
80	2.858	80	−2.858
85	1.977	85	−1.977
90	1.144	90	−1.144
95	.428	95	−.428
100	0	100	0

L. E. radius: 1.505

NACA 65$_2$-215

[Stations and ordinates given in percent of airfoil chord]

Upper surface		Lower surface	
Station	Ordinate	Station	Ordinate
0	0	0	0
.406	1.170	.594	−1.070
.645	1.422	.855	−1.282
1.132	1.805	1.368	−1.591
2.365	2.506	2.635	−2.134
4.848	3.557	5.152	−2.925
7.342	4.380	7.658	−3.532
9.841	5.060	10.159	−4.035
14.848	6.175	15.152	−4.829
19.863	7.018	20.137	−5.426
24.882	7.658	25.118	−5.868
29.904	8.123	30.096	−6.179
34.927	8.426	35.073	−6.366
39.952	8.569	40.048	−6.427
44.976	8.522	45.024	−6.332
50.000	8.271	50.000	−6.065
55.021	7.815	54.979	−5.625
60.039	7.189	59.961	−5.047
65.053	6.433	64.947	−4.373
70.062	5.572	69.938	−3.628
75.065	4.638	74.935	−2.848
80.063	3.658	79.937	−2.061
85.055	2.649	84.945	−1.308
90.040	1.660	89.960	−.626
95.020	.744	94.980	−.112
100.000	0	100.000	0

L. E. radius: 1.505
Slope of radius through L. E.: 0.084

NACA 65$_2$-415

[Stations and ordinates given in percent of airfoil chord]

Upper surface		Lower surface	
Station	Ordinate	Station	Ordinate
0	0	0	0
.318	1.206	.687	−1.008
.542	1.480	.958	−1.200
1.016	1.900	1.494	−1.472
2.231	2.680	2.769	−1.936
4.697	3.883	5.303	−2.599
7.184	4.794	7.816	−3.098
9.682	5.578	10.318	−3.510
14.697	6.842	15.303	−4.150
19.726	7.809	20.274	−4.625
24.764	8.550	25.236	−4.970
29.807	9.098	30.193	−5.205
34.854	9.455	35.146	−5.335
39.903	9.639	40.097	−5.355
44.953	9.617	45.047	−5.237
50.000	9.374	50.000	−4.962
55.043	8.910	54.957	−4.530
60.079	8.260	59.921	−3.976
65.106	7.462	64.894	−3.342
70.124	6.542	69.876	−2.654
75.131	5.532	74.869	−1.952
80.126	4.447	79.874	−1.263
85.109	3.320	84.891	−.628
90.080	2.175	89.920	−.107
95.040	1.058	94.960	.206
100.000	0	100.000	0

L. E. radius: 1.505
Slope of radius through L. E.: 0.168

NACA 65$_2$-415
$a=0.5$

[Stations and ordinates given in percent of airfoil chord]

Upper surface		Lower surface	
Station	Ordinate	Station	Ordinate
0	0	0	0
.245	1.233	.755	−.957
.464	1.520	1.036	−1.182
.927	1.965	1.573	−1.577
2.126	2.812	2.874	−1.776
4.574	4.099	5.426	−2.335
7.054	5.122	7.946	−2.746
9.549	5.985	10.451	−3.081
14.568	7.383	15.432	−3.591
19.611	8.459	20.389	−3.968
24.671	9.280	25.329	−4.232
29.743	9.883	30.257	−4.411
34.825	10.280	35.175	−4.508
39.916	10.470	40.084	−4.526
45.019	10.423	44.981	−4.431
50.152	10.106	49.848	−4.226
55.262	9.501	54.738	−3.929
60.307	8.672	59.693	−3.548
65.314	7.684	64.686	−3.104
70.294	6.573	69.706	−2.609
75.253	5.387	74.747	−2.083
80.199	4.157	79.801	−1.545
85.137	2.930	84.863	−1.014
90.077	1.755	89.923	−.527
95.027	.715	94.973	−.189
100.000	0	100.000	0

L. E. radius: 1.505
Slope of radius through L. E.: 0.238

NACA 65$_3$-018

[Stations and ordinates given in percent of airfoil chord]

Upper surface		Lower surface	
Station	Ordinate	Station	Ordinate
0	0	0	0
.50	1.337	.50	−1.337
.75	1.608	.75	−1.608
1.25	2.014	1.25	−2.014
2.5	2.751	2.5	−2.751
5.0	3.866	5.0	−3.866
7.5	4.733	7.5	−4.733
10	5.457	10	−5.457
15	6.606	15	−6.606
20	7.476	20	−7.476
25	8.129	25	−8.129
30	8.595	30	−8.595
35	8.886	35	−8.886
40	8.999	40	−8.999
45	8.901	45	−8.901
50	8.568	50	−8.568
55	8.008	55	−8.008
60	7.267	60	−7.267
65	6.395	65	−6.395
70	5.426	70	−5.426
75	4.396	75	−4.396
80	3.338	80	−3.338
85	2.295	85	−2.295
90	1.319	90	−1.319
95	.490	95	−.490
100	0	100	0

L. E. radius: 1.96

NACA 65$_3$-218

[Stations and ordinates given in percent of airfoil chord]

Upper surface		Lower surface	
Station	Ordinate	Station	Ordinate
0	0	0	0
.388	1.382	.612	−1.282
.625	1.673	.875	−1.533
1.110	2.116	1.390	−1.902
2.340	2.932	2.660	−2.560
4.819	4.178	5.181	−3.546
7.311	5.153	7.689	−4.305
9.809	5.971	10.191	−4.937
14.818	7.276	15.182	−5.980
19.835	8.270	20.165	−6.676
24.858	9.023	25.142	−7.233
29.884	9.566	30.116	−7.622
34.912	9.916	35.088	−7.856
39.942	10.070	40.058	−7.928
44.972	9.996	45.028	−7.806
50.000	9.671	50.000	−7.465
55.026	9.108	54.974	−6.913
60.047	8.338	59.953	−6.196
65.063	7.425	64.937	−5.365
70.073	6.398	69.927	−4.454
75.077	5.290	74.923	−3.500
80.074	4.133	79.926	−2.541
85.063	2.967	84.937	−1.621
90.046	1.835	89.954	−.801
95.023	.805	94.977	−.173
100.000	0	100.000	0

L. E. radius: 1.96
Slope of radius through L. E.: 0.084

NACA 65$_3$-418

[Stations and ordinates given in percent of airfoil chord]

Upper surface		Lower surface	
Station	Ordinate	Station	Ordinate
0	0	0	0
.278	1.418	.722	−1.218
.503	1.729	.997	−1.449
.973	2.309	1.527	−1.781
2.181	3.104	2.819	−2.360
4.639	4.481	5.361	−3.217
7.123	5.566	7.877	−3.870
9.619	6.478	10.381	−4.410
14.636	7.942	15.364	−5.250
19.671	9.061	20.329	−5.877
24.716	9.914	25.284	−6.334
29.768	10.536	30.232	−6.648
34.825	10.944	35.175	−6.824
39.884	11.140	40.116	−6.856
44.943	11.091	45.057	−6.711
50.000	10.774	50.000	−6.362
55.051	10.168	54.949	−5.818
60.094	9.408	59.906	−5.124
65.126	8.454	64.874	−4.334
70.146	7.368	69.854	−3.480
75.154	6.183	74.846	−2.603
80.147	4.927	79.853	−1.743
85.127	3.633	84.873	−.946
90.092	2.350	89.908	−.282
95.046	1.120	94.954	.144
100.000	0	100.000	0

L. E. radius: 1.96
Slope of radius through L. E.: 0.168

NACA 65$_3$-418
$a=0.5$

[Stations and ordinates given in percent of airfoil chord]

Upper surface		Lower surface	
Station	Ordinate	Station	Ordinate
0	0	0	0
.197	1.440	.803	−1.164
.411	1.766	1.089	−1.378
.868	2.271	1.632	−1.683
2.057	3.233	2.943	−2.197
4.498	4.716	5.507	−2.961
6.986	5.891	8.034	−3.515
9.459	6.882	10.541	−3.978
14.481	8.482	15.519	−4.690
19.533	9.709	20.467	−5.213
24.604	10.643	25.396	−5.595
29.691	11.325	30.309	−5.853
34.789	11.770	35.211	−5.998
39.899	11.970	40.101	−6.026
45.022	11.897	44.978	−5.905
50.152	11.506	49.848	−5.626
55.313	10.788	54.687	−5.216
60.364	9.820	59.636	−4.696
65.372	8.674	64.628	−4.094
70.347	7.397	69.653	−3.433
75.298	6.038	74.702	−2.734
80.232	4.636	79.768	−2.024
85.139	3.247	84.841	−1.331
90.089	1.930	89.911	−.702
95.030	.777	94.970	−.201
100.000	0	100.000	0

L. E. radius: 1.96
Slope of radius through L. E.: 0.233

NACA 65$_3$-618

[Stations and ordinates given in percent of airfoil chord]

Upper surface		Lower surface	
Station	Ordinate	Station	Ordinate
0	0	0	0
.172	1.446	.828	−1.146
.385	1.776	1.115	−1.356
.839	2.293	1.661	−1.651
2.026	3.268	2.974	−2.152
4.462	4.776	5.538	−2.880
6.936	5.971	8.064	−3.427
9.431	6.978	10.569	−3.876
14.455	8.602	15.545	−4.564
19.506	9.848	20.494	−5.072
24.574	10.803	25.426	−5.433
29.652	11.504	30.348	−5.672
34.738	11.972	35.262	−5.792
39.826	12.210	40.174	−5.784
44.915	12.186	45.085	−5.616
50.000	11.877	50.000	−5.289
55.077	11.293	54.923	−4.728
60.141	10.479	59.859	−4.053
65.189	9.482	64.811	−3.302
70.219	8.338	69.781	−2.506
75.230	7.075	74.770	−1.705
80.220	5.719	79.780	−.943
85.189	4.306	84.811	−.288
90.138	2.863	89.862	.239
95.068	1.433	94.932	.453
100.000	0	100.000	0

L. E. radius: 1.96
Slope of radius through L. E.: 0.268

NACA 65$_3$-618
$a=0.5$

[Stations and ordinates given in percent of airfoil chord]

Upper surface		Lower surface	
Station	Ordinate	Station	Ordinate
0	0	0	0
.059	1.469	.941	−1.055
.256	1.821	1.244	−1.289
.689	2.375	1.811	−1.693
1.846	3.449	3.154	−2.396
4.248	5.115	5.752	−2.869
6.706	6.448	8.294	−3.284
9.194	7.575	10.806	−3.219
14.225	9.404	15.775	−3.716
19.301	10.815	20.699	−4.071
24.407	11.898	25.593	−4.321
29.537	12.687	30.463	−4.479
34.684	13.209	35.316	−4.551
39.849	13.456	40.151	−4.540
45.034	13.395	44.966	−4.407
50.273	12.974	49.727	−4.154
55.468	12.173	54.532	−3.815
60.546	11.090	59.454	−3.404
65.557	9.806	64.443	−2.936
70.519	8.374	69.481	−2.428
75.445	6.851	74.555	−1.895
80.347	5.279	79.653	−1.361
85.230	3.720	84.761	−.846
90.138	2.233	89.867	−.391
95.046	.920	94.954	−.056
100.000	0	100.000	0

L. E. radius: 1.96
Slope of radius through L. E.: 0.349

NACA 65$_4$-021

[Stations and ordinates given in percent of airfoil chord]

Upper surface		Lower surface	
Station	Ordinate	Station	Ordinate
0	0	0	0
.50	1.522	.50	−1.522
.75	1.838	.75	−1.838
1.25	2.301	1.25	−2.301
2.5	3.154	2.5	−3.154
5.0	4.472	5.0	−4.472
7.5	5.498	7.5	−5.498
10	6.352	10	−6.352
15	7.700	15	−7.700
20	8.720	20	−8.720
25	9.487	25	−9.487
30	10.036	30	−10.036
35	10.375	35	−10.375
40	10.499	40	−10.499
45	10.366	45	−10.366
50	9.952	50	−9.952
55	9.277	55	−9.277
60	8.390	60	−8.390
65	7.360	65	−7.360
70	6.224	70	−6.224
75	5.024	75	−5.024
80	3.800	80	−3.800
85	2.598	85	−2.598
90	1.484	90	−1.484
95	.546	95	−.546
100	0	100	0

L. E. radius: 2.80

NACA 654-221

[Stations and ordinates given in percent of airfoil chord]

Upper surface		Lower surface	
Station	Ordinate	Station	Ordinate
0	0	0	0
.372	1.567	.628	−1.467
.608	1.902	.892	−1.762
1.090	2.402	1.410	−2.188
2.814	3.335	2.684	−2.963
4.791	4.783	5.209	−4.151
7.280	5.918	7.720	−5.070
9.778	6.865	10.222	−5.831
14.787	8.370	15.213	−7.024
19.808	9.514	20.192	−7.922
24.884	10.381	25.166	−8.591
29.865	11.007	30.135	−9.003
34.898	11.404	35.102	−9.344
39.982	11.570	40.068	−9.428
44.967	11.461	45.033	−9.271
50.000	11.055	50.000	−8.849
55.030	10.372	54.970	−8.182
60.054	9.461	59.946	−7.319
65.072	8.390	64.928	−6.330
70.084	7.195	69.916	−5.251
75.088	5.918	74.912	−4.128
80.084	4.595	79.916	−3.008
85.072	3.270	84.928	−1.924
90.052	2.000	89.948	−.966
95.028	.881	94.074	−.229
100.000	0	100.000	0

L. E. radius: 2.50
Slope of radius through L. E.: 0.084

NACA 654-421

[Stations and ordinates given in percent of airfoil chord]

Upper surface		Lower surface	
Station	Ordinate	Station	Ordinate
0	0	0	0
.247	1.601	.753	−1.401
.468	1.956	1.032	−1.676
.983	2.493	1.567	−2.095
2.135	3.505	2.855	−2.761
4.582	5.085	5.417	−3.821
7.062	6.329	7.938	−4.633
9.557	7.371	10.443	−5.303
14.575	9.034	15.425	−6.342
19.616	10.304	20.384	−7.120
24.668	11.271	25.332	−7.691
29.729	11.976	30.271	−8.088
34.796	12.433	35.204	−8.313
39.865	12.640	40.135	−8.356
44.934	12.556	45.066	−8.176
50.000	12.168	50.000	−7.746
55.059	11.487	54.941	−7.087
60.108	10.531	59.892	−6.247
65.145	9.419	64.855	−5.299
70.168	8.166	69.832	−4.278
75.176	6.811	74.824	−3.231
80.167	5.388	79.833	−2.204
85.143	3.940	84.857	−1.248
90.104	2.514	89.896	−.446
95.051	1.176	94.949	.088
100.000	0	100.000	0

L. E. radius: 2.50
Slope of radius through L. E.: 0.168

NACA 654-421 $a=0.5$

[Stations and ordinates given in percent of airfoil chord]

Upper surface		Lower surface	
Station	Ordinate	Station	Ordinate
0	0	0	0
.155	1.620	.845	−1.344
.368	1.991	1.187	−1.603
.813	2.553	1.687	−1.965
1.992	3.631	3.008	−2.595
4.414	5.315	5.586	−3.551
6.940	6.651	8.120	−4.275
9.471	7.773	10.620	−4.869
14.395	9.572	15.605	−5.780
19.455	10.951	20.545	−6.455
24.588	12.000	25.462	−6.953
29.639	12.765	30.361	−7.293
34.754	13.268	35.246	−7.486
39.882	13.470	40.118	−7.528
45.026	13.363	44.974	−7.370
50.211	12.890	49.789	−7.010
55.382	12.050	54.688	−6.484
60.421	10.942	59.579	−5.818
65.428	9.637	64.572	−5.057
70.398	8.193	69.602	−4.229
75.340	6.604	74.660	−3.360
80.264	5.097	79.736	−2.485
85.181	3.550	84.819	−1.634
90.100	2.095	89.900	−.867
95.034	.833	94.966	−.257
100.000	0	100.000	0

L. E. radius: 2.50
Slope of radius through L. E.: 0.233

NACA 65(215)-114

[Stations and ordinates given in percent of airfoil chord]

Upper surface		Lower surface	
Station	Ordinate	Station	Ordinate
0	0	0	0
.456	1.073	.544	−1.028
.701	1.300	.799	−1.230
1.195	1.642	1.305	−1.534
2.437	2.261	2.563	−2.075
4.929	3.186	5.071	−2.870
7.426	3.906	7.574	−3.482
9.926	4.508	10.074	−3.992
14.929	5.472	15.071	−4.800
19.936	6.206	20.064	−5.410
24.945	6.761	25.055	−5.865
29.955	7.161	30.045	−6.189
34.966	7.418	35.034	−6.388
39.977	7.534	40.023	−6.462
44.989	7.480	45.011	−6.384
50.000	7.242	50.000	−6.138
55.010	6.820	54.990	−5.724
60.018	6.246	59.982	−5.174
65.025	5.558	64.975	−4.528
70.029	4.779	69.971	−3.807
75.031	3.942	74.969	−3.046
80.029	3.065	79.971	−2.269
85.025	2.181	84.975	−1.509
90.019	1.326	89.981	−.810
95.009	.557	94.991	−.241
100.000	0	100.000	0

L. E. radius: 1.811
Slope of radius through L. E.: 0.042

NACA 65(421)-420

[Stations and ordinates given in percent of airfoil chord]

Upper surface		Lower surface	
Station	Ordinate	Station	Ordinate
0	0	0	0
.258	1.537	.742	−1.337
.482	1.864	1.018	−1.584
.950	2.374	1.550	−1.946
2.152	3.358	2.848	−2.614
4.603	4.866	5.397	−3.602
7.083	6.066	7.917	−4.370
9.579	7.060	10.421	−4.992
4.596	8.665	15.404	−5.978
19.634	9.885	20.366	−6.701
24.684	10.815	25.316	−7.235
29.742	11.494	30.258	−7.606
34.805	11.939	35.195	−7.819
39.871	12.140	40.129	−7.856
44.937	12.056	45.063	−7.676
50.000	11.672	50.000	−7.290
55.056	11.018	54.944	−6.035
60.103	10.120	59.897	−5.842
65.138	9.060	64.862	−4.940
70.160	7.861	69.840	−3.973
75.167	6.563	74.833	−2.988
80.159	5.200	79.841	−2.010
85.136	3.813	84.864	−1.121
90.098	2.441	89.902	−.378
95.049	1.150	94.951	.114
100.000	0	100.000	0

L. E. radius: 2.27
Slope of radius through L. E.: 0.168

NACA 66,1-212

[Stations and ordinates given in percent o airfoil chord]

Upper surface		Lower surface	
Station	Ordinate	Station	Ordinate
0	0	0	0
.424	.947	.576	−.847
.666	1.150	.884	−1.010
1.157	1.447	1.343	−1.238
2.395	1.986	2.605	−1.614
4.884	2.797	5.116	−2.165
7.379	3.441	7.621	−2.598
9.878	3.997	10.122	−2.963
14.884	4.885	15.116	−3.539
19.895	5.574	20.105	−3.982
24.909	6.112	25.091	−4.322
29.925	6.522	30.075	−4.578
34.943	6.816	35.057	−4.760
39.962	7.005	40.038	−4.863
44.981	7.093	45.019	−4.903
50.000	7.075	50.000	−4.869
55.019	6.939	54.981	−4.749
60.036	6.665	59.964	−4.528
65.051	6.195	64.949	−4.135
70.061	5.507	69.939	−3.563
75.066	4.663	74.934	−2.893
80.065	3.759	79.935	−2.167
85.058	2.770	84.942	−1.424
90.043	1.760	89.957	−.736
95.022	.792	94.978	−.160
100.000	0	100.000	0

L. E. radius: 0.898
Slope of radius through L. E.: 0.084

NACA 66(215)-016

[Stations and ordinates given in percent of airfoil chord]

Upper surface		Lower surface	
Station	Ordinate	Station	Ordinate
0	0	0	0
.5	1.184	.5	−1.184
.75	1.418	.75	−1.418
1.25	1.755	1.25	−1.755
2.5	2.378	2.5	−2.378
5.0	3.292	5.0	−3.292
7.5	4.007	7.5	−4.007
10	4.626	10	−4.026
15	5.605	15	−5.605
20	6.362	20	−6.362
25	6.950	25	−6.950
30	7.395	30	−7.395
35	7.706	35	−7.706
40	7.909	40	−7.909
45	7.997	45	−7.997
50	7.957	50	−7.957
55	7.780	55	−7.780
60	7.425	60	−7.425
65	6.832	65	−6.832
70	5.970	70	−5.970
75	4.966	75	−4.966
80	3.849	80	−3.849
85	2.728	85	−2.728
90	1.587	90	−1.587
95	.597	95	−.597
100	0	100	0

L. E. radius: 1.575

NACA 66(215)-216

[Stations and ordinates given in percent of airfoil chord]

Upper surface		Lower surface	
Station	Ordinate	Station	Ordinate
0	0	0	0
.401	1.280	.599	−1.180
.640	1.484	.880	−1.344
1.128	1.858	1.372	−1.644
2.362	2.560	2.638	−2.188
4.846	3.604	5.154	−2.972
7.340	4.428	7.660	−3.580
9.838	5.140	10.162	−4.106
14.845	6.276	15.155	−4.980
19.860	7.156	20.140	−5.564
24.879	7.844	25.121	−6.054
29.900	8.366	30.100	−6.422
34.924	8.736	35.076	−6.676
39.949	8.980	40.051	−6.838
44.974	9.092	45.026	−6.902
50.000	9.060	50.000	−6.854
55.025	8.878	54.975	−6.685
60.048	8.496	59.952	−6.354
65.067	7.862	64.933	−5.802
70.081	6.941	69.919	−4.997
75.087	5.860	74.913	−4.070
80.085	4.644	79.915	−3.052
85.075	3.305	84.925	−2.049
90.055	2.103	89.945	−1.069
95.028	.918	94.972	−.281
100.000	0	100.000	0

L. E. radius: 1.575
Slope of radius through L. E.: 0.084

NACA 66(215)-216 $a=0.6$

[Stations and ordinates given in percent of airfoil chord]

Upper surface		Lower surface	
Station	Ordinate	Station	Ordinate
0	0	0	0
.371	1.242	.629	−1.112
.607	1.501	.893	−1.319
1.091	1.838	1.409	−1.608
2.317	2.615	2.683	−2.127
4.794	3.701	5.206	−2.869
7.284	4.568	7.716	−3.441
9.781	5.308	10.219	−3.934
14.788	6.500	15.212	−4.702
19.806	7.428	20.194	−5.290
24.832	8.155	25.168	−5.741
29.862	8.708	30.138	−6.080
34.897	9.098	35.103	−6.312
39.936	9.356	40.064	−6.462
44.978	9.471	45.022	−6.523
50.023	9.431	49.977	−6.488
55.073	9.224	54.927	−6.336
60.141	8.800	59.859	−6.048
65.191	8.084	64.809	−5.574
70.198	7.068	69.802	−4.866
75.151	5.889	74.819	−4.037
80.148	4.585	79.852	−3.107
85.106	3.265	84.894	−2.177
90.061	1.937	89.939	−1.235
95.021	.762	94.979	−.432
100.000	0	100.000	0

L. E. radius: 1.575
Slope of radius through L. E.: 0.110

NACA 66(215)-416

[Stations and ordinates given in percent of airfoil chord]

Upper surface		Lower surface	
Station	Ordinate	Station	Ordinate
0	0	0	0
.303	1.268	.697	−1.068
.532	1.541	.968	−1.261
1.008	1.952	1.492	−1.524
2.225	2.734	2.775	−1.990
4.698	3.510	5.307	−2.646
7.180	4.243	7.820	−3.147
9.677	5.049	10.323	−3.581
14.691	6.942	15.309	−4.250
19.720	7.948	20.280	−4.764
24.757	8.736	25.248	−5.156
29.801	9.336	30.199	−5.448
34.848	9.765	35.152	−5.645
39.898	10.050	40.102	−5.766
44.949	10.187	45.051	−5.807
50.000	10.163	50.000	−5.751
55.050	9.970	54.950	−5.590
60.096	9.596	59.904	−5.282
65.135	8.991	64.865	−4.771
70.161	7.912	69.839	−4.024
75.174	6.753	74.826	−3.173
80.170	5.437	79.830	−2.253
85.150	4.065	84.850	−1.373
90.111	2.617	89.889	−.549
95.056	1.226	94.944	.038
100.000	0	100.000	0

L. E. radius: 1.575
Slope of radius through L. E.: 0.168

NACA 66-006

[Stations and ordinates given in percent of airfoil chord]

Upper surface		Lower surface	
Station	Ordinate	Station	Ordinate
0	0	0	0
.50	.461	.50	−.461
.75	.554	.75	−.554
1.25	.693	1.25	−.693
2.5	.918	2.5	−.918
5.0	1.257	5.0	−1.257
7.5	1.524	7.5	−1.524
10	1.752	10	−1.752
15	2.119	15	−2.119
20	2.401	20	−2.401
25	2.618	25	−2.618
30	2.782	30	−2.782
35	2.899	35	−2.899
40	2.971	40	−2.971
45	3.000	45	−3.000
50	2.985	50	−2.985
55	2.925	55	−2.925
60	2.815	60	−2.815
65	2.611	65	−2.611
70	2.316	70	−2.316
75	1.953	75	−1.953
80	1.543	80	−1.543
85	1.107	85	−1.107
90	.665	90	−.665
95	.262	95	−.262
100	0	100	0

L. E. radius: 0.223

NACA 66-009

[Stations and ordinates given in percent of airfoil chord]

Upper surface		Lower surface	
Station	Ordinate	Station	Ordinate
0	0	0	0
.50	.687	.50	−.687
.75	.824	.75	−.824
1.25	1.030	1.25	−1.030
2.5	1.368	2.5	−1.368
5.0	1.880	5.0	−1.880
7.5	2.283	7.5	−2.283
10	2.626	10	−2.626
15	3.178	15	−3.178
20	3.601	20	−3.601
25	3.927	25	−3.927
30	4.173	30	−4.173
35	4.348	35	−4.348
40	4.457	40	−4.457
45	4.499	45	−4.499
50	4.475	50	−4.475
55	4.381	55	−4.381
60	4.204	60	−4.204
65	3.882	65	−3.882
70	3.428	70	−3.428
75	2.877	75	−2.877
80	2.263	80	−2.263
85	1.611	85	−1.611
90	.961	90	−.961
95	.374	95	−.374
100	0	100	0

L. E. radius: 0.530

NACA 66-206

[Stations and ordinates given in percent of airfoil chord]

Upper surface		Lower surface	
Station	Ordinate	Station	Ordinate
0	0	0	0
.461	.509	.539	−.499
.707	.622	.793	−.482
1.202	.798	1.298	−.584
2.447	1.102	2.553	−.730
4.941	1.572	5.059	−.940
7.439	1.947	7.561	−1.099
9.939	2.268	10.061	−1.234
14.942	2.791	15.058	−1.445
19.947	3.196	20.053	−1.604
24.954	3.513	25.046	−1.723
29.962	3.754	30.038	−1.810
34.971	3.929	35.029	−1.869
39.981	4.042	40.019	−1.900
44.990	4.095	45.010	−1.905
50.000	4.088	50.000	−1.882
55.009	4.020	54.991	−1.830
60.018	3.886	59.982	−1.744
65.026	3.641	64.974	−1.581
70.031	3.288	69.969	−1.344
75.034	2.848	74.966	−1.058
80.034	2.339	79.996	−.747
85.031	1.780	84.969	−.434
90.028	1.182	89.977	−.148
95.012	.578	94.988	.054
100.000	0	100.000	0

L. E. radius: 0.223
Slope of radius through L. E.: 0.084

NACA 66-209

[Stations and ordinates given in percent of airfoil chord]

Upper surface		Lower surface	
Station	Ordinate	Station	Ordinate
0	0	0	0
.442	.735	.558	−.685
.686	.892	.814	−.752
1.179	1.135	1.321	−.921
2.420	1.552	2.580	−1.180
4.912	2.194	5.088	−1.562
7.409	2.705	7.591	−1.857
9.908	3.141	10.092	−2.107
14.912	3.850	15.088	−2.504
19.921	4.396	20.079	−2.804
24.931	4.821	25.069	−3.031
29.944	5.145	30.056	−3.201
34.957	5.378	35.043	−3.318
39.971	5.528	40.029	−3.386
44.986	5.594	45.014	−3.404
50.000	5.578	50.000	−3.373
55.014	5.476	54.986	−3.296
60.027	5.275	59.973	−3.133
65.038	4.912	64.962	−2.852
70.046	4.400	69.954	−2.456
75.050	3.772	74.950	−1.982
80.050	3.058	79.950	−1.466
85.044	2.283	84.956	−.937
90.034	1.477	89.965	−.443
95.018	.660	94.982	−.058
100.000	0	100.000	0

L. E. radius: 0.580
Slope of radius through L. E.: 0.084

NACA 66-210

[Stations and ordinates given in percent of airfoil chord]

Upper surface		Lower surface	
Station	Ordinate	Station	Ordinate
0	0	0	0
.436	.806	.564	−.706
.670	.980	.821	−.840
1.171	1.245	1.329	−1.031
2.412	1.699	2.588	−1.327
4.902	2.401	5.098	−1.769
7.399	2.958	7.601	−2.110
9.898	3.432	10.102	−2.389
14.903	4.202	15.097	−2.856
19.912	4.796	20.088	−3.204
24.924	5.257	25.076	−3.467
29.937	5.608	30.063	−3.664
34.952	5.862	35.048	−3.802
39.968	6.024	40.032	−3.882
44.984	6.095	45.016	−3.905
50.000	6.074	50.000	−3.868
55.016	5.960	54.984	−3.770
60.030	5.736	59.970	−3.594
65.042	5.332	64.958	−3.272
70.051	4.759	69.949	−2.815
75.056	4.071	74.944	−2.281
80.055	3.289	79.945	−1.697
85.049	2.445	84.951	−1.099
90.037	1.570	89.963	−.536
95.019	.724	94.981	−.092
100.000	0	100.000	0

L. E. radius: 0.662
Slope of radius through L. E.: 0.084

NACA 66$_1$-012

[Stations and ordinates given in percent of airfoil chord]

Upper surface		Lower surface	
Station	Ordinate	Station	Ordinate
0	0	0	0
.5	.906	.5	−.906
.75	1.087	.75	−1.087
1.25	1.358	1.25	−1.358
2.5	1.808	2.5	−1.808
5.0	2.496	5.0	−2.496
7.5	3.037	7.5	−3.037
10	3.496	10	−3.496
15	4.234	15	−4.234
20	4.801	20	−4.801
25	5.238	25	−5.238
30	5.568	30	−5.568
35	5.803	35	−5.803
40	5.947	40	−5.947
45	6.000	45	−6.000
50	5.965	50	−5.965
55	5.836	55	−5.836
60	5.588	60	−5.588
65	5.139	65	−5.139
70	4.515	70	−4.515
75	3.767	75	−3.767
80	2.944	80	−2.944
85	2.083	85	−2.083
90	1.234	90	−1.234
95	.474	95	−.474
100	0	100	0

L. E. radius: 0.962

NACA 66$_1$-212

[Stations and ordinates given in percent of airfoil chord]

Upper surface		Lower surface	
Station	Ordinate	Station	Ordinate
0	0	0	0
.424	.953	.576	−.953
.666	1.154	.834	−1.014
1.156	1.462	1.344	−1.348
2.395	1.991	2.605	−1.619
4.883	2.809	5.117	−2.177
7.379	3.459	7.621	−2.611
9.878	4.011	10.122	−2.977
14.883	4.895	15.117	−3.559
19.894	5.596	20.106	−4.004
24.908	6.132	25.092	−4.342
29.925	6.539	30.075	−4.595
34.943	6.838	35.057	−4.773
39.962	7.018	40.038	−4.876
44.981	7.096	45.019	−4.905
50.000	7.068	50.000	−4.862
55.019	6.931	54.981	−4.741
60.036	6.659	59.964	−4.517
65.051	6.169	64.949	−4.109
70.061	5.487	69.939	−3.543
75.066	4.661	74.934	−2.871
80.065	3.739	79.935	−2.147
85.057	2.755	84.943	−1.409
90.043	1.750	89.957	−.716
95.022	.739	94.978	−.157
100.000	0	100.000	0

L. E. radius: 0.962
Slope of radius through L. E.: 0.084

NACA 66$_2$-015

[Stations and ordinates given in percent of airfoil chord]

Upper surface		Lower surface	
Station	Ordinate	Station	Ordinate
0	0	0	0
.5	1.122	.5	−1.122
.75	1.343	.75	−1.343
1.25	1.675	1.25	−1.675
2.5	2.235	2.5	−2.235
5.0	3.100	5.0	−3.100
7.5	3.781	7.5	−3.781
10	4.358	10	−4.358
15	5.286	15	−5.286
20	5.995	20	−5.995
25	6.543	25	−6.543
30	6.956	30	−6.956
35	7.250	35	−7.250
40	7.430	40	−7.430
45	7.495	45	−7.495
50	7.450	50	−7.450
55	7.283	55	−7.283
60	6.959	60	−6.959
65	6.372	65	−6.372
70	5.576	70	−5.576
75	4.632	75	−4.632
80	3.596	80	−3.596
85	2.530	85	−2.530
90	1.489	90	−1.489
95	.566	95	−.566
100	0	100	0

L. E. radius: 1.426

NACA 66$_2$-215

[Stations and ordinates given in percent of airfoil chord]

Upper surface		Lower surface	
Station	Ordinate	Station	Ordinate
0	0	0	0
.406	1.168	.594	−1.068
.646	1.409	.854	−1.269
1.134	1.778	1.366	−1.564
2.370	2.417	2.630	−2.045
4.855	3.418	5.145	−2.781
7.349	4.202	7.651	−3.354
9.848	4.872	10.152	−3.833
14.854	5.957	15.146	−4.611
19.868	6.790	20.132	−5.198
24.886	7.437	25.114	−5.647
29.905	7.927	30.094	−5.983
34.929	8.280	35.071	−6.220
39.952	8.501	40.048	−6.359
44.976	8.590	45.024	−6.400
50.000	8.553	50.000	−6.347
55.023	8.378	54.977	−6.188
60.045	8.030	59.955	−5.898
65.063	7.402	64.937	−5.342
70.078	6.547	69.925	−4.603
75.081	5.626	74.919	−3.736
80.079	4.393	79.921	−2.801
85.070	3.202	84.930	−1.886
90.052	2.005	89.948	−.971
95.026	.881	94.974	−.249
100.000	0	100.000	0

L. E. radius: 1.435
Slope of radius through L. E.: 0.084

NACA 66$_2$-415

[Stations and ordinates given in percent of airfoil chord]

Upper surface		Lower surface	
Station	Ordinate	Station	Ordinate
0	0	0	0
.314	1.206	.686	−1.006
.544	1.407	.966	−1.187
1.019	1.873	1.481	−1.445
2.241	2.592	2.759	−1.848
4.711	3.718	5.289	−2.454
7.199	4.617	7.801	−2.921
9.696	5.381	10.304	−3.313
14.709	6.624	15.291	−3.932
19.736	7.581	20.264	−4.397
24.771	8.320	25.229	−4.749
29.812	8.897	30.188	−5.009
34.857	9.309	35.143	−5.189
39.904	9.571	40.096	−5.287
44.952	9.685	45.048	−5.305
50.000	9.666	50.000	−5.244
55.046	9.473	54.954	−5.093
60.090	9.100	59.910	−4.816
65.126	8.431	64.874	−4.311
70.150	7.518	69.850	−3.630
75.162	6.419	74.838	−2.839
80.159	5.187	79.841	−2.003
85.139	3.872	84.861	−1.180
90.104	2.519	89.896	−.451
95.053	1.190	94.947	.068
100.000	0	100.000	0

L. E. radius: 1.435
Slope of radius through L. E.: 0.168

NACA 663-018

[Stations and ordinates given in percent of airfoil chord]

Upper surface		Lower surface	
Station	Ordinate	Station	Ordinate
0	0	0	0
.5	1.323	.5	−1.323
.75	1.571	.75	−1.571
1.25	1.952	1.25	−1.952
2.5	2.646	2.5	−2.646
5.0	3.690	5.0	−3.690
7.5	4.513	7.5	−4.513
10	5.210	10	−5.210
15	6.333	15	−6.333
20	7.188	20	−7.188
25	7.848	25	−7.848
30	8.346	30	−8.346
35	8.701	35	−8.701
40	8.918	40	−8.918
45	8.998	45	−8.998
50	8.942	50	−8.942
55	8.733	55	−8.733
60	8.323	60	−8.323
65	7.580	65	−7.580
70	6.507	70	−6.507
75	5.451	75	−5.451
80	4.206	80	−4.206
85	2.934	85	−2.934
90	1.714	90	−1.714
95	.646	95	−.646
100	0	100	0

L. E. radius: 1.956

NACA 663-218

[Stations and ordinates given in percent of airfoil chord]

Upper surface		Lower surface	
Station	Ordinate	Station	Ordinate
0	0	0	0
.389	1.368	.611	−1.268
.928	1.636	.872	−1.490
1.115	2.054	1.385	−1.840
2.846	2.828	2.654	−2.456
4.827	4.002	5.173	−3.370
7.320	4.983	7.680	−4.085
9.818	5.724	10.182	−4.690
14.825	7.004	15.175	−5.658
19.841	7.982	20.159	−6.300
24.868	8.742	25.137	−6.952
29.887	9.317	30.113	−7.373
34.914	9.731	35.086	−7.671
39.942	9.989	40.058	−7.847
44.971	10.093	45.029	−7.903
50.000	10.045	50.000	−7.839
55.028	9.828	54.972	−7.658
60.054	9.394	59.946	−7.262
65.075	8.610	64.925	−6.550
70.089	7.568	69.911	−5.624
75.095	6.345	74.905	−4.555
80.093	5.001	79.907	−3.409
85.081	3.606	84.919	−2.280
90.060	2.230	89.940	−1.196
95.030	.961	94.970	−.329
100.000	0	100.000	0

L. E. radius: 1.955
Slope of radius through L. E.: 0.084

NACA 663-418

[Stations and ordinates given in percent of airfoil chord]

Upper surface		Lower surface	
Station	Ordinate	Station	Ordinate
0	0	0	0
.280	1.405	.720	−1.205
.509	1.692	.991	−1.412
.981	2.147	1.519	−1.719
2.194	3.000	2.806	−2.256
4.656	4.806	5.344	−3.042
7.140	5.847	7.860	−3.651
9.636	6.231	10.364	−4.163
14.651	7.609	15.349	−4.977
19.683	8.778	20.317	−5.589
24.726	9.633	25.274	−6.053
29.775	10.287	30.225	−6.399
34.829	10.759	35.171	−6.639
39.885	11.059	40.115	−6.775
44.943	11.188	45.057	−6.808
50.000	11.148	50.000	−6.736
55.056	10.928	54.944	−6.543
60.107	10.404	59.893	−6.180
65.149	9.639	64.851	−5.619
70.178	8.639	69.822	−4.861
75.191	7.238	74.809	−3.658
80.185	5.794	79.815	−2.610
85.162	4.276	84.838	−1.584
90.120	2.744	89.880	−.676
95.060	1.275	94.940	−.011
100.000	0	100.000	0

L. E. radius: 1.955
Slope of radius through L. E.: 0.168

NACA 664-021

[Stations and ordinates given in percent of airfoil chord]

Upper surface		Lower surface	
Station	Ordinate	Station	Ordinate
0	0	0	0
.5	1.525	.5	−1.525
.75	1.804	.75	−1.804
1.25	2.240	1.25	−2.240
2.5	3.045	2.5	−3.045
5.0	4.269	5.0	−4.269
7.5	5.233	7.5	−5.233
10	6.052	10	−6.052
15	7.369	15	−7.369
20	8.376	20	−8.376
25	9.153	25	−9.153
30	9.738	30	−9.738
35	10.154	35	−10.154
40	10.407	40	−10.407
45	10.500	45	−10.500
50	10.434	50	−10.434
55	10.186	55	−10.186
60	9.692	60	−9.692
65	8.793	65	−8.793
70	7.610	70	−7.610
75	6.251	75	−6.251
80	4.796	80	−4.796
85	3.324	85	−3.324
90	1.924	90	−1.924
95	.717	95	−.717
100	0	100	0

L. E. radius: 2.550

NACA 664-221

[Stations and ordinates given in percent of airfoil chord]

Upper surface		Lower surface	
Station	Ordinate	Station	Ordinate
0	0	0	0
.872	1.570	.628	−1.470
.610	1.809	.890	−1.729
1.095	2.342	1.405	−2.128
2.323	3.226	2.677	−2.854
4.800	4.580	5.200	−3.948
7.291	5.653	7.709	−4.805
9.788	6.565	10.212	−5.531
14.797	8.039	15.203	−6.698
19.815	9.170	20.185	−7.578
24.840	10.047	25.160	−8.257
29.869	10.709	30.131	−8.765
34.900	11.188	35.100	−9.123
39.933	11.478	40.067	−9.336
44.967	11.595	45.033	−9.405
50.000	11.537	50.000	−9.331
55.032	11.281	54.968	−9.091
60.063	10.703	59.937	−8.621
65.087	9.823	64.913	−7.703
70.103	8.581	69.897	−6.637
75.109	7.145	74.891	−5.355
80.106	5.591	79.894	−3.999
85.092	3.996	84.908	−2.550
90.067	2.440	89.933	−1.406
95.034	1.032	94.966	−.400
100.000	0	100.000	0

L. E. radius: 2.550
Slope of radius through L. E.: 0.084

NACA 67,1-215

[Stations and ordinates given in percent of airfoil chord]

Upper surface		Lower surface	
Station	Ordinate	Station	Ordinate
0	0	0	0
.402	1.213	.598	−1.113
.642	1.460	.858	−1.320
1.128	1.867	1.372	−1.653
2.361	2.577	2.639	−2.205
4.848	3.557	5.152	−2.925
7.344	4.321	7.656	−3.473
9.845	4.947	10.155	−3.913
14.854	5.954	15.146	−4.608
19.869	6.735	20.131	−5.143
24.887	7.348	25.113	−5.558
29.908	7.825	30.092	−5.881
34.930	8.185	35.070	−6.125
39.953	8.430	40.047	−6.288
44.976	8.570	45.024	−6.380
50.000	8.600	50.000	−6.394
55.024	8.516	54.976	−6.326
60.047	8.302	59.953	−6.160
65.068	7.985	64.932	−5.875
70.086	7.373	69.914	−5.429
75.098	6.515	74.902	−4.725
80.100	5.385	79.900	−3.748
85.092	3.999	84.908	−2.563
90.071	2.537	89.929	−1.503
95.037	1.103	94.963	−.471
100.000	0	100.000	0

L. E. radius: 1.528
Slope of radius through L. E.: 0.084

NACA 747A315

[Stations and ordinates given in percent of airfoil chord]

Upper surface		Lower surface	
Station	Ordinate	Station	Ordinate
0	0	0	0
.229	1.305	.771	−1.081
.449	1.599	1.051	−1.207
.911	2.065	1.589	−1.473
2.109	2.935	2.891	−1.927
4.564	4.264	5.436	−2.518
7.053	5.286	7.947	−2.952
9.558	6.140	10.442	−3.304
14.599	7.497	15.401	−3.843
19.668	8.503	20.332	−4.247
24.758	9.242	25.242	−4.546
29.867	9.731	30.133	−4.773
35.001	9.982	34.999	−4.926
40.200	9.962	39.800	−5.020
45.375	9.572	44.625	−5.040
50.447	8.904	49.553	−5.014
55.463	8.200	54.537	−4.930
60.435	7.324	59.565	−4.772
65.360	6.305	64.634	−4.509
70.241	5.254	69.759	−4.110
75.130	4.286	74.870	−3.502
80.073	3.295	79.927	−2.743
85.088	2.257	84.912	−1.915
90.016	1.289	89.984	−1.097
95.004	.481	94.996	−.405
100.000	0	100.000	0

L. E. radius: 1.544
Slope of radius through L. E.: 0.232

NACA 747A415

[Stations and ordinates given in percent of airfoil chord]

Upper surface		Lower surface	
Station	Ordinate	Station	Ordinate
0	0	0	0
.183	1.518	.817	−.994
.398	1.822	1.102	−1.160
.852	2.406	1.648	−1.406
2.041	3.016	2.959	−1.822
4.487	4.411	5.513	−2.349
6.972	5.488	8.028	−2.730
9.476	6.390	10.524	−3.038
14.521	7.827	15.479	−3.501
19.598	8.897	20.402	−3.845
24.698	9.687	25.302	−4.095
29.818	10.216	30.182	−4.286
34.954	10.497	35.046	−4.411
40.176	10.490	39.824	−4.485
45.364	10.121	44.636	−4.498
50.447	9.516	49.553	−4.462
55.474	8.753	54.526	−4.381
60.454	7.859	59.546	−4.235
65.393	6.878	64.607	−3.992
70.278	5.838	69.727	−3.622
75.164	4.783	74.836	−3.063
80.107	3.692	79.893	−2.344
85.066	2.592	84.934	−1.578
90.087	1.546	89.963	−.838
95.015	.639	94.985	−.247
100.000	0	100.000	0

L. E. radius: 1.544
Slope of radius through L. E.: 0.274

IV—PREDICTED CRITICAL MACH NUMBERS

	Page
Critical Mach number chart	372
Variation of critical Mach number with low-speed section lift coefficient:	
For the NACA 0006, 0009, and 0012 airfoil sections	373
For several NACA 14-series airfoil sections of various thicknesses	373
For several NACA 24-series airfoil sections of various thicknesses	374
For several NACA 44-series airfoil sections of various thicknesses	374
For several NACA 230-series airfoil sections of various thicknesses	375
For several NACA 63-series airfoil sections of various thicknesses, cambered for various design lift coefficients	375
For several NACA 63-series symmetrical airfoil sections of various thicknesses	376
For several NACA 63-series airfoil sections of various thicknesses, cambered for a design lift coefficient of 0.2	376
For several NACA 63-series airfoil sections of various thicknesses, cambered for a design lift coefficient of 0.4	377
For two NACA 63-series airfoil sections of different thicknesses, cambered for a design lift coefficient of 0.6	377
For several NACA 64-series symmetrical airfoil sections of various thicknesses	378
For several NACA 64-series airfoil sections of various thicknesses, cambered for a design lift coefficient of 0.1	378
For several NACA 64-series airfoil sections of various thicknesses, cambered for a design lift coefficient of 0.2	379
For several NACA 64-series airfoil sections of various thicknesses, cambered for a design lift coefficient of 0.4	379
For two NACA 64-series airfoil sections of different thicknesses, cambered for a design lift coefficient of 0.6	380
Variation of critical Mach number with low-speed section lift coefficient—Continued	
For several NACA 65-series symmetrical airfoil sections of various thicknesses	380
For several NACA 65-series airfoil sections with a thickness ratio of 0.18 and cambered for various design lift coefficients	381
For several NACA 65-series airfoil sections of various thicknesses, cambered for a design lift coefficient of 0.2	381
For several NACA 65-series airfoil sections of various thicknesses, cambered for a design lift coefficient of 0.4	382
For several NACA 65-series airfoil sections with mean line of the type $a=0.5$ and cambered for a design lift coefficient of 0.4	382
For two NACA 65-series airfoil sections of different thicknesses, cambered for a design lift coefficient of 0.6	383
For two NACA 65-series airfoil sections with mean line of the type $a=0.5$, with different thicknesses, and cambered for a design lift coefficient of 0.6	383
For several NACA 66-series symmetrical airfoil sections of various thicknesses	384
For several NACA 66-series airfoil sections of various thicknesses, cambered for a design lift coefficient of 0.2	384
For two NACA 66-series airfoil sections of different thicknesses, cambered for a design lift coefficient of 0.4	385
For several NACA 66-series airfoil sections with a thickness ratio of 0.16 and cambered for various design lift coefficients	385
For several NACA 6-series airfoil sections with different positions of minimum pressure and various thicknesses, cambered for various design lift coefficients	386
For two NACA 7-series airfoil sections with a thickness ratio of 0.15 and cambered for different design lift coefficients	386

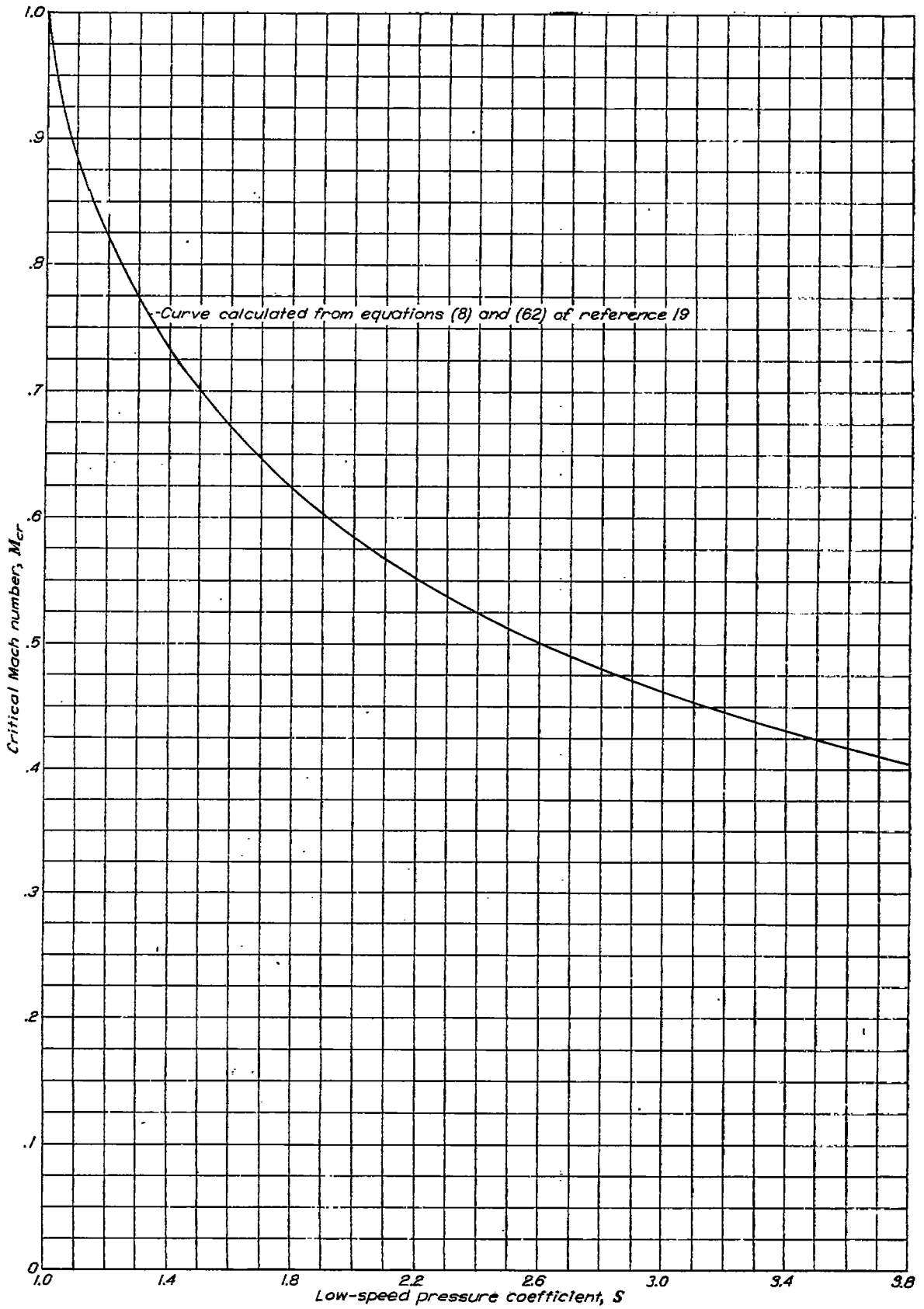

Critical Mach number chart.

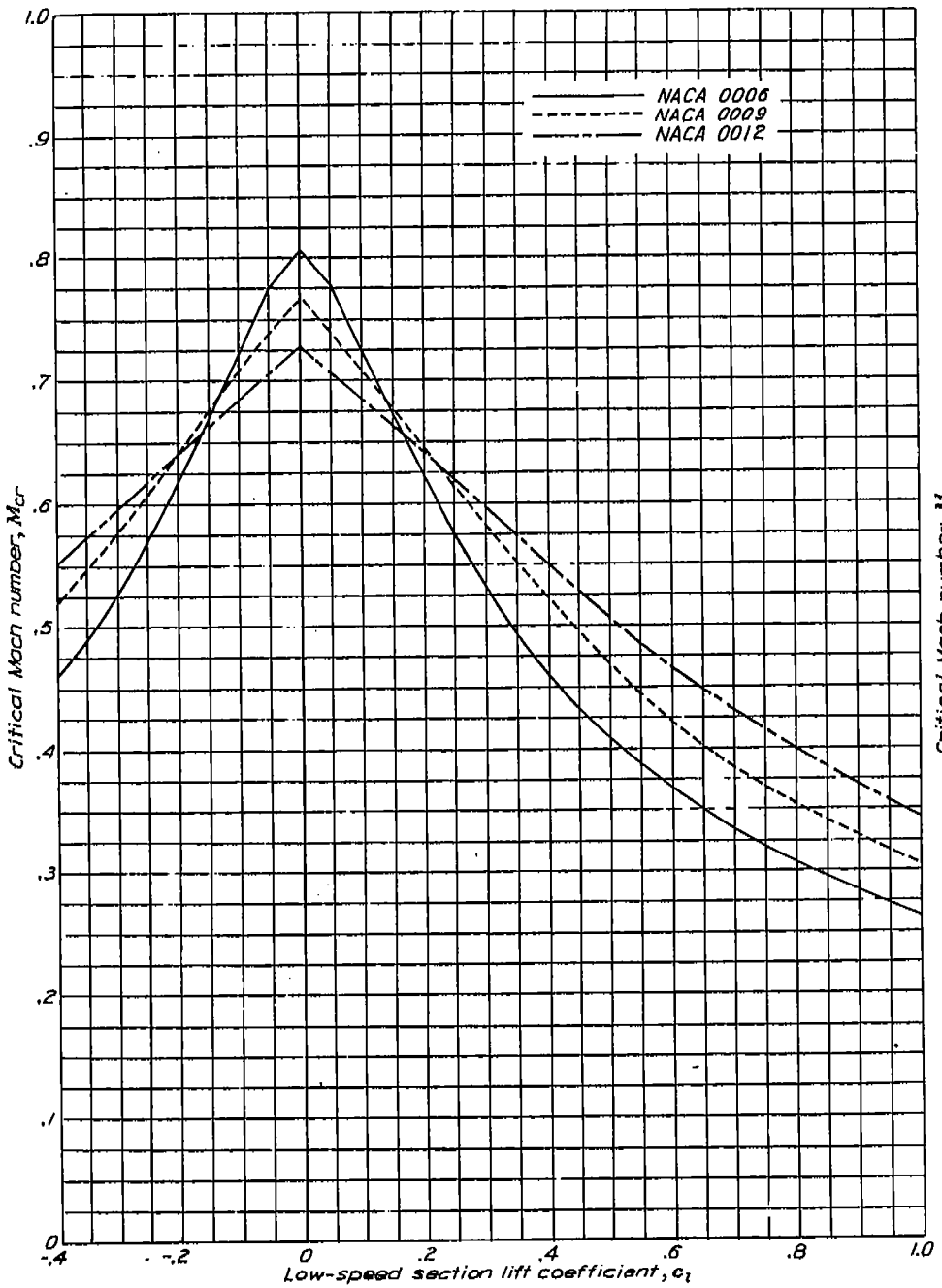

Variation of critical Mach number with low-speed section lift coefficient for the NACA 0006, 0009, and 0012 airfoil sections.

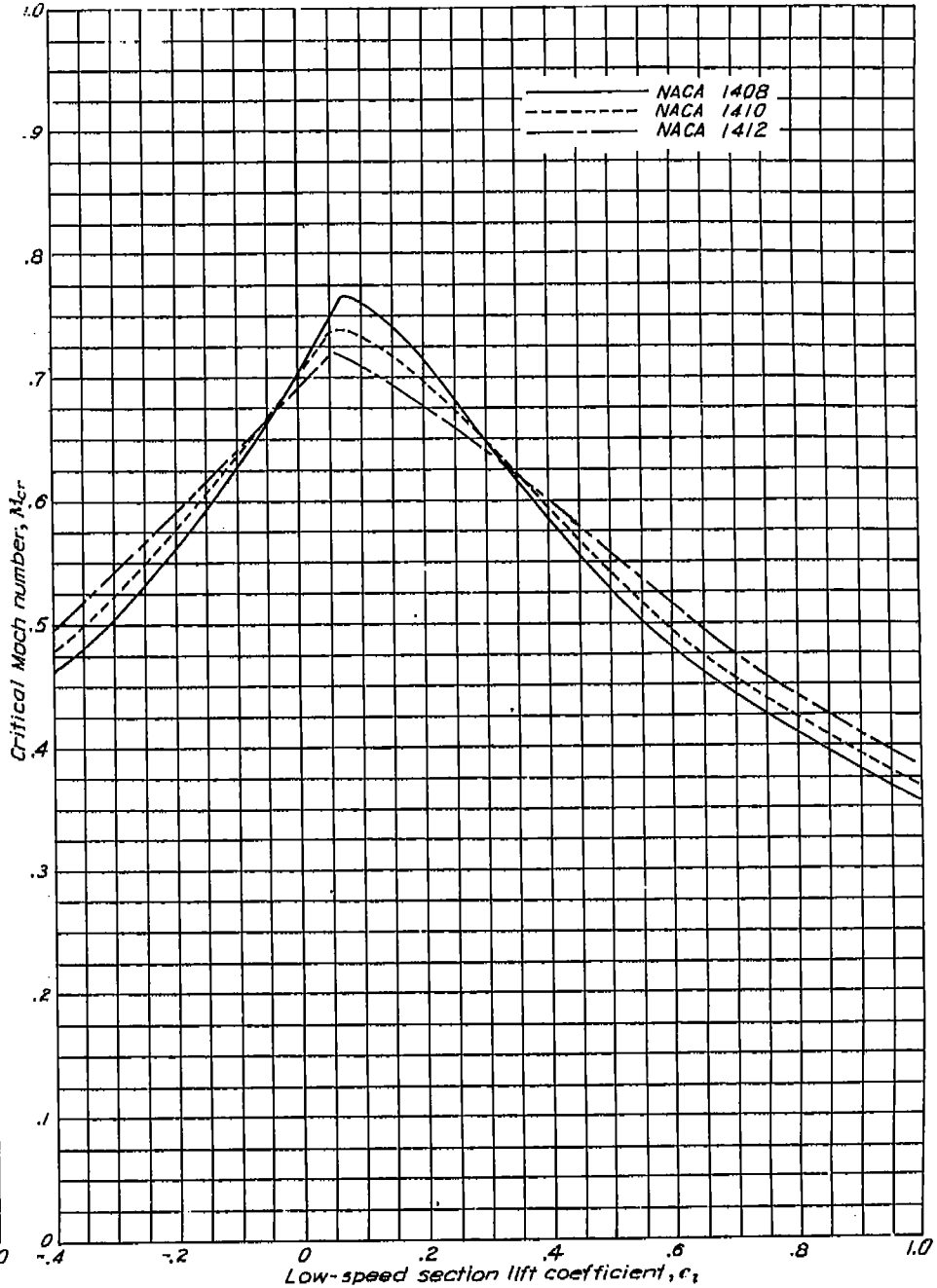

Variation of critical Mach number with low-speed section lift coefficient for several NACA 14-series airfoil sections of various thicknesses.

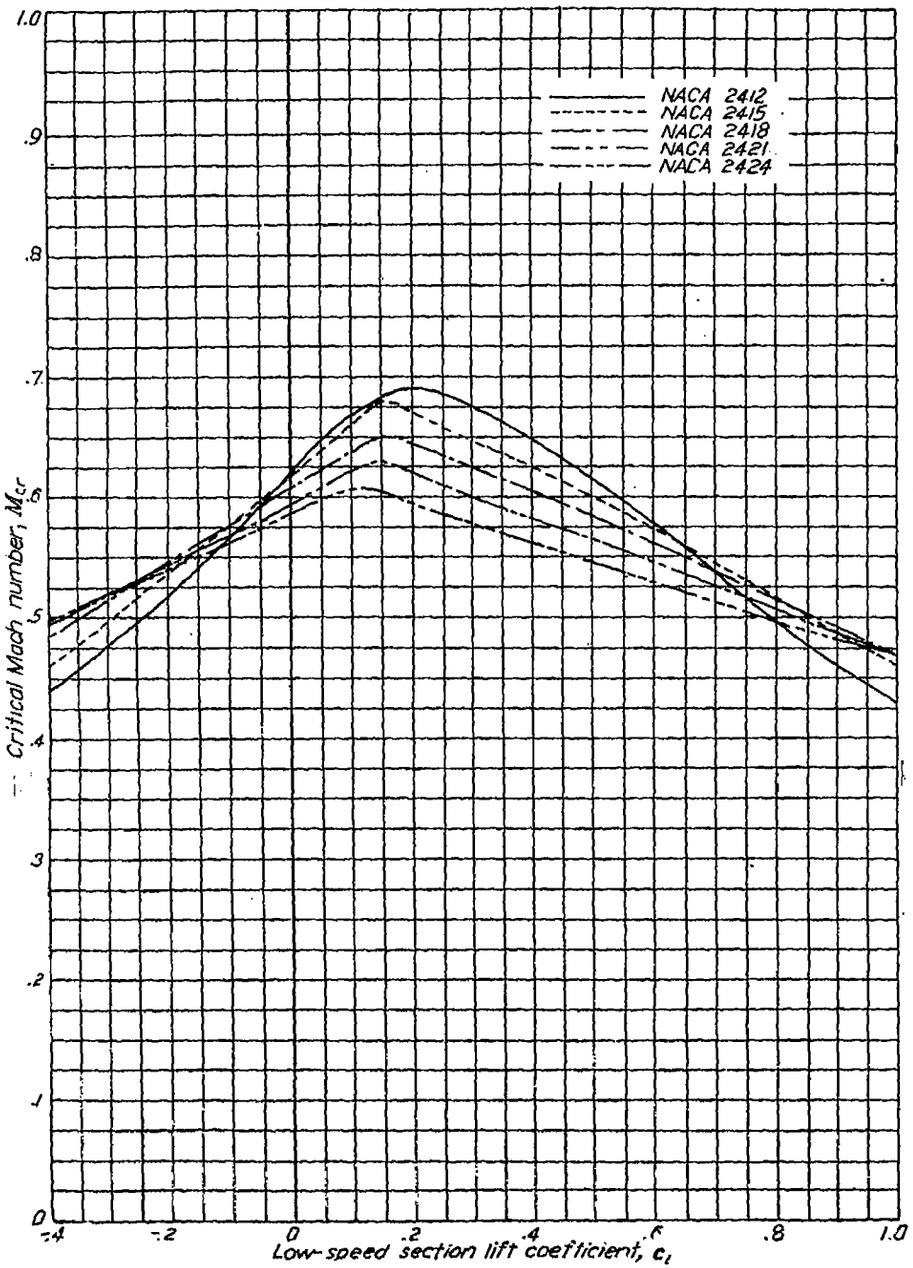

Variation of critical Mach number with low-speed section lift coefficient for several NACA 24 series airfoil sections of various thicknesses.

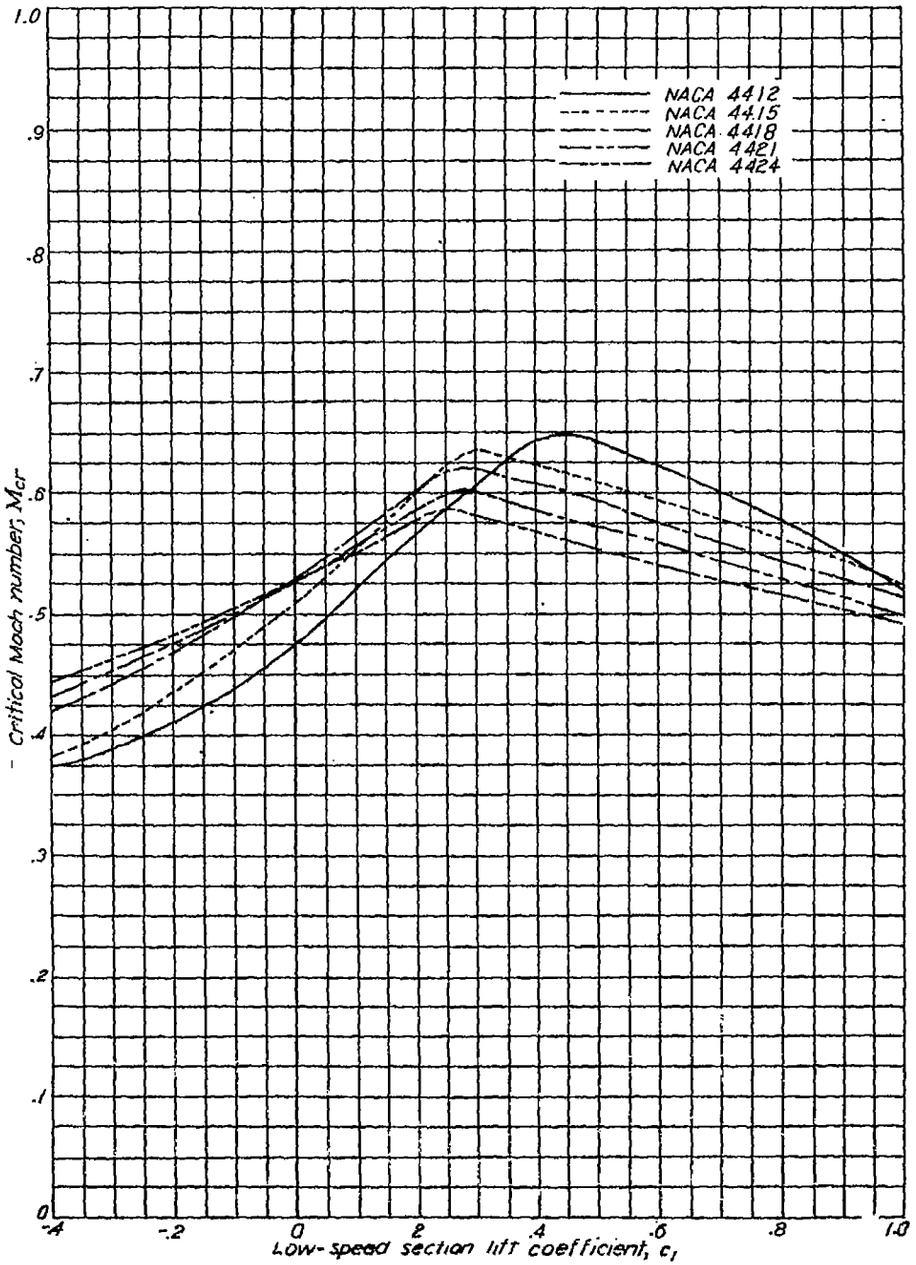

Variation of critical Mach number with low-speed section lift coefficient for several NACA 44-series airfoil sections of various thicknesses.

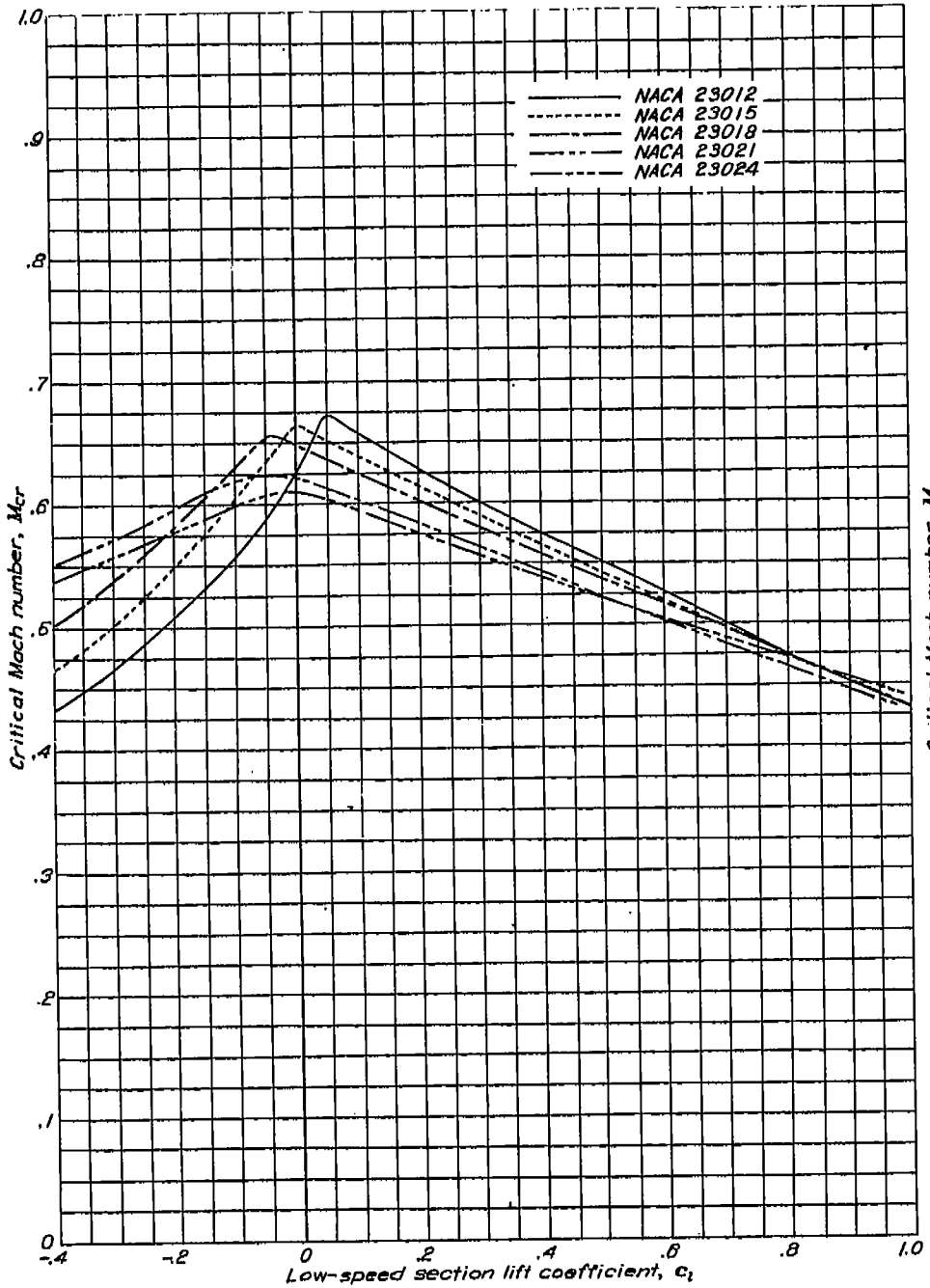

Variation of critical Mach number with low-speed section lift coefficient for several NACA 230-series airfoil sections of various thicknesses.

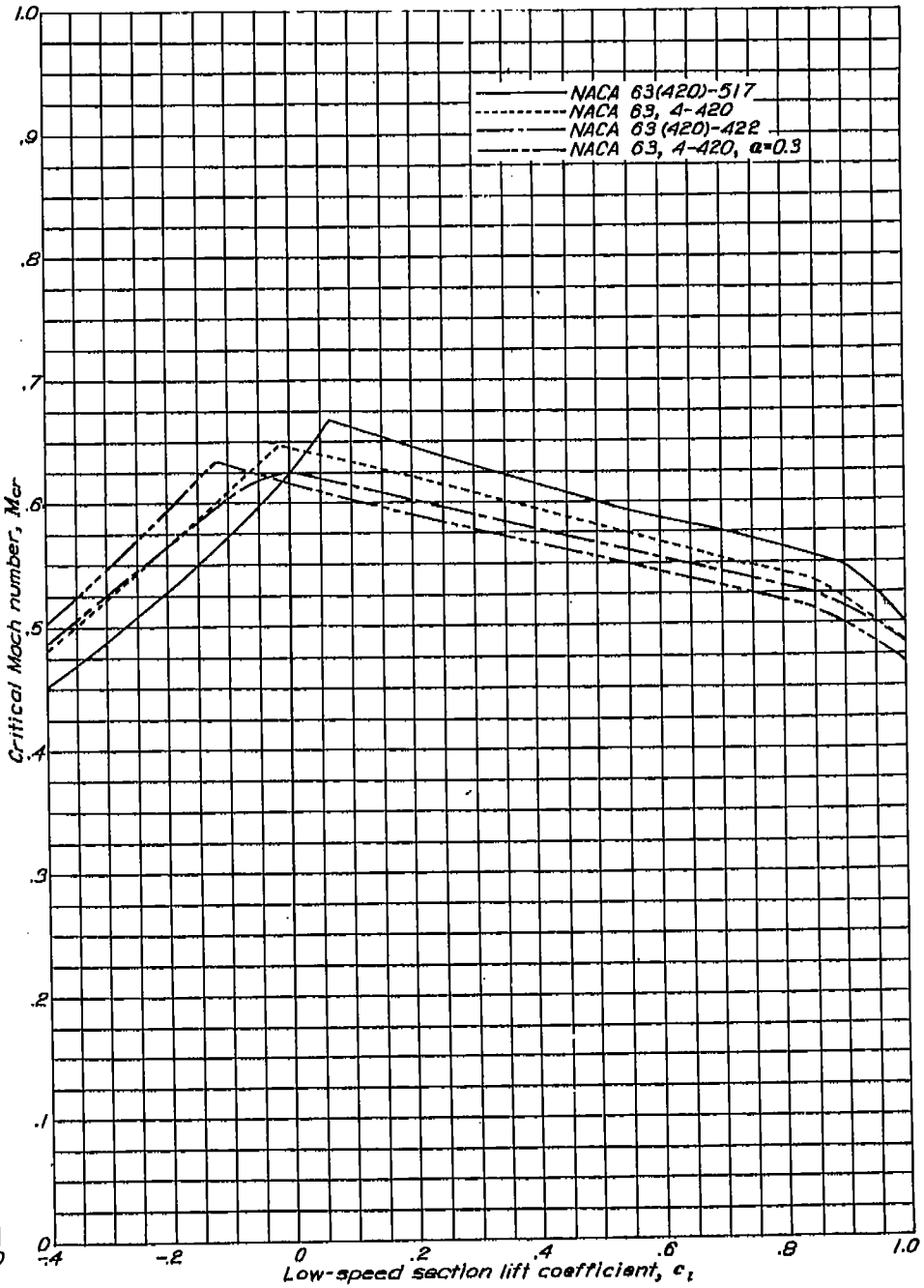

Variation of critical Mach number with low-speed section lift coefficient for several NACA 63-series airfoil sections of various thicknesses, cambered for various design lift coefficients.

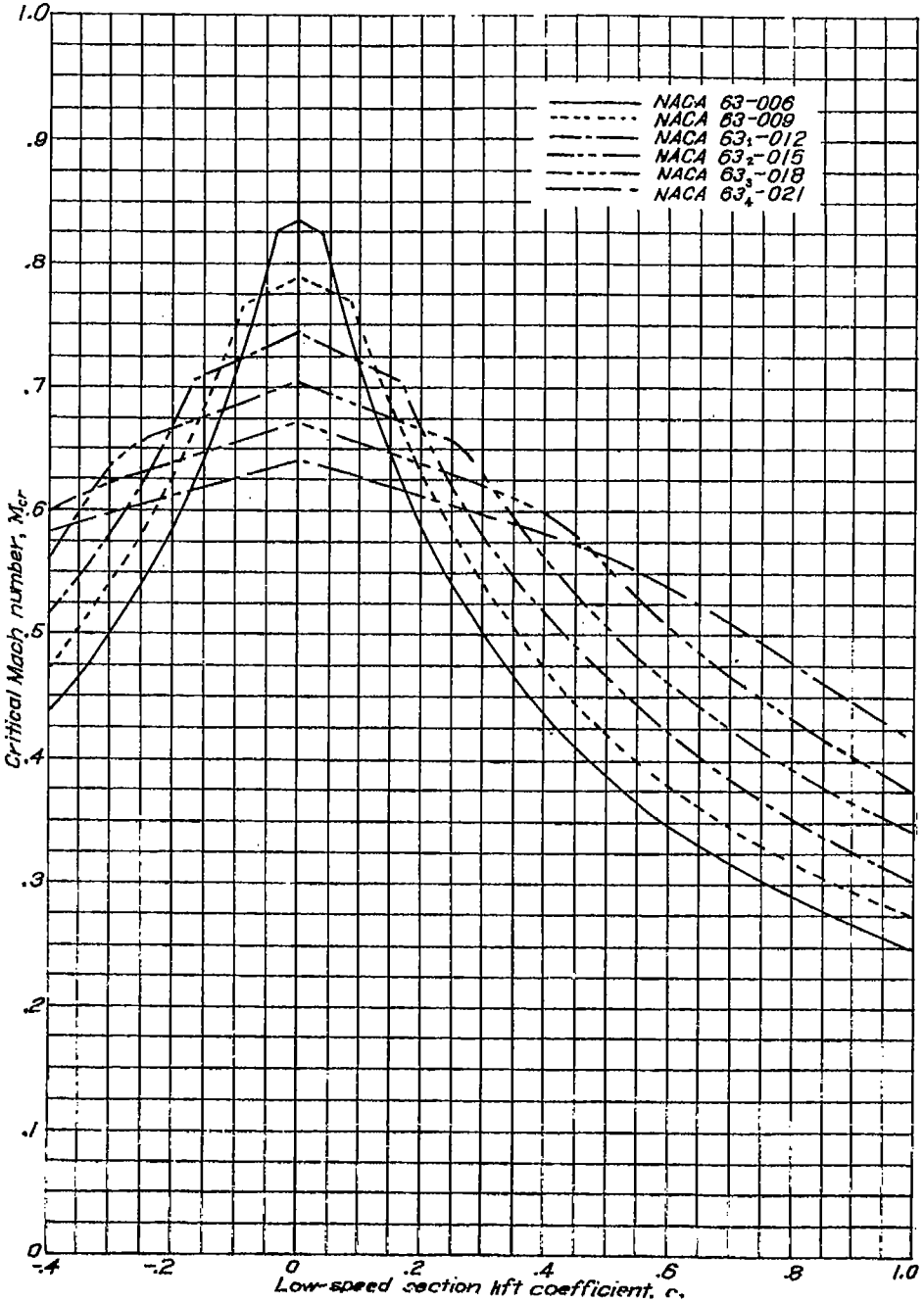

Variation of critical Mach number with low-speed section lift coefficient for several NACA 63-series symmetrical airfoil sections of various thicknesses.

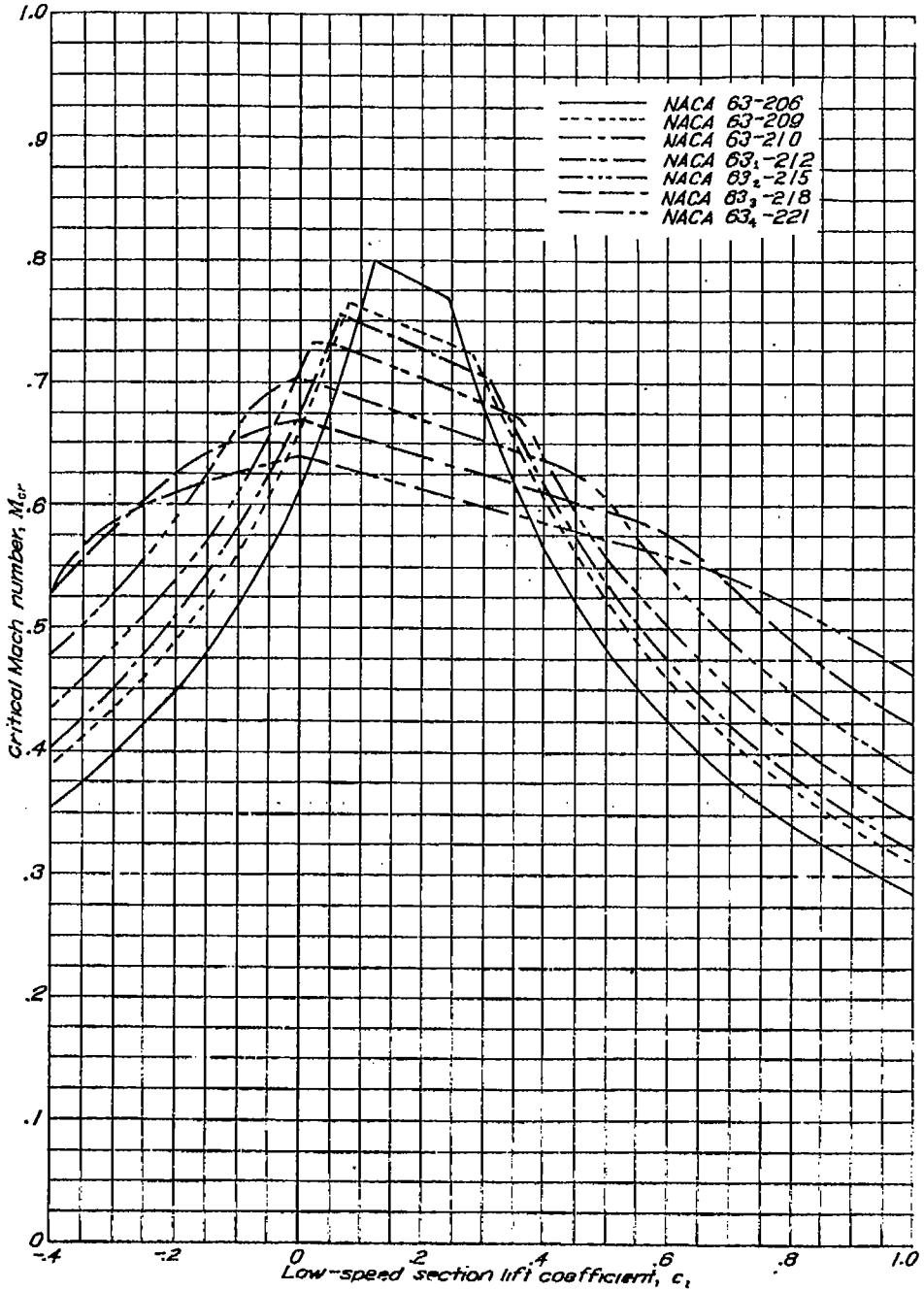

Variation of critical Mach number with low-speed section lift coefficient for several NACA 63-series airfoil sections of various thicknesses, cambered for a design lift coefficient of 0.2.

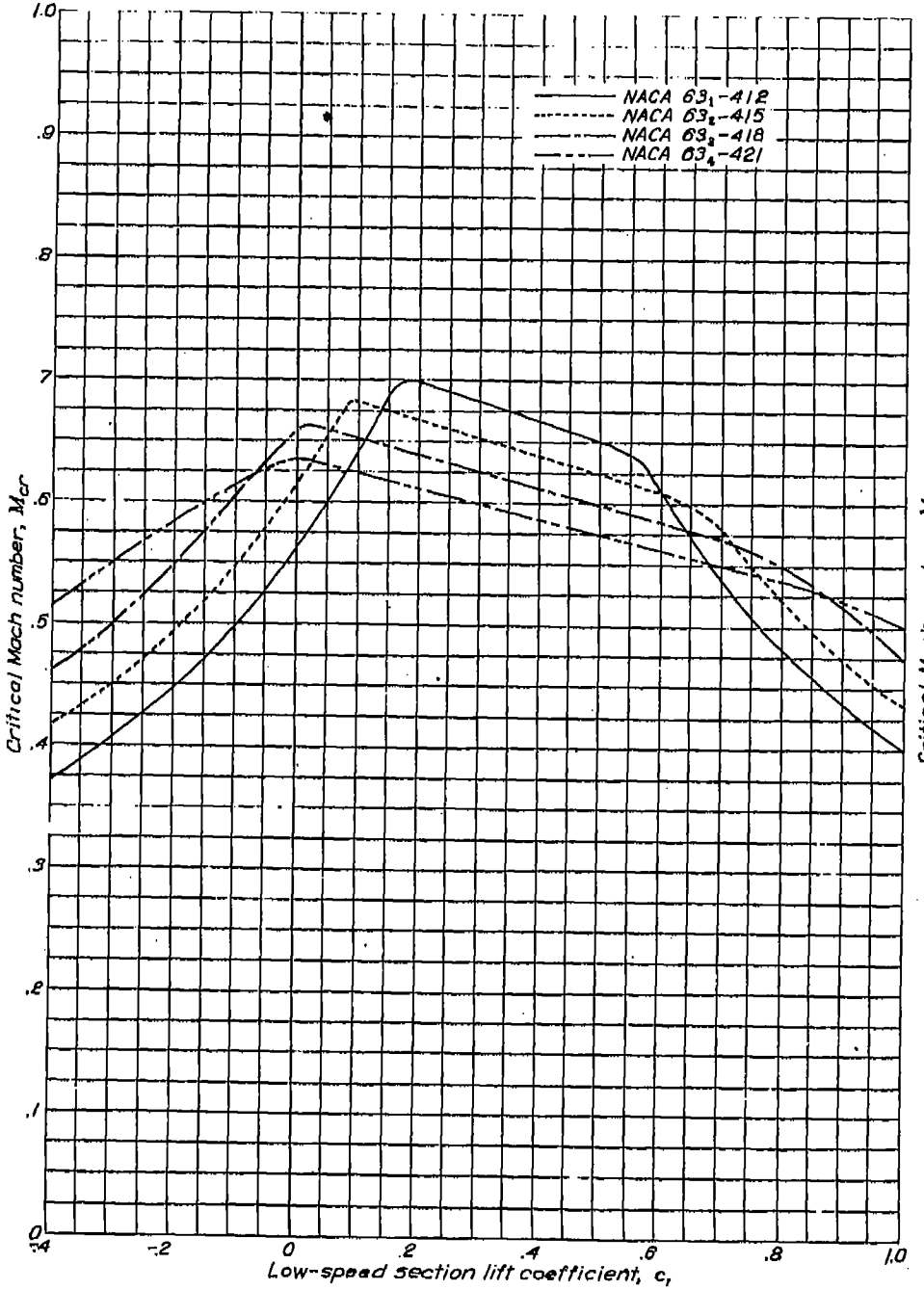

Variation of critical Mach number with low-speed section lift coefficient for several NACA 63-series airfoil sections of various thicknesses, cambered for a design lift coefficient of 0.4.

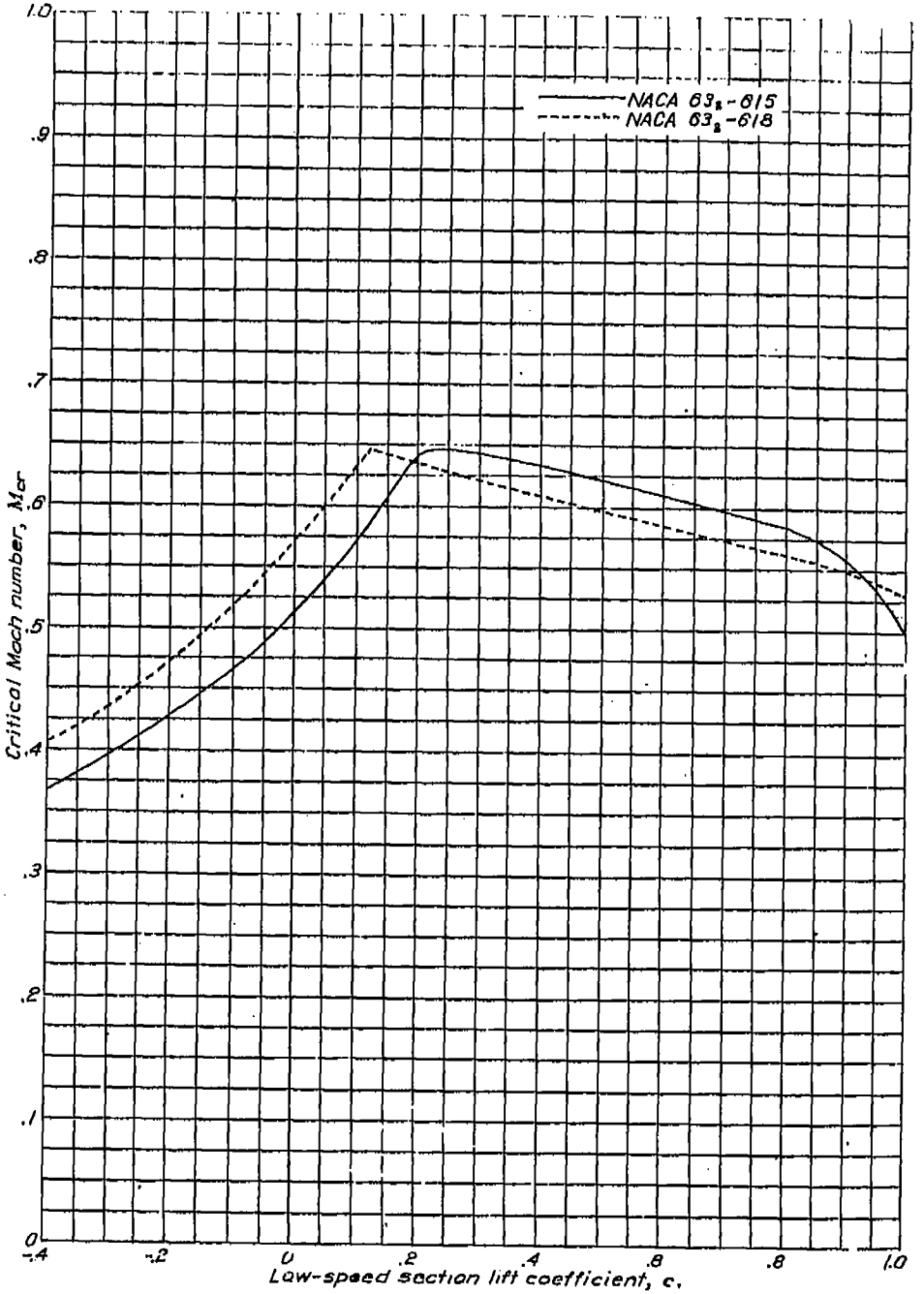

Variation of critical Mach number with low-speed section lift coefficient for two NACA 63-series airfoil sections of different thicknesses, cambered for a design lift coefficient of 0.6.

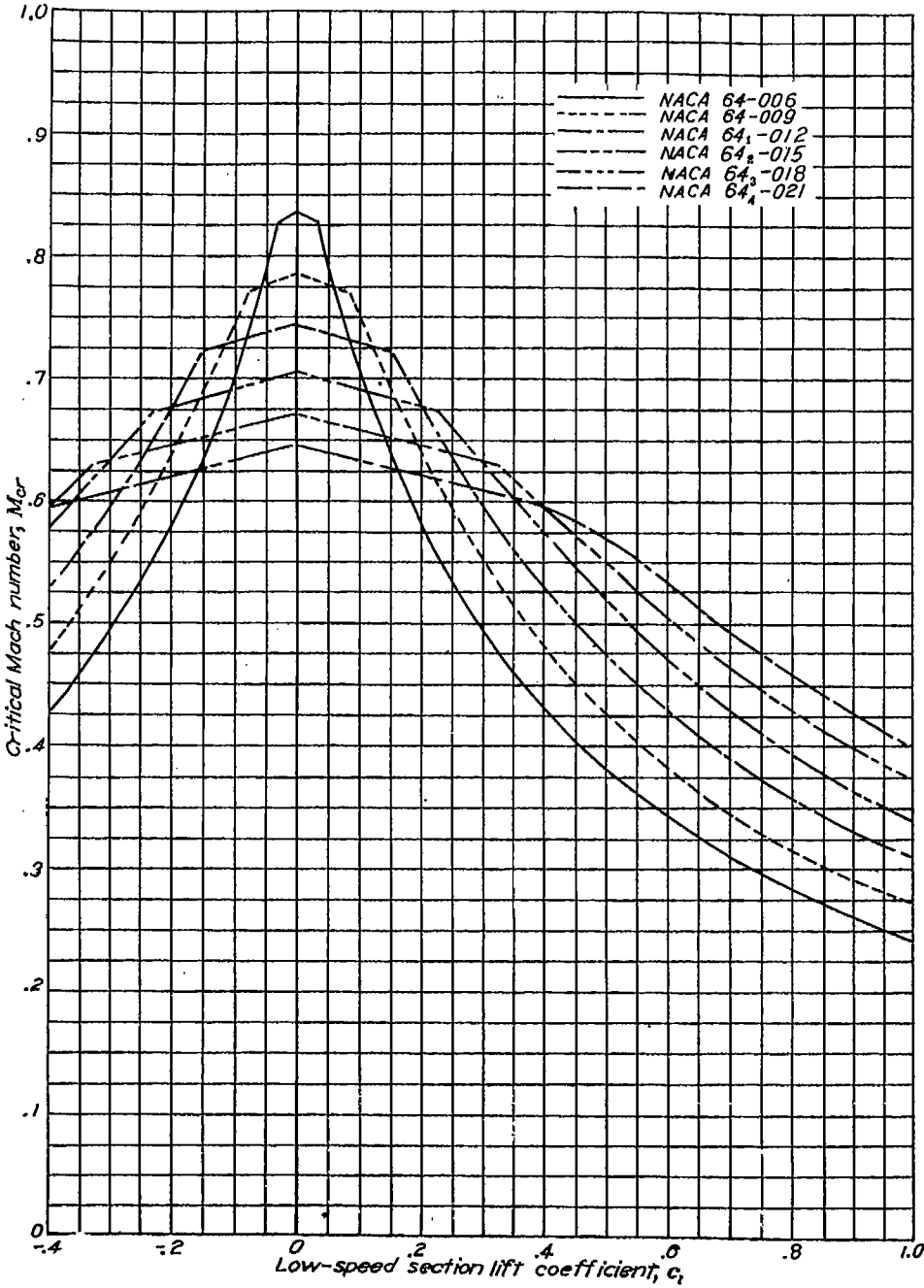

Variation of critical Mach number with low-speed section lift coefficient for several NACA 64-series symmetrical airfoil sections of various thicknesses.

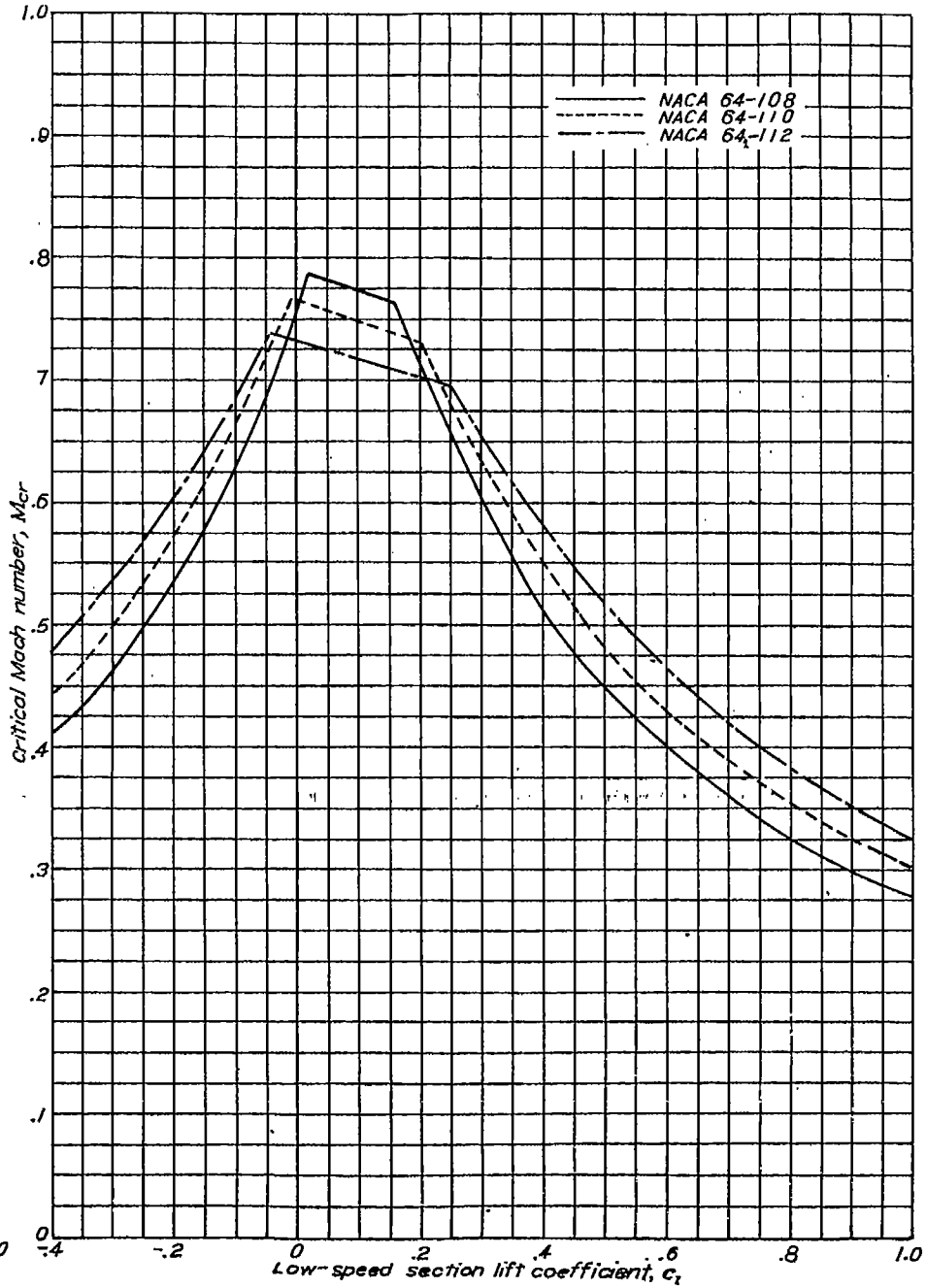

Variation of critical Mach number with low-speed section lift coefficient for several NACA 64-series airfoil sections of various thicknesses, cambered for a design lift coefficient of 0.1.

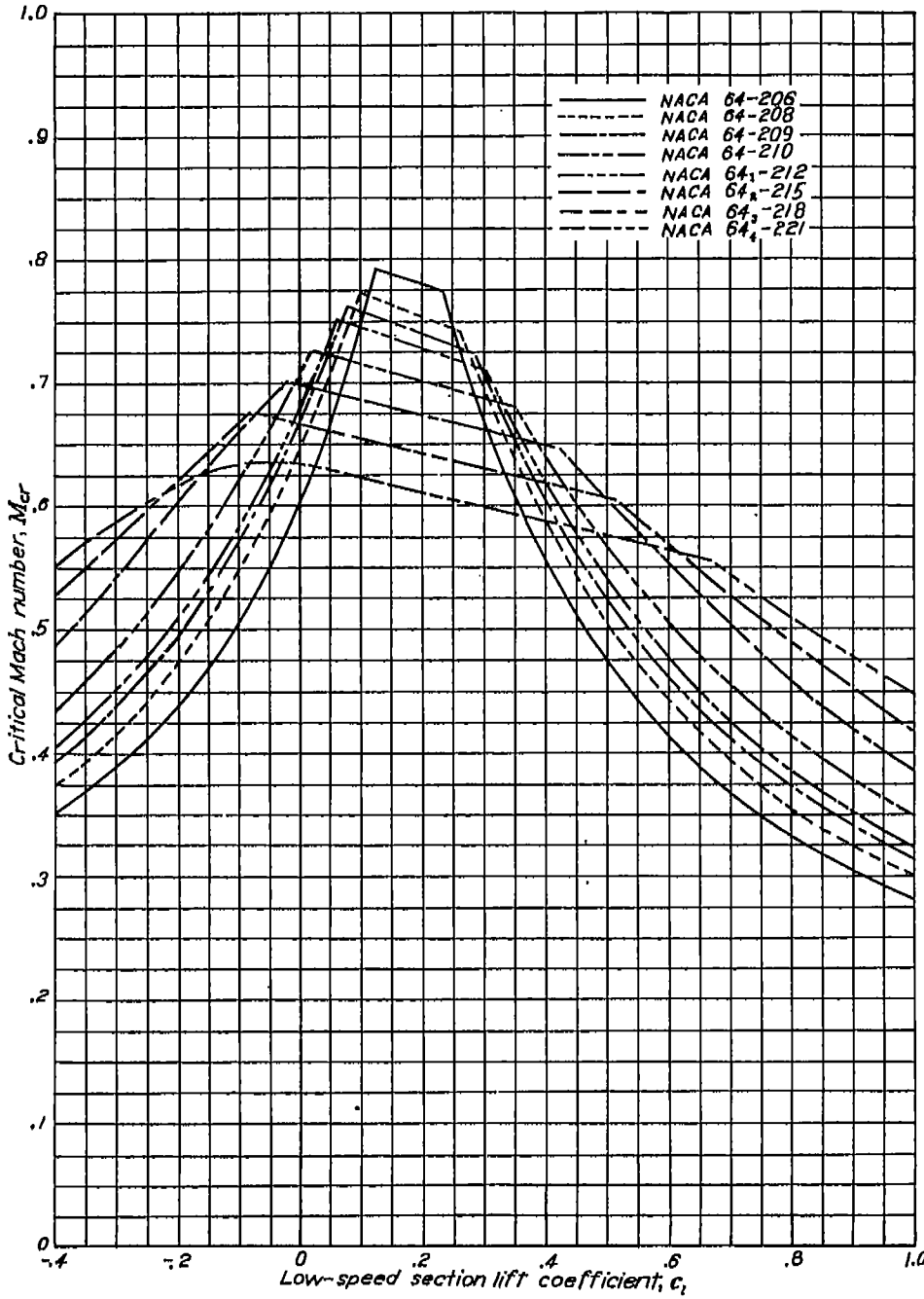

Variation of critical Mach number with low-speed section lift coefficient for several NACA 64-series airfoil sections of various thicknesses, cambered for a design lift coefficient of 0.2.

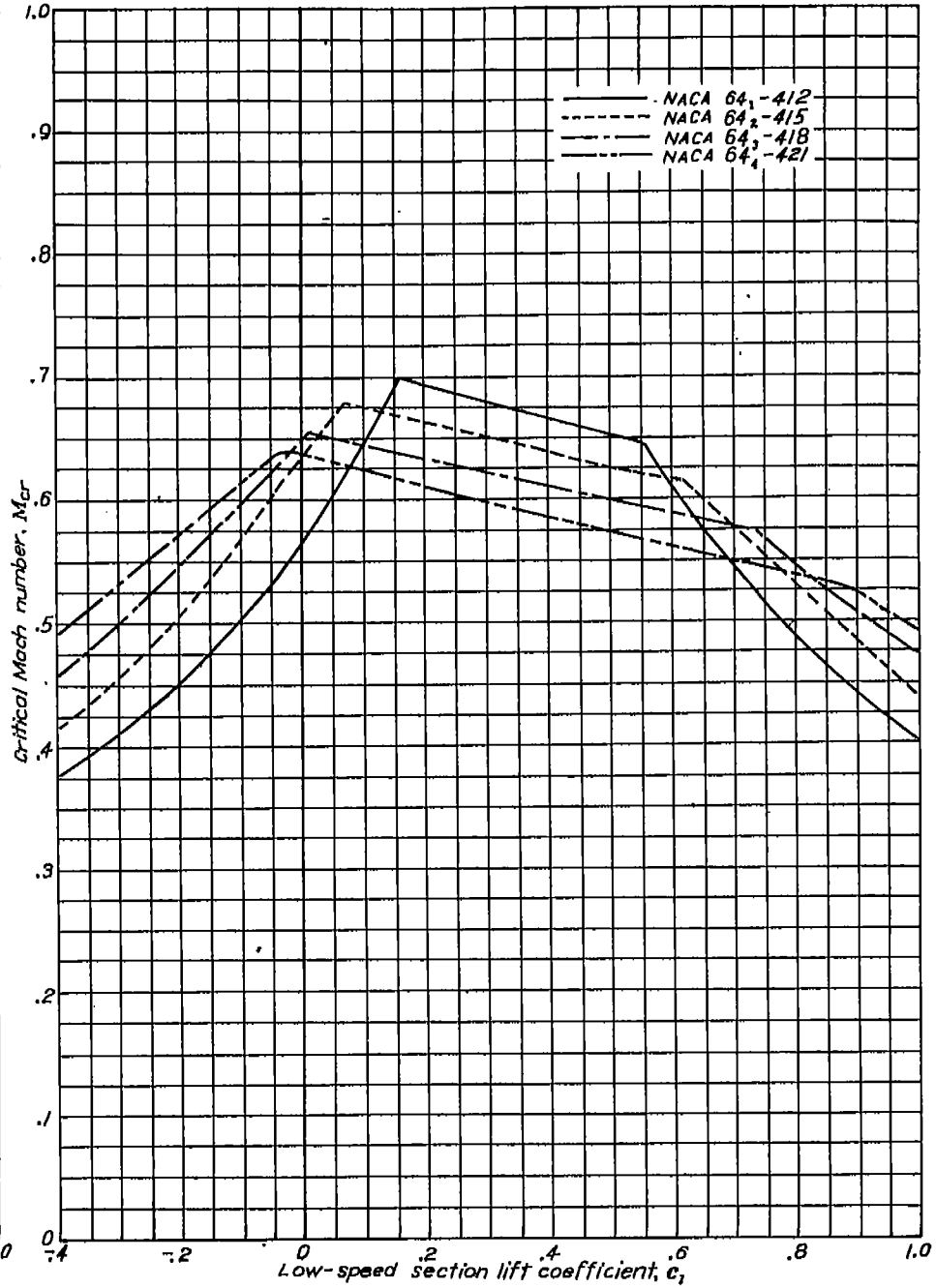

Variation of critical Mach number with low-speed section lift coefficient for several NACA 64-series airfoil sections of various thicknesses, cambered for a design lift coefficient of 0.4.

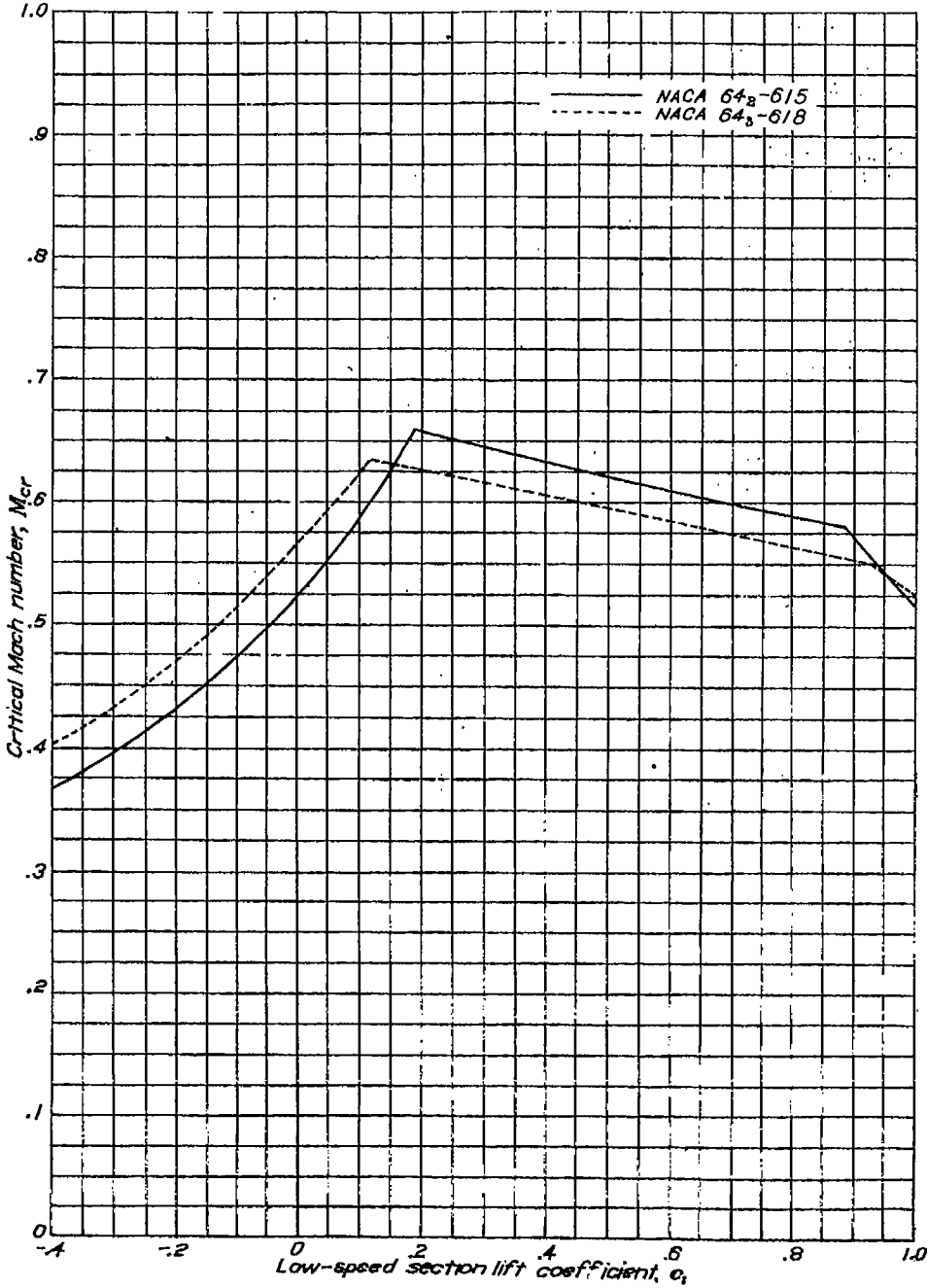

Variation of critical Mach number with low-speed section lift coefficient for two NACA 64-series airfoil sections of different thicknesses, cambered for a design lift coefficient of 0.6.

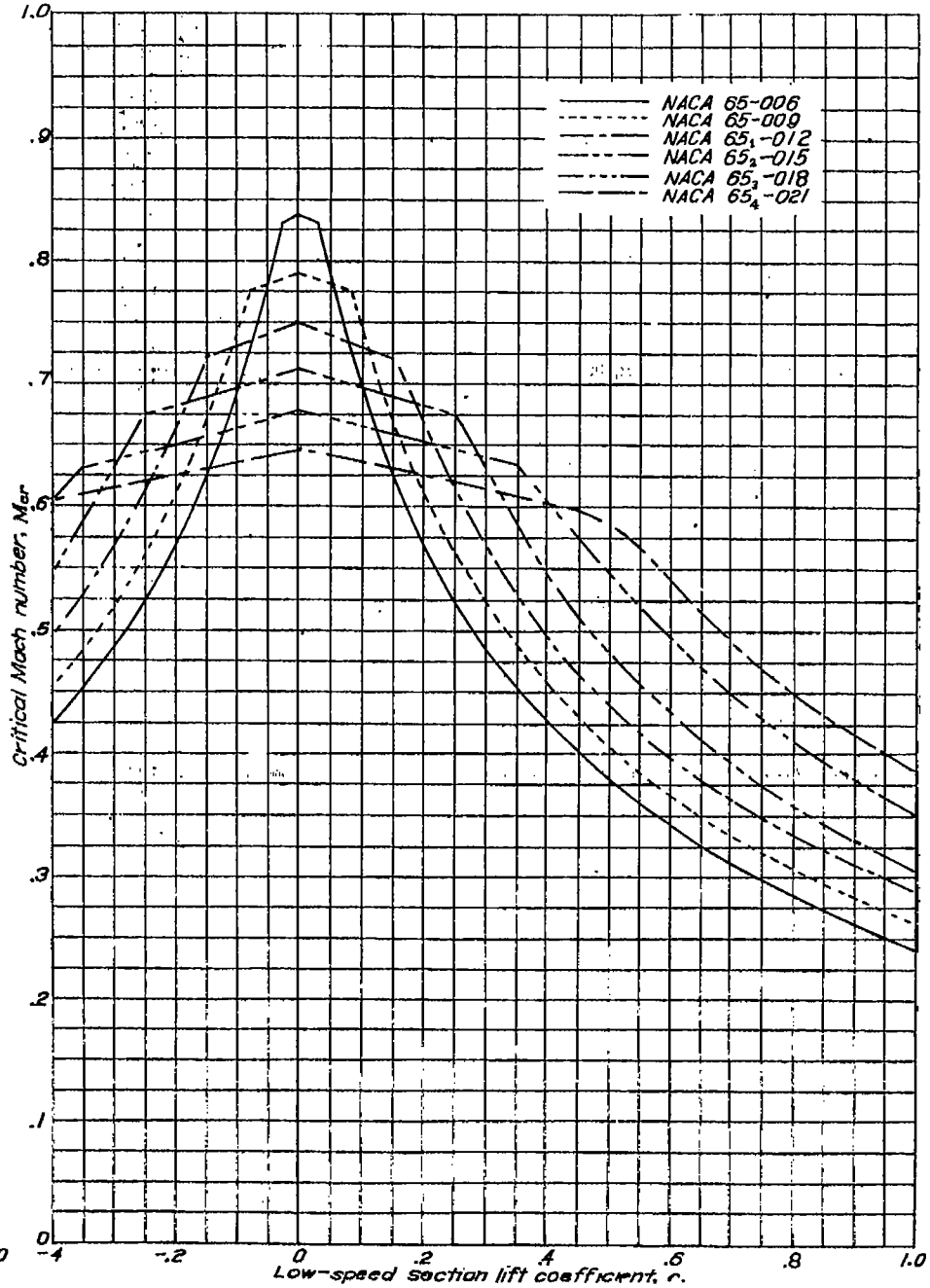

Variation of critical Mach number with low-speed section lift coefficient for several NACA 65-series symmetrical airfoil sections of various thicknesses.

838101—50——25

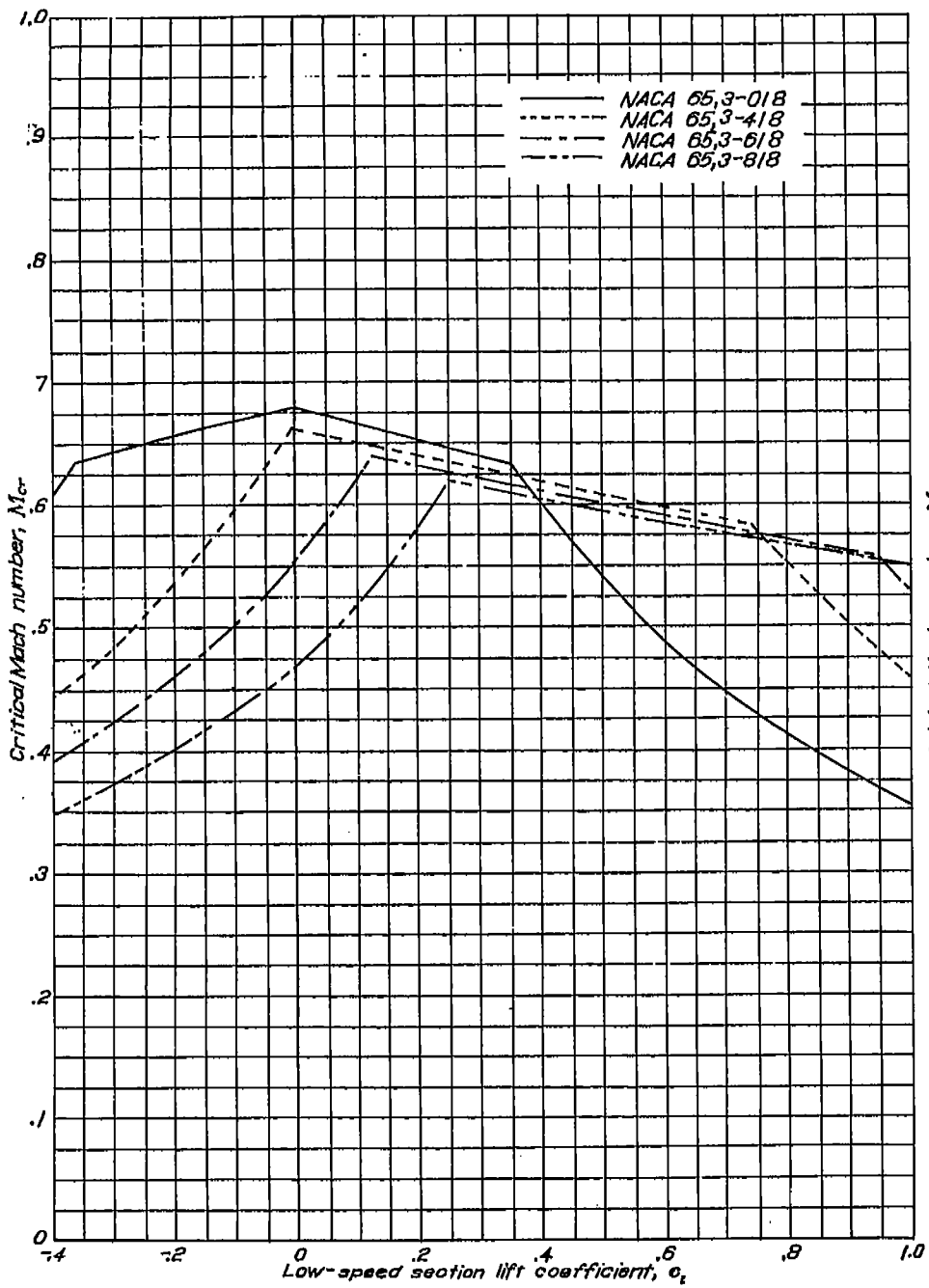

Variation of critical Mach number with low-speed section lift coefficient for several NACA 65-series airfoil sections with a thickness ratio of 0.18 and cambered for various design lift coefficients.

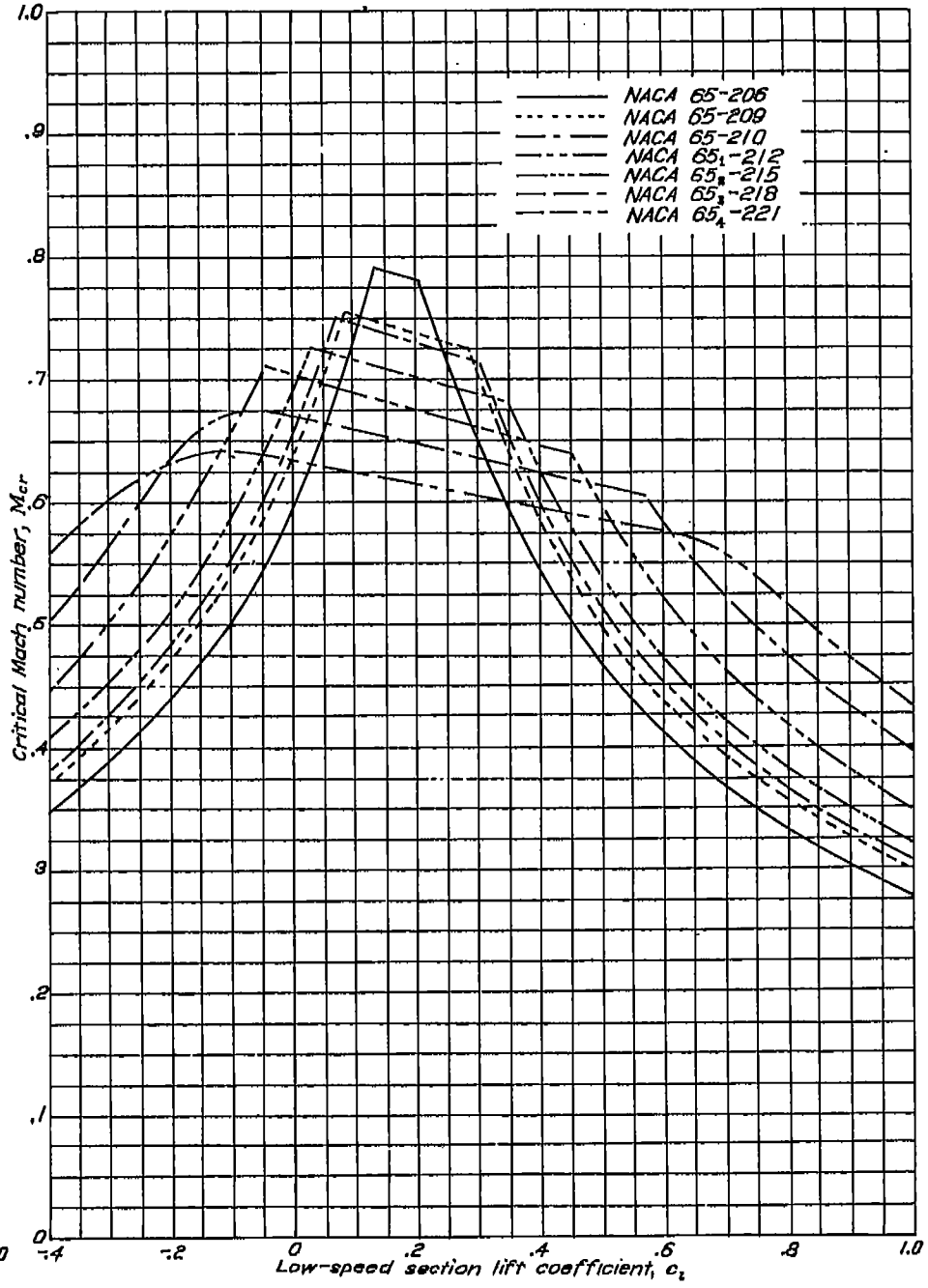

Variation of critical Mach number with low-speed section lift coefficient for several NACA 65-series airfoil sections of various thicknesses, cambered for a design lift coefficient of 0.2.

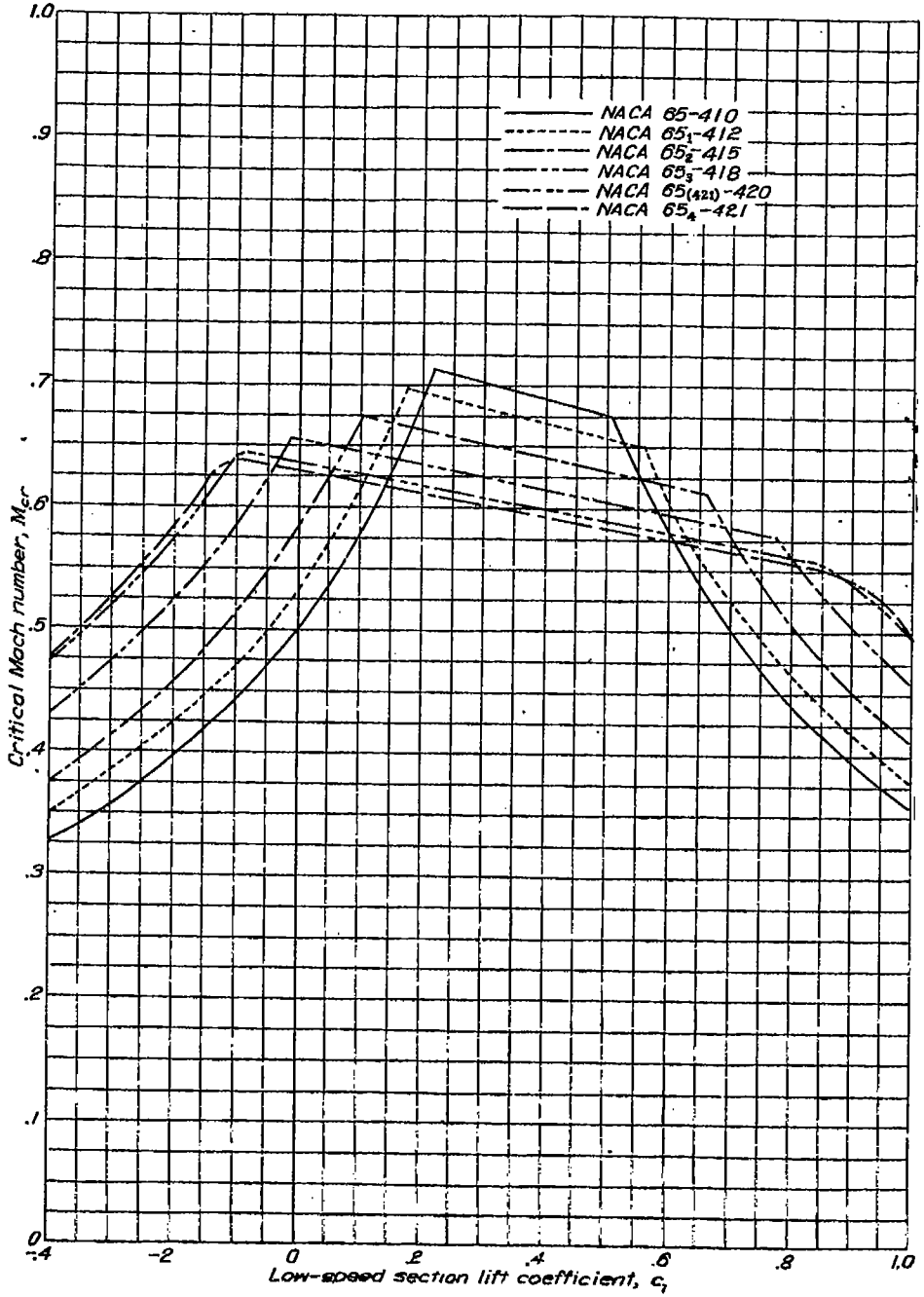

Variation of critical Mach number with low-speed section lift coefficient for several NACA 65-series airfoil sections of various thicknesses, cambered for a design lift coefficient of 0.4.

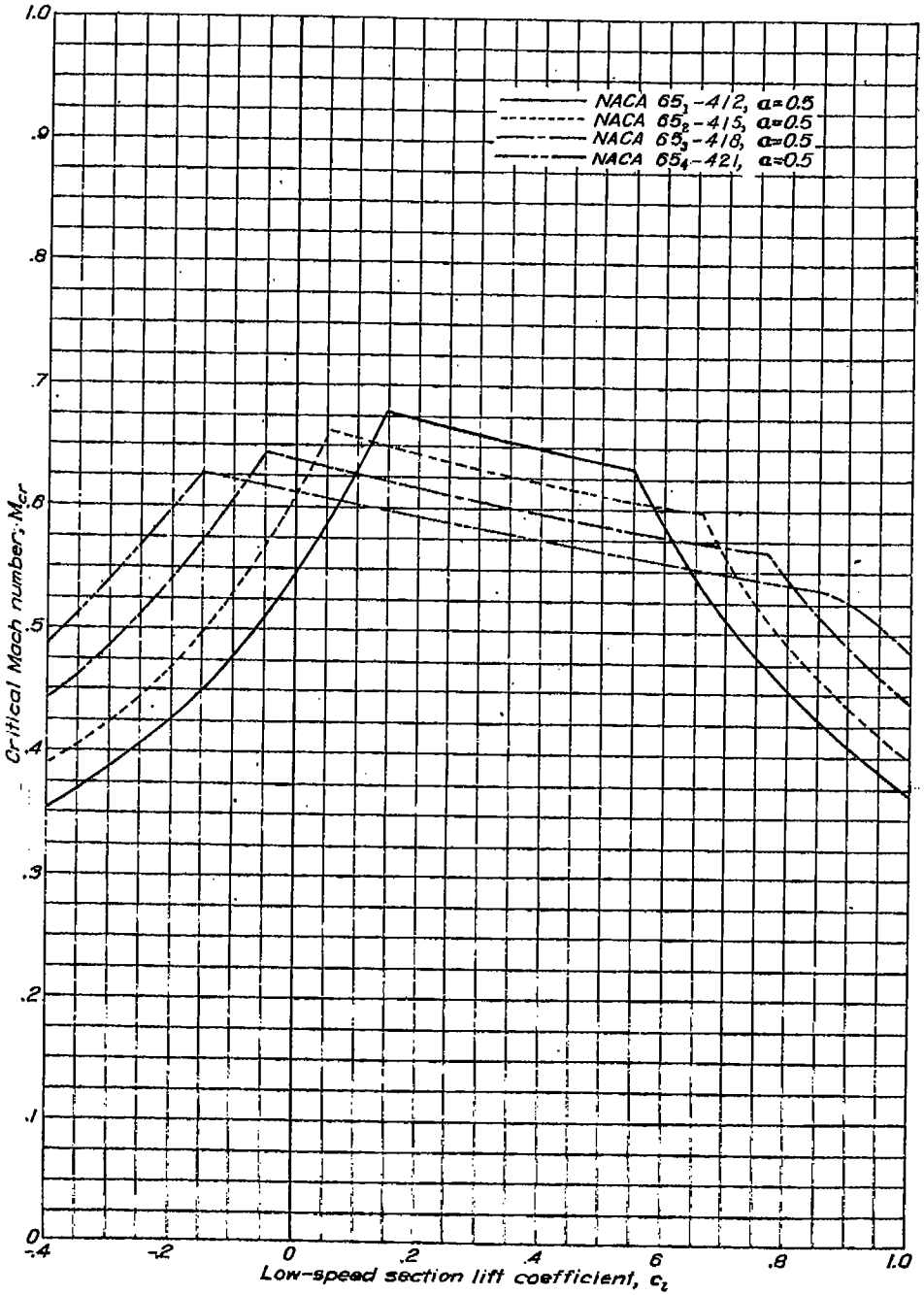

Variation of critical Mach number with low-speed section lift coefficient for several NACA 65-series airfoil sections with mean line of the type a=0.5 and cambered for a design lift coefficient of 0.4.

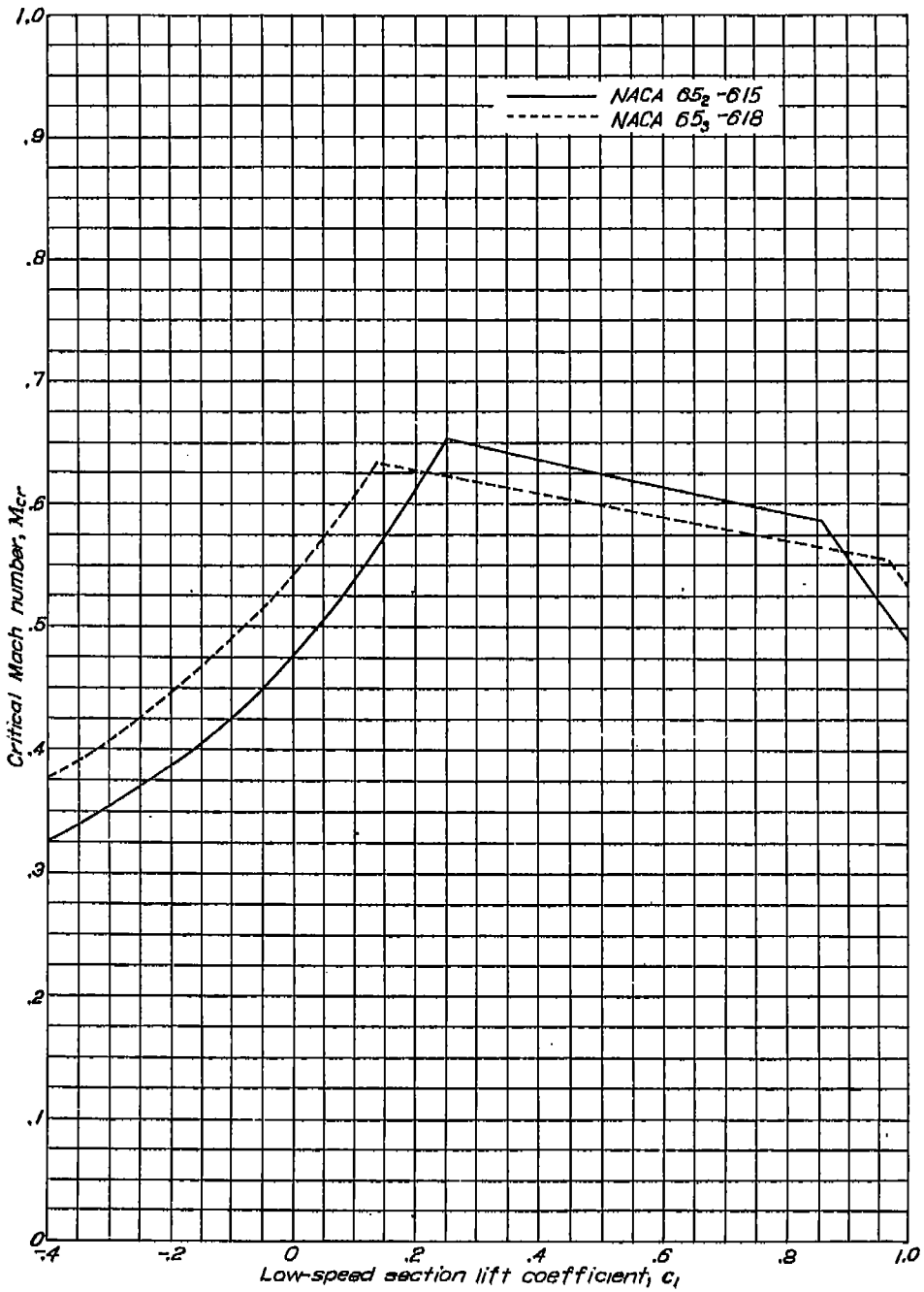

Variation of critical Mach number with low-speed section lift coefficient for two NACA 65-series airfoil sections of different thicknesses, cambered for a design lift coefficient of 0.6.

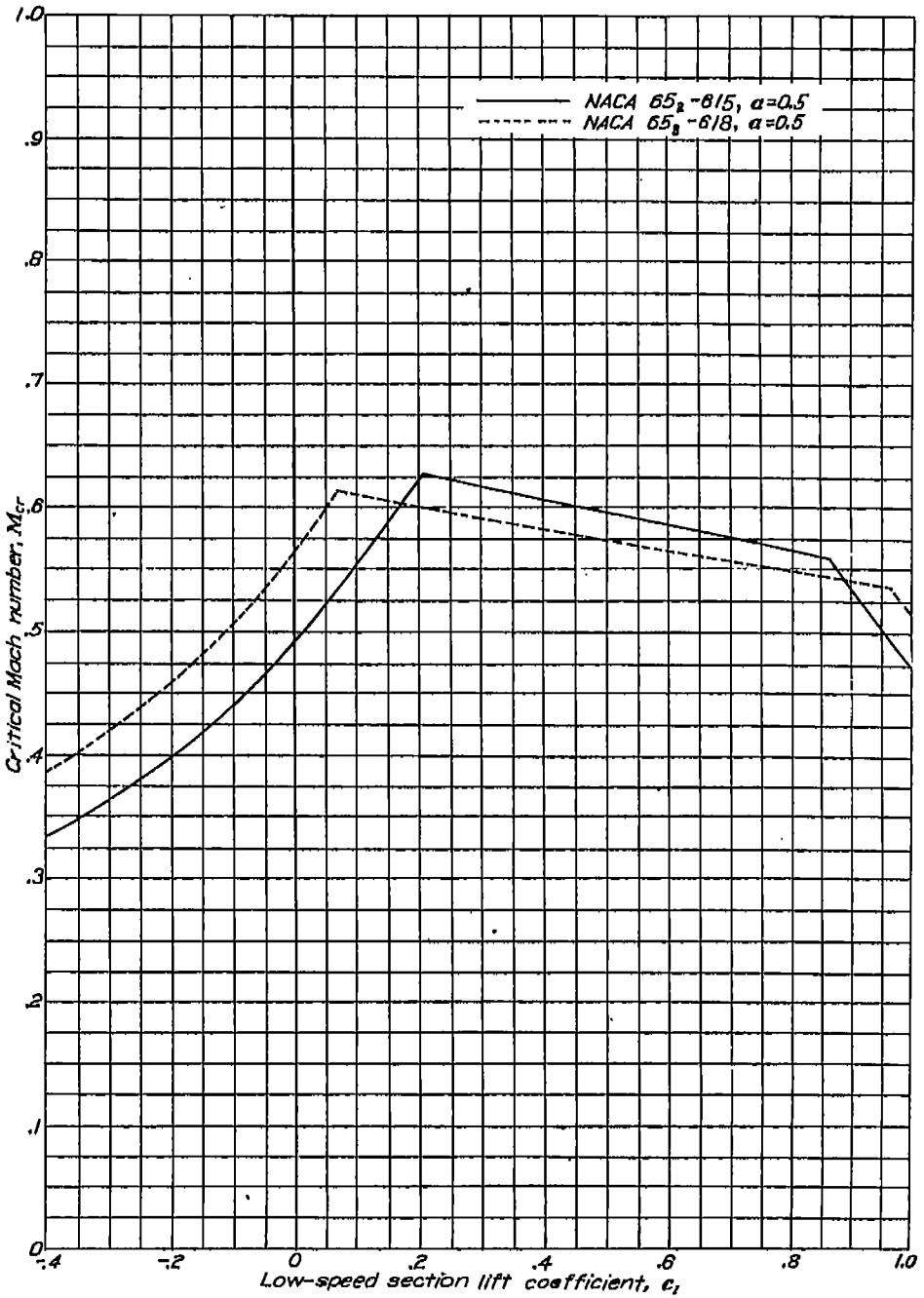

Variation of critical Mach number with low-speed section lift coefficient for two NACA 65-series airfoil sections with mean line of the type $a=0.5$, with different thicknesses, and cambered for a design lift coefficient of 0.6.

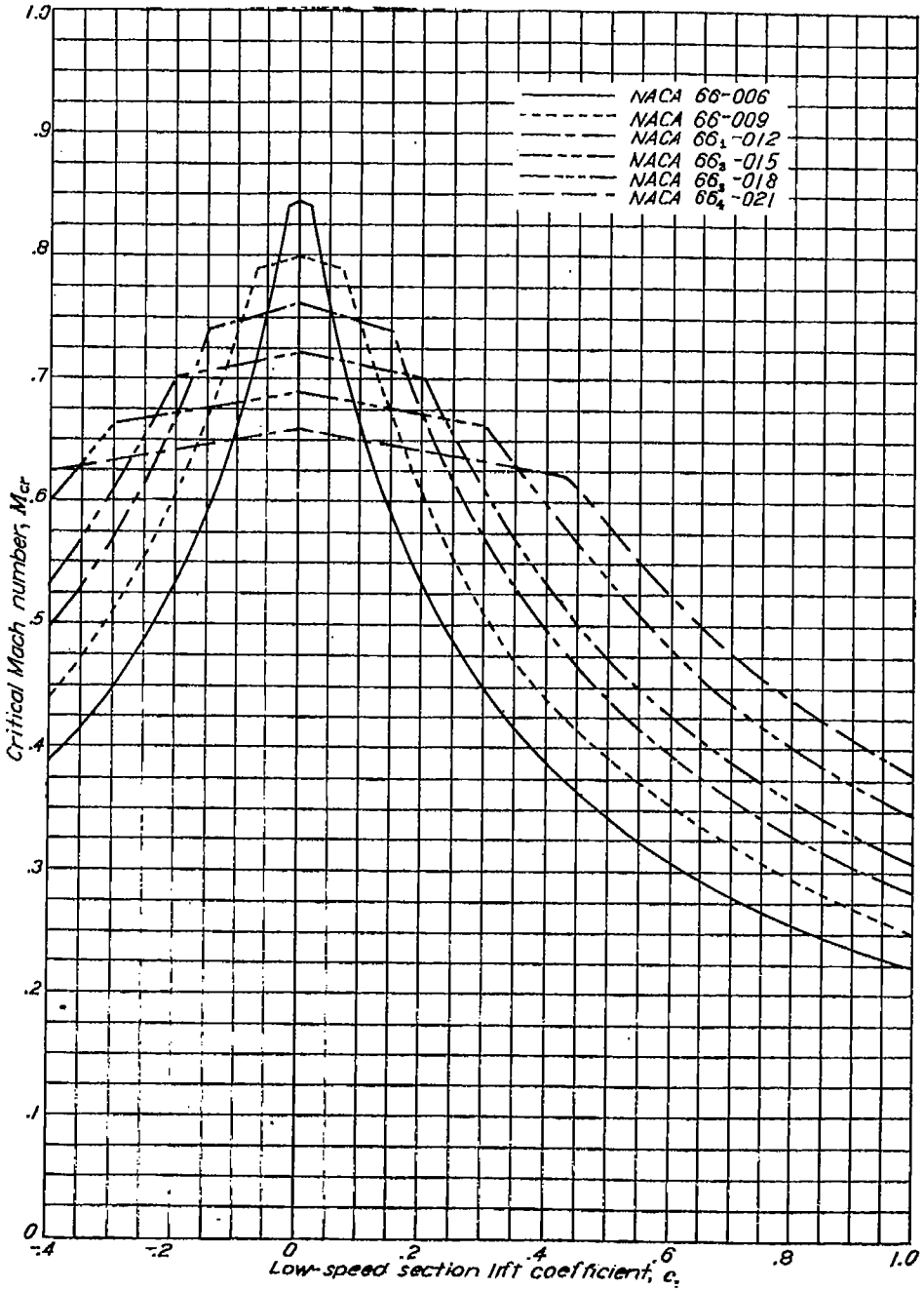

Variation of critical Mach number with low-speed section lift coefficient for several NACA 66-series symmetrical airfoil sections of various thicknesses.

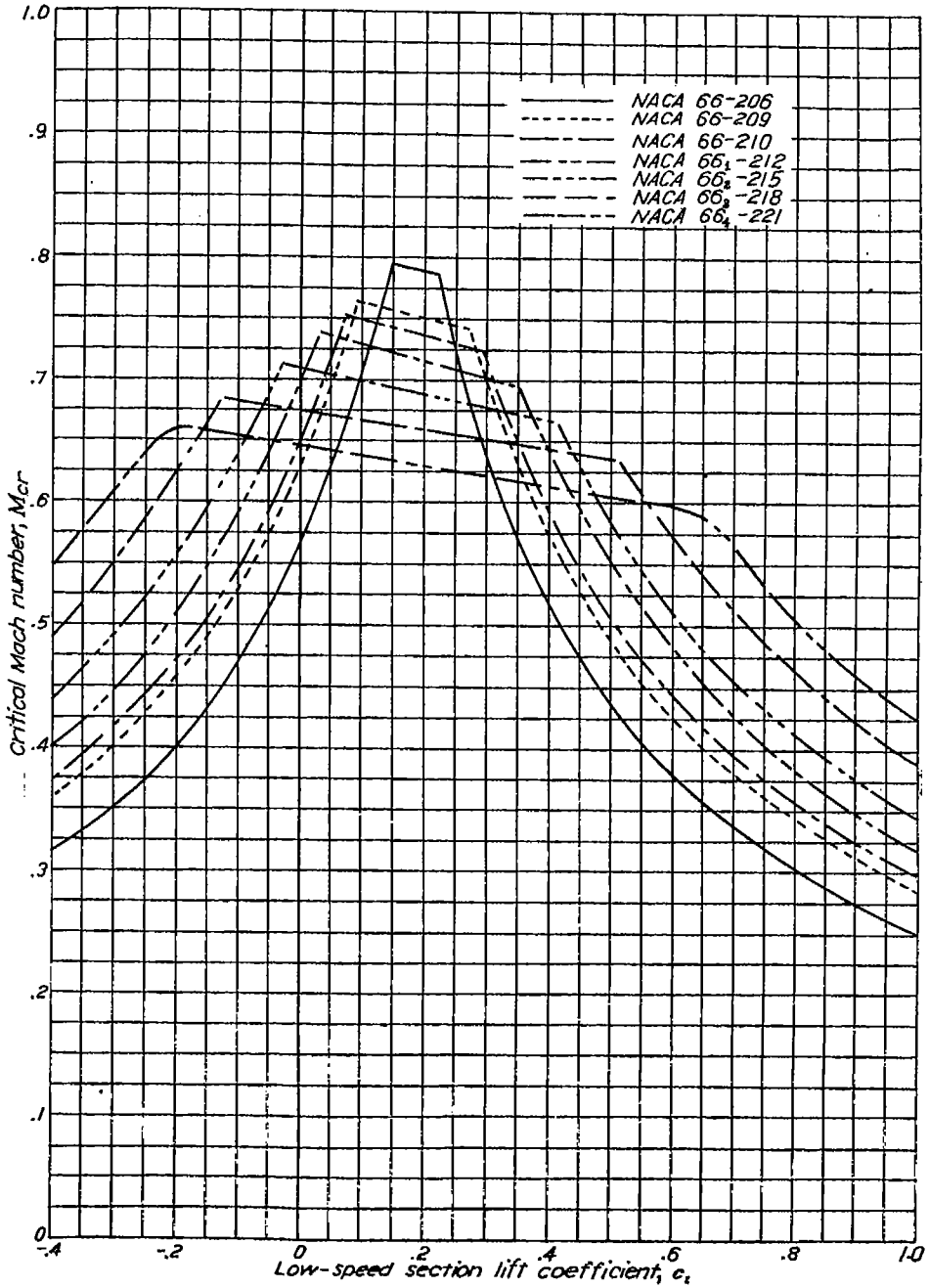

Variation of critical Mach number with low-speed section lift coefficient for several NACA 66-series airfoil sections of various thicknesses, cambered for a design lift coefficient of 0.2.

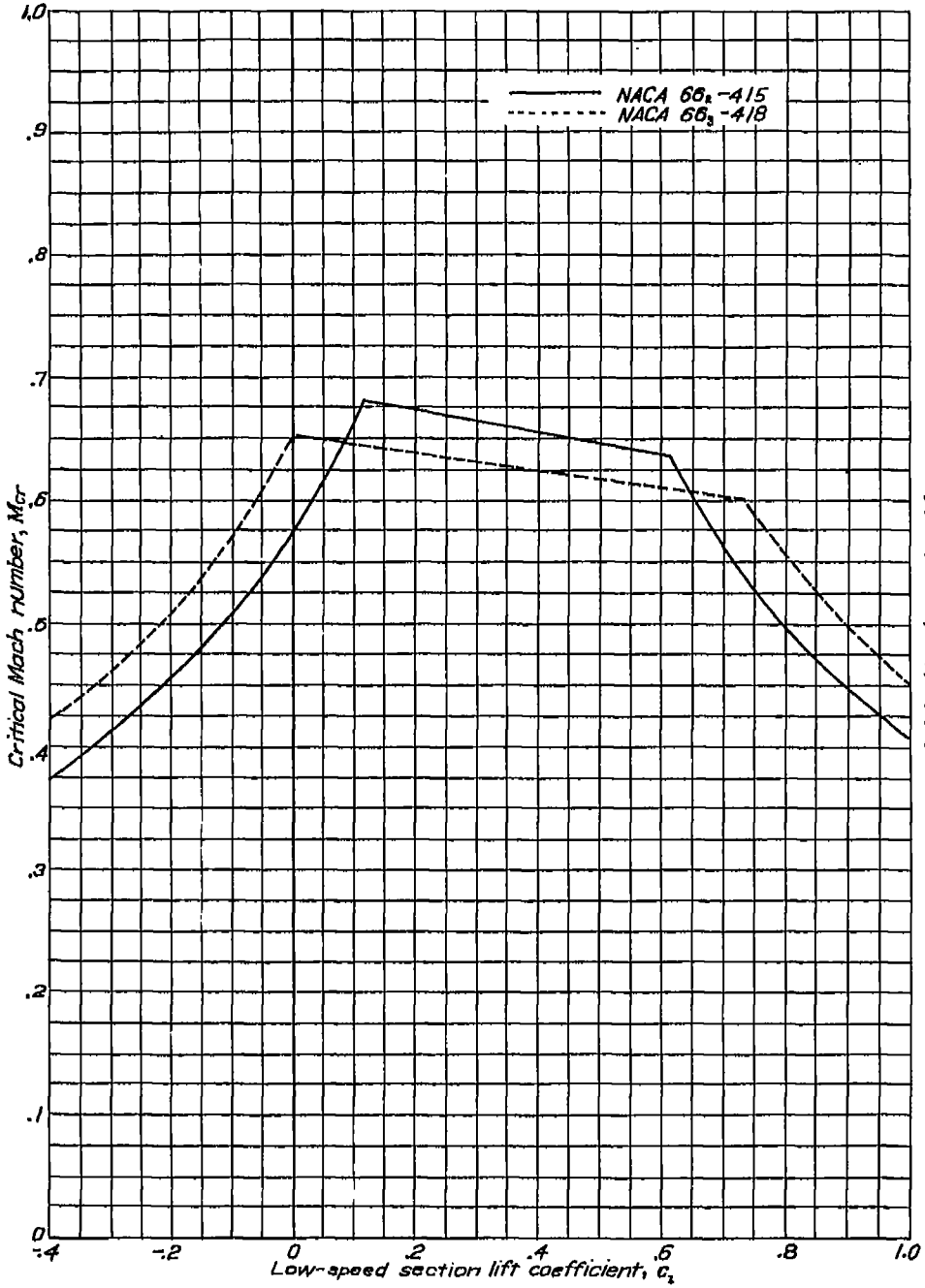

Variation of critical Mach number with low-speed section lift coefficient for two NACA 66-series airfoil sections of different thicknesses, cambered for a design lift coefficient of 0.4.

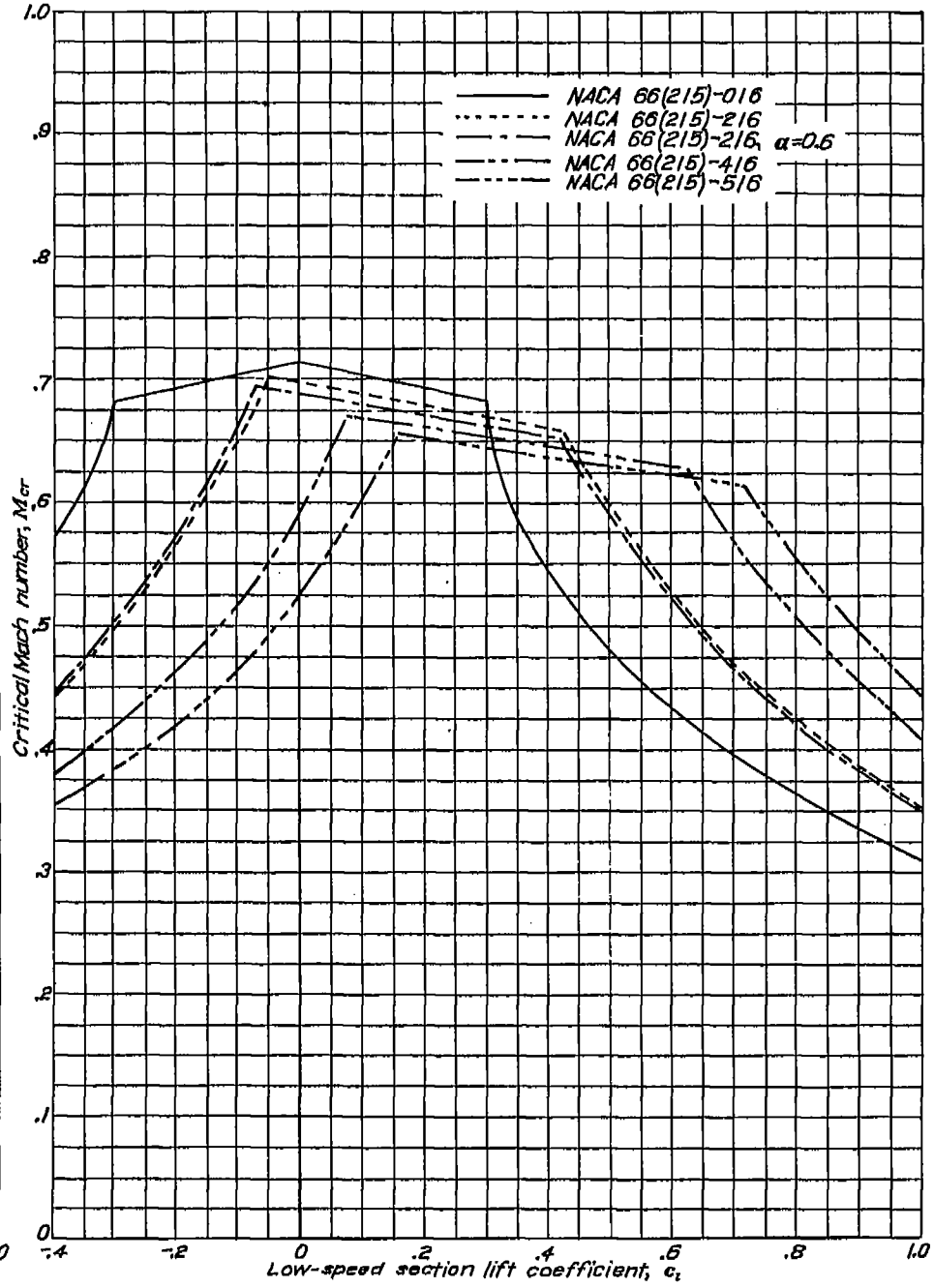

Variation of critical Mach number with low-speed section lift coefficient for several NACA 66-series airfoil sections with a thickness ratio of 0.16 and cambered for various design lift coefficients.

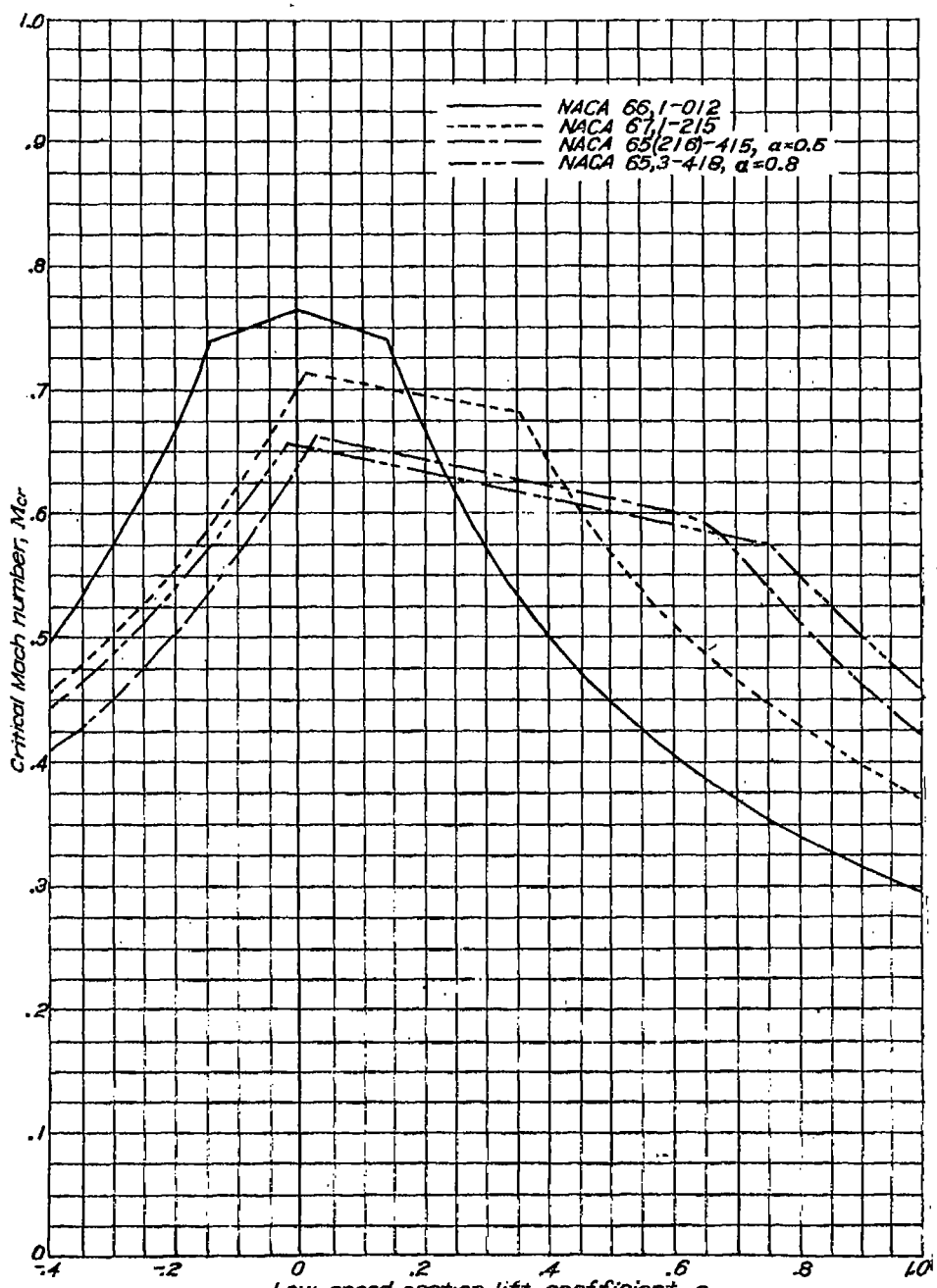

Variation of critical Mach number with low-speed section lift coefficient for several NACA 6-series airfoil sections with different positions of minimum pressure and various thicknesses, cambered for various design lift coefficients.

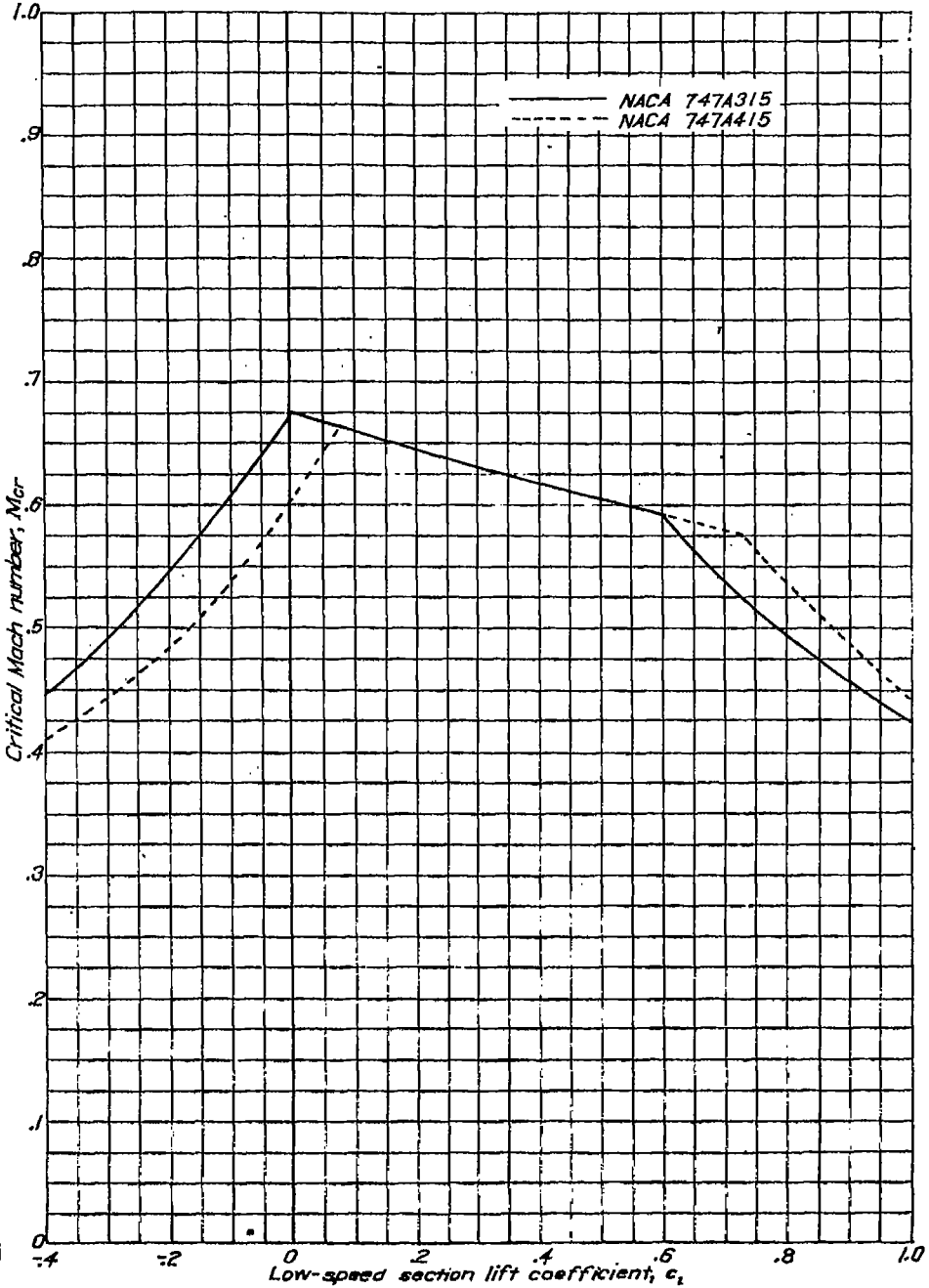

Variation of critical Mach number with low-speed section lift coefficient for two NACA 7-series airfoil sections with a thickness ratio of 0.15 and cambered for different design lift coefficients.

V—AERODYNAMIC CHARACTERISTICS OF VARIOUS AIRFOIL SECTIONS

	Page
NACA 0006	389
NACA 0009	390
NACA 1408	391
NACA 1410	392
NACA 1412	393
NACA 2412	394
NACA 2415	395
NACA 2418	396
NACA 2421	397
NACA 2424	398
NACA 4412	399
NACA 4415	400
NACA 4418	401
NACA 4421	402
NACA 4424	403
NACA 23012	404
NACA 23015	405
NACA 23018	406
NACA 23021	407
NACA 23024	408
NACA 63,4–420	409
NACA 63,4–420 with 0.25c slotted flap	
(a) Configuration	410
(b) Aerodynamic characteristics with hinge location 1	411
(c) Aerodynamic characteristics with hinge location 2	412
NACA 63,4–420, α=0.3	413
NACA 63(420)–422	414
NACA 63(420)–517	415
NACA 63–006	416
NACA 63–009	417
NACA 63–206	418
NACA 63–209	419
NACA 63–210	420
NACA 63_1–012	421
NACA 63_1–212	422
NACA 63_1–412	423
NACA 63_2–015	424
NACA 63_2–215	425
NACA 63_2–415	426
NACA 63_2–615	427
NACA 63_3–018	428
NACA 63_3–218	429
NACA 63_3–418	430
NACA 63_3–618	431
NACA 63_4–021	432
NACA 63_4–221	433
NACA 63_4–421	434
NACA 64–006	435
NACA 64–009	436
NACA 64–108	437
NACA 64–110	438
NACA 64–206	439
NACA 64–208	440
NACA 64–209	441
NACA 64–210	442
NACA 64_1–012	443
NACA 64_1–112	444
NACA 64_1–212	445
NACA 64_1–412	446
NACA 64_2–015	447
NACA 64_2–215	448
NACA 64_2–415	449
NACA 64_3–018	450
NACA 64_3–218	451
NACA 64_3–418	452
NACA 64_3–618	453
NACA 64_4–021	454
NACA 64_4–221	455
NACA 64_4–421	456
NACA 65,3–018	457
NACA 65,3–418, α=0.8	458
NACA 65,3–618	459
NACA 65,3–618 with 0.20c sealed plain flap	460
NACA 65(216)–415, α=0.5	461
NACA 65–006	462
NACA 65–009	463
NACA 65–206	464
NACA 65–209	465
NACA 65–210	466
NACA 65–410	467
NACA 65_1–012	468
NACA 65_1–212	469
NACA 65_1–212 with 0.20c split flap (lift and moment characteristics)	470
NACA 65_1–212, α=0.6	471
NACA 65_1–412	472
NACA 65_2–015	473
NACA 65_2–215	474
NACA 65_2–415	475
NACA 65_2–415, α=0.5	476
NACA 65_3–018	477
NACA 65_3–118 with 0.309c double slotted flap	
(a) Configuration	478
(b) Aerodynamic characteristics	479
NACA 65_3–218	480
NACA 65_3–418	481
NACA 65_3–418, α=0.5	482
NACA 65_3–618	483
NACA 65_3–618, α=0.5	484
NACA 65_4–021	485
NACA 65_4–221	486
NACA 65_4–421	487
NACA 65_4–421, α=0.5	488
NACA $65_{(215)}$–114	489
NACA $65_{(420)}$–420	490
NACA 66,1–212	491
NACA 66,1–212 with 0.20c split flap (lift and moment characteristics)	492
NACA 66(215)–016	493
NACA 66(215)–216	494
NACA 66(215)–216 with 0.20c sealed plain flap	495
NACA 66(125)–216 with 0.20c split flap (lift and moment characteristics)	496
NACA 66(215)–216, α=0.6	497
NACA 66(215)–216, α=0.6 with 0.30c slotted and 0.10c plain flap	
(a) Airfoil-flap configuration	498
(b) Flap configuration	498
(c) Aerodynamic characteristics. Slotted flap retracted	499
(d) Lift and moment characteristics. Slotted flap deflected 22°	500
(e) Lift and moment characteristics. Slotted flap deflected 27°	501
(f) Lift and moment characteristics. Slotted flap deflected 32°	502
(g) Lift and moment characteristics. Slotted flap deflected 37°	503
NACA 66(215)–416	504

	Page
NACA 66-006	505
NACA 66-009	506
NACA 66-206	507
NACA 66-209	508
NACA 66-210	509
NACA 66_1-012	510
NACA 66_1-212	511
NACA 66_2-015	512
NACA 66_2-215	513
NACA 66_2-415	514
NACA 66_3-018	515
NACA 66_3-218	516
NACA 66_3-418	517
NACA 66_4-021	518
NACA 66_4-221	519
NACA 67,1-215	520
NACA 747A315	521
NACA 747A415	522

NACA 0006

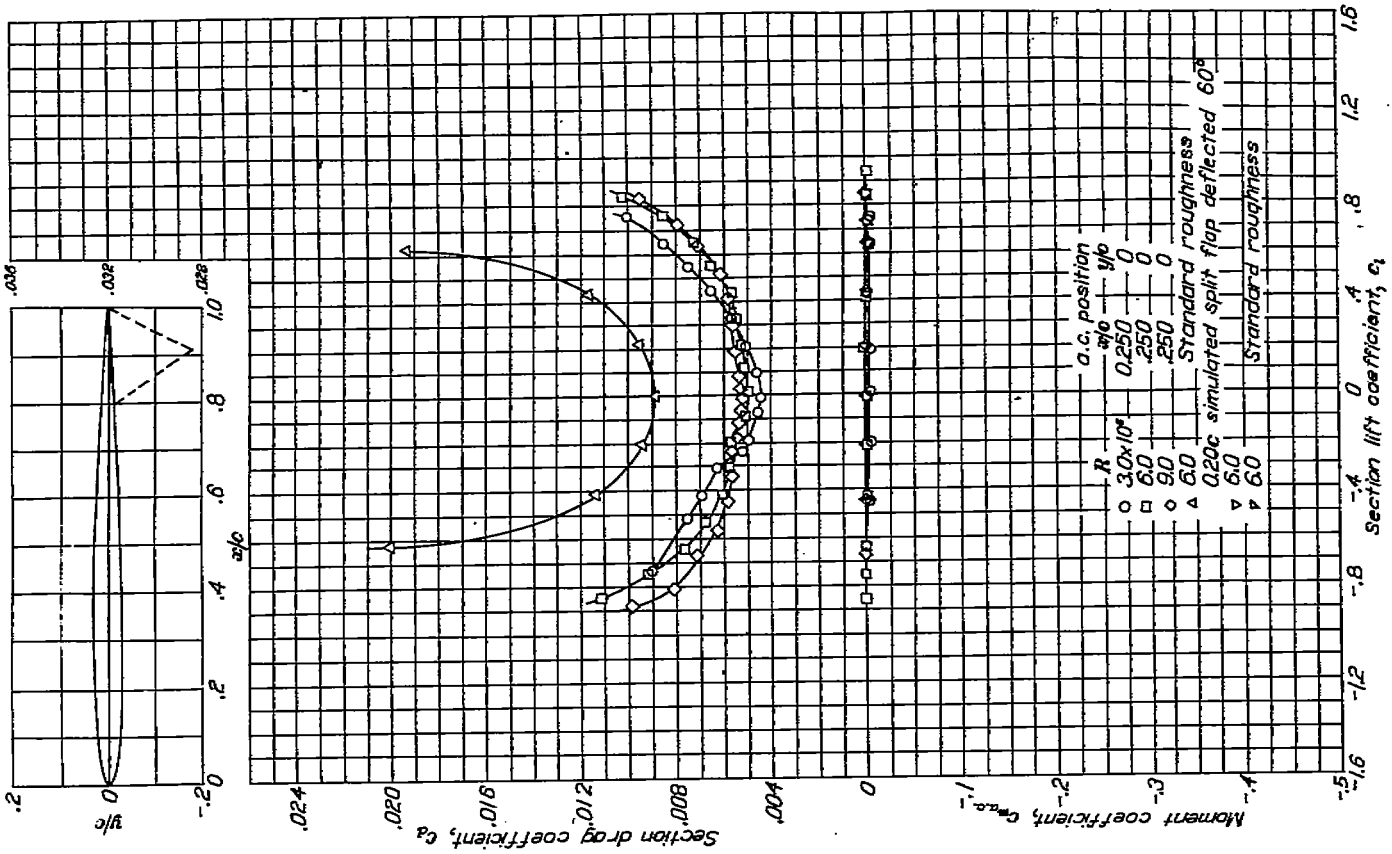

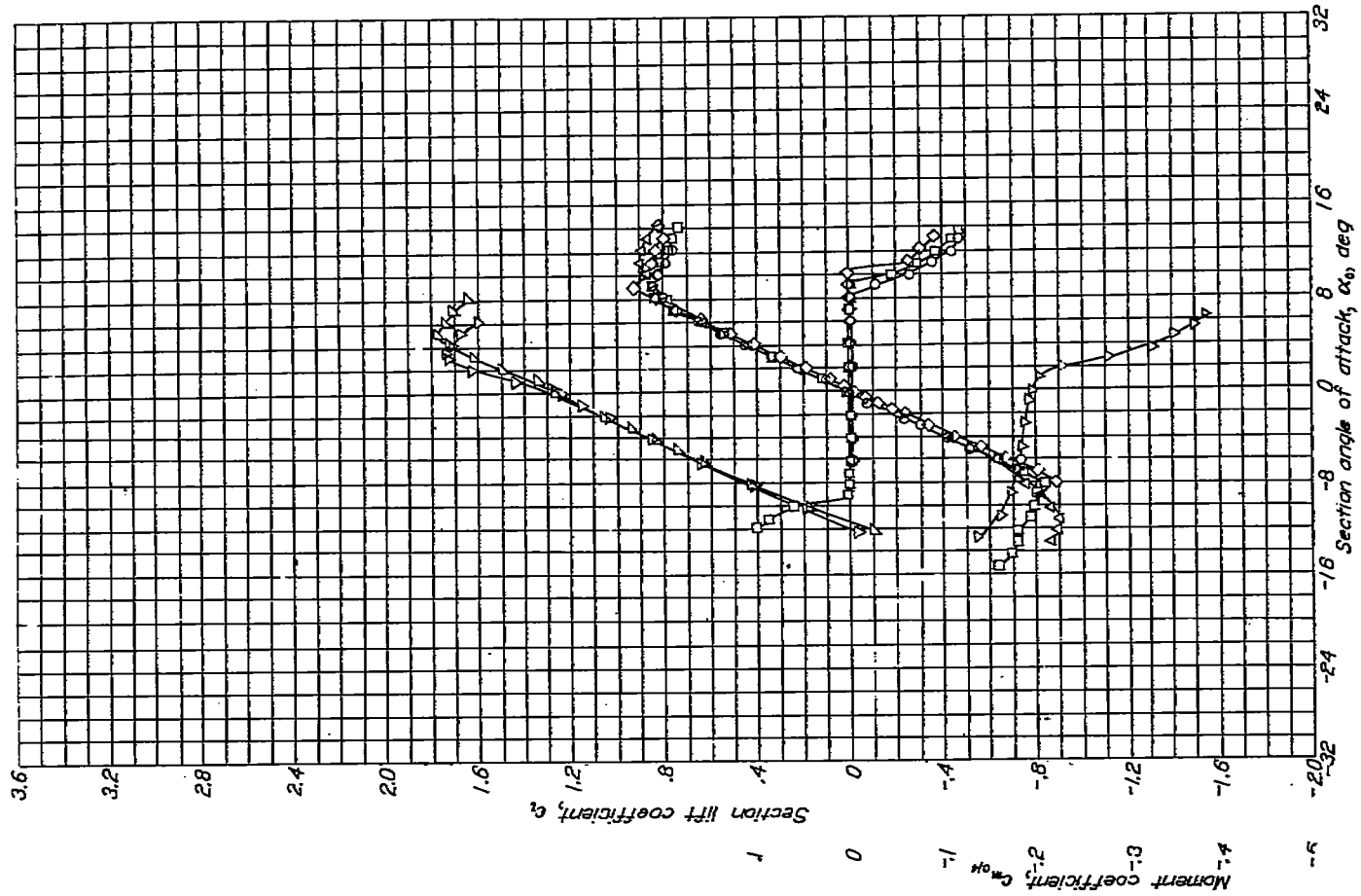

Aerodynamic characteristics of the NACA 0006 airfoil section, 24-inch chord.

NACA 0009

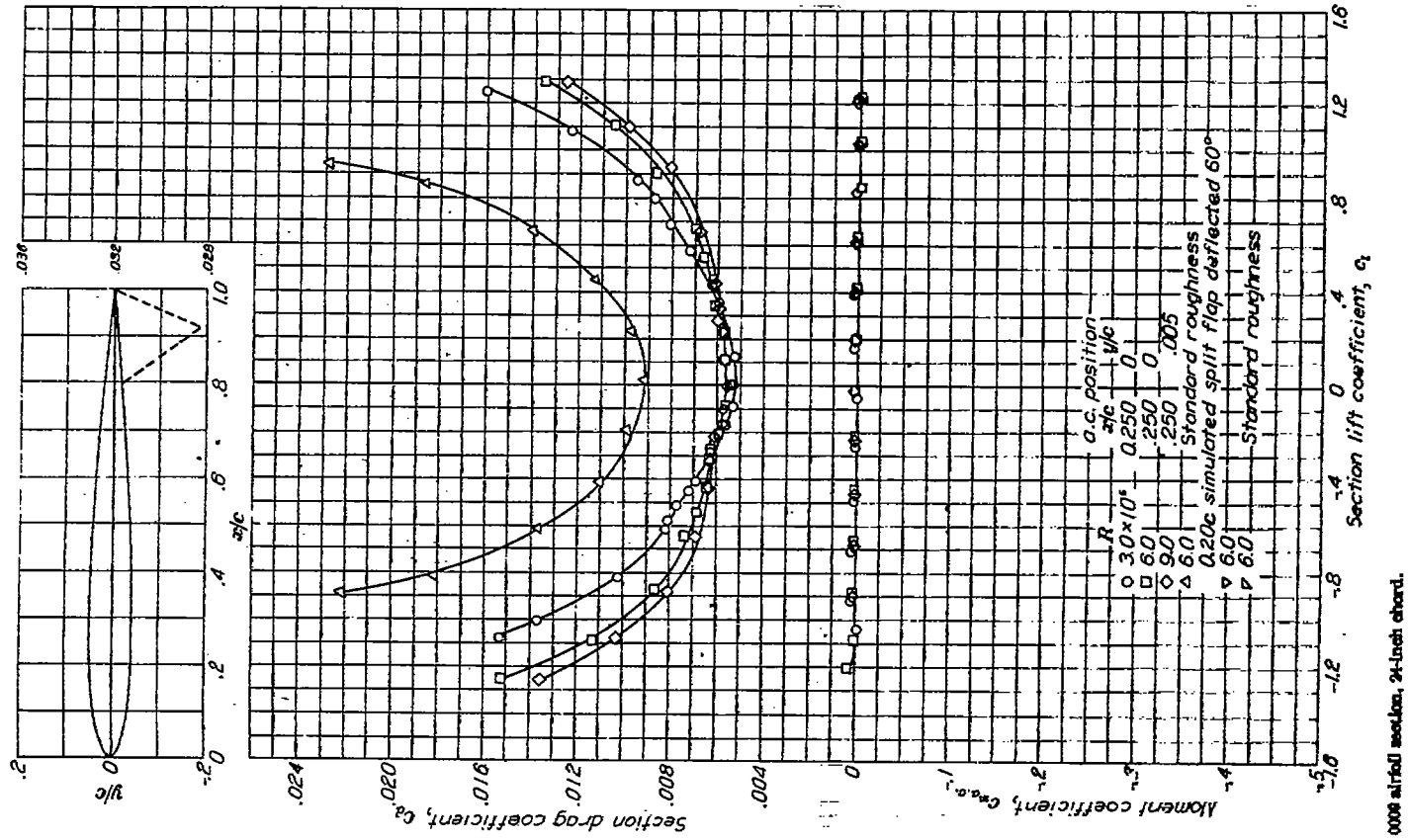

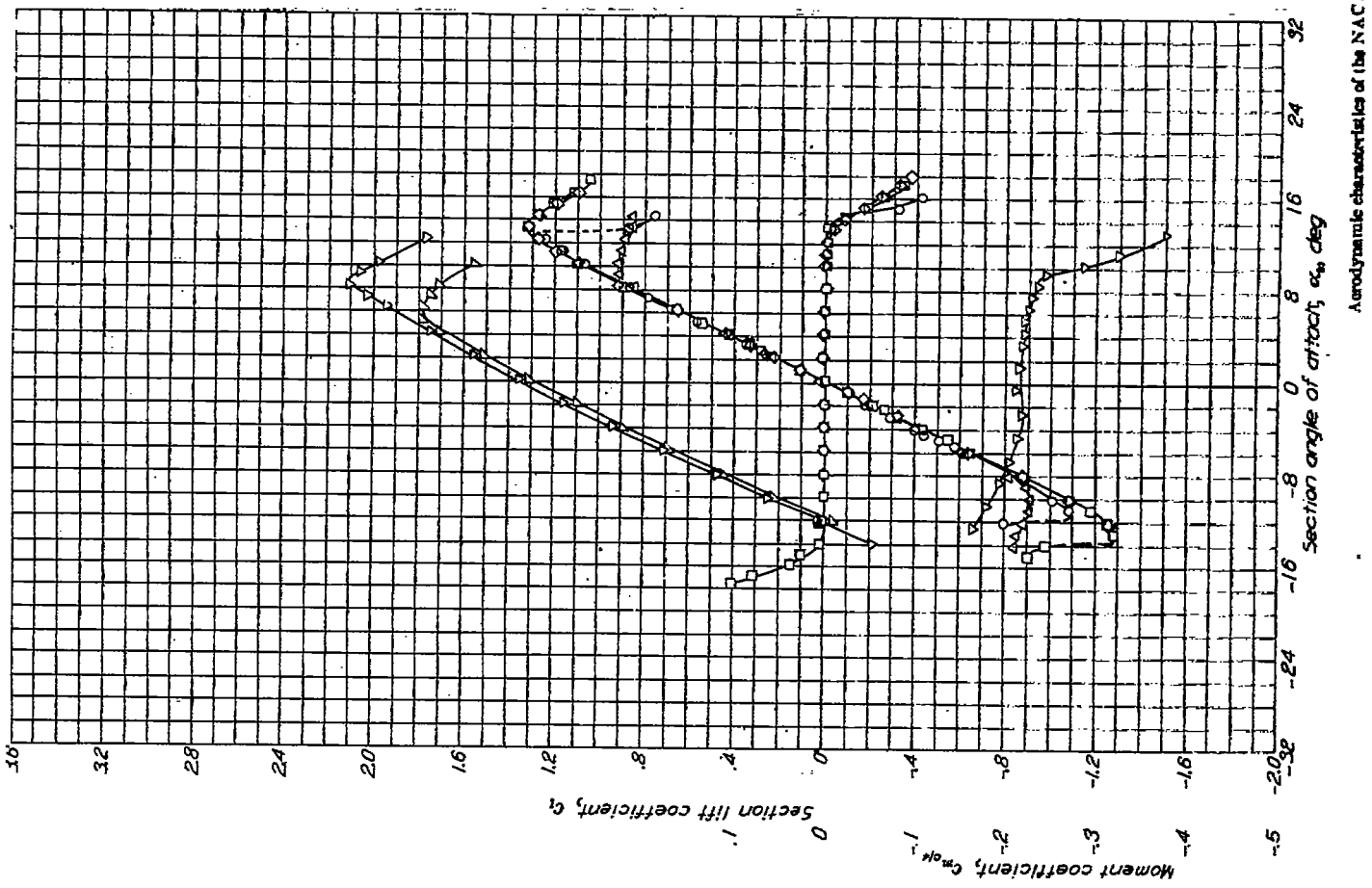

Aerodynamic characteristics of the NACA 0009 airfoil section, 24-inch chord.

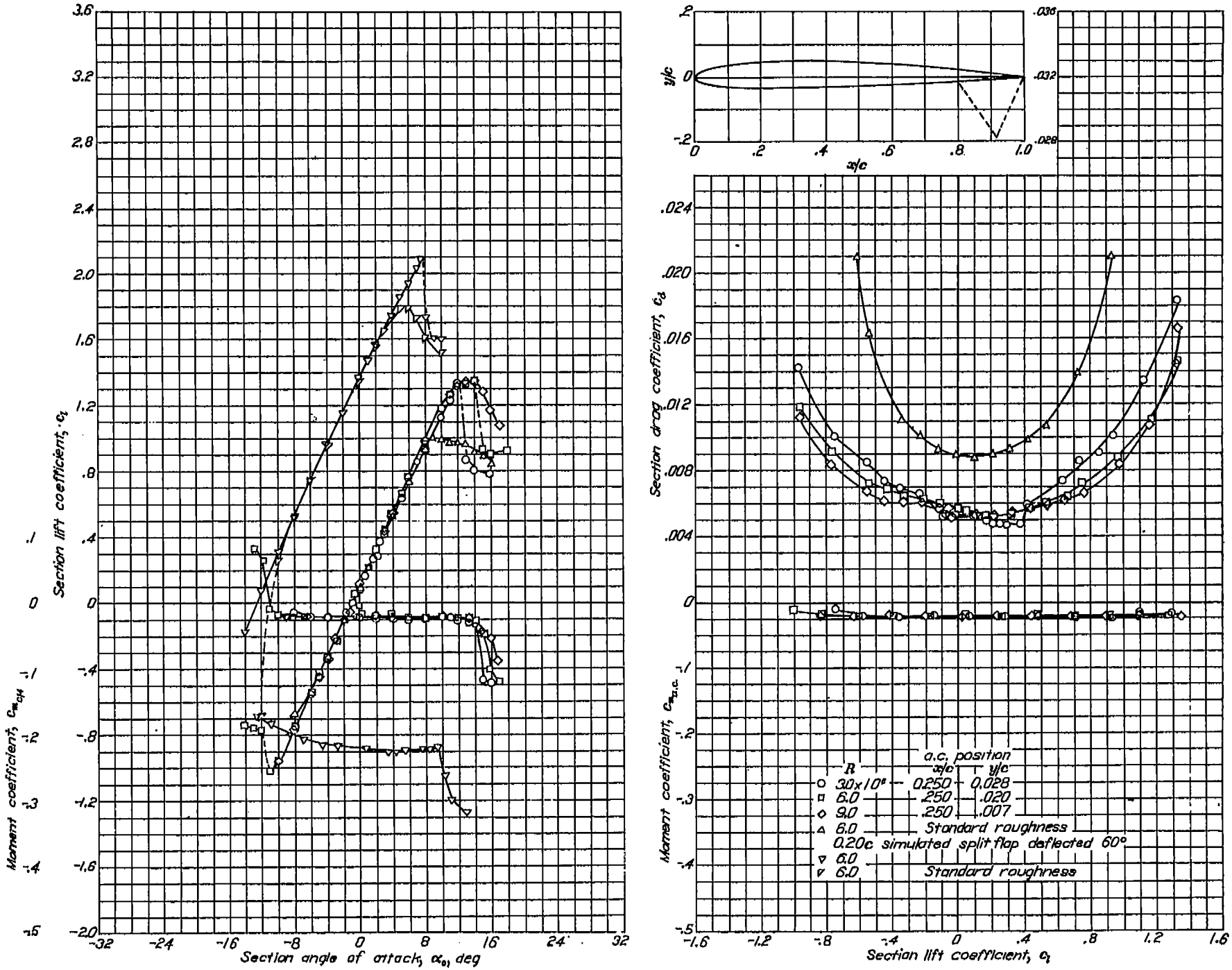

Aerodynamic characteristics of the NACA 1408 airfoil section, 24-inch chord.

NACA 1410

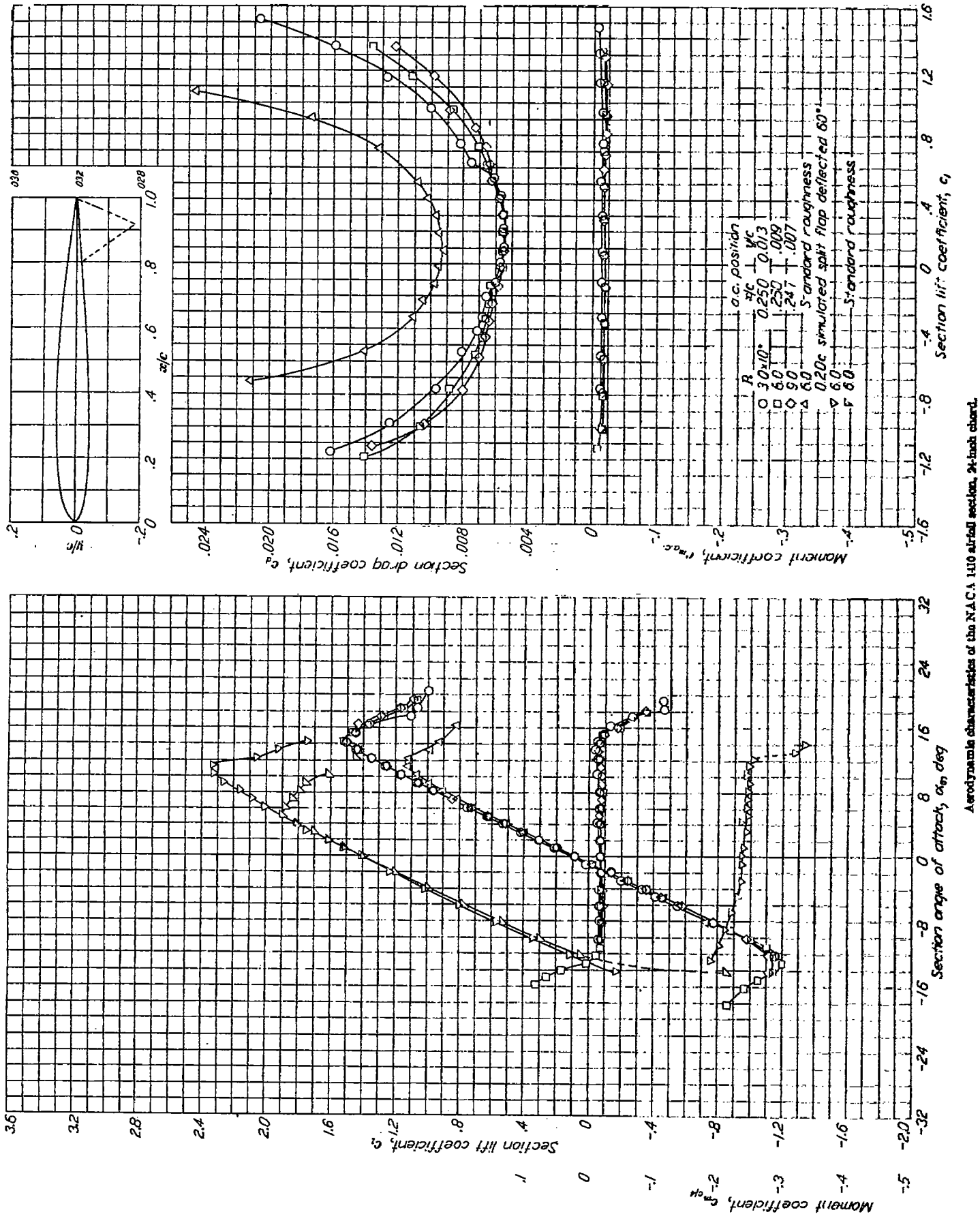

Aerodynamic characteristics of the NACA 1410 airfoil section, 24-inch chord.

NACA 1412

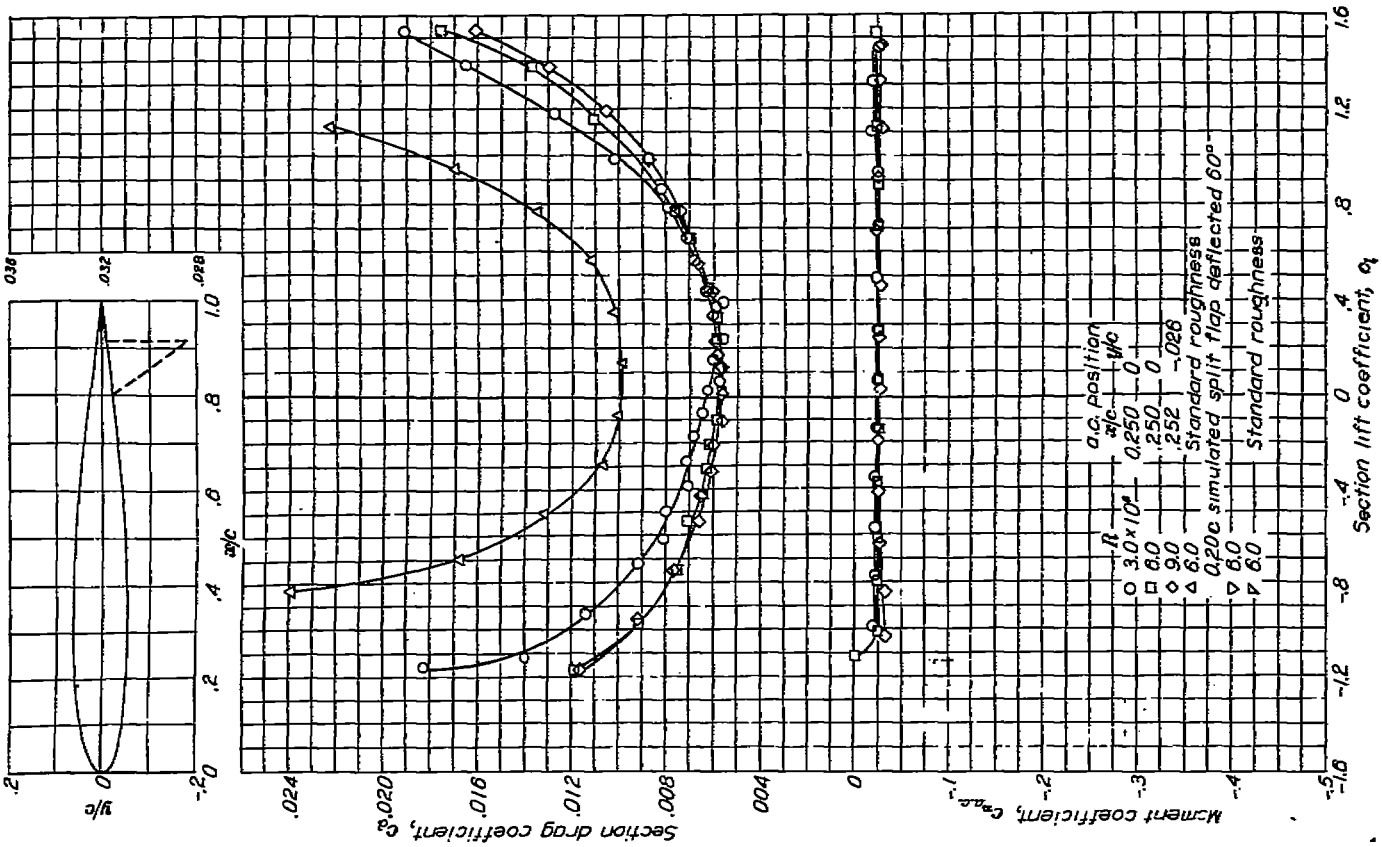

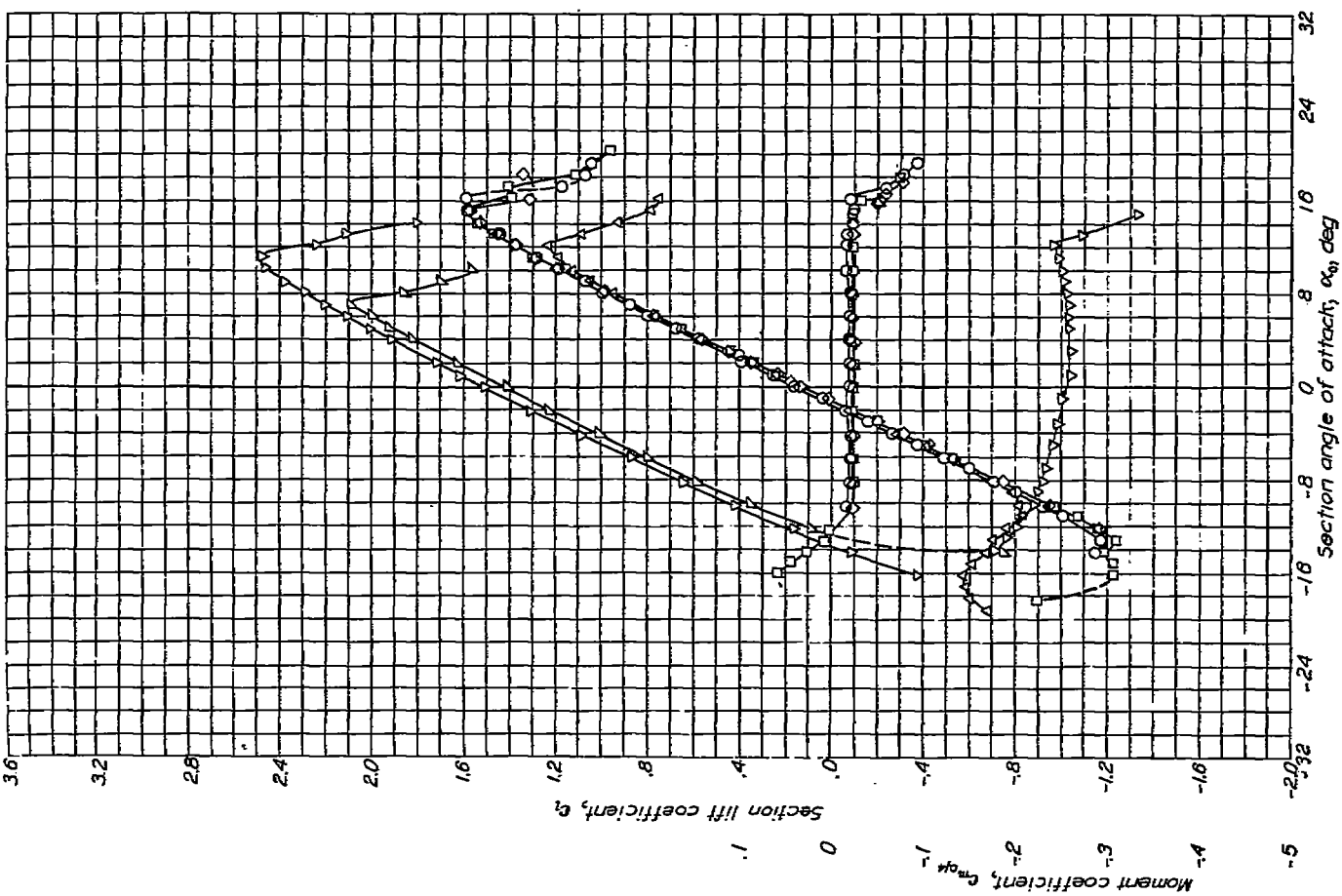

Aerodynamic characteristics of the NACA 1412 airfoil section, 24-inch chord.

NACA 2412

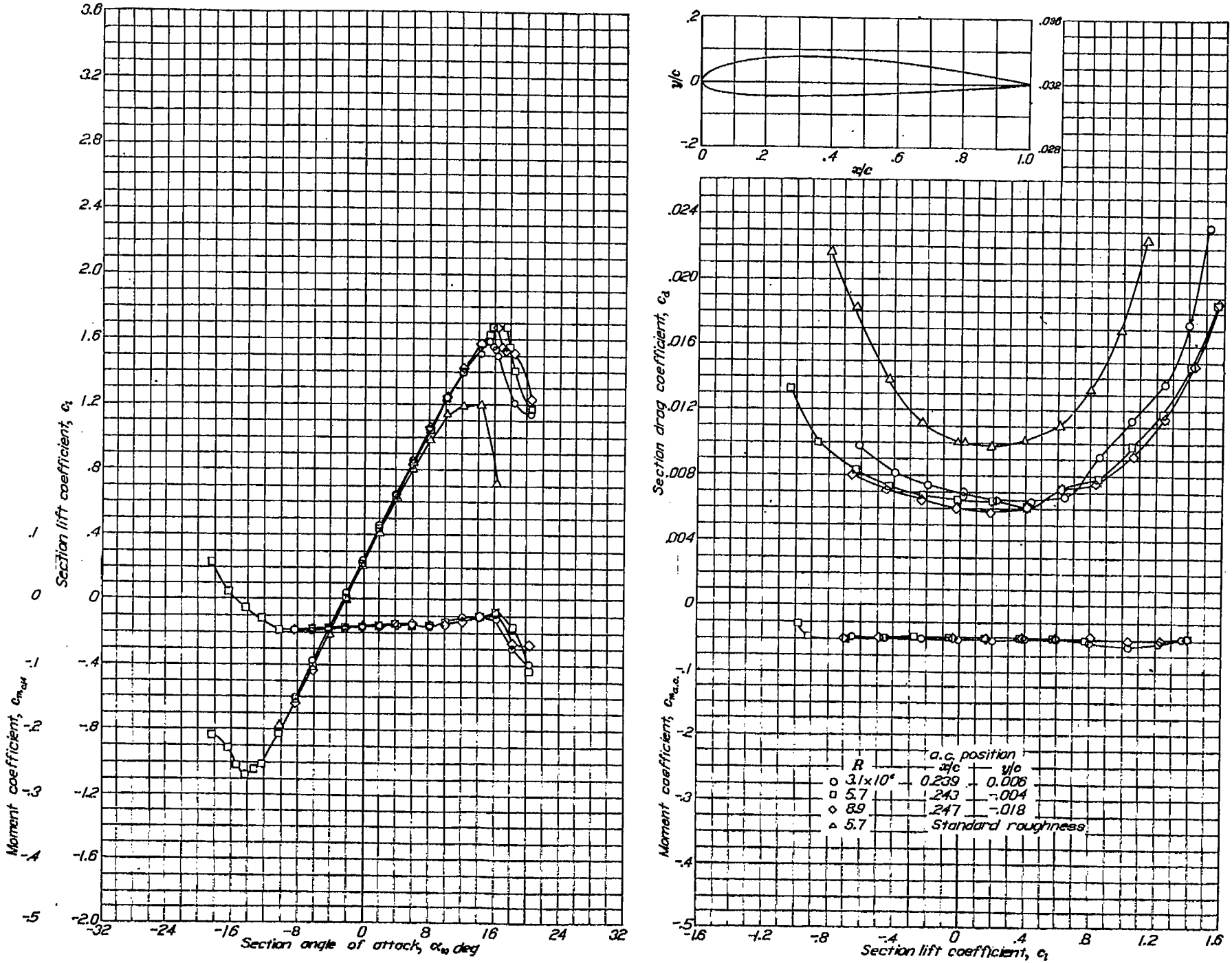

Aerodynamic characteristics of the NACA 2412 airfoil section, 24-inch chord.

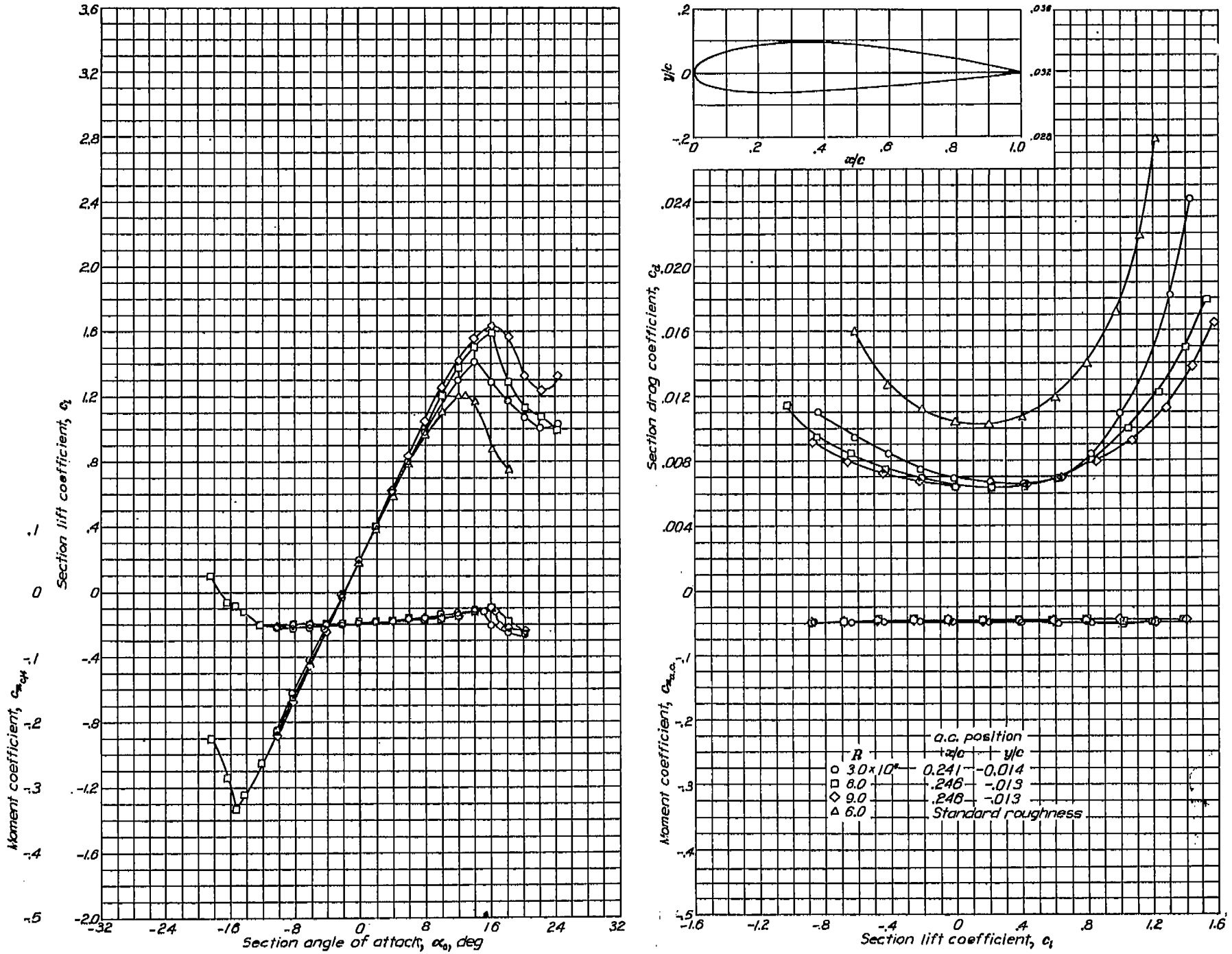

Aerodynamic characteristics of the NACA 2415 airfoil section, 24-inch chord.

NACA 2418

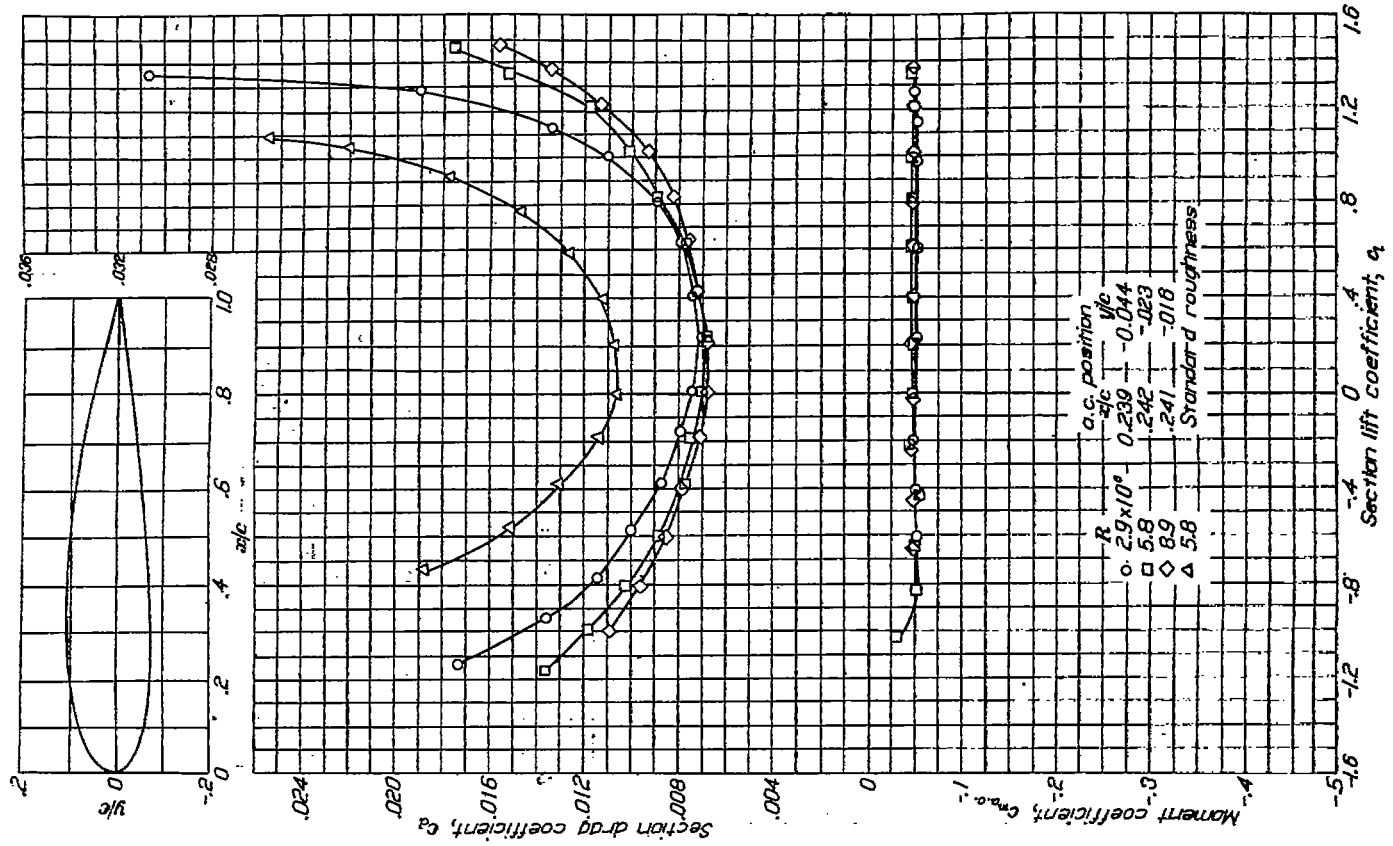

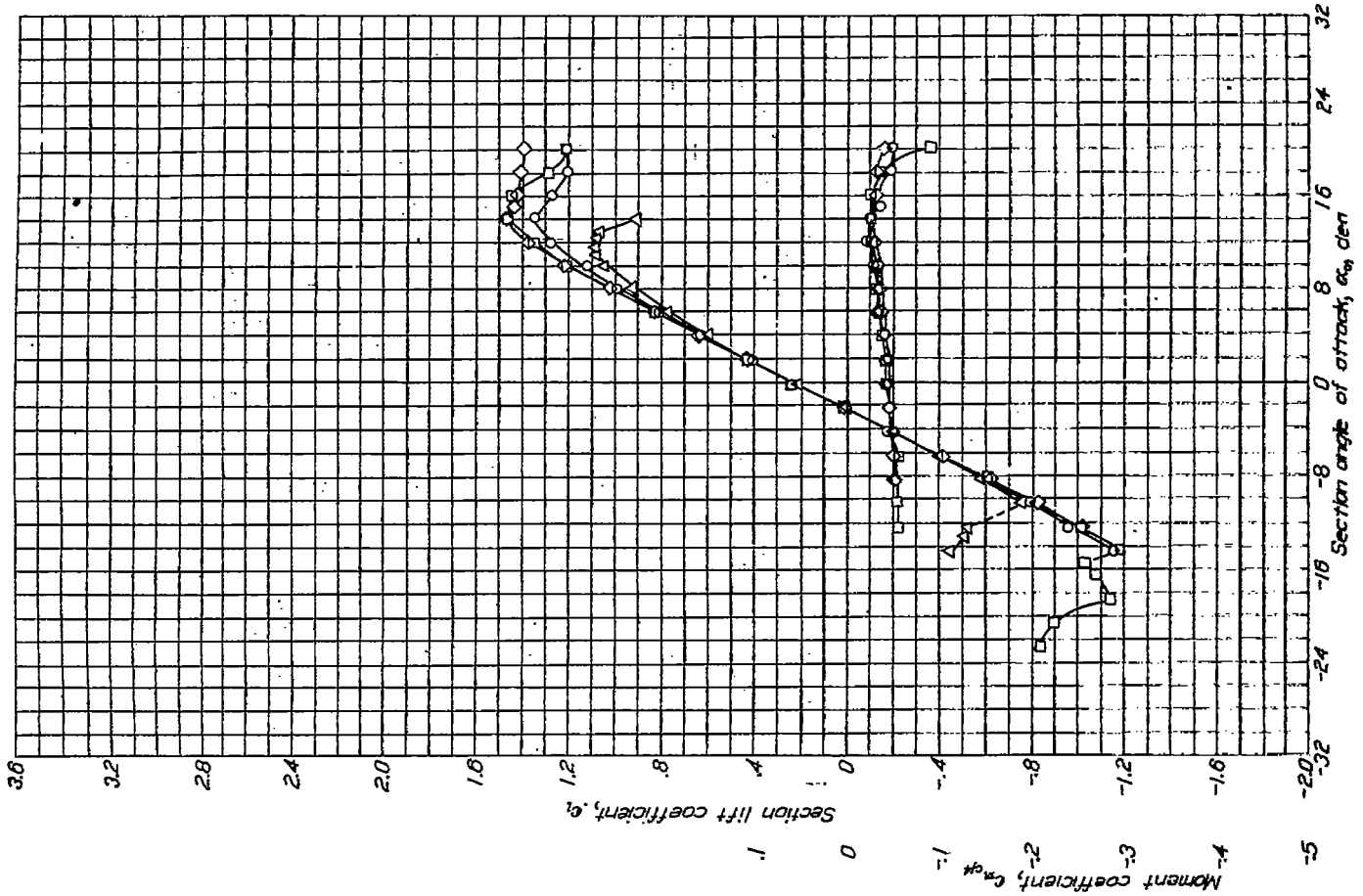

Aerodynamic characteristics of the NACA 2418 airfoil section, 24-inch chord.

NACA 2421

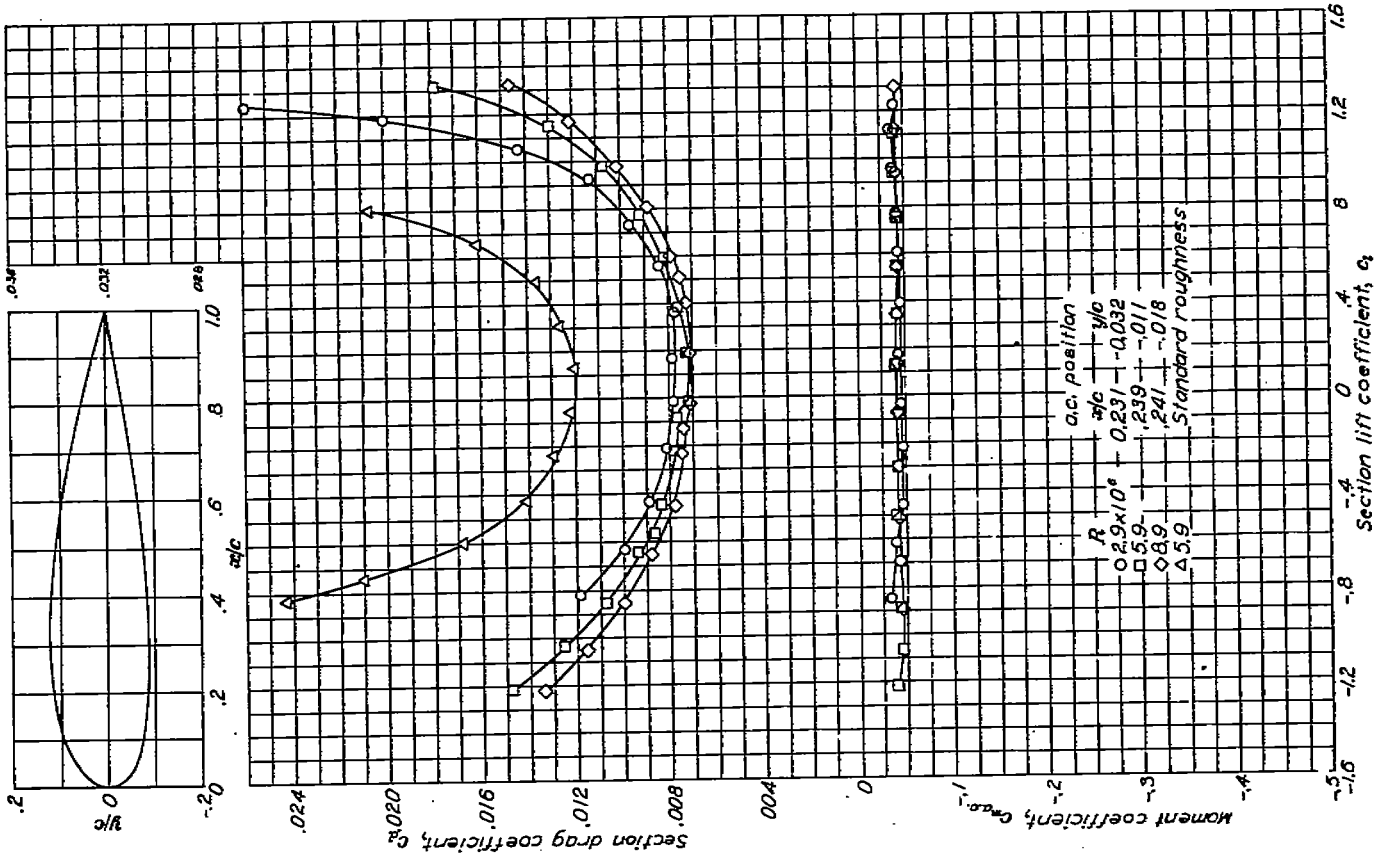

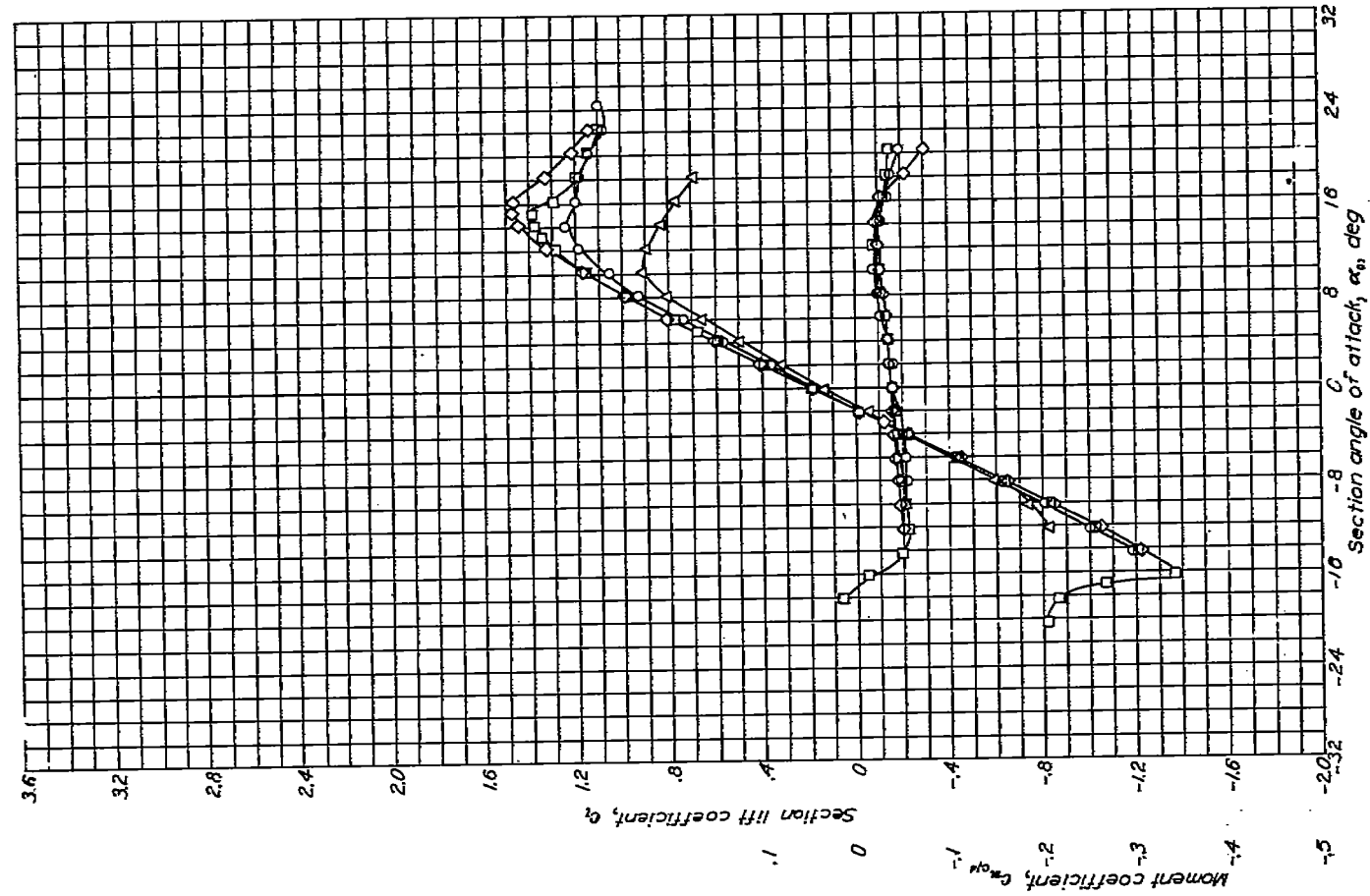

Aerodynamic characteristics of the NACA 2421 airfoil section, 24-inch chord.

NACA 2424

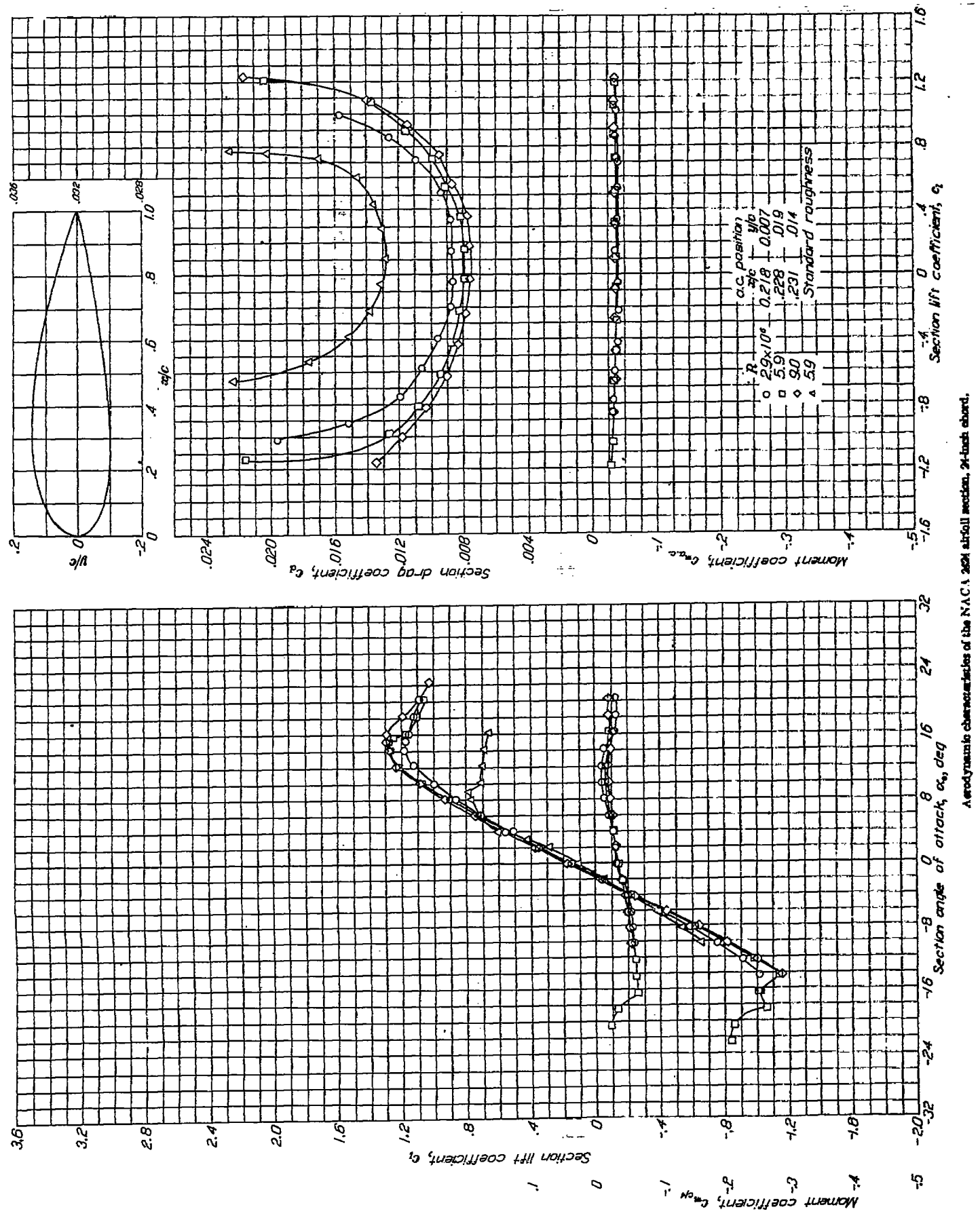

Aerodynamic characteristics of the NACA 2424 airfoil section, 24-inch chord.

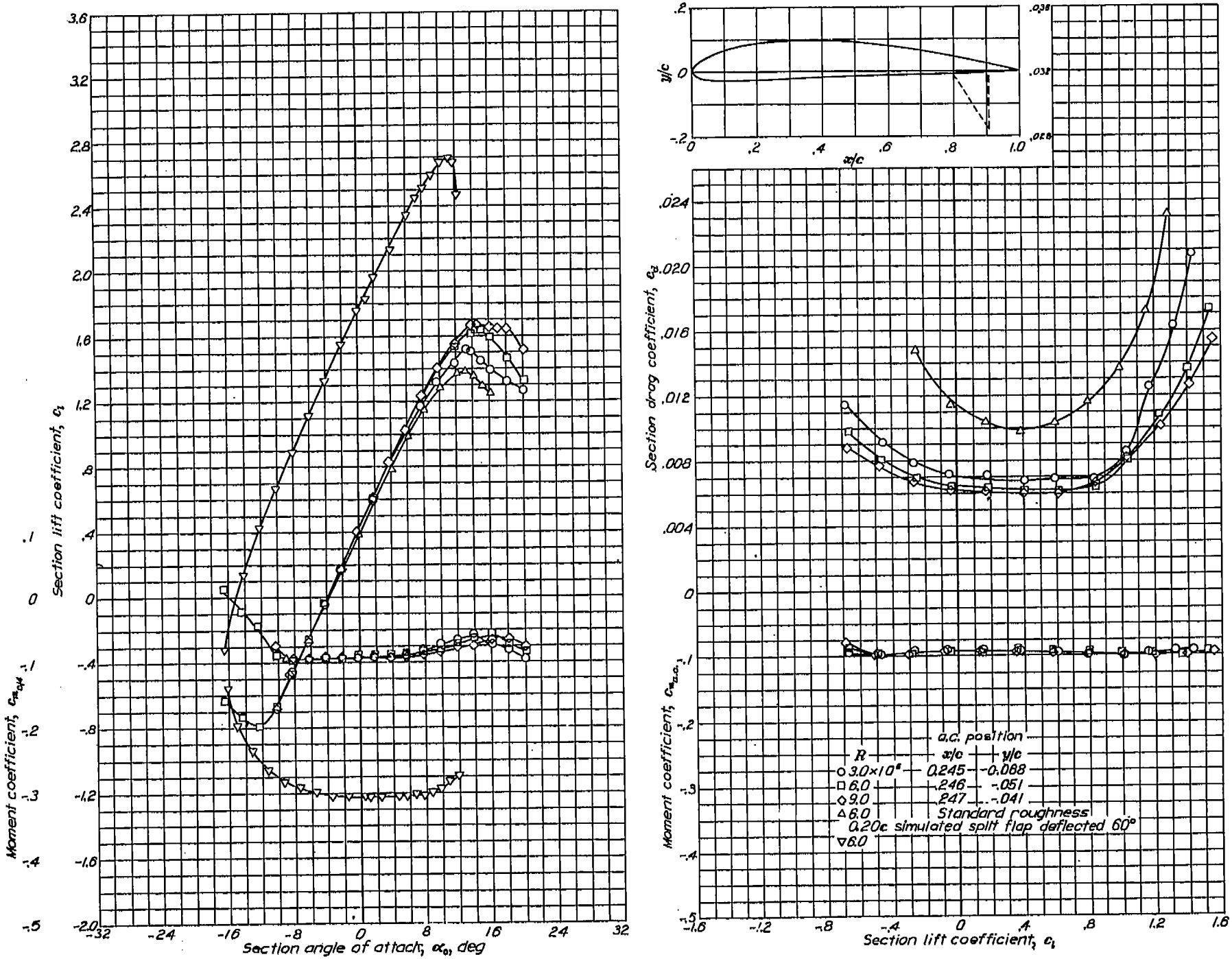

Aerodynamic characteristics of the NACA 4412 airfoil section, 24-inch chord.

NACA 4415

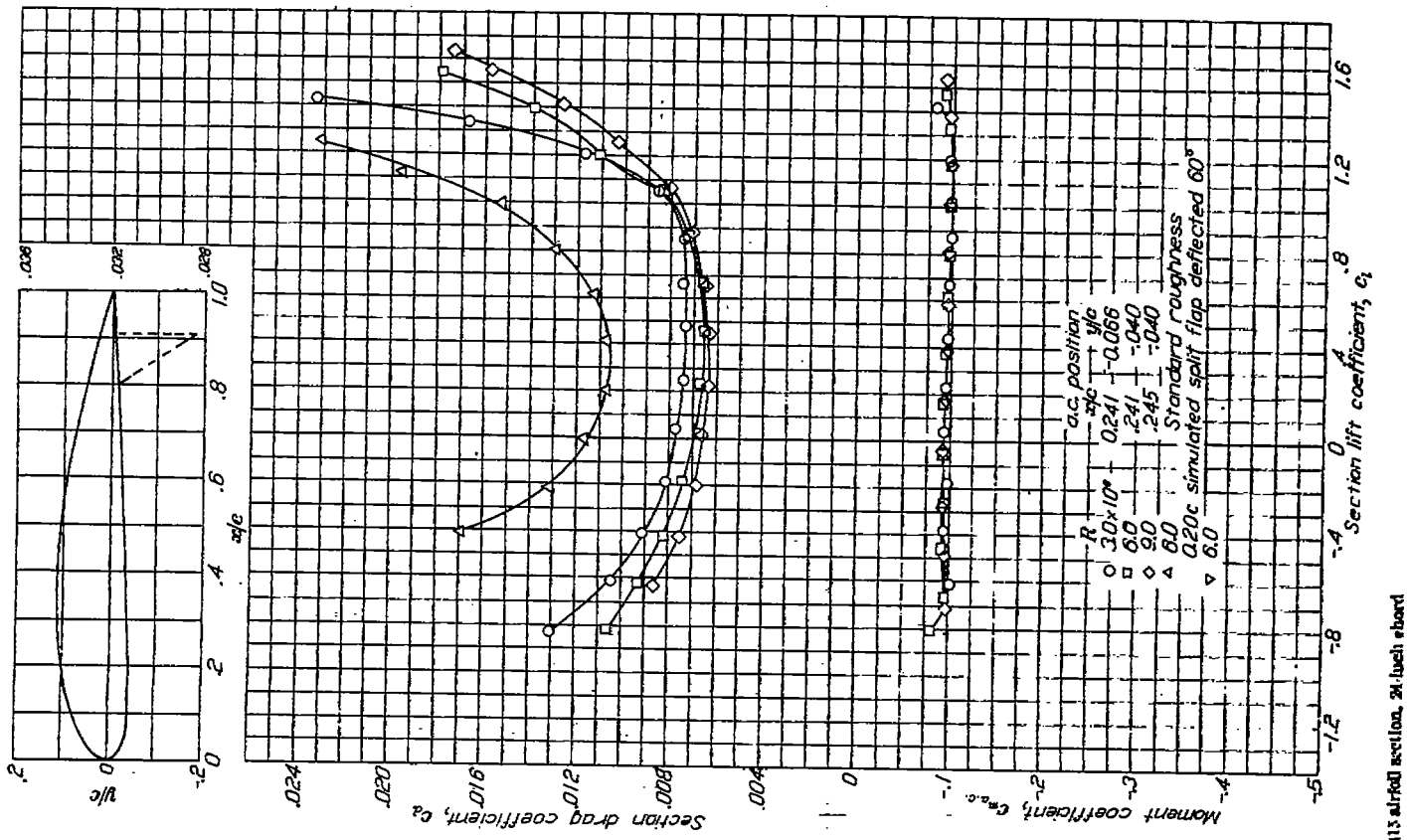

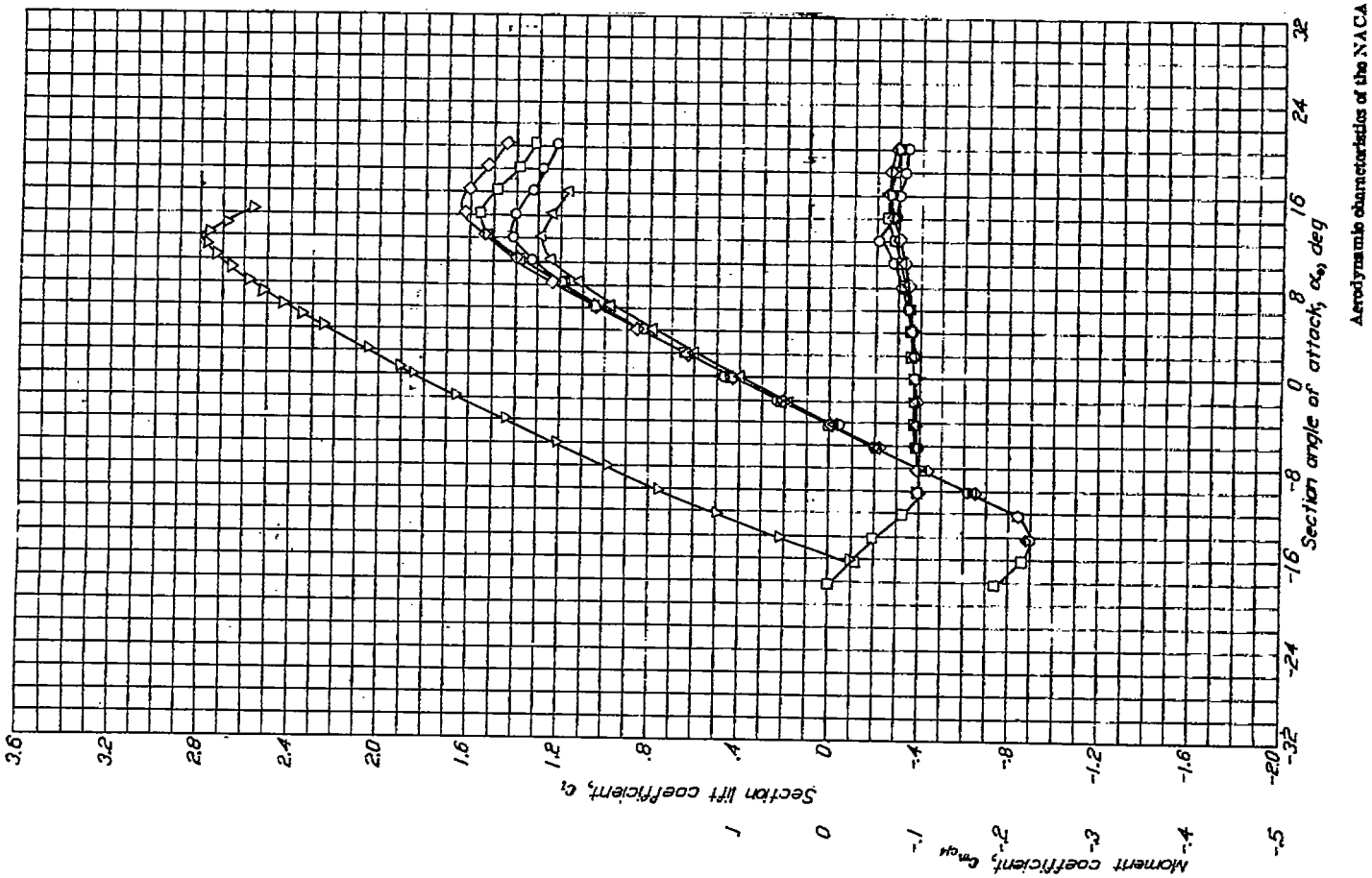

Aerodynamic characteristics of the NACA 4415 airfoil section, 24-inch chord

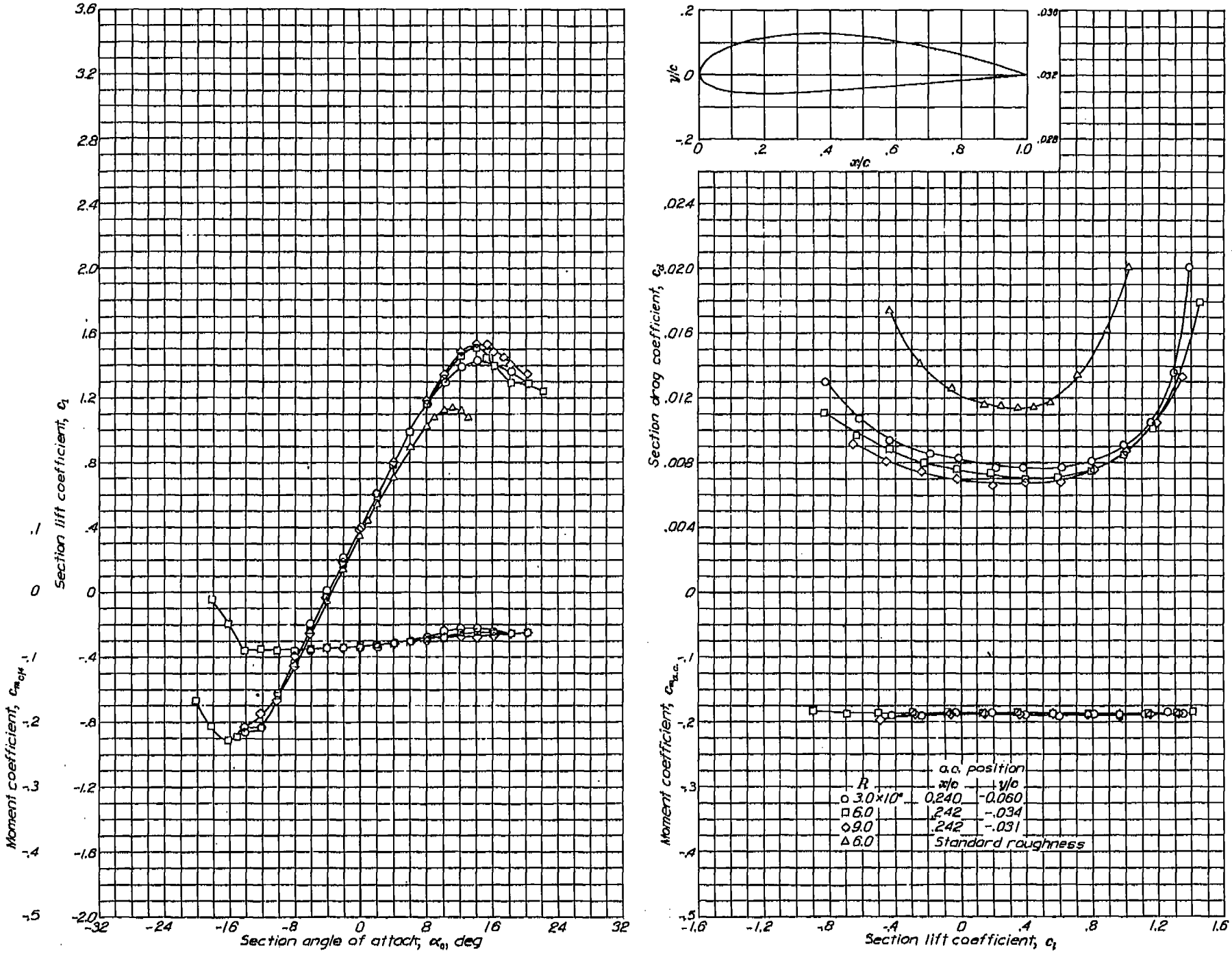

Aerodynamic characteristics of the NACA 4418 airfoil section, 24-inch chord.

NACA 4421

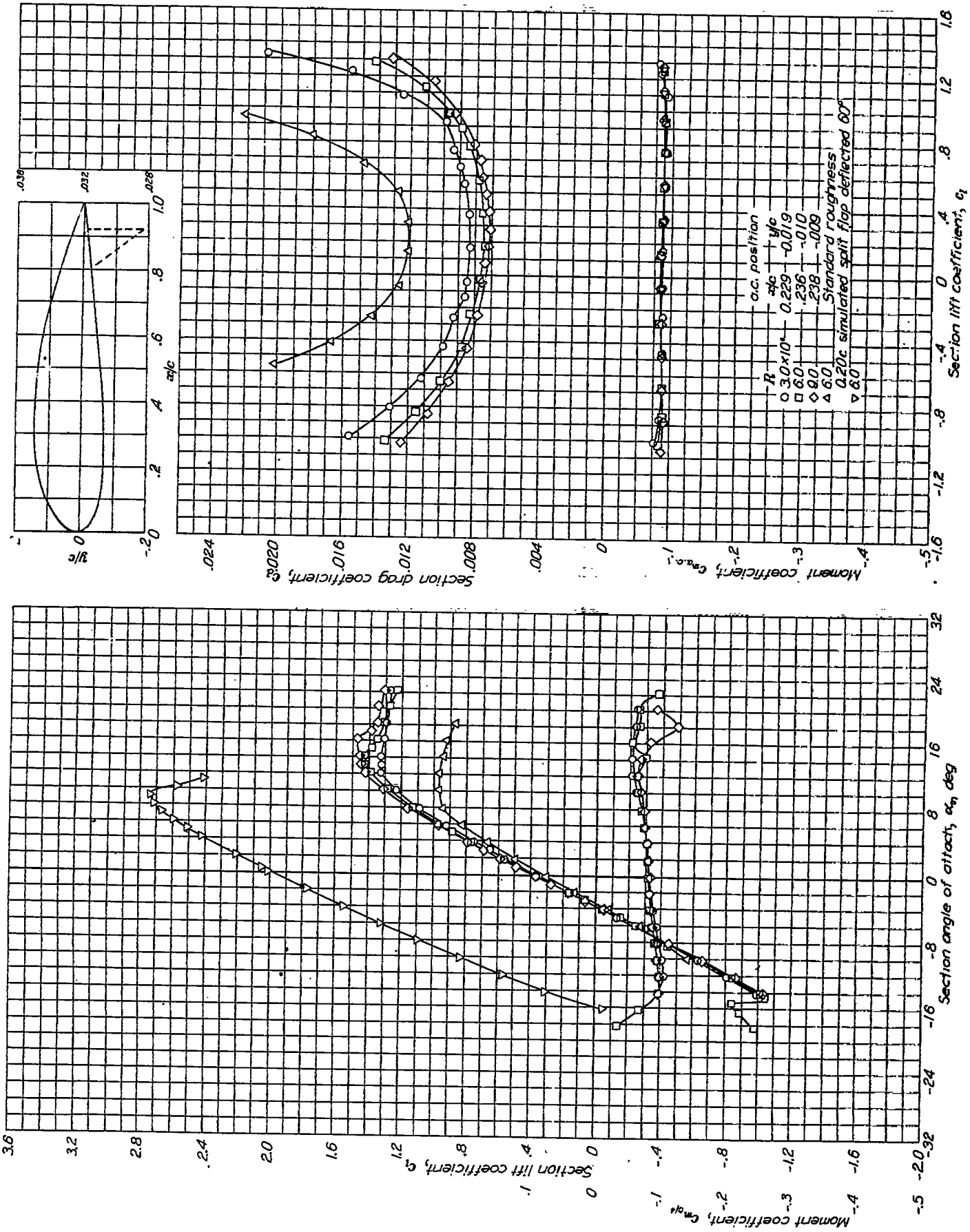

Aerodynamic characteristics of the NACA 4421 airfoil section, 24-inch chord.

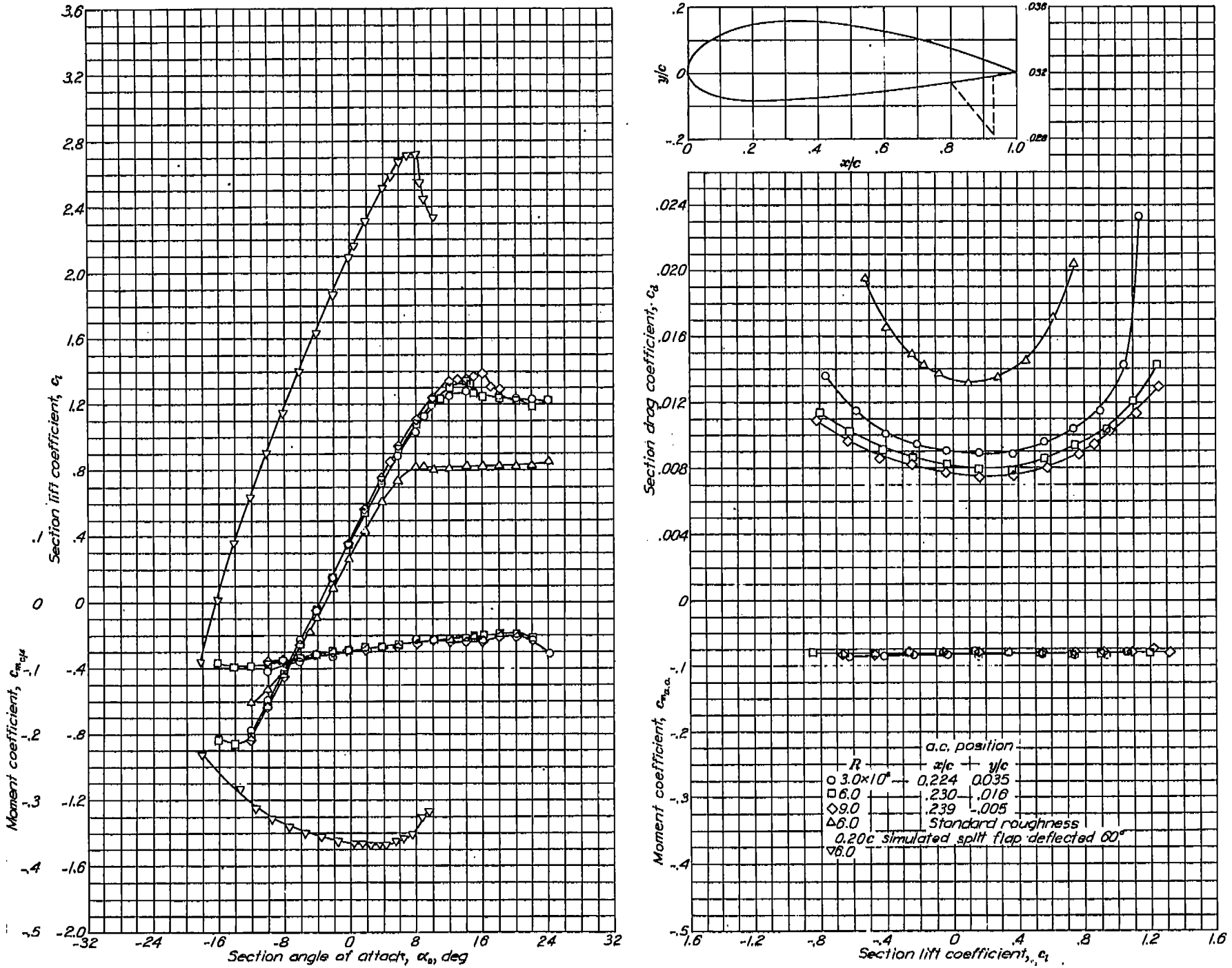

Aerodynamic characteristics of the NACA 4424 airfoil section, 24-inch chord.

NACA 23012

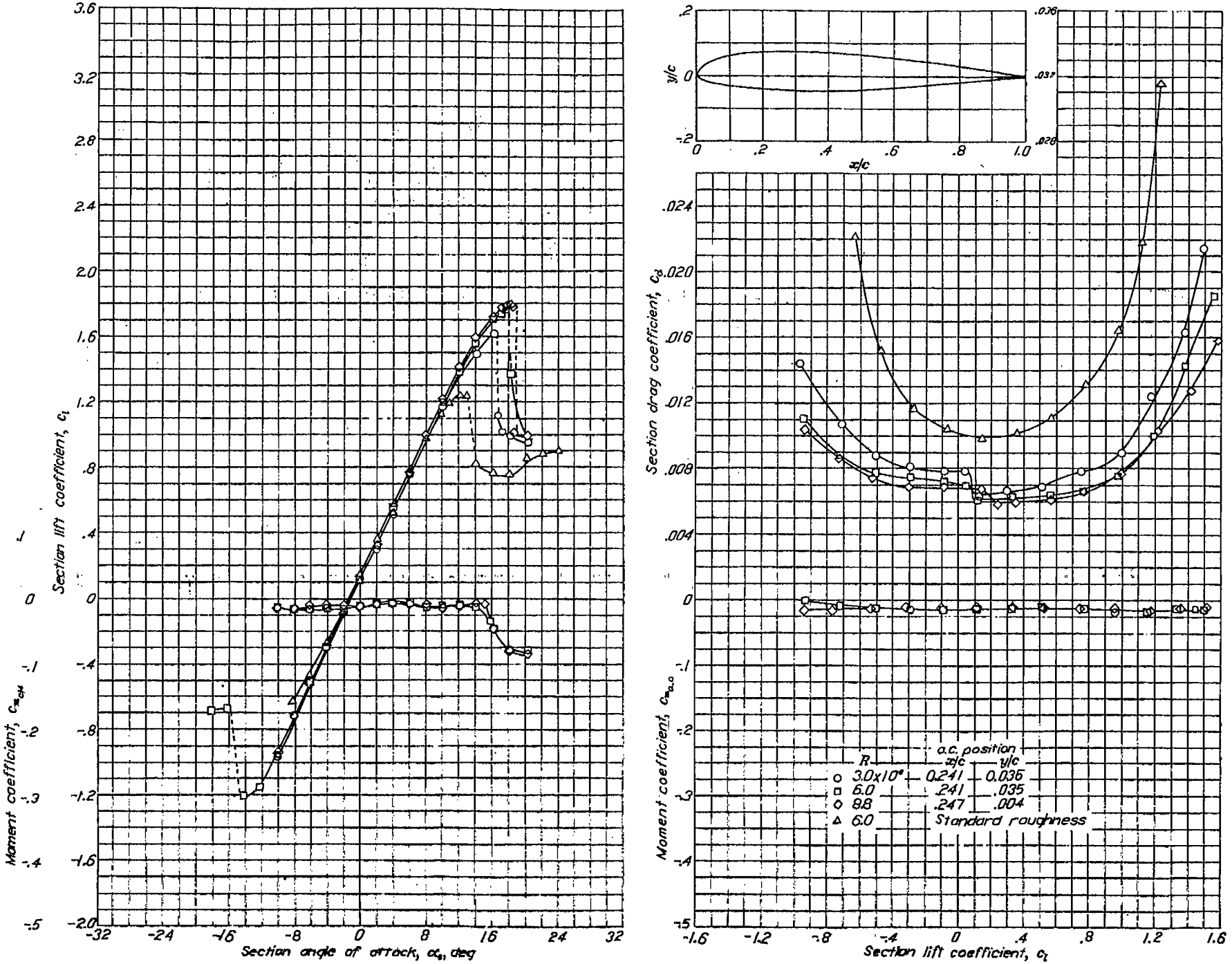

Aerodynamic characteristics of the NACA 23012 airfoil section, 24-inch chord.

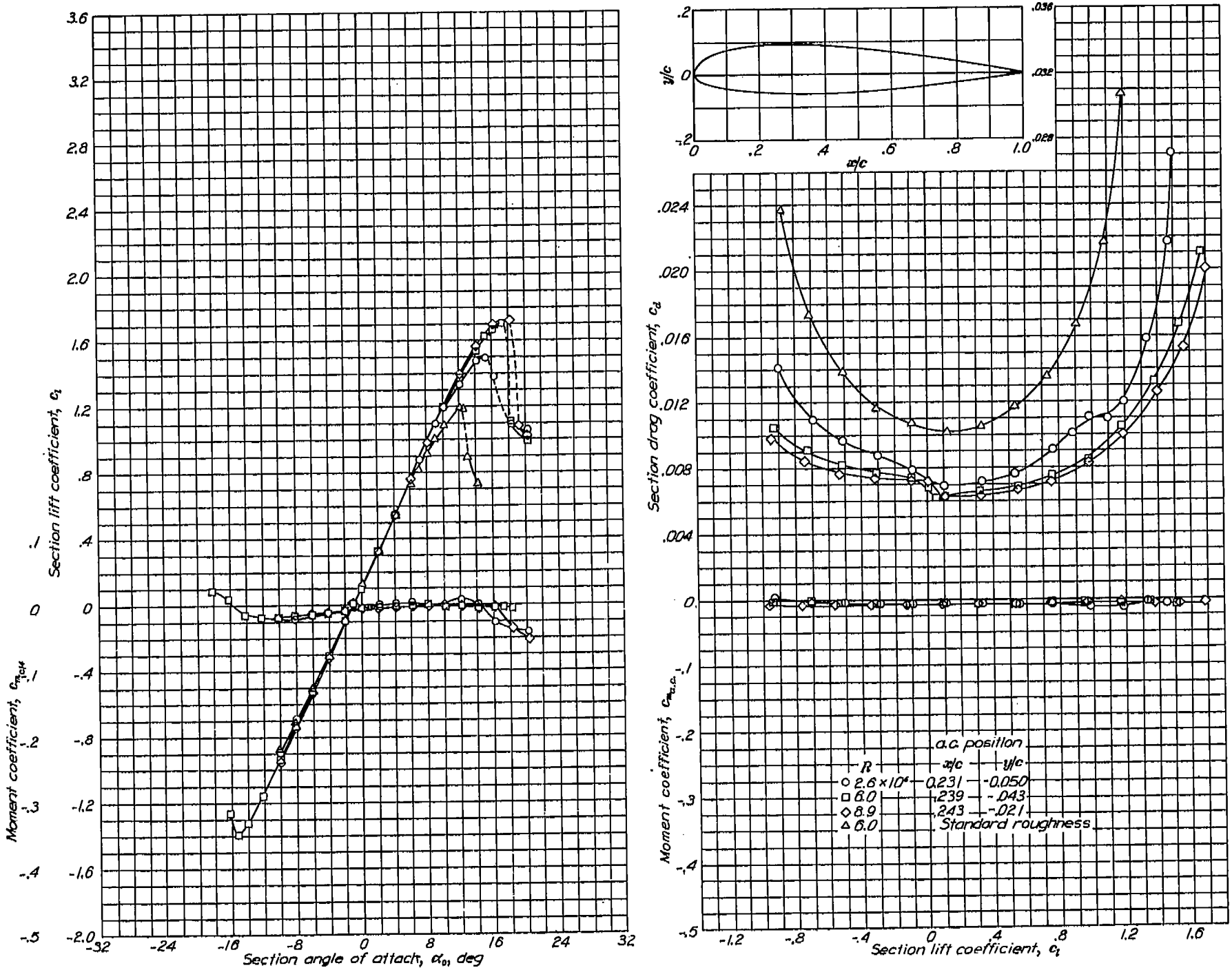

Aerodynamic characteristics of the NACA 23015 airfoil section, 24-inch chord.

NACA 23018

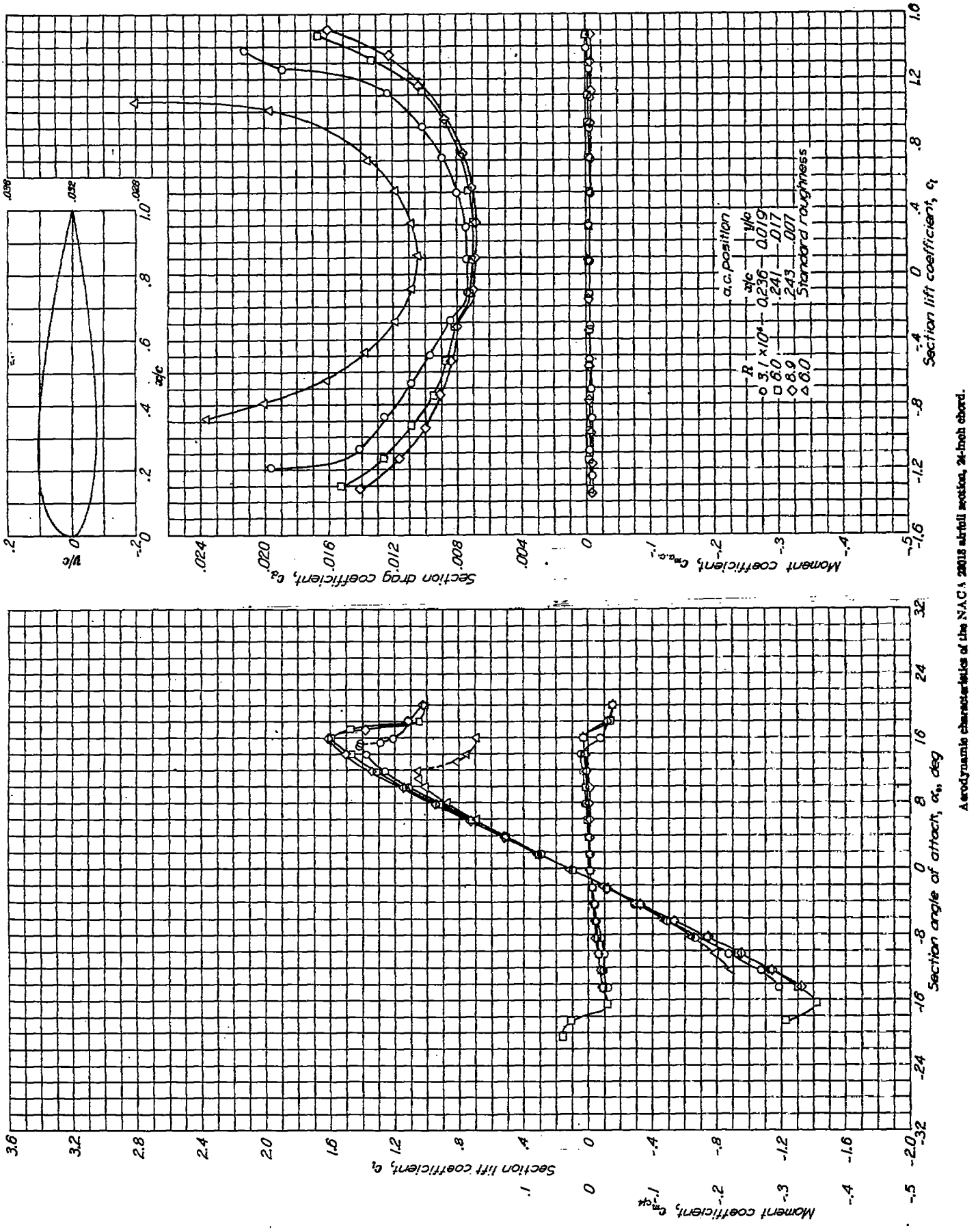

Aerodynamic characteristics of the NACA 23018 airfoil section, 24-inch chord.

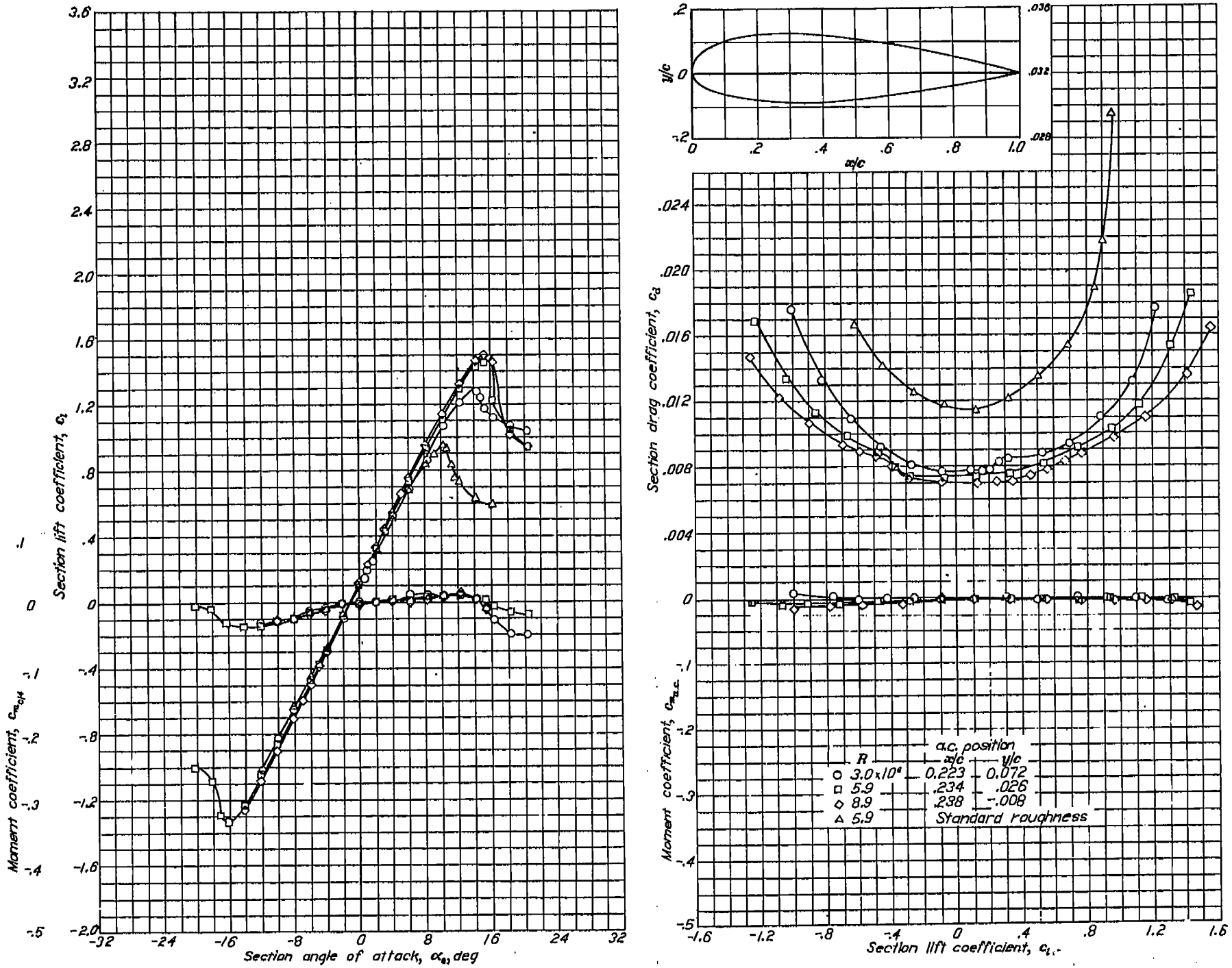

Aerodynamic characteristics of the NACA 23021 airfoil section, 24-inch chord.

NACA 23024

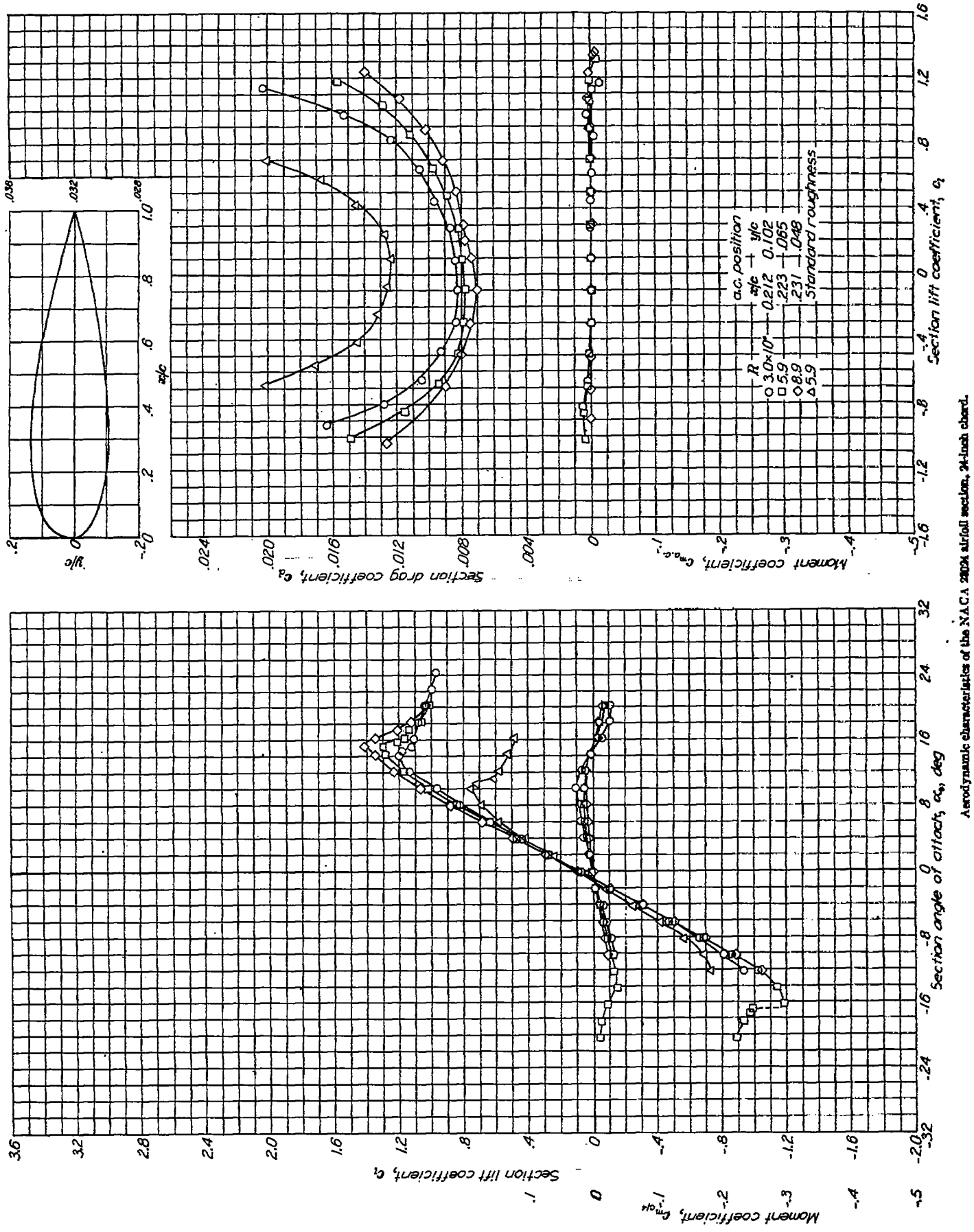

Aerodynamic characteristics of the NACA 23024 airfoil section, 24-inch chord.

NACA 63,4-420

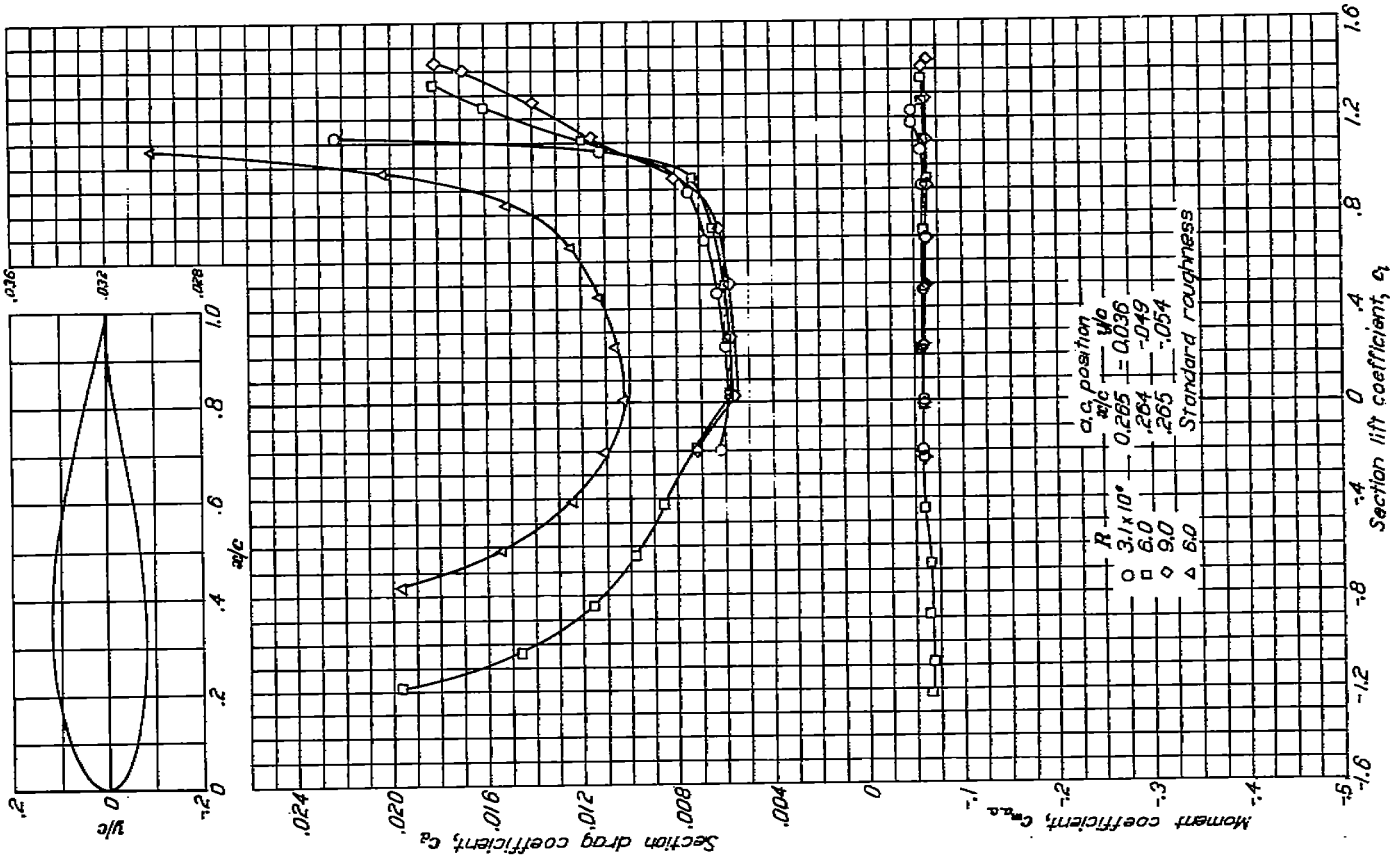

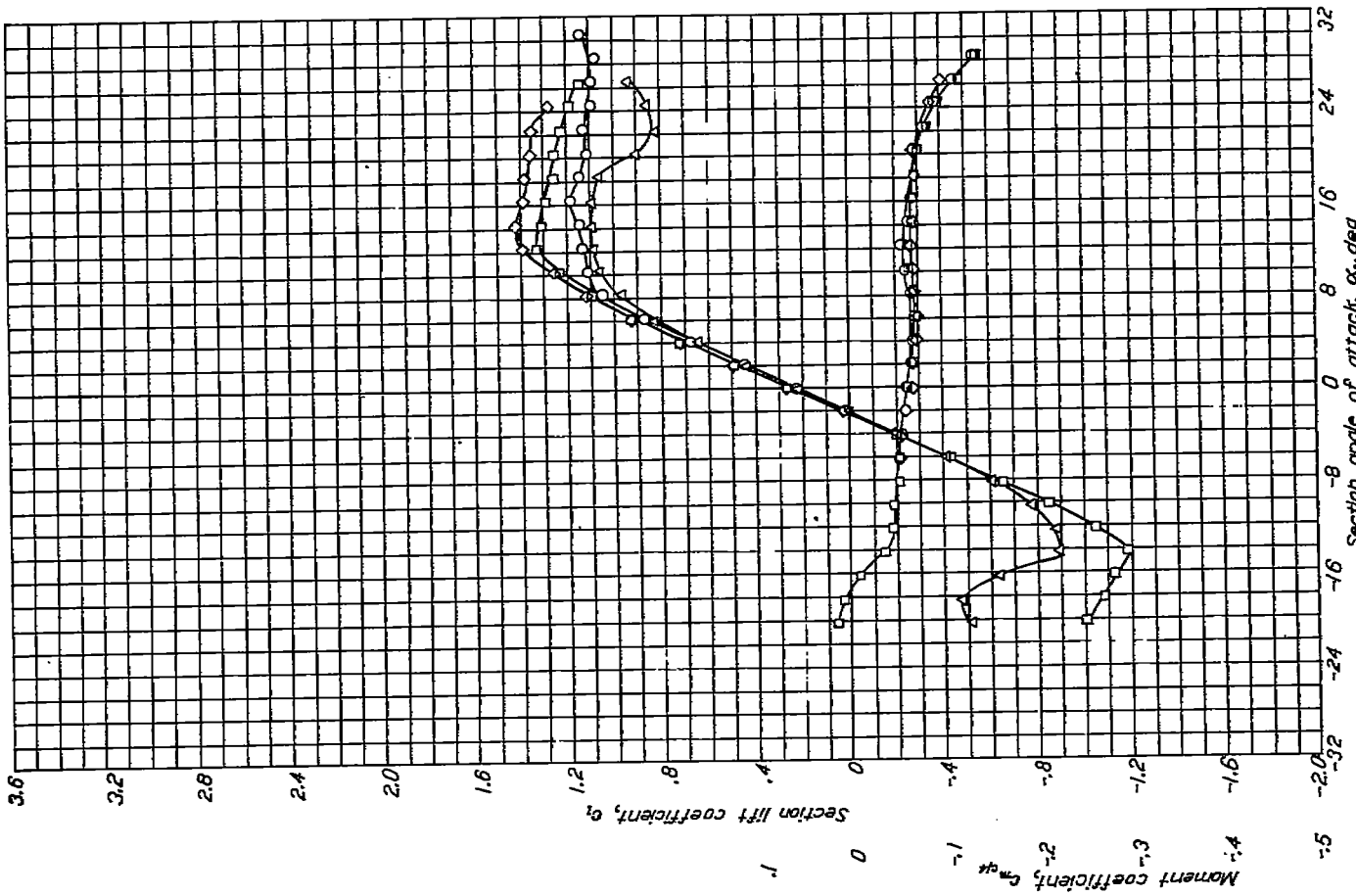

Aerodynamic characteristics of the NACA 63,4-420 airfoil section, 24-inch chord.

NACA 63,4-420 with flap

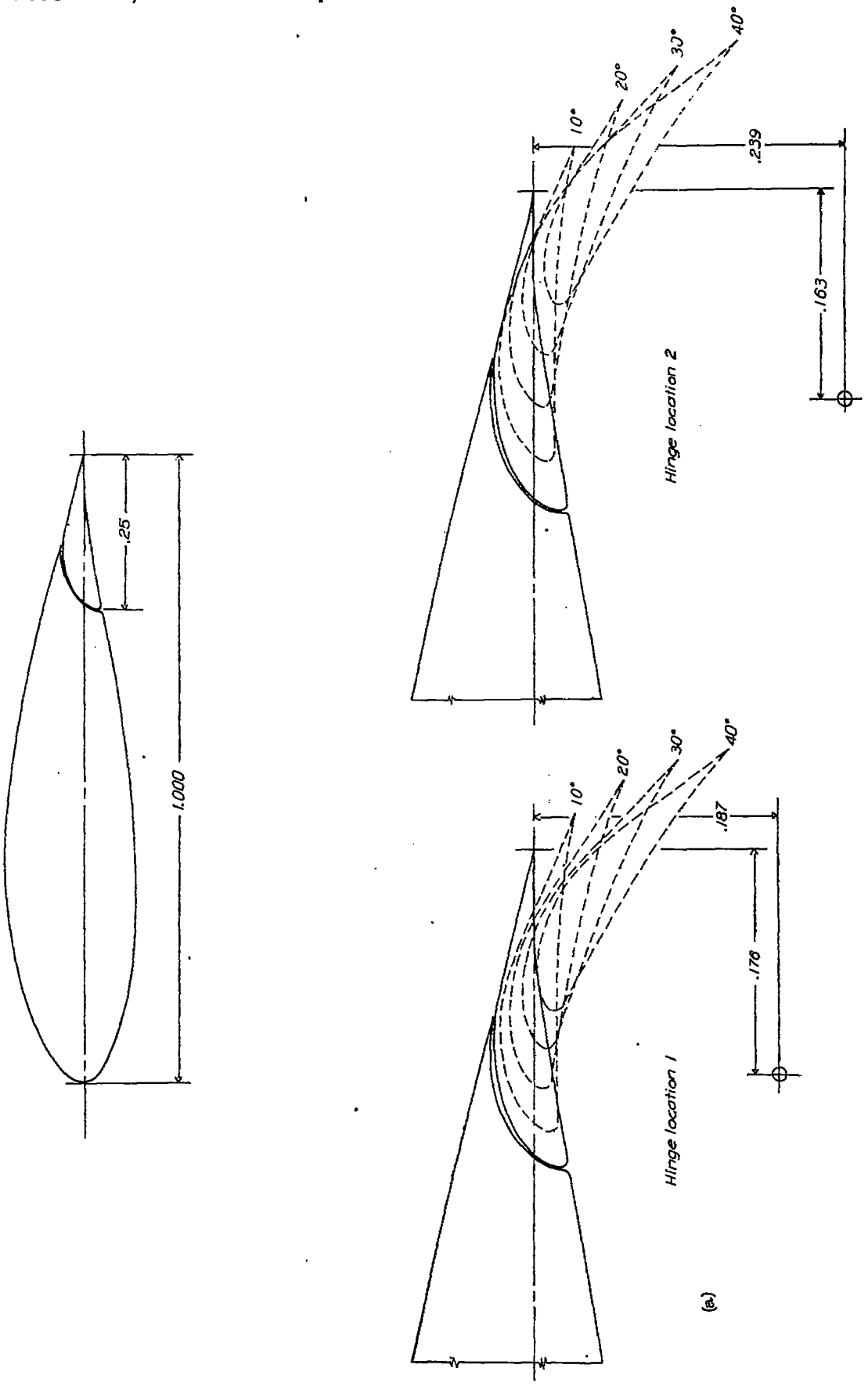

(a) Configuration.

NACA 63,4-420 airfoil section with 0.25c slotted flap.

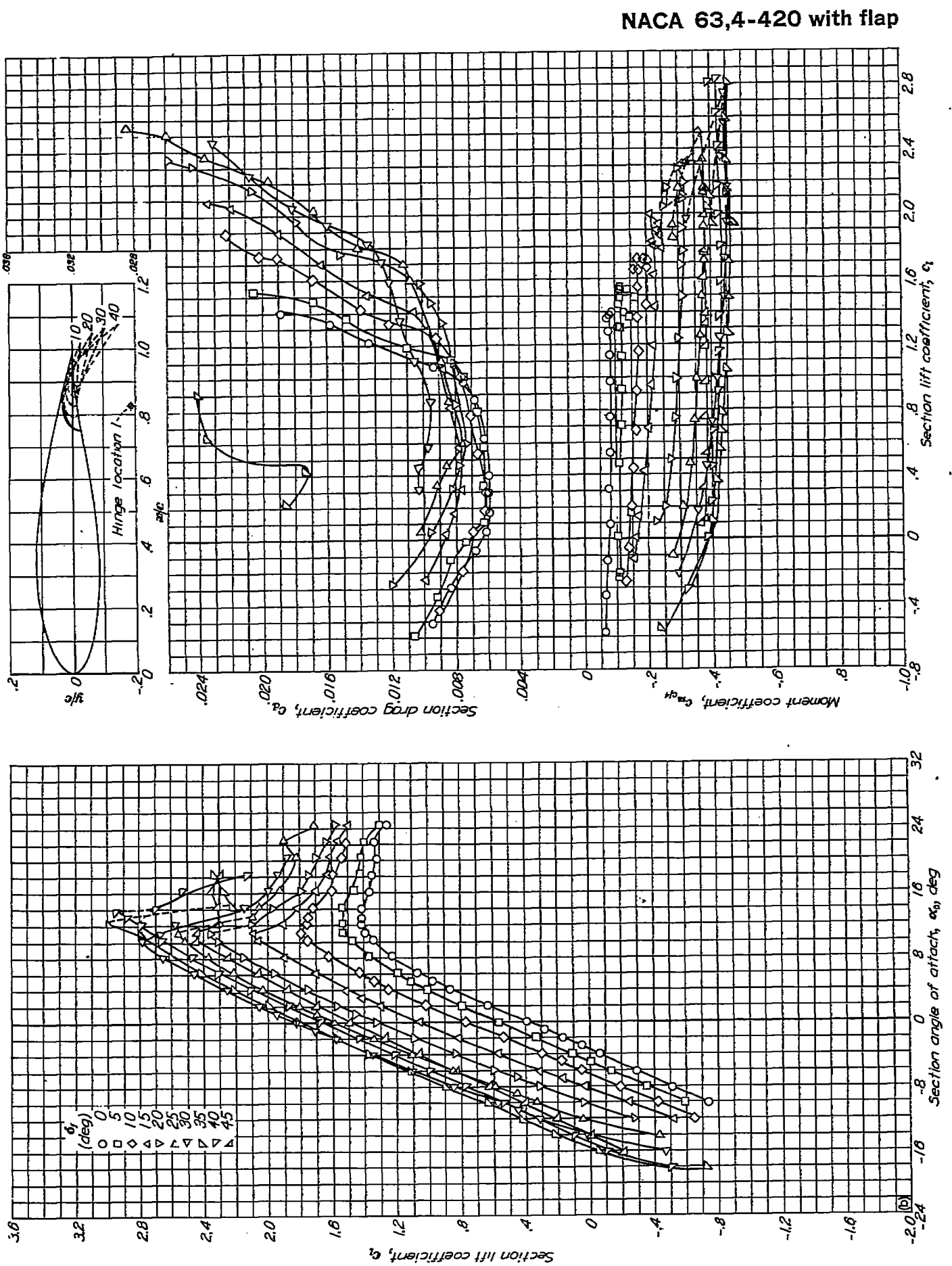

(b) Aerodynamic characteristics with hinge location 1.; $R = 6 \times 10^6$.
NACA 63,4-420 airfoil section with 0.25c slotted flap.

NACA 63,4-420 with flap

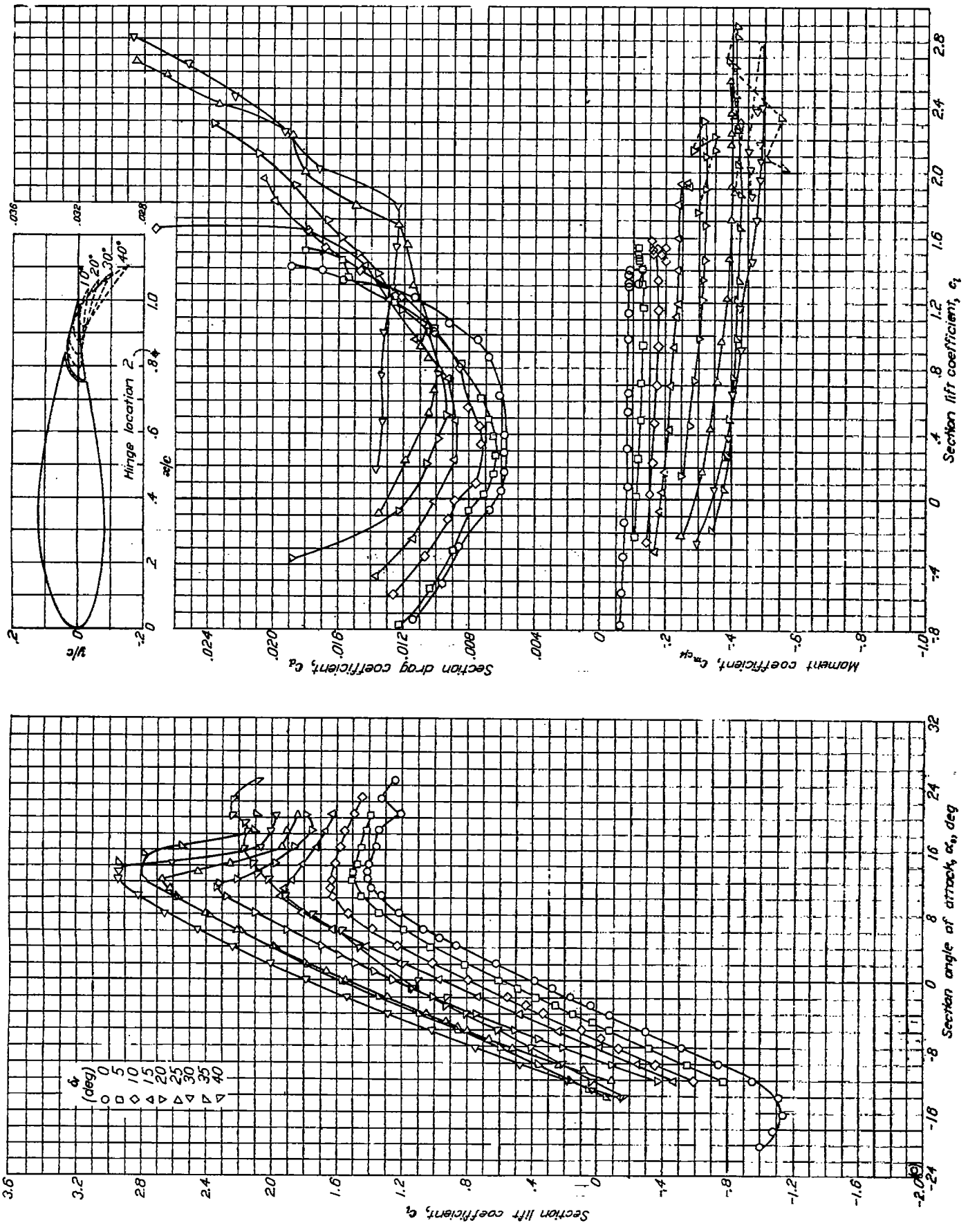

(c) Aerodynamic characteristics with hinge location 2. $R = 6 \times 10^6$. NACA 63,4-420 airfoil section with 0.20c slotted flap.

NACA 63,4-420, $a = 0.3$

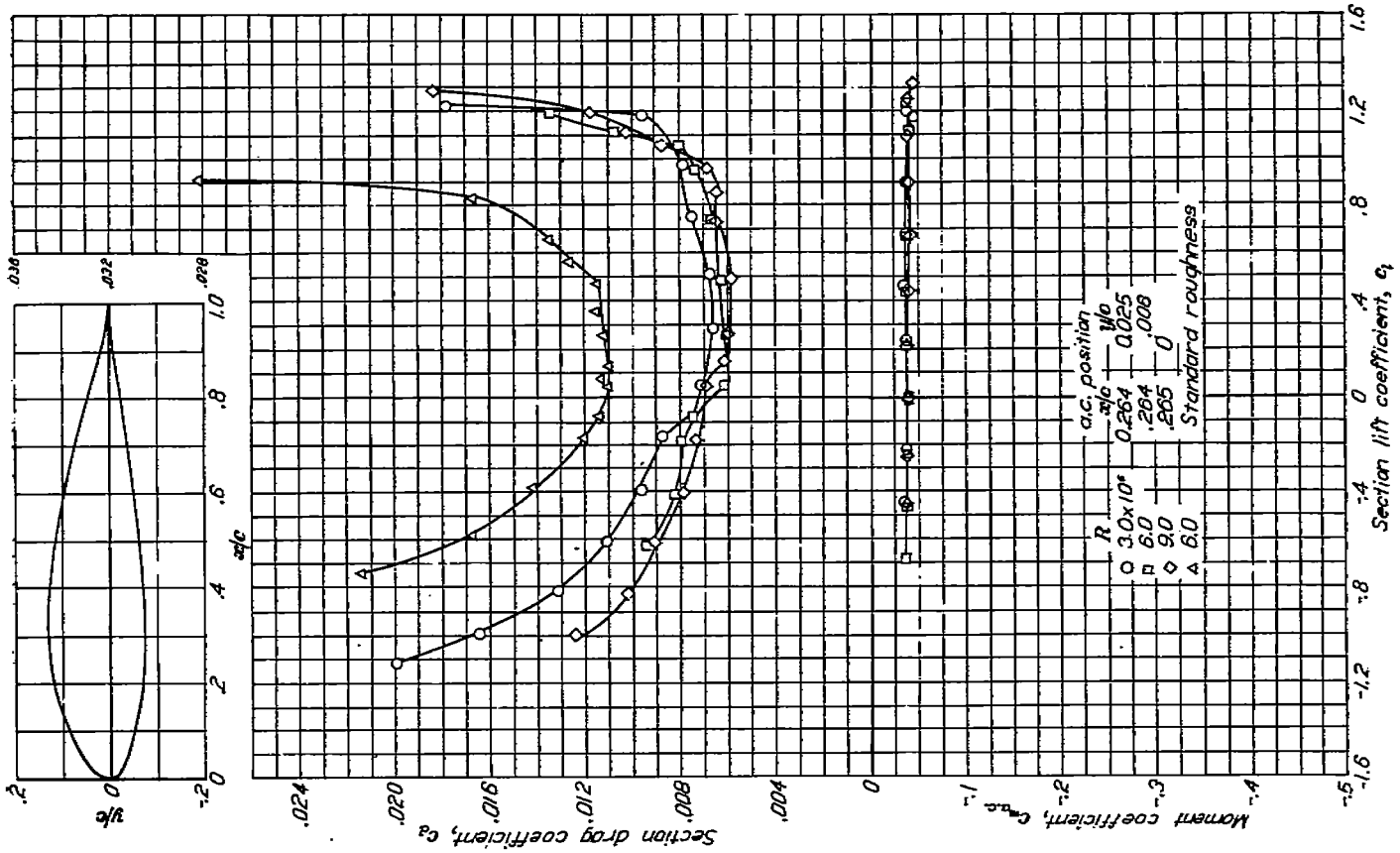

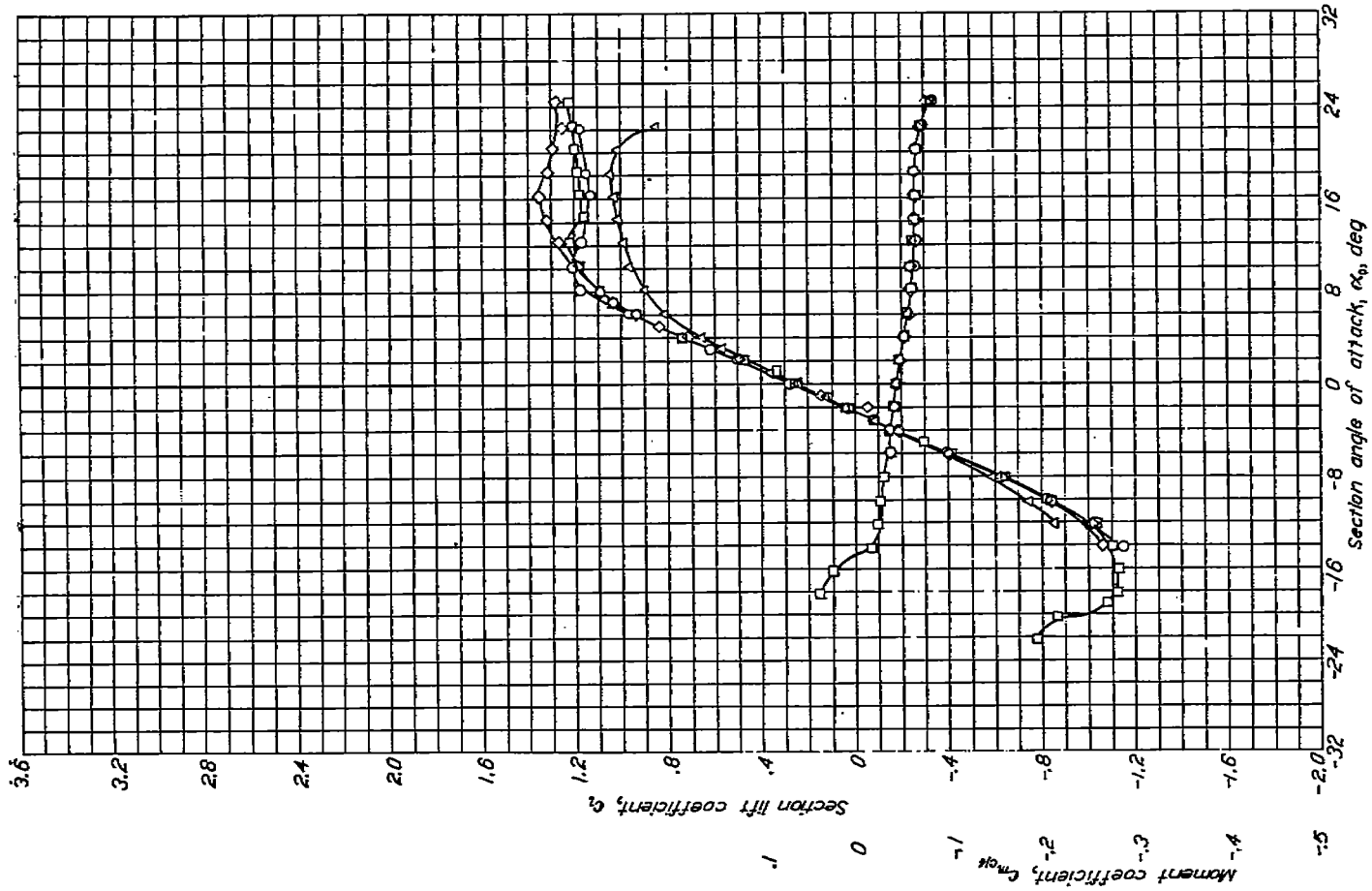

Aerodynamic characteristics of the NACA 63,4-420, $a = 0.3$ airfoil section, 24-inch chord.

NACA 63(420)-422

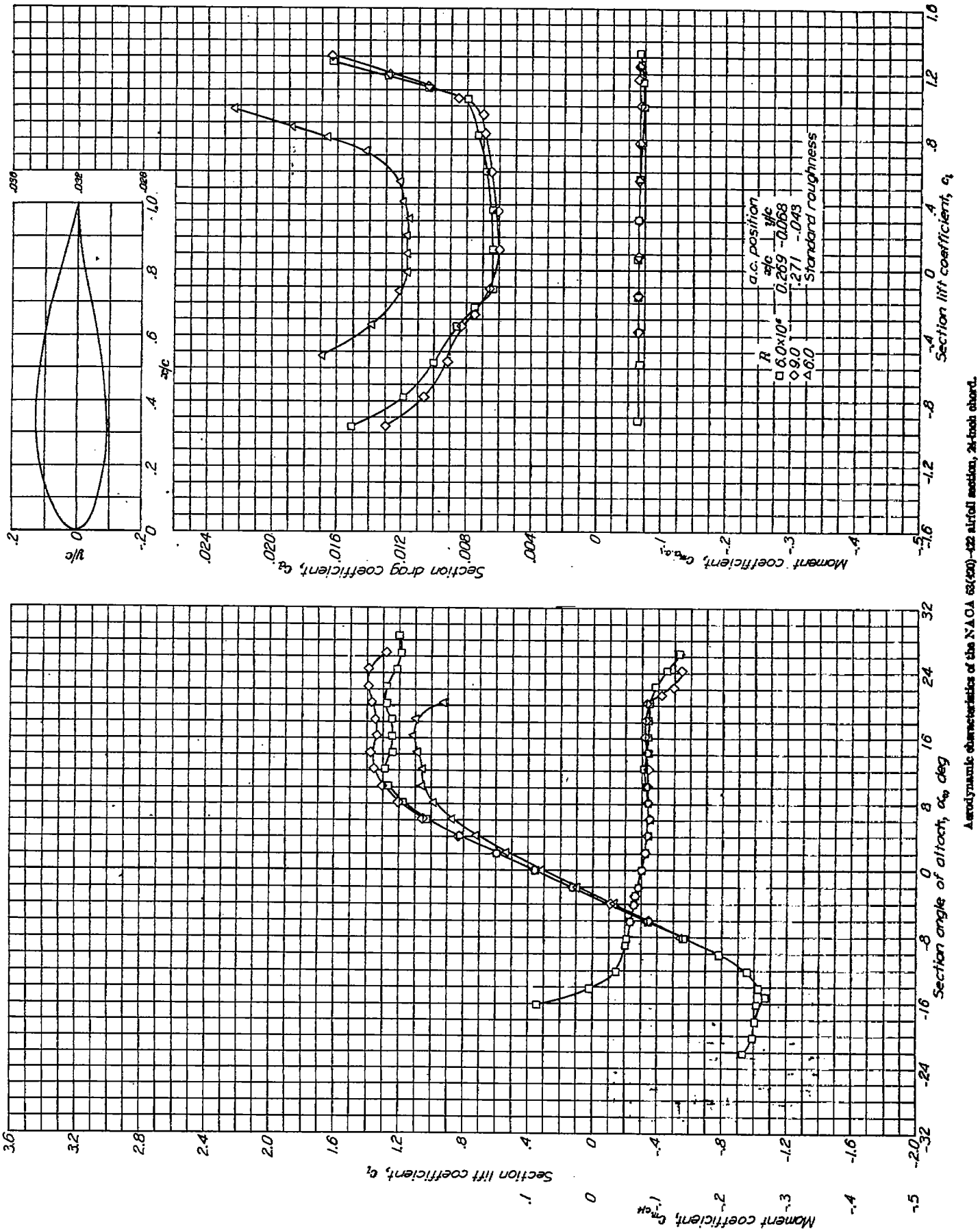

Aerodynamic characteristics of the NACA 63(420)-422 airfoil section, 24-inch chord.

NACA 63(420)-517

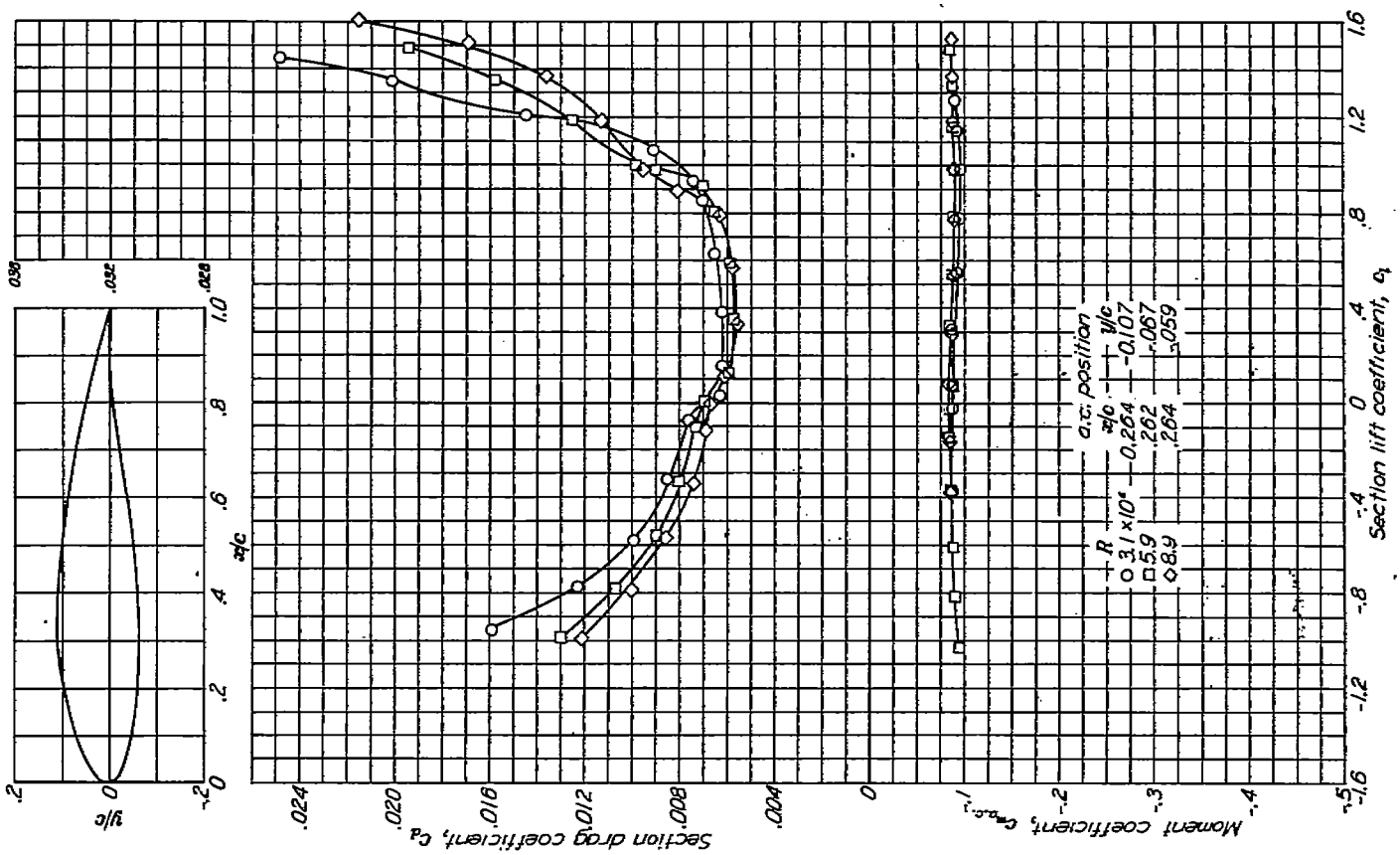

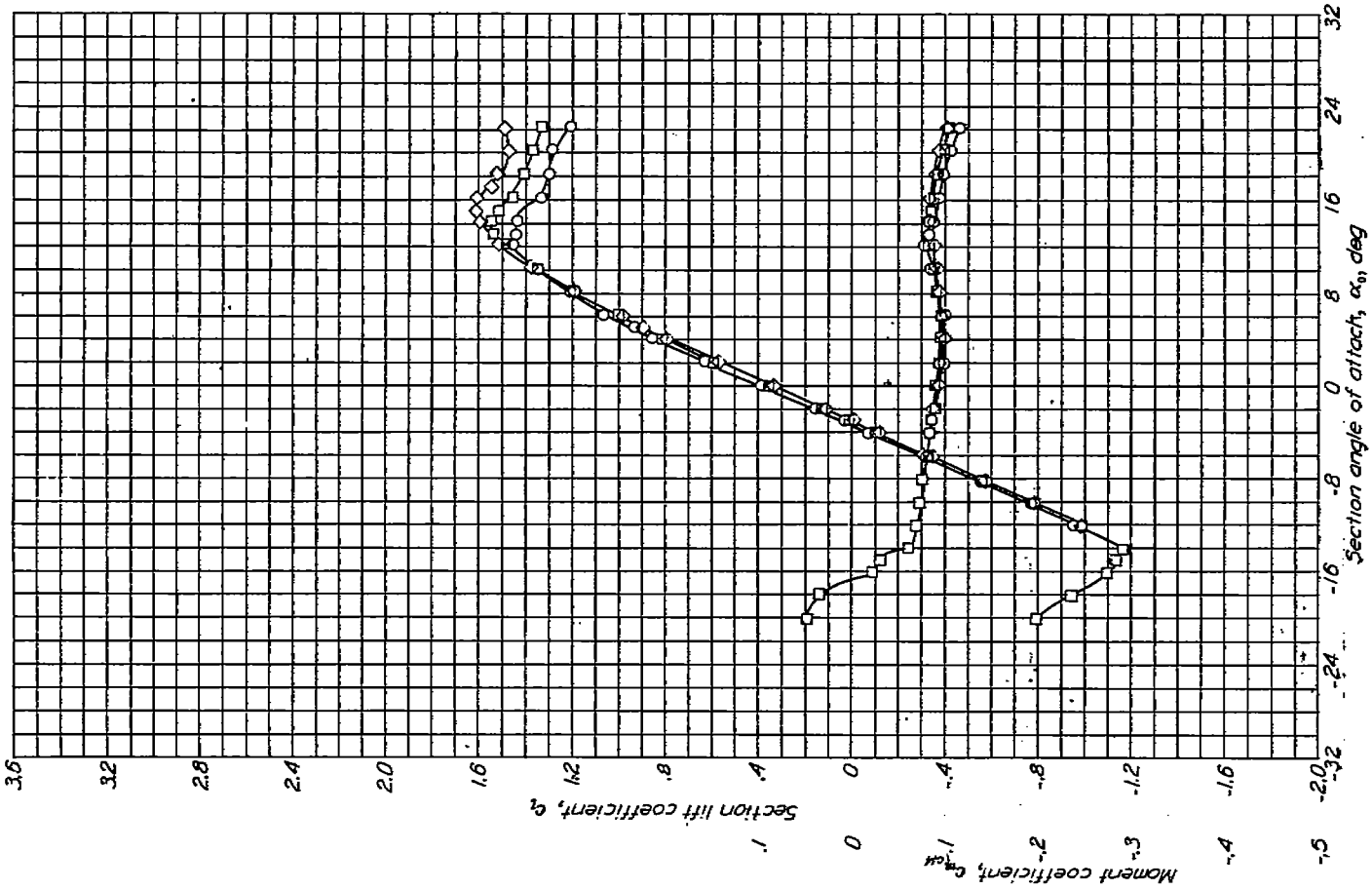

Aerodynamic characteristics of the NACA 63(420)-517 airfoil section, 24-inch chord.

NACA 63-006

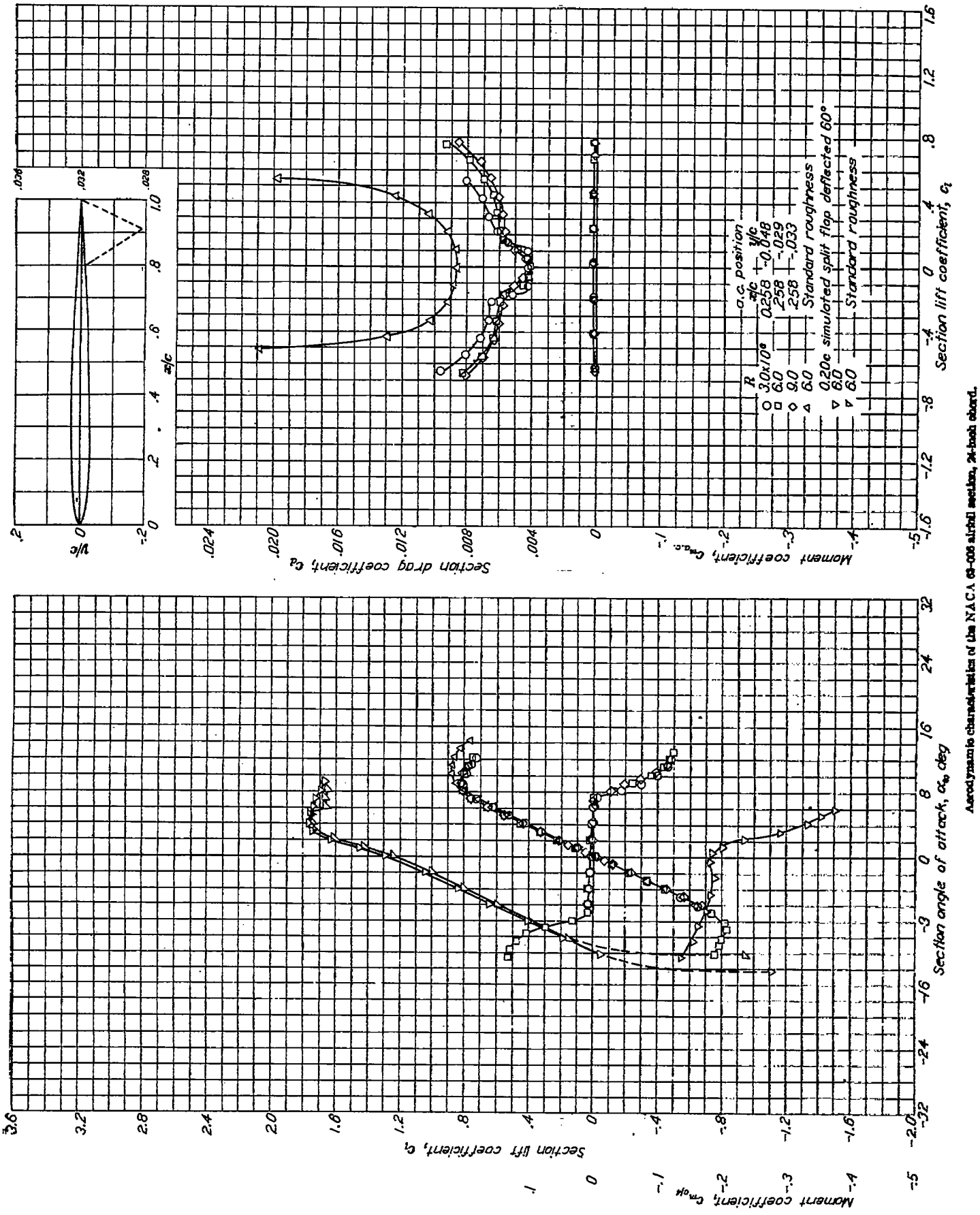

Aerodynamic characteristics of the NACA 63-006 airfoil section, 24-inch chord.

NACA 63-009

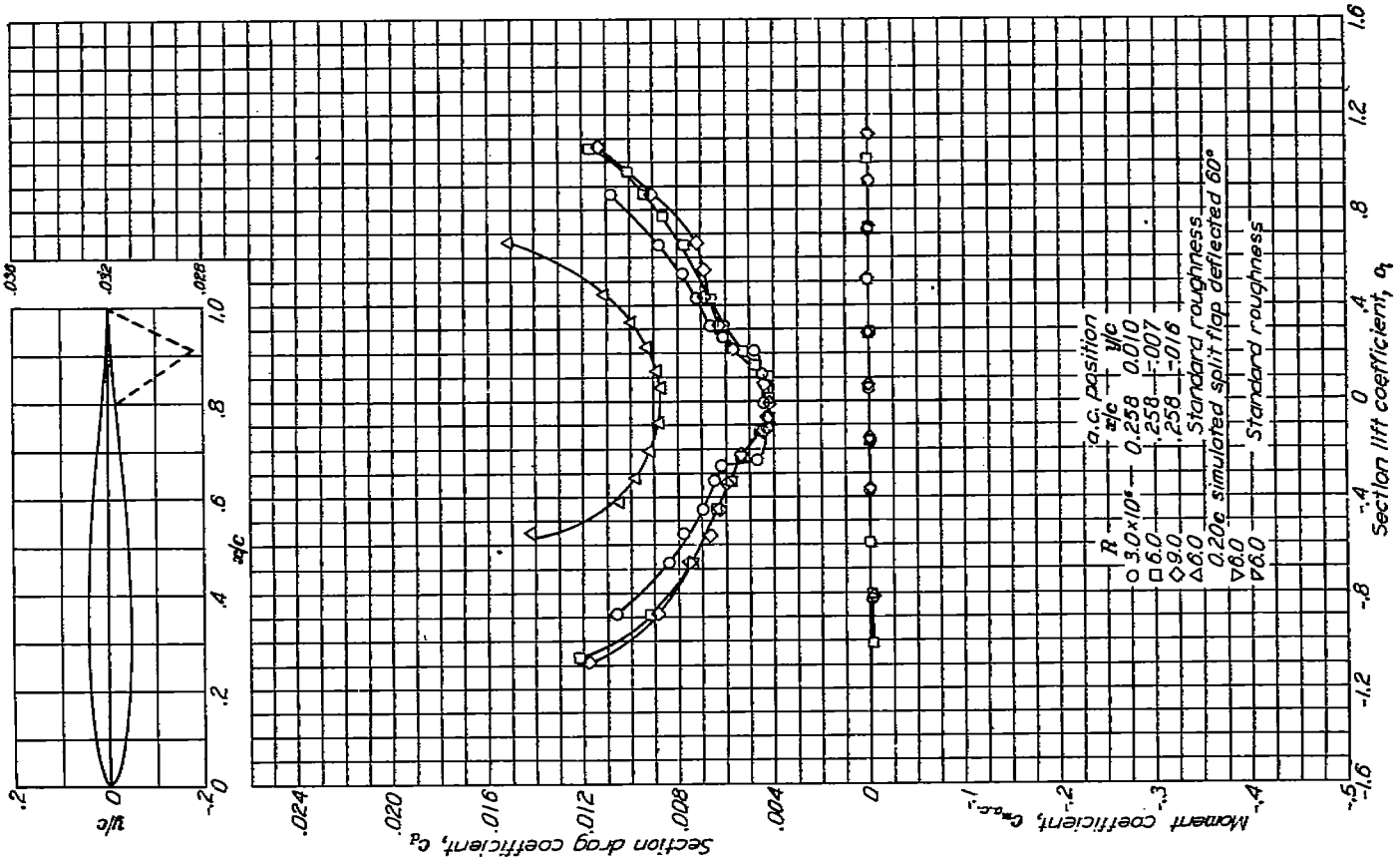

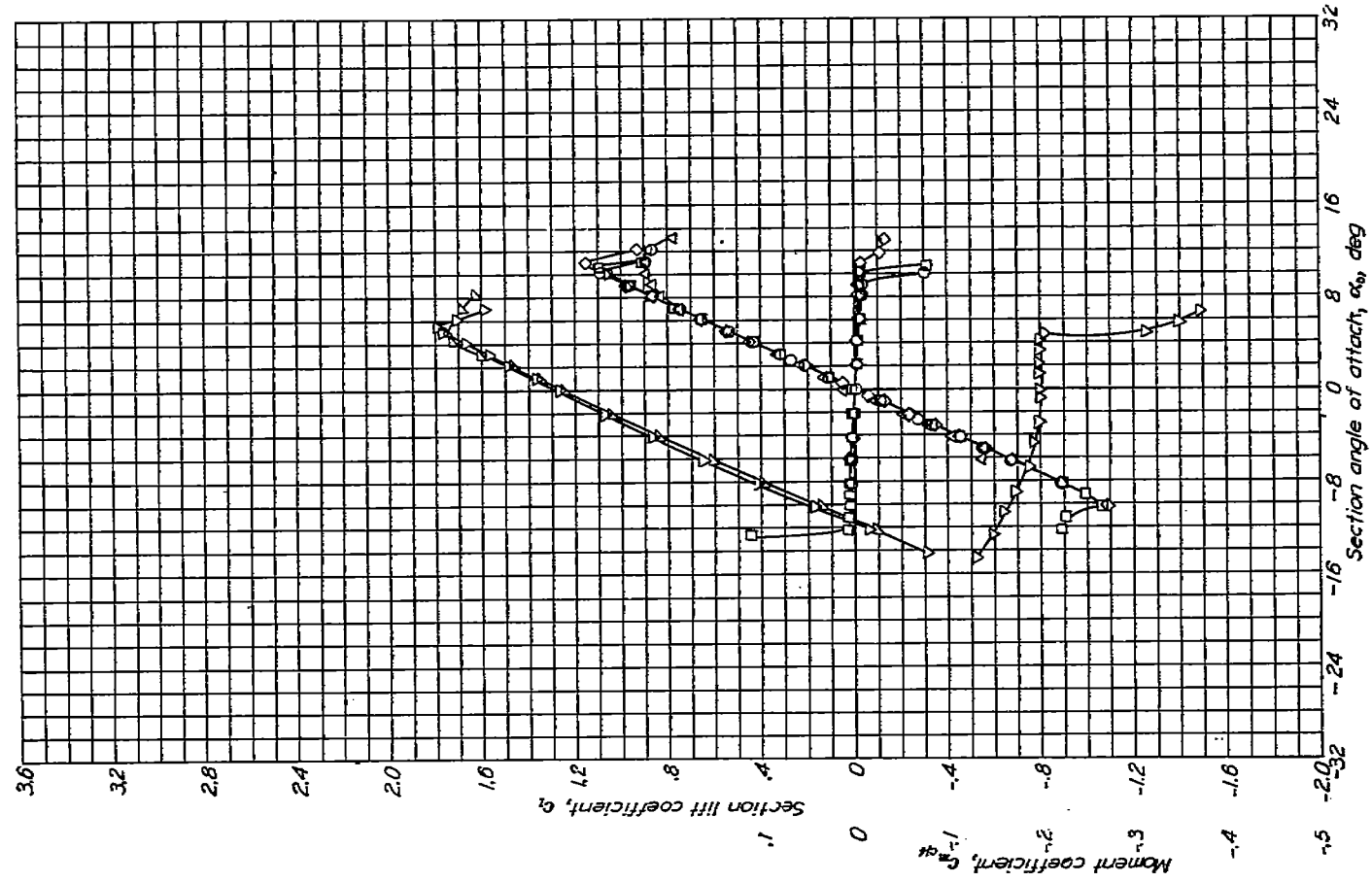

Aerodynamic characteristics of the NACA 63-009 airfoil section, 24-inch chord.

NACA 63-206

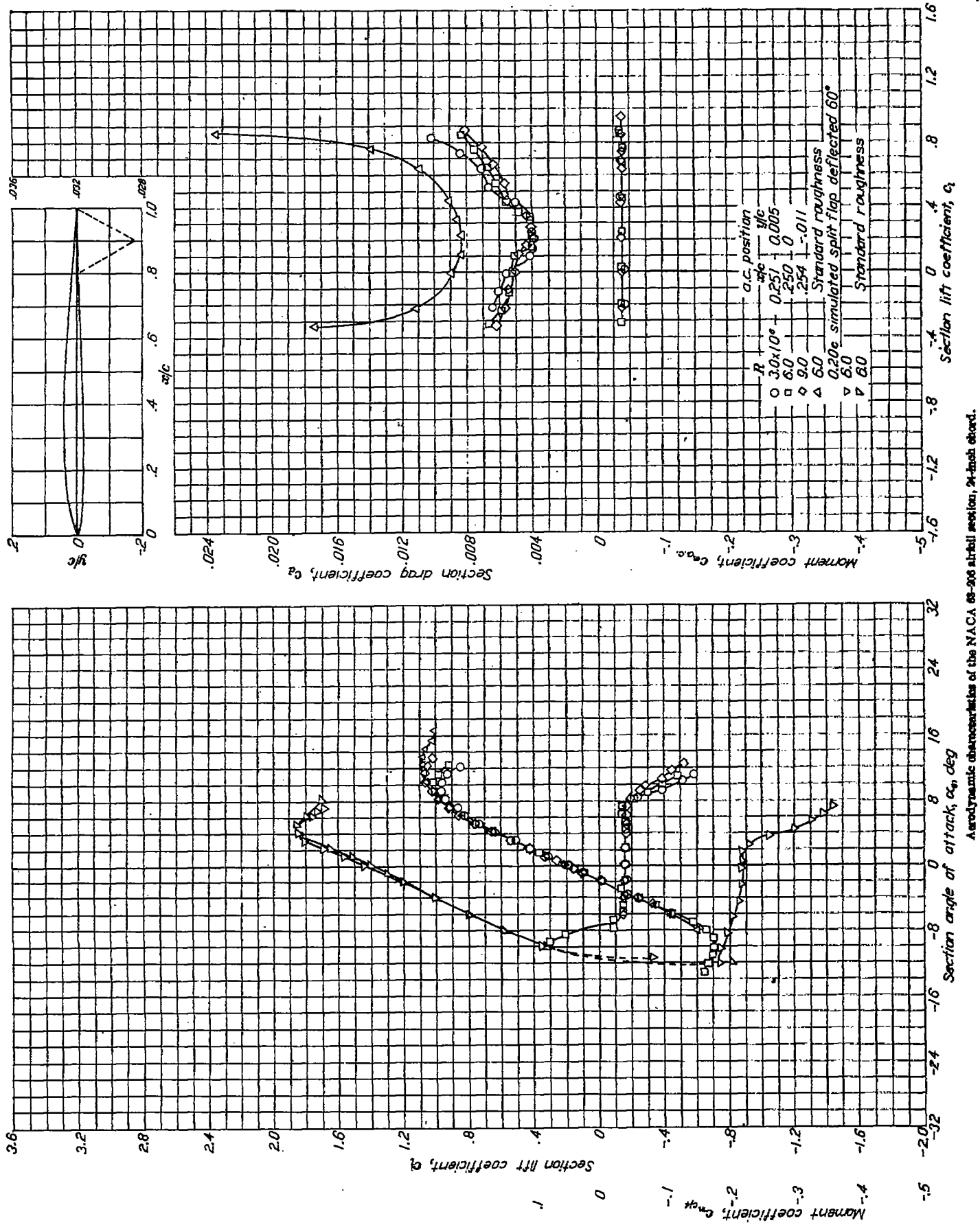

Aerodynamic characteristics of the NACA 63-206 airfoil section, 24-inch chord.

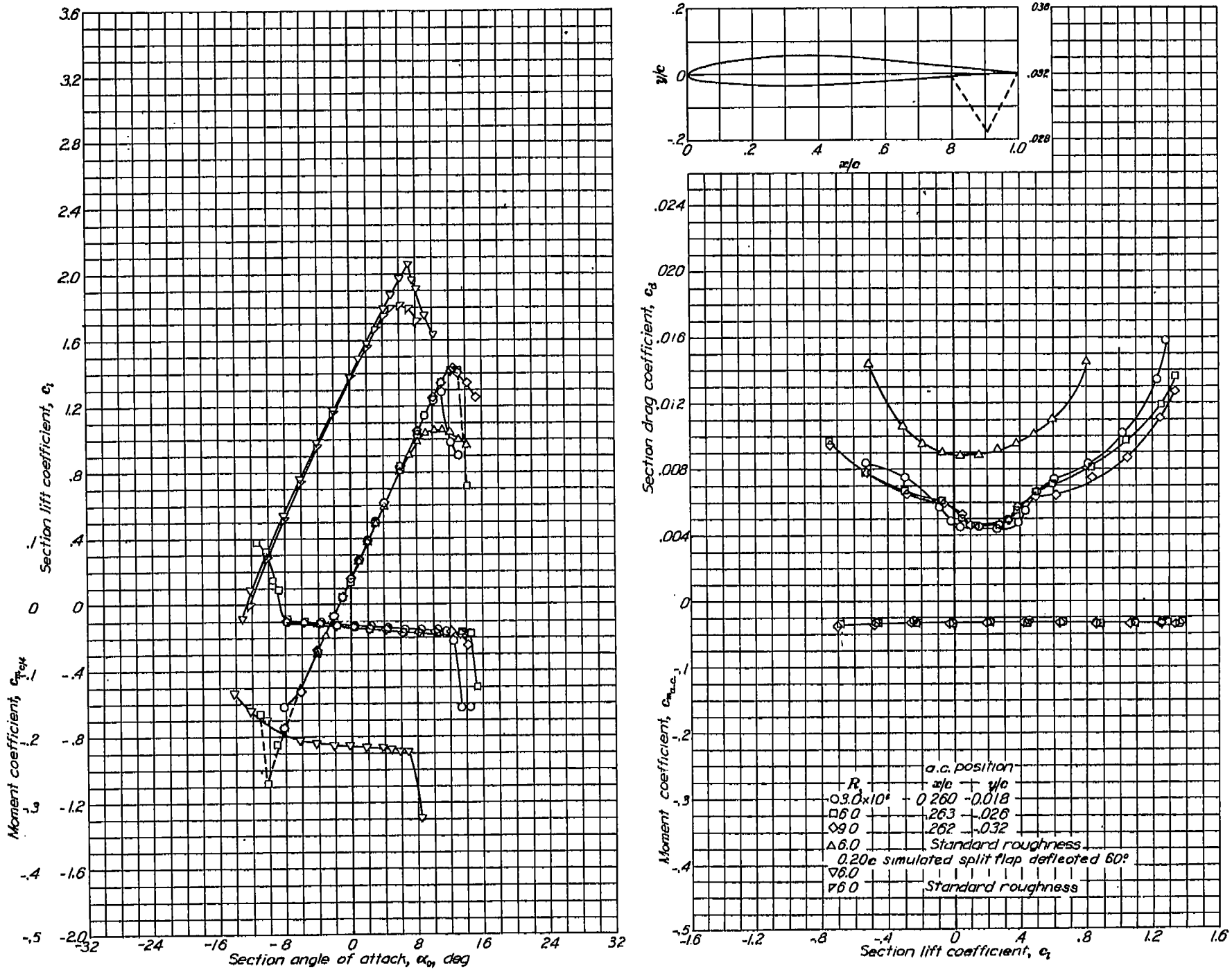

Aerodynamic characteristics of the NACA 63-209 airfoil section, 24-inch chord.

NACA 63-210

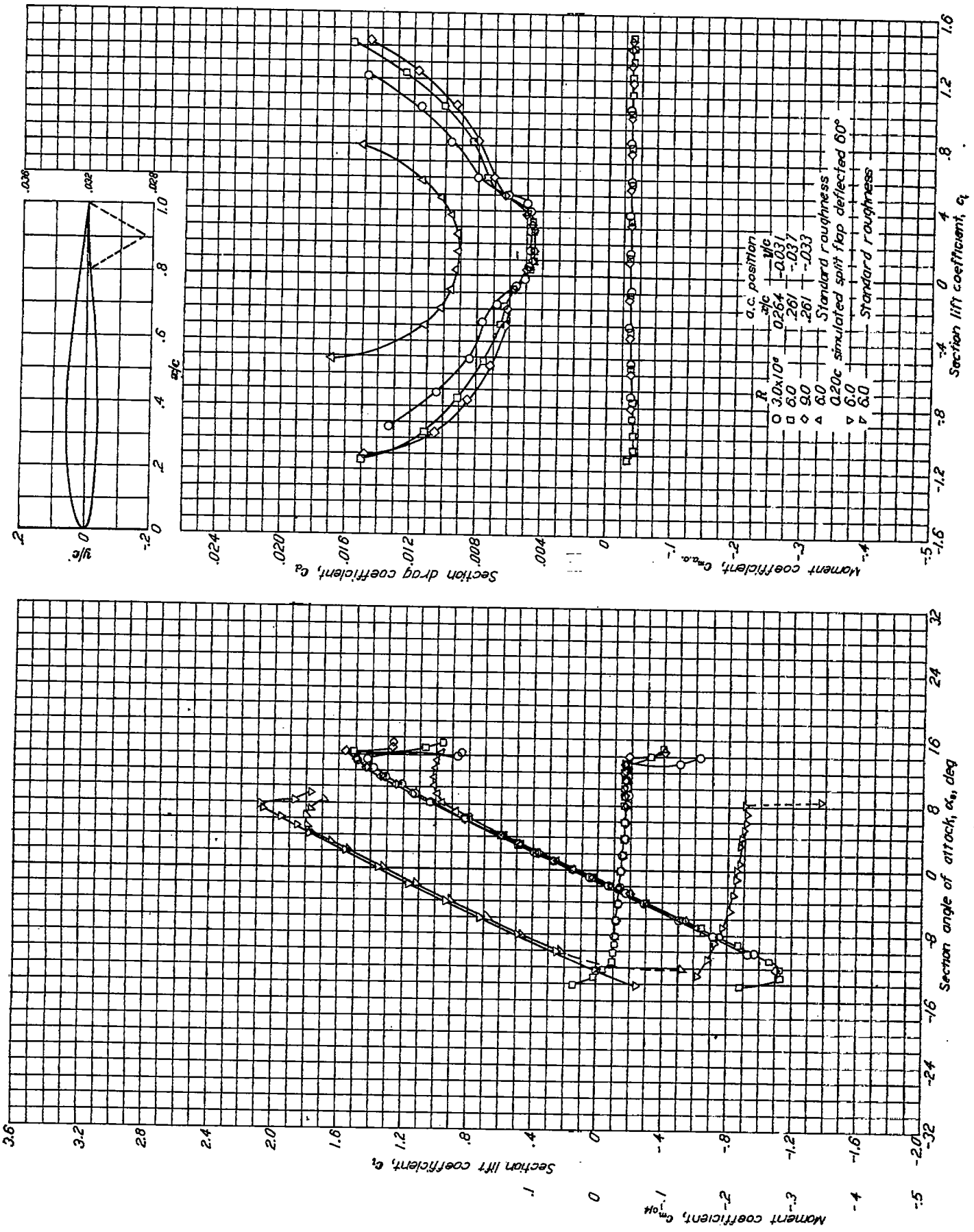

Aerodynamic characteristics of the NACA 63-210 airfoil section, 24-inch chord.

NACA 631-012

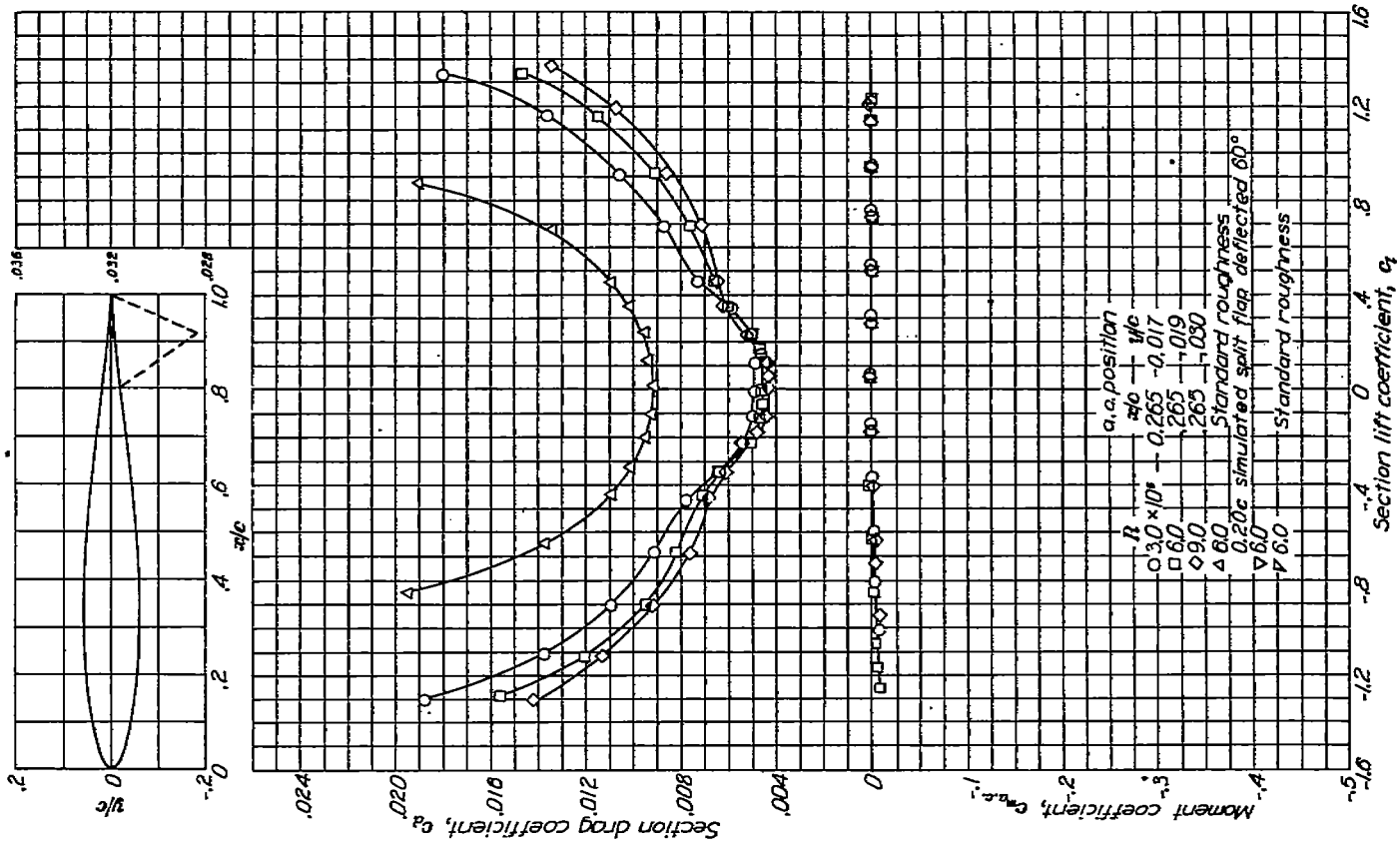

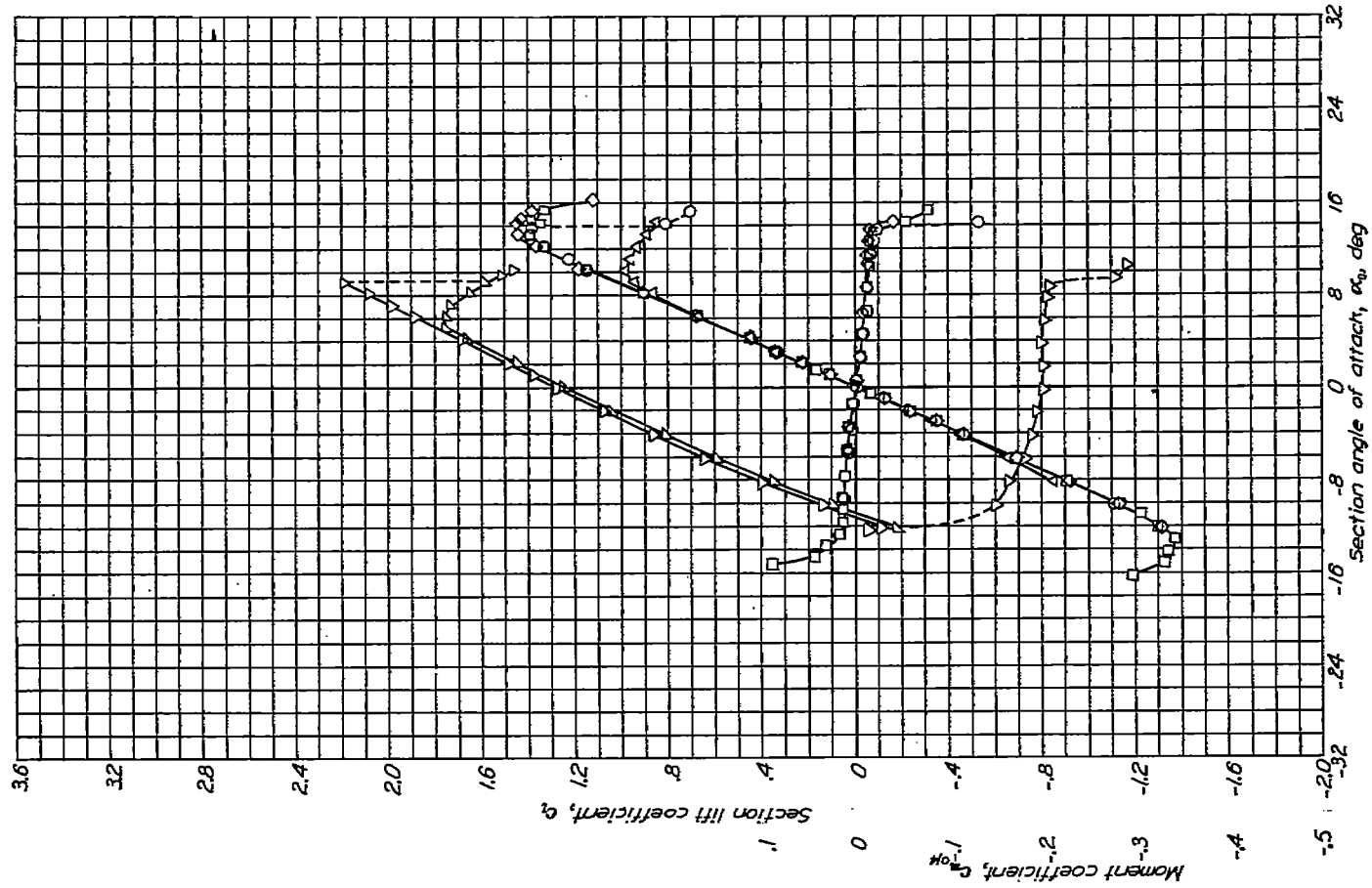

Aerodynamic characteristics of the NACA 631-012 airfoil section, 24-inch chord.

NACA 63$_1$-212

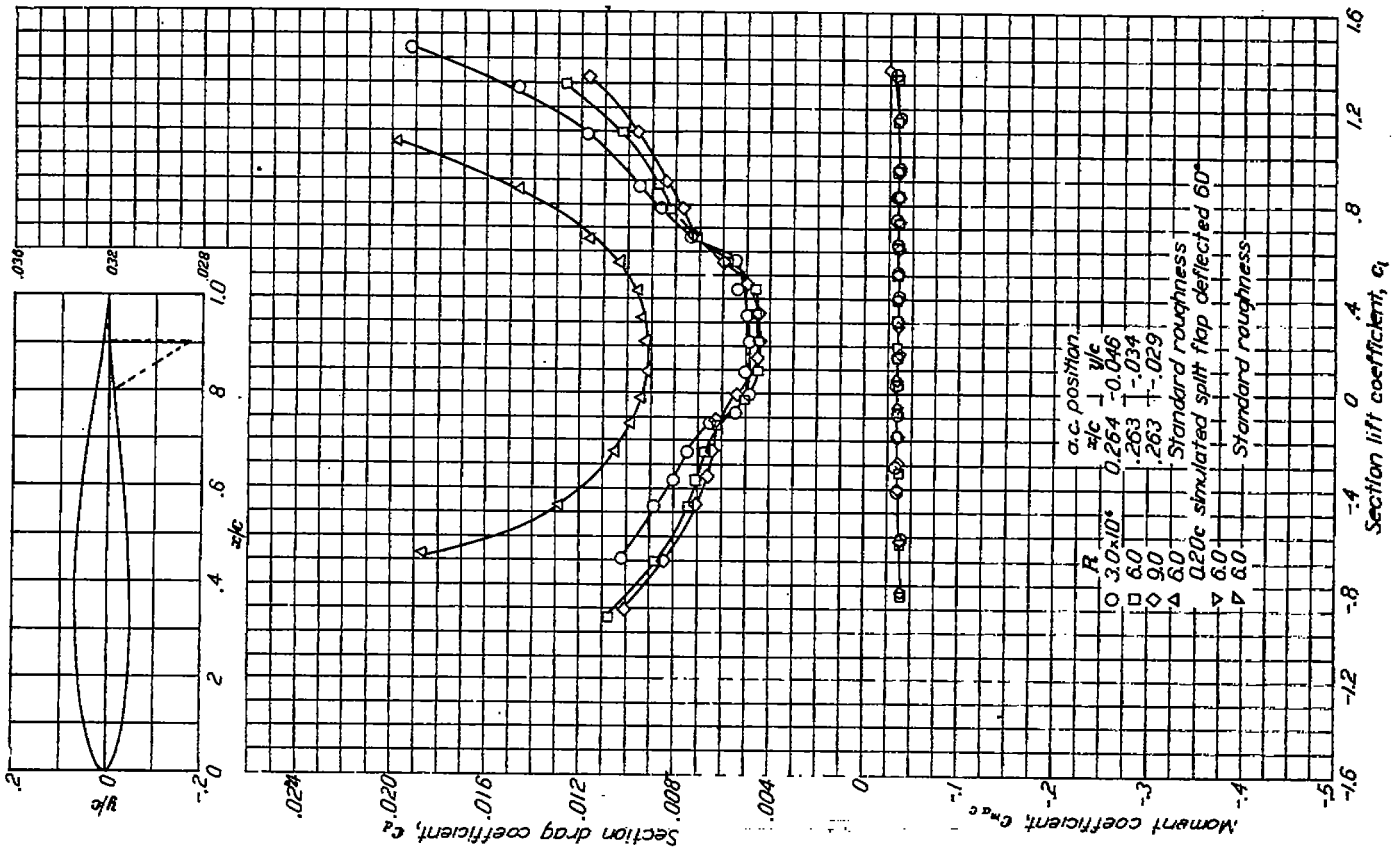

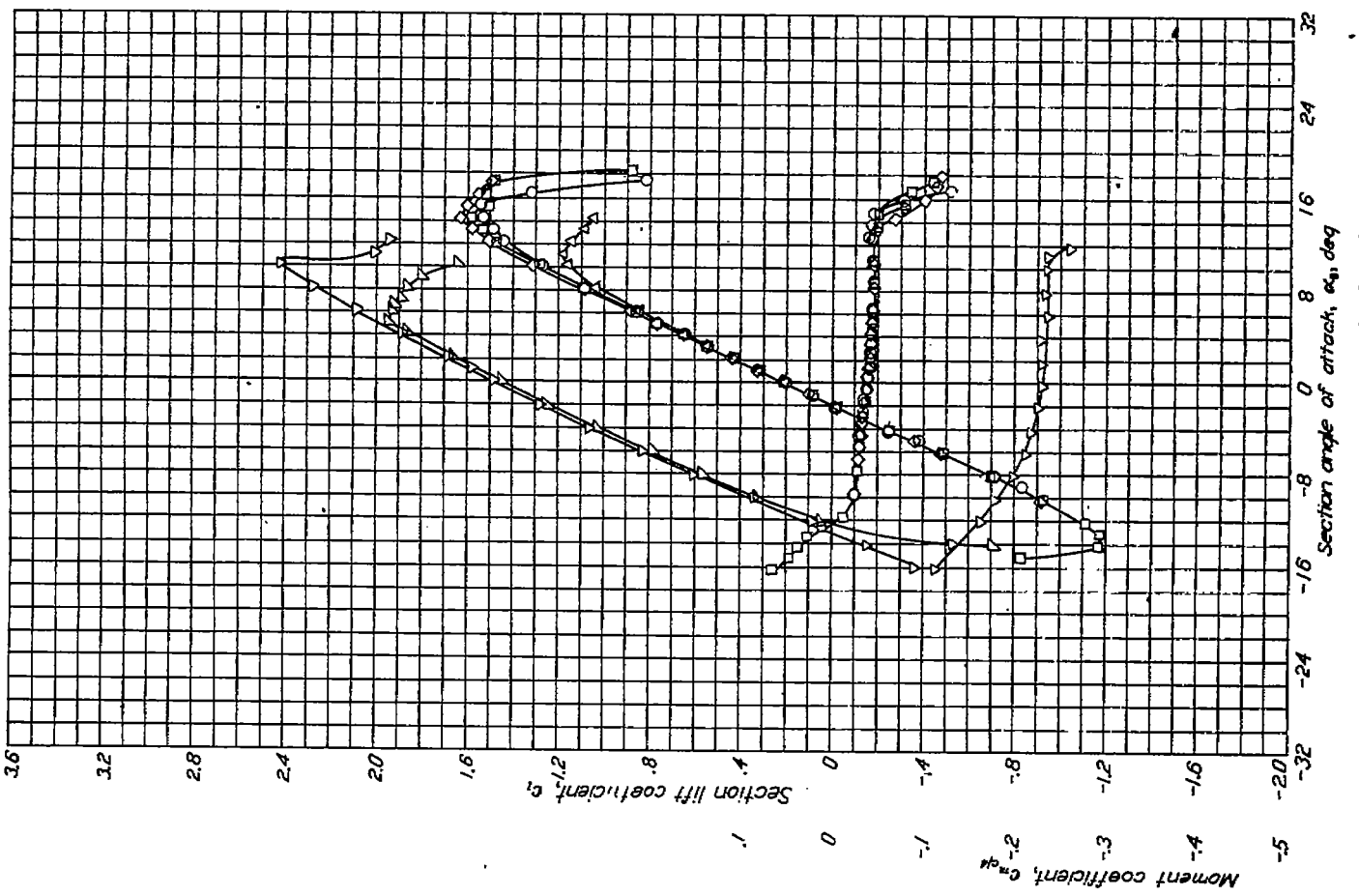

Aerodynamic characteristics of the NACA 63$_1$-212 airfoil section, 24-inch chord.

NACA 63$_1$-412

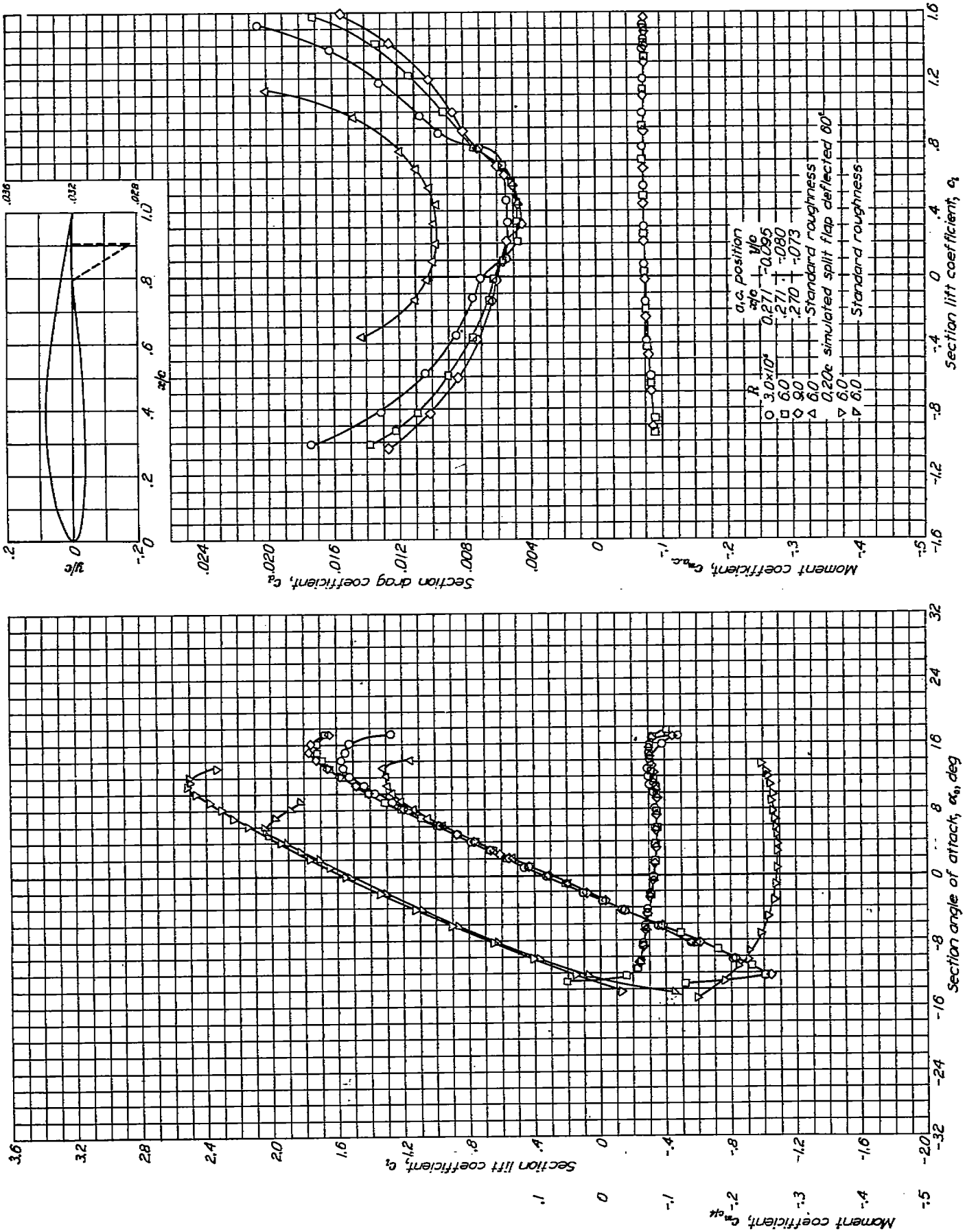

Aerodynamic characteristics of the NACA 63$_1$-412 airfoil section, 24-inch chord.

NACA 63$_2$-015

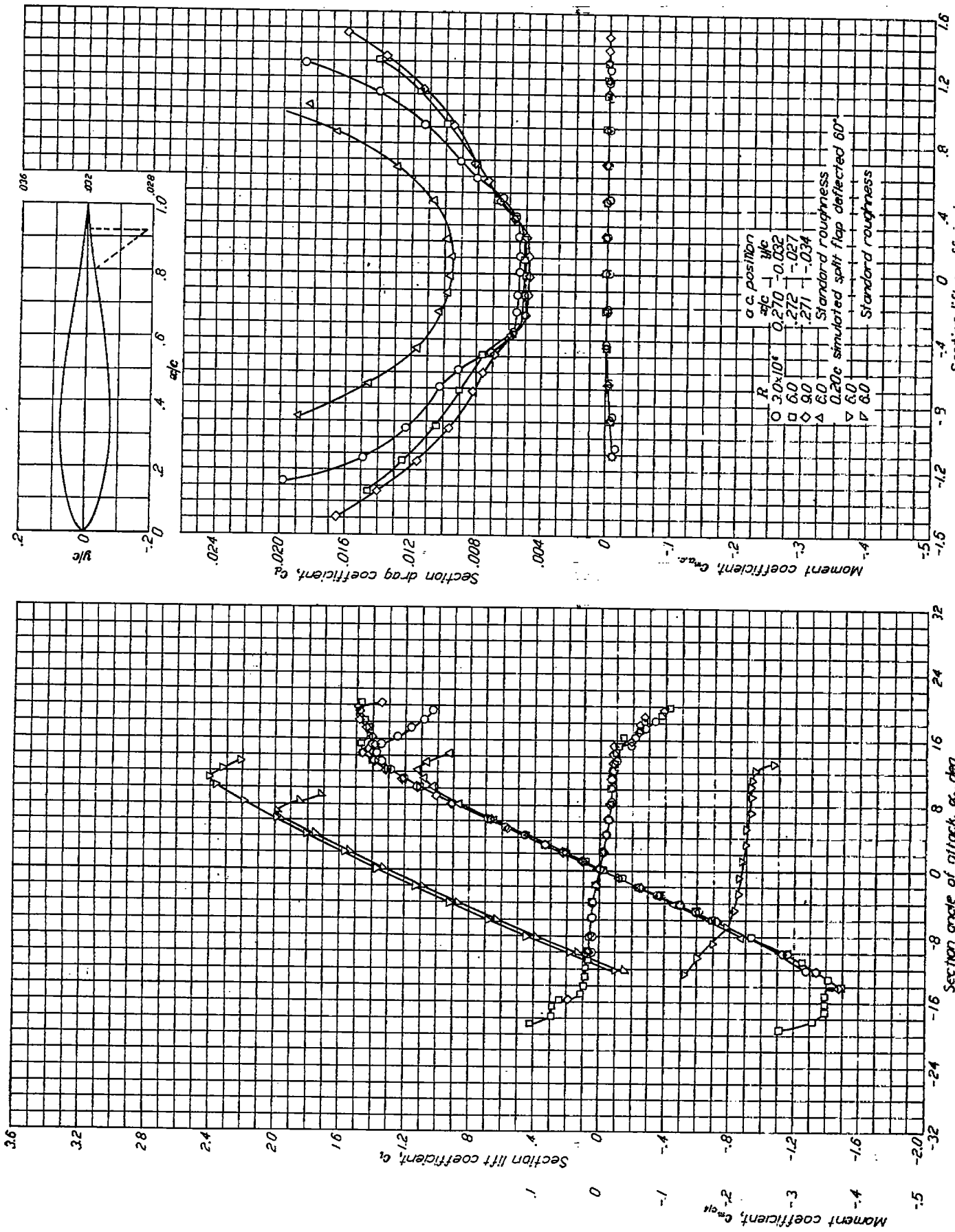

Aerodynamic characteristics of the NACA 63$_2$-015 airfoil section, 24-inch chord.

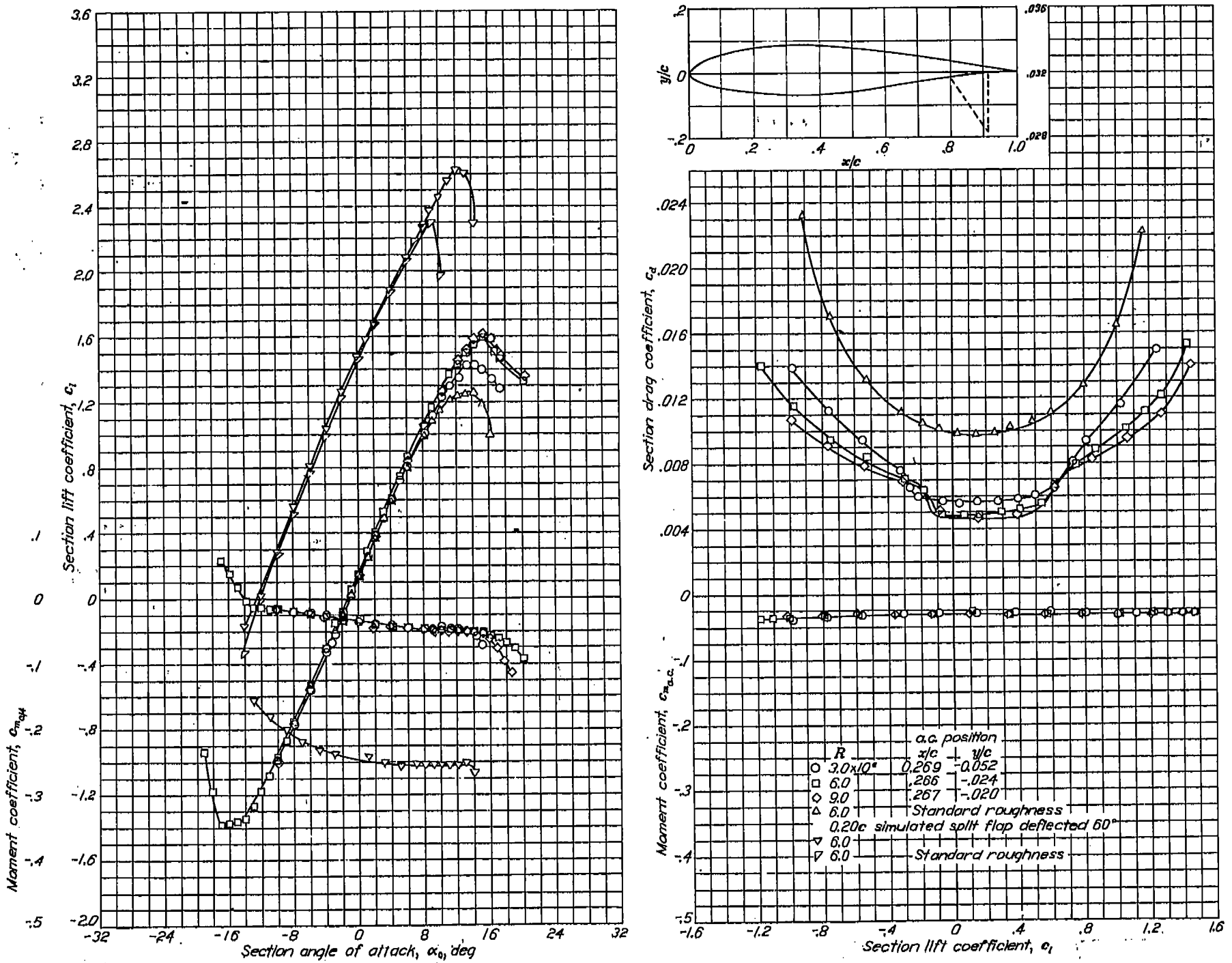

Aerodynamic characteristics of the NACA 63$_3$-215 airfoil section, 24-inch chord.

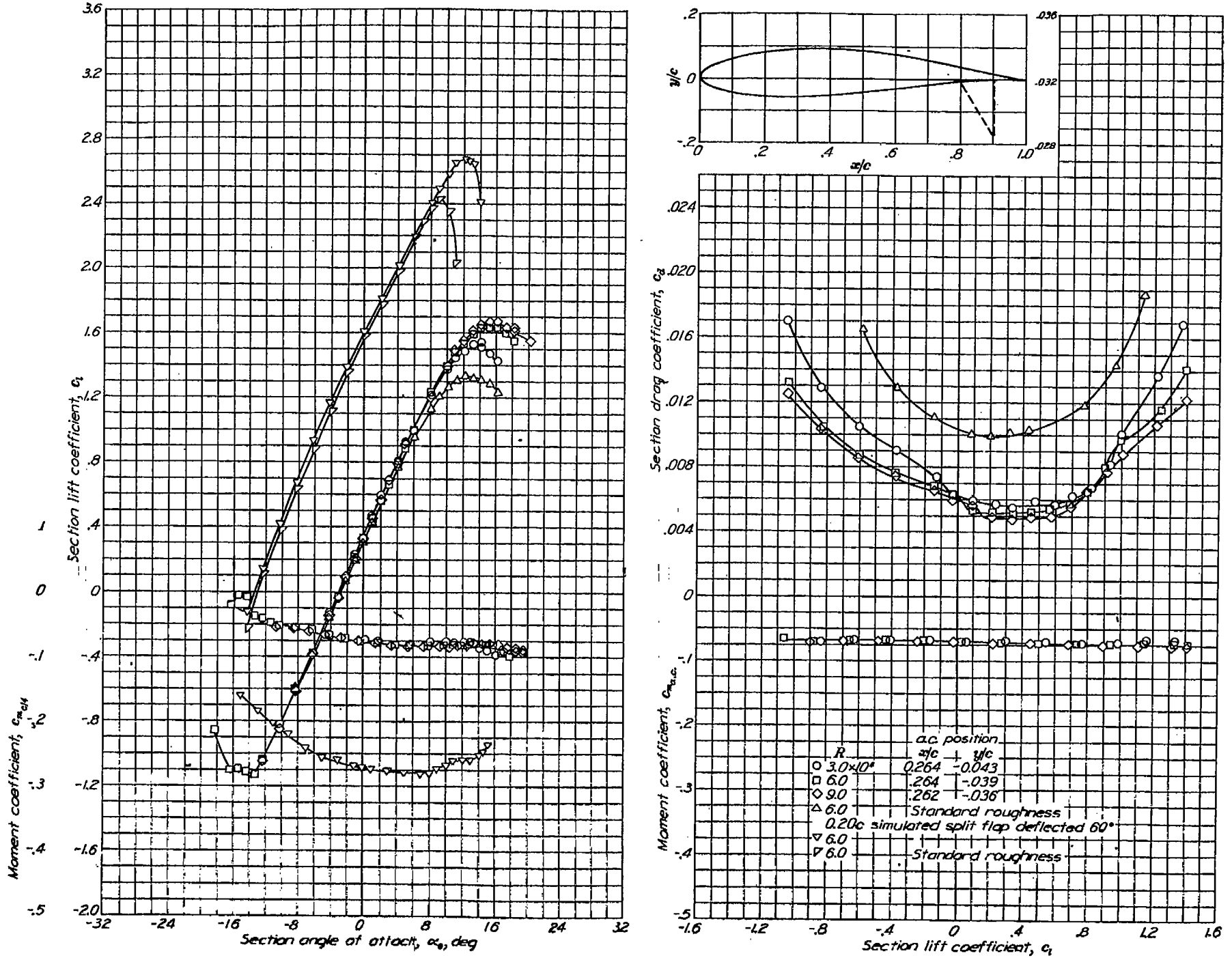

Aerodynamic characteristics of the NACA 63₃-415 airfoil section. 24-inch chord.

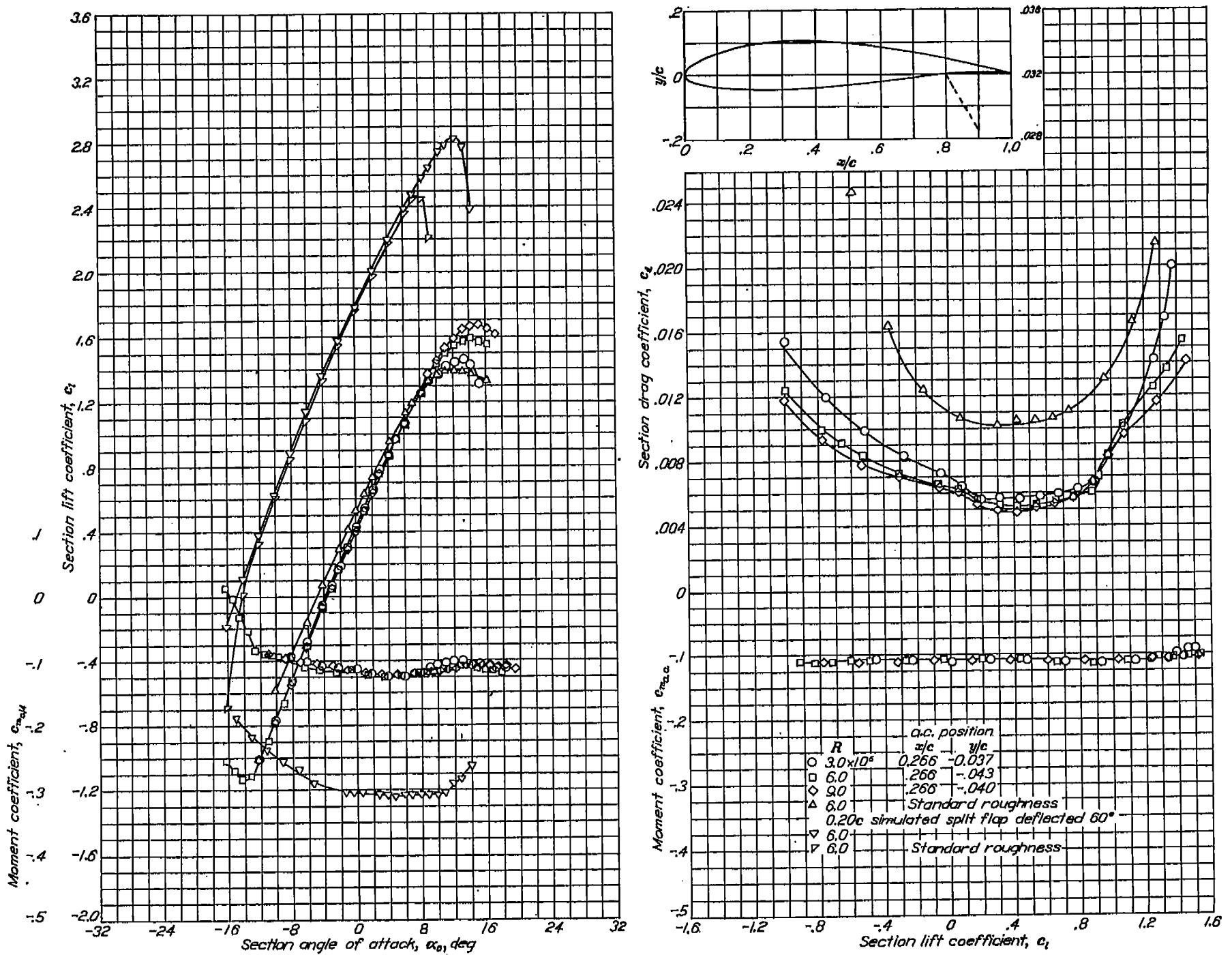

Aerodynamic characteristics of the NACA 63₂-615 airfoil section, 24-inch chord.

NACA 63$_3$-018

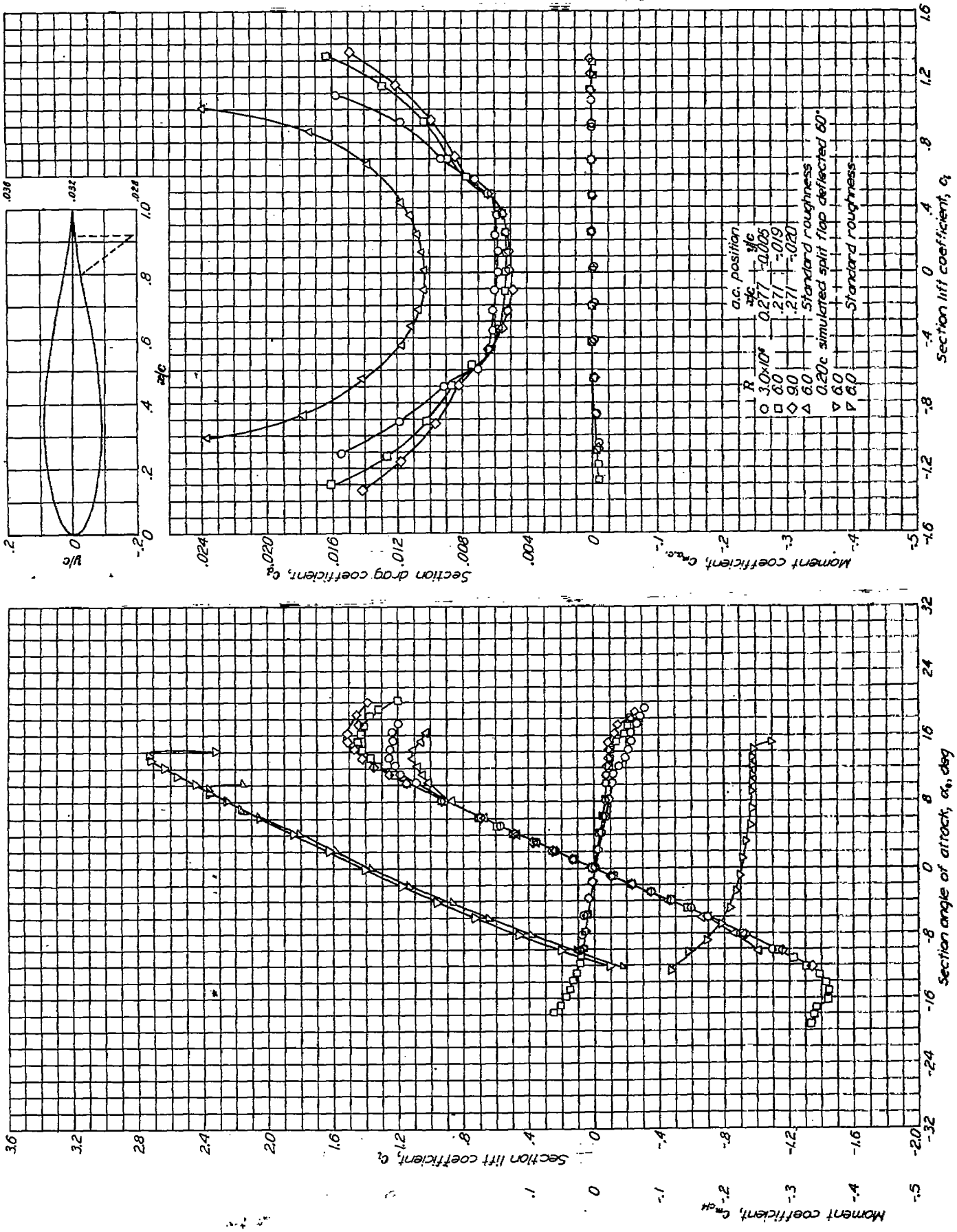

Aerodynamic characteristics of the NACA 63$_3$-018 airfoil section, 24-inch chord.

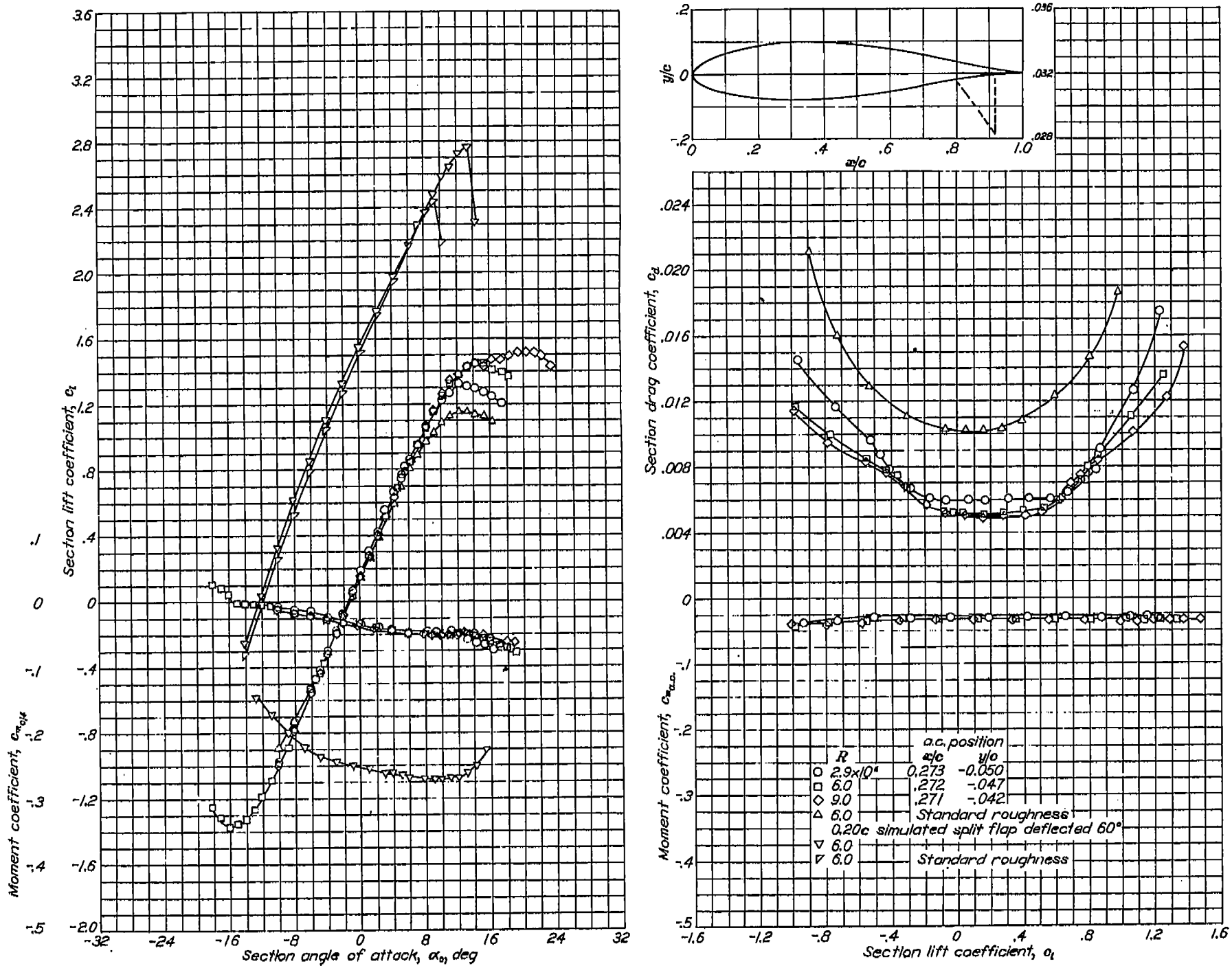

Aerodynamic characteristics of the NACA 63₃-218 airfoil section, 24-inch chord.

NACA 63$_3$-418

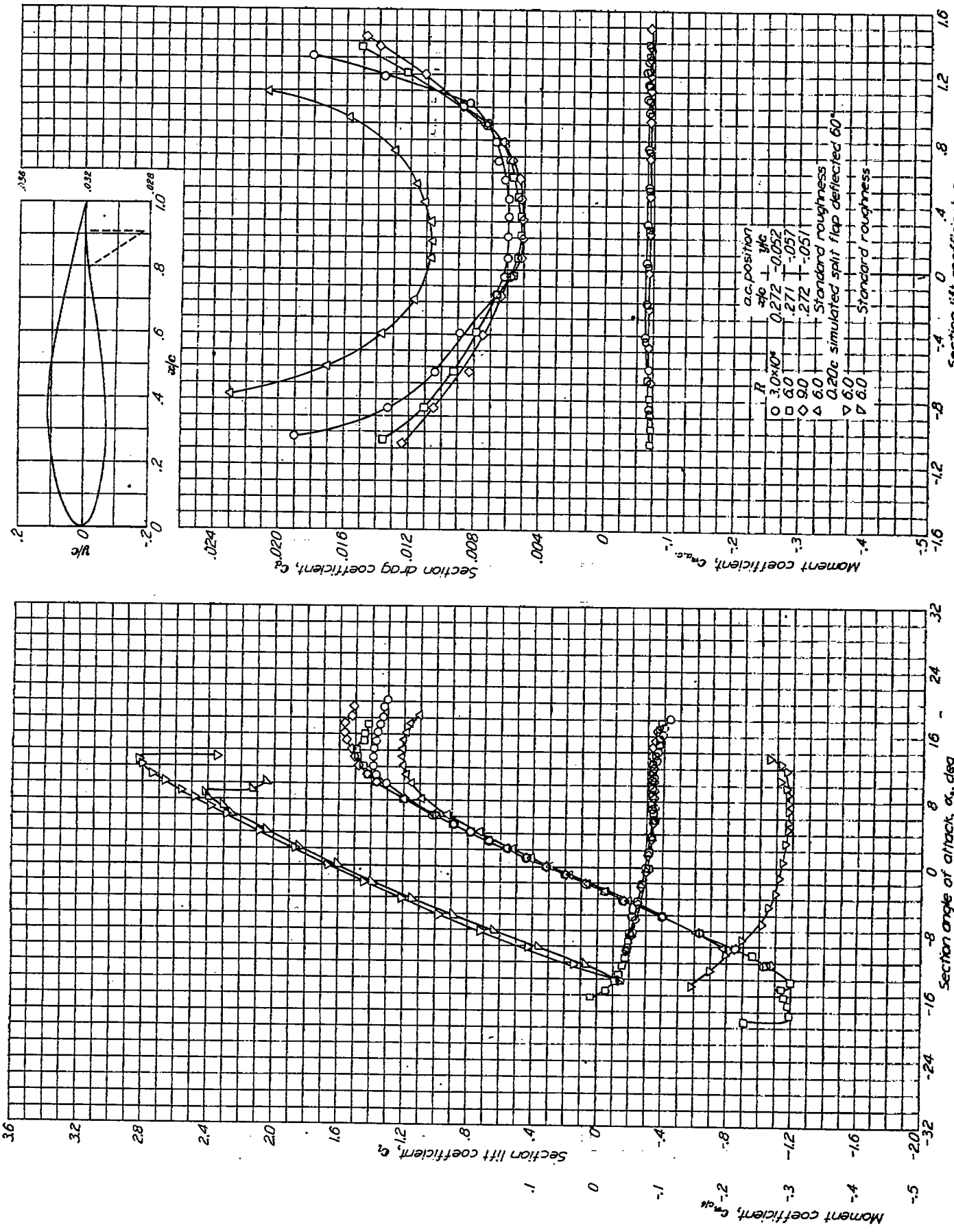

Aerodynamic characteristics of the NACA 63$_3$-418 airfoil section, 24-inch chord.

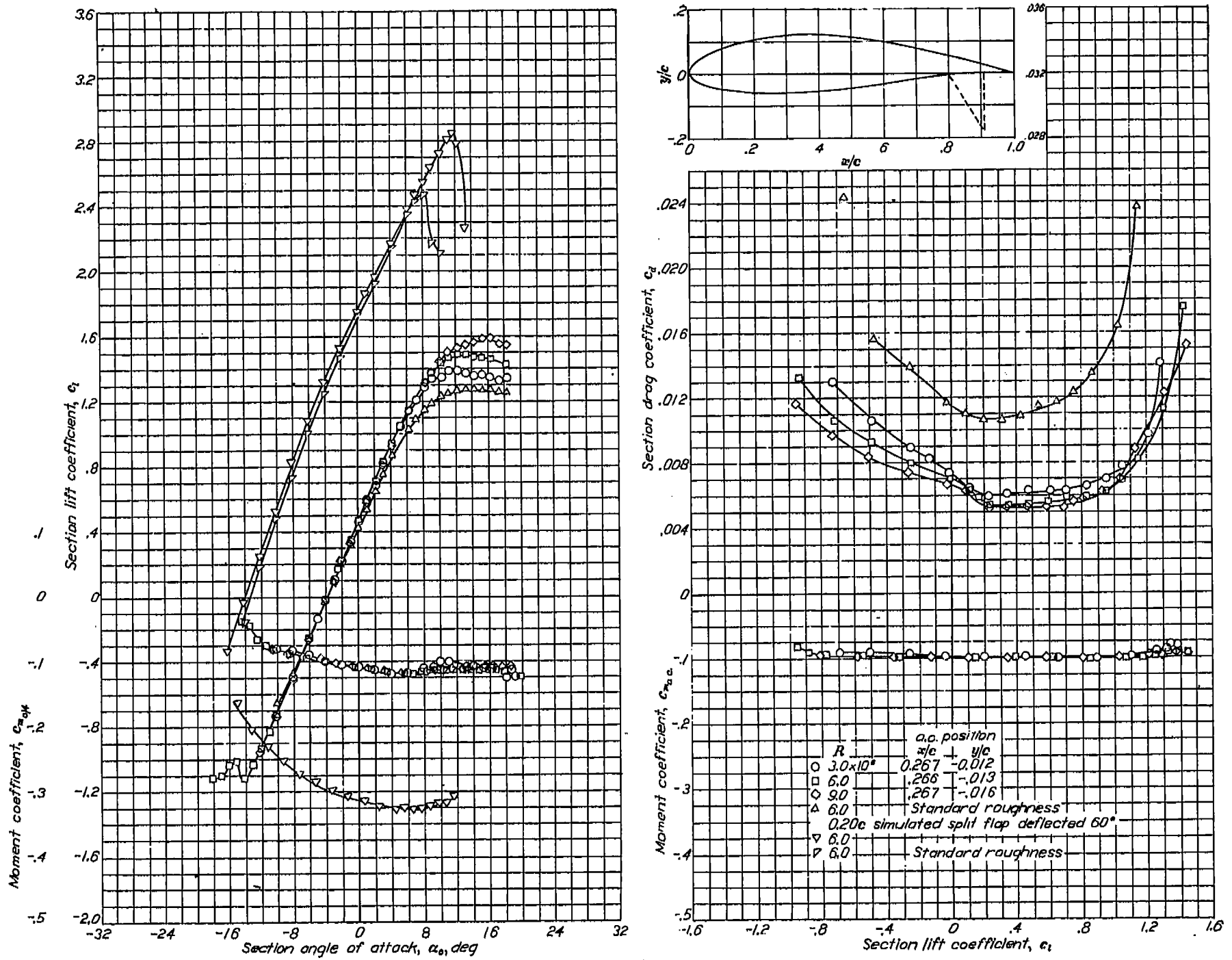

Aerodynamic characteristics of the NACA 633-618 airfoil section, 24-inch chord.

NACA 63$_4$-021

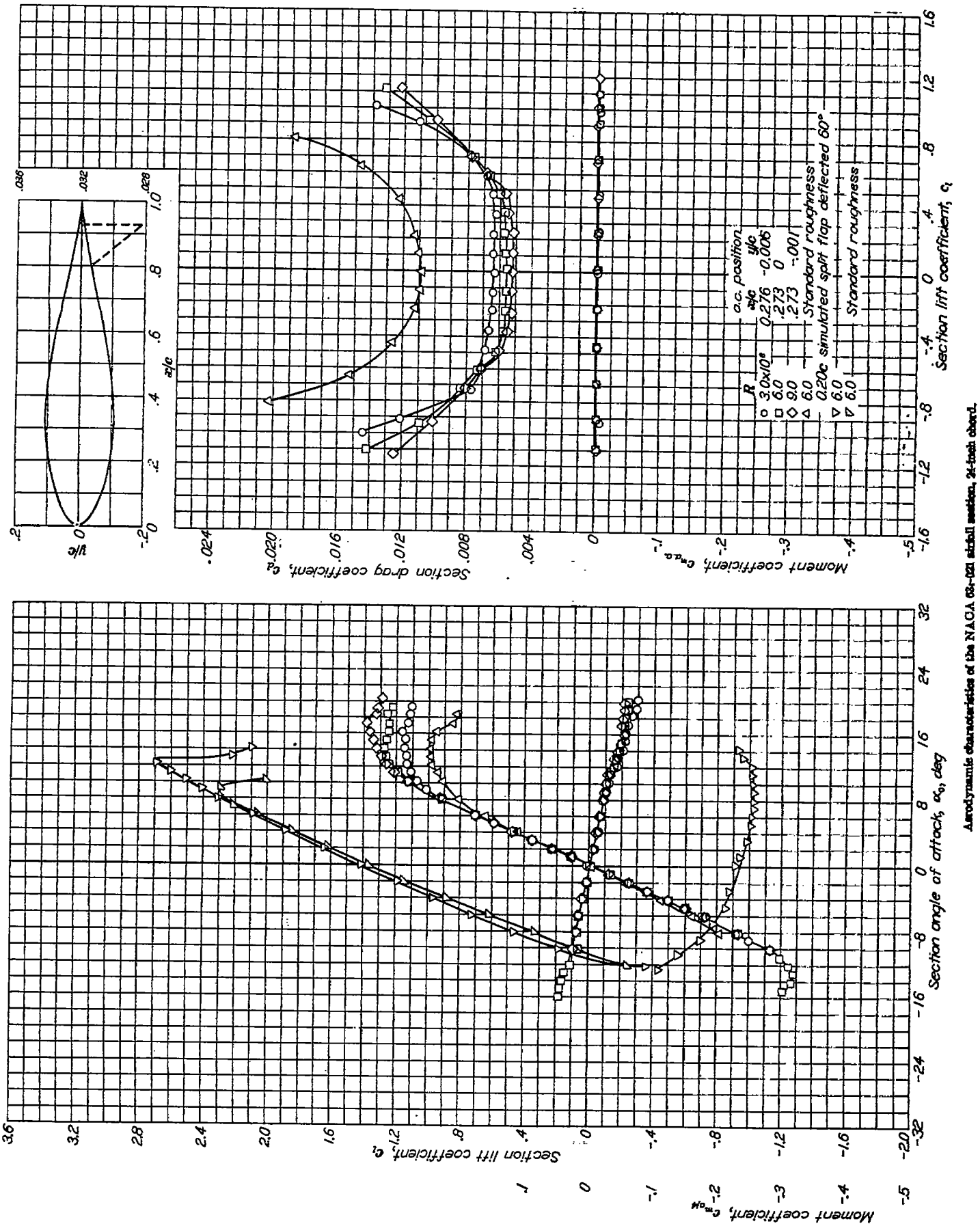

Aerodynamic characteristics of the NACA 63-021 airfoil section, 24-inch chord.

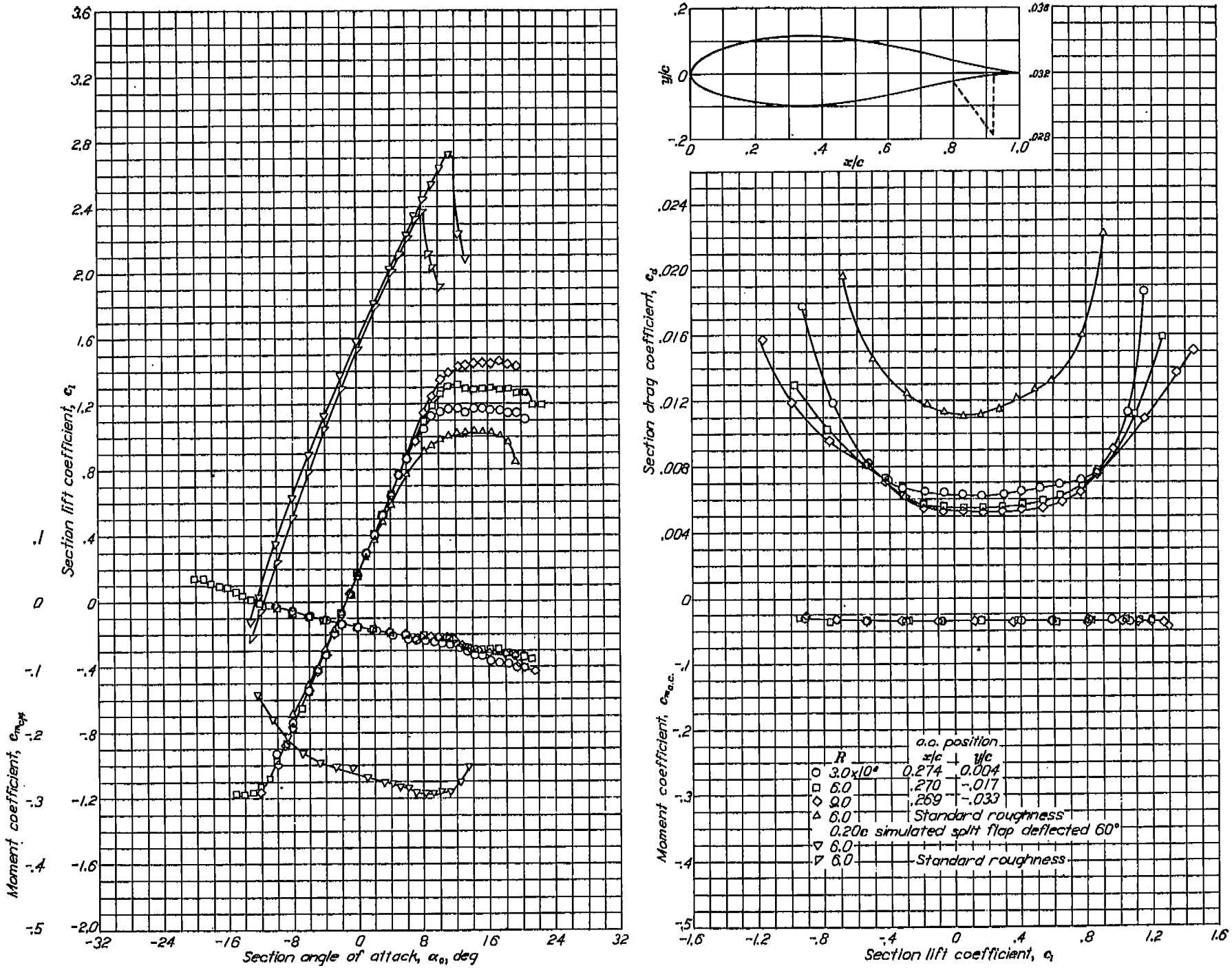

Aerodynamic characteristics of the NACA 63₄-221 airfoil section, 24-inch chord.

NACA 63$_4$-421

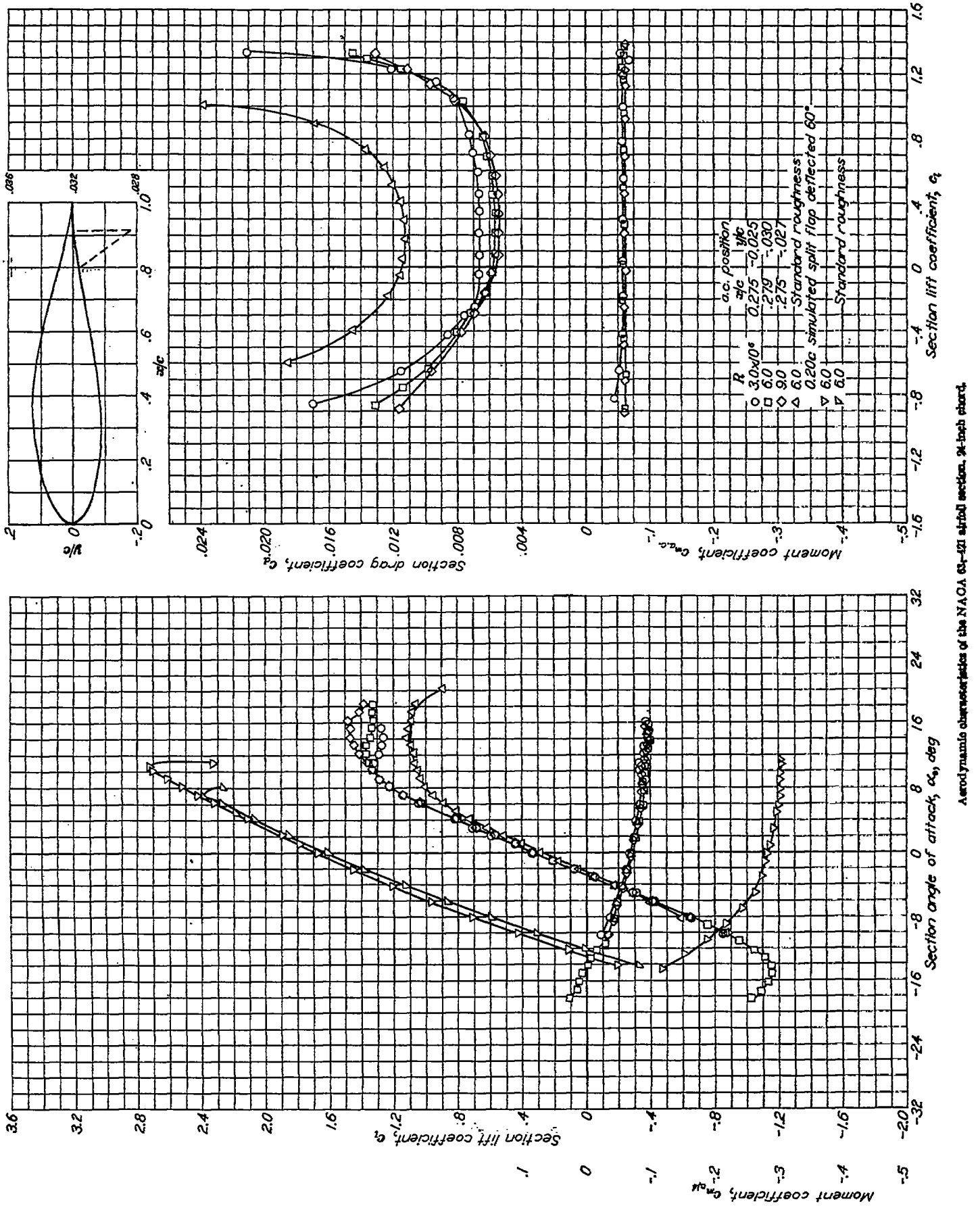

Aerodynamic characteristics of the NACA 63$_4$-421 airfoil section. 24-inch chord.

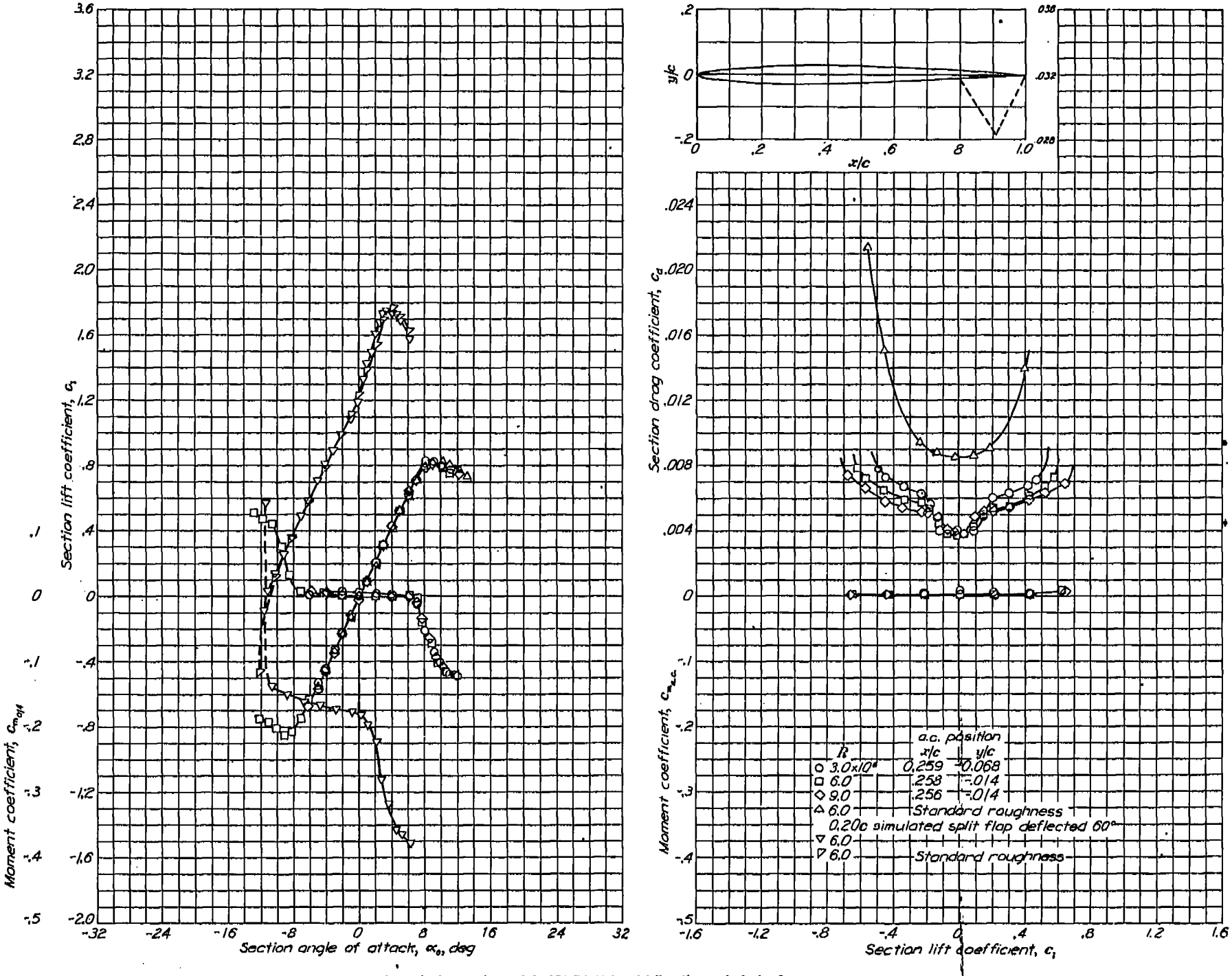

Aerodynamic characteristics of the NACA 64-006 airfoil section, 24-inch chord.

NACA 64-009

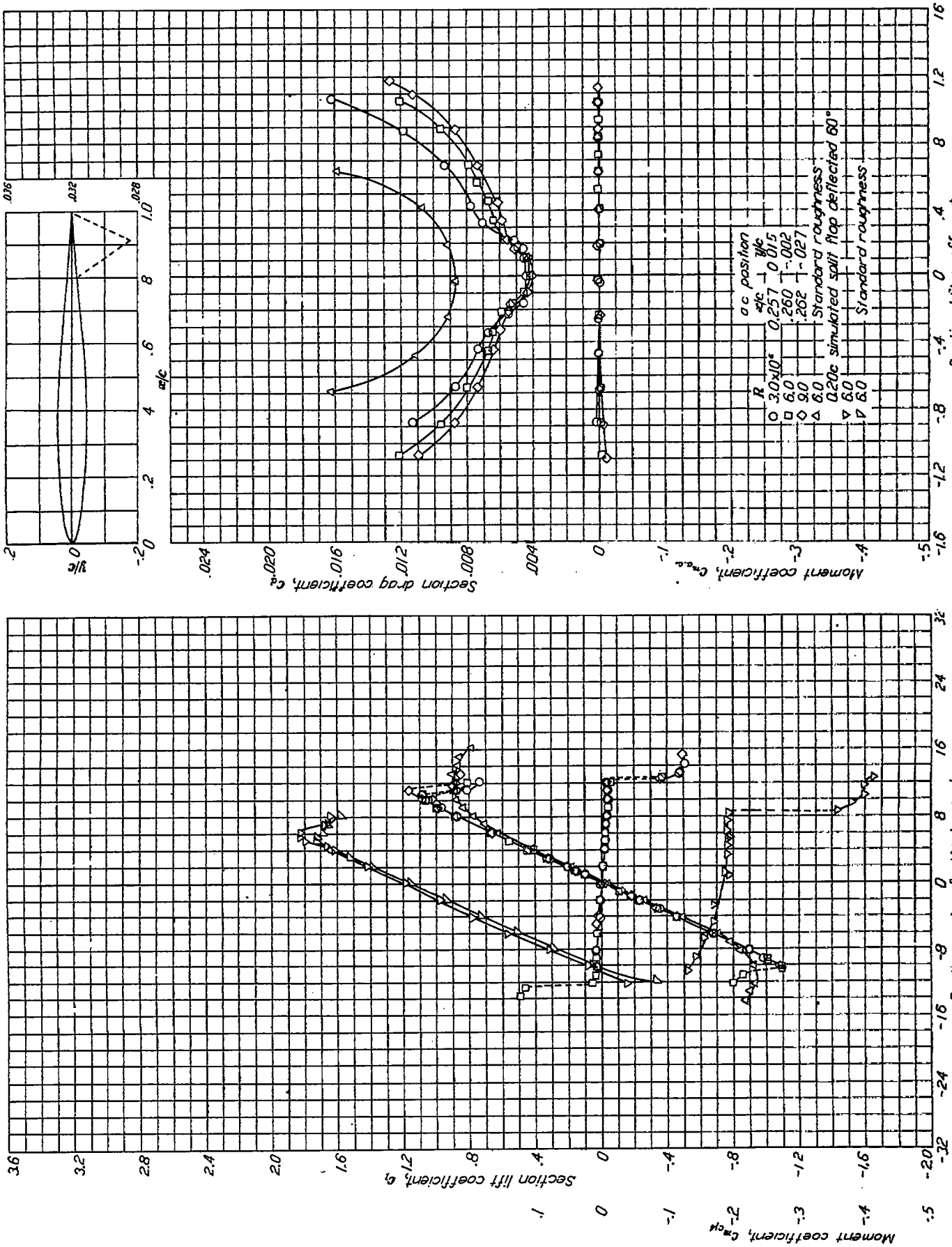

Aerodynamic characteristics of the NACA 64-009 airfoil section, 24-inch chord.

NACA 64-108

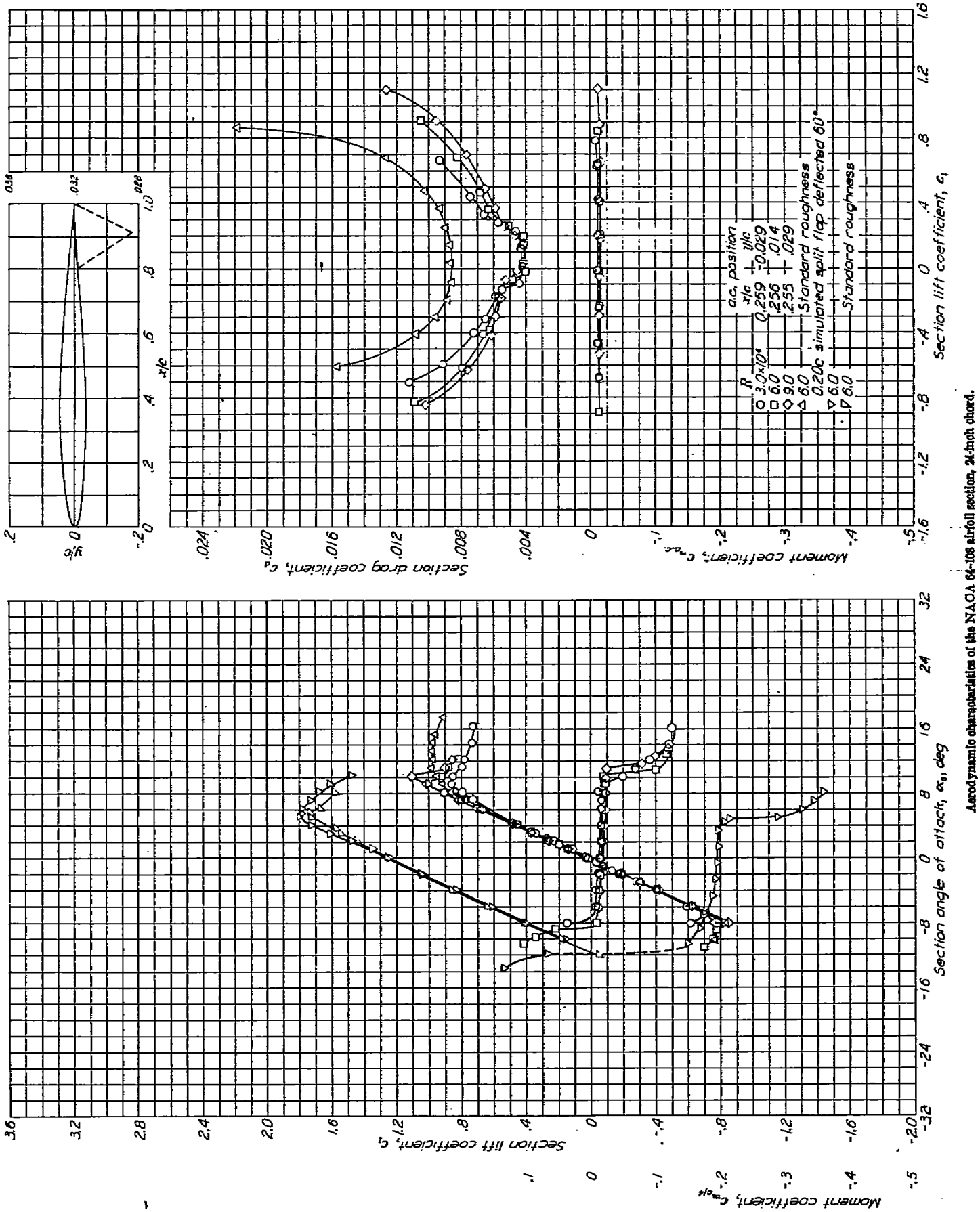

Aerodynamic characteristics of the NACA 64-108 airfoil section, 24-inch chord.

NACA 64-110

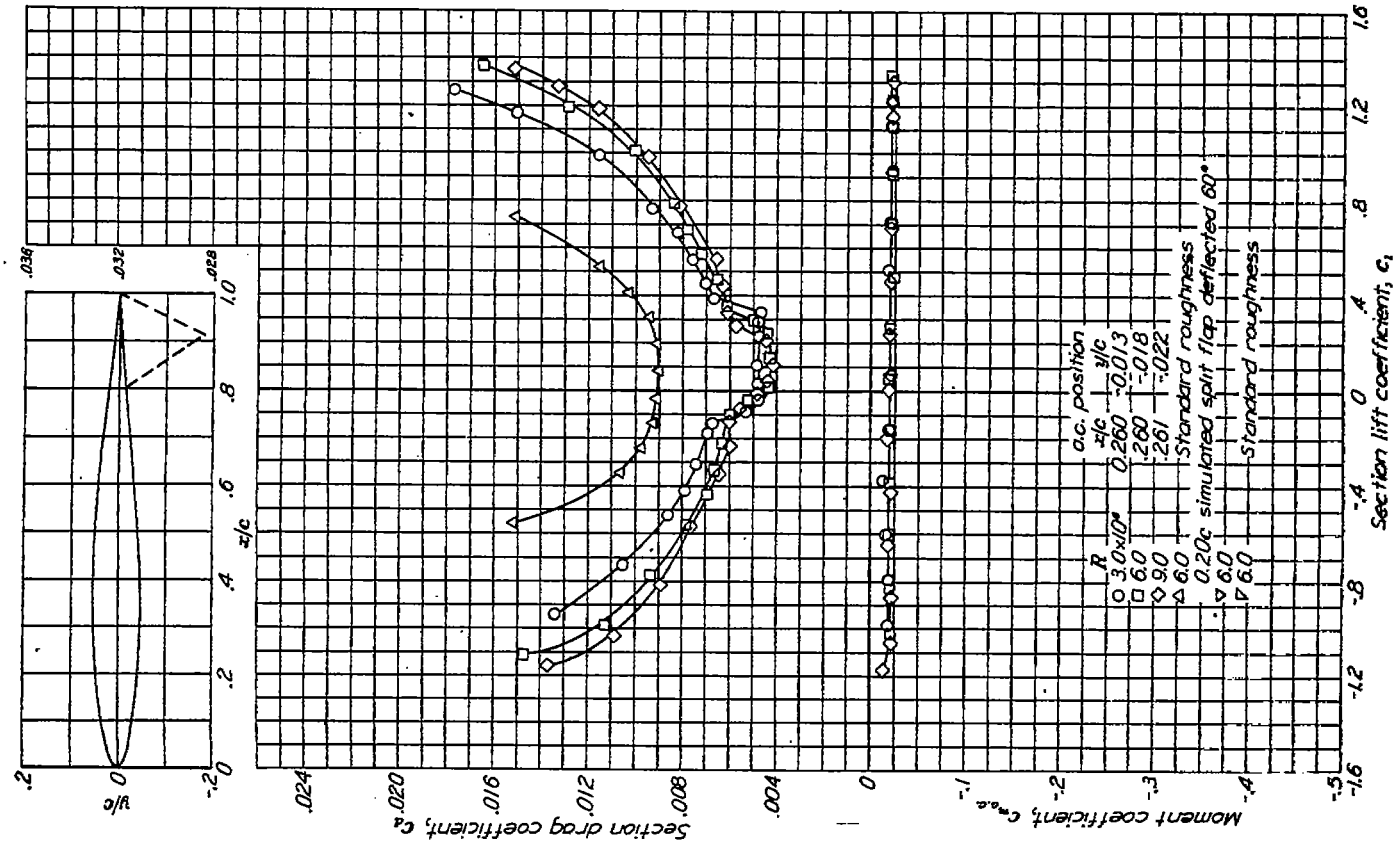

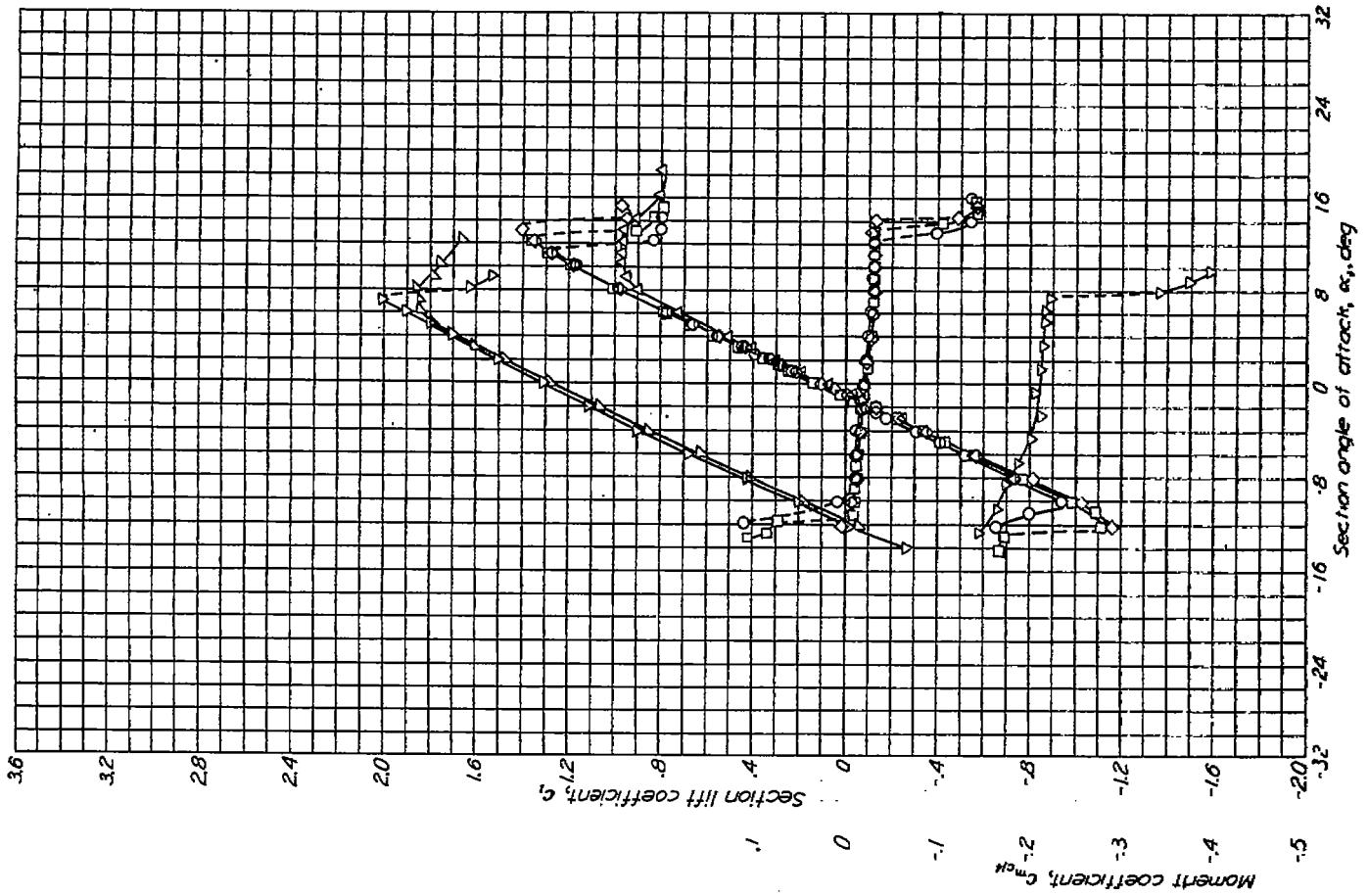

Aerodynamic characteristics of the NACA 64-110 airfoil section, 24-inch chord.

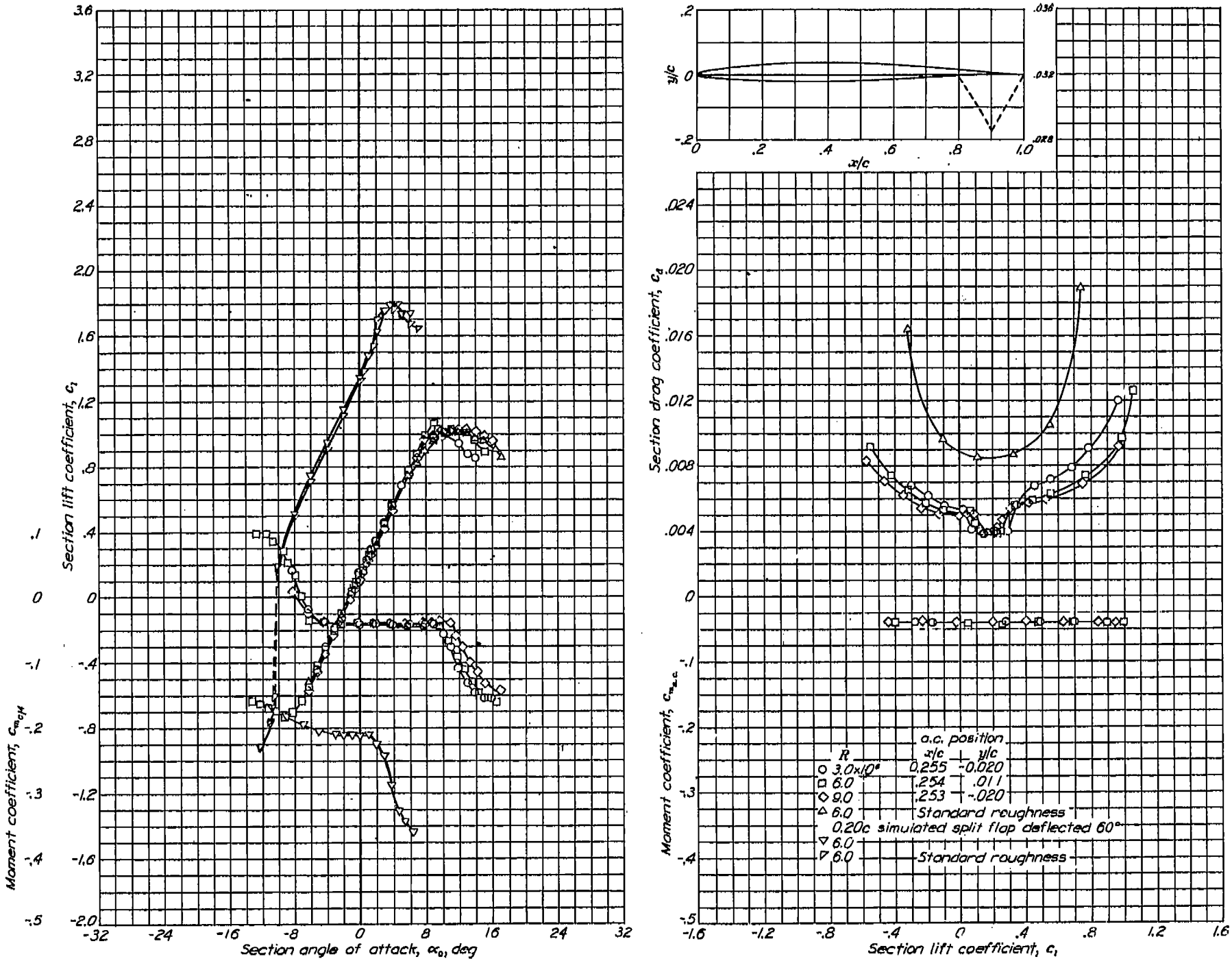

Aerodynamic characteristics of the NACA 64-206 airfoil section, 24-inch chord.

NACA 64-208

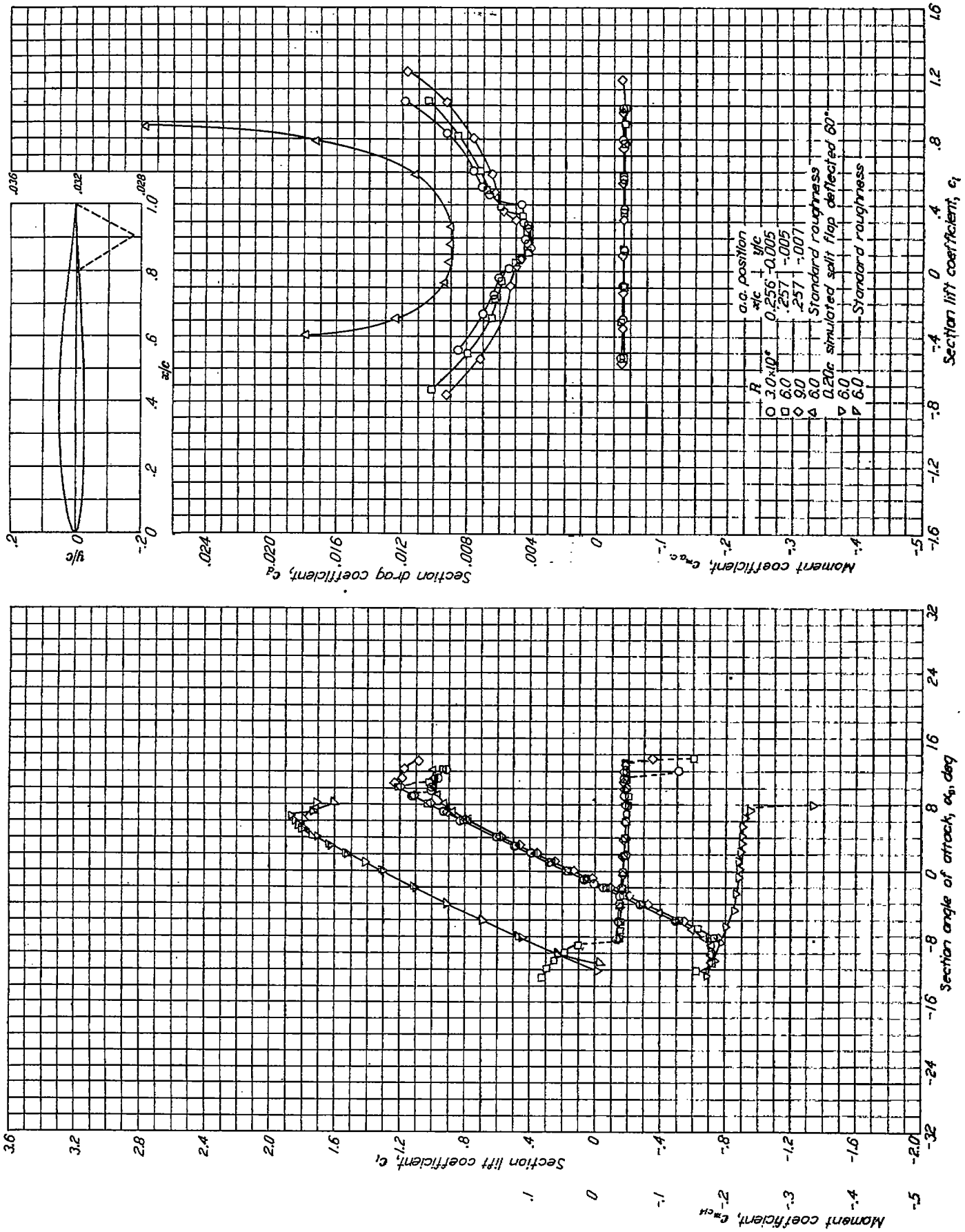

Aerodynamic characteristics of the NACA 64-208 airfoil section, 24-inch chord.

NACA 64-209

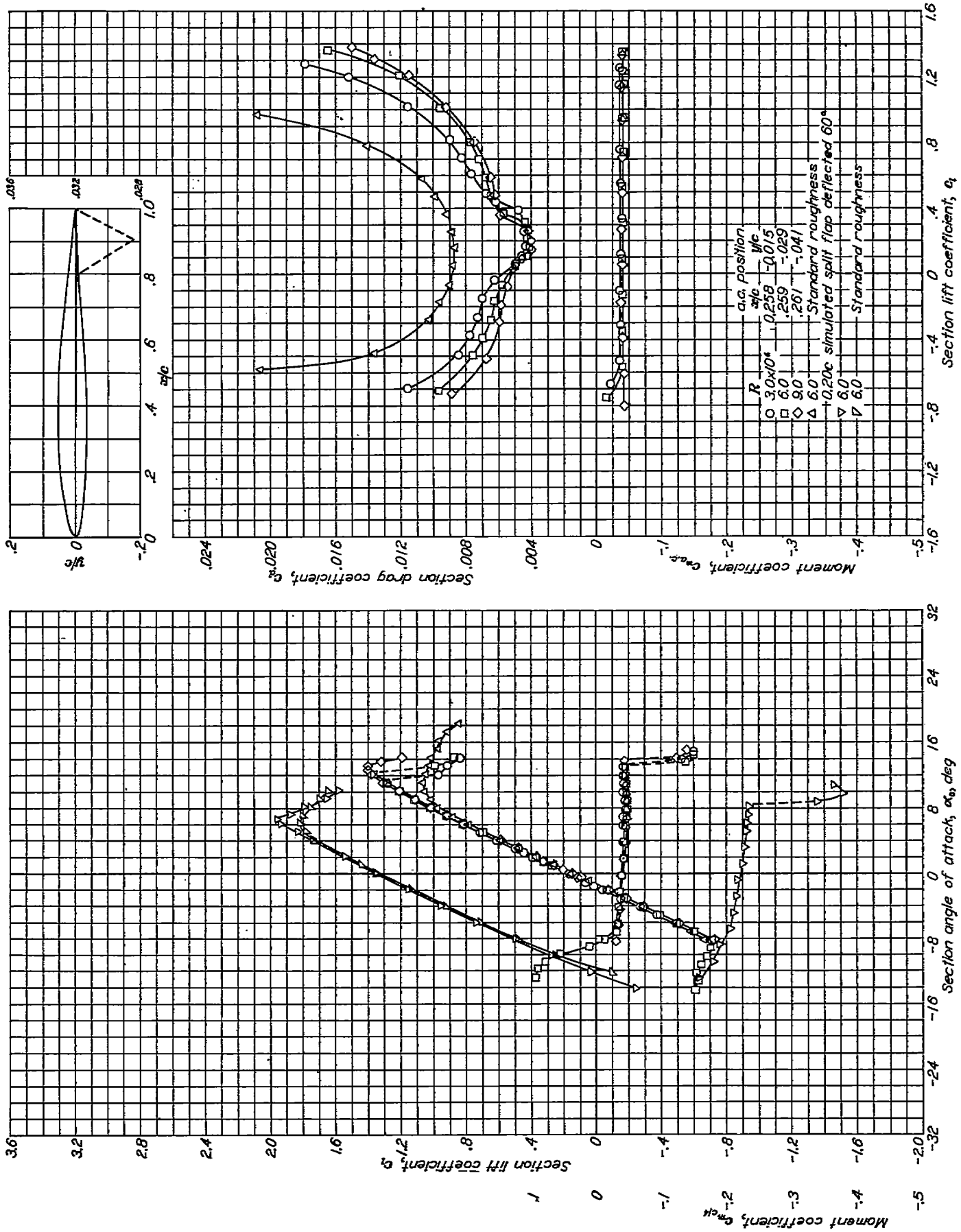

Aerodynamic characteristics of the NACA 64-209 airfoil section, 24-inch chord.

NACA 64-210

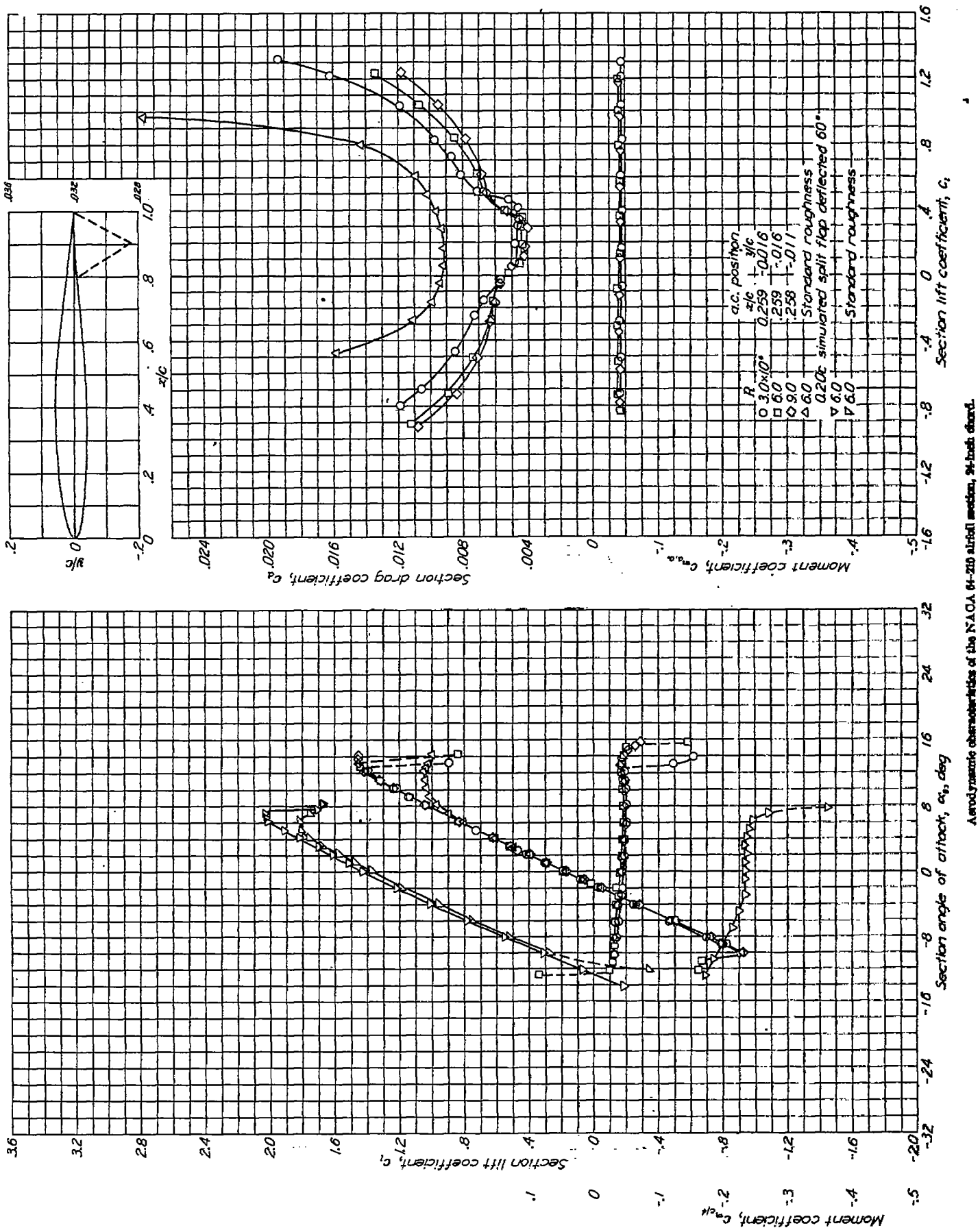

Aerodynamic characteristics of the NACA 64-210 airfoil section, 24-inch chord.

NACA 64$_1$-012

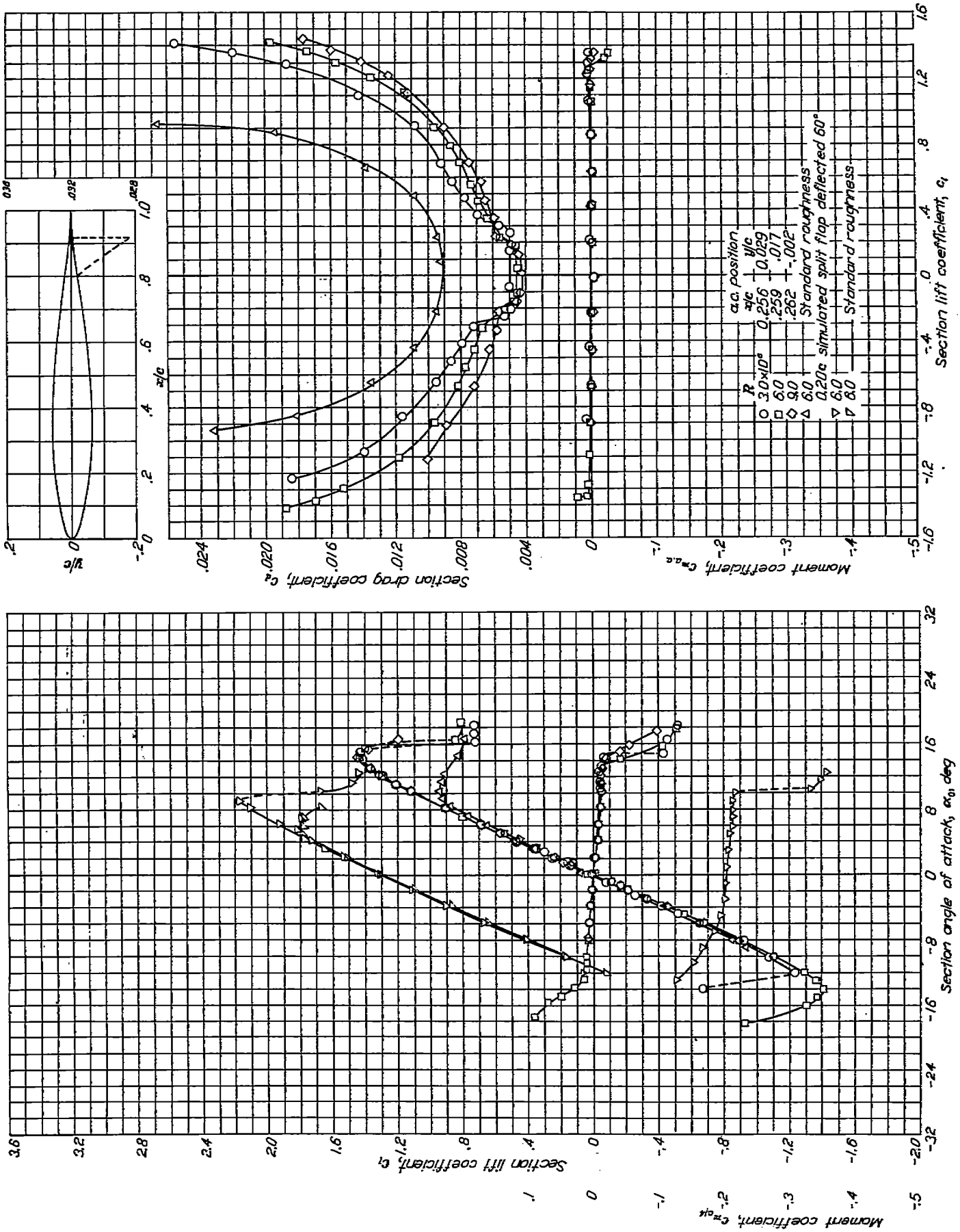

Aerodynamic characteristics of the NACA 64-012 airfoil section, 24-inch chord.

NACA 64$_1$-112

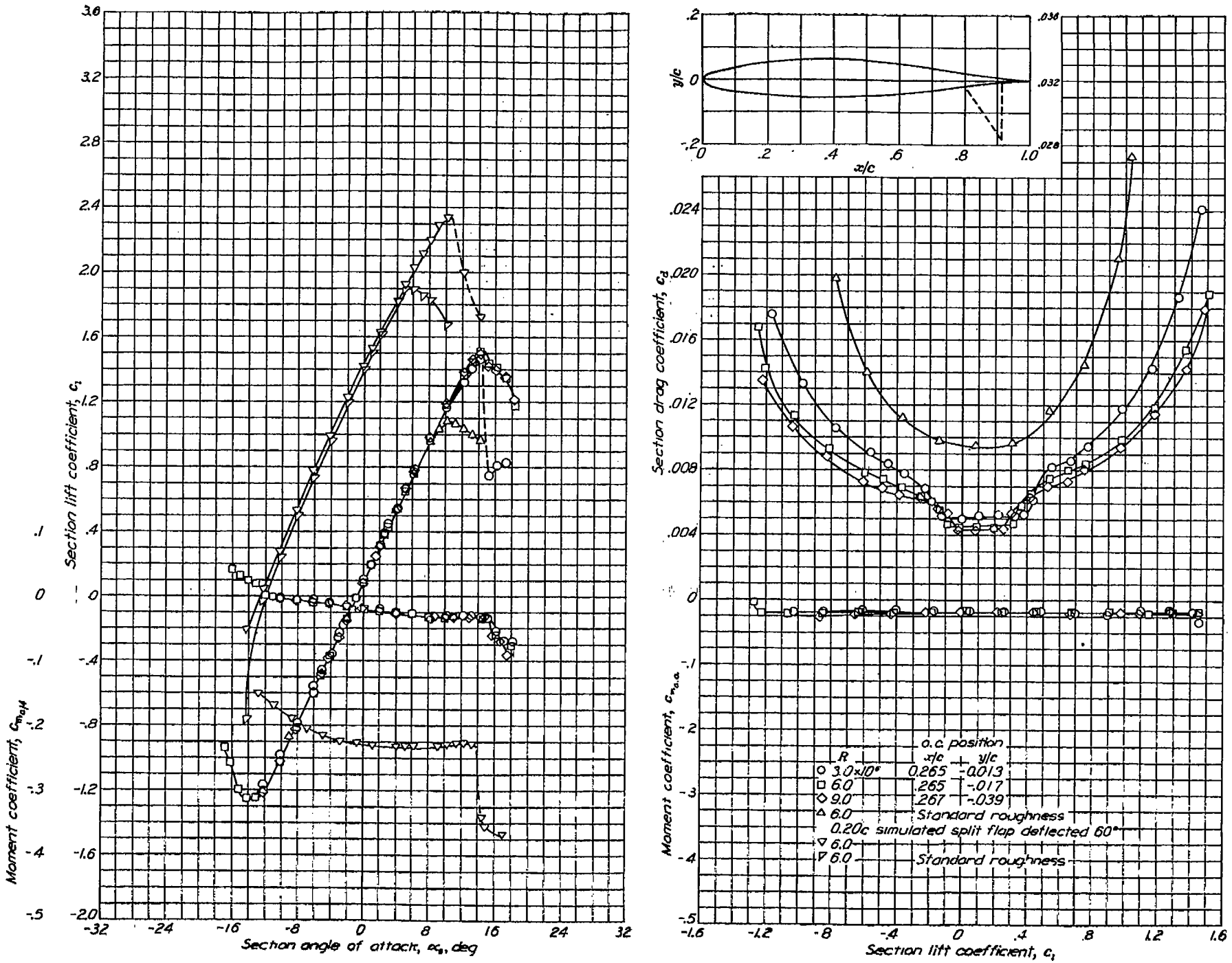

Aerodynamic characteristics of the NACA 64$_1$-112 airfoil section, 24-inch chord.

NACA 64₁-212

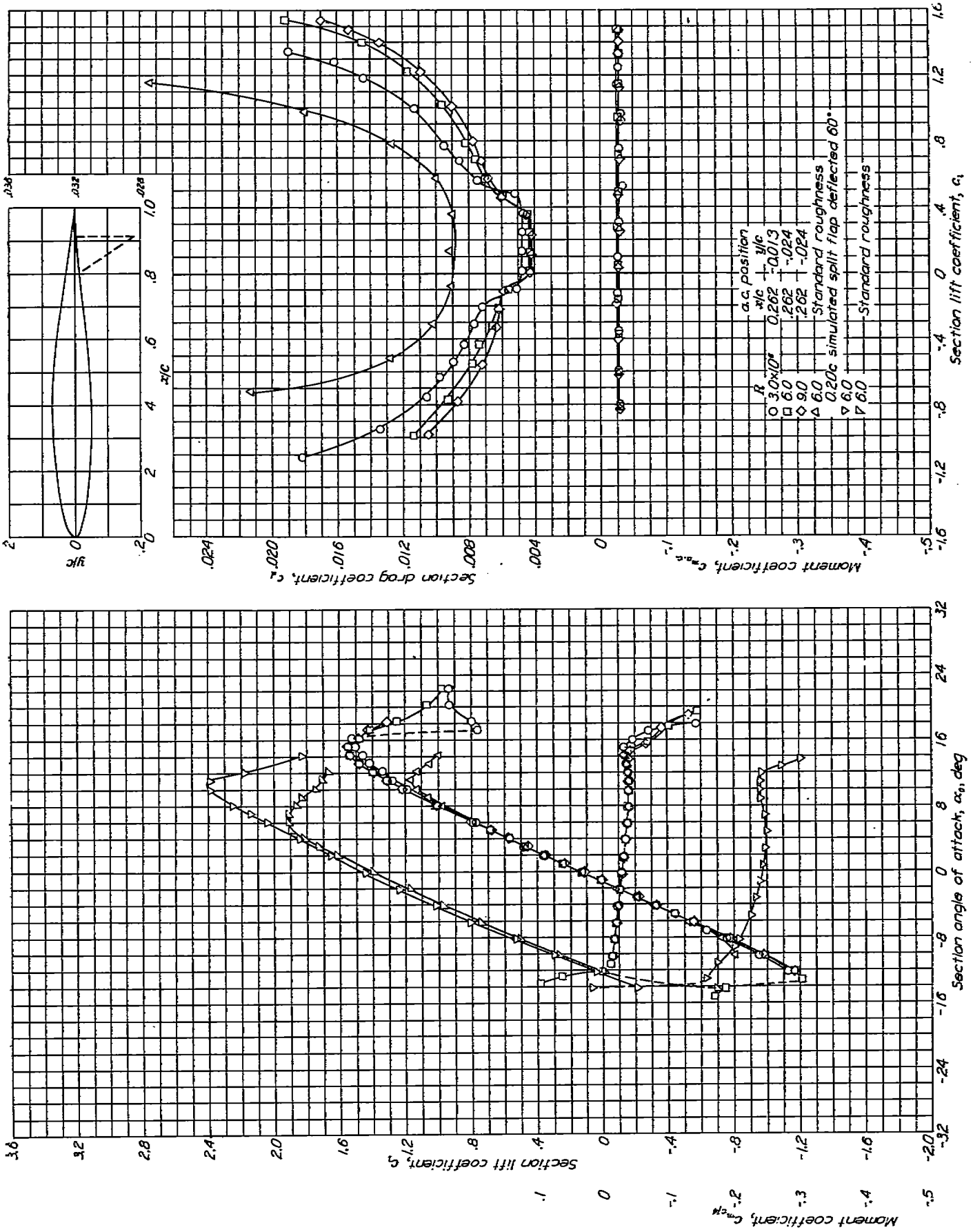

Aerodynamic characteristics of the NACA 64₁-212 airfoil section, 24-inch chord.

NACA 64$_1$-412

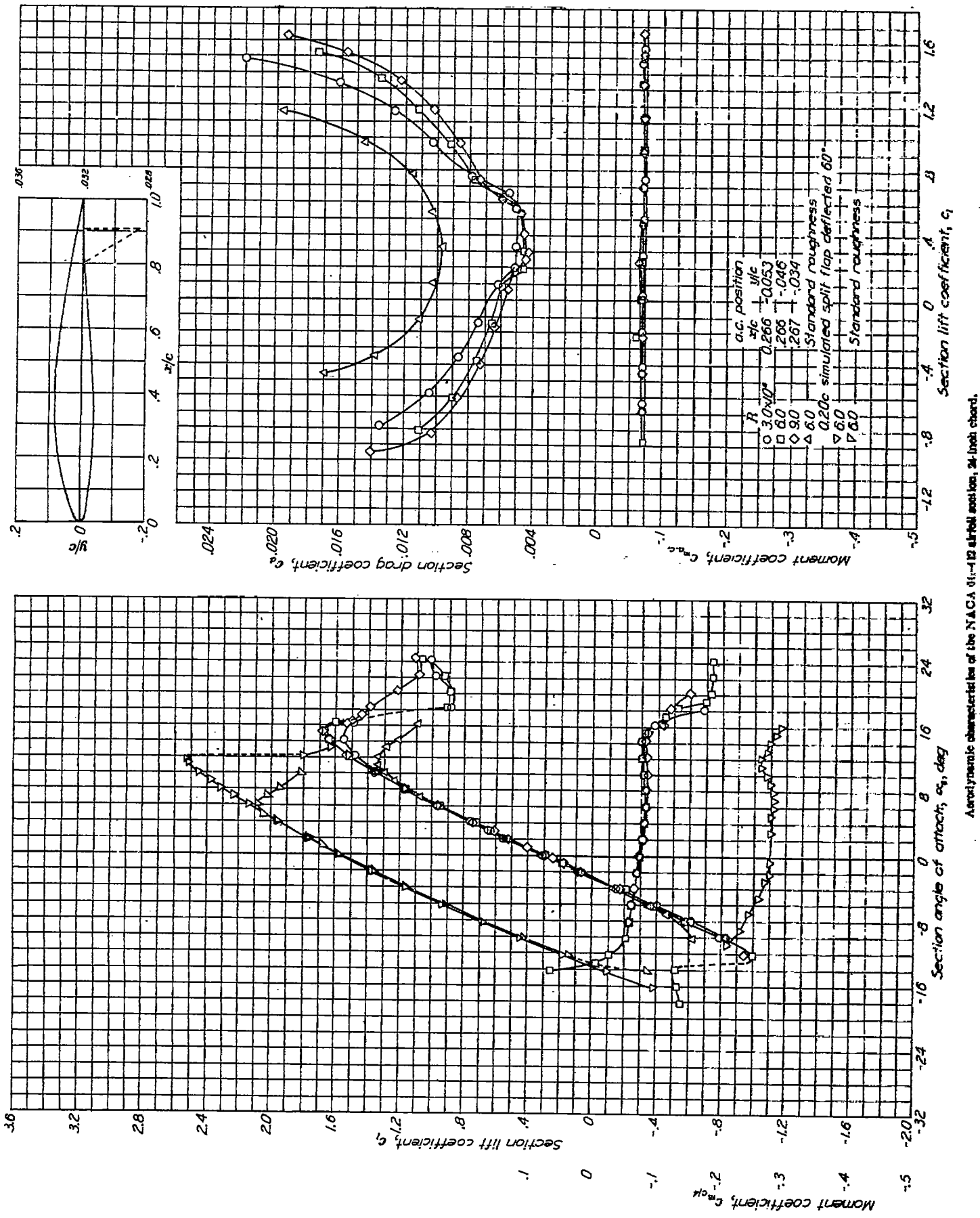

Aerodynamic characteristics of the NACA 64$_1$-412 airfoil section, 24-inch chord.

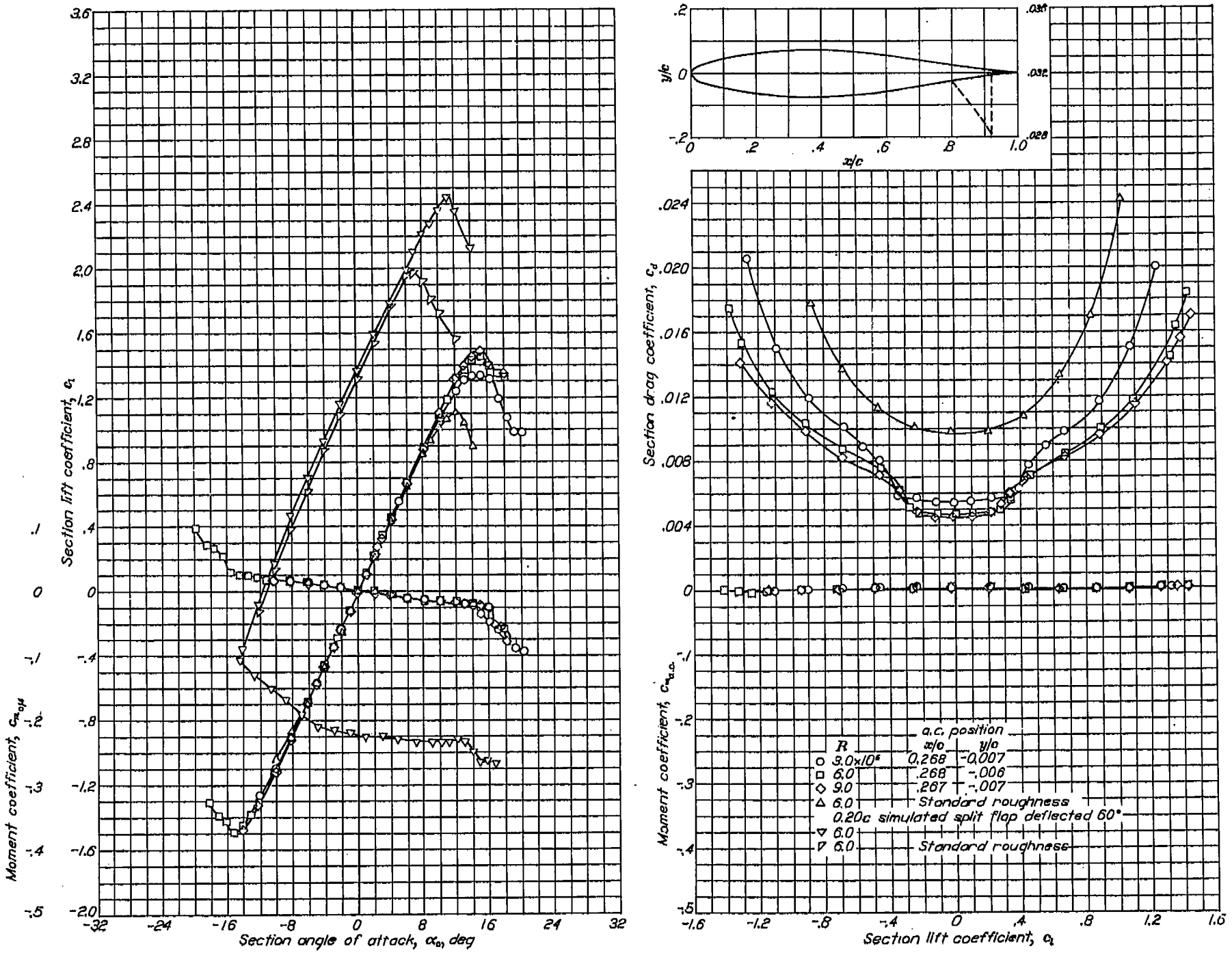

Aerodynamic characteristics of the NACA 642-015 airfoil section, 24-inch chord.

NACA 64$_2$-215

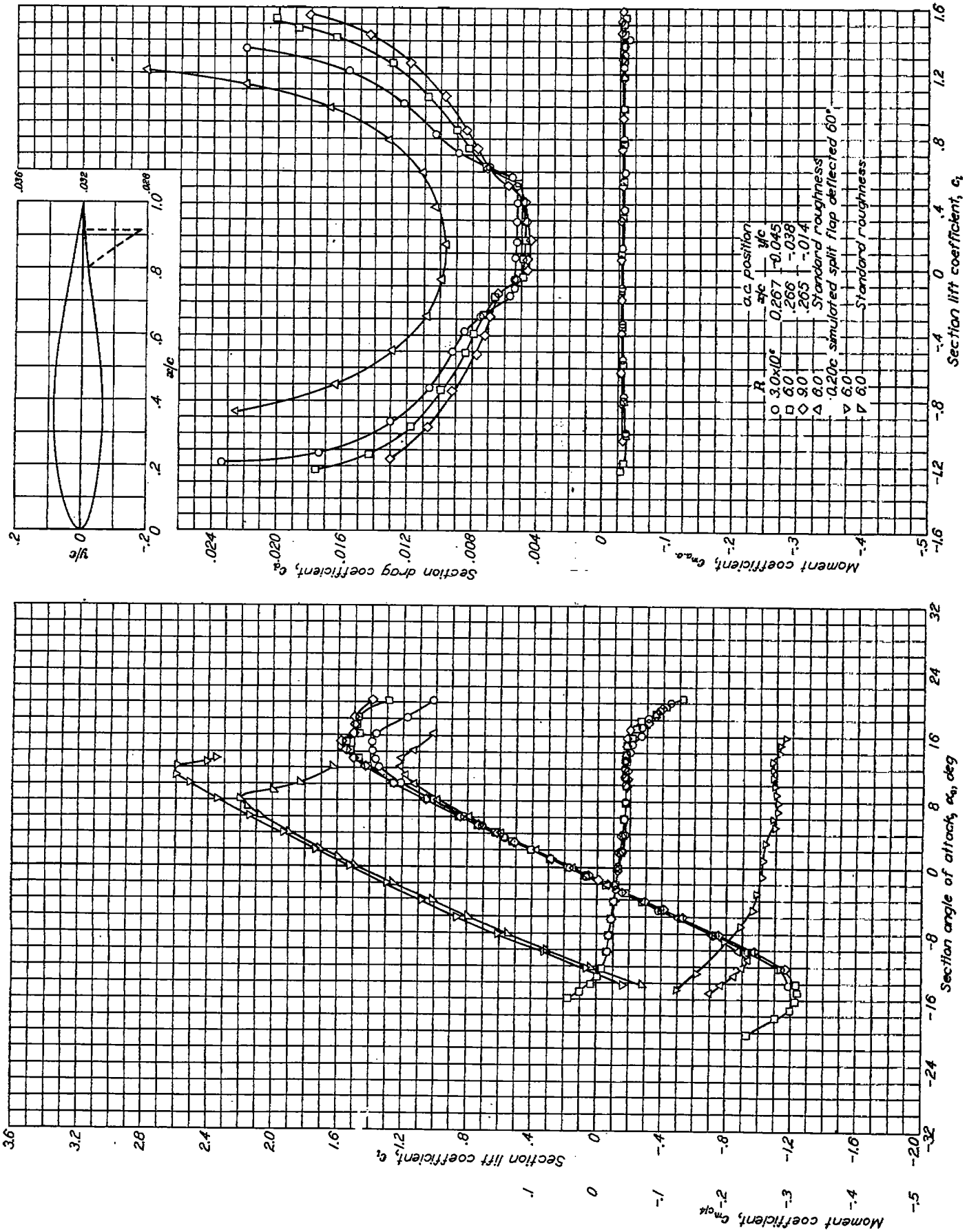

Aerodynamic characteristics of the NACA 64$_2$-215 airfoil section, 24-inch chord.

NACA 64$_2$-415

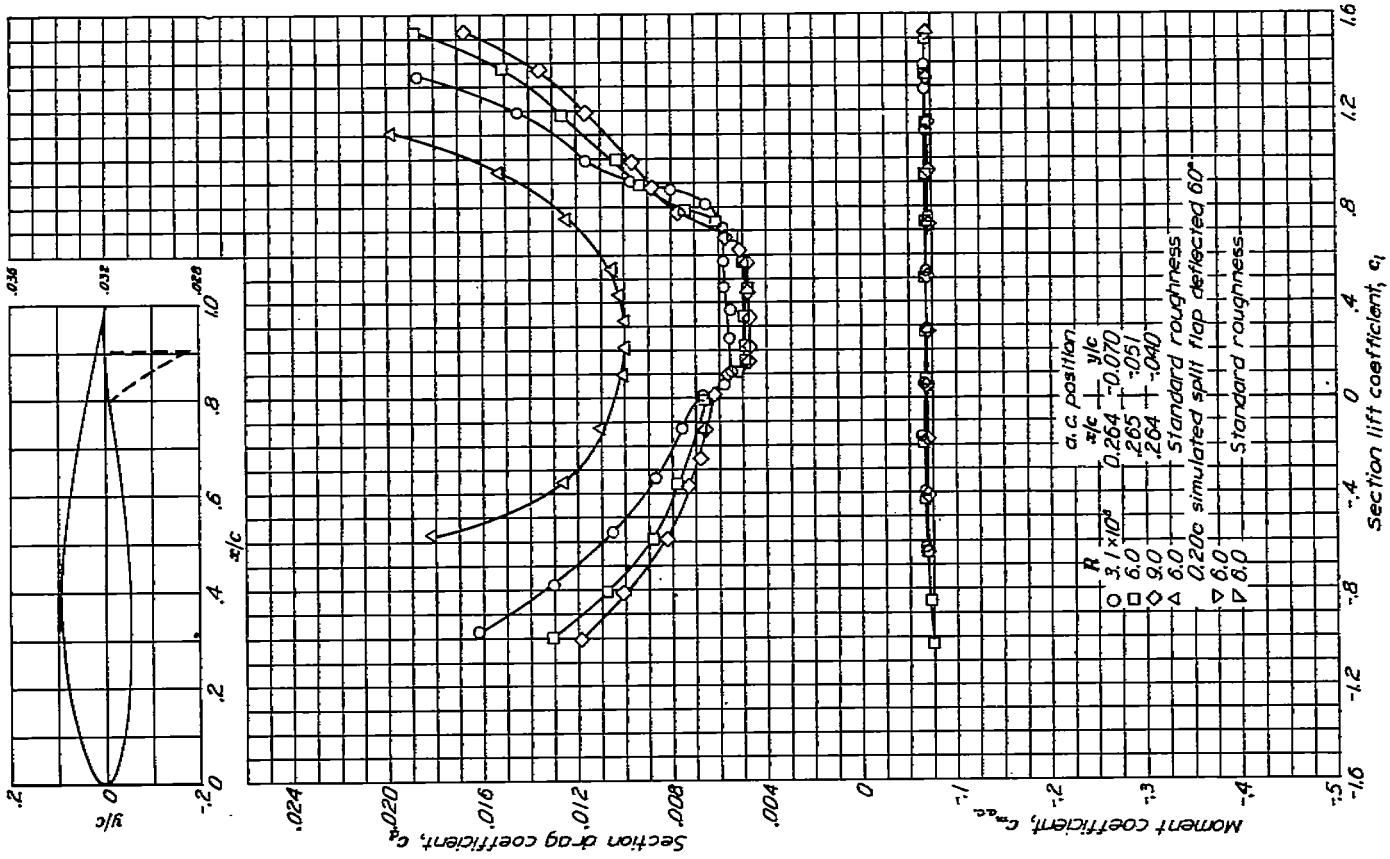

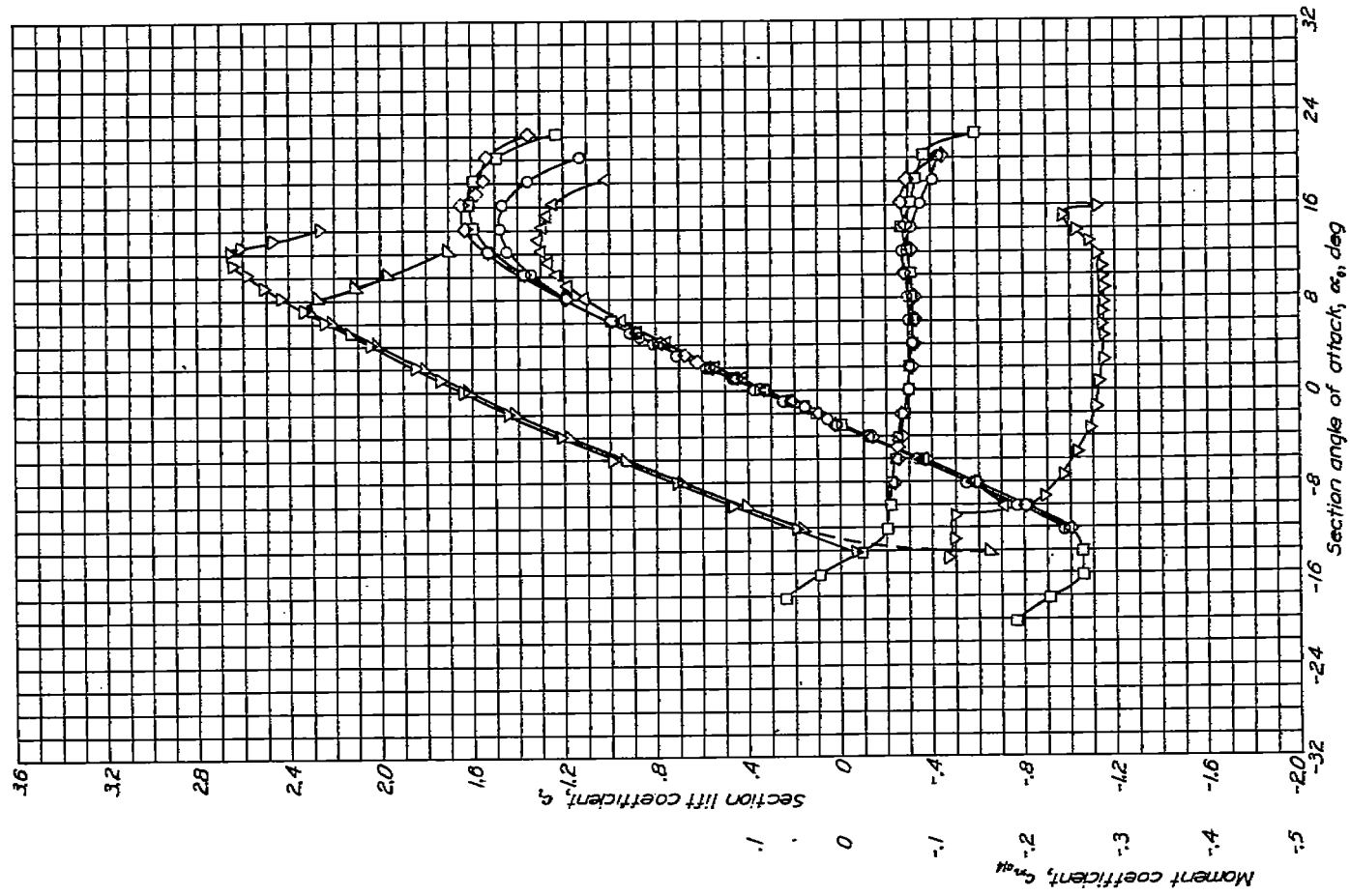

Aerodynamic characteristics of the NACA 64-415 airfoil section, 24-inch chord.

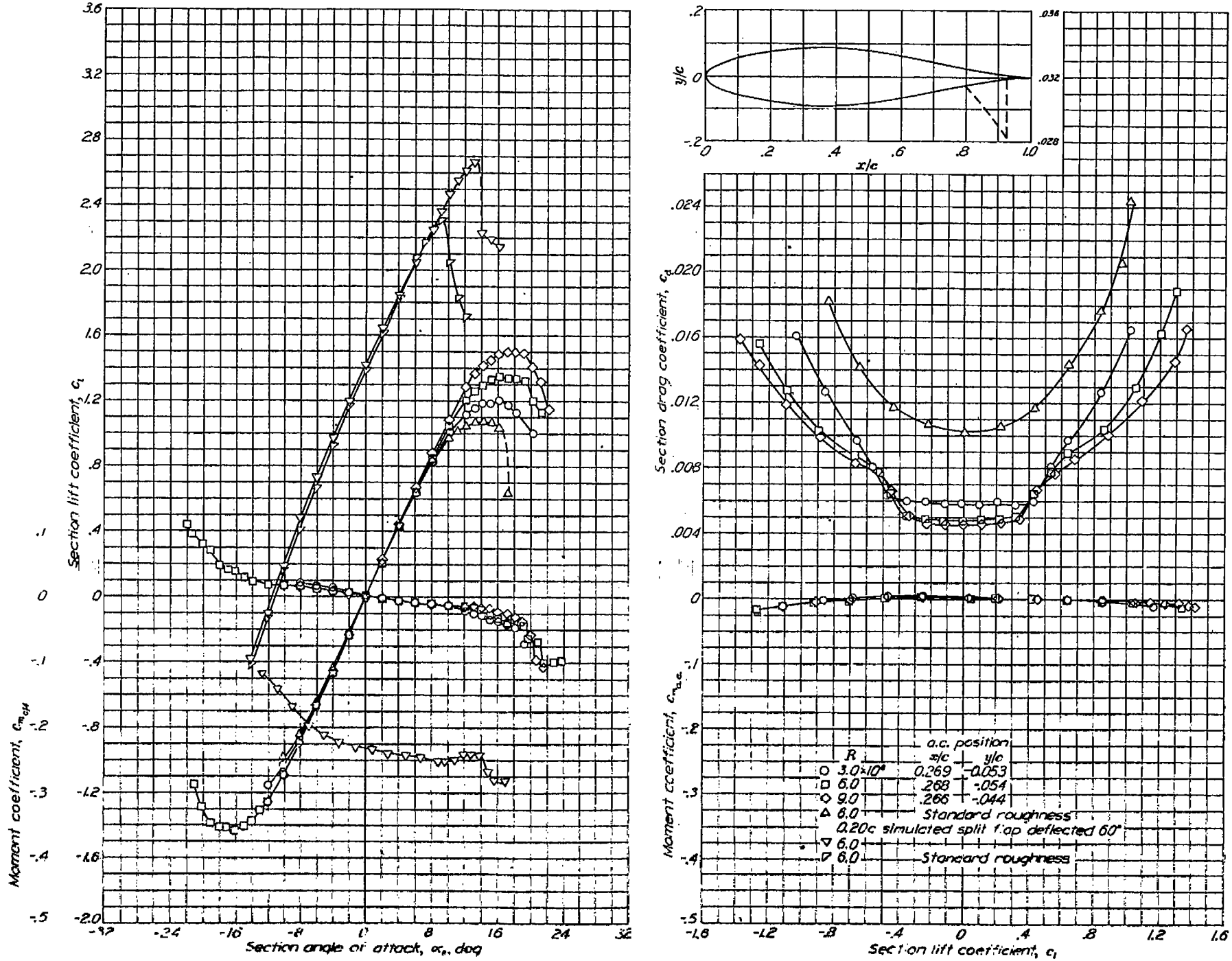

Aerodynamic characteristics of the NACA 64s-018 airfoil section, 24-inch chord.

NACA 64$_3$-218

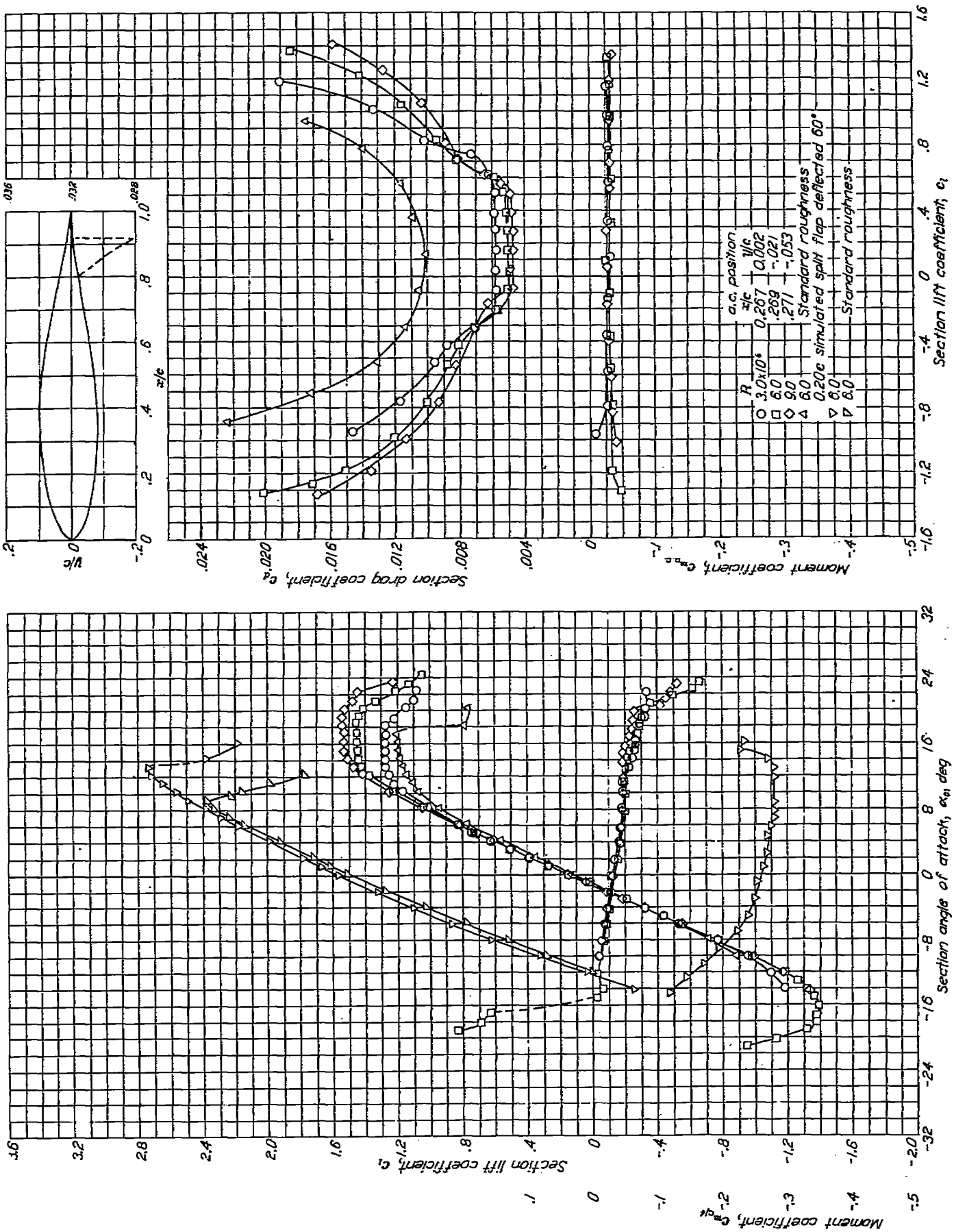

Aerodynamic characteristics of the NACA 64$_3$-218 airfoil section, 24-inch chord.

NACA 64$_3$-418

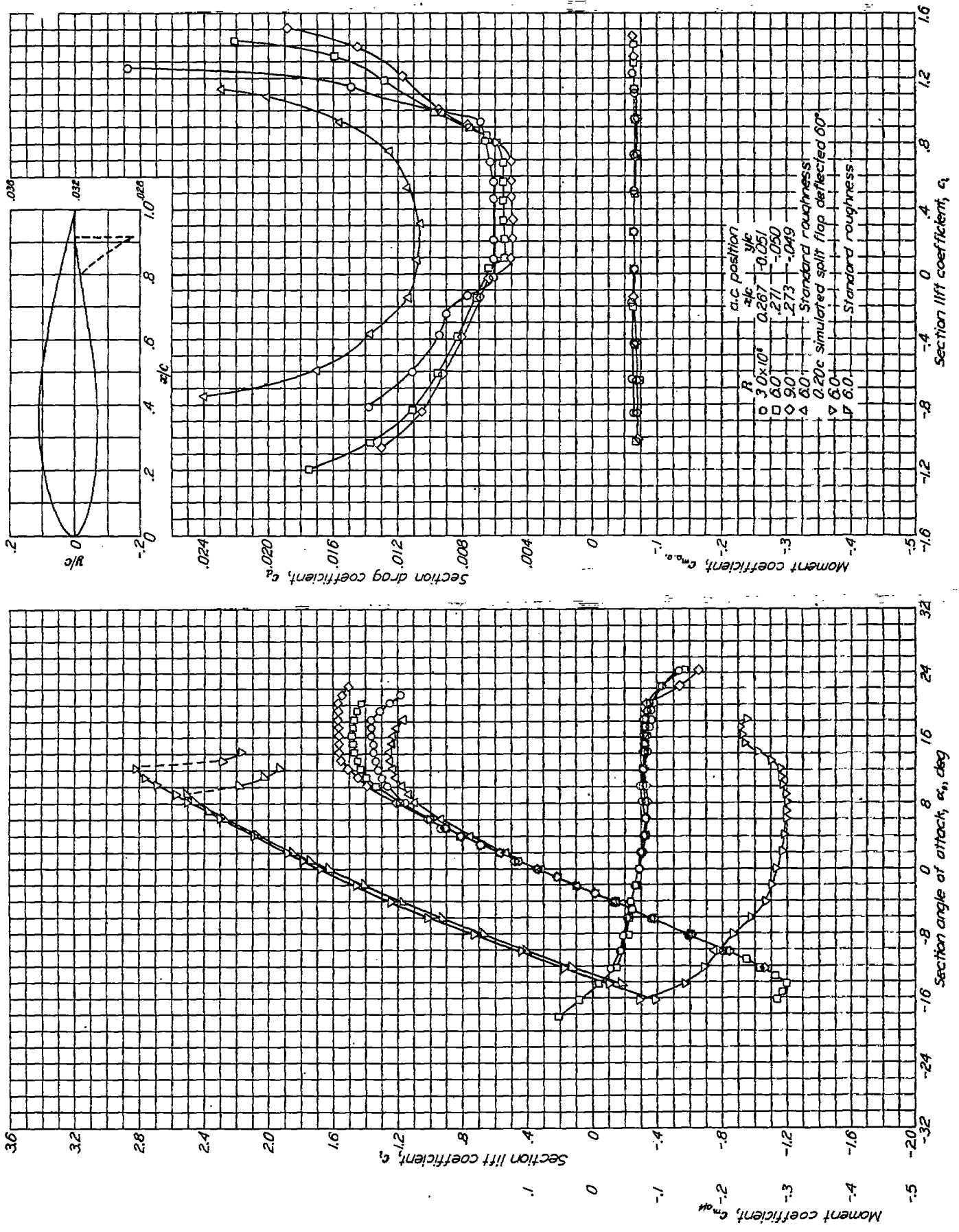

Aerodynamic characteristics of the NACA 64$_3$-418 airfoil section, 24-inch chord.

NACA 643-618

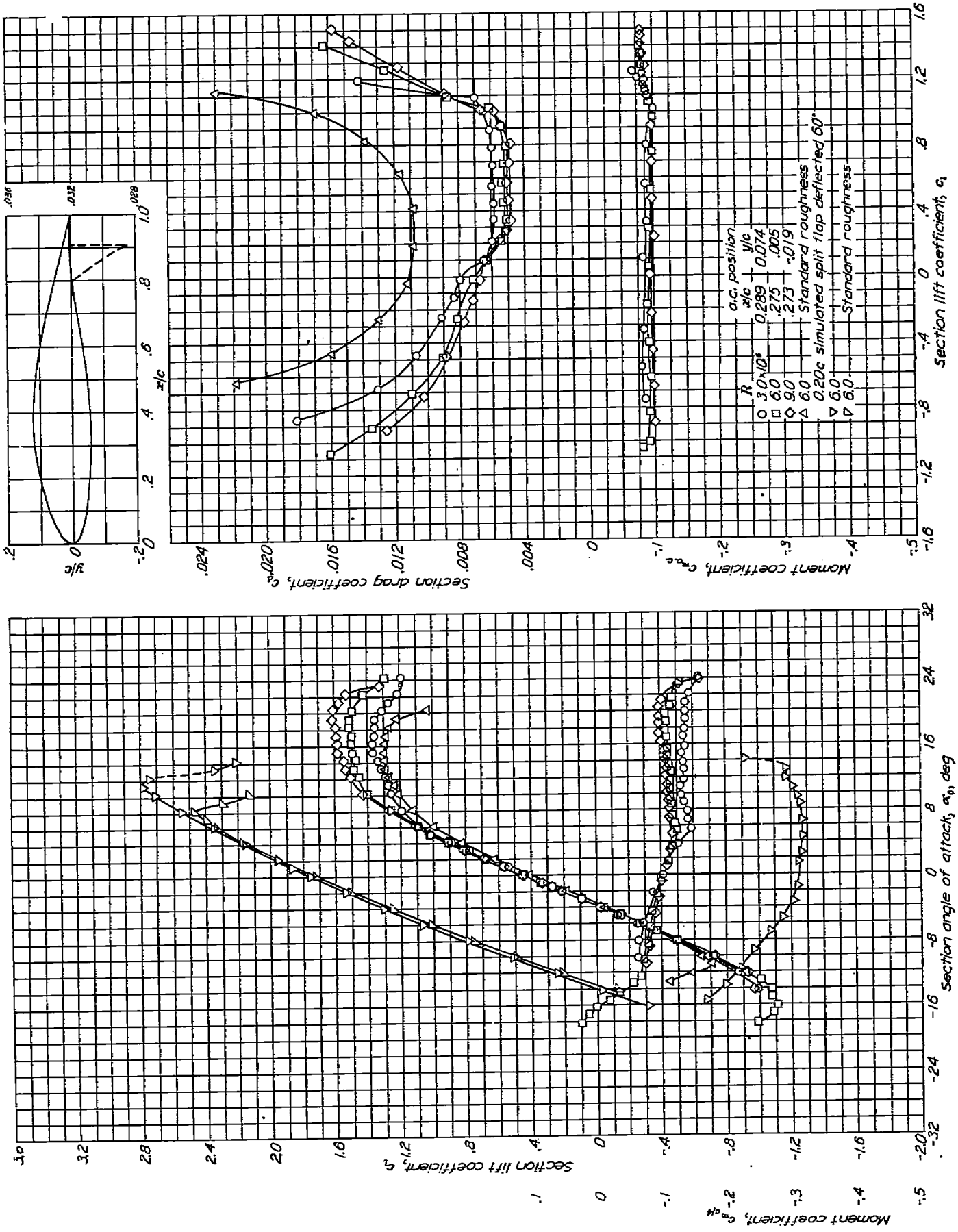

Aerodynamic characteristics of the NACA 643-618 airfoil section, 24-inch chord.

NACA 64₄-021

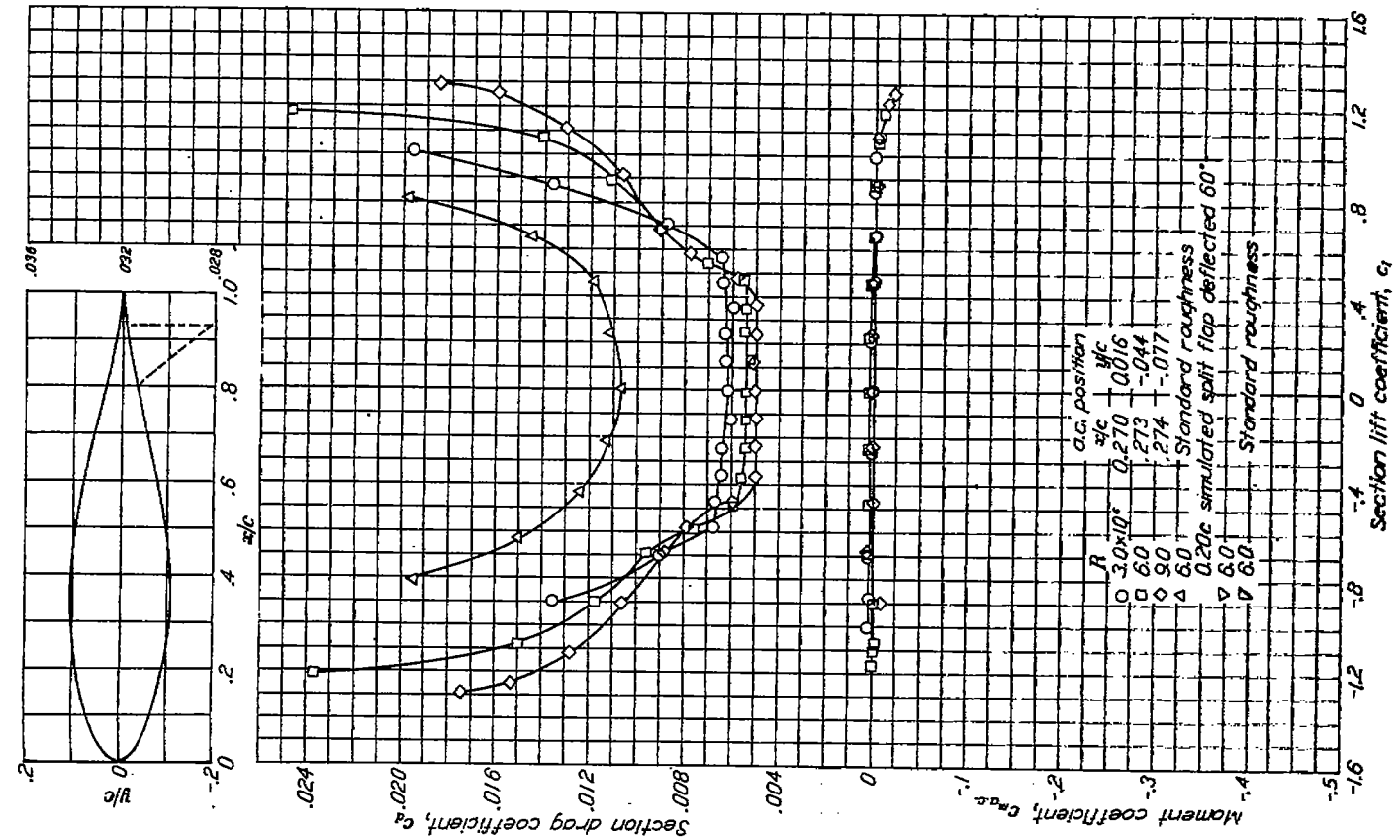

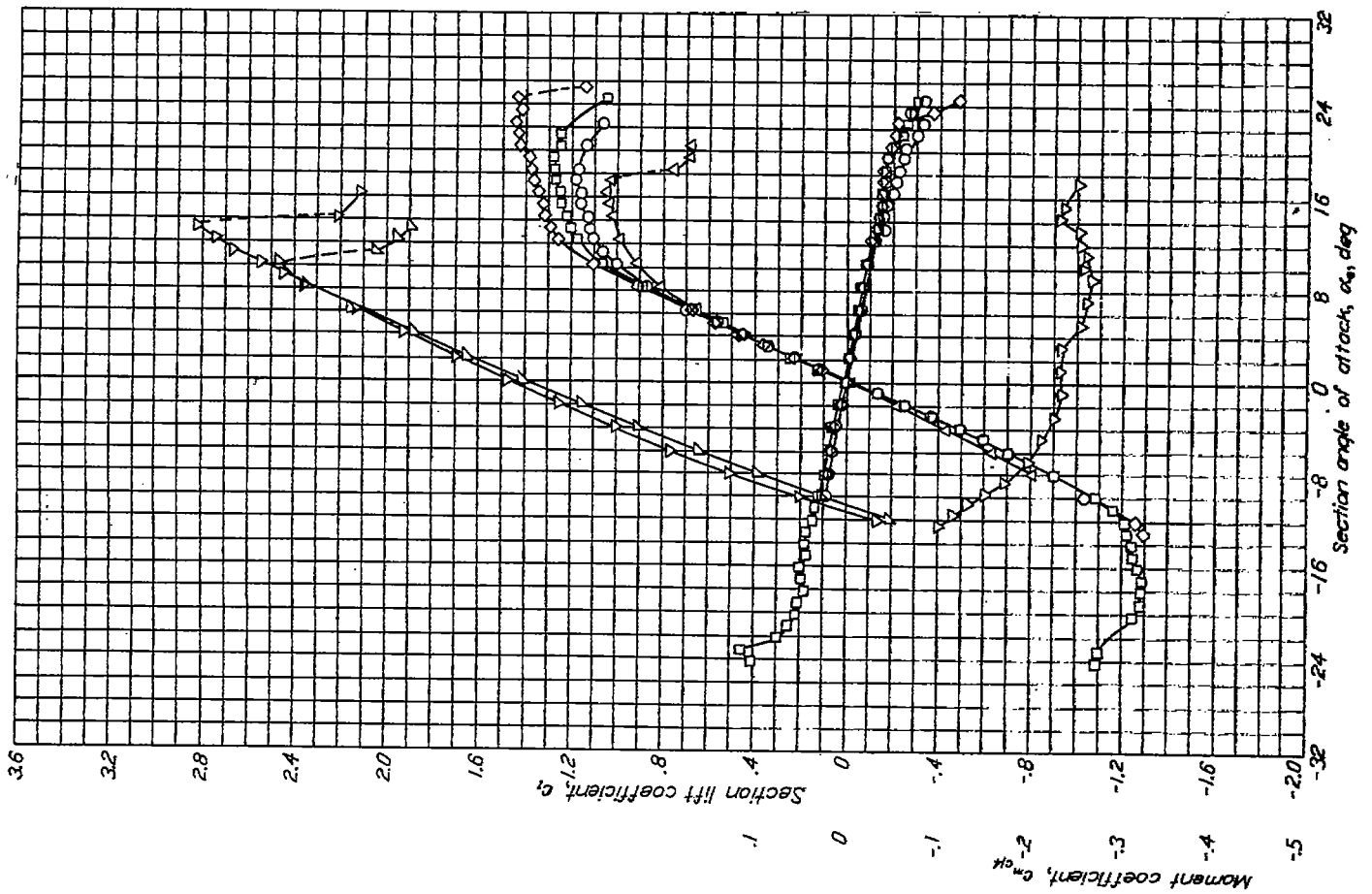

Aerodynamic characteristics of the NACA 64₄-021 airfoil section, 24-inch chord.

NACA 64₄-221

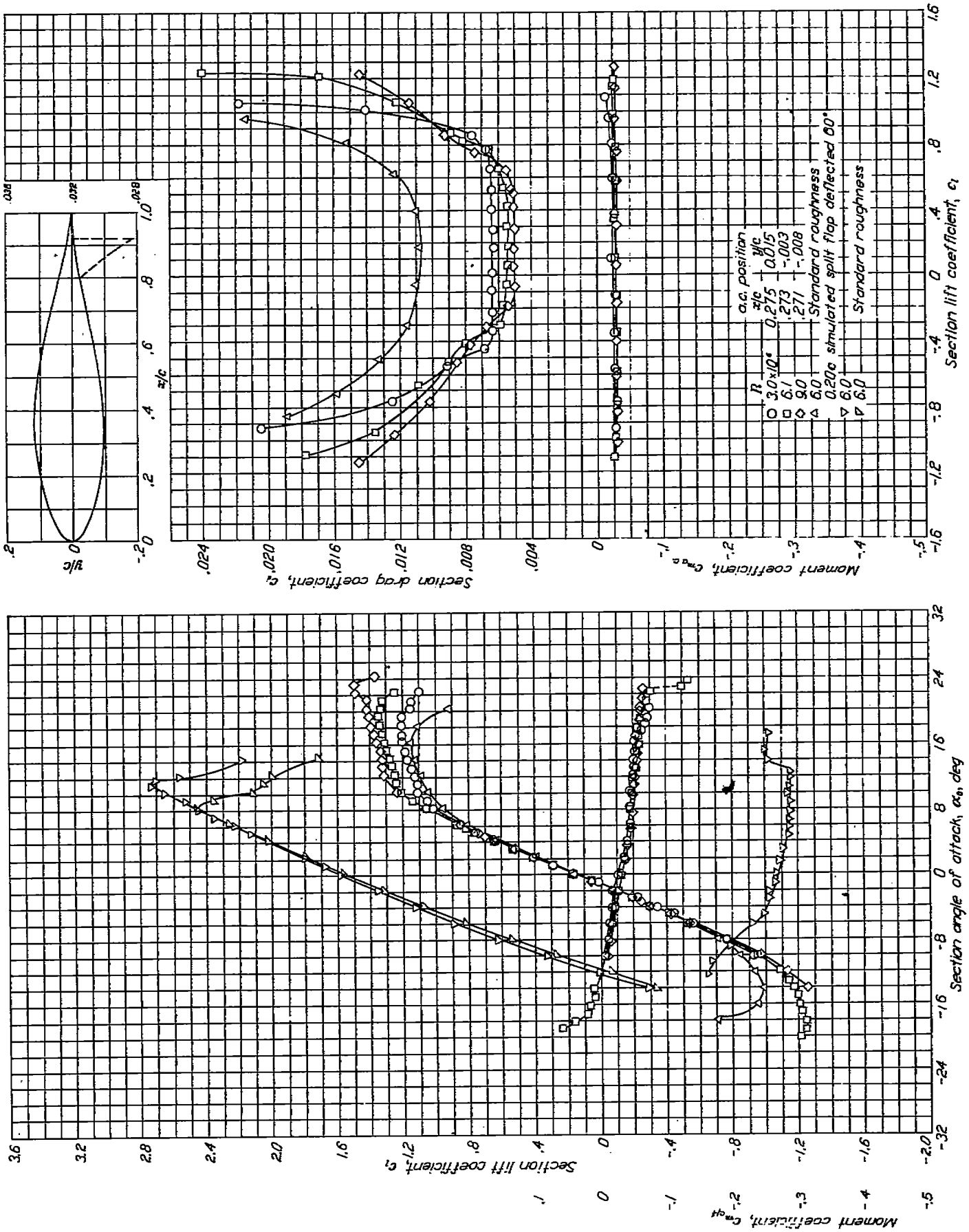

Aerodynamic characteristics of the NACA 64₄-221 airfoil section, 24-inch chord.

NACA 64$_4$-421

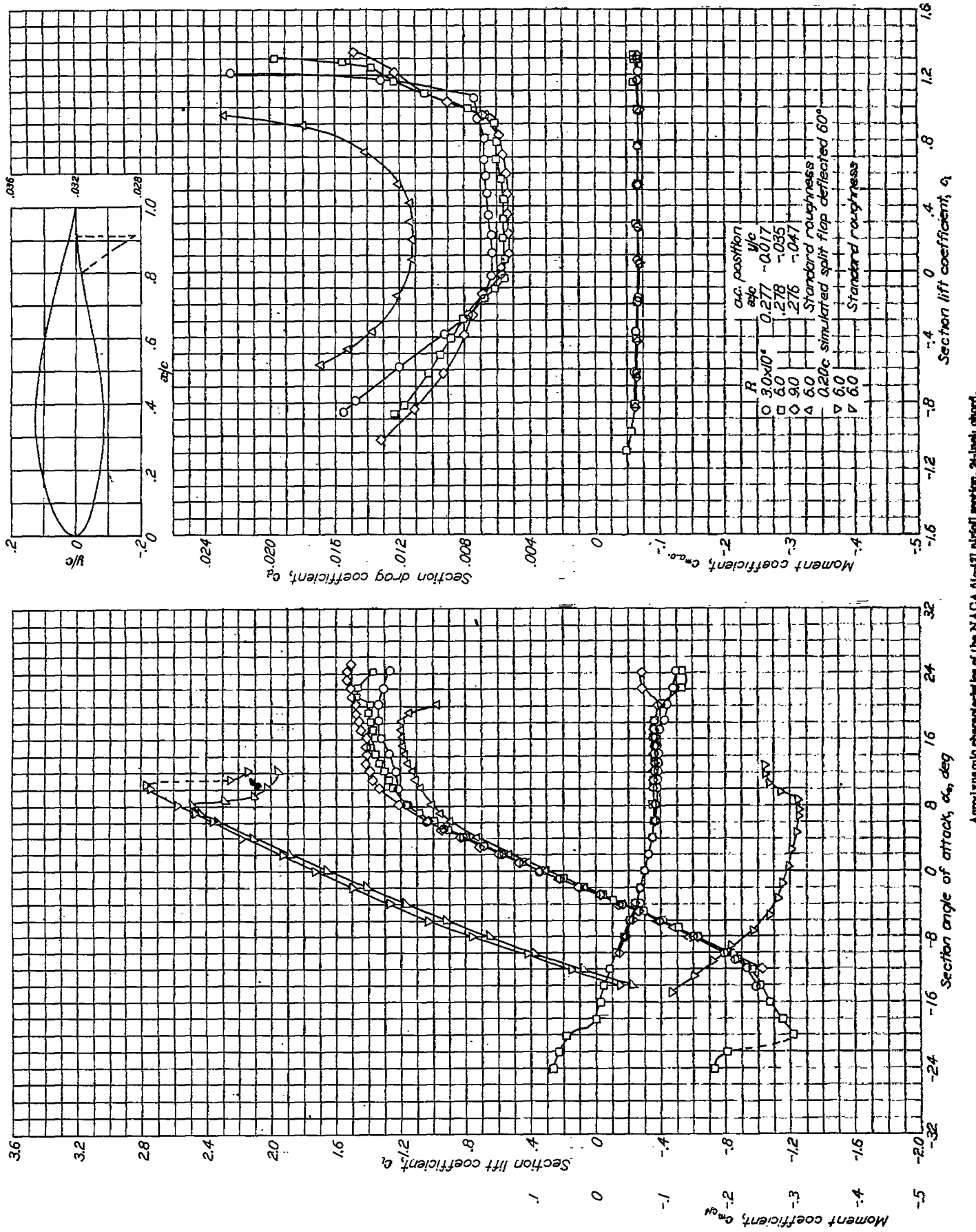

Aerodynamic characteristics of the NACA 64$_4$-421 airfoil section, 24-inch chord.

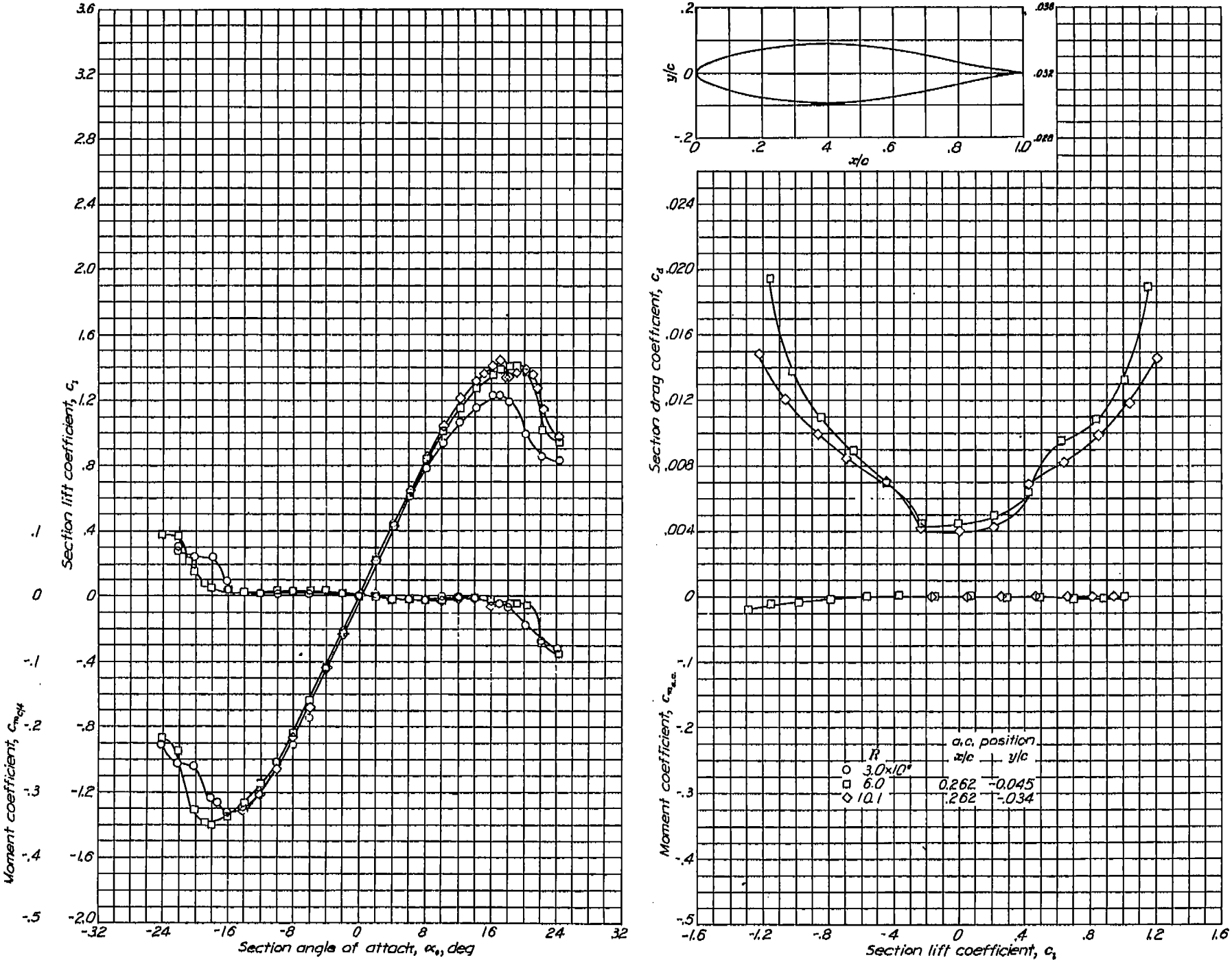

Aerodynamic characteristics of the NACA 65,3-018 airfoil section, 24-inch chord.

NACA 65,3-418, $a = 0.8$

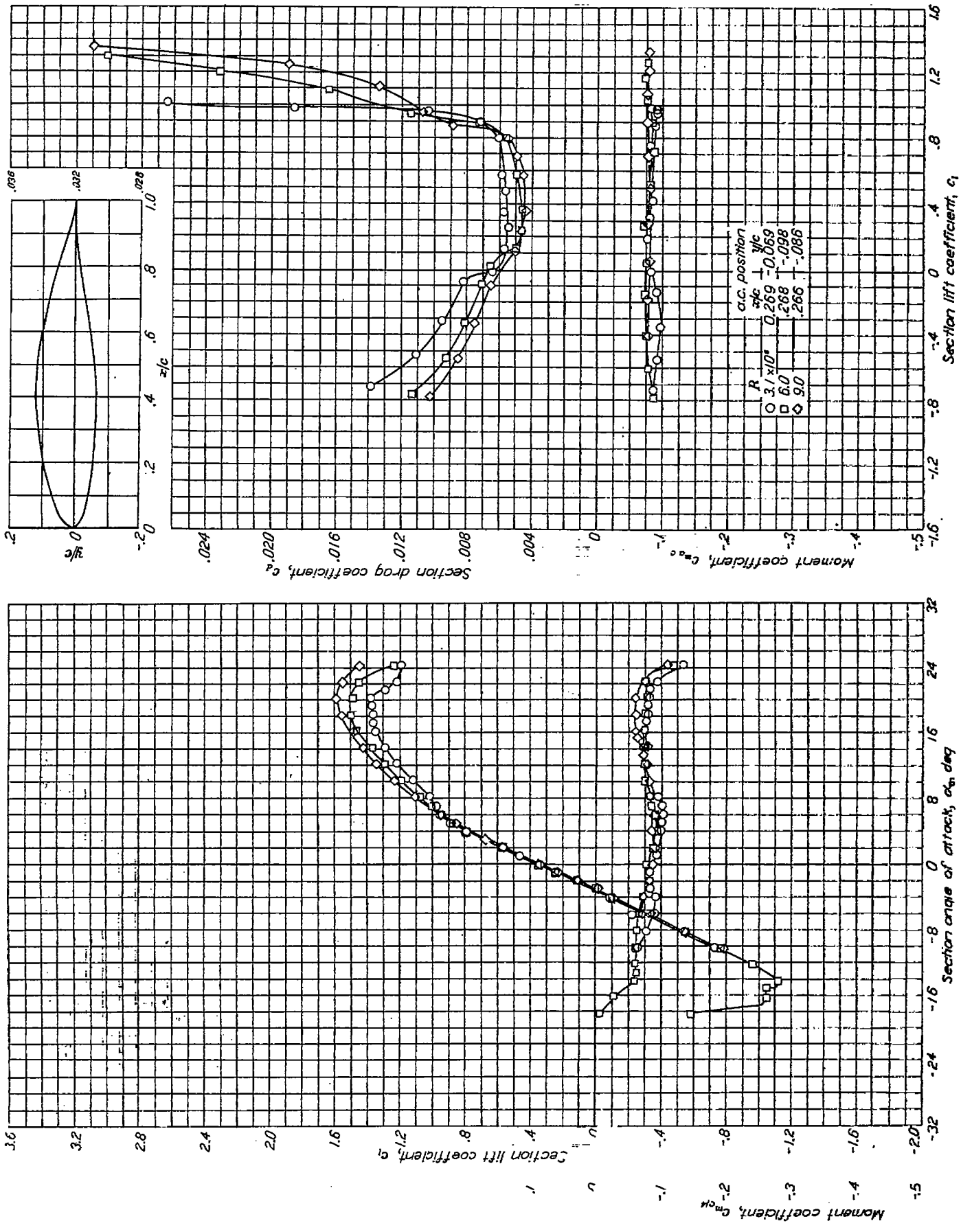

Aerodynamic characteristics of the NACA 65,3-418, $a = 0.8$ airfoil section, 24-inch chord.

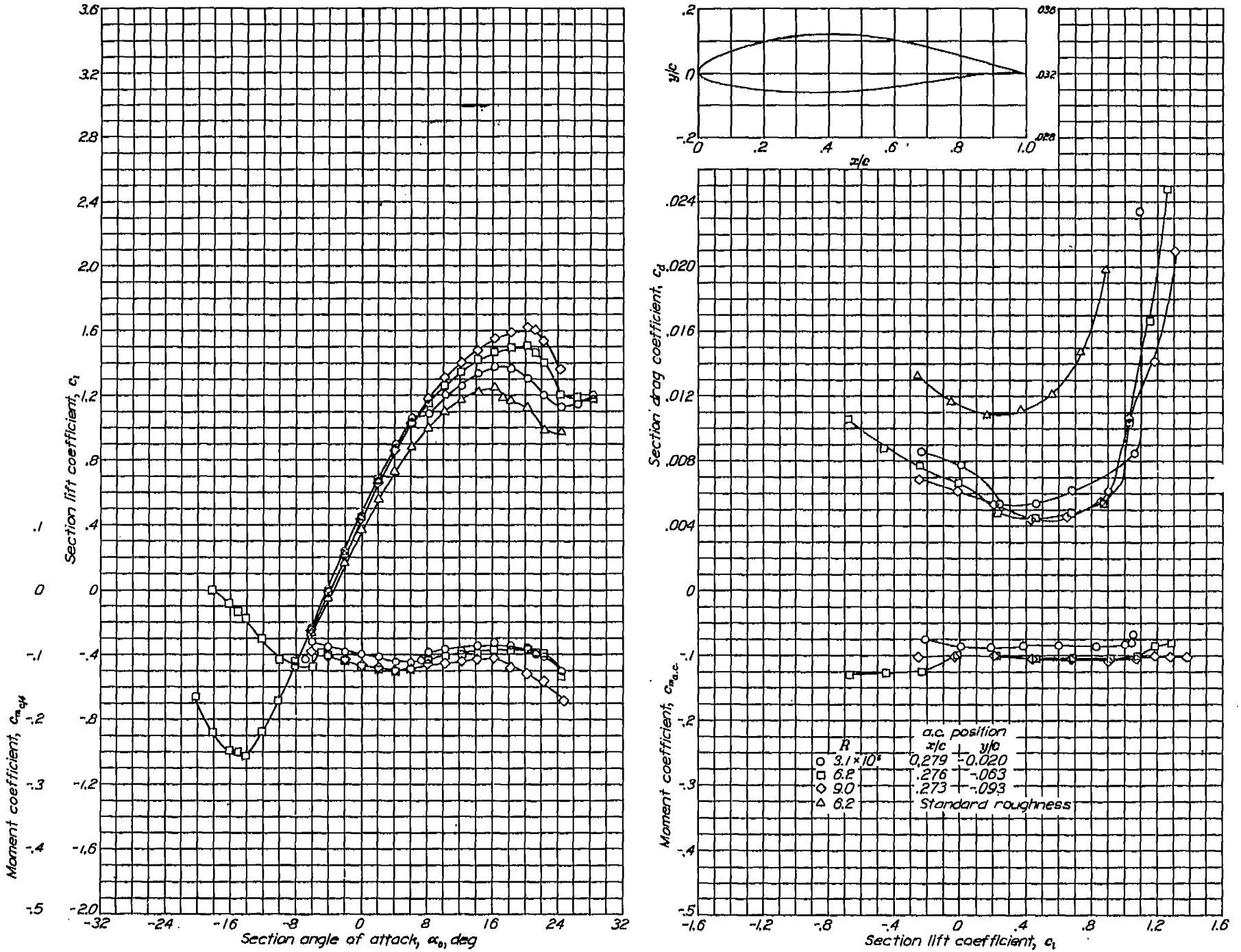

Aerodynamic characteristics of the NACA 65,3-618 airfoil section, 24-inch chord.

NACA 65,3-618 with flap

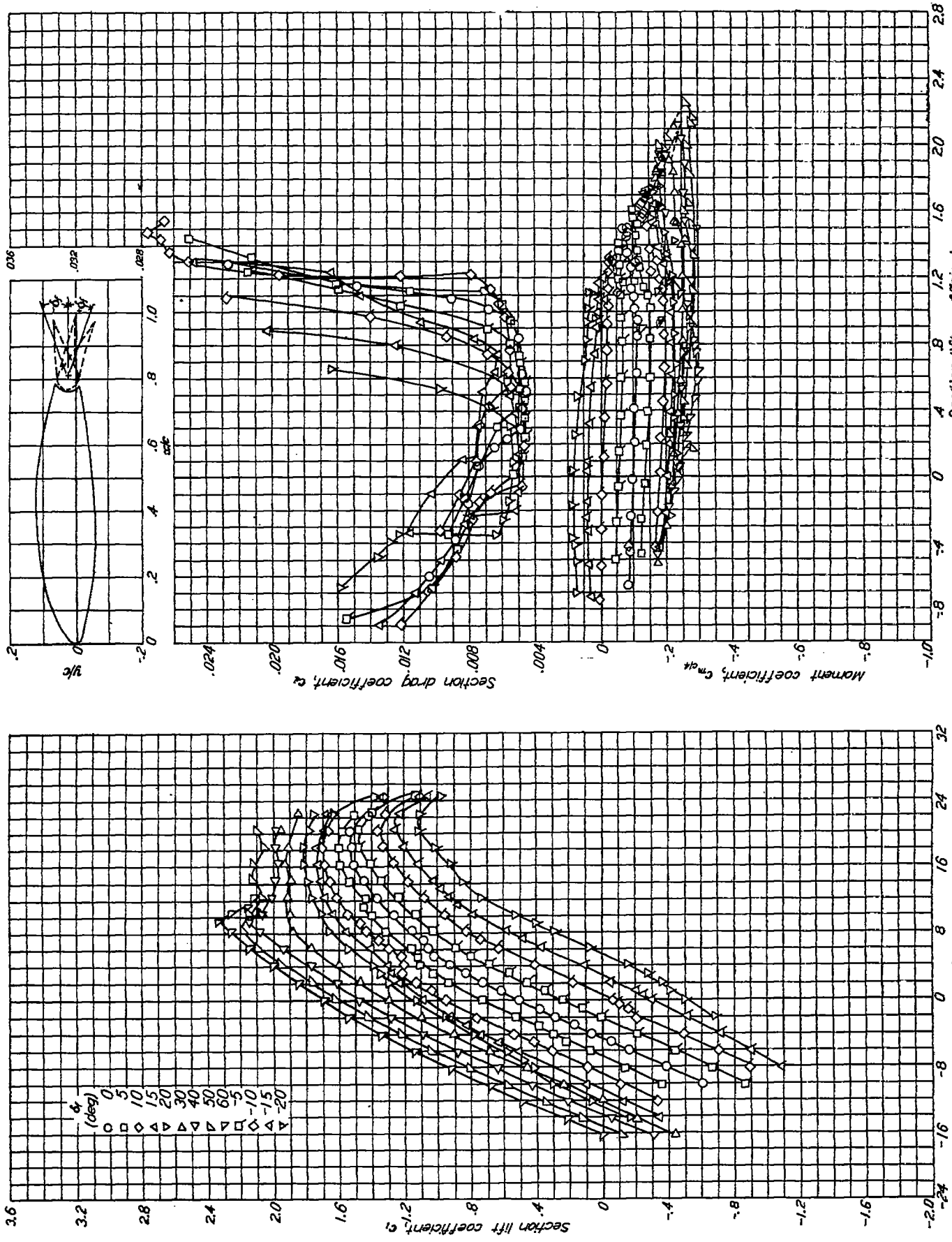

Aerodynamic characteristics of the NACA 65,3-618 airfoil section with 0.20c sealed plain flap. R=6X10⁶.

NACA 65(216)-415, $a = 0.5$

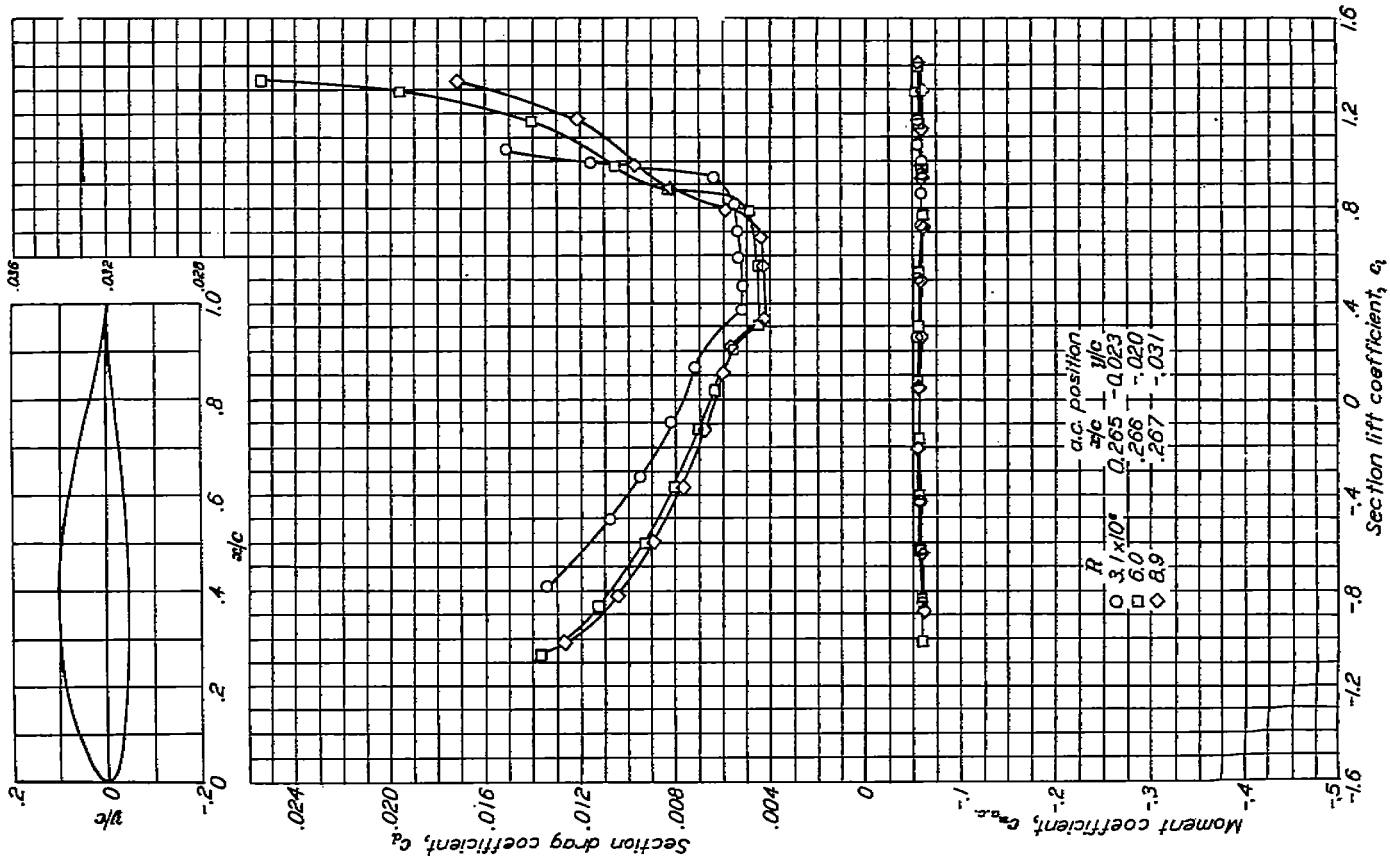

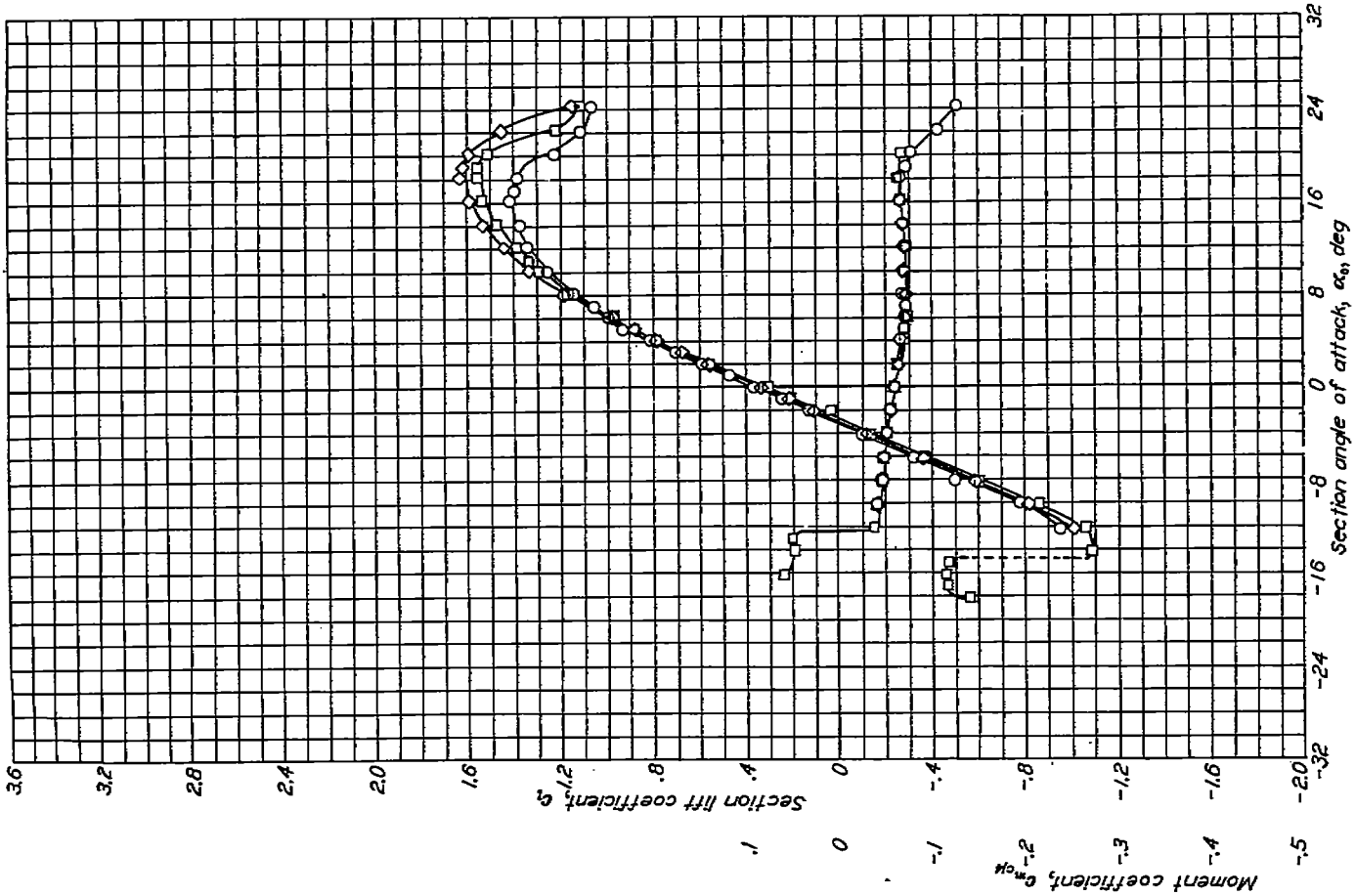

Aerodynamic characteristics of the NACA 65(210)-415, $a = 0.5$ airfoil section, 24-inch chord.

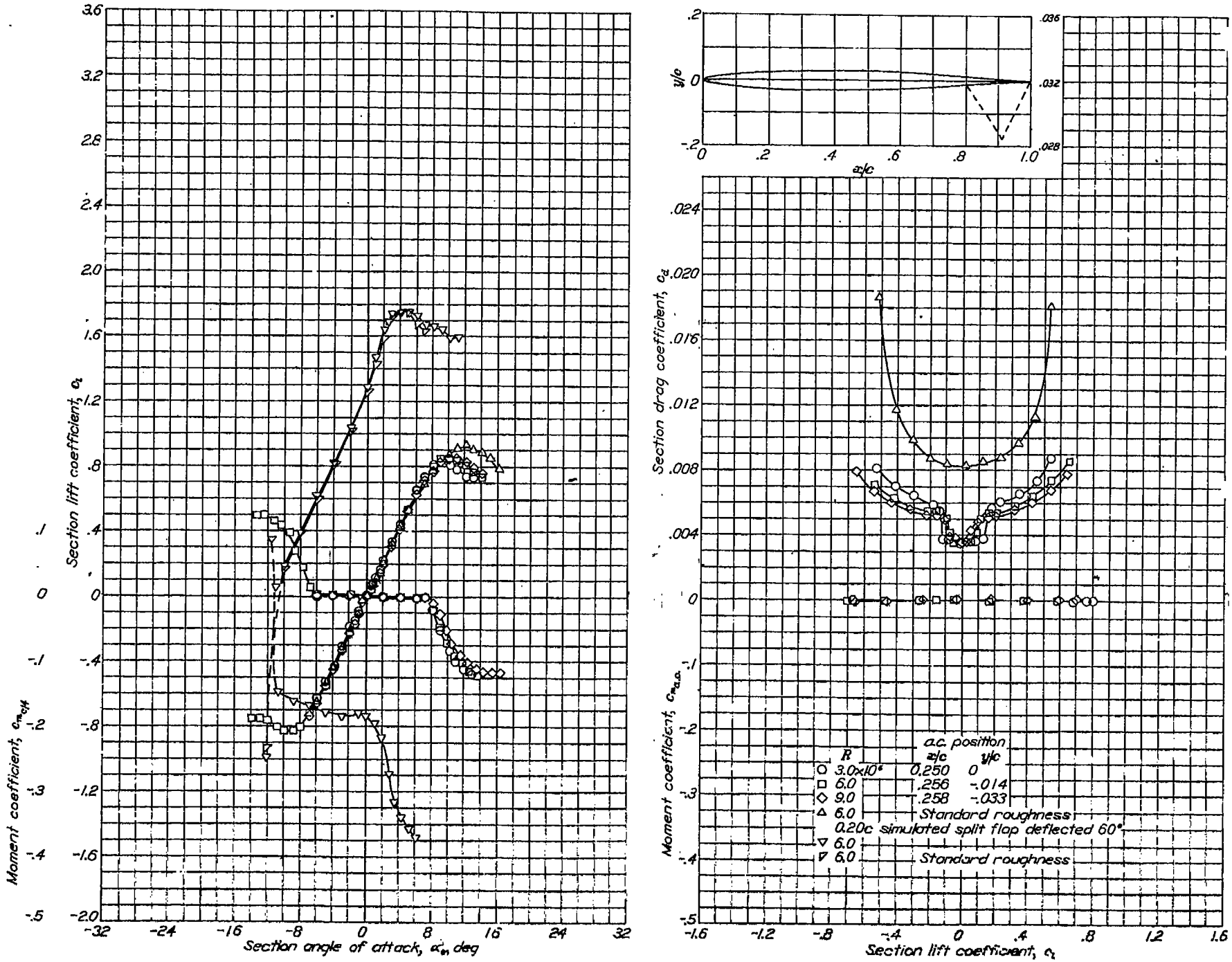

Aerodynamic characteristics of the NACA 65-006 airfoil section, 24-inch chord.

NACA 65-009

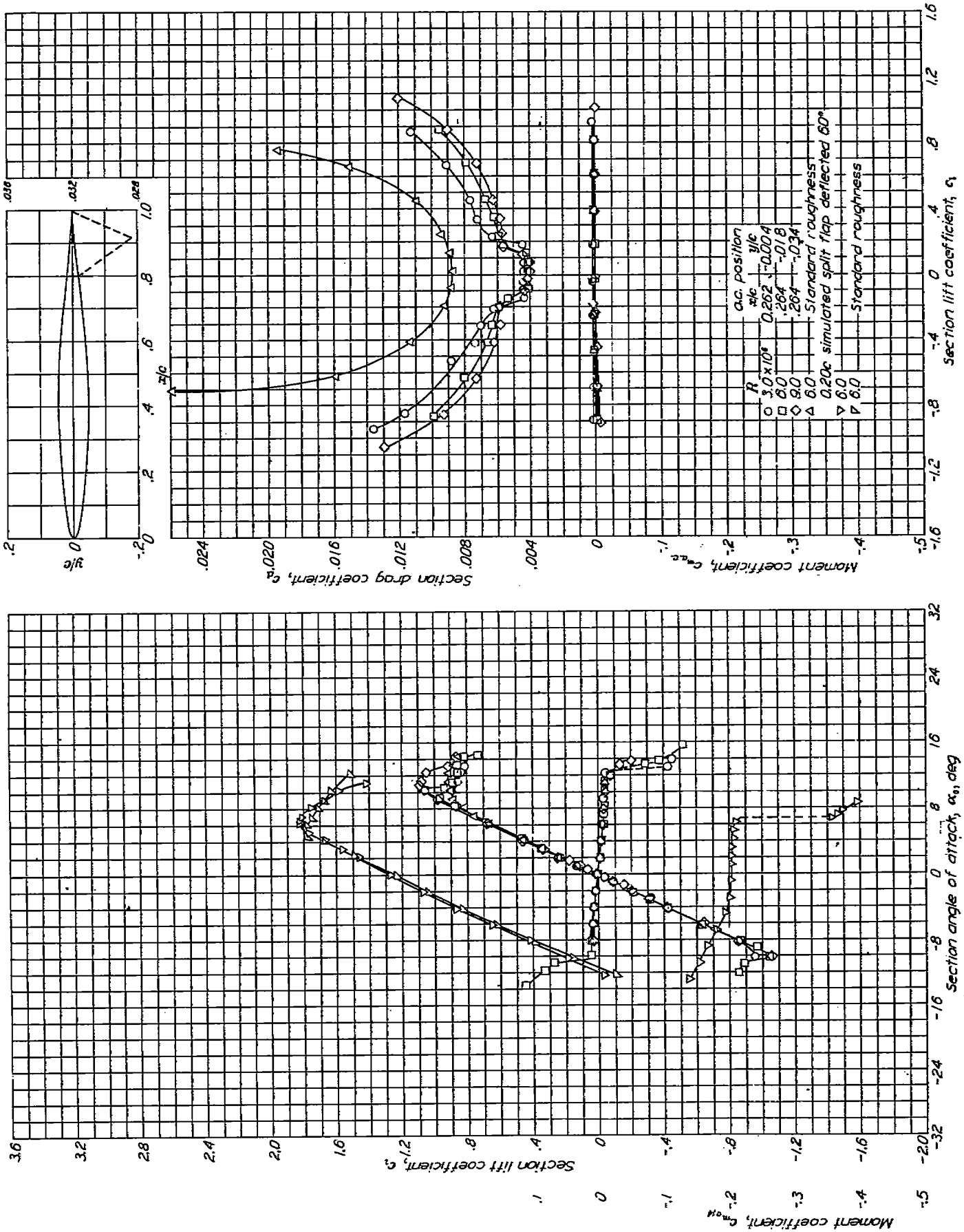

Aerodynamic characteristics of the NACA 65-009 airfoil section, 24-inch chord.

NACA 65-206

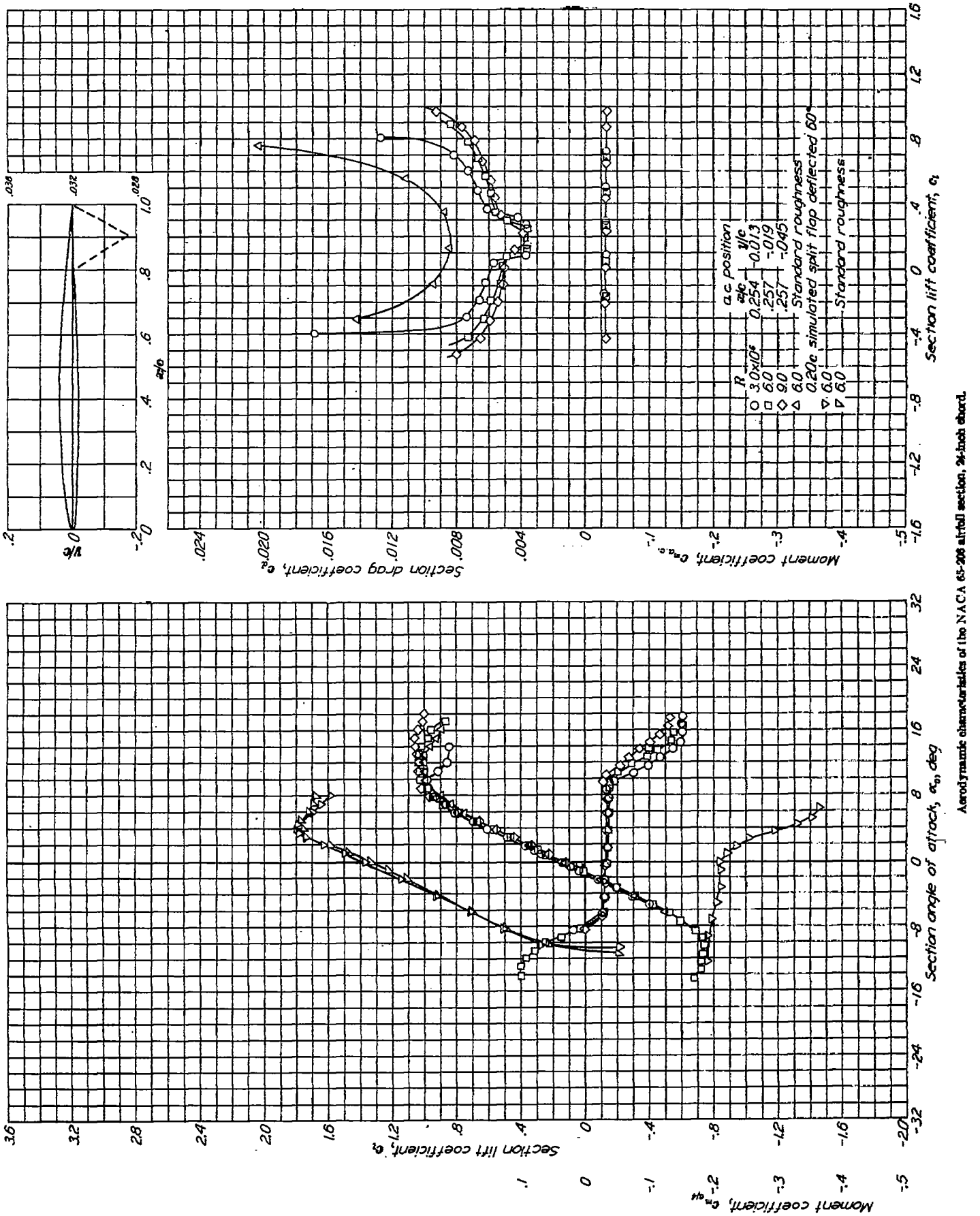

Aerodynamic characteristics of the NACA 65-206 airfoil section, 24-inch chord.

NACA 65-209

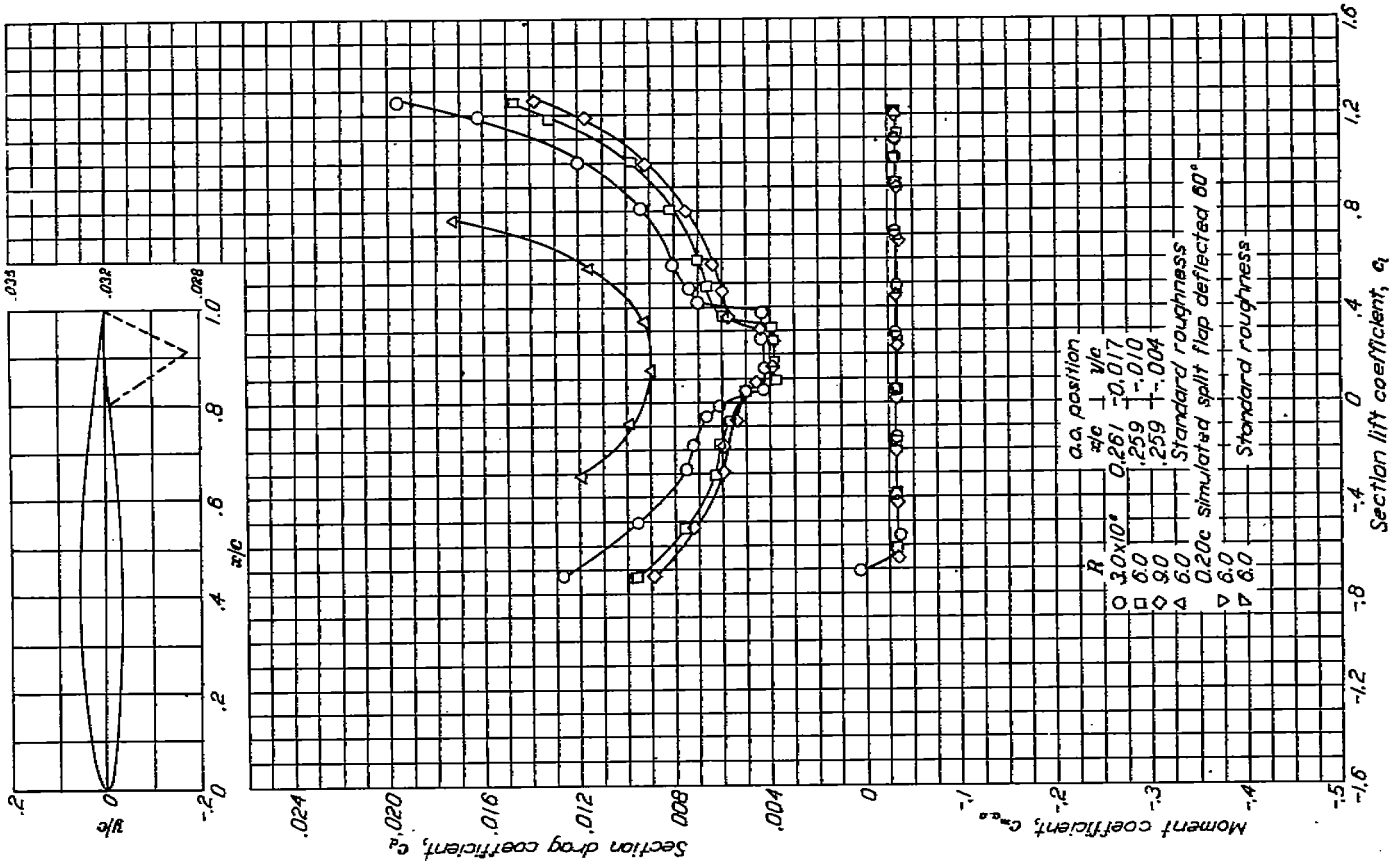

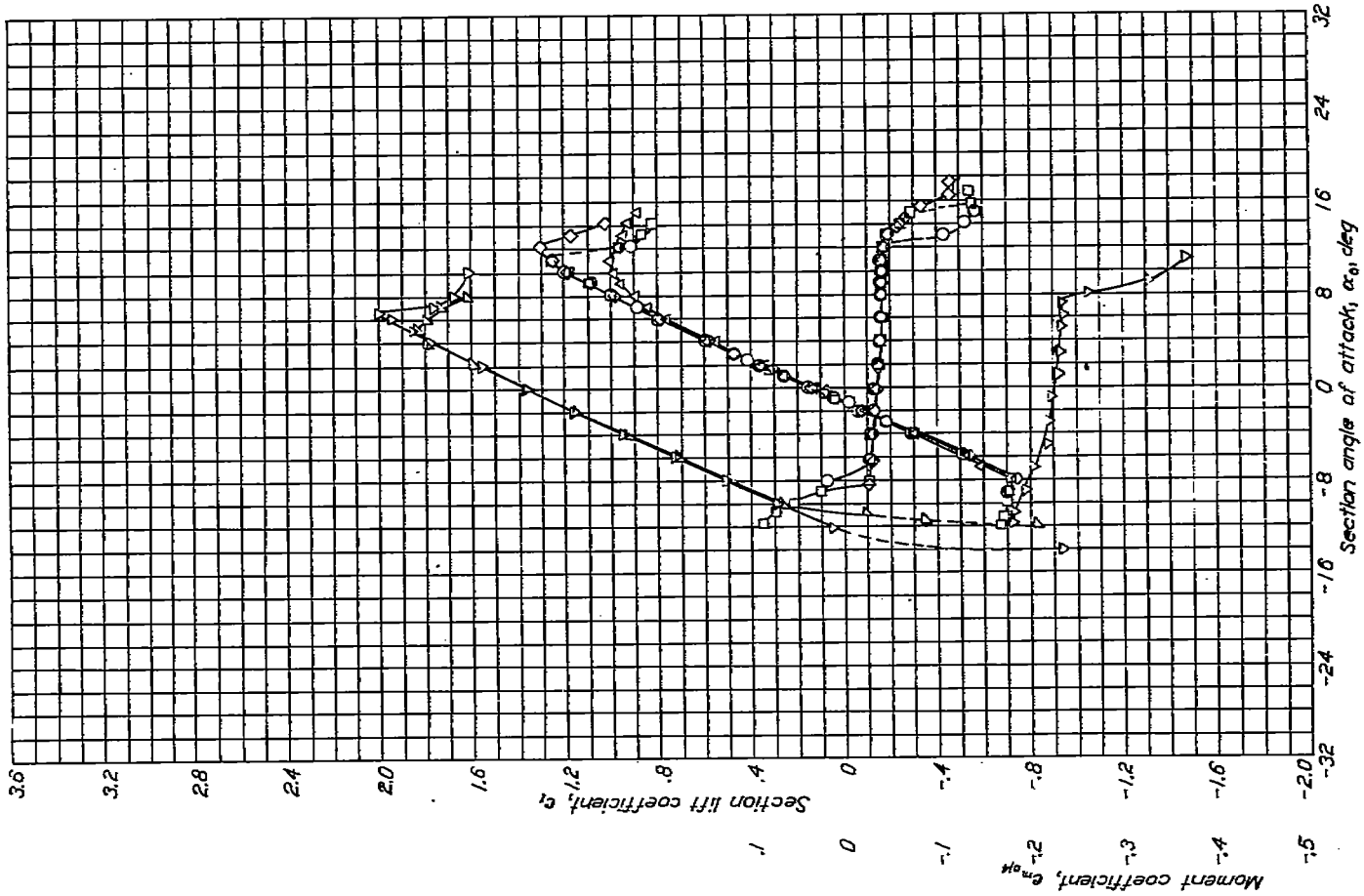

Aerodynamic characteristics of the NACA 65-209 airfoil section, 24-inch chord.

NACA 65-210

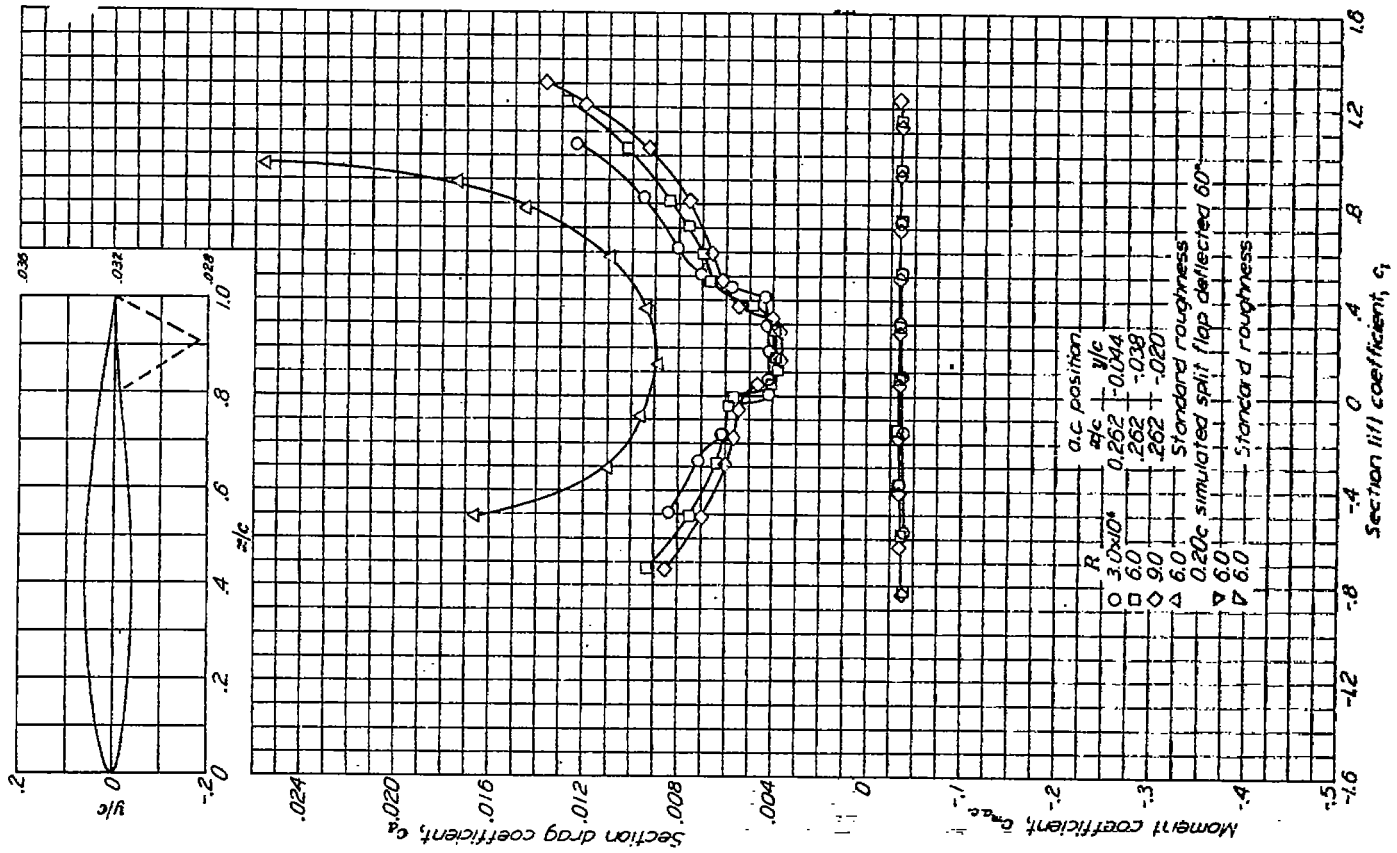

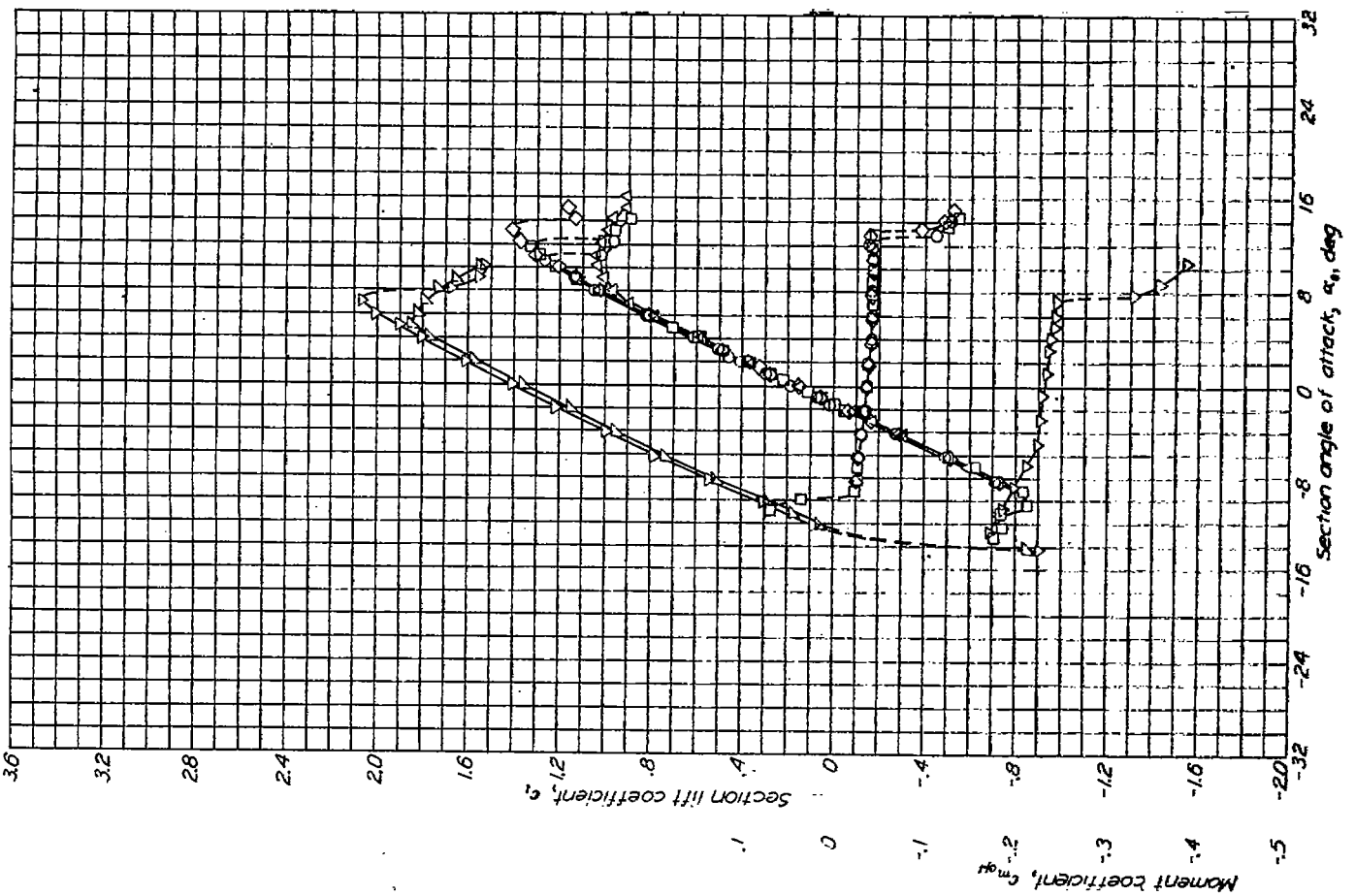

Aerodynamic characteristics of the NACA 65-210 airfoil section, 24-inch chord.

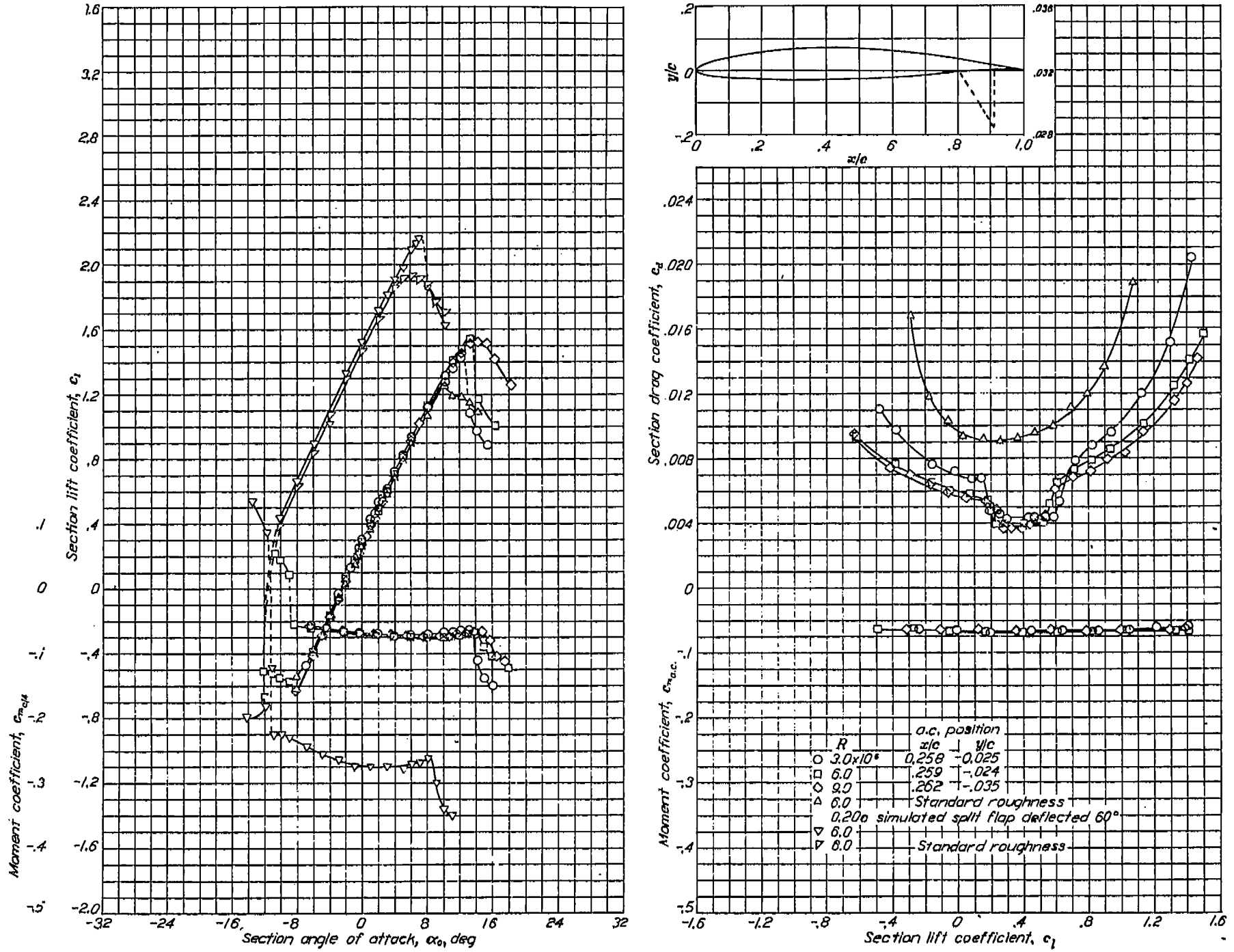

Aerodynamic characteristics of the NACA 65-410 airfoil section, 24-inch chord.

NACA 65$_1$-012

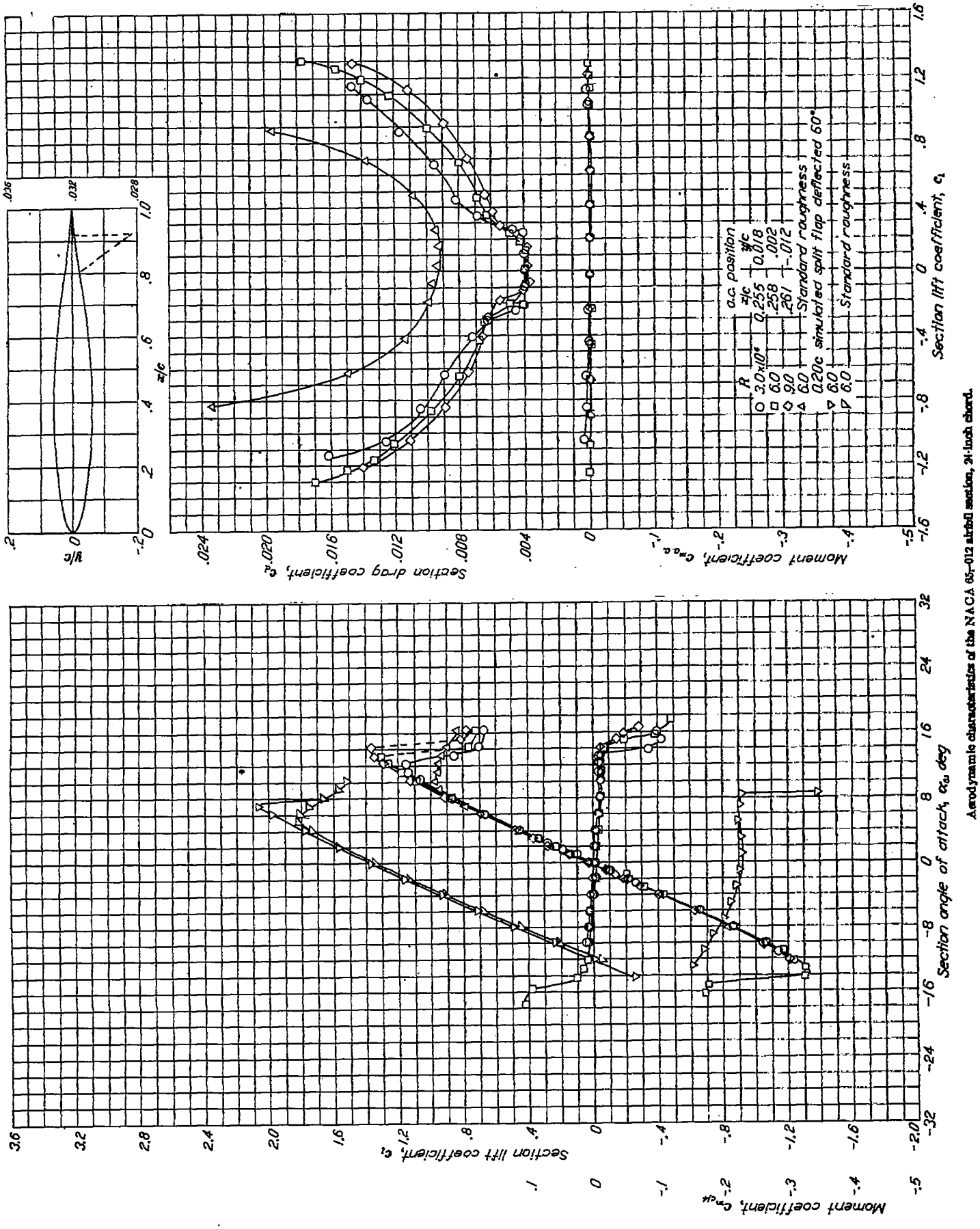

Aerodynamic characteristics of the NACA 65$_1$-012 airfoil section, 24-inch chord.

NACA 65₁-212

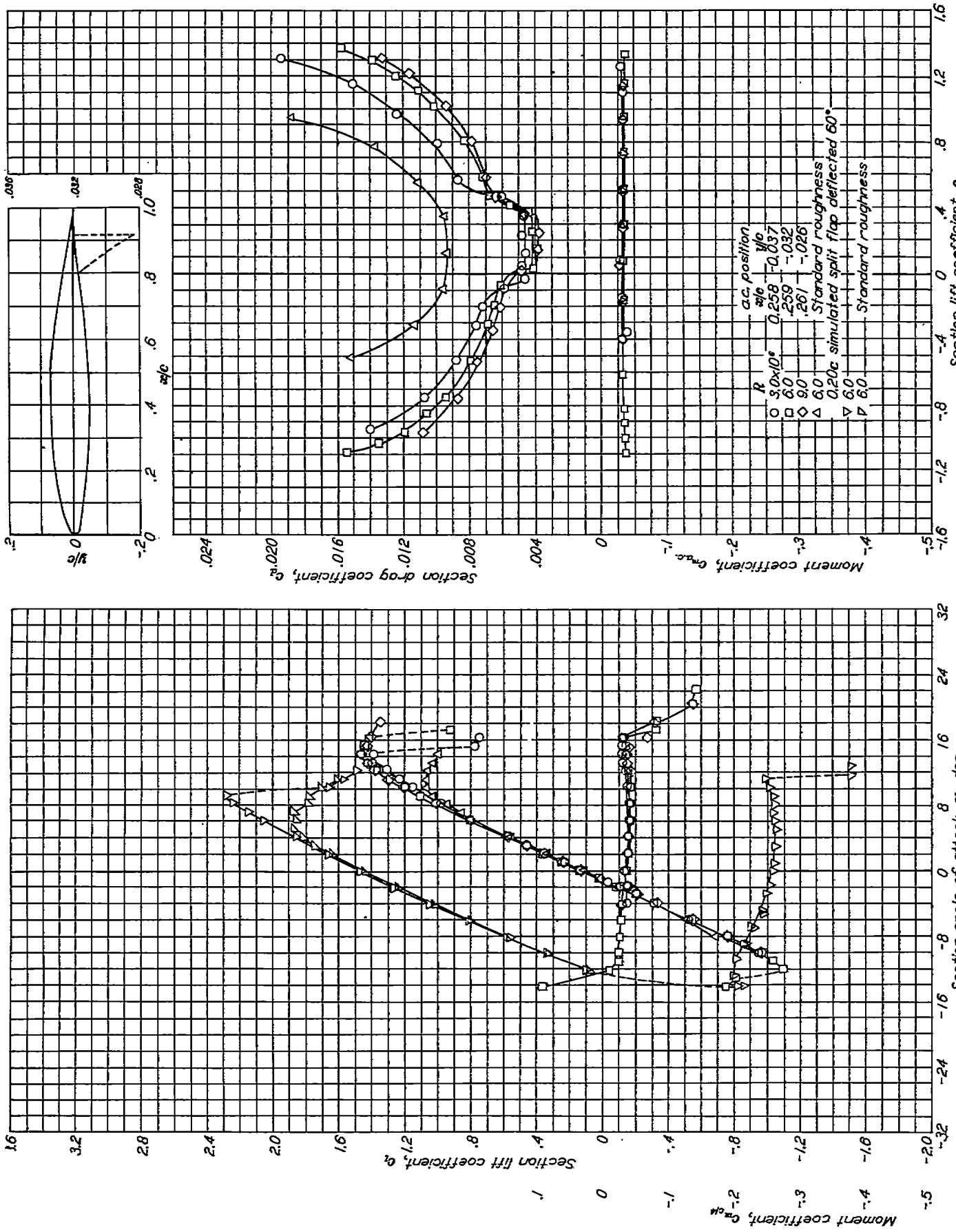

Aerodynamic characteristics of the NACA 65₁-212 airfoil section, 24-inch chord.

NACA 65$_1$-212 with flap

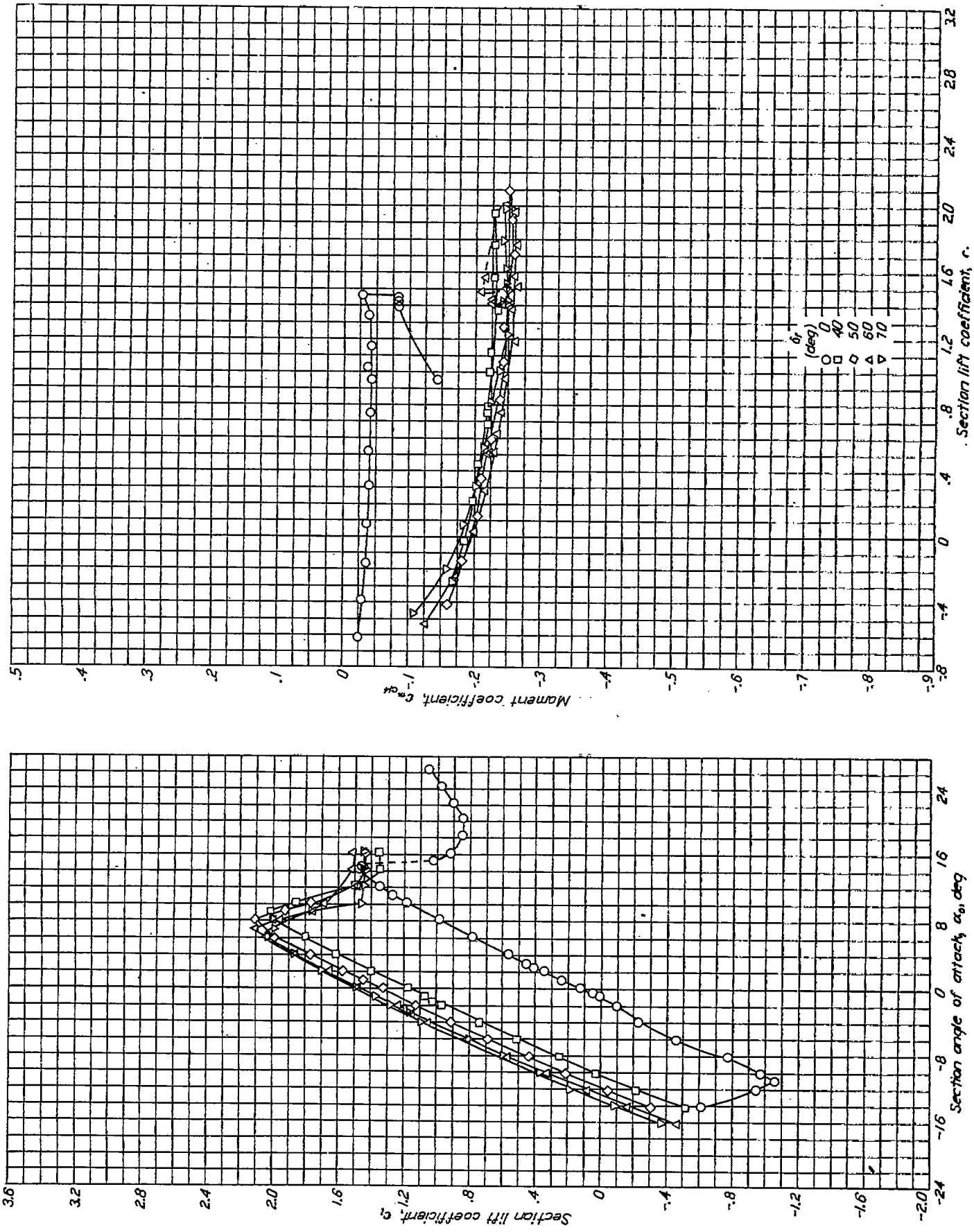

Lift and moment characteristics of the NACA 65-212 airfoil section with 0.20c split flap. R=6×10^6.

NACA 65$_1$-212, $a = 0.6$

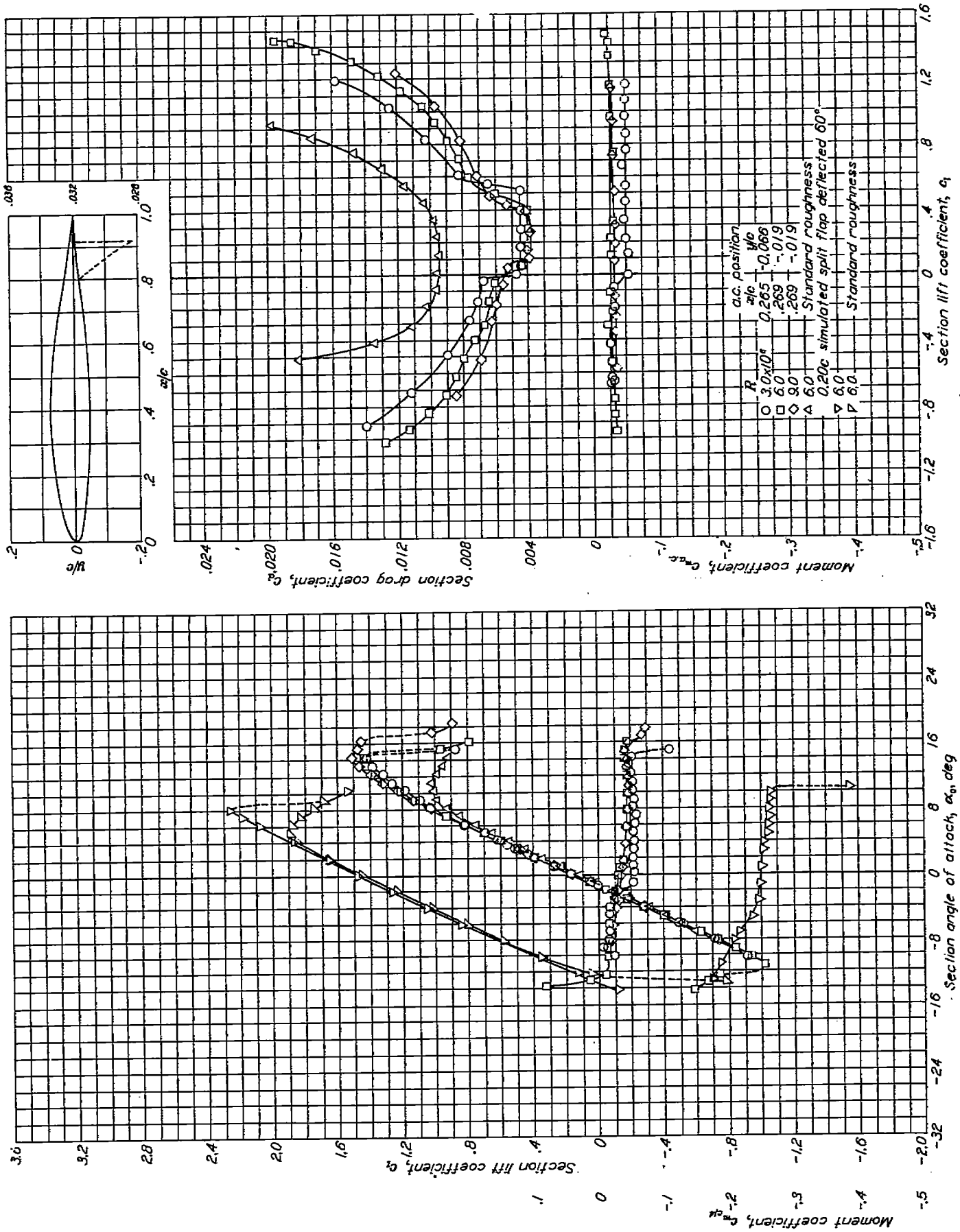

Aerodynamic characteristics of the NACA 65$_1$-212, a=0.6 airfoil section, 24-inch chord.

NACA 65$_1$-412

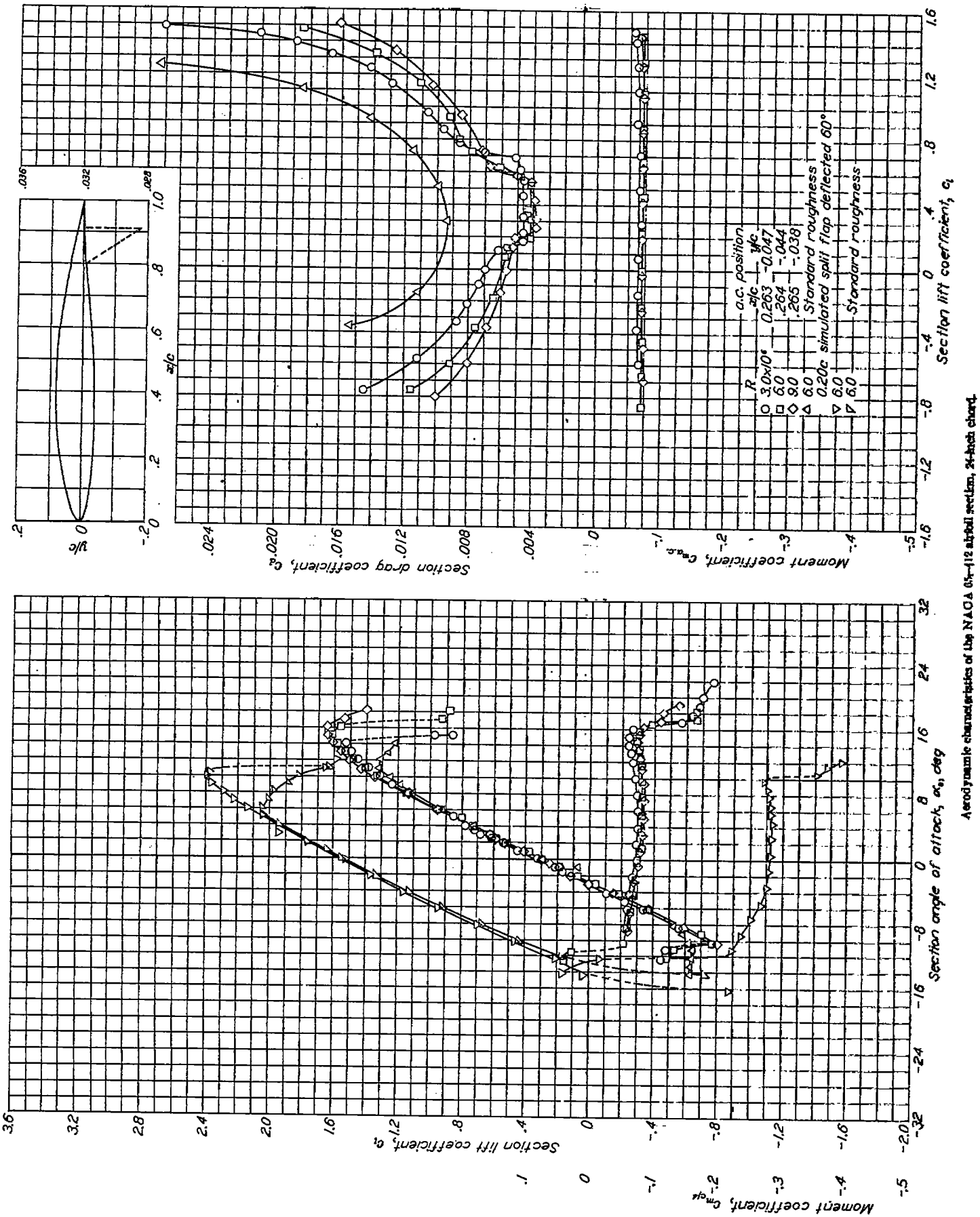

Aerodynamic characteristics of the NACA 65$_1$-412 airfoil section, 24-inch chord.

NACA 65$_2$-015

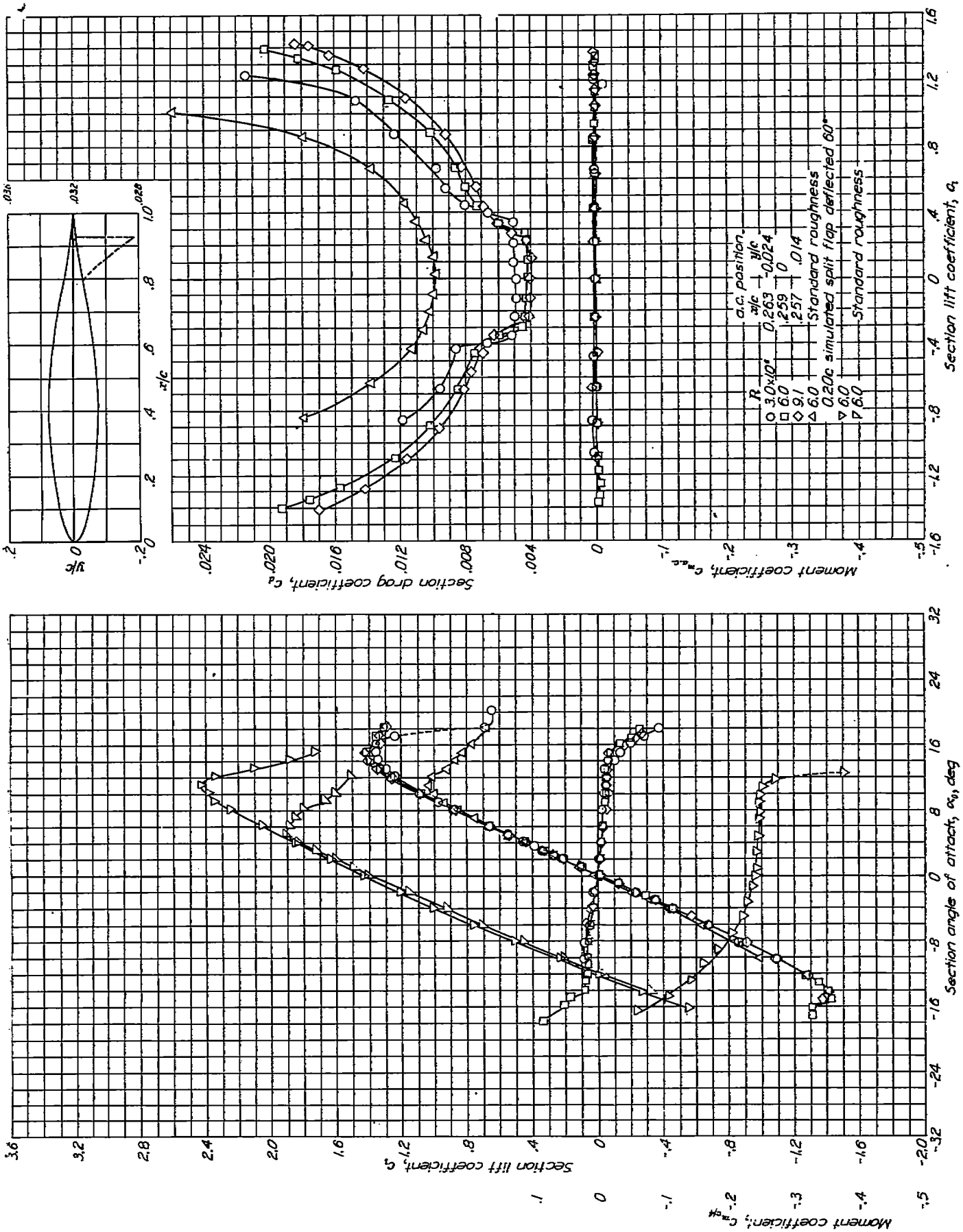

Aerodynamic characteristics of the NACA 65$_2$-015 airfoil section, 24-inch chord.

NACA 65$_2$-215

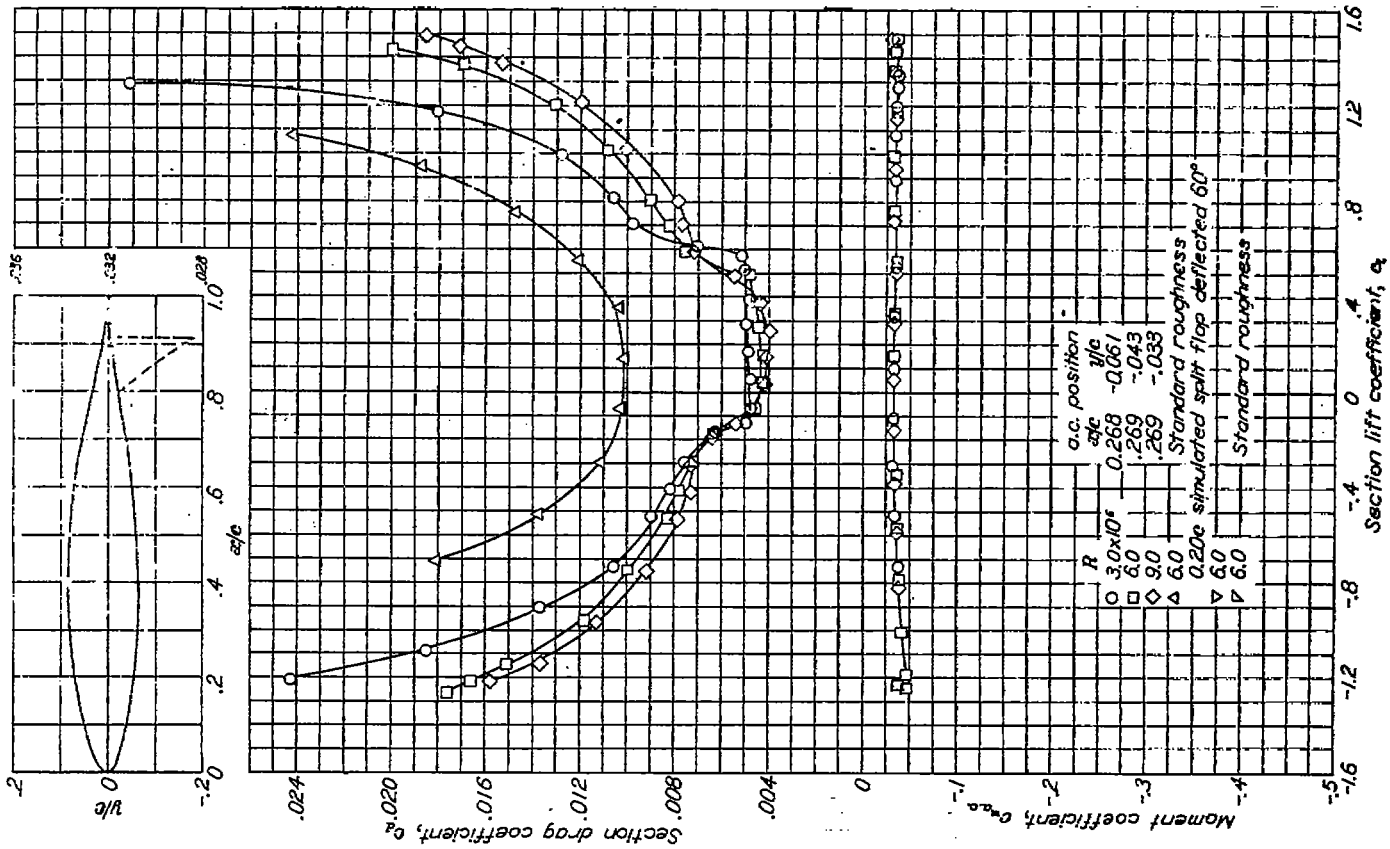

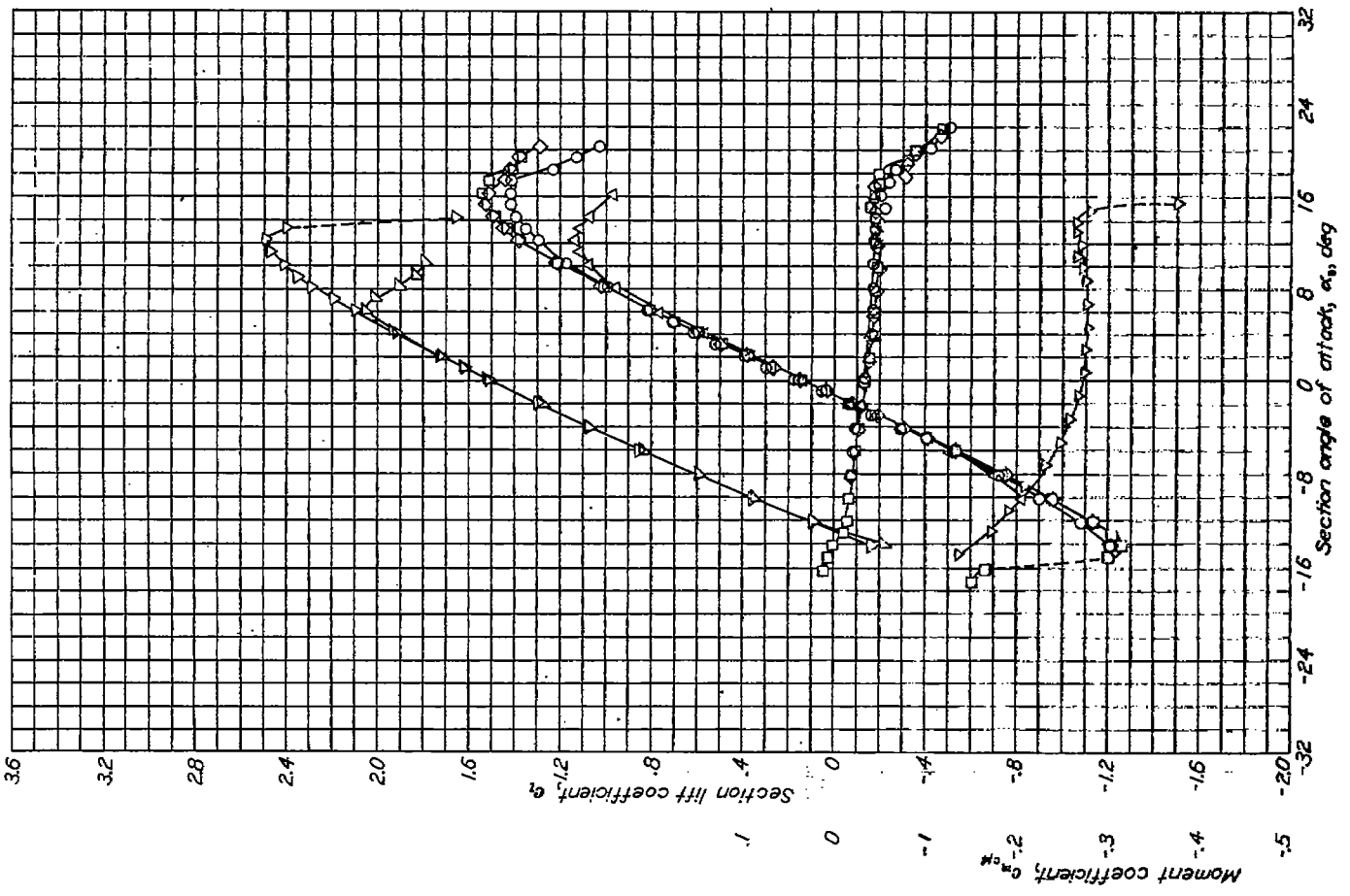

Aerodynamic characteristics of the NACA 65$_2$-215 airfoil section, 24 inch chord.

NACA 65$_2$-415

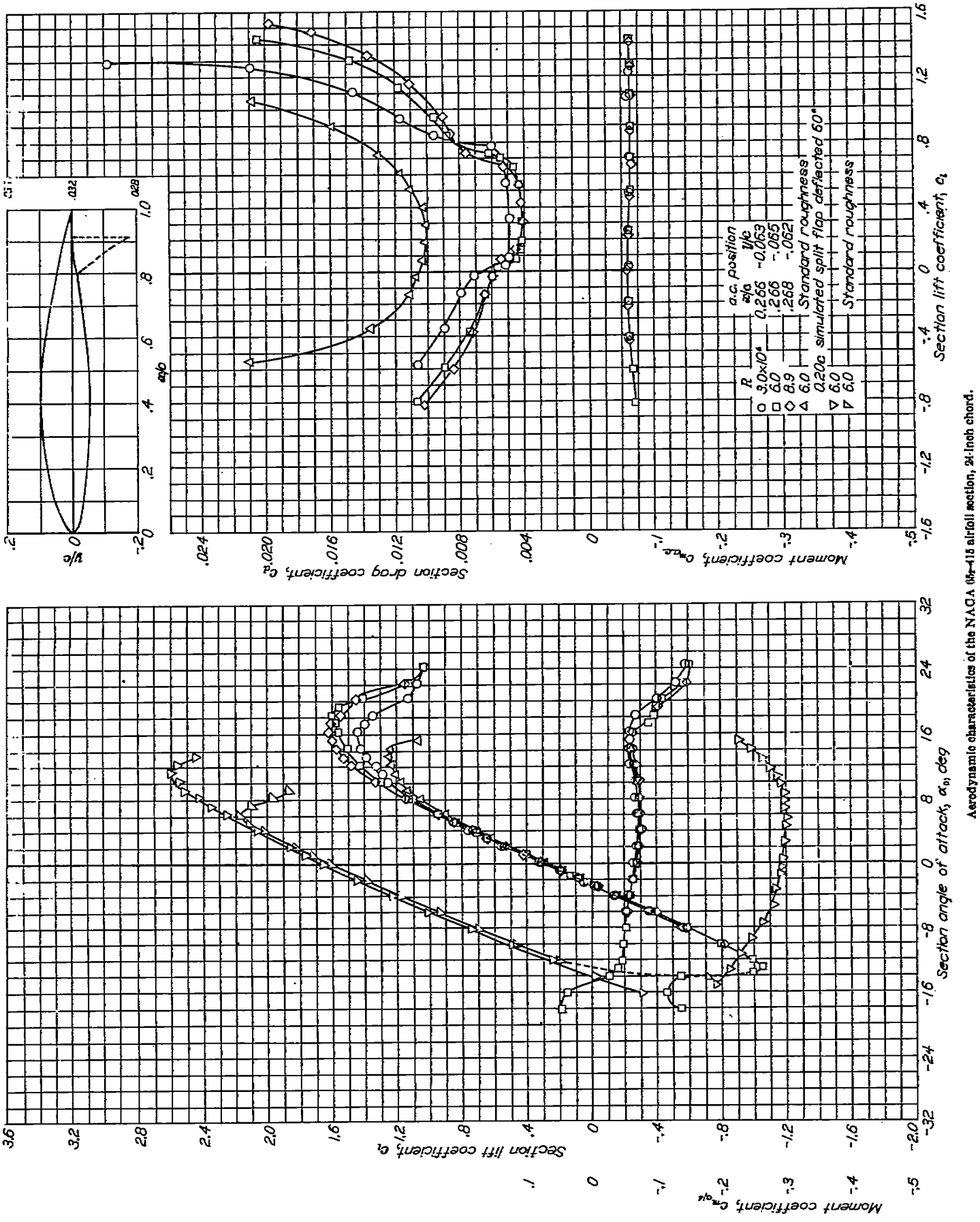

Aerodynamic characteristics of the NACA 65$_2$-415 airfoil section, 24-inch chord.

NACA 65$_2$-415, $a = 0.5$

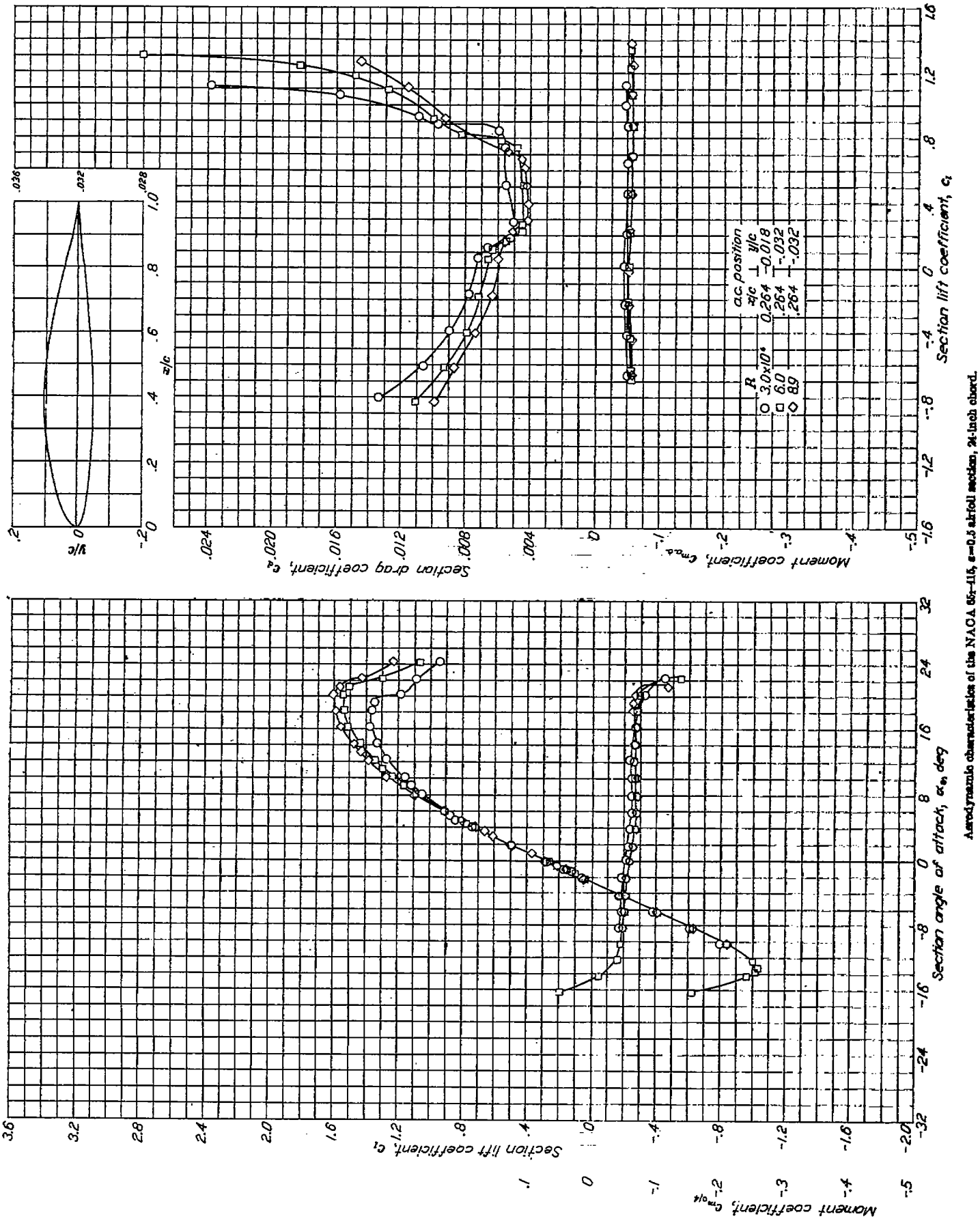

Aerodynamic characteristics of the NACA 65$_2$-415, a=0.5 airfoil section, 24-inch chord.

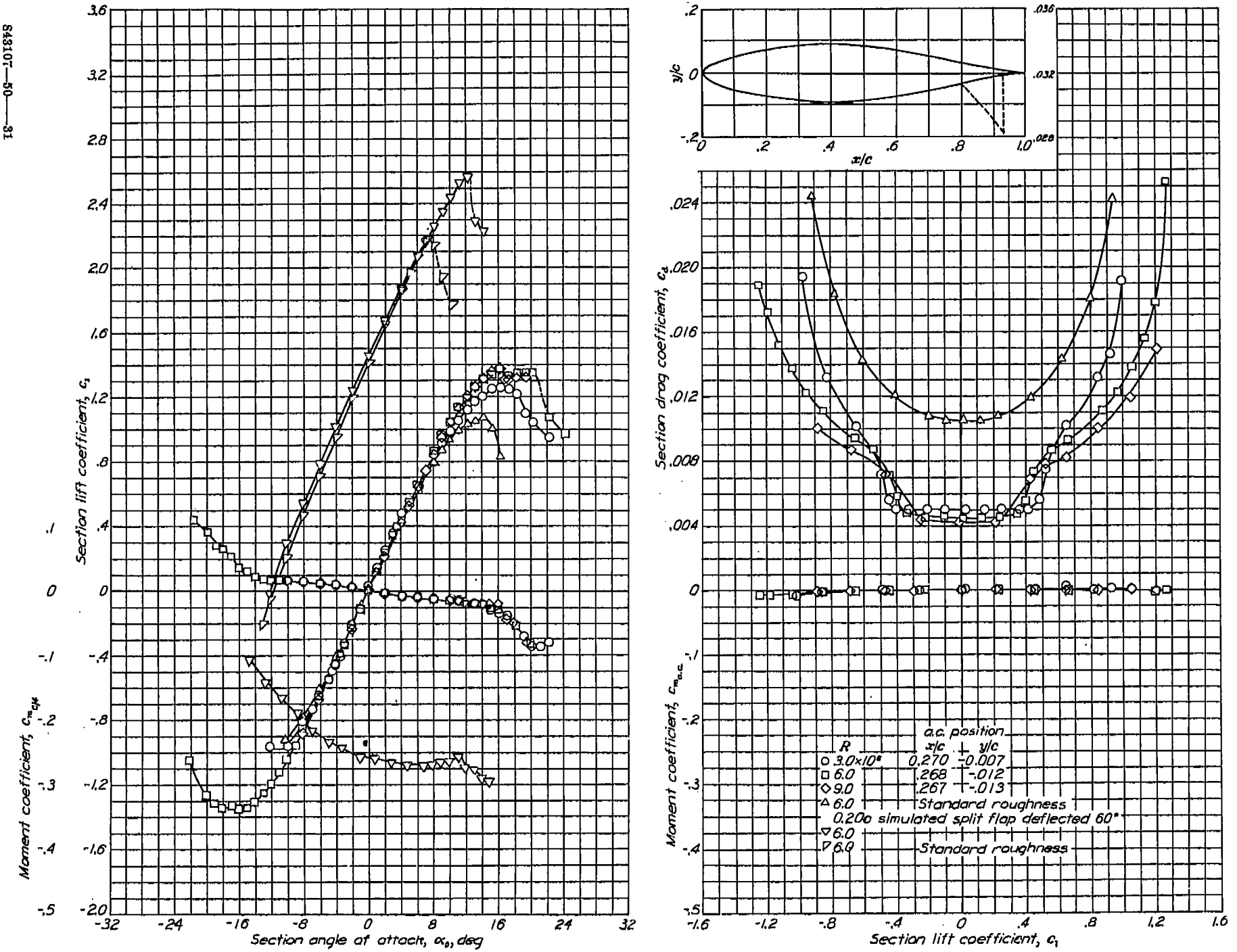

Aerodynamic characteristics of the NACA 65₁-018 airfoil section, 24-inch chord.

S4810T—50——31

NACA 65$_3$-118 with flap

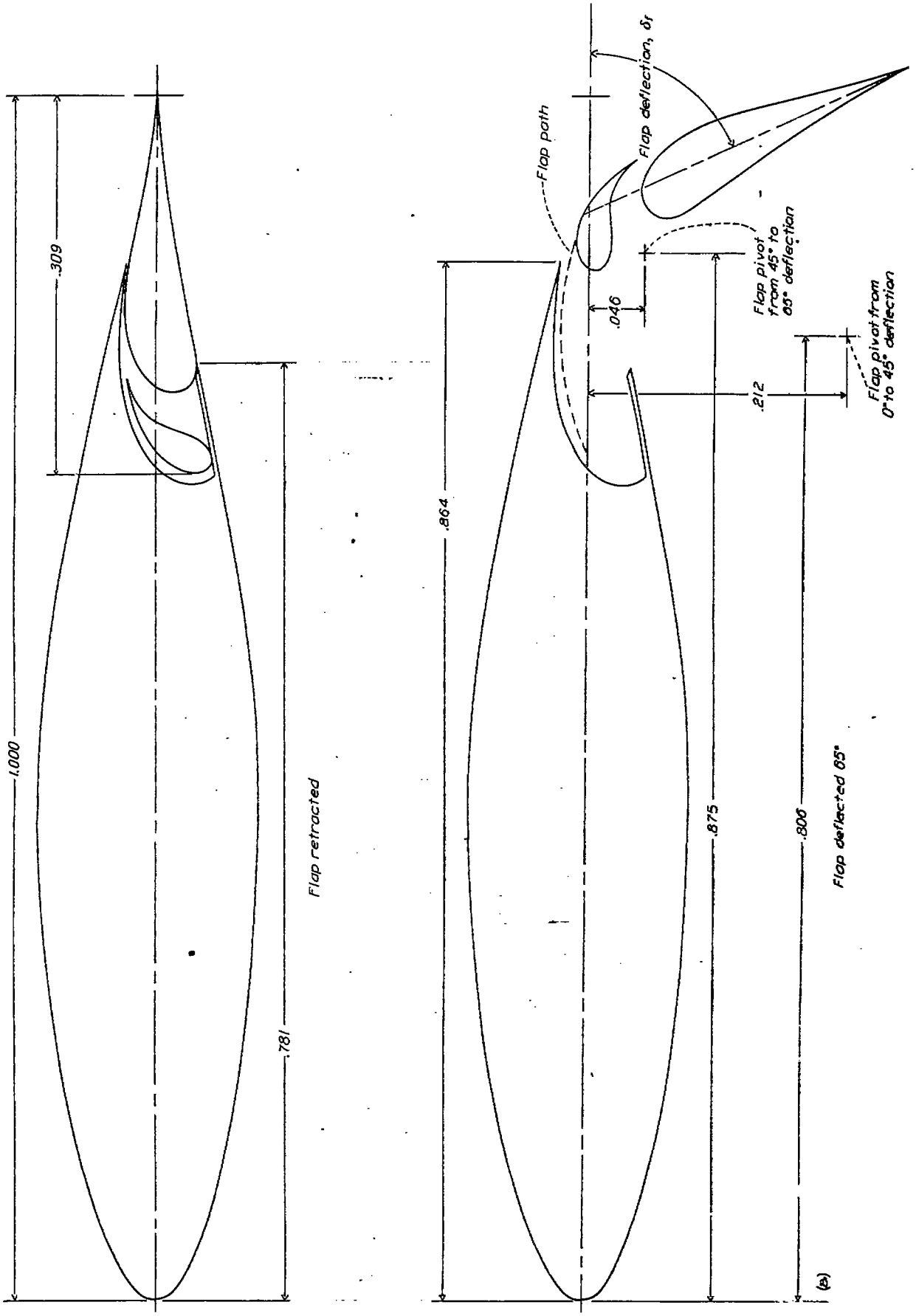

(a) Configuration.

NACA 65$_3$-118 airfoil section with 0.30c single slotted flap.

NACA 65₃-118 with flap

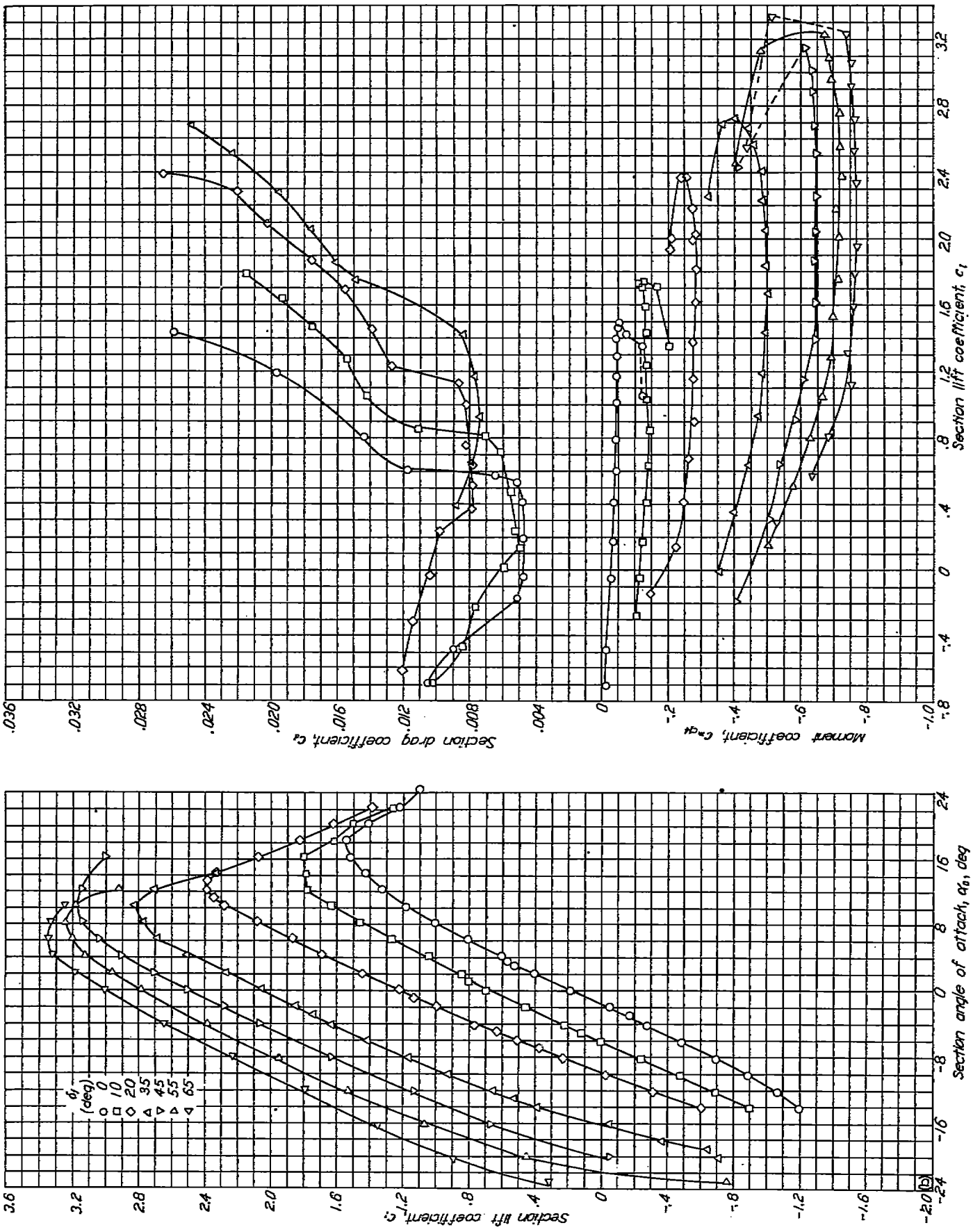

(b) Aerodynamic characteristics. $R=6\times10^6$.

NACA 65₃-118 airfoil section with 0.30c double slotted flap.

NACA 65$_3$-218

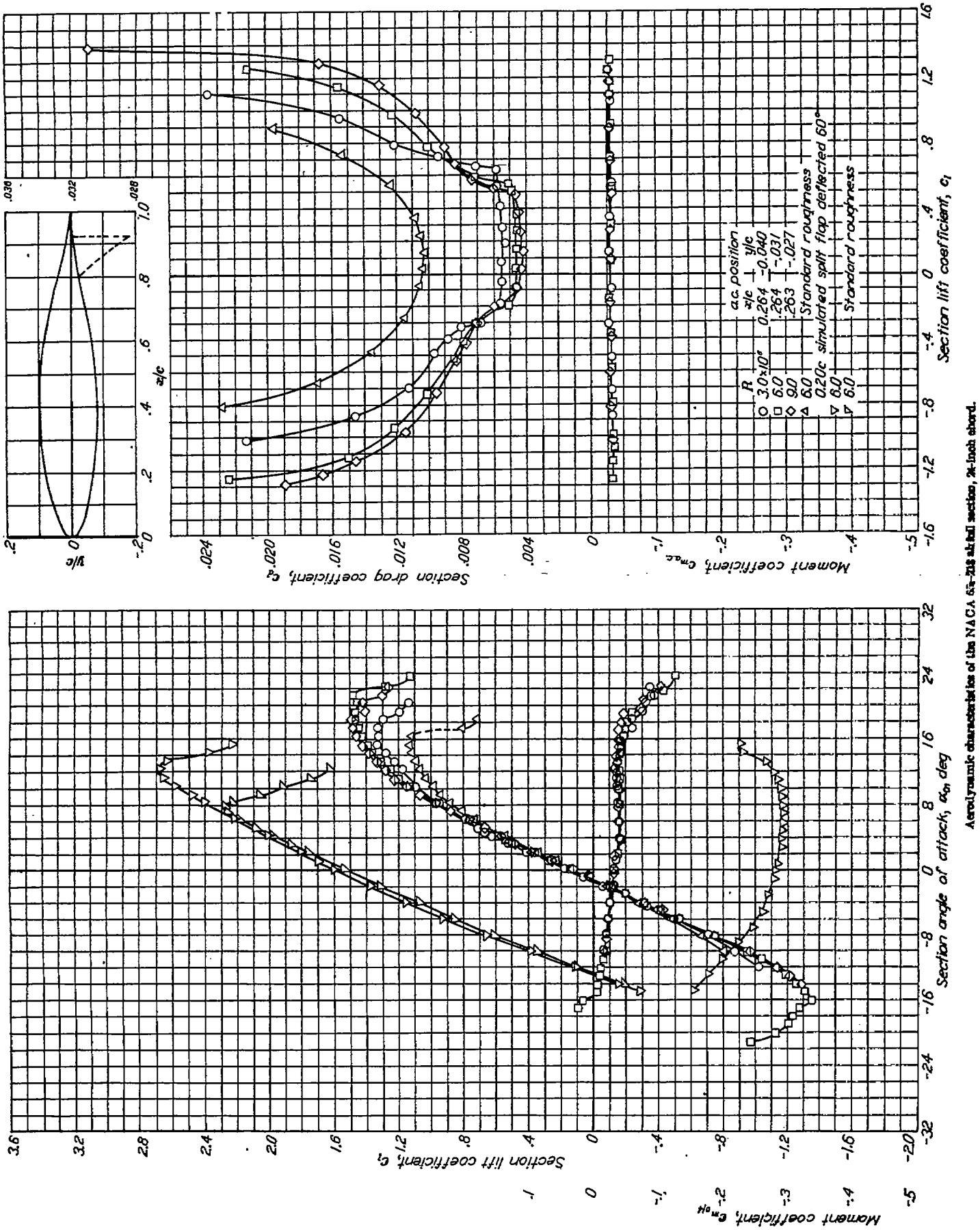

Aerodynamic characteristics of the NACA 65$_3$-218 airfoil section, 24-inch chord.

NACA 65$_3$-418

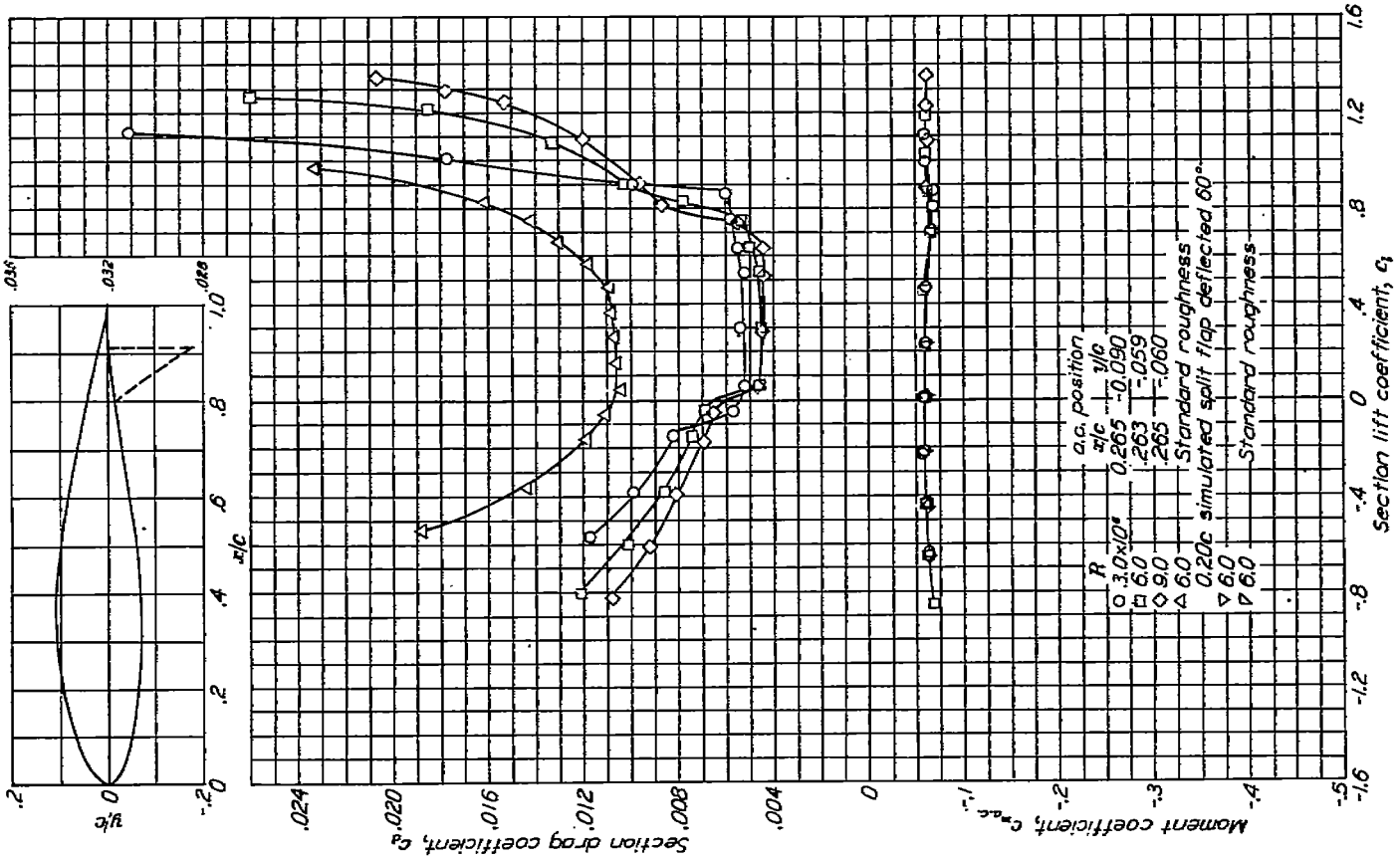

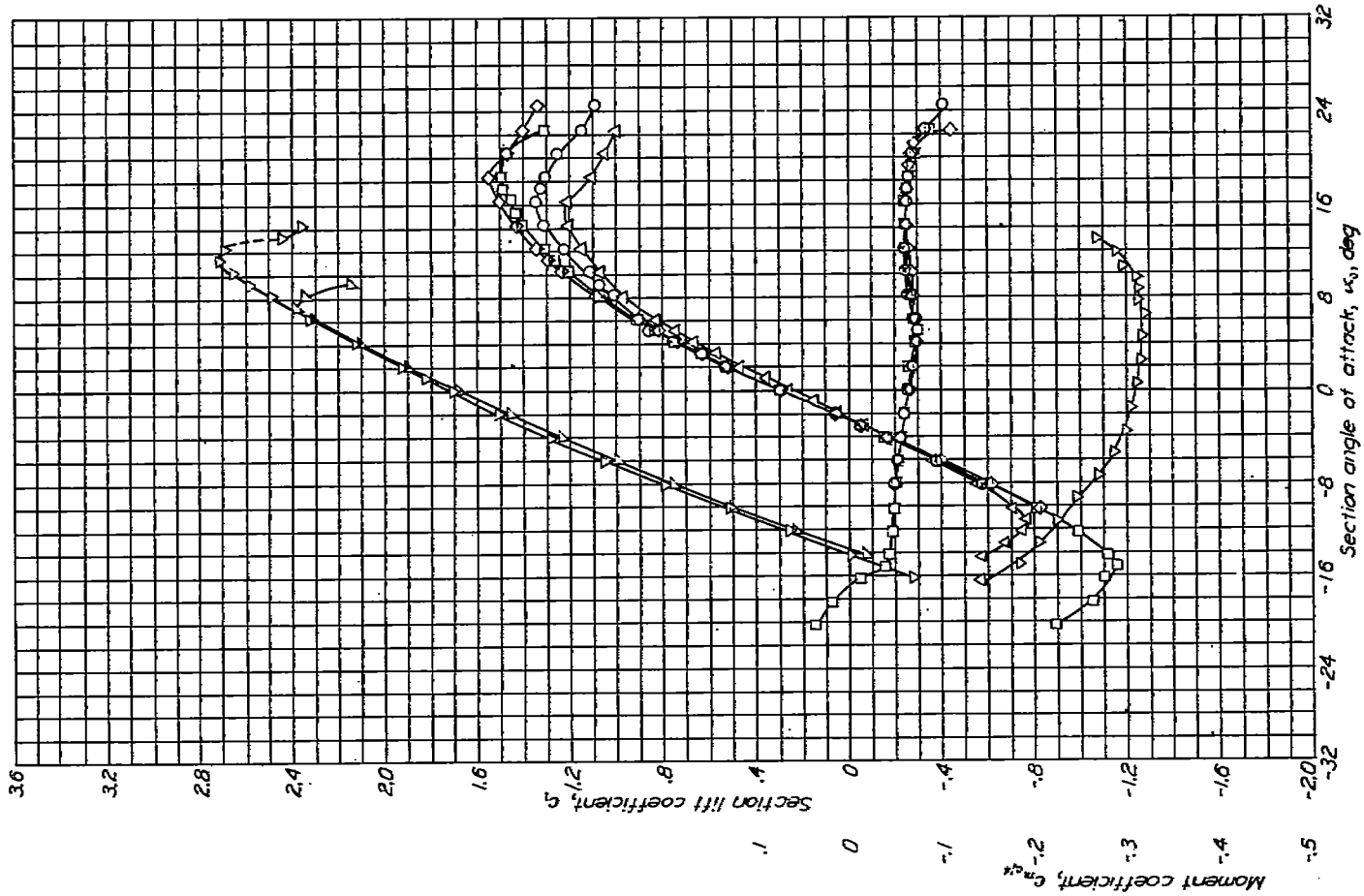

Aerodynamic characteristics of the NACA 65$_3$-418 airfoil section, 24-inch chord.

NACA 65$_3$-418, $a = 0.5$

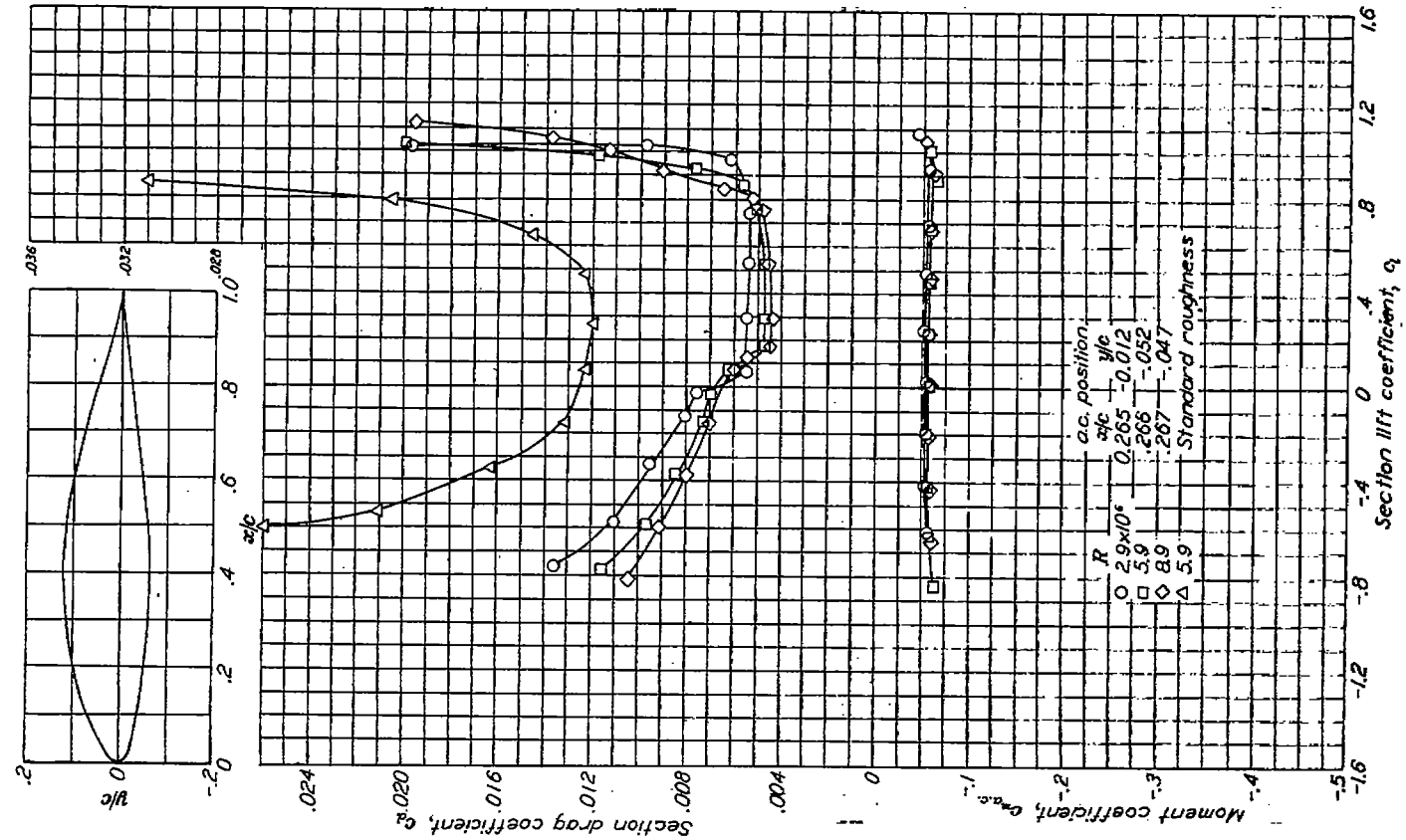

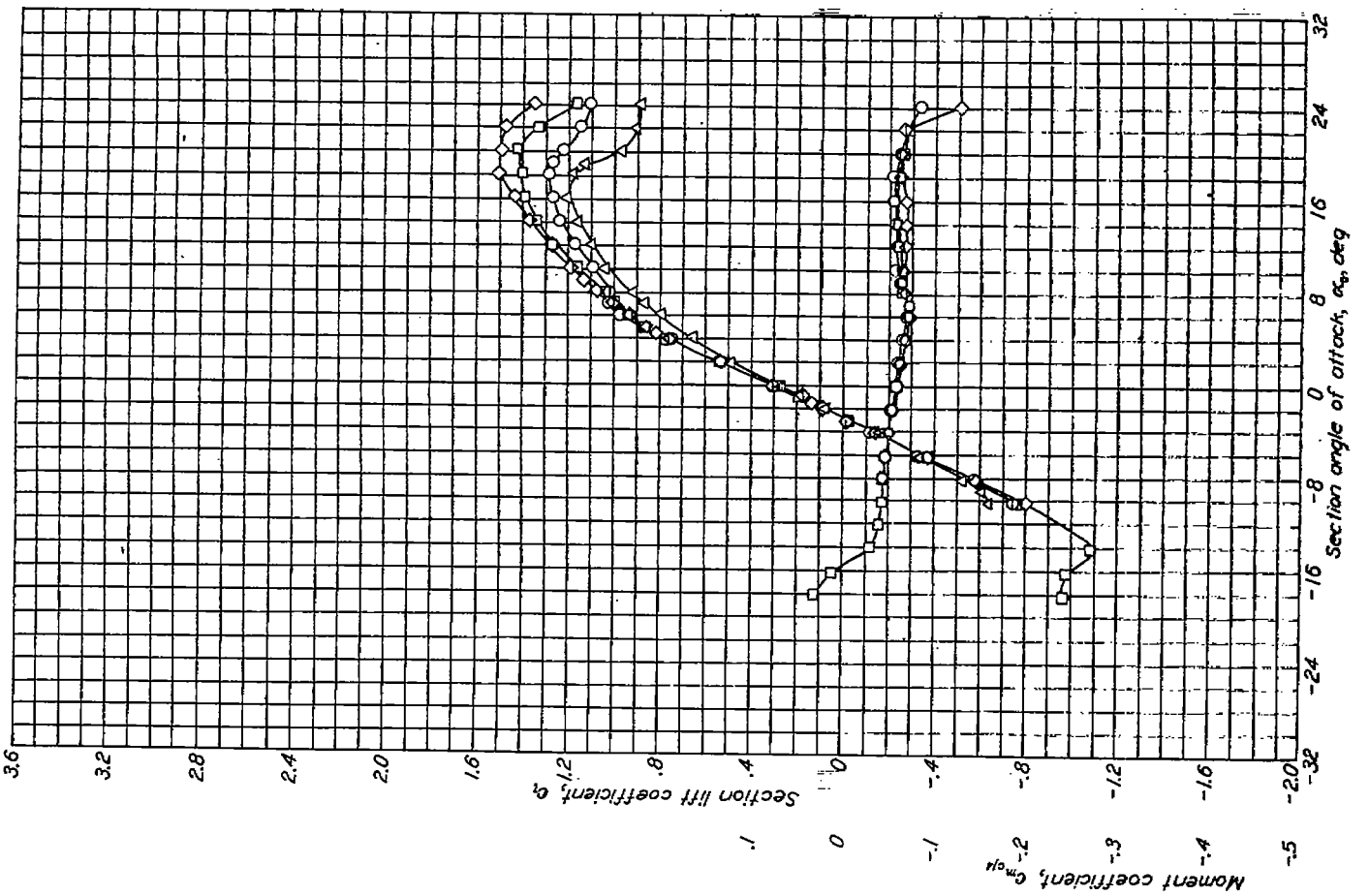

Aerodynamic characteristics of the NACA 65$_3$-418, $a = 0.5$ airfoil section, 24-inch chord.

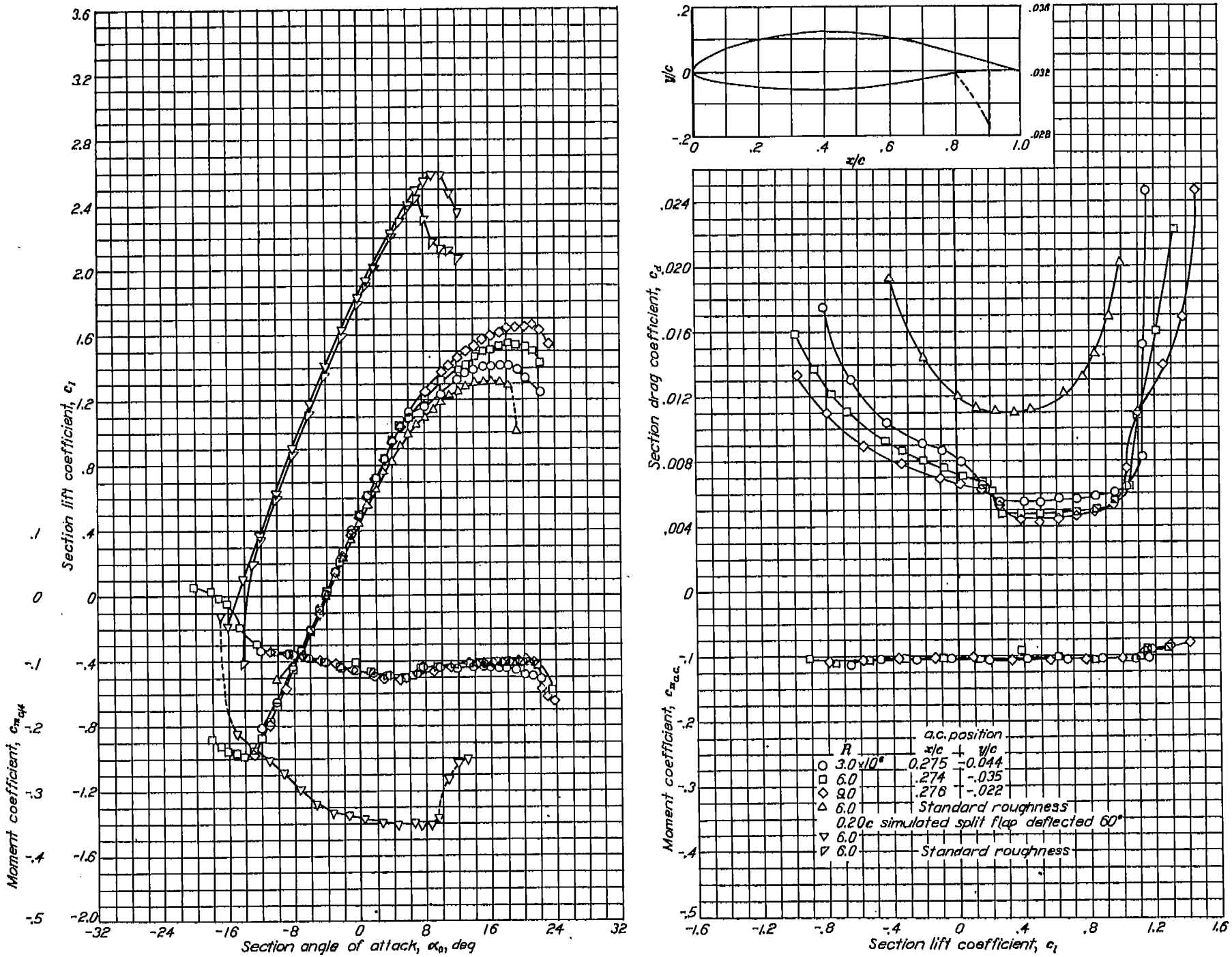

Aerodynamic characteristics of the NACA 65₃-618 airfoil section, 24-inch chord.

NACA 65$_3$-618, $a = 0.5$

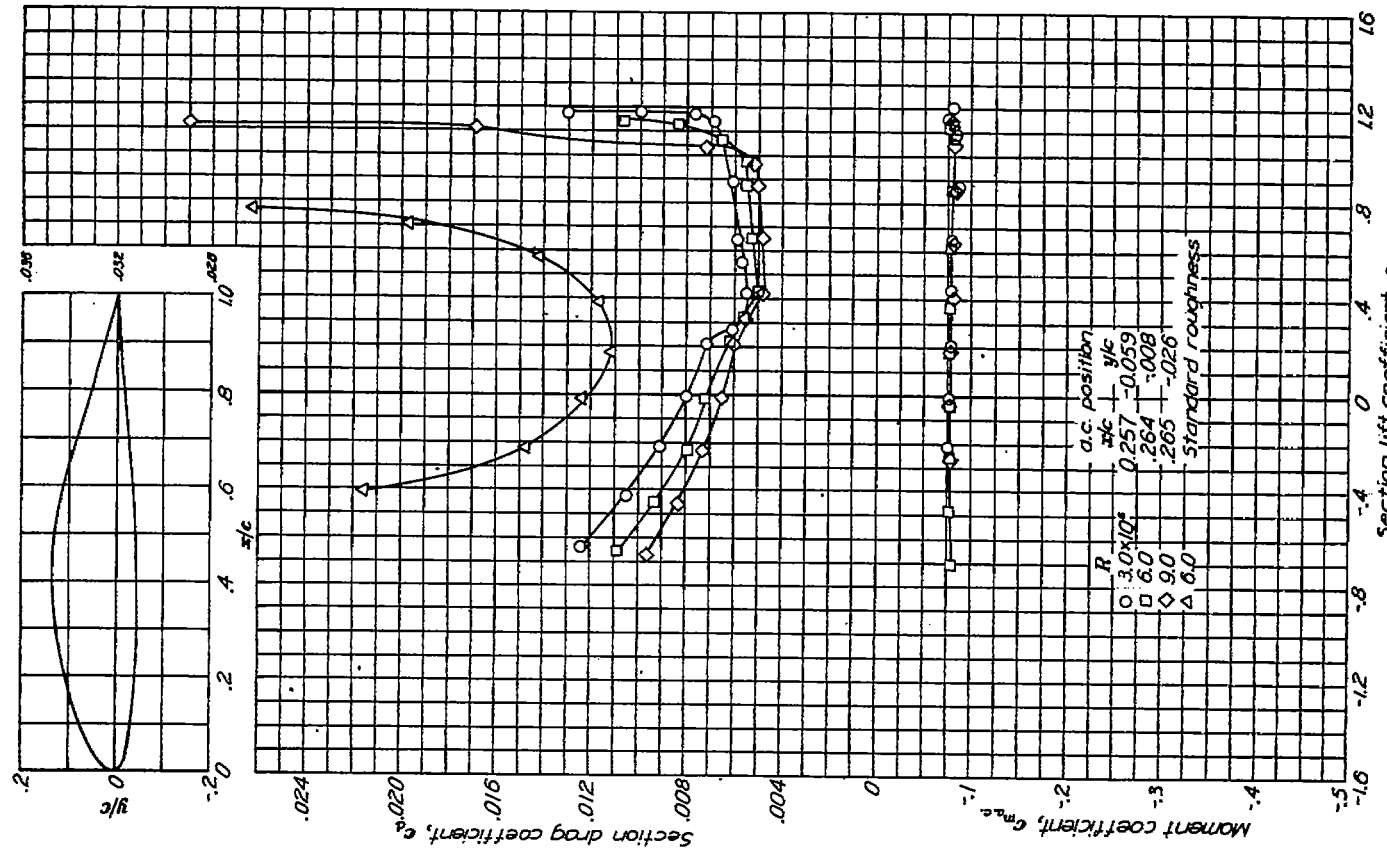

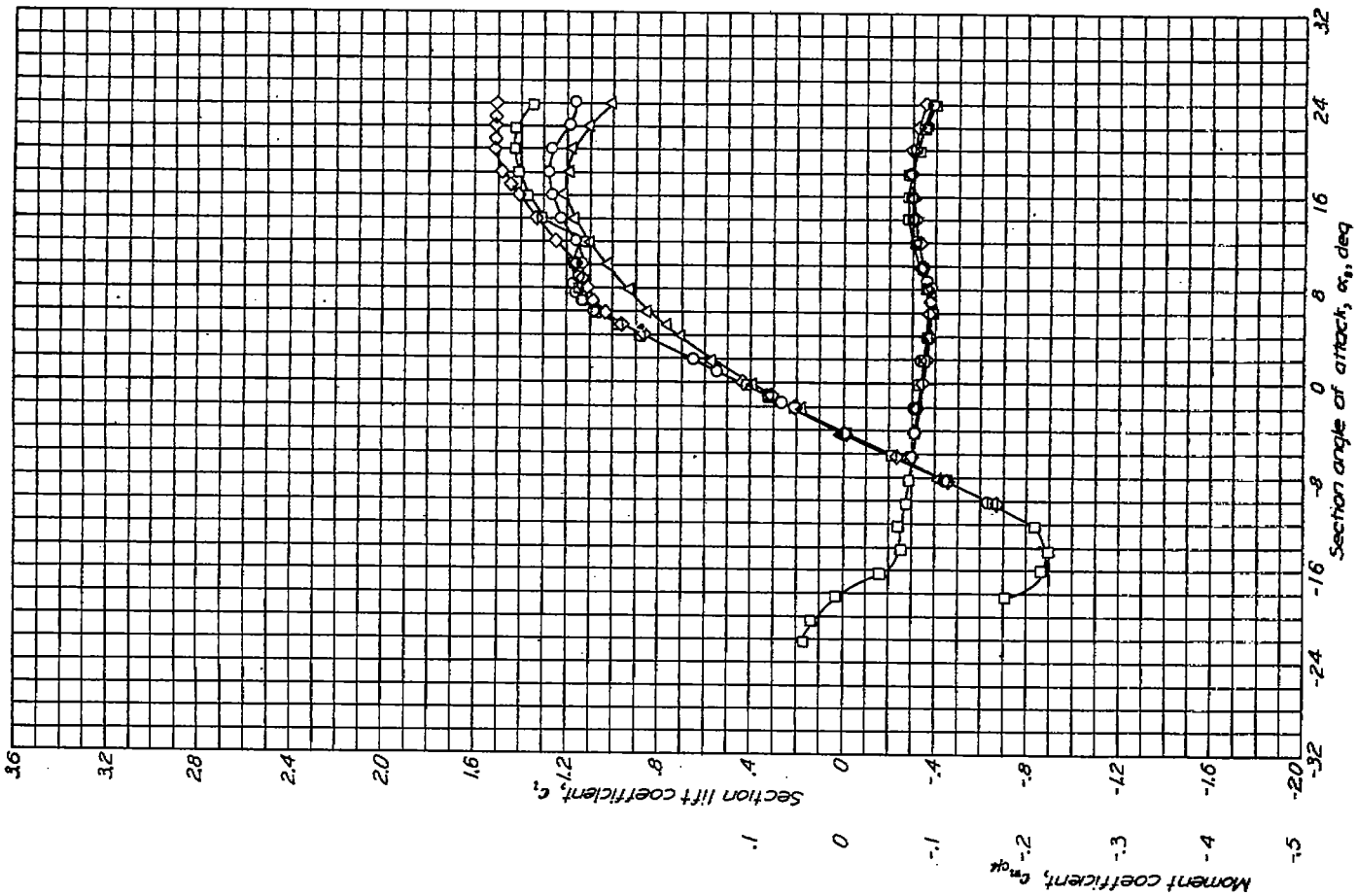

Aerodynamic characteristics of the NACA 65$_3$-618, $a = 0.5$ airfoil section, 24-inch chord.

S43107—50——32

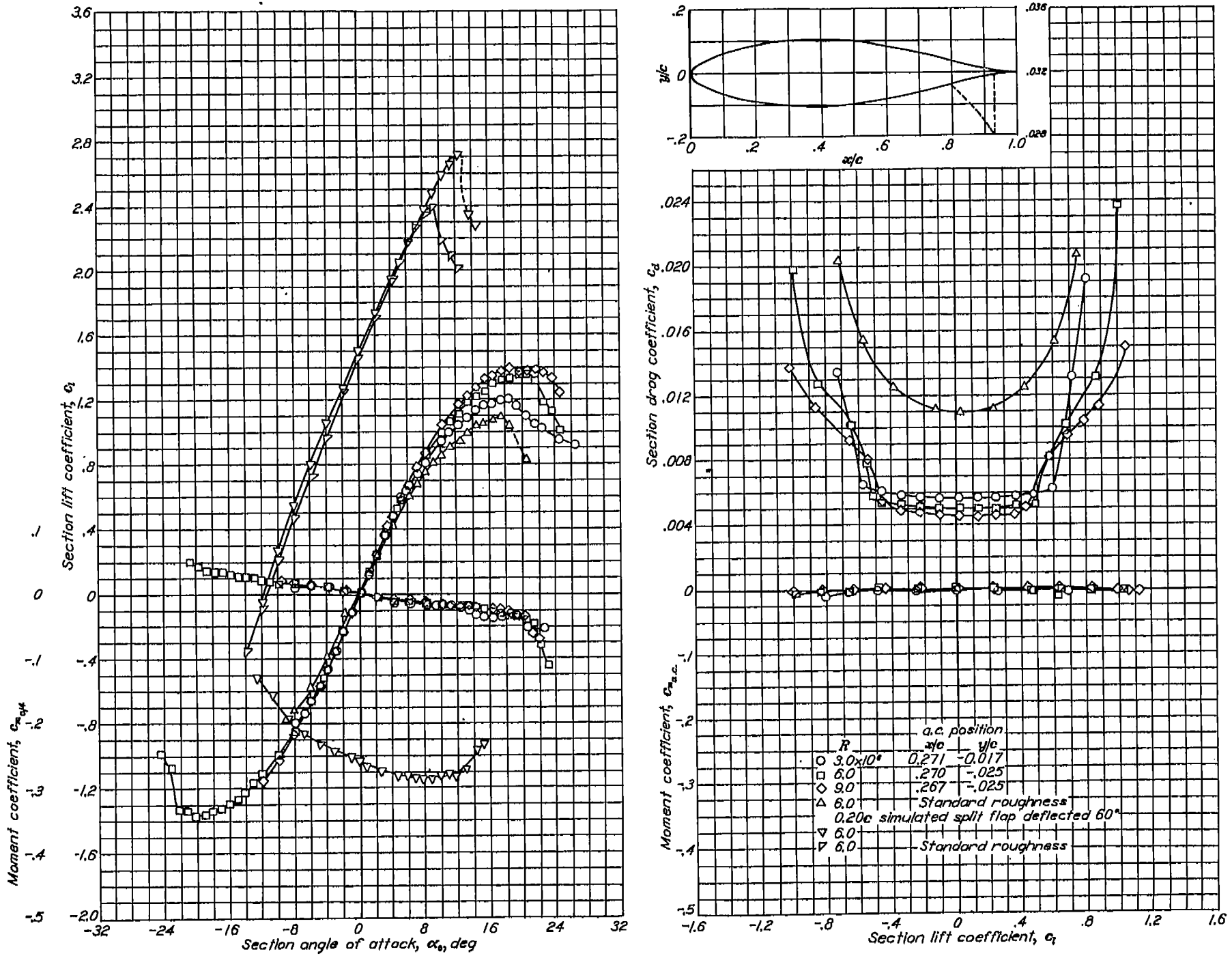

Aerodynamic characteristics of the NACA 654-021 airfoil section, 24-inch chord.

NACA 654-221

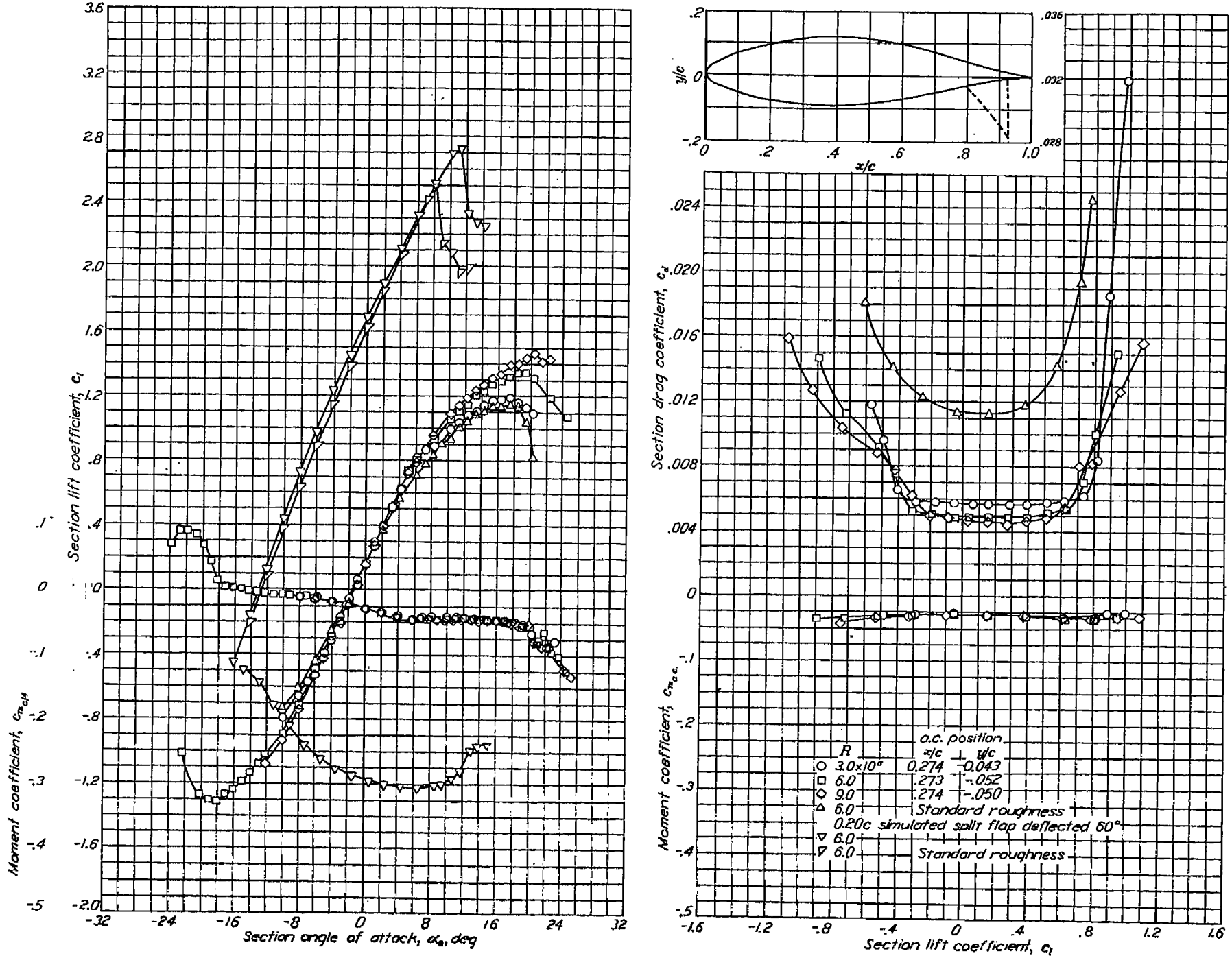

Aerodynamic characteristics of the NACA 654-221 airfoil section. 24-inch chord.

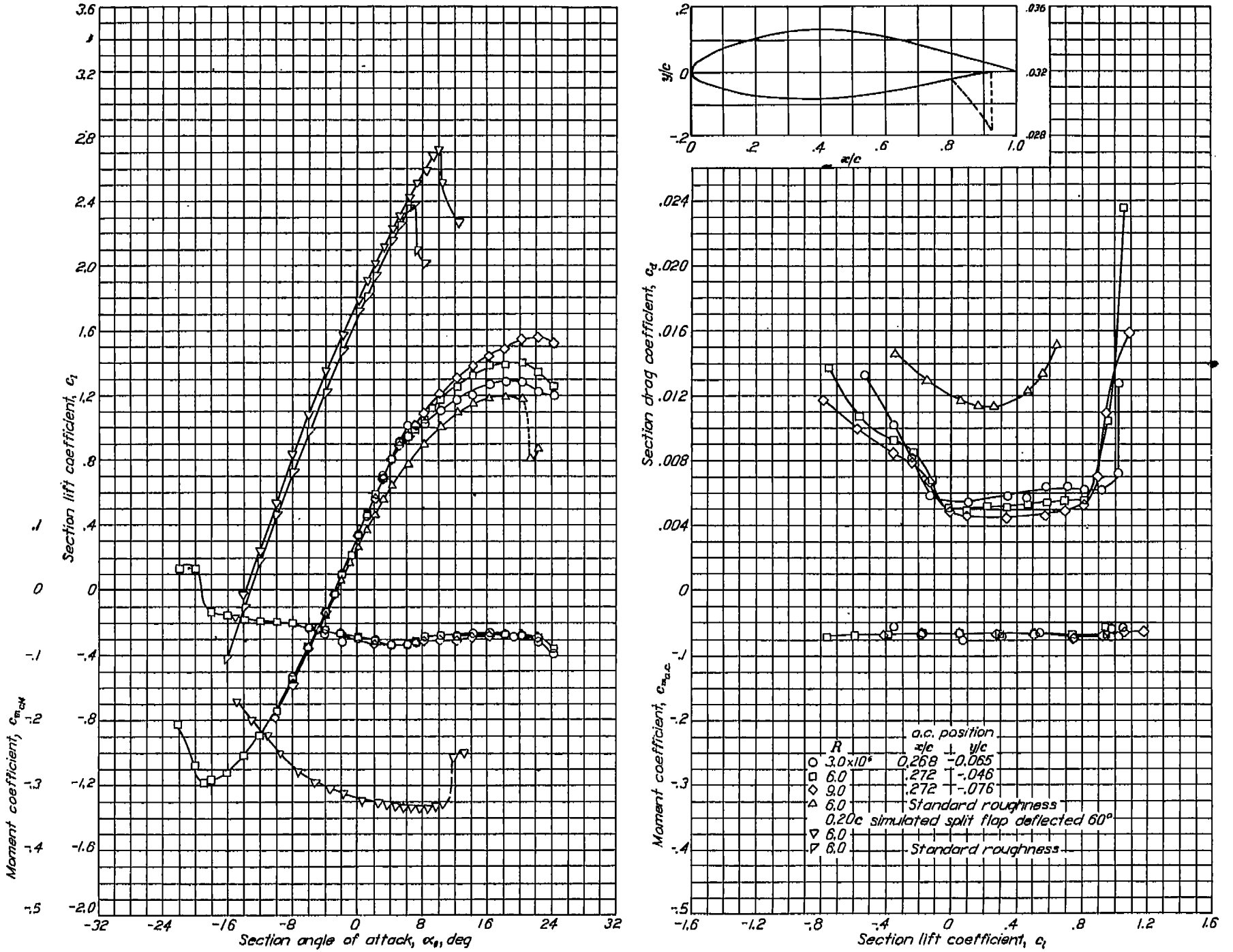

Aerodynamic characteristics of the NACA 654-421 airfoil section, 24-inch chord.

NACA 654-421, $a = 0.5$

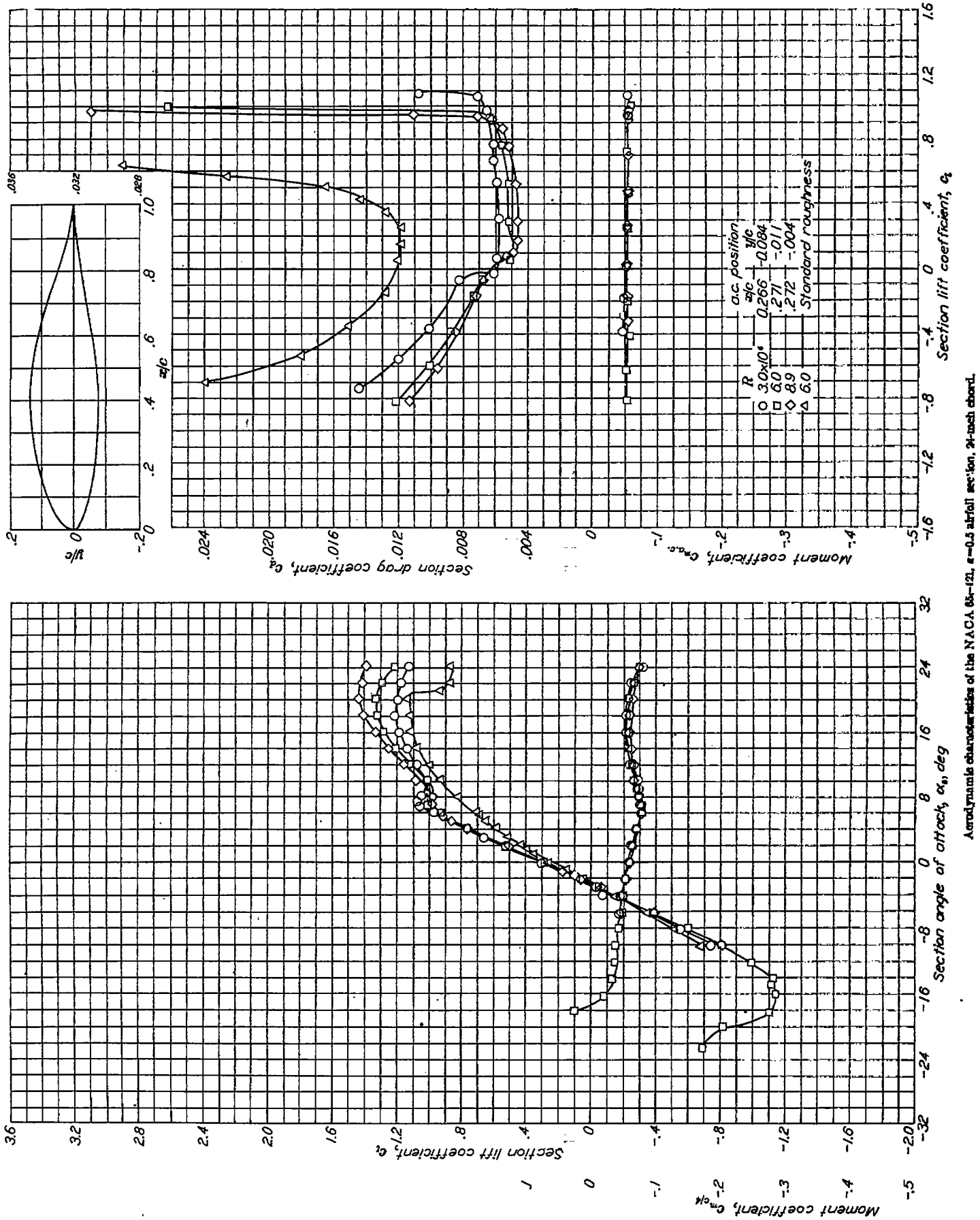

Aerodynamic characteristics of the NACA 654-421, $a = 0.5$ airfoil section, 24-inch chord.

NACA 65(215)-114

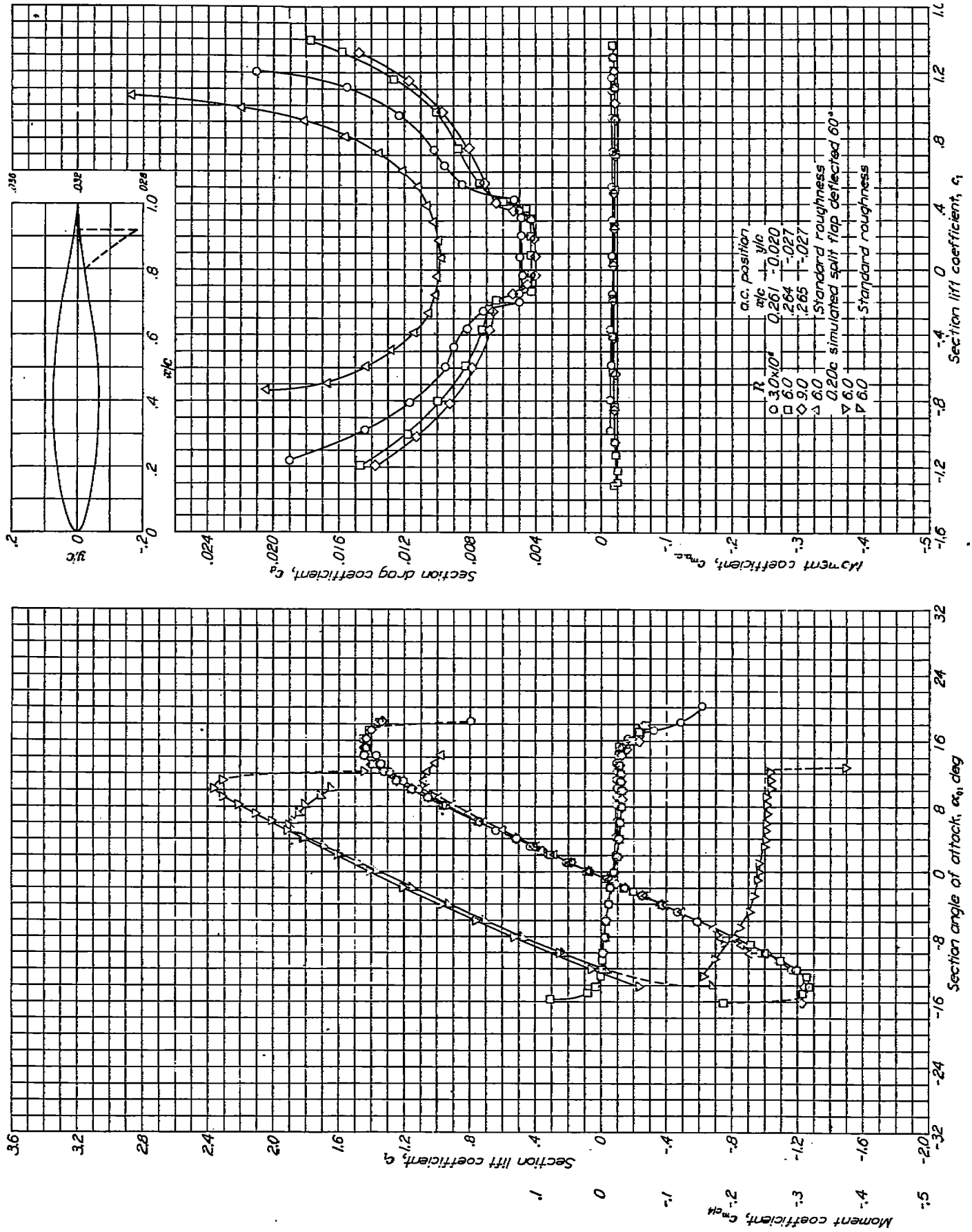

Aerodynamic characteristics of the NACA 65-(215)-114 airfoil section, 24 inch chord.

NACA 65(421)-420

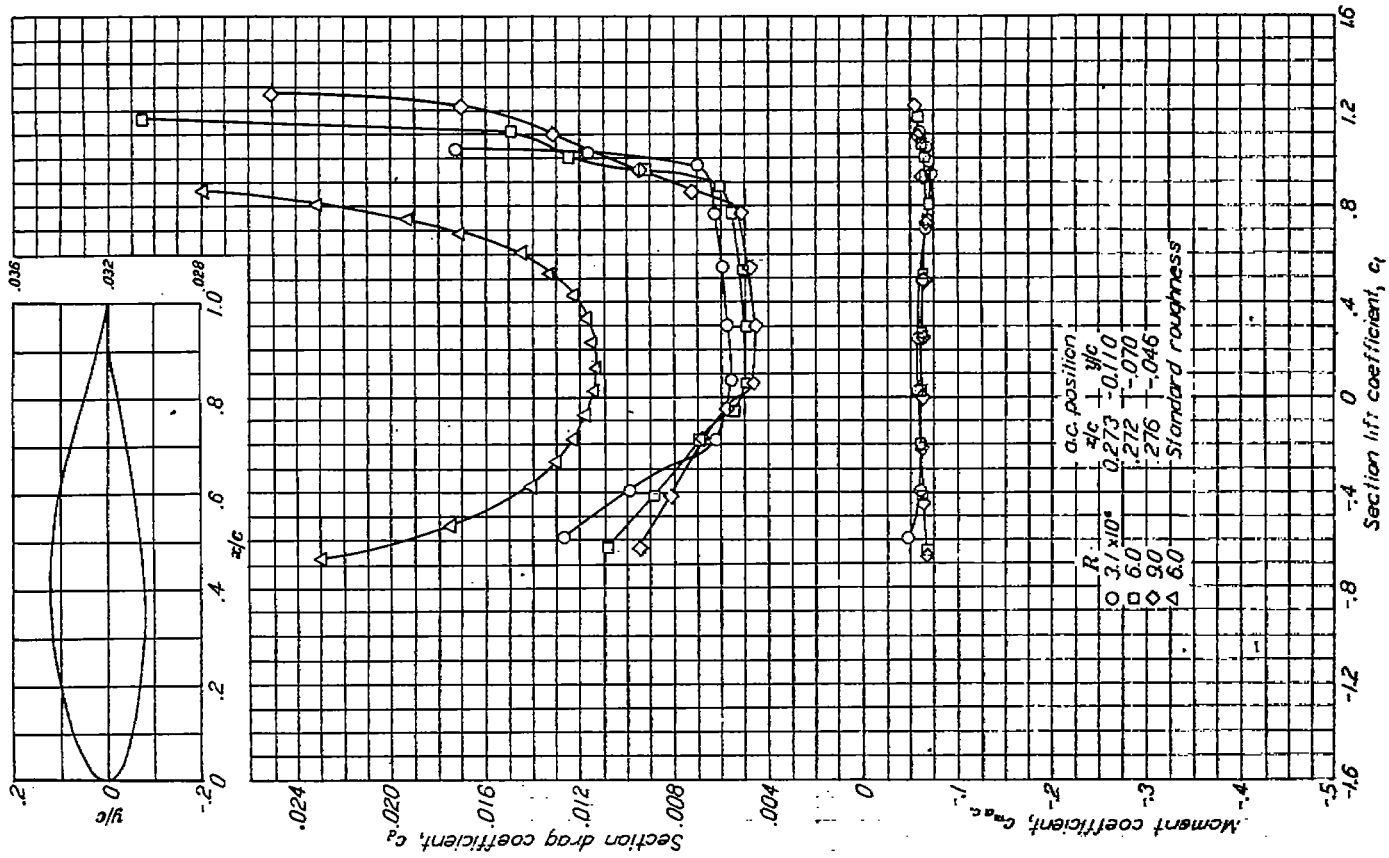

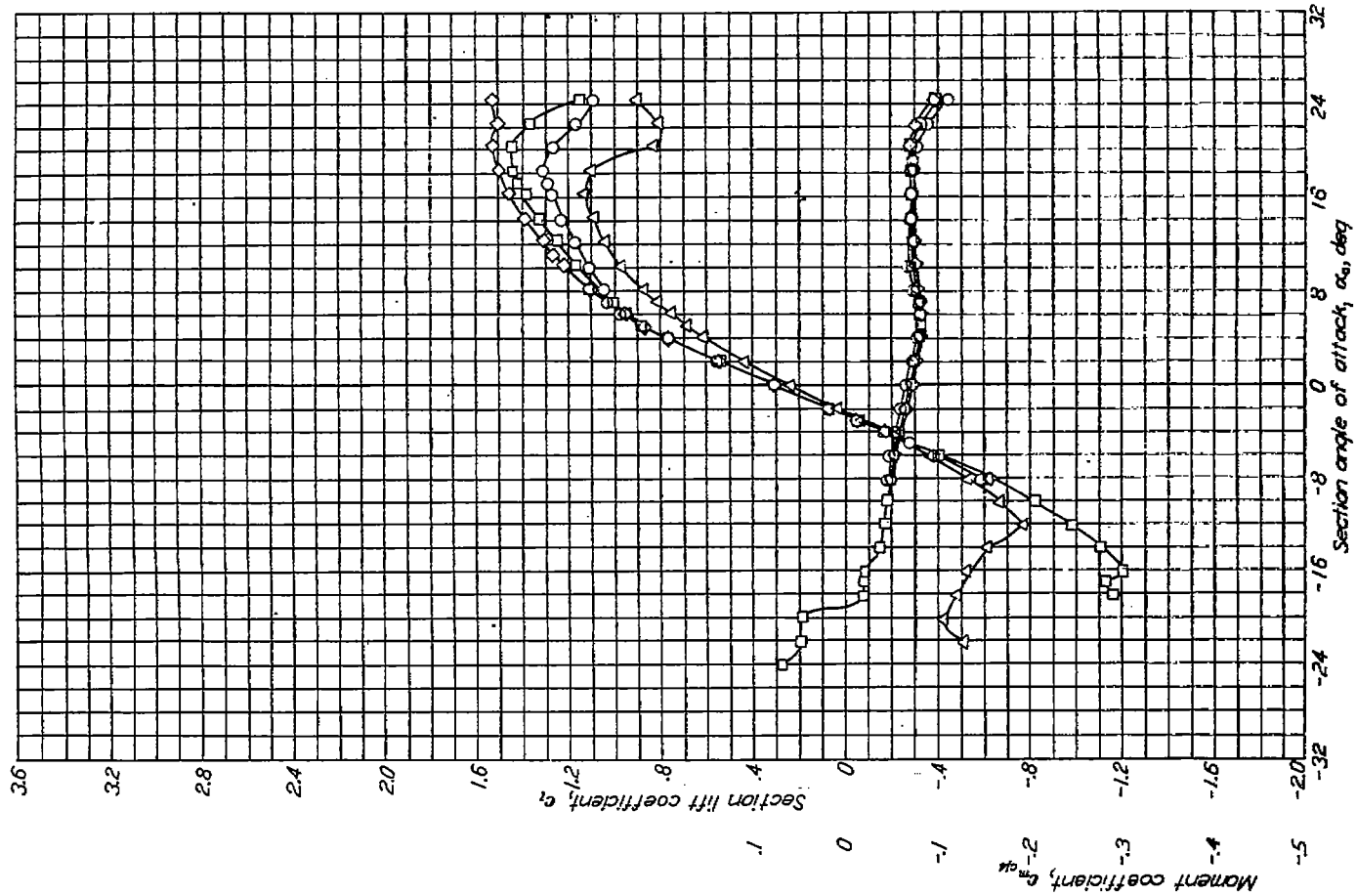

Aerodynamic characteristics of the NACA 63(421)-420 airfoil section, 24-inch chord.

NACA 66,1-212

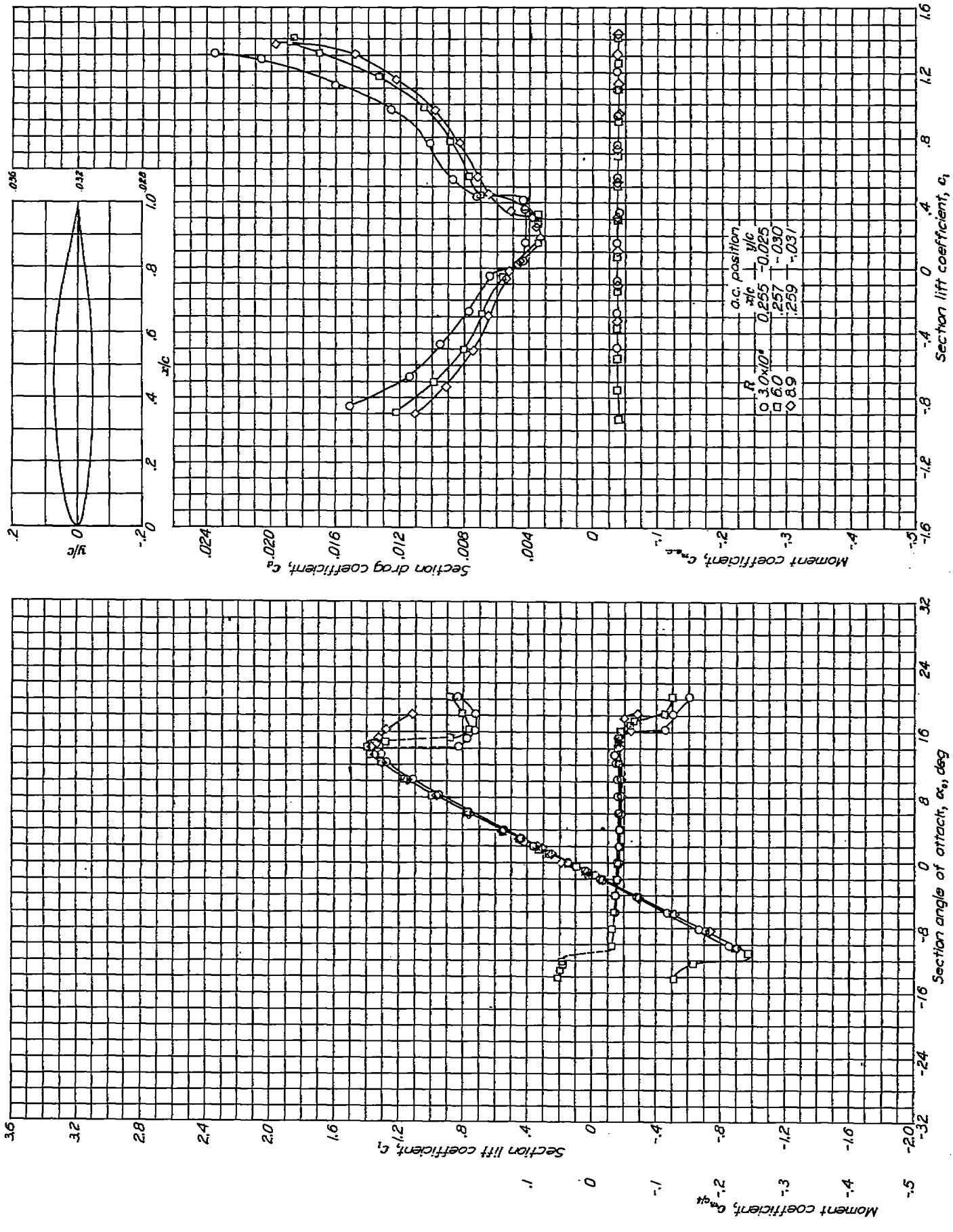

Aerodynamic characteristics of the NACA 66,1-212 airfoil section, 24-inch chord.

NACA 66,1-212 with flap

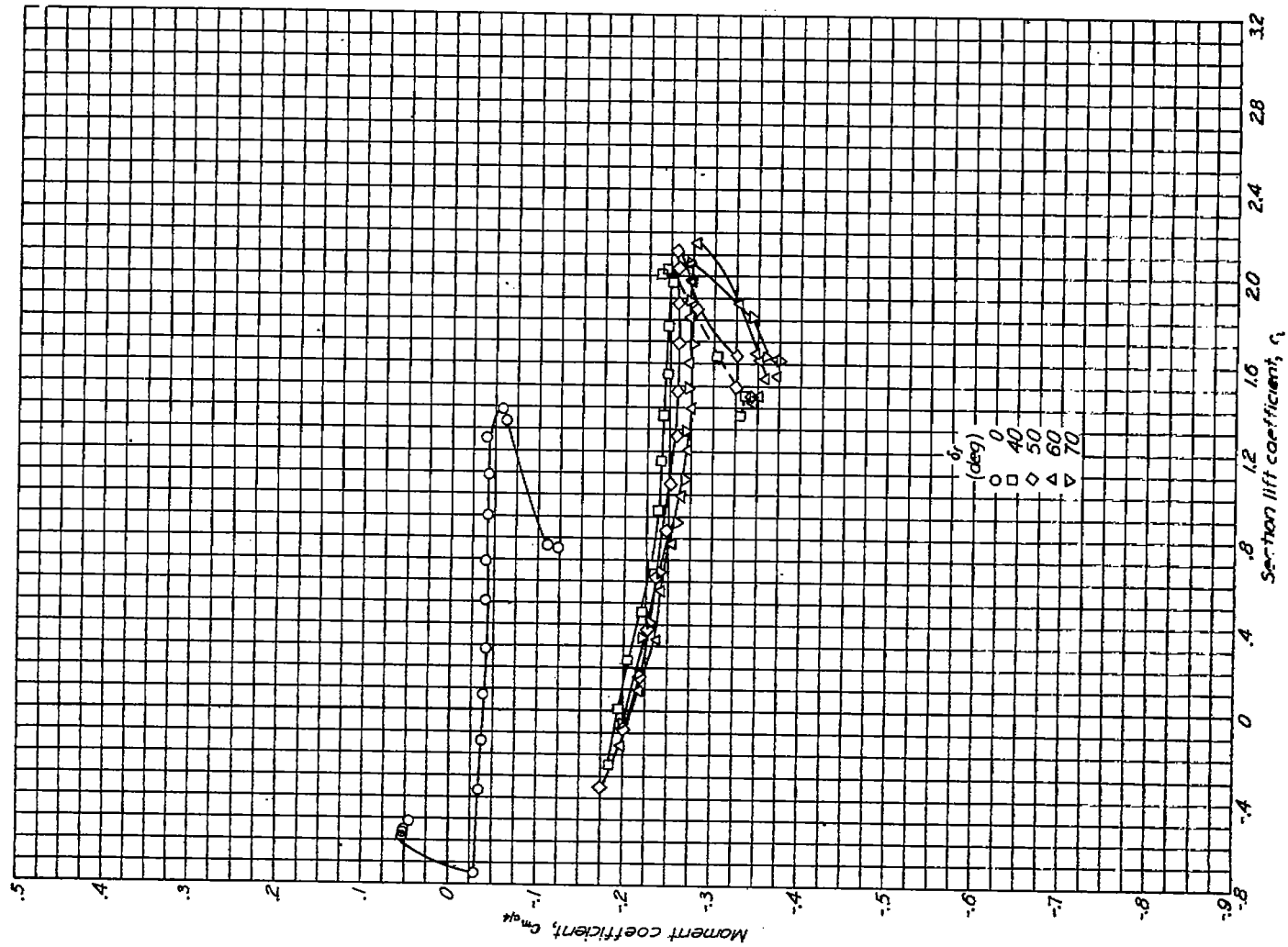

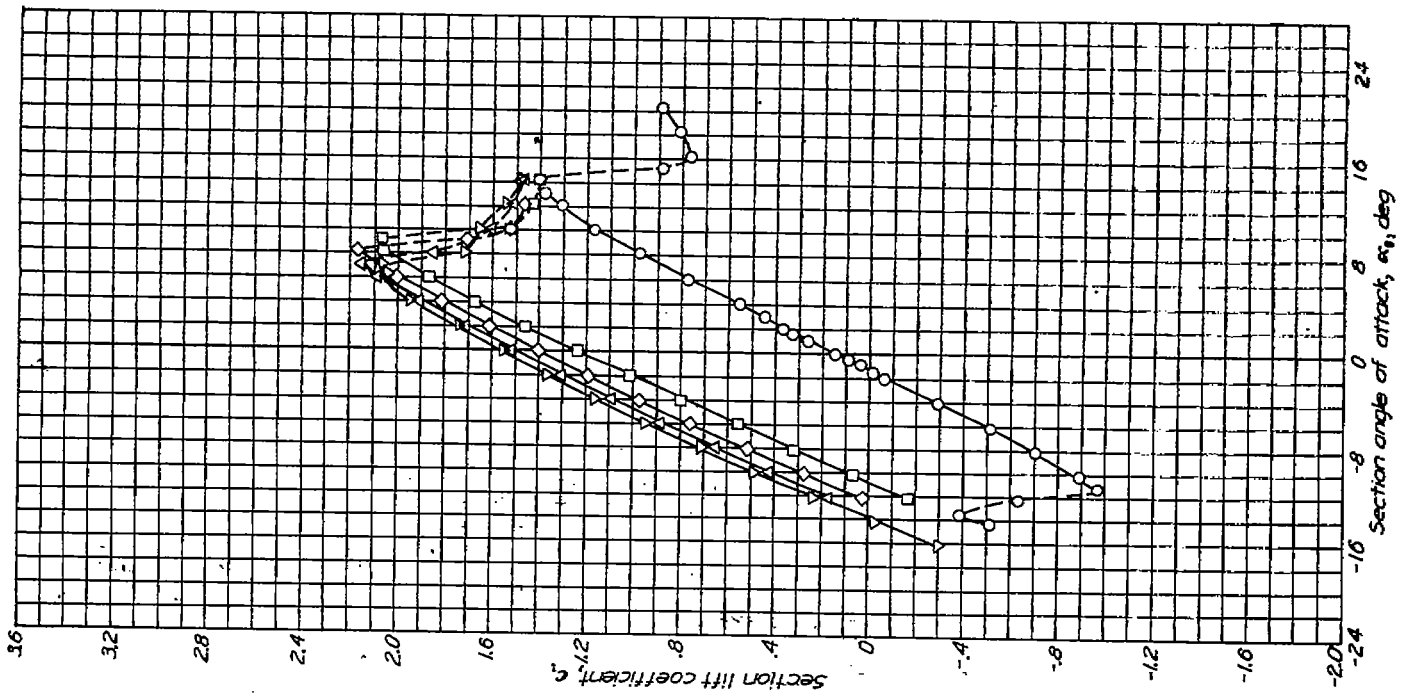

Lift and moment characteristics of the NACA 66,1-212 airfoil section with 0.20c split flap. $R=6\times10^6$.

NACA 66(215)-016

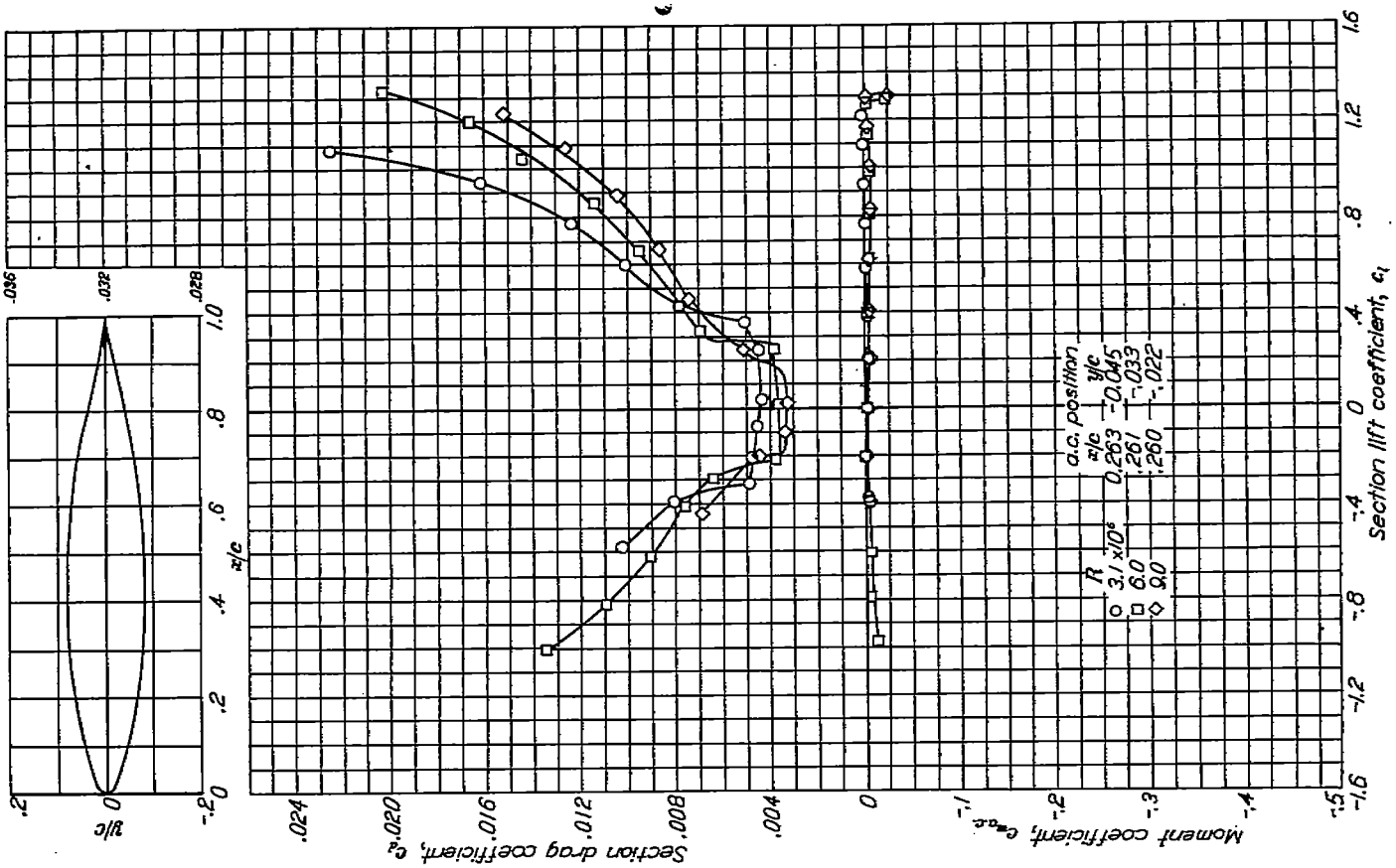

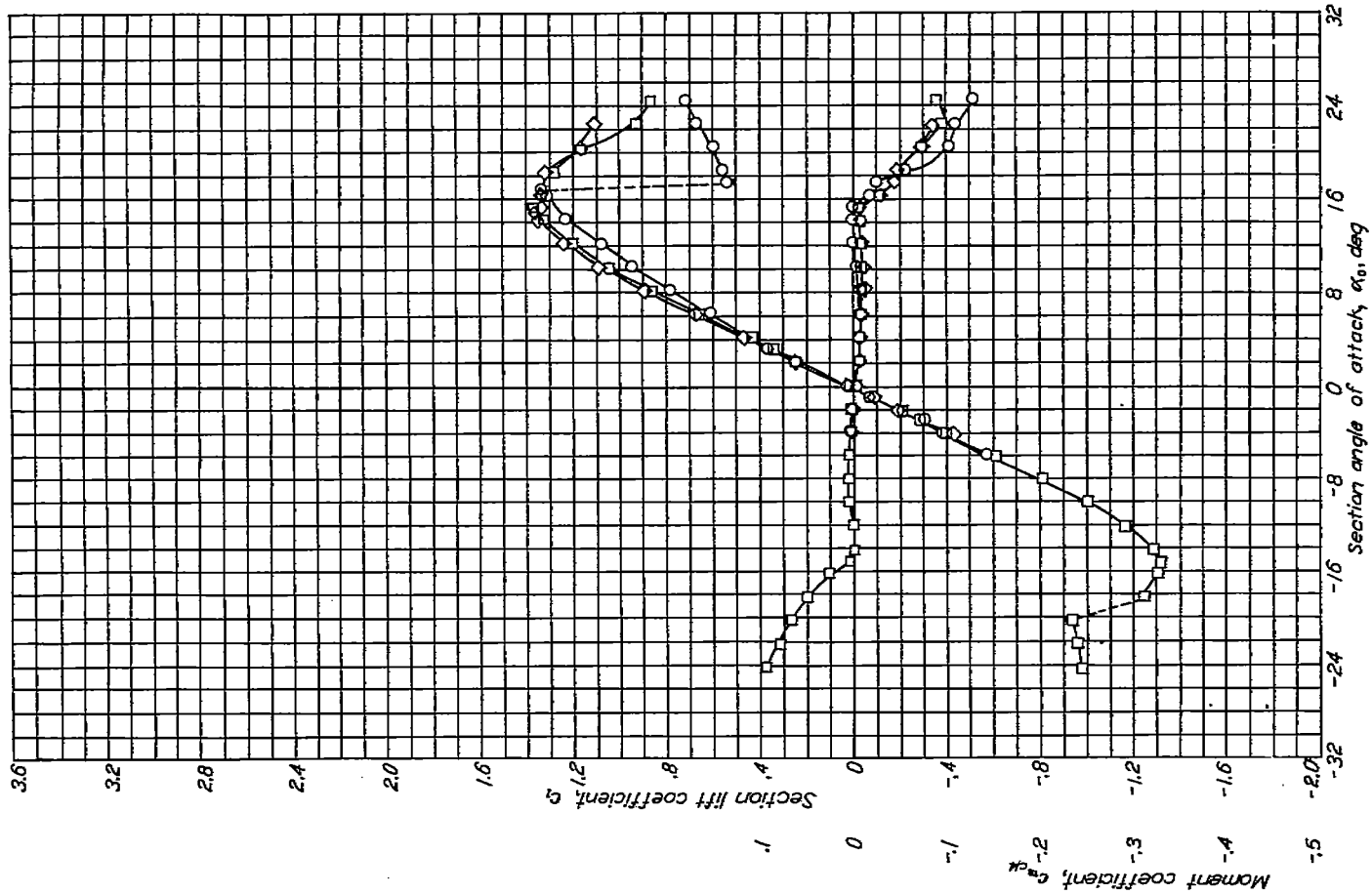

Aerodynamic characteristics of the NACA 66(215)-016 airfoil section, 24-inch chord.

NACA 66(215)-216

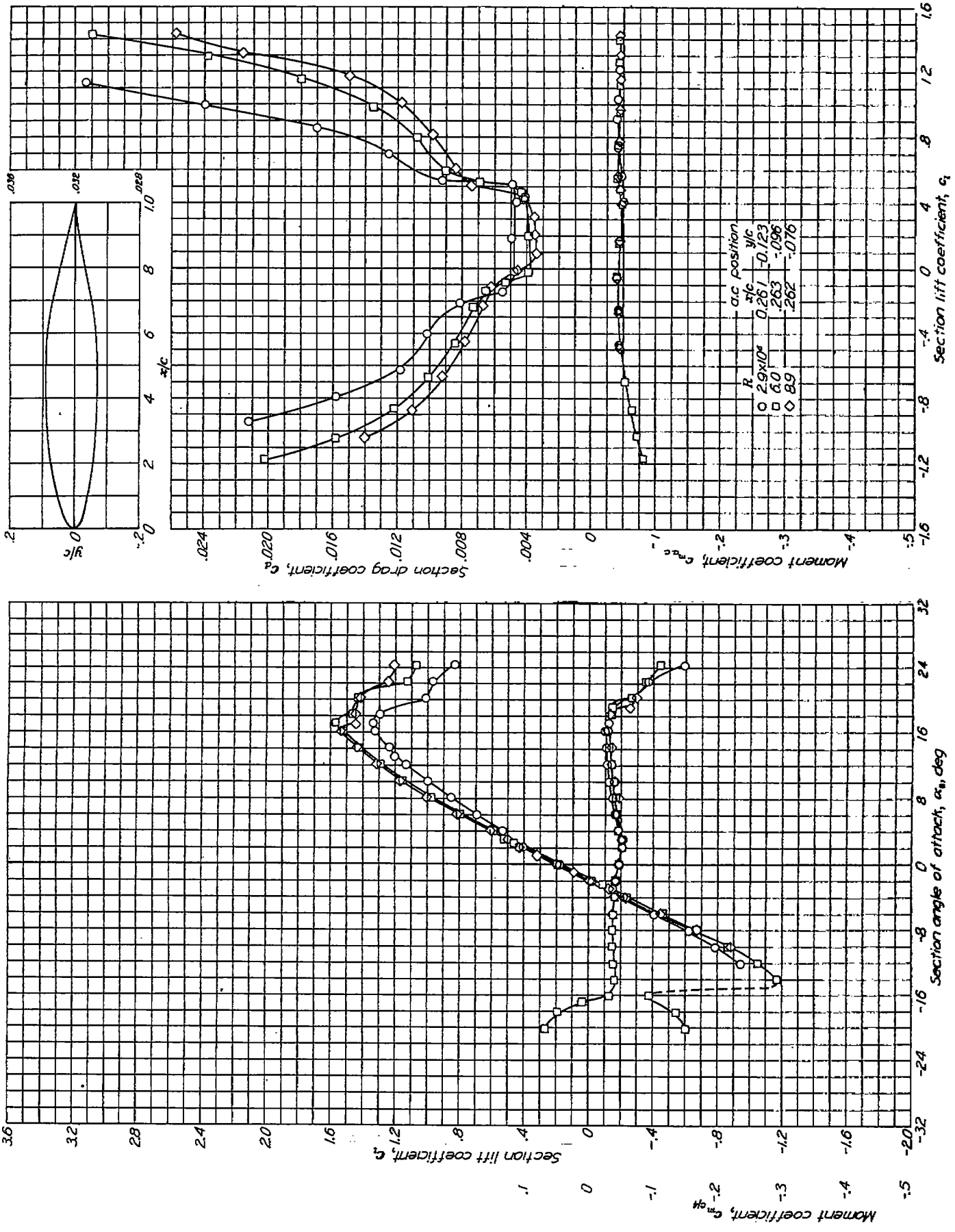

Aerodynamic characteristics of the NACA 66(215)-216 airfoil section, 24-inch chord.

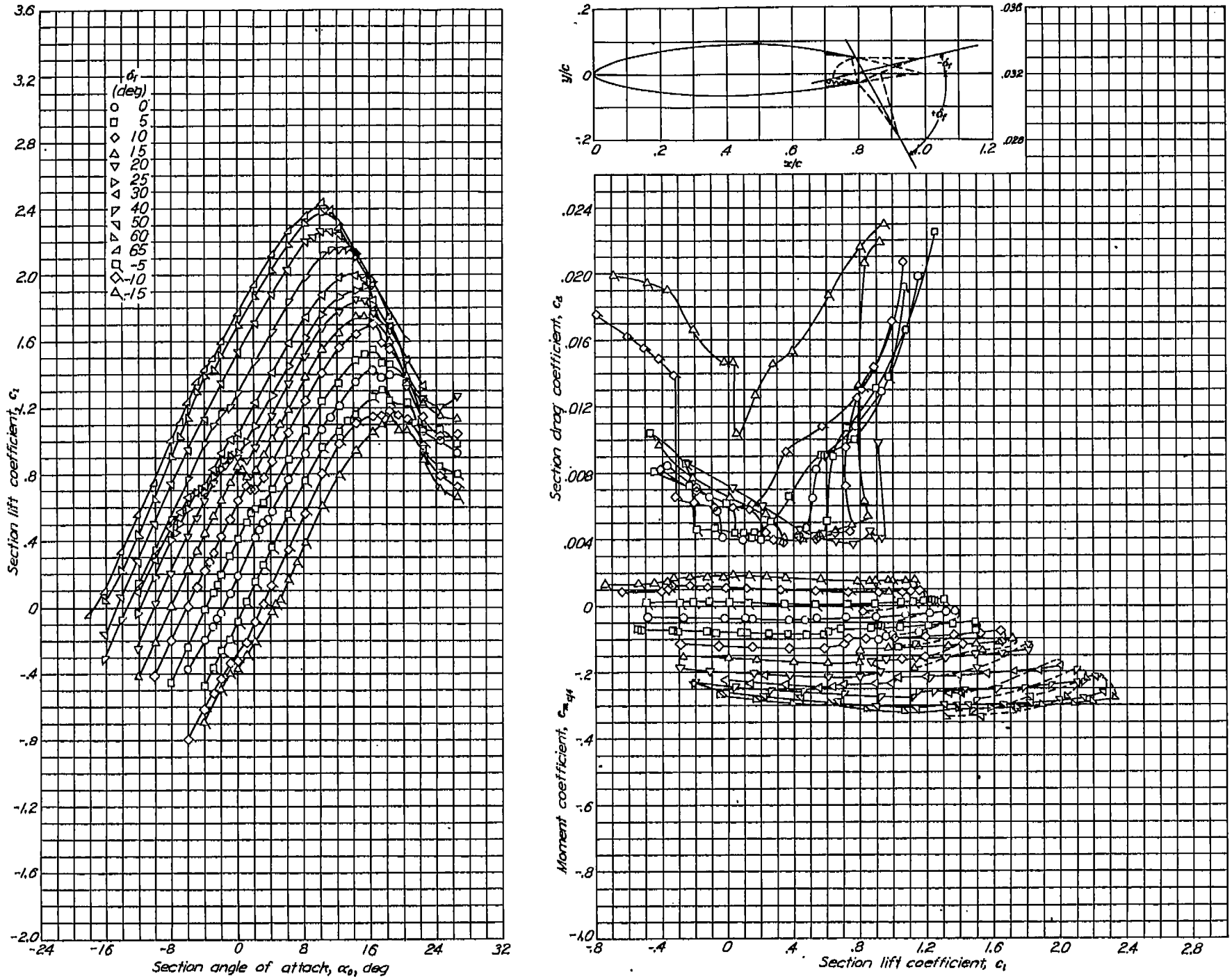

Aerodynamic characteristics of the NACA 66(215)-216 airfoil section with 0.20c sealed plain flap. $R=6\times10^6$.

NACA 66(215)-216 with flap

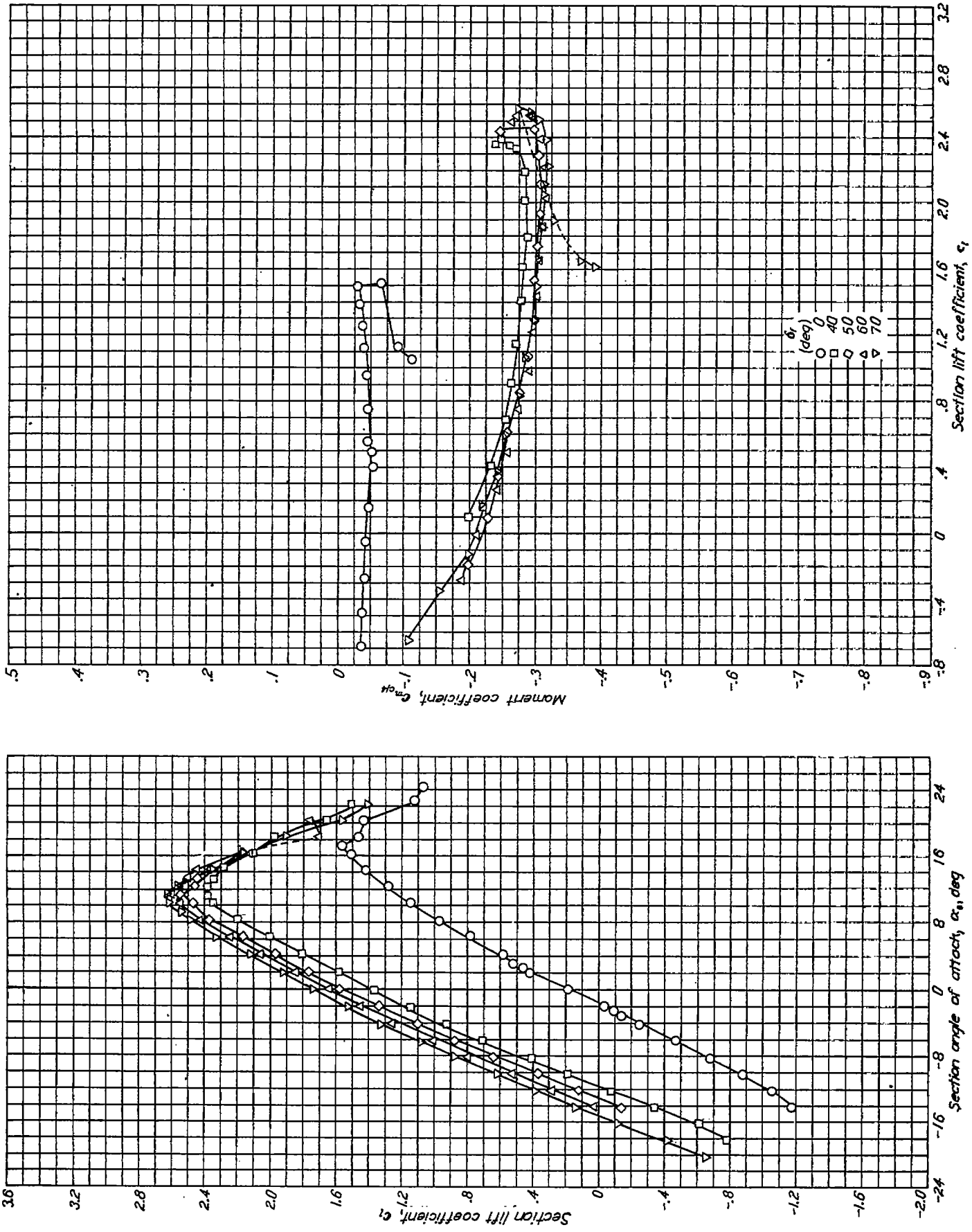

Lift and moment characteristics of the NACA 66(215)-216 airfoil section with 0.20c split flap. $R = 6 \times 10^6$.

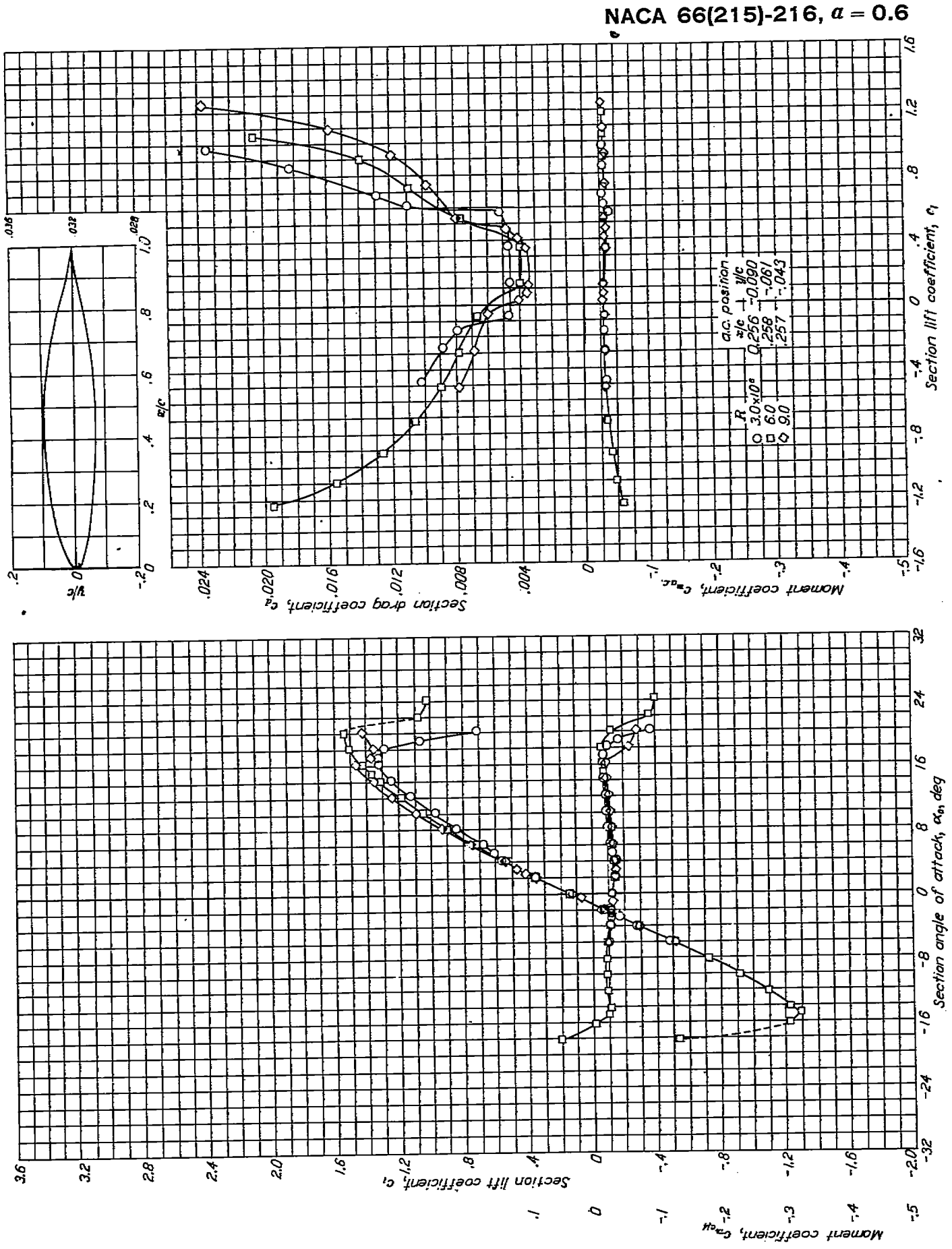

Aerodynamic characteristics of the NACA 66(216)-216, α=0.6 airfoil section, 24-inch chord.

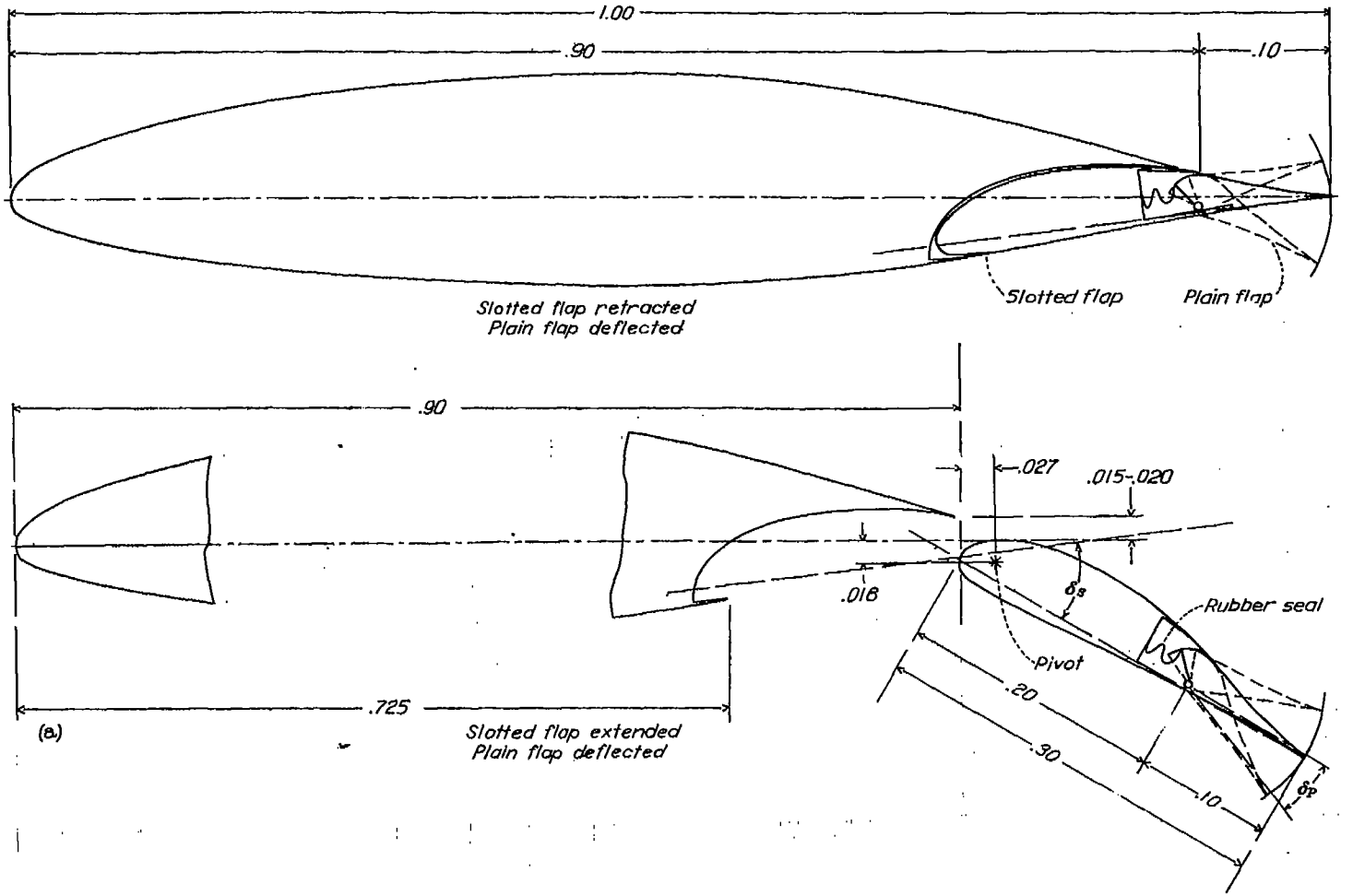

(a) Airfoil-flap configuration.

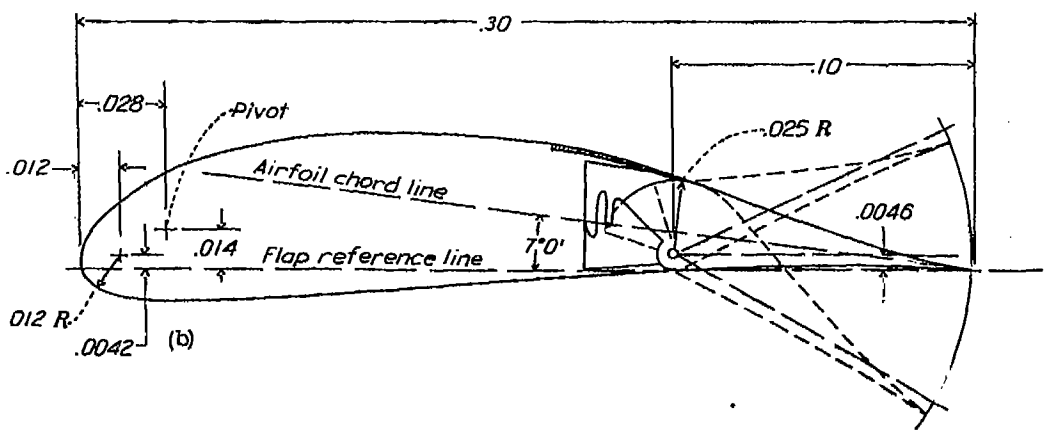

(b) Flap configuration.

NACA 66(215)-216, $a=0.6$ airfoil section with 0.30c slotted and 0.10c plain flap

Flap coordinates			
Upper surface		Lower surface	
Abscissa	Ordinate	Abscissa	Ordinate
0.5	1.54	0.5	−0.58
1.04	2.04	1.04	−.83
2.08	2.75	2.08	−1.00
4.16	3.75	4.16	−1.00
6.25	4.28	6.25	−.92
8.33	4.53	8.33	−.79
10.41	4.68	10.41	−.62
12.50	4.50	12.50	−.45
14.58	4.33	14.58	−.33
16.66	4.06	16.66	−.21
18.75	3.54	18.75	−.06
20.29	3.04	20.29	0
22.91	2.06	22.91	.10
25.00	1.27	25.00	.17
27.08	.62	27.08	.14
29.16	.15	29.16	.004
30.00	0	30.00	0

NACA 66(215)-216, $a = 0.6$ with flap

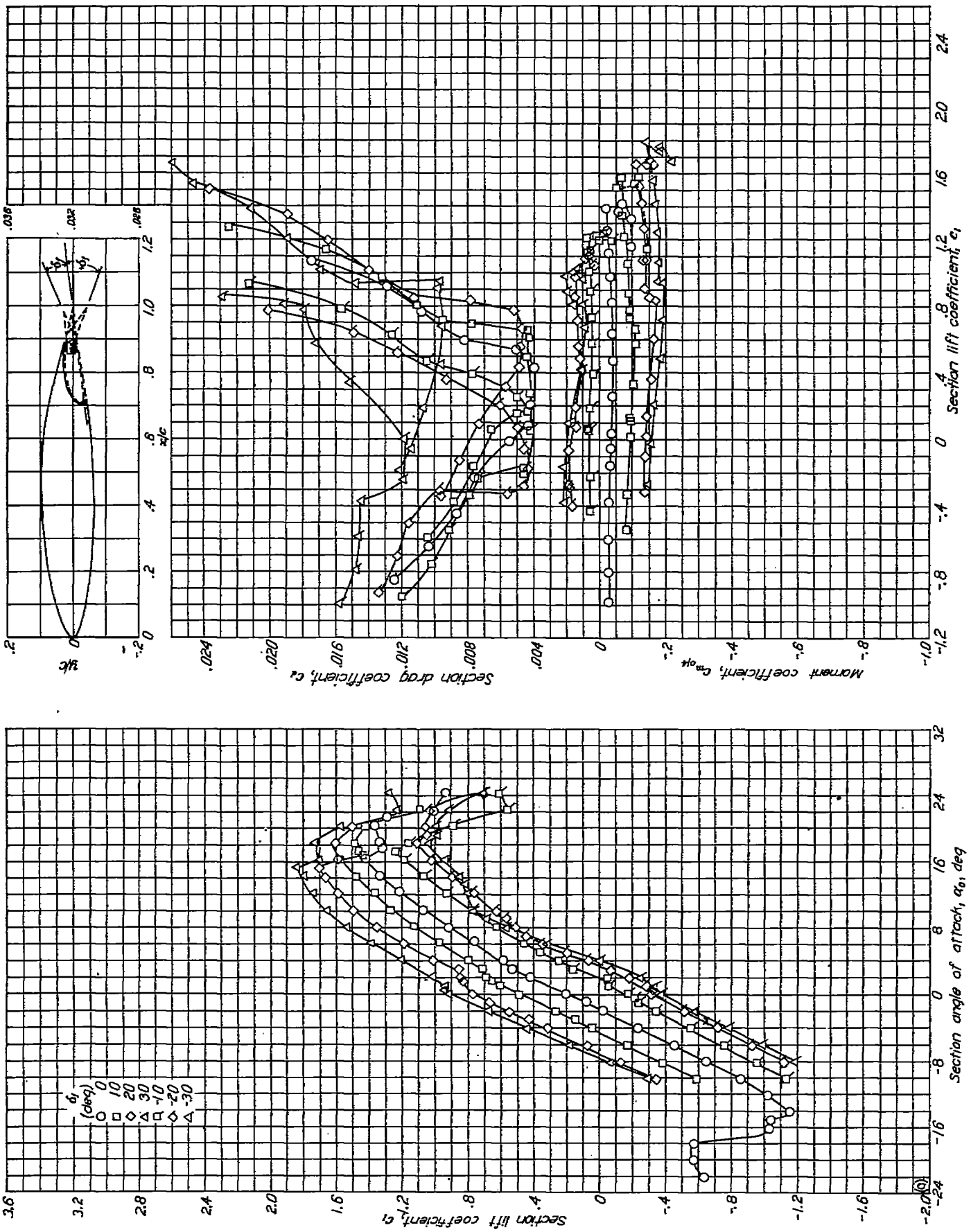

(a) Aerodynamic characteristics. Slotted flap retracted; $R = 6 \times 10^6$.
NACA 66(215)-216, $a = 0.6$ airfoil section with 0.80c slotted and 0.10c plain flap.

NACA 66(215)-216, $a = 0.6$ with flap

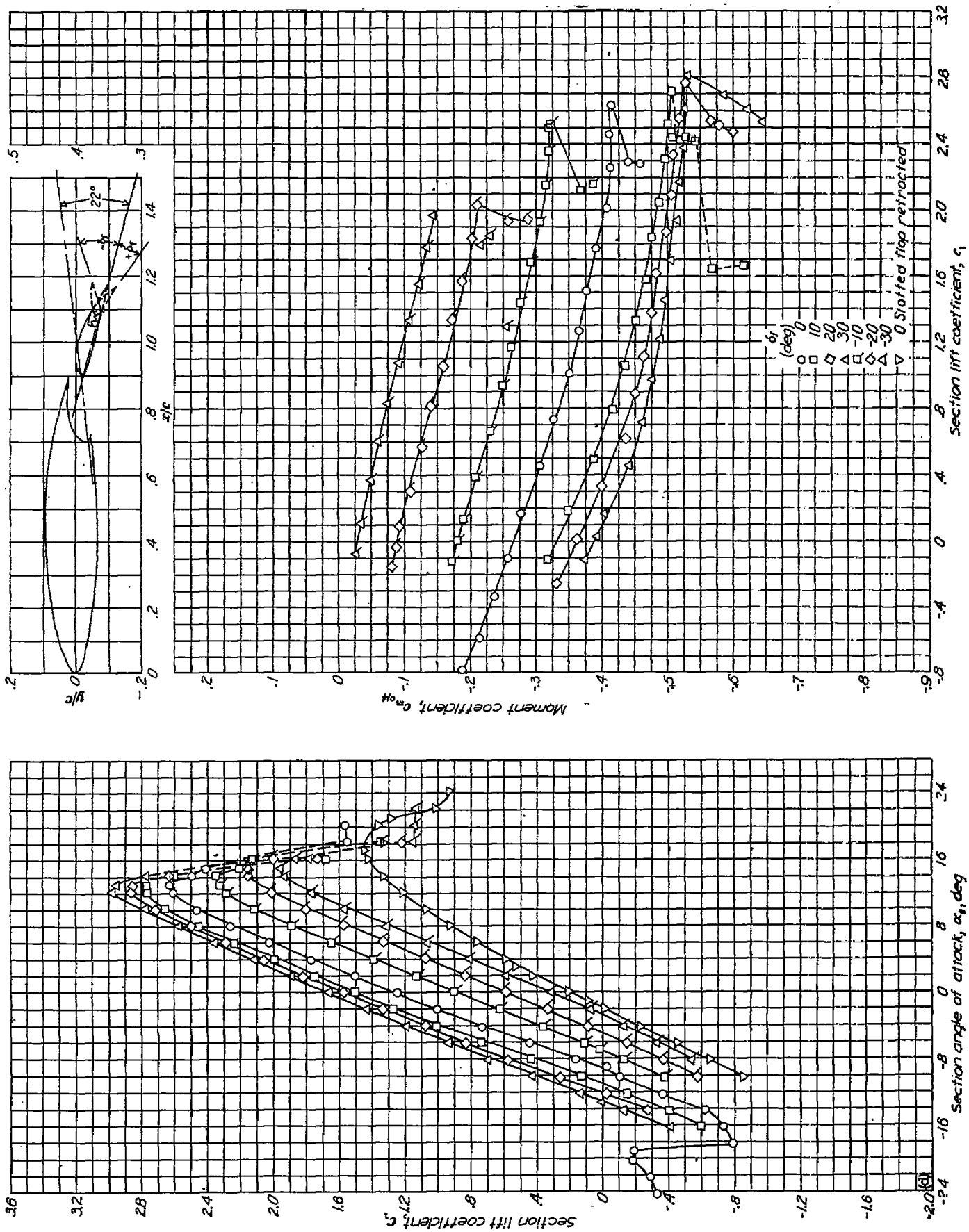

(d) Lift and moment characteristics. Slotted flap deflected 22°; $R = 6 \times 10^6$.
NACA 66(215)-216, $a = 0.6$ airfoil section with 0.30c slotted and 0.10c plain flap.

NACA 66(215)-216, $\alpha = 0.6$ with flap

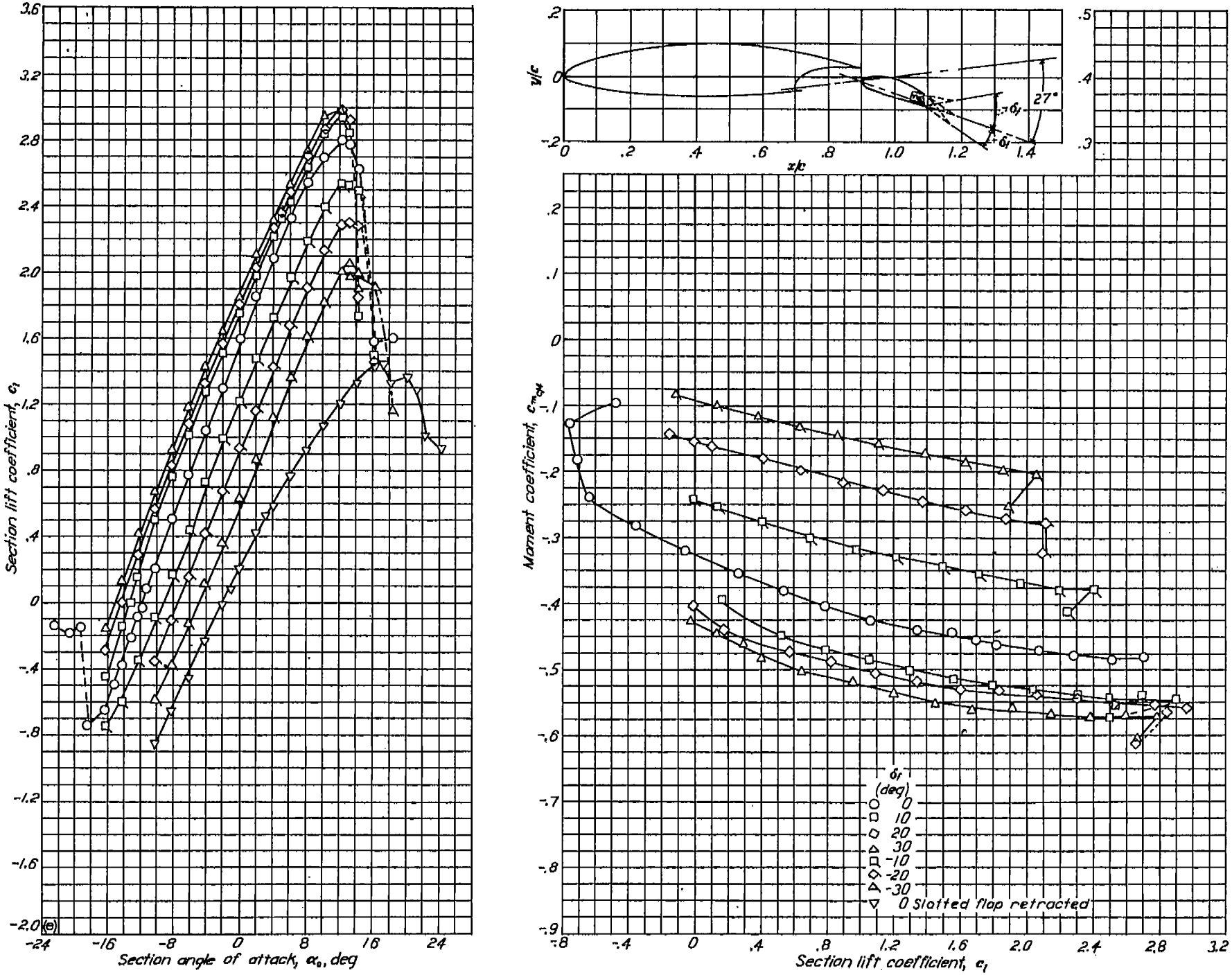

(e) Lift and moment characteristics. Slotted flap deflected 27°; R=6×10⁶.
NACA 66(215)-216, a=0.6 airfoil section with 0.30c slotted and 0.10c plain flap.

NACA 66(215)-216, $a = 0.6$ with flap

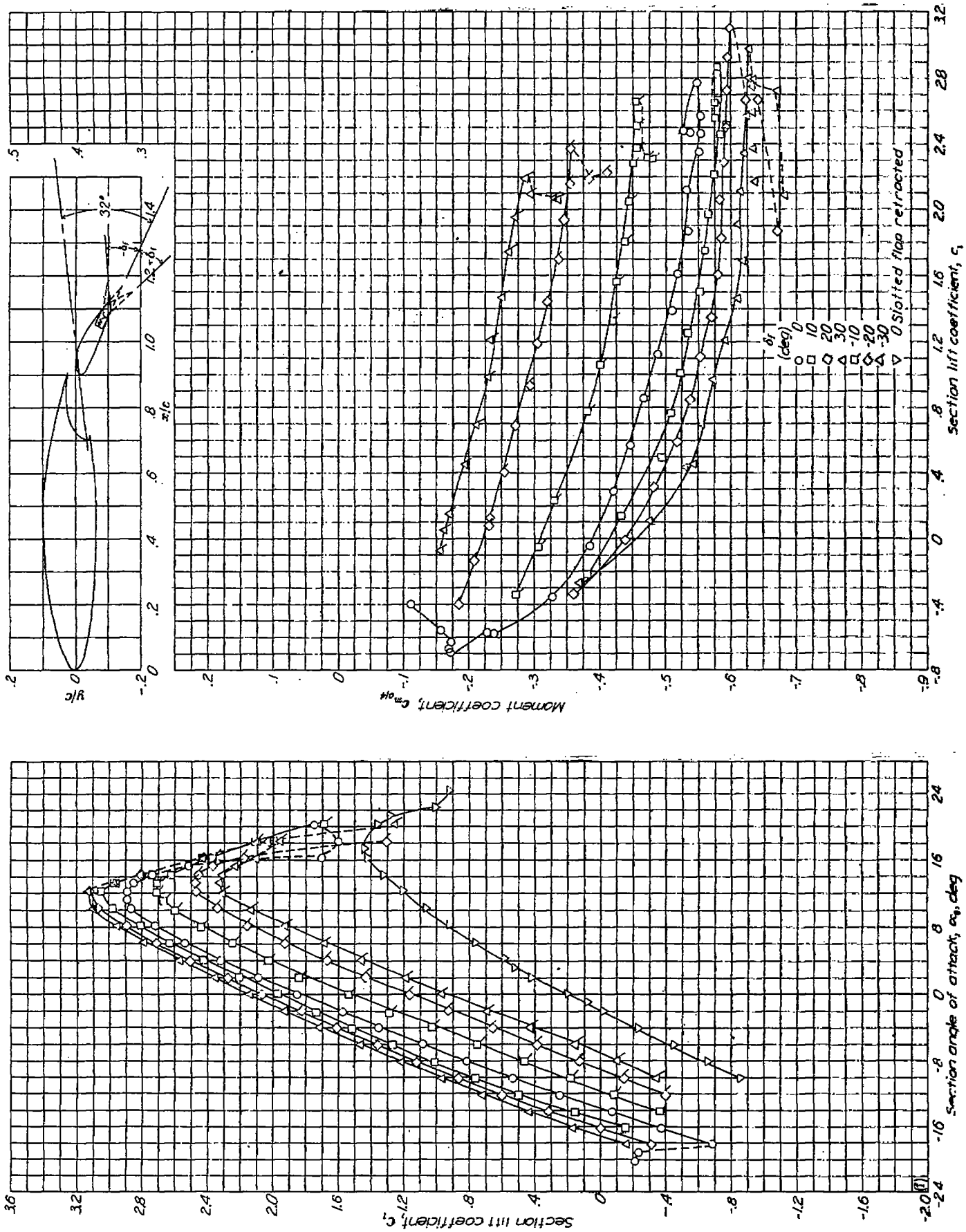

(1) Lift and moment characteristics. Slotted flap deflected 32°; $R = 6 \times 10^6$.
NACA 66(215)-216, $a = 0.6$ airfoil section with 0.30c slotted and 0.30c plain flap.

NACA 66(215)-216, $a = 0.6$ with flap

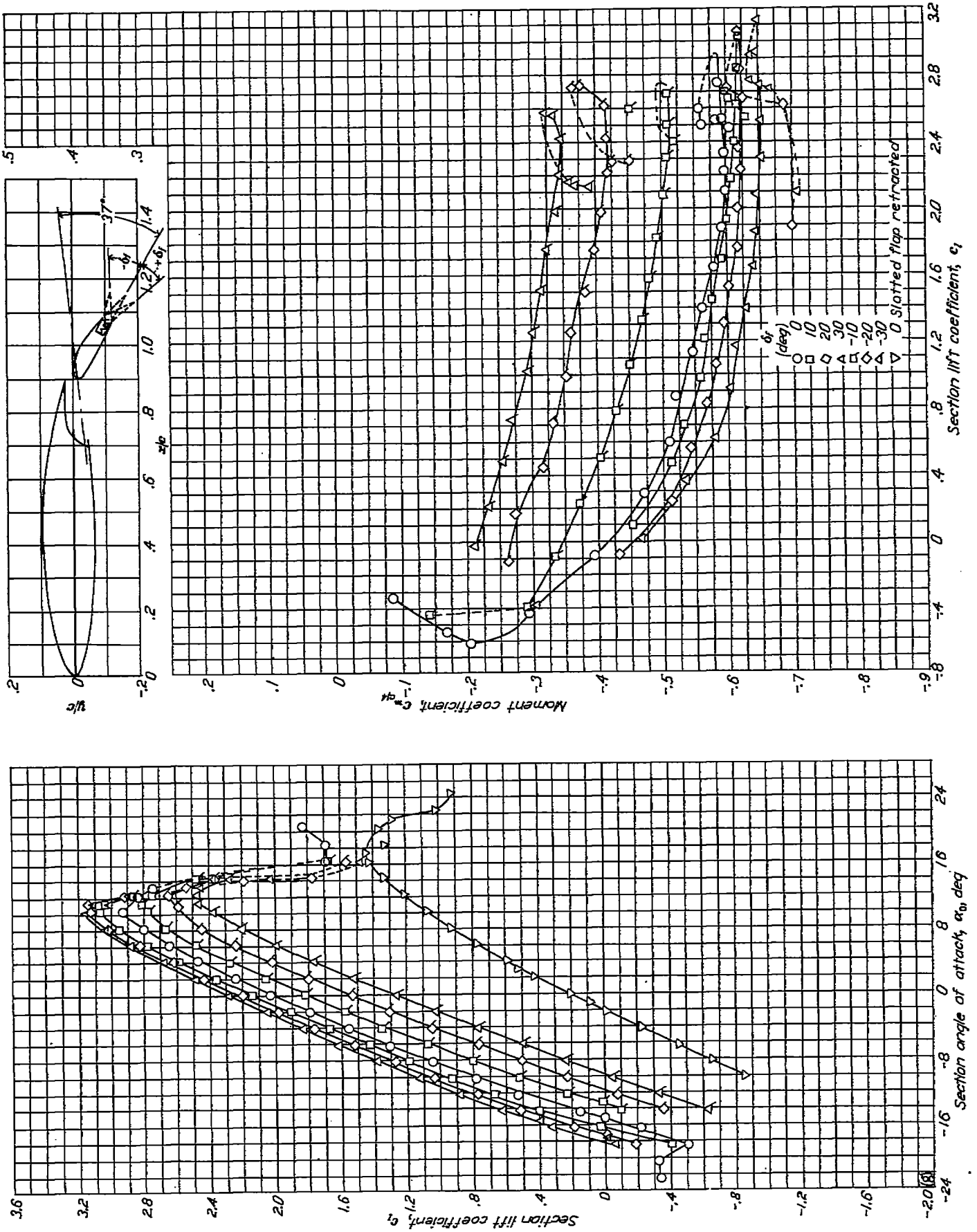

(g) Lift and moment characteristics. Slotted flap deflected 87°; $R = 6 \times 10^6$.
NACA 66(215)-216, $a = 0.6$ airfoil section with 0.80c slotted and 0.10c plain flap.

NACA 66(215)-416

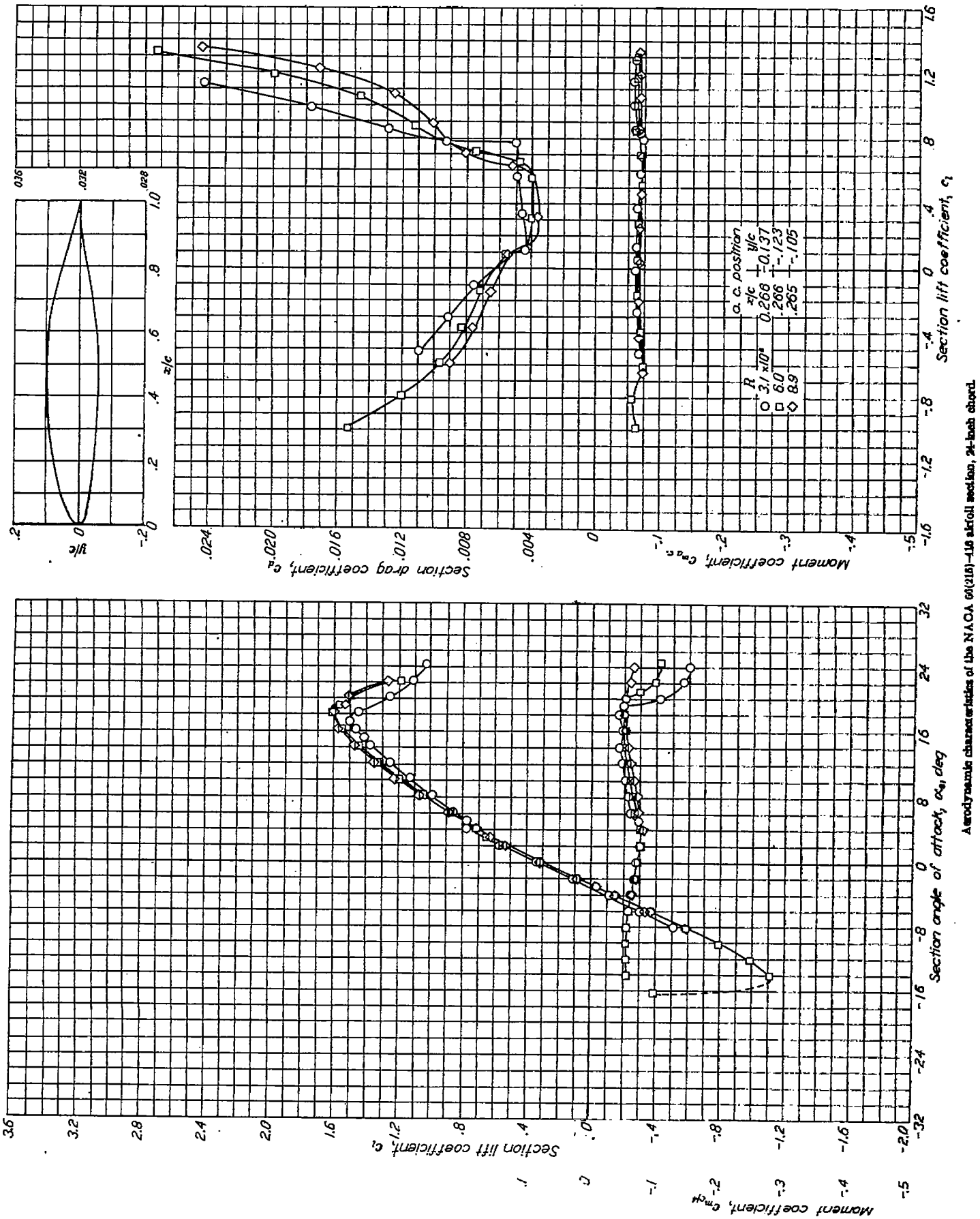

Aerodynamic characteristics of the NACA 66(215)-416 airfoil section, 24-inch chord.

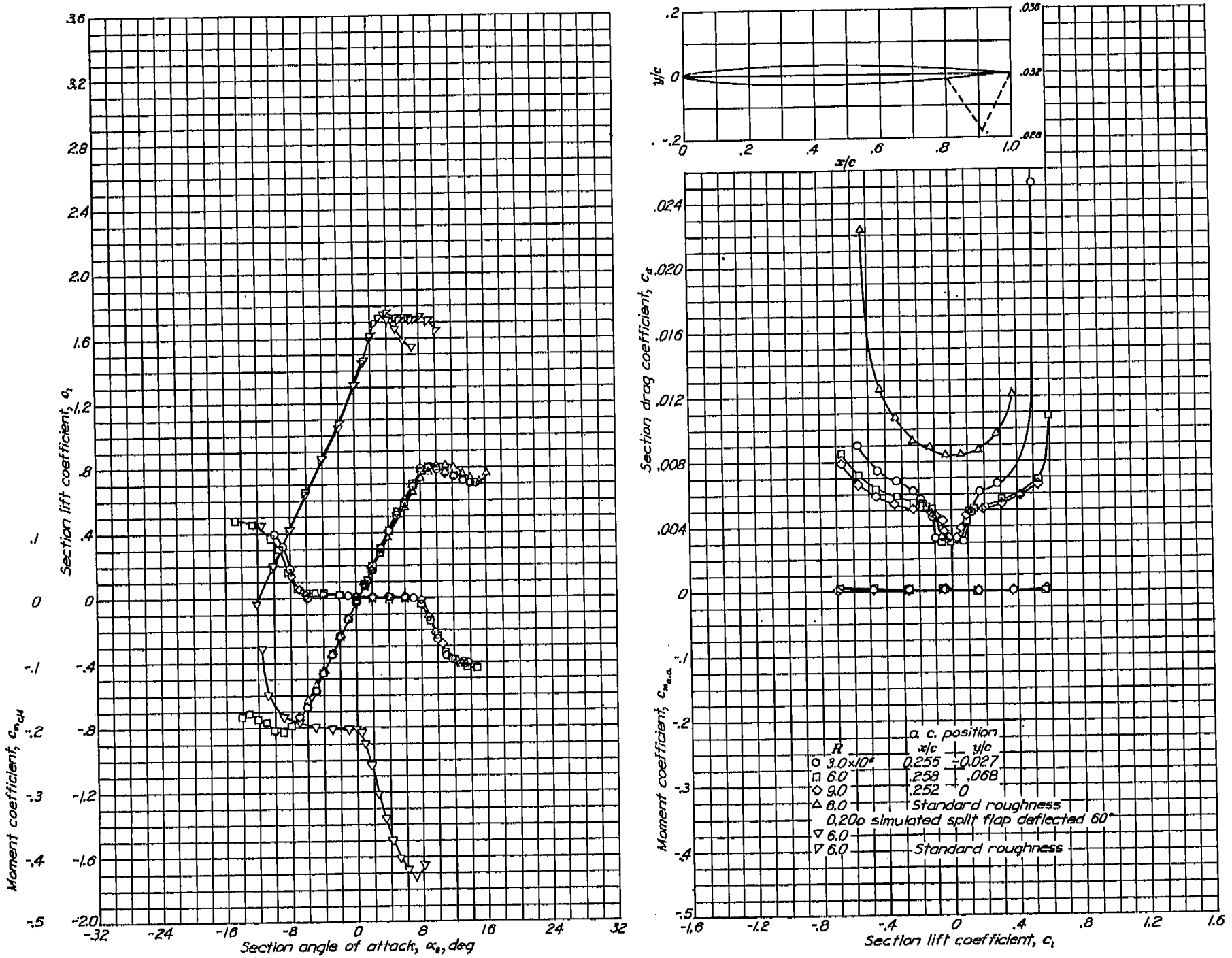

Aerodynamic characteristics of the NACA 66-006 airfoil section, 24-inch chord.

NACA 66-009

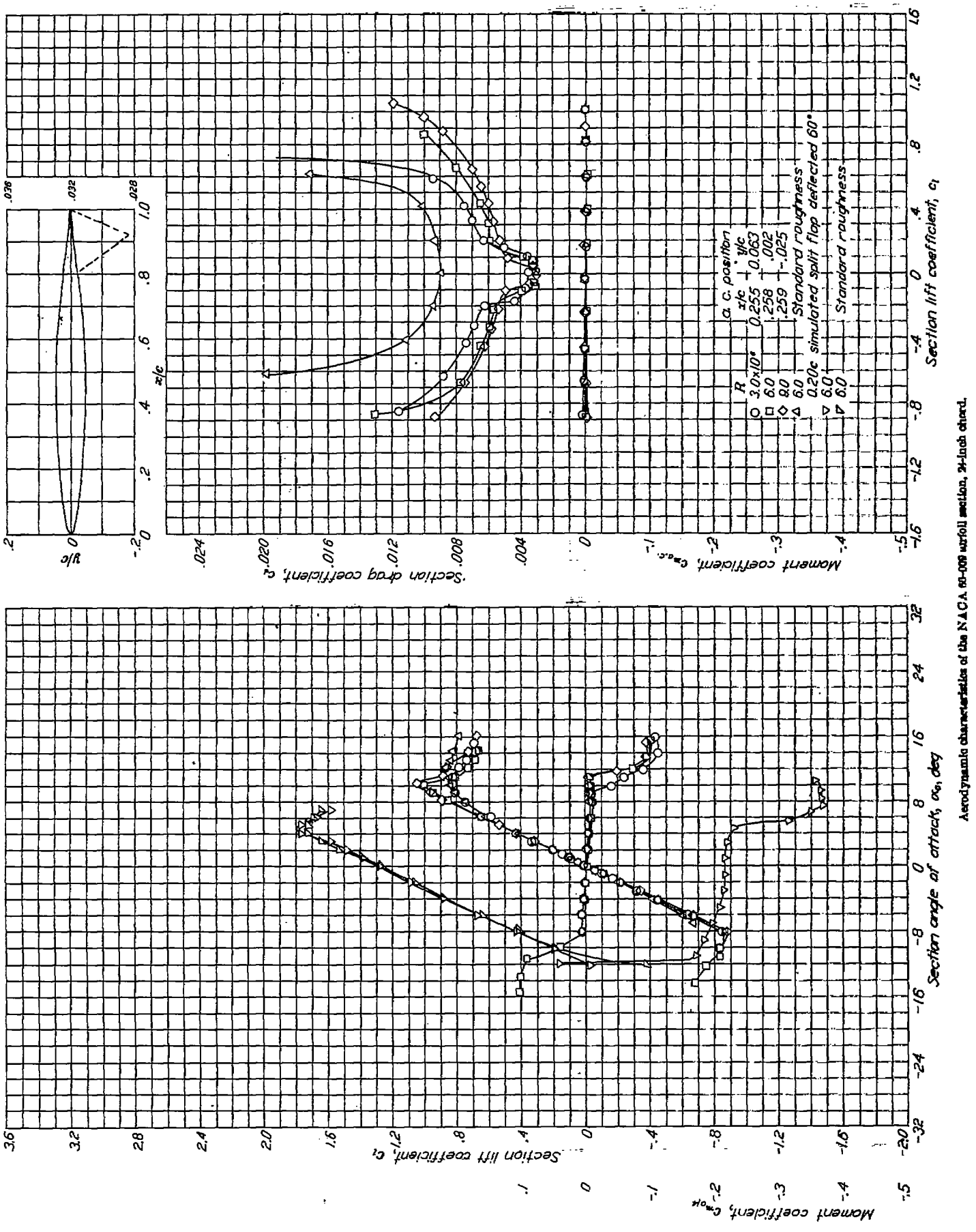

Aerodynamic characteristics of the NACA 66-009 airfoil section, 24-inch chord.

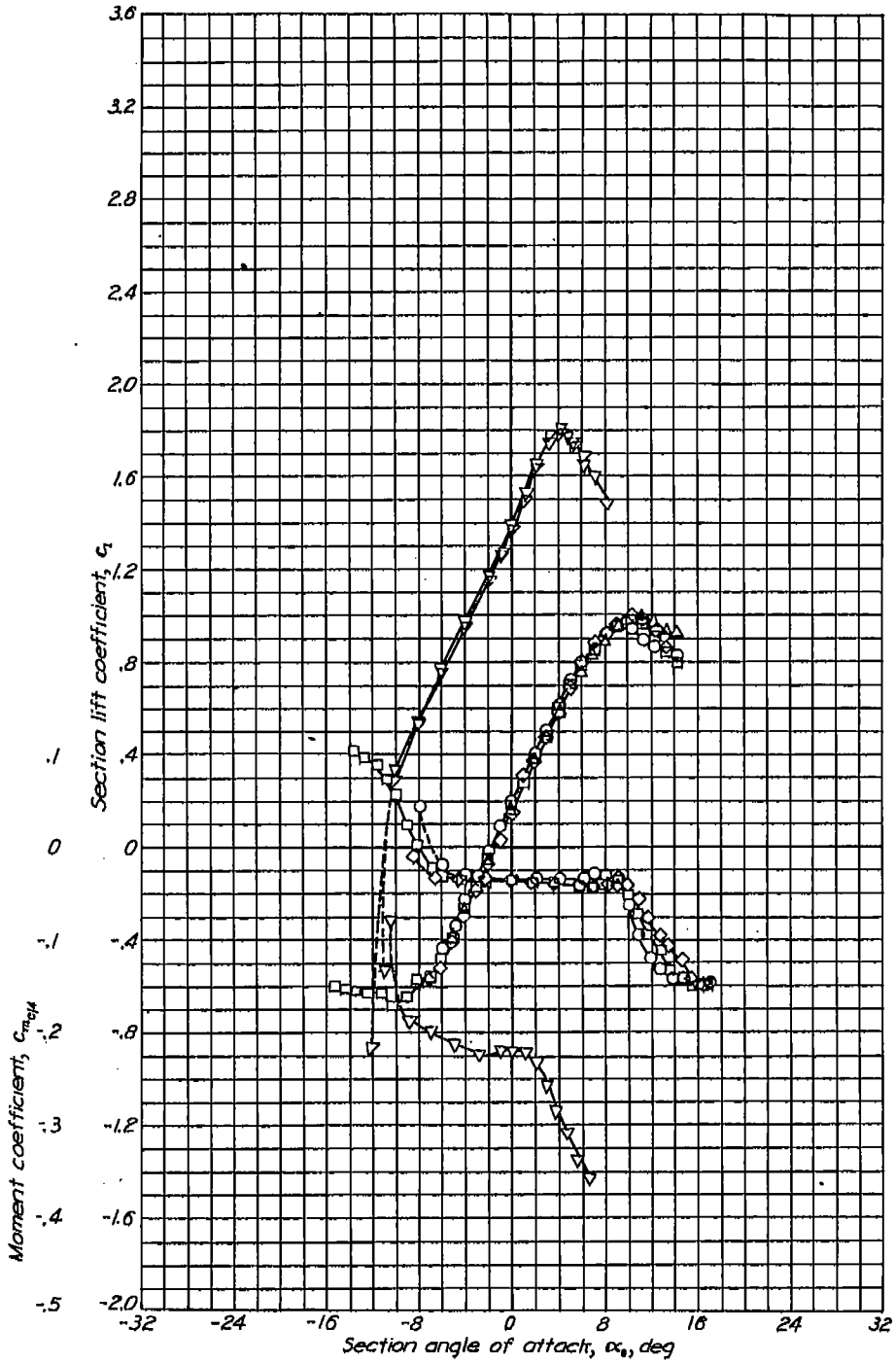

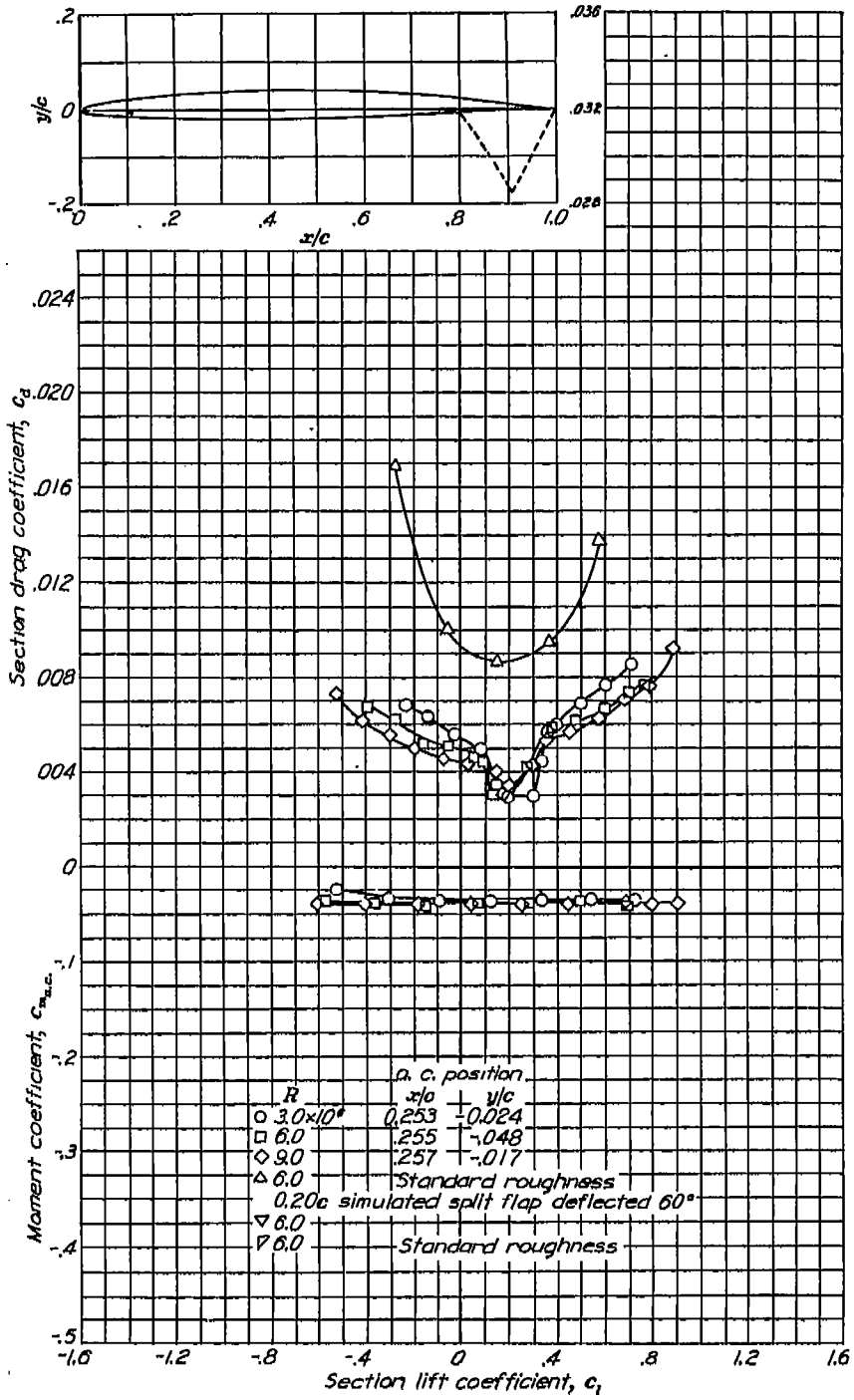

Aerodynamic characteristics of the NACA 66-206 airfoil section, 24-inch chord.

NACA 66-209

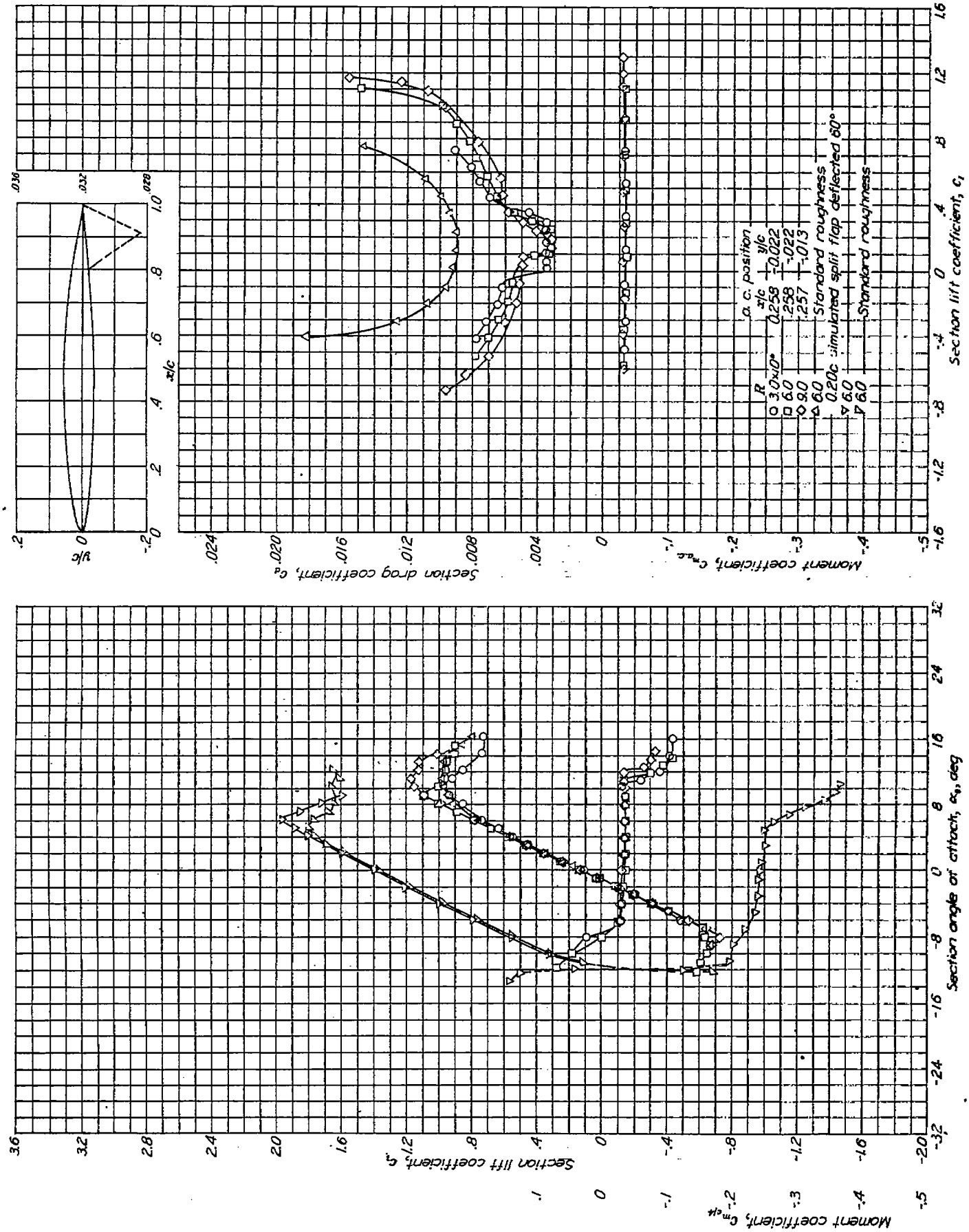

Aerodynamic characteristics of the NACA 66-209 airfoil section, 24-inch chord.

NACA 66-210

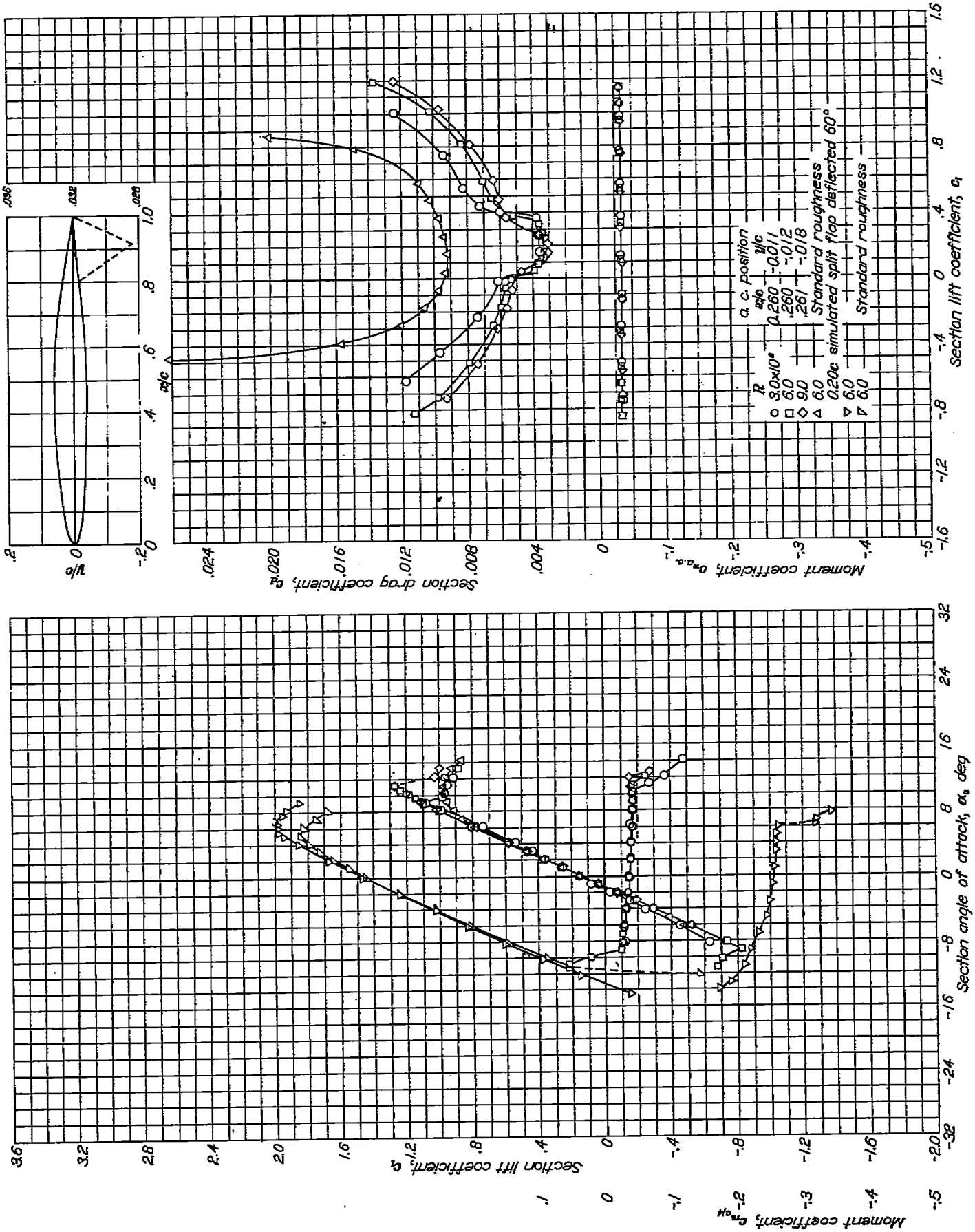

Aerodynamic characteristics of the NACA 66-210 airfoil section, 24-inch chord.

NACA 66$_1$-012

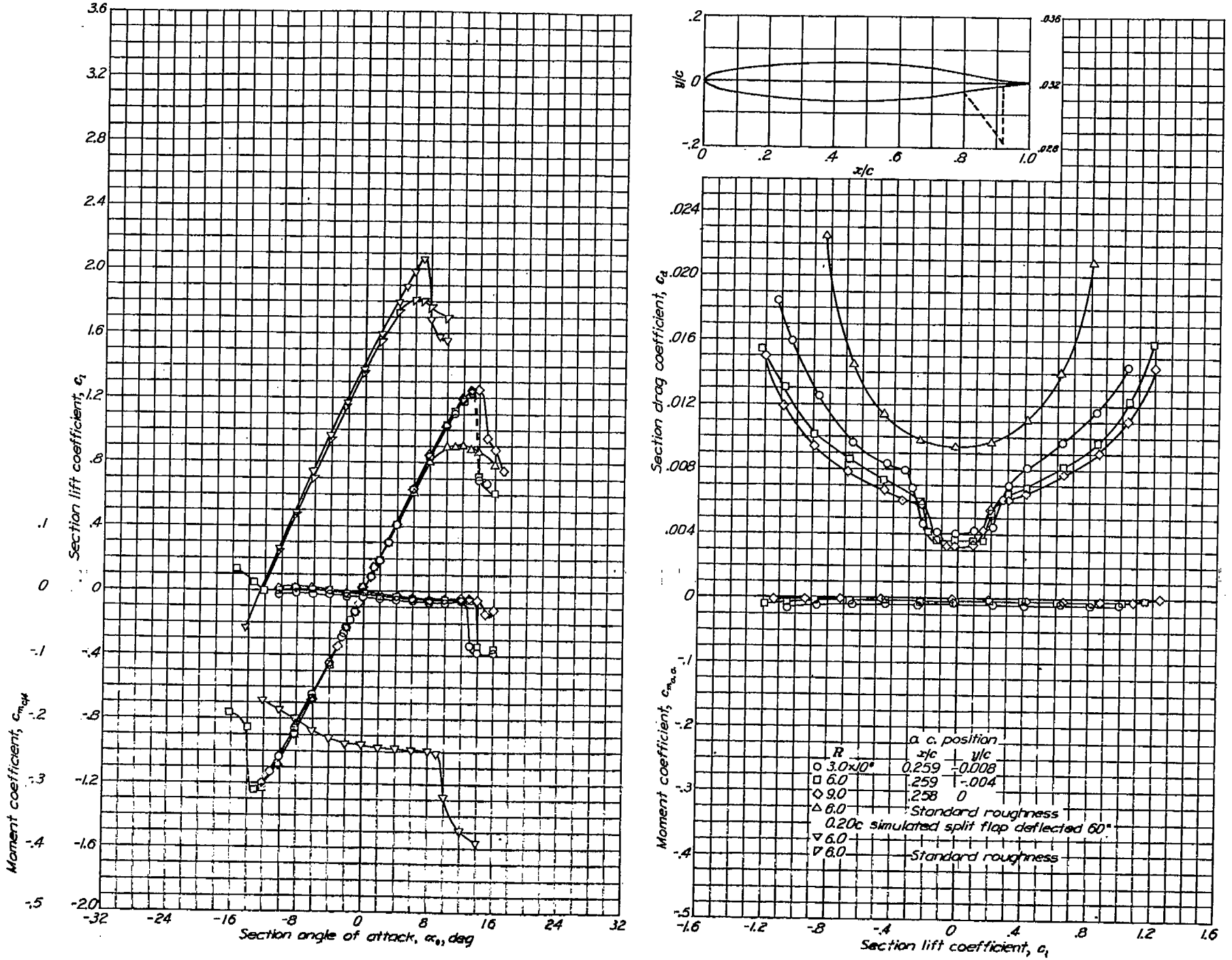

Aerodynamic characteristics of the NACA 66$_1$-012 airfoil section, 24-inch chord.

NACA 66$_1$-212

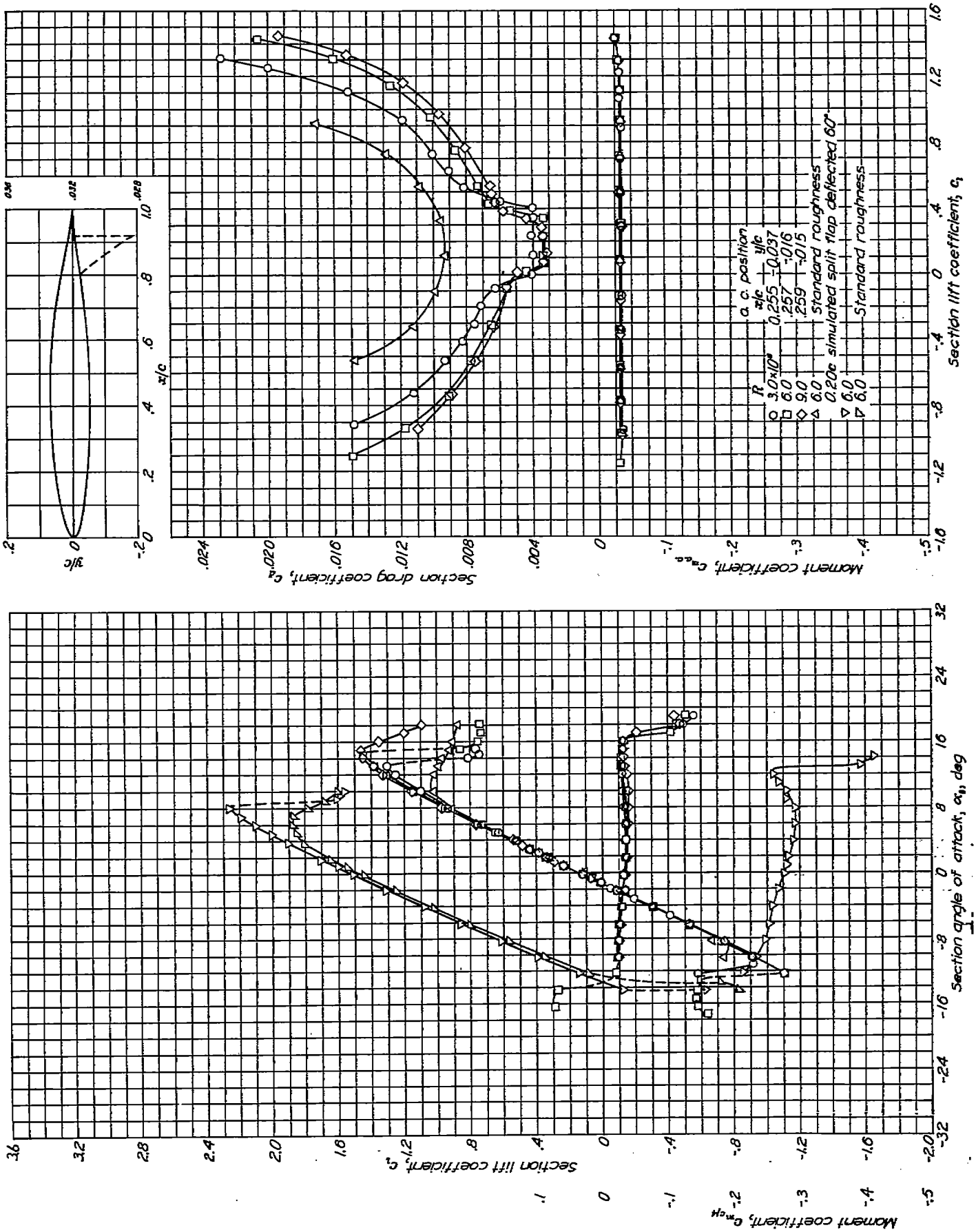

Aerodynamic characteristics of the NACA 66$_1$-212 airfoil section, 24-inch chord.

NACA 66$_2$-015

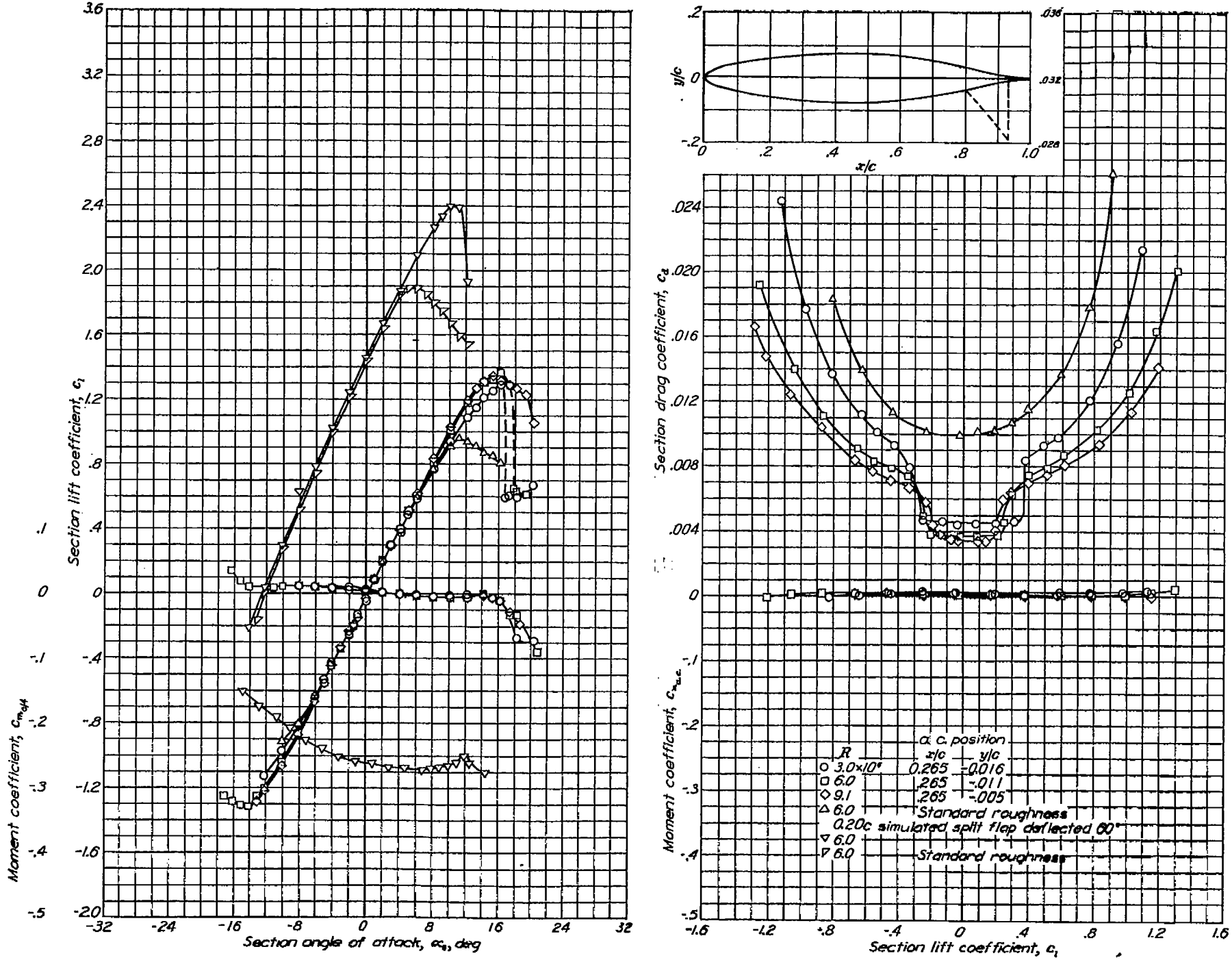

Aerodynamic characteristics of the NACA 66$_2$-015 airfoil section, 24-inch chord.

NACA 66$_2$-215

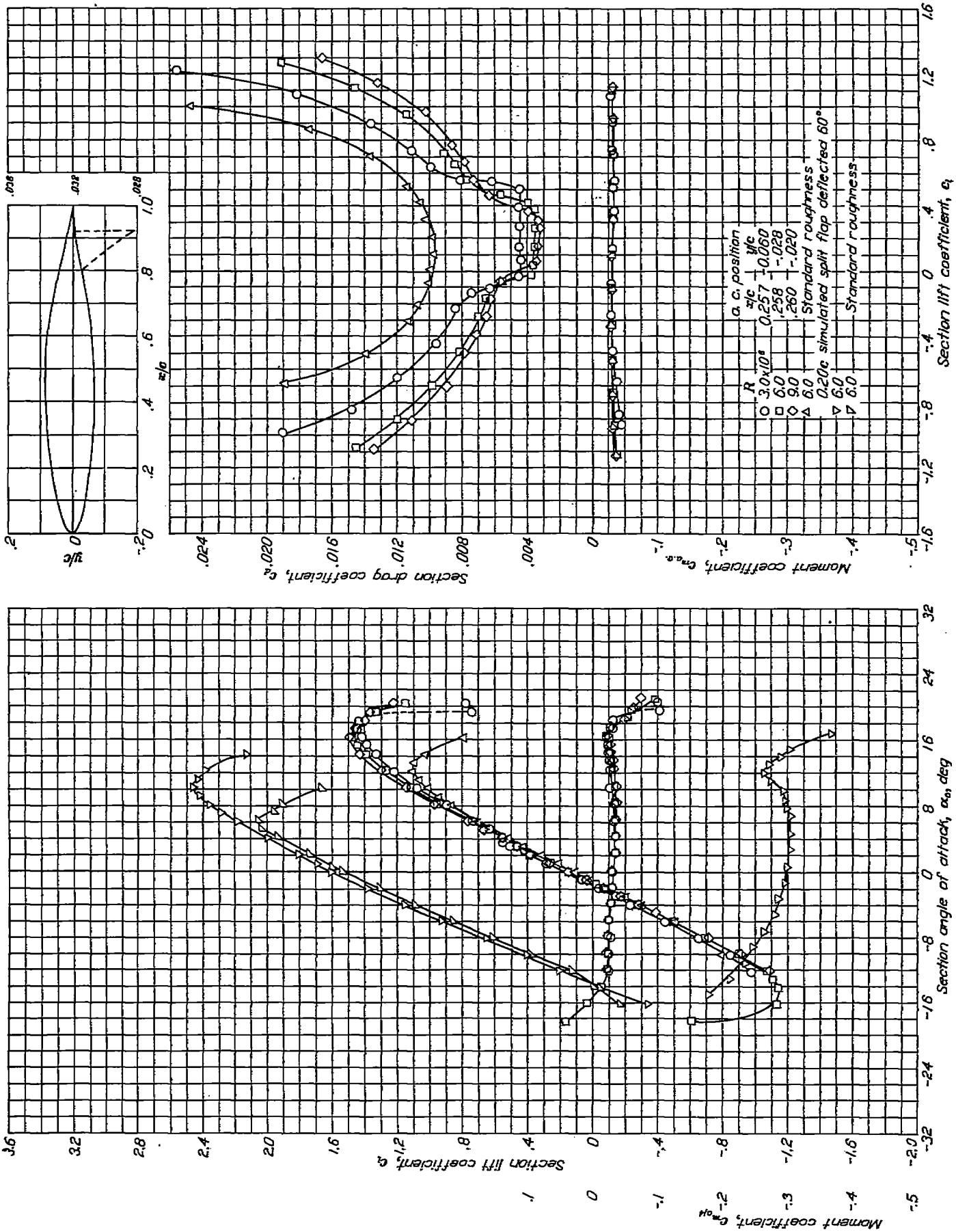

Aerodynamic characteristics of the NACA 66$_2$-215 airfoil section, 24-inch chord.

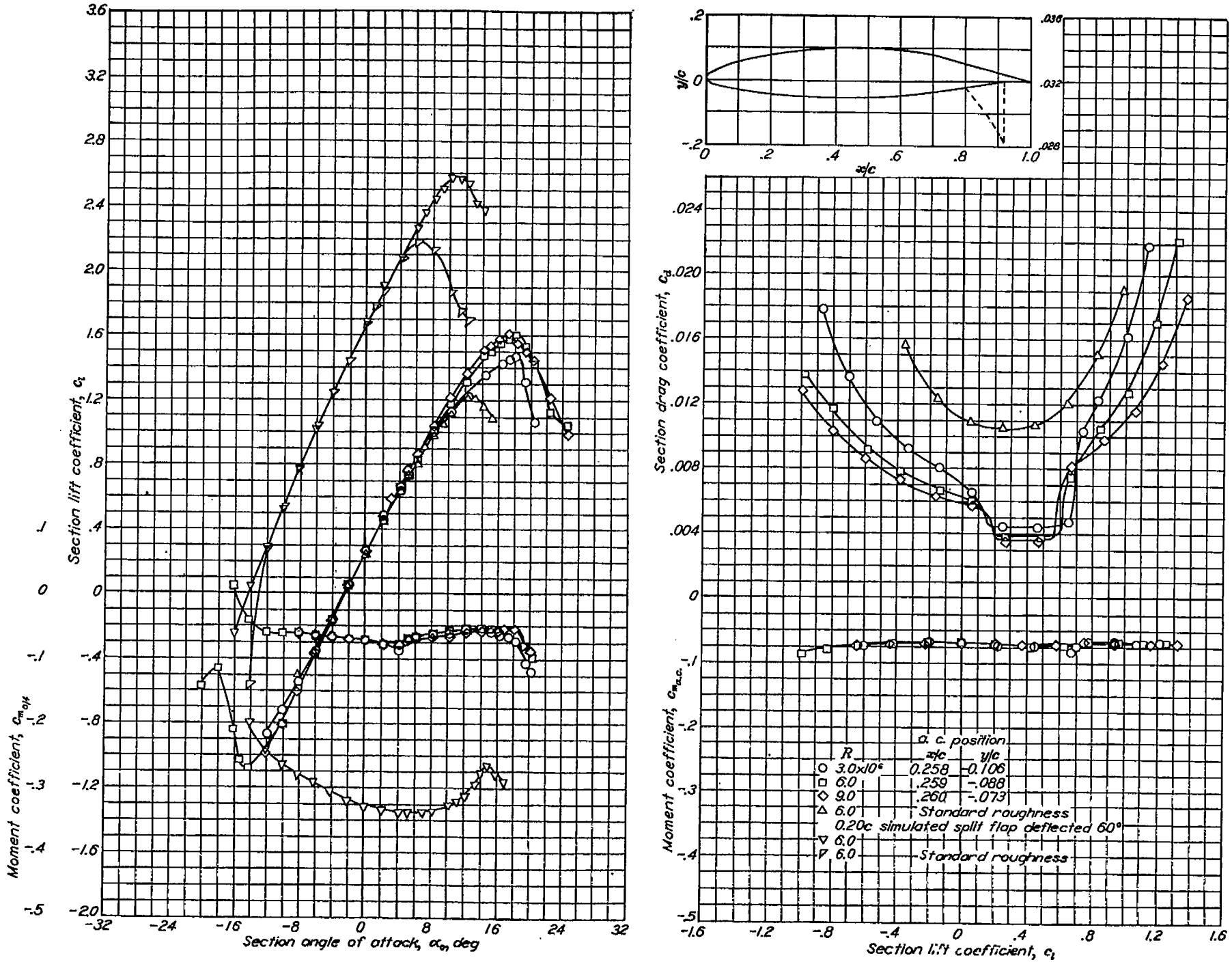

Aerodynamic characteristics of the NACA 66$_2$-415 airfoil section, 24-inch chord.

NACA 66$_3$-018

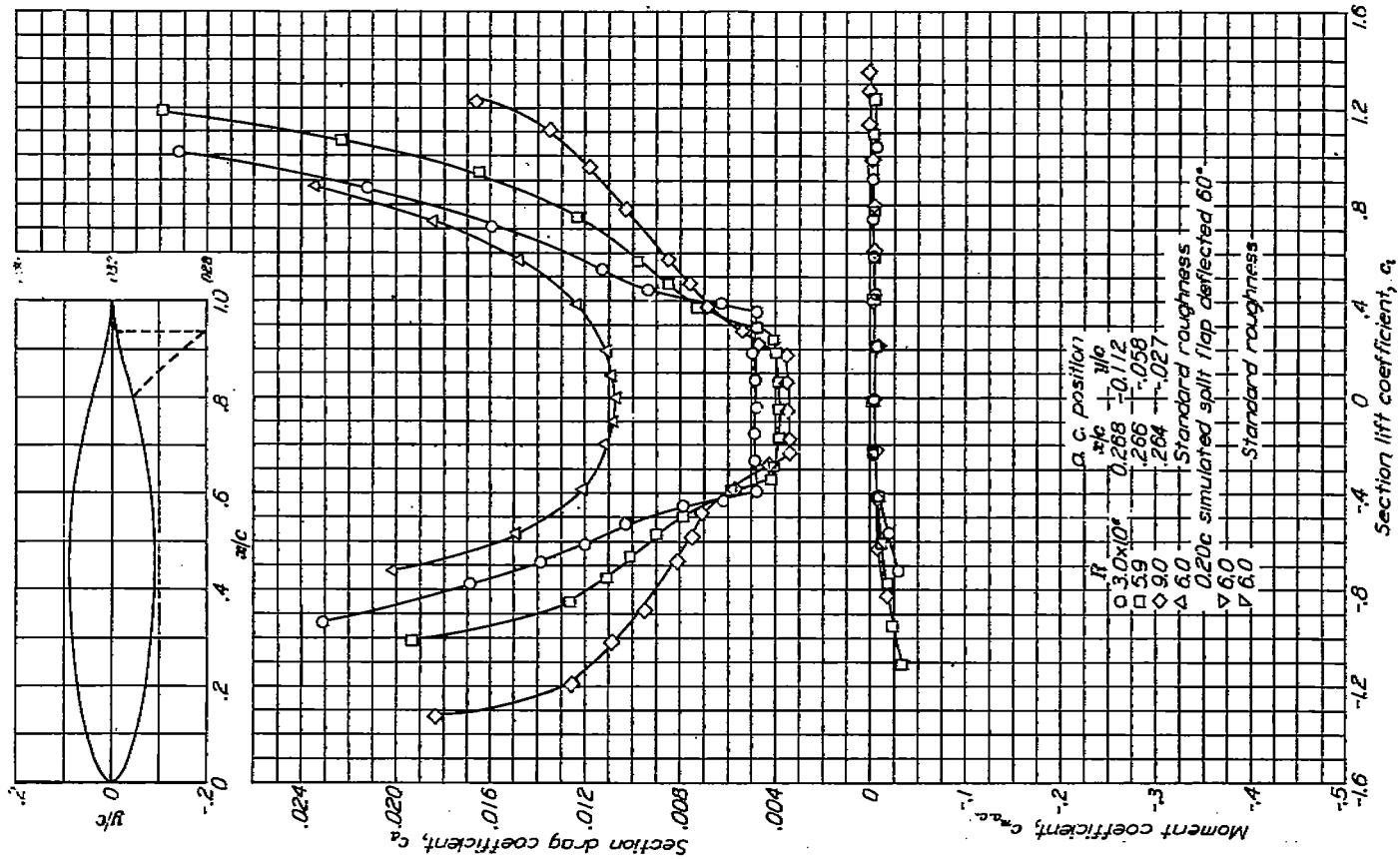

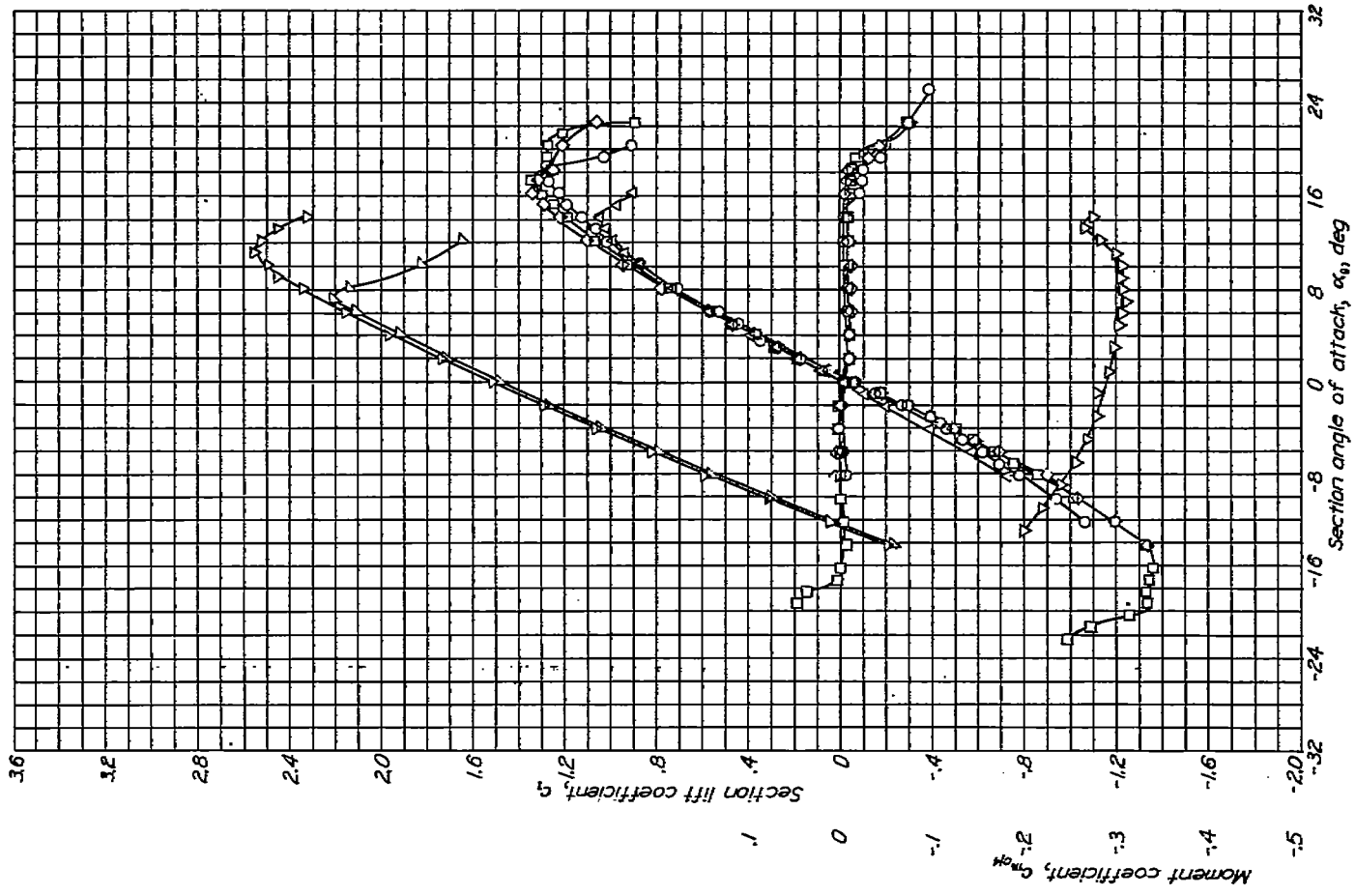

Aerodynamic characteristics of the NACA 66$_3$-018 airfoil section, 24-inch chord.

NACA 66$_3$-218

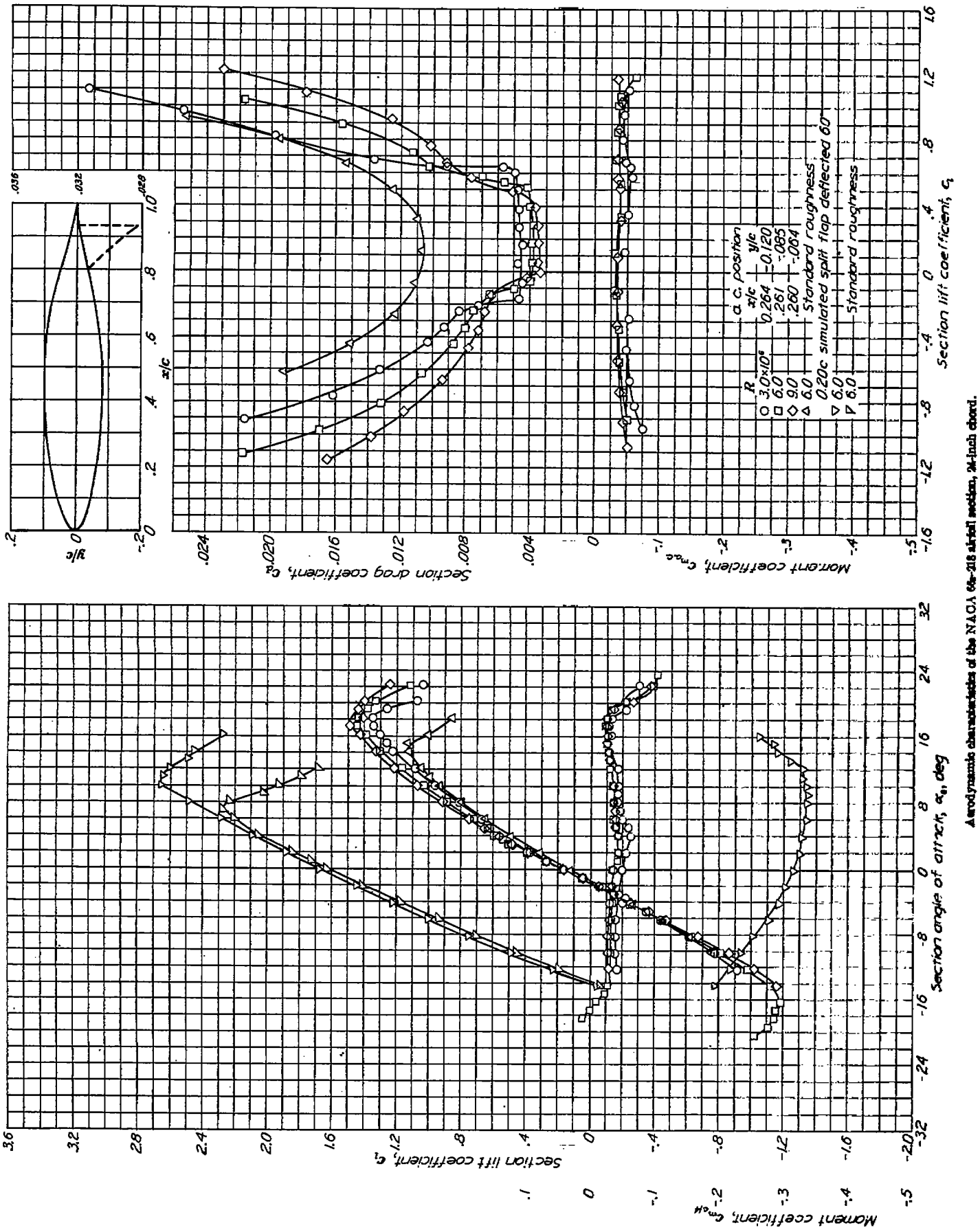

Aerodynamic characteristics of the NACA 66$_3$-218 airfoil section, 24-inch chord.

NACA 66$_3$-418

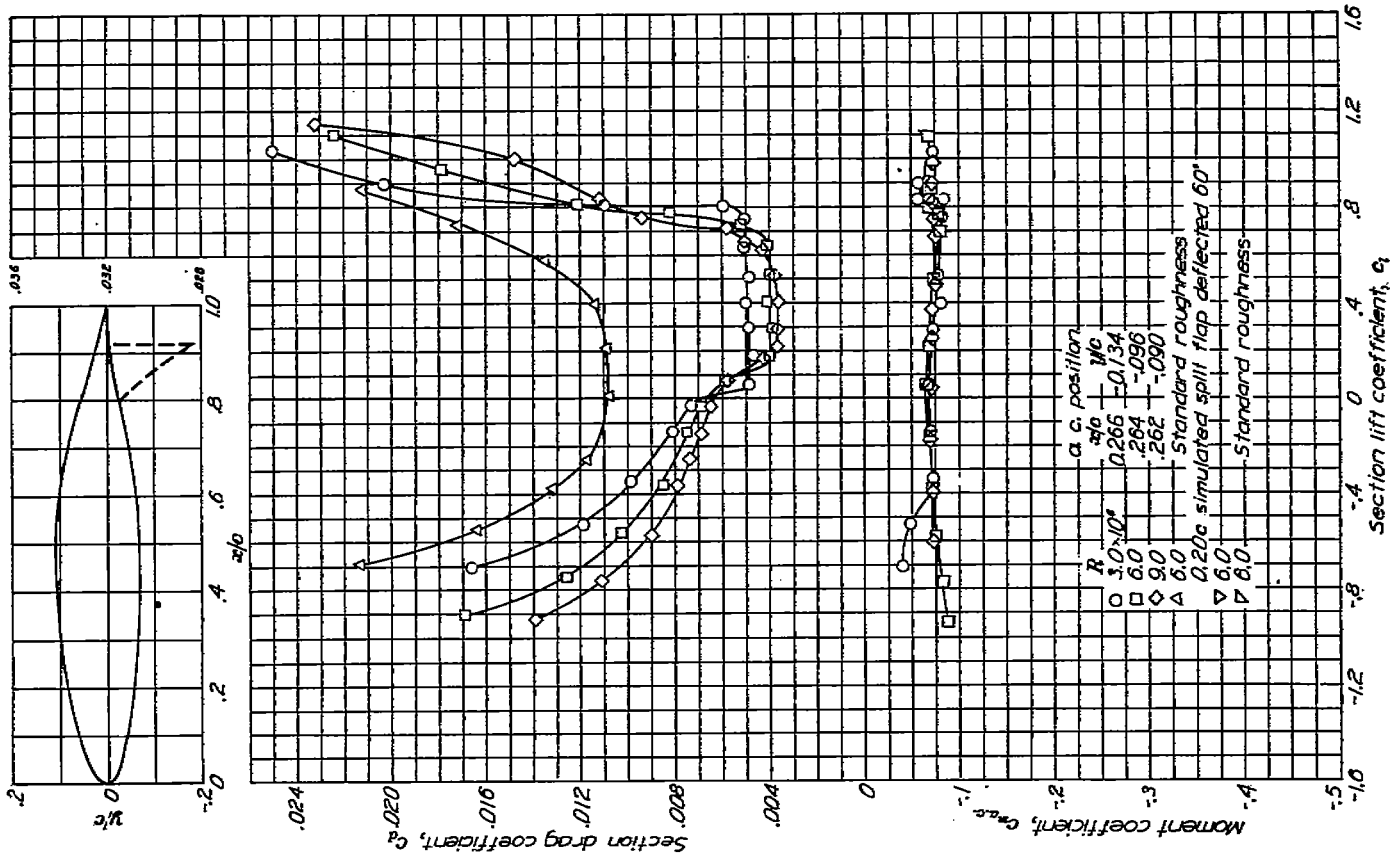

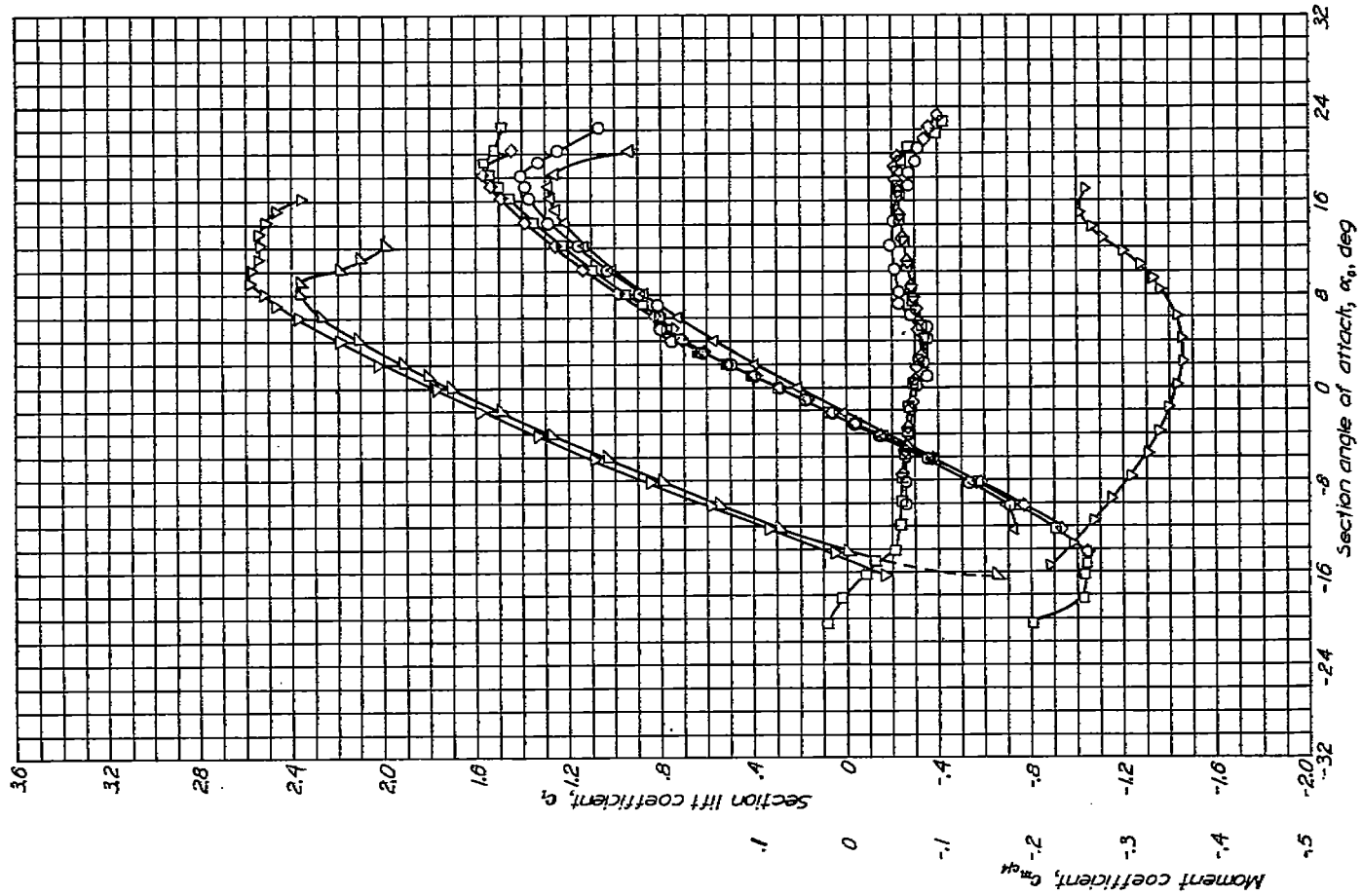

Aerodynamic characteristics of the NACA 66-418 airfoil section, 24-inch chord.

NACA 664-021

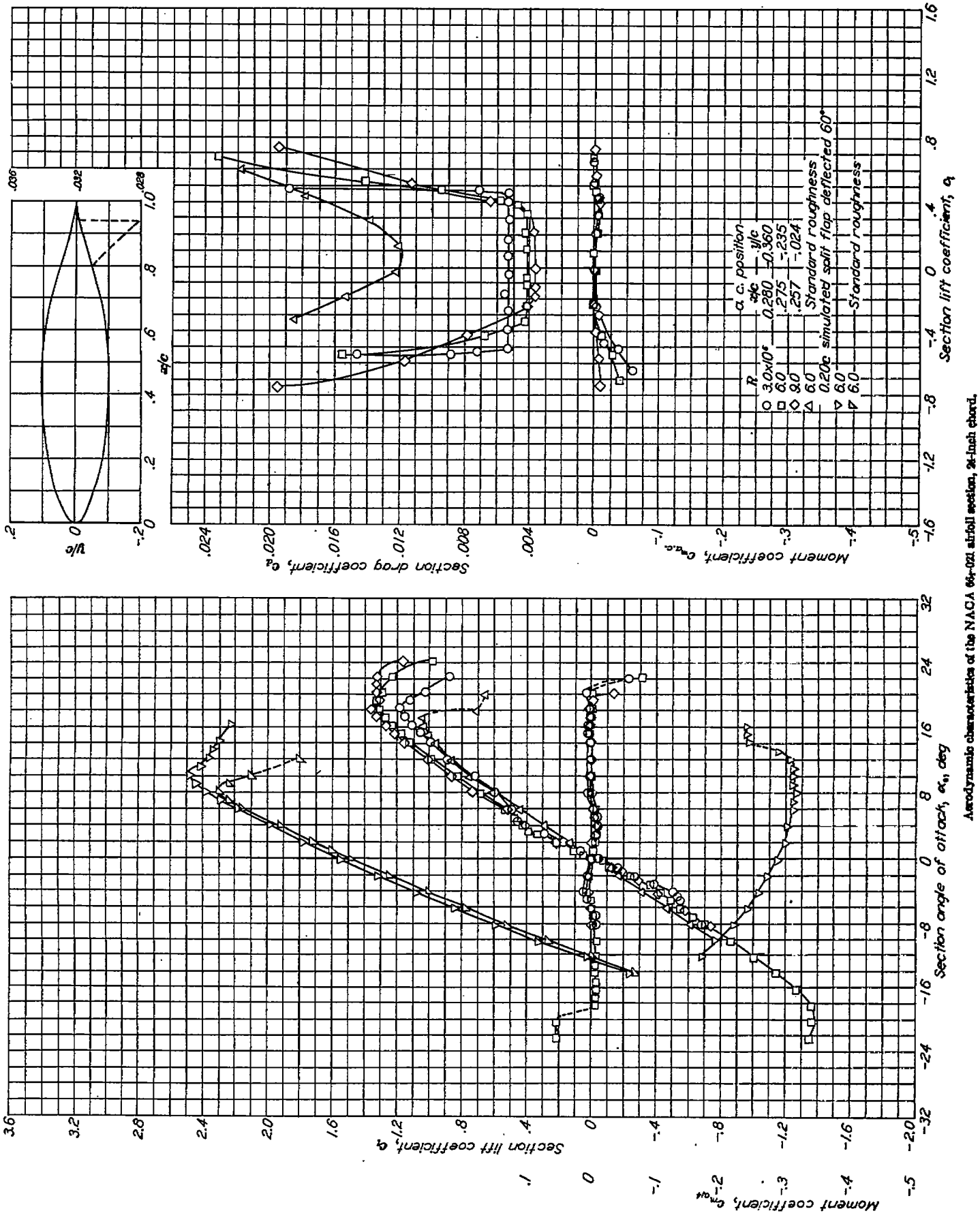

Aerodynamic characteristics of the NACA 64-021 airfoil section, 24-inch chord.

NACA 664-221

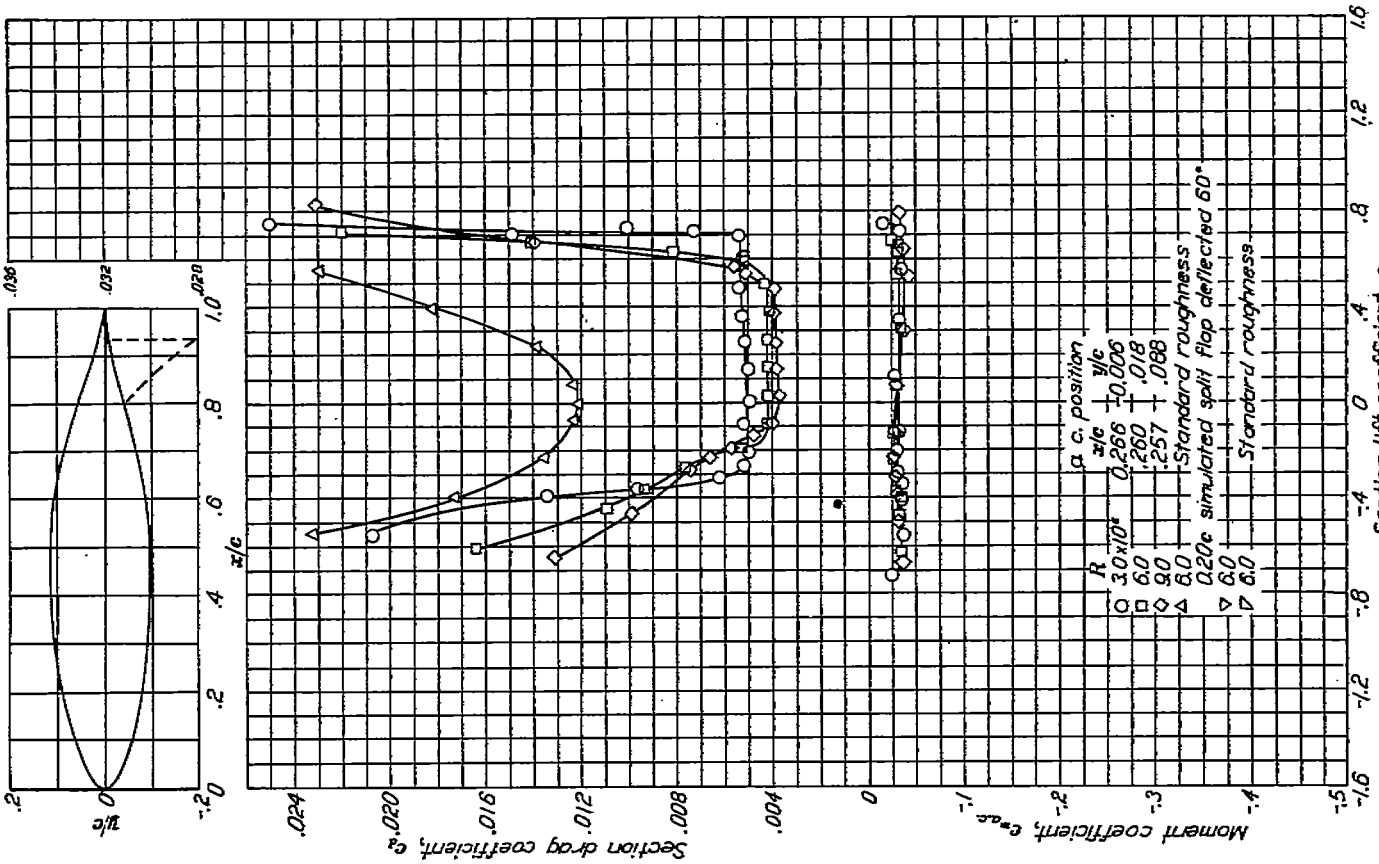

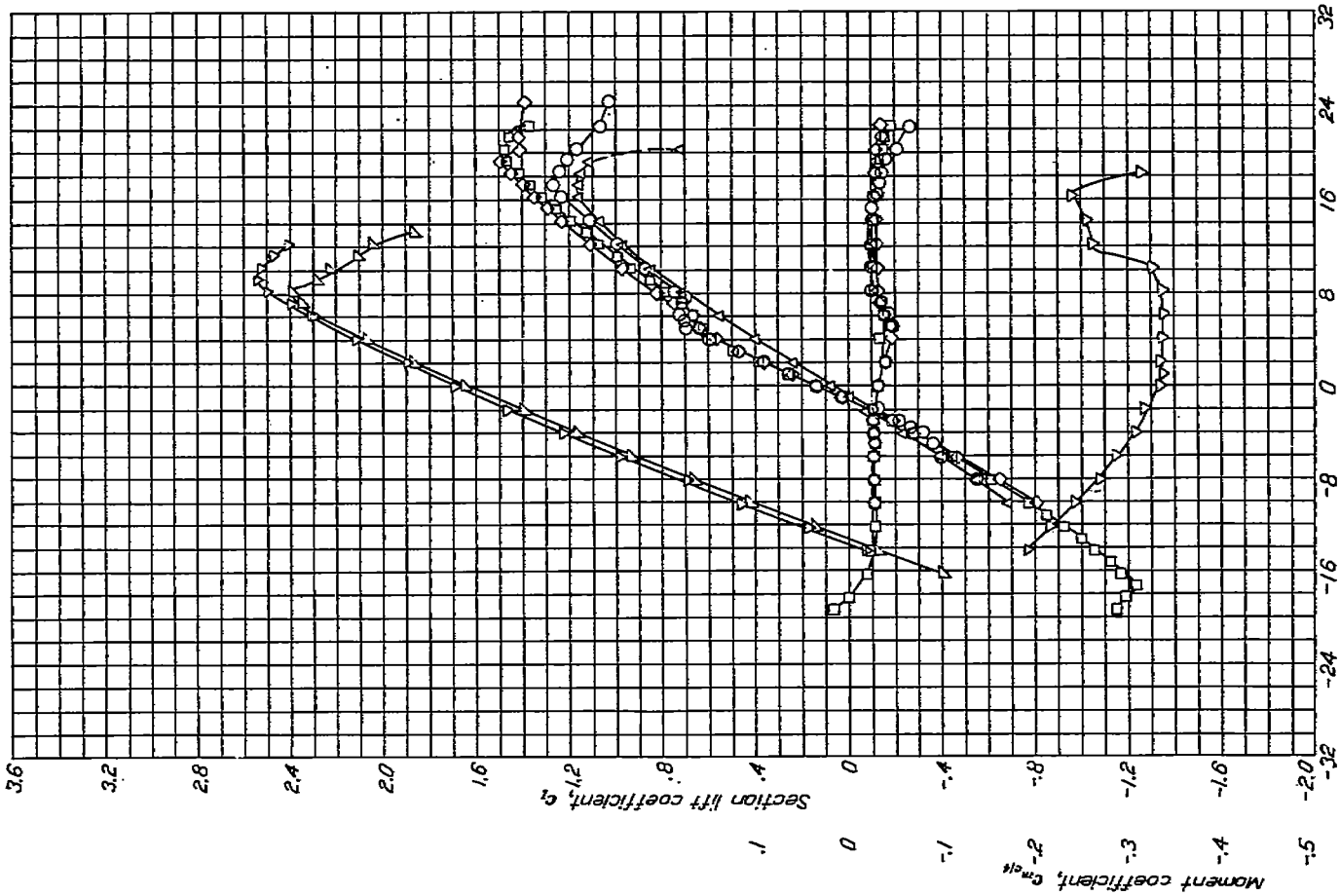

Aerodynamic characteristics of the NACA 66-221 airfoil section, 24-inch chord.

NACA 67,1-215

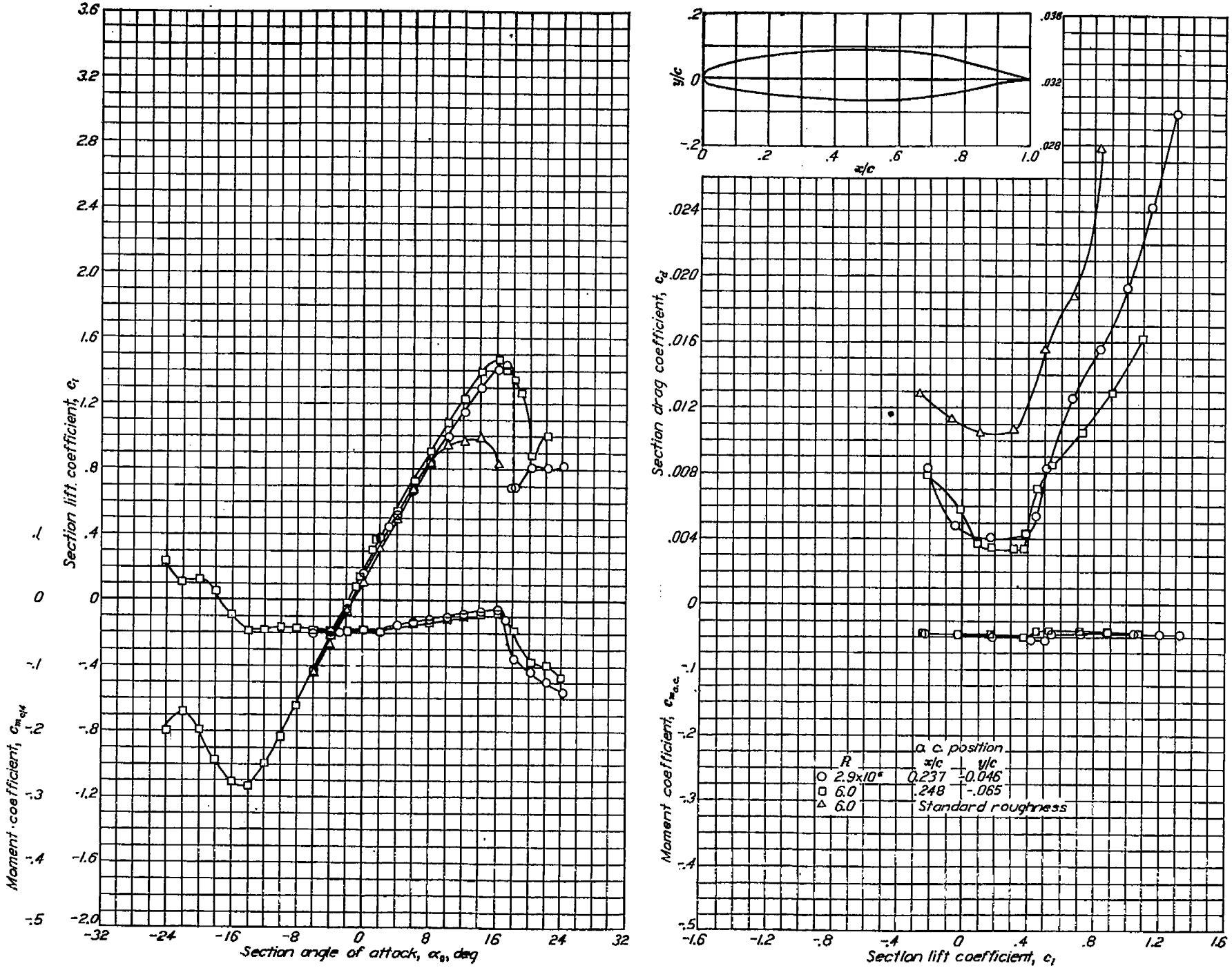

Aerodynamic characteristics of the NACA 67,1-215 airfoil section, 24-inch chord.

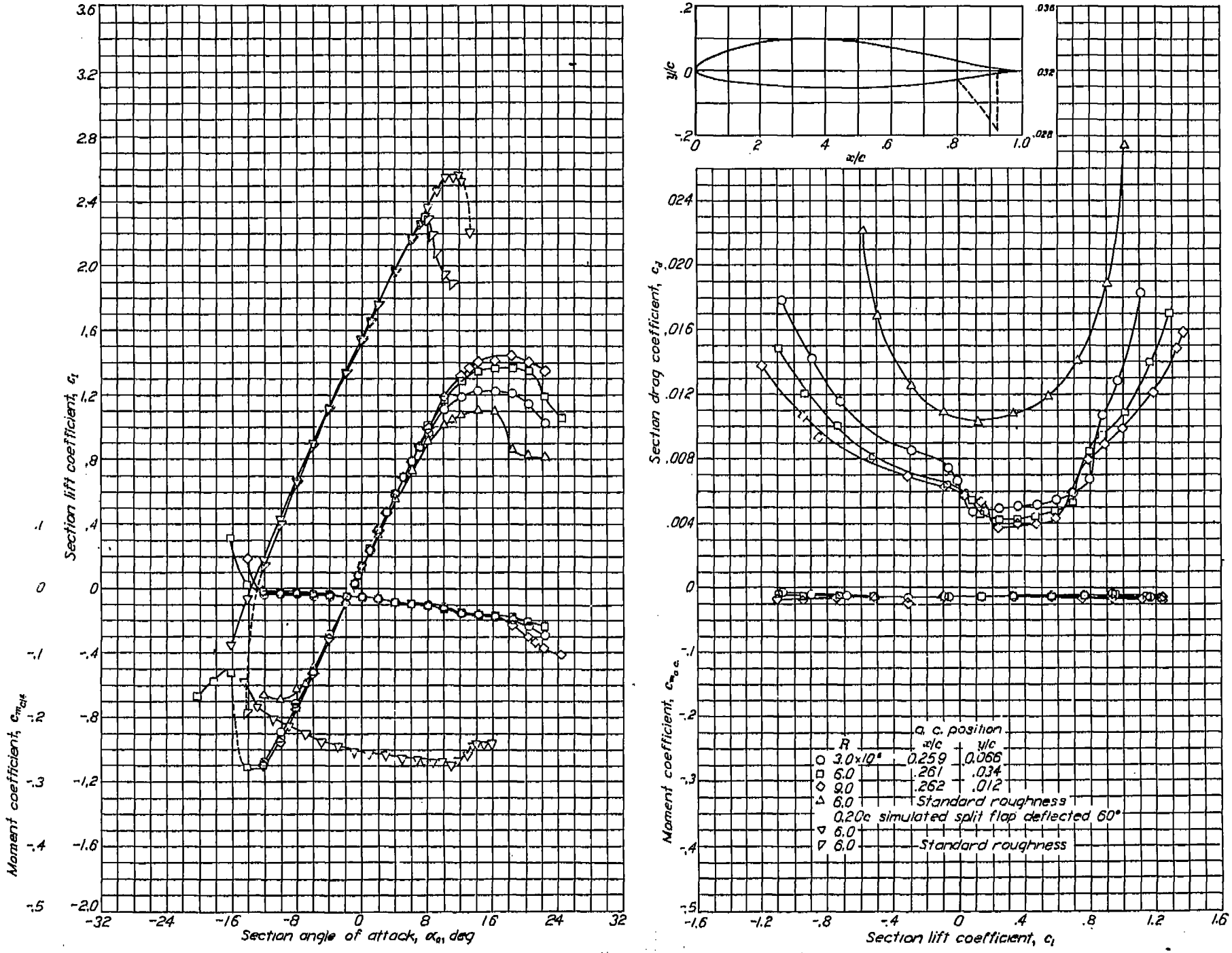

Aerodynamic characteristics of the NACA 747A315 airfoil section, 24-inch chord.

NACA 747A415

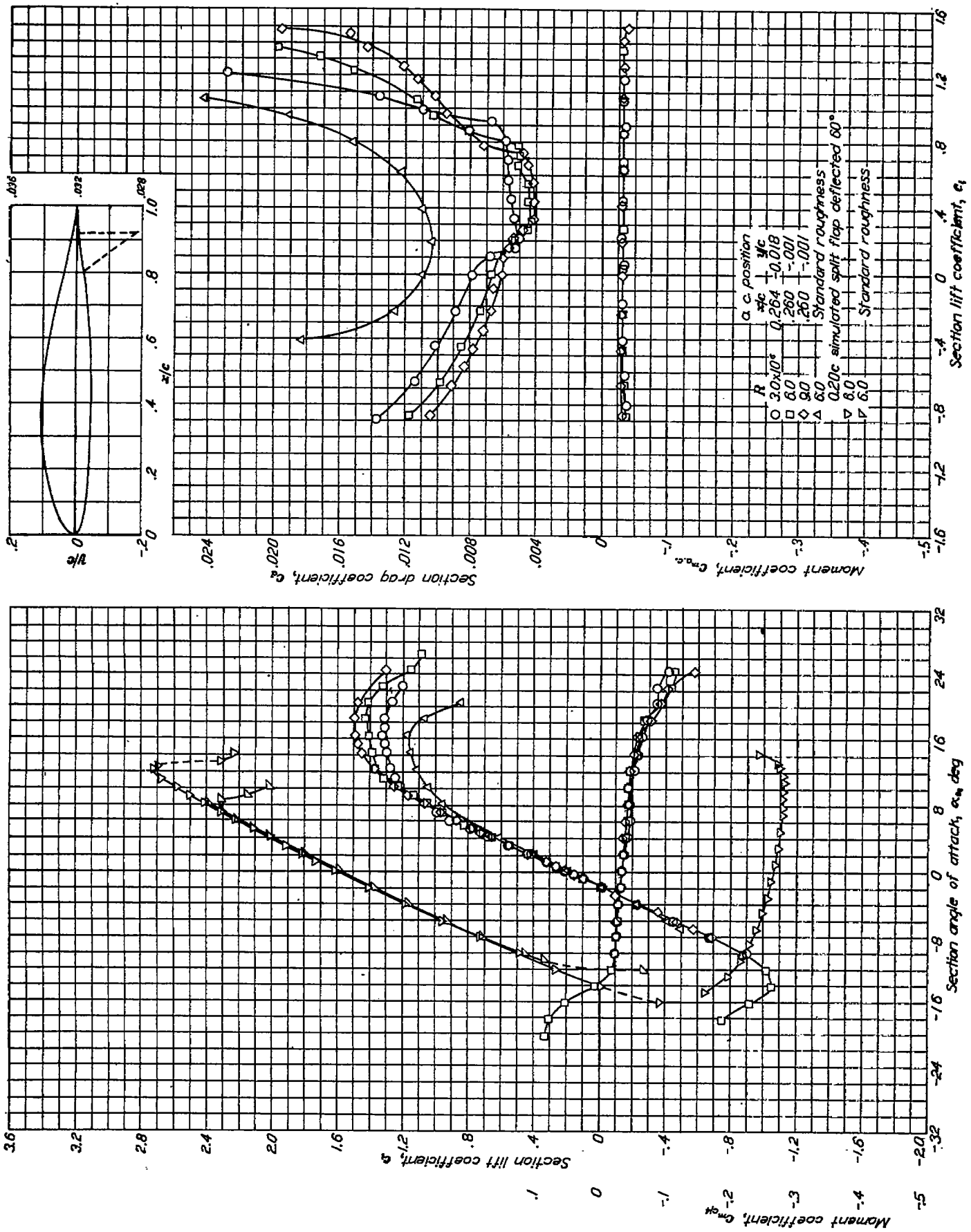

Aerodynamic characteristics of the NACA 747A415 airfoil section, 24-inch chord.